frontiers | Research Topics

Bacteriophage and host interactions

Edited by
Alicja Wegrzyn and Sylwia Bloch

Coordinated by
Kotsoana Peter Montso

Published in
Frontiers in Microbiology

ISSN 1664-8714
ISBN 978-2-8325-5015-1
DOI 10.3389/978-2-8325-5015-1

About Frontiers

Frontiers is more than just an open access publisher of scholarly articles: it is a pioneering approach to the world of academia, radically improving the way scholarly research is managed. The grand vision of Frontiers is a world where all people have an equal opportunity to seek, share and generate knowledge. Frontiers provides immediate and permanent online open access to all its publications, but this alone is not enough to realize our grand goals.

Frontiers journal series

The Frontiers journal series is a multi-tier and interdisciplinary set of open-access, online journals, promising a paradigm shift from the current review, selection and dissemination processes in academic publishing. All Frontiers journals are driven by researchers for researchers; therefore, they constitute a service to the scholarly community. At the same time, the *Frontiers journal series* operates on a revolutionary invention, the tiered publishing system, initially addressing specific communities of scholars, and gradually climbing up to broader public understanding, thus serving the interests of the lay society, too.

Dedication to quality

Each Frontiers article is a landmark of the highest quality, thanks to genuinely collaborative interactions between authors and review editors, who include some of the world's best academicians. Research must be certified by peers before entering a stream of knowledge that may eventually reach the public - and shape society; therefore, Frontiers only applies the most rigorous and unbiased reviews. Frontiers revolutionizes research publishing by freely delivering the most outstanding research, evaluated with no bias from both the academic and social point of view. By applying the most advanced information technologies, Frontiers is catapulting scholarly publishing into a new generation.

What are Frontiers Research Topics?

Frontiers Research Topics are very popular trademarks of the *Frontiers journals series*: they are collections of at least ten articles, all centered on a particular subject. With their unique mix of varied contributions from Original Research to Review Articles, Frontiers Research Topics unify the most influential researchers, the latest key findings and historical advances in a hot research area.

Find out more on how to host your own Frontiers Research Topic or contribute to one as an author by contacting the Frontiers editorial office: frontiersin.org/about/contact

Bacteriophage and host interactions

Topic editors
Alicja Wegrzyn — University of Gdansk, Poland
Sylwia Bloch — University of Gdansk, Poland

Topic coordinator
Kotsoana Peter Montso — Stellenbosch University, South Africa

Citation
Wegrzyn, A., Bloch, S., Montso, K. P., eds. (2024). *Bacteriophage and host interactions*. Lausanne: Frontiers Media SA. doi: 10.3389/978-2-8325-5015-1

Table of contents

frontiers | Frontiers in Microbiology

TYPE Editorial
PUBLISHED 31 May 2024
DOI 10.3389/fmicb.2024.1422076

OPEN ACCESS

EDITED AND REVIEWED BY
Sangryeol Ryu,
Seoul National University, Republic of Korea

*CORRESPONDENCE
Sylwia Bloch
✉ sylwia.bloch@ug.edu.pl

RECEIVED 23 April 2024
ACCEPTED 24 May 2024
PUBLISHED 31 May 2024

CITATION
Bloch S and Wegrzyn A (2024) Editorial: Bacteriophage and host interactions. *Front. Microbiol.* 15:1422076. doi: 10.3389/fmicb.2024.1422076

Editorial: Bacteriophage and host interactions

Sylwia Bloch[1]* and Alicja Wegrzyn[2]

[1]Department of Molecular Biology, University of Gdansk, Gdansk, Poland, [2]University Center for Applied and Interdisciplinary Research, University of Gdansk, Gdansk, Poland

KEYWORDS

bacteriophages, phage-host interactions, phage therapy, lytic and lysogenic cycles, pathogenic bacteria

Editorial on the Research Topic
Bacteriophage and host interactions

Bacteriophages (shortly phages) are defined as viruses that infect bacteria. They play a crucial role in many ecosystems by affecting the bacterial communities (Dion et al., 2020). This phenomenon is tightly bound with the fact that phages have complex interactions with their hosts. They are unable to carry out most of the biological processes on their own and need a live bacterial cell to multiply efficiently. As a result, phages have an influence on host abundance, diversity, physiology, and metabolism. For these reasons, bacteriophages are considered as a drivers of microbial diversity and may be use as means to understand many molecular mechanisms in biological processes. Over the last two decades, phages have been also intensively studied for their usage in biotechnology, medicine, food industry, and agriculture (Naureen et al., 2020; Albrycht et al., 2022). Application of bacteriophages in many areas of life undoubtedly requires, for safety reasons, a deep analysis of complex phage-bacteria interactions.

This Research Topic has been devoted to works that aim to help researchers understand the network of various interactions between bacteriophages and their hosts. The current Research Topic consists of fourteen articles. These articles are extremely interesting and well-representing the diversity of the studies on biology and biotechnology of bacteriophages.

Phages develop some strategies to adapt to different environmental conditions (Dennehy and Abedon, 2020). In the first article, Laguno-Castro et al. demonstrated that the adaptive pathway of phage Qβ, in the face of similar variations of *Escherichia coli* cells density, depends on temperature. They showed that in the conditions of the reduction of host availability, Qβ chooses the same adaptive strategy at 30 and 43°C, which is related to the improvement of its entry into bacterial cell. The authors concluded that the adaptation of Qβ to low bacterial cells availability involves different mutational pathway depending on the balance between fitness advantages and costs of replication at each temperature.

Through a series of interactions between phage-encoded receptor binding proteins (RBPs) and receptors located on the cell surface, the virus recognizes a sensitive bacteria (Bertozzi Silva et al., 2016). The work by Forrest et al. presented the evidence of genetic dependencies between *sap, csaB* and the sporulation proteins Spo0A, Spo0B, and Spo0F of *Bacillus anthracis* with the RBPs of the AP50c and W1 bacteriophages. Thanks to these results, we understood better the mechanisms of attachment and entry strategies of phages infecting the *Bacillus anthracis* bacterium.

One of challenges of molecular engineering is how to introduce foreign DNA to environmental bacterial cells. An excellent solution to this problem is the P1 bacteriophage (Westwater et al., 2002). The third article, published by Giermasińska-Buczek et al., focused on the interactions of P1 with an environmental epiphytic isolate *Pantoea agglomerans* L15. The authors demonstrated that the L15 can be a host for the phage P1. Moreover, based on analysis of the L15 interaction with the P1 *c1-100* Tn9 mutant, they have discovered the influence of antibiotic selection pressure on overcoming the barriers protecting bacterial cells from foreign DNA.

Bacteria evade viral infections by developing various defense systems (Egido et al., 2022). In the review article, Akritidou and Thurtle-Schmidt described the composition, structure, and function of overcoming lysogenization defect (OLD) nucleases that contain an ABC ATPase and Toprim domains. The authors also highlighted the role of OLD proteins in the anti-phage defense systems, such as the Gabija system and retrons.

Our understanding of phage-host interactions is extremely important to effectively use bacteriophages against pathogenic bacteria in a wide range of sectors of our life. Several articles in the Research Topic addressed this issue. In the review article, Glizniewicz et al. presented different phage-mediated strategies for combating polymicrobial biofilms. They also summarized the advantages and disadvantages of phage therapy, and familiarized the reader with the perspectives of such form of treatment.

The next article related to phage therapy, published by Pacios et al., focused on improving the lytic activity of phage vB_KpnS_VAC35 against two bacteremia-causing isolates of *Klebsiella pneumoniae*. The authors demonstrated that bacterial cells exposed to mucin and the *N*-acetyl cysteine exhibited a significant reduction in the frequency of phage resistance compared to mucin-treated bacteria. Determining the dependences between the mucoid environment and the difficulties in applying phage therapy allowed researchers to create a promising approach based on the application of mucolytic agents together with phages against *K. pneumoniae* infections.

In turn, the work by Chen et al. described the identification and characterization of phage vB_KpP_HS106 which infects 26 *K. pneumoniae* strains isolated from dairy farms in Shanghai. The great advantages of this virus are a good tolerance to extreme environments and the ability to efficient reduction of *K. pneumoniae* in milk and chicken meat. Therefore, HS106 has a prospects as biocontrol agent used against *K. pneumoniae* in foods.

Another phage with antimicrobial potential has been presented by Cui et al.. The vB_PaeP_ASP23 infects *Pseudomonas aeruginosa* strain L64 which causes hemorrhagic pneumonia in minks. Interestingly, the authors also confirmed the lytic activity of lysin and holin of the ASP23 against some tested Gram-negative and -positive bacteria, respectively. In this case, all three, ASP23, LysASP and recombinant phage HolASP can be considered as promising antimicrobial tools in the mink farming industry.

In the next article, Zou et al. described a novel phage MA9V-1 infecting *Chryseobacterium indologenes* which is the primary agent of root rot of *Panax notoginseng*. MA9V-1 exhibited a quick adsorption rate (>75% in 8 min) and a brief latent period (20 min). Moreover, the phage particles were stable in a relative broad range of temperatures (30–60°C). The authors suggested that these features of MA9V-1 make this virus promising in its use for preventing the diseases of medical plants.

Other studies on the control of plant diseases were presented in the article by Borowicz et al.. The researchers characterized the dickeyocin P2D1of *Dickeya dadantii* strain 3937, a representant of plant pathogenic Soft Rot *Pectobacteriaceae* (SRP). Interestingly, P2D1 could kill eight different *Dickeya* ssp. Moreover, this tailocin was stable at temperatures between 4 and 50°C, in pHs ranking from 3.5 to 12, and in osmotic conditions generated by NaCl (0.01–1 M). All of these features indicate that the newly identified dickeyocin would be a grate tool in controlling SRP infections in crops.

One of the biggest challenges in designing bacteriophage-based therapy is to identify the most appropriate phage which will be effective in the fight against pathogenic bacteria. A promising solution to this problem may be the water-in-oil droplet-mediated method described in the work by Hoshino et al.. This approach is based on the combination of droplet technology with a fluorescent YOYO-1 dye that stains the virus particles. Such an innovative method will enable researchers to isolate previously unidentified viruses for known host when applied to environmental samples.

Quite different approach was presented in the article by Aggarwal et al.. The authors have developed an *in-silico* tool, named PhageTB, for the prediction of phage-bacteria interactions with high accuracy. Interestingly, this bioinformatics tool contains three modules: host for phage, phage-host interaction and phage for host. We believe that PhageTB will be an effective method for prediction of phage-based therapy against bacterial infections.

It should also be mentioned that the pathogenicity of some bacteria is related to the presence of prophages in their genomes. In the next article, Mangieri et al. characterized inducible prophages from three shiga toxin producing *E. coli* strains. Interestingly, the authors indicated that some factors in cheese making process, such as NaCl and lactic acid, can be considered as potential stressors to induce phage release. Unfortunately, such a phenomenon promotes the shiga toxins transmission among bacteria and affects the safety of the cheese manufacturing.

In turn, the work by Li et al. described the role of spontaneous induction of newly identified prophage phi485 in avian pathogenic *E. coli* strain DE458. This study reveals that the deletion of phi458 leads to a strong decreased of biofilm formation and increased colonization abilities and virulence of DE458Δphi458. Undoubtedly, this report will allow us to better understand the relationship between the spontaneous induction of prophages and the pathogenicity of *E. coli* bacteria.

This Research Topic of articles includes articles describing a number of new and interesting phenomena regarding the complex networks of various dependencies between bacteriophages and their hosts. Readers are encouraged to get acquainted with details of the works published in the frame of this Research Topic as they provide a very valuable knowledge about pathogenic bacteria, phages and their potential applications in many areas of our life.

Author contributions

SB: Writing—original draft. AW: Writing—review & editing.

Funding

The author(s) declare that no financial support was received for the research, authorship, and/or publication of this article.

Conflict of interest

The authors declare that the research was conducted in the absence of any commercial or financial relationships that could be construed as a potential conflict of interest.

The author(s) declared that they were an editorial board member of Frontiers, at the time of submission. This had no impact on the peer review process and the final decision.

Publisher's note

References

Albrycht, K., Rynkiewicz, A. A., Harasymczuk, M., Barylski, J., and Zielezinski, A. (2022). Daily reports on phage-host interactions. *Front. Microbiol.* 13:946070. doi: 10.3389/fmicb.2022.946070

Bertozzi Silva, J., Storms, Z., and Sauvageau, D. (2016). Host receptors for bacteriophage adsorption. *FEMS Microbiol. Lett.* 363:fnw002. doi: 10.1093/femsle/fnw002

Dennehy, J. J., and Abedon, S. T. (2020). "Bacteriophage ecology," in *Bacteriophages: Biology, Technology, Therapy*, eds. D. R. Harper, S. T. Abedon, B. H. Burrowes, and M. L. McConville (Cham: Springer International Publishing), 1–42.

Dion, M. B., Oechslin, F., and Moineau, S. (2020). Phage diversity, genomics and phylogeny. *Nat. Rev. Microbiol.* 18, 125–138. doi: 10.1038/s41579-019-0311-5

Egido, J. E., Costa, A. R., Aparicio-Maldonado, C., Haas, P. J., and Brouns, S. J. J. (2022). Mechanisms and clinical importance of bacteriophage resistance. *FEMS Microbiol. Rev.* 46:fuab048. doi: 10.1093/femsre/fuab048

Naureen, Z., Dautaj, A., Anpilogov, K., Camilleri, G., Dhuli, K., Tanzi, B., et al. (2020). Bacteriophages presence in nature and their role in the natural selection of bacterial populations. *Acta Biomed.* 91:e2020024. doi: 10.23750/abm.v91i13-S.10819

Westwater, C., Schofield, D. A., Schmidt, M. G., Norris, J. S., and Dolan, J. W. (2002). Development of a P1 phagemid system for the delivery of DNA into gram-negative bacteria. *Microbiology* 14(Pt 4), 943–950. doi: 10.1099/00221287-148-4-943

frontiers | Frontiers in Microbiology

TYPE Original Research
PUBLISHED 14 November 2022
DOI 10.3389/fmicb.2022.1049341

OPEN ACCESS

EDITED BY
Alicja Wegrzyn,
Polish Academy of Sciences,
Poland

REVIEWED BY
Jens Andre Hammerl,
Bundesinstitut für Risikobewertung,
Germany
Sylwia Bloch,
University of Gdansk,
Poland

*CORRESPONDENCE
Qing Liu
liuq@usst.edu.cn
Fang Tang
tfalice@126.com

SPECIALTY SECTION
This article was submitted to Phage Biology, a section of the journal Frontiers in Microbiology

RECEIVED 20 September 2022
ACCEPTED 24 October 2022
PUBLISHED 14 November 2022

CITATION
Li D, Liang W, Hu Q, Ren J, Xue F, Liu Q and Tang F (2022) The effect of a spontaneous induction prophage, phi458, on biofilm formation and virulence in avian pathogenic *Escherichia coli*. *Front. Microbiol.* 13:1049341. doi: 10.3389/fmicb.2022.1049341

The effect of a spontaneous induction prophage, phi458, on biofilm formation and virulence in avian pathogenic *Escherichia coli*

Dezhi Li[1,2], Wei Liang[3], Qingyue Hu[1], Jianluan Ren[2], Feng Xue[2], Qing Liu[1]*and Fang Tang[2]*

[1]School of Health Science and Engineering, University of Shanghai for Science and Technology, Shanghai, China, [2]MOE Joint International Research Laboratory of Animal Health and Food Safety, Key Laboratory of Animal Bacteriology, Ministry of Agriculture, College of Veterinary Medicine, Nanjing Agricultural University, Nanjing, China, [3]The Fourth Affiliated Hospital of Guangxi Medical University, Liuzhou, Guangxi, China

Prophage sequences are present in most bacterial genomes and account for up to 20% of its host genome. Integration of temperate phages may have an impact on the expression of host genes, while some prophages could turn into the lytic cycle and affect bacterial host biological characteristics. We investigated the role of spontaneous induction prophages in avian pathogenic *Escherichia coli* (APEC), which is the causative agent of avian colibacillosis in poultry, and considered a potential zoonotic bacterium related to the fact it serves as an armory of extraintestinal pathogenic *E. coli*. We found that APEC strain DE458 had a high spontaneous induction rate *in vivo* and *in vitro*. The released phage particles, phi458, were isolated, purified, and sequenced, and the deletion mutant, DE458Δphi458, was constructed and characterized. Biofilm formation of DE458Δphi458 was strongly decreased compared to that of the wild-type strain ($p<0.01$). In addition, while the addition of DNase (100μg/ml) did not affect prophage release but could digest eDNA, it significantly reduced the biofilm production of DE458 biofilm to a level close to that of DE458Δphi458. Compared to DE458, the adhesion and invasion abilities of DE458Δphi458 increased by approximately 6–20 times ($p<0.05$). The virulence of DE458Δphi458 was enhanced by approximately 10-fold in chickens based on a 50% lethal dose. Furthermore, avian infection assays showed that the bacterial loads of DE458Δphi458 in the lung and liver were increased by 16.5- and 10-fold ($p<0.05$), respectively, compared with those of the WT strain. The qRT-PCR revealed that deletion of phi458 led to upregulation of type I fimbriate-related gene *fimH* and curli-related gene *csgC* by 3- and 2.8-fold, respectively ($p<0.01$). Our study revealed that phi458 promoted biofilm formation by spontaneously inducing and decreasing virulence by repressing virulence genes.

KEYWORDS

avian pathogenic *Escherichia coli*, prophage, spontaneous induction, virulence, biofilm formation

Introduction

Bacteriophages (phages), naturally occurring viruses that infect bacteria, outnumber bacteria by more than a factor of ten (Brussow and Hendrix, 2002). According to their lifecycles, phages are divided into two groups: lytic phages and lysogenic phages. Lysogenic phages, also called temperate phages, have DNA that is integrated into the bacterial genome or maintained as an episome after infecting bacteria (Feiner et al., 2015). With the advances in whole genome sequencing platforms, it has been proven that most bacterial genomes contain prophage sequences at proportions as high as 20% (Casjens, 2003).

It is worth noting that prophage sequences can also be excised from the bacterial genome when faced with extrinsic factors (e.g., UV radiation, ROS, pH, and heat) or intrinsic factors (stalled replication forks and ROS; Luchnik, 1979). These factors could upregulate the expressions of SOS genes and lead to expression of anti-repressors. The phage repressor protein was cleaved by binding to the antirepressor protein (Crowl et al., 1981). Then, the expressions of lytic phage genes can facilitate prophage excision from the bacterial genome and formation of phage particles (Nanda et al., 2015). Spontaneous prophage induction, an important but uncommon phenomenon, is the spontaneous activation of lytic genes even in the absence of the noninducing factors mentioned above (Santiviago et al., 2010; Nanda et al., 2014).

The influence of spontaneous prophages on bacterial fitness has been studied in a variety of bacterial species. For example, the prophage, Rs551, in *Ralstonia solanacearum*, could reduce the virulence and enhance the competitiveness of its host. Further study found that the presence of the CII phage repressor in Rs551 inhibited the expressions of genes related to twitching motility, extracellular polysaccharide production, and virulence (Ahmad et al., 2017). Similarly, integration of PhiRSM also led to a decline in *R. solanacearum* virulence; the difference was that the CI repressor caused this phenomenon (Addy et al., 2012). In *E. coli* K-12, deletion of all nine prophages resulted in decreased biofilm formation and impaired the ability to adapt to adverse environments. These nine prophages in *E. coli* K-12 were unable to form infectious virus particles, but seven of them were shown to excise spontaneously (Wang et al., 2010). In Shiga toxin-producing *E. coli* (STEC), spontaneous induction of prophages contributed to the entire bacterial population infecting host epithelial cells. Further study found that the type 3 secretion system in STEC, which is required for colonization, is negatively controlled by CII (Robinson et al., 2006; Shimizu et al., 2009).

Avian pathogenic *E. coli* (APEC), a major extraintestinal pathogenic *Escherichia coli* (ExPEC), is the causative agent of avian colibacillosis and causes huge economic loss in the poultry industry worldwide (Kathayat et al., 2021). neonatal meningitis *E. coli* (NMEC) is another important ExPEC which infects the central nervous system of newborns with a high morbidity and mortality (Nielsen et al., 2018). According to comparative genomics and phylogenetic group studies, both APEC and NMEC appeared obvious phylogenetic overlaps and shared some genes related to pathogenicity (for example, salmochelin and type I fimbriae; Ewers et al., 2007; Mitchell et al., 2015). In addition, some highly pathogenic APEC had been proved to be capable of inducing bacteremia or meningitis in mouse models (Tivendale et al., 2010). Therefore, APEC strains are presumed to be an armory of NMEC and be a potential zoonotic bacterium.

Integration of prophages not only brings new genes to the host but also has a stochastic impact on gene expressions (Canchaya et al., 2004). Spontaneous prophage induction may have an impact on the fitness of the bacterial host (Nanda et al., 2015). However, the role of prophages in APEC strains remains largely unknown. Thus, we searched for APEC strains with spontaneous prophage induction *in vitro* and *in vivo*. DE458 was shown to have a high spontaneous rate, and its released phage particles, phi458, were isolated, purified, and sequenced. To investigate the role of this spontaneously inducible prophage phi458 on bacterial fitness, a phi458 deletion mutant was constructed, and the biological properties of the strains were studied.

Materials and methods

Bacterial strains and culture conditions

The bacterial strains and prophages used in this work are listed in Table 1. The APEC strain, DE458, was isolated from a duck with clinical neurological symptoms and belongs to the phylogenetic *E. coli* reference (ECOR) Group B2.

E. coli strains were grown overnight at 37°C or 28°C in Luria-Bertani (LB) medium with shaking at 180 rpm. When necessary, the medium was supplemented with appropriate antibiotics [e.g., ampicillin (Amp, 100 μg/ml); kanamycin (Kan, 20 μg/ml); and chloramphenicol (Cm, 30 μg/ml)].

TABLE 1 Bacterial strains, phages and plasmids used in this study.

Strain, plasmids or phage	Description	Source
DE458	Wild-type APEC strain isolated, O2 serotype	This study
DE458Δphi458	Phi458 deletion mutant	This study
MC1061	The indicator bacteria	This study
pKD46	Express λ red recombinase, Amp	Datsenko and Wanner (2000)
pKD4	Template plasmid, Kan	Datsenko and Wanner (2000)
pCP20	Yeast Flp recombinase gene, FLP, Cm, Amp	Takara
Phi458	Prophage induced from DE458	Takara

Screening for spontaneous prophage induction

First, nalidixic acid was used to screen out the strain that could release phage particles under chemical conditions. Chemical phage induction assays were performed as previously described (DeMarini and Lawrence, 1992). Nalidixic acid suspended in sodium bicarbonate solution was sterilized with a 0.22-μm-pore-size membrane filter and added to log-phase growing cultures ($OD_{600} = 0.5$) at a final concentration of 1 μg/ml. After 3 h of incubation, the cultures were centrifuged at 5000 rpm for 10 min, and the supernatants were collected and passed through a 0.22-μm filter. To confirm the presence of phages in the supernatants, the *E. coli* strain, MC1061, was used as an indicator host for phages, and the double-layer agar method was used.

Second, the strains identified in the previous step were used to screen out the strains that exhibited spontaneous induction phenomena. A single colony of each strain was cultured in LB medium at 37°C for 12 h, and then, the cultured supernatants were collected and filtered. MC1061 was also used as an indicator strain to confirm the presence of phage particles as described previously.

Phage isolation, purification, and propagation

A single plaque on the double-layer agar plate was picked and incubated in 5 ml of LB medium with the addition of indicator strain MC1061. Phages were purified three times by the double-layer agar method. Finally, SM buffer was added to the double-layer agar plate, which was full of plaques, and incubated 4°C for 12 h. The SM buffer was collected and the bacteria were filtered out with a 0.22-μm filter.

TEM analysis

Phages were cultured in double-layer plates at 37°C for 10–12 h. A plate with an abundance of plaques was added to 3 ml of doubly deionized H_2O. Phages were slightly shaken for 10 min to fully wash them off. The suspensions were centrifuged at 5,000 rpm for 10 min, spotted onto a copper grid, and negatively stained with 2% uranyl acetate. The phage morphologies were observed by TEM (H 7650; Hitachi, Japan).

Induction rates in different environments

To measure the excision rates of phi458 at different temperatures, single DE458 colonies were picked and cultured overnight at 28°C or 42°C for 12 h. To determine the excision rate of phi458 when DE458 interacts with cells, the procedure used was similar to that used for the adhesion assays. DF-1 cells are derived from ELL chicken embryos and are a passable chicken fibroblast cell line which are widely used in bacterial infection model, animal virus research, and many other fields. In summary, chicken embryo fibroblast DF-1 cell monolayers were cultured in sterilized 24-well plates with DMEM (containing 10% fetal bovine serum) at 37°C in a humidified chamber containing 5% CO_2. Then, the log-phase bacterial cultures were harvested after centrifugation and washing twice with ice-cold DMEM to remove the LB medium and phage particles that had been released. The bacterial suspensions were infected with DF-1 cells (according to an infection multiplicity of 100) for 4 h at 37°C under a 5% CO_2-humidified atmosphere.

Bacterial DNA under different environmental conditions was extracted and used as a template for qPCR with a one-step qRT-PCR SYBR Green kit (Vazyme). Quantitative real-time PCR was used to determine the prophage excision rates (Lunde et al., 2003). The amounts of bacterial genome that absence of phi458 were measured using the primers flanking phi458 (Table 2); PCR products were generated only if the genome lacked phi458 due to the size of phi458. The relative number of the target gene was normalized to the reference gene, *purA*. Reactions and analyses were performed with an ABI PRISM 7300 Fast Real-time PCR machine.

Isolation of DNA from phage particles for genome sequence analysis

Purified phage particles were collected by PEG-8000 precipitation, and DNA was then isolated from the phage particles by phenol extraction. The extraction of bacterial DNA was performed using a Mega Bacterial DNA Kit (D3350-01) according to the manufacturer's protocol. The phi458 genomic DNA was sent to Shanghai Weina Biotechnology Co., Ltd. for whole genome sequencing. The next-generation sequencing (NGS) and MiSeq (Illumina) were used for genome sequencing. Raw sequenced reads were filtered for low-quality reads and assembled using Unicycler v 0.43 with a flagged minimum contig length of 1,000 bp. The assembled phi458 genome was annotated using RAST.[1] VirulenceFinder was used to determine the presence of virulence genes.[2]

Construction of DE458Δphi458

To investigate the role of phi458 in the DE458 genome, we constructed a DE458 mutant lacking phi458. The phi458 deletion mutant was generated based on the lambda Red-mediated recombination system (Datsenko and Wanner, 2000). First, the flanking regions of phi458 were amplified using plasmid pKD4 as a template with primers. Second, to replace the prophage region, the

1 https://rast.nmpdr.org/rast.cgi
2 https://cge.cbs.dtu.dk/services/

TABLE 2 Primers used in this study.

Primer	Sequence (5′ to 3′)	Target gene
K1	CAGTCATAGCCGAATAGCCT	pKD4
K2	CGGTGCCCTGAATGAACTGC	pKD4
Kt	CGGCCACAGTCGATGAATCC	pKD4
pKD46-F	GATACCGTCCGTTCTTTCCTT	pKD46-
pKD46-R	TGATGATACCGCCTGCCTTACT	
pCP20-F	ATTGGGTACTGTGGGTTTAGTGGTT	pCP20
pCP20-R	TTGGCTTATCCCAGGAATCTGTC	
Phi458-Mu-F	TGGGACTTGTGAGCGCAGTGTTGATGGGGTAATGCTTTGAATTAGAAGCGGATTCTTATAGTGTAGGCTGGAGCTGCTTC	Phi458
Phi458-Mu-R	TCTGGCACTCTCCGTGCTGGCAGAAGTCGCCTCTGTACGTCTCCATCAGGAGGAGGATTCCATATGAATATCCTCCTTAG	
qPCR-phi458-F	TGGGACTTGTGAGCGCAG	Deletion of
qPCR-phi458-R	TCTGGCACTCTCCGTGCT	phi458
RT-*fimH*-F	CTTATGGCGGCGTGTTATCT	*fimH*
RT-*fimH*-R	CGGCTTATCCGTTCTCGAATTA	
RT-*csgC*-F	CCATTGCTTTGACGAAGTTGAG	*csgC*
RT-*csgC*-R	GCGGCCATTGTTGTGATAAAT	
RT-*eaeH*-F	GTACCCTGAAGGCCACTAAATC	*eaeH*
RT-*eaeH*-R	GACTGCGTTCCGGTAGTAAAG	
RT-*ibeA*-F	ATGACGGTGGGAACAAGAGAA	*ibeA*
RT-*ibeA*-R	ATACCCCTATTGAATCCGCAT	
RT-*aufG*-F	CTGGATCAGCAACCTGGATATT	*aufG*
RT-*aufG*-R	CCCACACATCCGGCATATTA	
RT-*yqiL*-F	AGATCAGACGGTGAACTTTGG	*yqiL*
RT-*yqiL*-R	TCCCGTAATCACATAGCGTAAAT	
RT-*ompA*-F	TGGGTGTTTCCTACCGTTTC	*ompA*
RT-*ompA*-R	GAGTGAAGTGCTTGGTCTGT	
RT-*fepA*-F	CAATGCGCCAGAACATAAAGAG	*fepA*
RT-*fepA*-R	TGTCGAGGTTGCCATACAAG	
RT-*tsh*-F	CACAACCATCCAGGCAGATAA	*tsh*
RT-*tsh*-R	TGTGCCTTCTTCAAGGGTAAA	
RT-*yadC*-F	GGGTCAGGTTCGTTCTTCTC	*yadC*
RT-*yadC*-R	GTGACAGTAGTACCCAGGAATG	

PCR products were transformed into APEC strain DE458 harboring plasmid pKD46 by electroporation. The mutant was selected on LB plates with kan and confirmed by PCR using primers K1 and K2 combined with primers T-phi458-1 and T-phi458-2. Third, plasmid pCP20 was transferred into the mutant to remove the kan resistance region. Finally, the strain was serially subcultured in LB at 42°C to eliminate plasmid pCP20, which was confirmed by PCR. Thus, we obtained the phi458 deletion mutant and named it DE458Δphi458. The primers used are listed in Table 2.

Growth curve

Growth was determined by turbidity measurements at 600 nm (OD_{600}). Each strain was grown to log phase in LB medium at 37°C. After centrifugation and washing twice with ice-cold PBS, the cells were resuspended in PBS to an OD_{600} of 1.0. Then, 200 µl-suspensions were transferred into Erlenmeyer flasks containing 20 ml of LB. The OD_{600} values were monitored every hour for 16 h. The experiment was performed three times.

Biofilm formation assays

As previously described (Li et al., 2020), biofilms were determined by crystal violet staining. Briefly, the bacterial suspensions were subjected to an exponential period ($OD_{600} = 0.6$) and then diluted 1:100 in LB medium. Next, 200 µl aliquots were added to 96-well polystyrene microplates and incubated at 37°C for 36 h. The plates were washed with PBS, and 200 µl of methanol was added to the wells to fix the biofilms for 15 min. After drying at room temperature, the biofilms were stained with 1% (w/v) crystal violet for 15 min. After washing with double-distilled water (ddH_2O) and drying for 1 h, the stained bacteria were dissolved in 0.2 ml of 95% ethanol for 30 min. The optical densities at a wavelength of 600 nm were determined. Samples were performed

in triplicate, and LB medium alone was used as the negative control. The experiments were repeated three times.

Determination of the median lethal dose (LD_{50})

To assess the virulence levels, 97-day-old chickens were used to measure the 50% median lethal doses (LD_{50}) of WT and DE458Δphi458. For each strain, 48 chickens were divided into six groups and challenged intratracheally with 1×10^8 to 1×10^3 CFU of bacteria diluted in 1 ml of PBS. The number of dead chickens was recorded within 7 days, and the LD_{50} values were calculated according to the modified Karber method.

Adhesion and invasion assays

The adhesion and invasion abilities of the strains were determined as previously described (Fu et al., 2022). For the adherence and invasion experiments, chicken embryo fibroblast DF-1-cell monolayers were cultivated in sterilized 24-well plates with DMEM (containing 10% fetal bovine serum) at 37°C in a humidified chamber containing 5% CO_2. Then, the log-phase bacterial cultures were harvested, washed twice with ice-cold PBS, and resuspended in DMEM to remove the LB medium. Bacterial suspensions were infected with DF-1 cells (according to an infection multiplicity of 100) for 2 h at 37°C under a 5% CO_2-humidified atmosphere. For the adhesion assays, after washing three times with ice-cold PBS, the adherent bacteria were lysed with 0.5% Triton X-100 for 10 min and analyzed by the plate counting method. For the invasion assays, the steps were similar to those use for the adhesion assays. After washing out the nonadherent bacteria, the cells were subsequently treated with gentamicin (100 μg/ml) for 1 h to kill the adherent bacteria. The remaining numbers of bacteria that invaded DF-1 cells were determined in the same way as in the adhesion assays. All assays were performed in triplicate and repeated at least three times.

Analysis of phage cytotoxicity in DF-1 cells

Chicken embryo fibroblast DF-1-cell monolayers were prepared as previously described with some modifications (Henein et al., 2016). DF-1 cells were cultured in 24-well cell culture plates with DMEM (containing 10% fetal bovine serum) at 37°C in a humidified chamber containing 5% CO_2. When the cells were 80% confluent on the plates, 200 μl of trypsin was added to each well. After 3–5 min of incubation, the cells were suspended in DMEM and centrifuged at 500 × g for 5 min. The supernatants were discarded, and the pellets were resuspended in 2 ml of fresh DMEM.

For trypan blue exclusion assay: DF-1-cell suspensions and 50 μl of purified phage were mixed and incubated in 24-well cell culture plates for 24 h at 37°C under a 5% CO_2-humidified atmosphere. DMEM and SM were used as the negative controls. After trypsinization, the cell viabilities were measured with Trypan blue assays. In brief, 4 μl of 0.4% trypan blue solution in PBS was added to the cell suspensions, and the cell numbers were immediately counted under an inverted light microscope. Five squares of view were used for each sample. All assays were performed in triplicate and repeated at least three times. For lactate dehydrogenase (LDH) release: LDH values were measured with a colorimetric assay kit (#ab102526, Abcam, United States). These assays were conducted according to the manufacturer's protocol.

Bacterial colonization *in vivo*

The strains were cultured to an OD_{600} value of 0.6, washed twice with ice-cold PBS and suspended in an appropriate volume of PBS to ensure that the suspension concentration was 1×10^8 CFU. Two groups of chickens were challenged intratracheally with WT or mutant strain bacterial suspensions (0.1 ml/chicken). At 24 h post-infection, the chickens were euthanized and dissected. The bacterial loads in the lung, heart, and liver were determined by the plate counting method.

RNA isolation and qRT-PCR

The DE458 and DE458Δphi458 were cultured to an OD_{600} value of 0.6. Then, total RNA was extracted from the bacteria using an E.Z.N.A. bacterial RNA isolation kit (Omega, Beijing, China). HiScript II QRT Supermix (Vazyme Biotech) were used for the cDNA synthesis. The mRNA transcription levels were examined using a One-Step qRT-PCR SYBR Green kit (Vazyme Biotech). The endogenous reference gene *DnaE* was chosen as an internal control, and the $2^{-\Delta\Delta Ct}$ method was used to calculate the mRNA relative expression level. The primers used are listed in Table 2.

Ethics statement

The chickens used in the study were obtained from a poultry farm in Anhui Province and housed in cages with a 12 h light/dark cycle. The animal study protocol was approved by the Ethical Committee for Animal Experiments of Nanjing Agricultural University (SYXK(SU)2017-0007), Nanjing, China.

Statistical analyses

The data obtained in this study were analyzed using the GraphPad Prism Software package (GraphPad Software, La Jolla, CA, United States). Mann–Whitney *U*-tests were used to analyze the *in vivo* colonization data. The other data were analyzed by unpaired *t*-tests.

Accession number

The sequence of phi458 was submitted to GenBank database (accession number OP434518).

Results

Screening for APEC strains with spontaneous prophage induction

Escherichia coli is divided into four main phylogenetic groups (A, B1, B2, and D), and extraintestinal pathogenic *E. coli* mainly belong to groups B2 and D (Clermont et al., 2000; Zhu Ge et al., 2014; Cordoni et al., 2016). Therefore, 29 strains belonging to B2 or D were selected as screening objects to determine the role of prophages in extraintestinal pathogenic *E. coli*. The results showed that 9 of 29 strains could release phages, and 4 strains exhibited spontaneous induction (Table 3). Among these four strains, DE456 released the largest number of phage particles in LB media (3.5×10^5 PFU/mL), while DE458 was the most after adding Nalidixic acid (4.2×10^7 PFU/mL; Supplementary Table S1).

TABLE 3 APEC strains used in prophage induction experiments.

Strain	ECOR group	Strain	ECOR group	Strain	ECOR group
DE033#	B2	DE139	B2	DE232	D
DE039	D	DE161	D	DE296#*	B2
DE044#	D	DE168	B2	DE297	B2
DE066	D	DE169#*	D	DE298	B2
DE068	B2	DE182#	B2	DE346	B2
DE126	B2	DE183#	B2	DE456#*	D
DE130	D	DE210	D	DE458#*	D
DE142	B2	DE220	D	IMT5155	B2
DE132#	D	DE224	D		
DE134	D	DE231	D		

#Prophage induction of *Escherichia coli* strains after nalidixic acid 1 μg/ml was added.
*Phage particles were released by spontaneous induction in LB medium at 37°C.

The prophage in DE458 had a high spontaneous induction rate *in vivo*

To investigate whether the stains that exhibited spontaneous induction *in vitro* could also release phage particles *in vivo*, systemic infection assays were conducted (Gao et al., 2021). After 24 h post-infection, the numbers of phage particles were measured in the selected organs with the double-layer agar plate method. Among the four strains which exhibited spontaneous induction, no phage particles were detected in liver and heart except for DE458 and the number of phages in lung is shown in Supplementary Figure S1. DE458 had a higher spontaneous induction rate *in vivo* than the other three stains. In particular, maximum colonization was observed in the lung (2.0×10^3 PFU/g), and the lowest colony counts were obtained in the heart (25 PFU/g); the colony numbers in the liver were 100 PFU/g (Figure 1A). The plaques of phi458 showed clear medium-sized plaque spots (0.1 cm, Figure 1B). The transmission electron microscopy results showed that phi458 belongs to the *Siphoviridae* family of long-tailed phages (Figure 1C). Therefore, DE458 was selected as the subsequent research object. To investigate the role of this spontaneously inducible prophage phi458 on bacterial fitness, a phi458 deletion mutant was constructed, and the biological properties of the strains were studied.

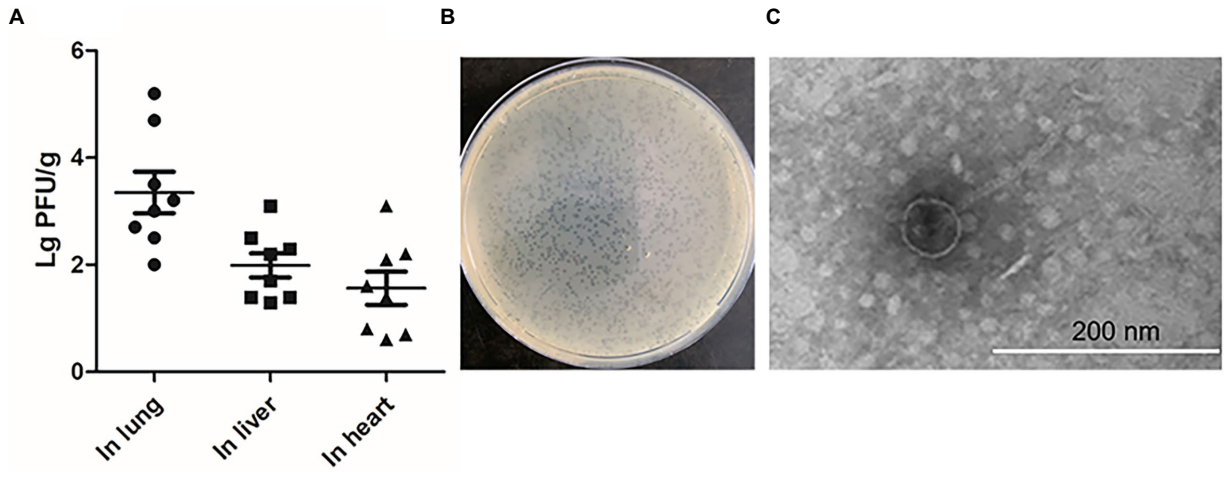

FIGURE 1
The production of phage during infection *in vivo*. **(A)** The chickens were infected with 5×10^{6}CFU of WT DE458 through the air sacs. After 24 h post-infection, phage particles re-isolation from the lung, live and heart were determined by the double-layer agar method. Each data point repressed a sample from an individual chicken. **(B)** Plaque morphology of phi458. **(C)** Transmission electron microscopy (TEM) images of purified phage phi458.

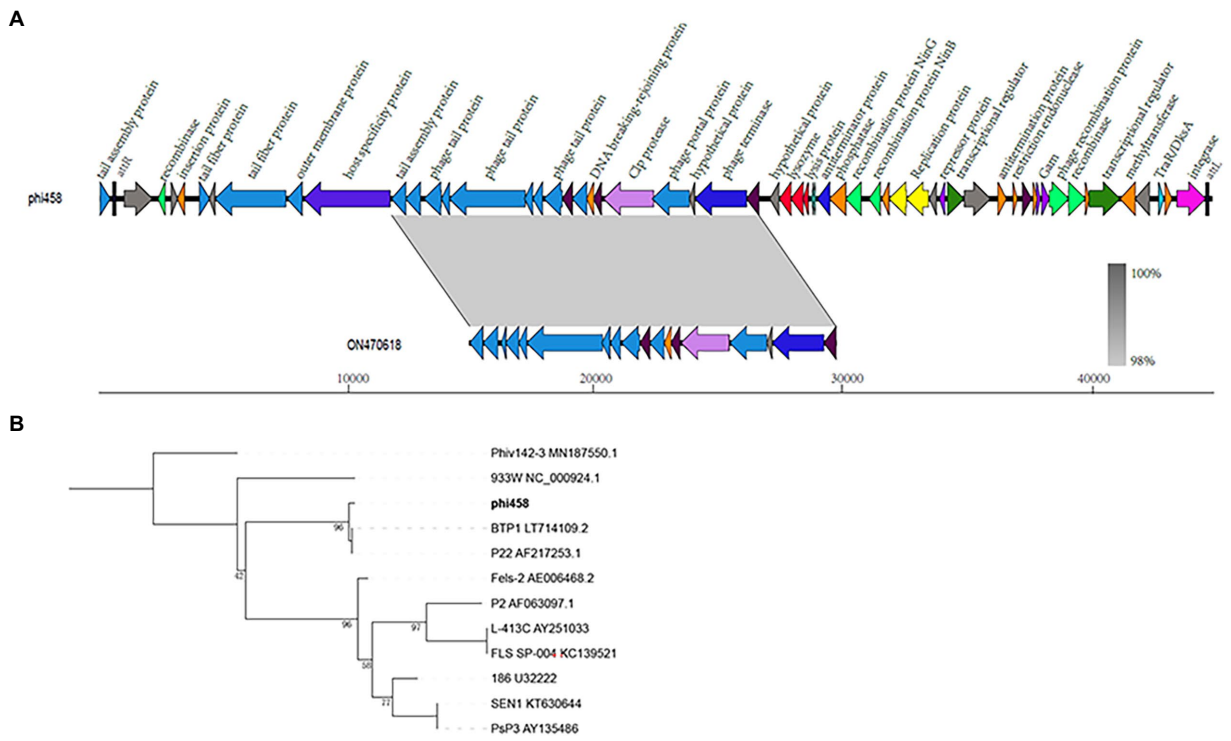

FIGURE 2
Bioinformation analysis of phi458. **(A)** The structure of prophage phi458. Phi458 is an intact phage and shares a 32% nucleotide sequence identity with *Escherichia* phage vB_EcoS-813R6. The unbroken line represents the length of the sequence. ORFs that are classified in the same functional categories are in the same color. **(B)** Phylogenetic trees of sequence of integrase. Neighbor-joining tree analysis based on the alignment of the amino acid sequence of the integrase. The numbers at the nodes indicate the bootstrap probabilities of that particular branch.

Genomic characterization

The genome size of prophage phi458 was 44.8 kb, and there were 60 open reading frames, including integrase, lysin, repressor, terminase, portal, protease, tail, transposase, and recombinase. Phi458 shared a 32% nucleotide sequence identity with *Escherichia* phage vB_EcoS-813R6 (Figure 2A). Although in this sequence the similarity was very high, it was regrettable that only have partial genome of *Escherichia* phage vB_EcoS-813R6 (14.9 kb) in NCBI and could not find more information for analysis.

Twenty prophages which could transferred into lytic cycle were selected to compare with phi458 (Supplementary Table S2). As more than half of them shared the integrase gene, the phylogenetic trees obtained using the integrase sequence exhibited similar topologies and supported assignment of phi458 to a sublineage shared by *Salmonella* phage BTP1 and *Salmonella* phage P22 (Figure 2B).

The spontaneous induction rates of DE458 increased when incubated with DF-1 or grown at 42°C.

As the body temperature of chickens is around 42°C, we measured the spontaneous inductions rates at 28°C and 42°C by qPCR. As shown in Figure 3, compared with the induction rate of DE458 at 28°C, the induction proportion was increased by 1.5-fold at 42°C. Furthermore, when DE458 was incubated with DF-1 cells, the induction proportion increased from 2×10^{-5} to 4×10^{-4} ($p < 0.01$). The results indicated that higher temperatures and interactions with host cells could promote phi458 release.

Phi458 contributed to biofilm formation of APEC strain DE458

Biofilm formation is an important factor in pathogenic bacteria and is crucial for bacteria to resists in nature (Klemm et al., 2010; Gao et al., 2019). Thus, the ability of strains to form biofilms was measured in 96-well microtiter plates. As shown in Figure 4A, biofilm formation of DE458Δphi458 showed a strong decrease compared to that of the WT strain ($p < 0.01$). In addition, while addition of DNase (100 μg/ml) did not affect prophage release but could digest eDNA, it significantly reduced the biofilm production of DE458 biofilm to a level close to that of DE458Δphi458. DE458Δphi458 biofilms were not significantly affected after addition of DNase. Furthermore, phi458 could be induced in

mature biofilms at a concentration of 5×10^6 PFU/mL, while no phages could be detected in DE458Δphi458 (Figure 4B). These data suggested that induction of prophage phi458 in DE458 contributes to biofilm formation by releasing eDNA.

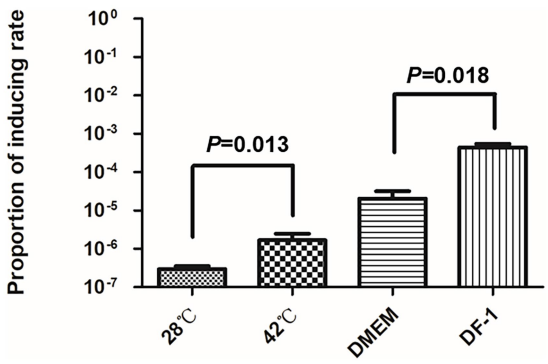

FIGURE 3
Prophage inducting rate in different environment. Quantitative real-time PCR was used to determine the prophage excision rate. The amount of bacterial genome that was lost of phi458 was measured using primers flanking of phi458, it only gave PCR products if the genome lack of phi458. The relative number of the target gene was normalized to reference gene *purA*. The columns represent the means and standard deviations of three experiments. Unpaired *t*-test were performed for significance.

Deletion of phi458 increased adhesion and invasion

To assess the effects of phi458 on adhesion and invasion, assays were conducted on the DF-1-cell line. Compared with the WT strain, the numbers of DE458Δphi458 that adhered to DF-1 cells increased from 9.4×10^4 CFU/ml to 1.9×10^6 CFU/ml, while the amounts of invasive bacteria increased from 4.2×10^3 CFU/ml to 2.8×10^4 CFU/ml (Figure 5). In summary, the ability of the mutant strain to adhere to and invade DF-1 cells increased by approximately 6–20 times ($p < 0.05$ by unpaired *t*-tests).

Deletion of phi458 enhanced the virulence of APEC strain DE458

To investigate the effect of phi458 *in vivo*, chickens were used to evaluate the LD_{50} values of DE458 and its mutant strains. The chickens were challenged intratracheally with the different strains, and the mortalities were recorded daily for 7 days. The LD_{50} values of the phi458 mutant and WT strains were 1.3×10^5 CFU and 1.8×10^6 CFU, respectively (Table 4). The virulence of the wild-type strain was approximately 10-fold weaker than that of DE458Δphi458 ($p < 0.001$). The results indicated that the presence of phi458 led to virulence attenuation in chickens.

In order to know if phi458 affects the growth of its carrier strain DE458, the growth curves were determined. The growth curves of the prophage deletion mutant DE458Δphi458 and WT strains did

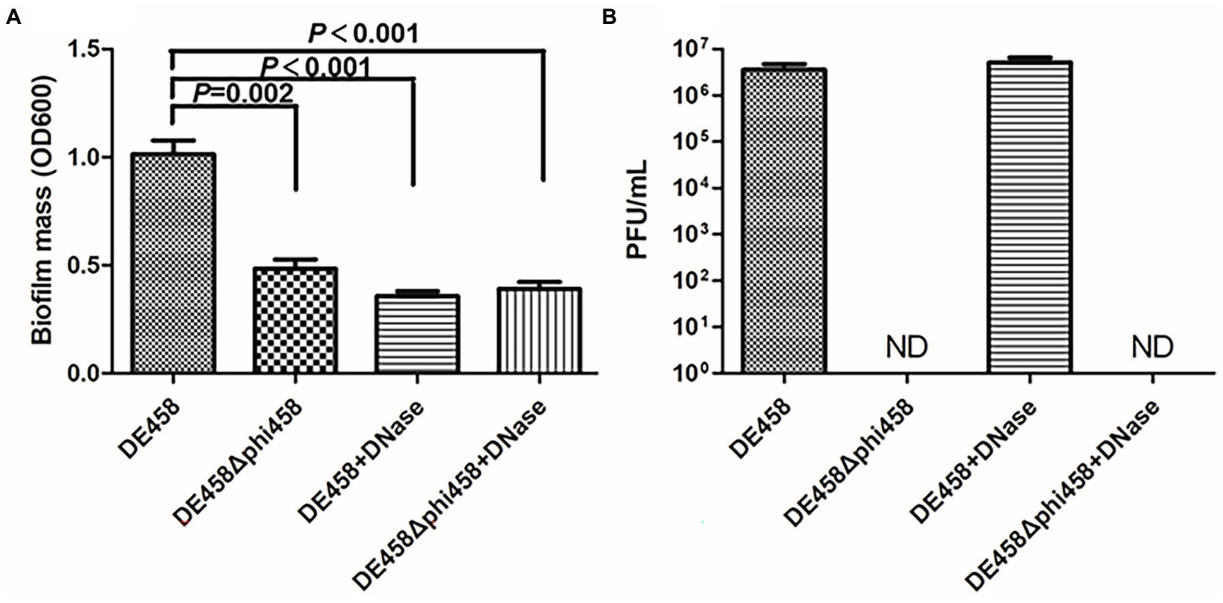

FIGURE 4
Phi458 increased biofilm formation. **(A)** Biofilm formation abilities of DE458 and its mutant strain DE458Δphi458. The biomass of each strain was measured in the absence or presence of DNase for 36 h. **(B)** The concentration of phage particles phi458 in the supernatant. After 36 h cultivation, the phage in supernatant was filtrated and calculated by the double-layer method. Data are the averages of six replicate wells in 96-well plates from three independent experiments. Error bars indicate standard deviations. Unpaired *t*-test were performed for significance.

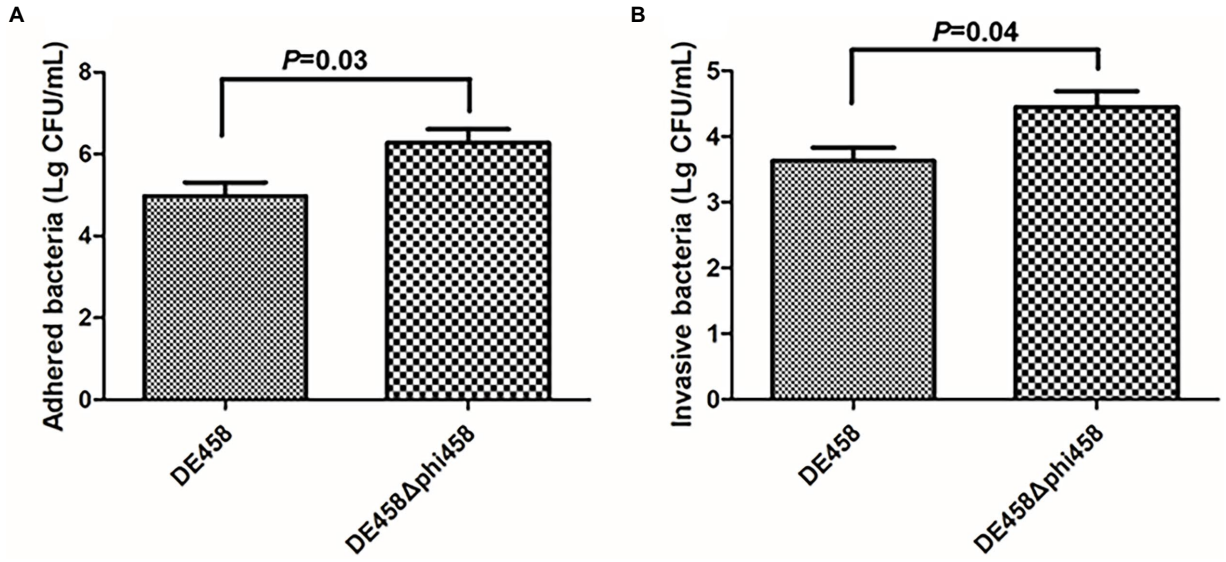

FIGURE 5
(A,B) Adherence and invasion assay. Both adherence and invasion of DF-1 cells by the mutant were significantly increased, as compared to the wild-type strain DE458. Values are the average of three independent experiments. Error bars indicate standard deviations. Unpaired *t*-test were performed for significance.

TABLE 4 Calculations of LD_{50}.

Challenge dose (CFU)	Dead chicks (*n*)/injected chicks (*n*)	
	DE458	DE458Δphi458
1×10^{8}	8/8	8/8
1×10^{7}	7/8	8/8
1×10^{6}	4/8	6/8
1×10^{5}	2/8	5/8
1×10^{4}	1/8	2/8
1×10^{3}	0/8	0/8
LD_{50}	1.8×10^{6} CFU	1.3×10^{5} CFU

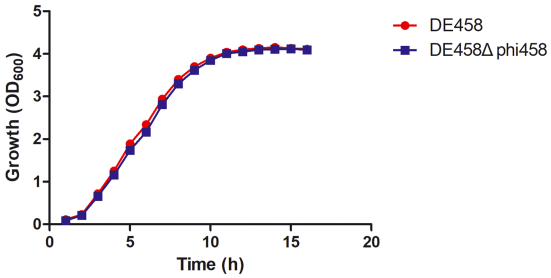

FIGURE 6
Growth curves of different APEC strains. The wild-type strain DE458 and phi458 mutant strain DE458Δphi458 were grown in LB at 37°C. Growth was determined by measuring the OD_{600}. The OD_{600} values were monitored every hour for 16 h. The data represented the average of three independent assays. Unpaired *t*-test were performed for significance.

not show significant differences in LB medium (Figure 6), indicating that the increase of virulence in prophage deletion mutant DE458Δphi458 was not due to the change of growth rate.

Deletion of phi458 increased colonization *in vivo*

To assess the effect of phi458 on colonization ability *in vivo*, a systemic infection experiment was performed. At 24 h post-infection, the bacterial loads in selected organs were measured. As shown in Figure 7, the bacterial loads of DE458 in the lung, liver, and heart were 4.0×10^{4} CFU/g, 6.3×10^{3} CFU/g, and 2.5×10^{4} CFU/g, respectively. However, the bacterial loads of DE458Δphi458 were 6.6×10^{5} CFU/g ($p<0.05$), 6.2×10^{4} CFU/g ($p<0.05$), and 1.3×10^{5} CFU/g, respectively. The results showed that the colonization ability of DE458Δphi458 increased by approximately 8–40 times compared to that of DE458.

In addition, no genes related to bacterial pathogenicity were found in phi458, as predicted by VirulenceFinder, and phi458 was not cytotoxic to cells (Figure 8), suggesting that phi458 might affect the virulence of DE458 by regulating virulence genes in DE458 rather than itself.

Deletion of phi458 increased the expression levels of *fimH* and *csgC*

To investigate the regulatory mechanism of phi458 on the virulence of DE458, the transcription levels of the virulence genes were screened by qRT-PCR. As shown in Figure 9, the

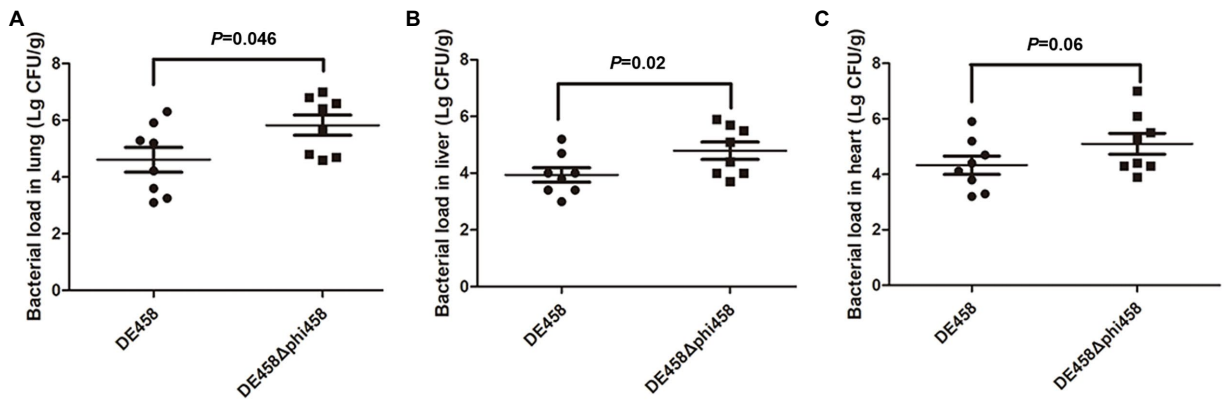

FIGURE 7
Bacterial colonization during infection *in vivo*. Chickens were changed with strains (5x10^{6}CFU for each strain) through the respiratory tract. After 24 h post-infection, the bacterial loads in **(A)** lung, **(B)** liver, and **(C)** hear was counted. Each data point repressed a sample from an individual chicken. The Mann–Whitney *U* test was used to analyze the data.

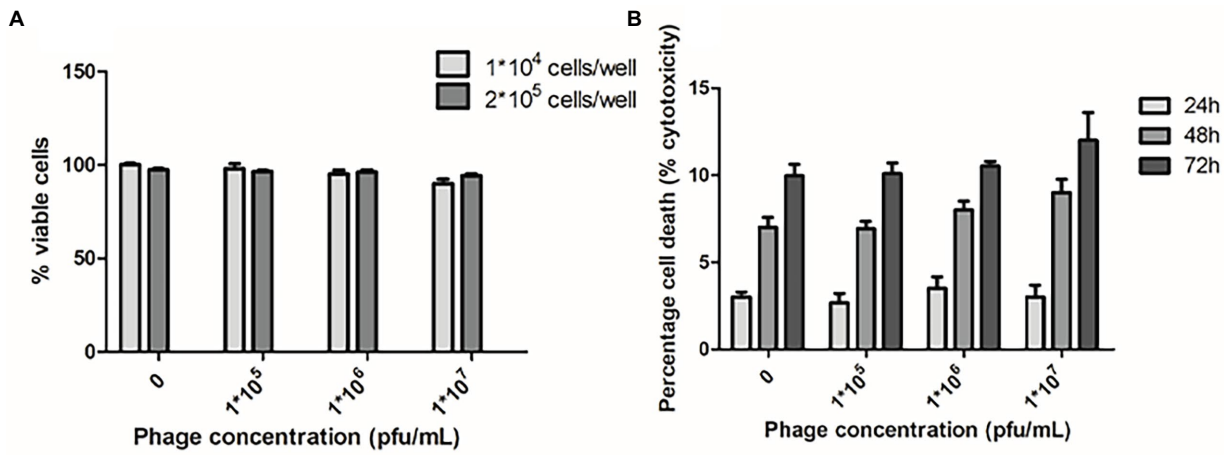

FIGURE 8
Cytotoxic assays. **(A)** Chicken embryo fibroblast DF-1 cells viability following 24 h exposure to phi458 in DMEM by trypan blue exclusion assay. **(B)** LDH release of chicken embryo fibroblast DF-1 cells following exposure to phi458. Data are the mean of 3 replicates ±SD.

transcription levels of *fimH* and *csgC* were upregulated 3-fold and 2.8-fold in DE458Δphi458, respectively. The results suggest that phi458 affected the virulence of DE458 by regulating the expressions of *fimH* and *csgC*.

Discussion

Currently, the effect of spontaneous prophage induction on the fitness of the bacterial host has been proved in different bacterial strains or species. For example, the phage 933 W could release from STEC, as it carrying exotoxins, the spontaneous induction of phage 933 W facilitates the its bacterial host to infect cells (Livny and Friedman, 2004). The induction of phage DMS3 (in *Pseudomonas aeruginosa* PA14) or Pf4 (in *P. aeruginosa* PAO1) could increase the biofilm formation capacities of the bacterial host (Webb et al., 2003; Zegans et al., 2009). Our study found that APEC strain DE458 had a high spontaneous induction rate *in vitro* and *in vivo*. The released phage particles phi458 were isolated and sequenced. The impact of inducible prophage phi458 on bacterial fitness was investigated in this study.

In nature, bacteria can resist various adverse environments by forming biofilms (Hanlon et al., 2004). As shown in Figure 4A, the biofilms produced by DE458Δphi458 were significantly reduced compared to those produced by the wild-type strain. This result indicated that the presence of phi458 enhanced biofilm formation. Biofilm formation requires various extracellular polymeric substances (Kim et al., 2022), and the spontaneous induction of prophages leads to accumulation of extracellular DNA (eDNA), which contributes to biofilm production (Shen et al., 2018). To test

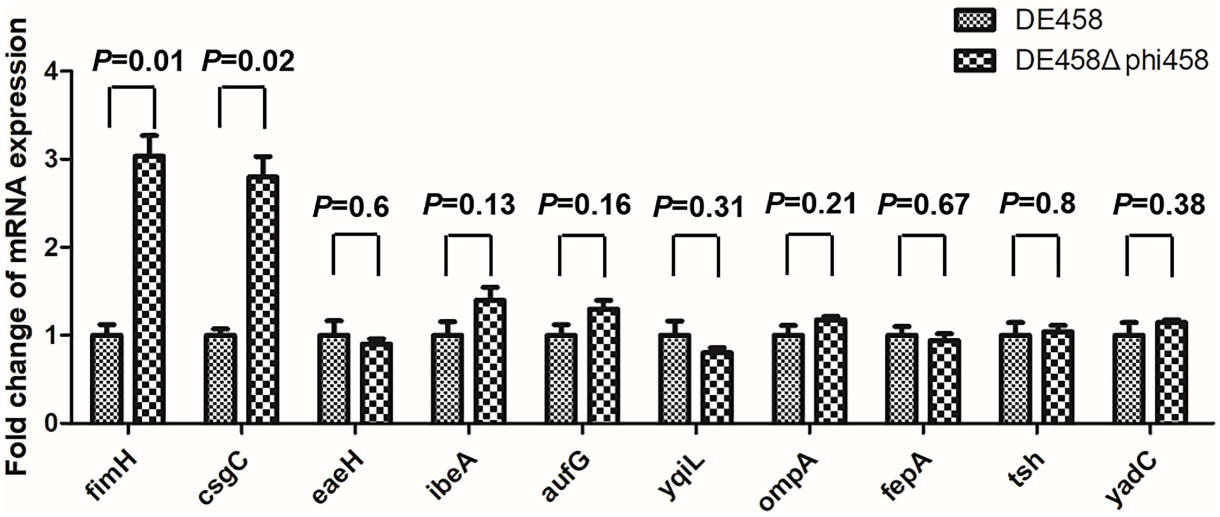

FIGURE 9
Quantification of virulence genes. The expression level of important virulence genes for APEC infection in strains DE458 and DE458Δphi458 were determined by qRT-PCR. The acquired cycle threshold was normalized to the housekeeping gene *dnaE*. Data were presented as the mean±SD of three independent experiments. Each experiment is composed of four individual measurements. Unpaired *t*-test were performed for significance.

whether a similar mechanism exists in the observed phi458-dependent enhanced biofilm production, DNase was added to the biofilm assay, which significantly decreased the biofilm formation of DE458 to a level close to that of DE458Δphi458. However, the biomass of the DE458Δphi458 biofilm was not significantly changed by the addition of DNase (Figure 4A). Furthermore, phi458 could be induced in mature biofilms at a concentration of 5×10^6 PFU/mL, while no phages could be detected in DE458Δphi458 (Figure 4B). These data strongly indicated that prophage phi458 enhances biofilm production by spontaneous activation. Meanwhile, the phage production provides DE458 with a competitive advantage over a sensitive host (Supplementary Table S1).

To investigate the effect of phi458 *in vivo*, we first examined its induction *in vivo*. Our study showed that phi458 had a high spontaneous induction rate *in vivo* (Figure 1). Extrinsic factors, such as pH, temperature, and organic carbon, can affect the expression level of RecA and induce the SOS response, resulting in the prophage switching to a lytic life cycle (Nanda et al., 2015). In chickens, the body temperature is approximately 42°C, and oxidative stress exists. In order to know which factors may induce prophage phi458 entry into a lytic cycle, we measured the induction rates of DE458 in different environments. The results showed that DE458 had a high induction rate when incubated at 42°C or interacted with DF-1 cells (Figure 3).

An essential step in APEC infection consists of adhesion and invasion of host cells (Klemm et al., 2010). Therefore, we tested the influence of phi458 on the adhesion and invasion ability of DE458. The ability of DE458Δphi458 to adhere to and invade DF-1 cells was increased by approximately 6–20 times (Figure 5). It has been reported that integration of a prophage into a bacterial genome can alter host gene regulation and cause changes in adhesion properties. For example, prophage D3112 in *P. aeruginosa* can inhibit the expression level of the bacterial host gene, *pilB*, which is associated with type IV pilus function and bacterial adhesion ability (Chung et al., 2014). A similar phenomenon was also found in APEC; phiv142-3 regulated the formation of flagella and I fimbriae and contributed accordingly to the adhesion ability (Li et al., 2018).

As previous results suggested that phi458 may affect the colonization ability of DE458 *in vivo*, we determined the colony numbers of mutant and WT strains at 24 h post-infection. As shown in Figure 7, the colonization ability of mutant strain DE458Δphi458 increased compared with that of the WT strain. The results indicate that phi458 affects the colonization ability of DE458. Our main concern is whether phi458 has an effect on bacterial virulence, and we determined the bacterial virulence in chickens. The results showed that the LD_{50} of the mutant strain decreased 10-fold in chickens compared to that of the WT strain, indicating that the integration of phi458 attenuated the virulence of APEC strain DE458.

The prophage affects virulence mainly in two ways: One possibility, prophages can encode some cellular toxins, and release of prophages is a hallmark of several pathogenic bacteria (Goshorn and Schlievert, 1989; Yamaguchi et al., 2000; Sakaguchi et al., 2005). The other possibility, the acquisition and excision of prophages can have an impact on the gene expressions of bacterial hosts, for instance, genes related to motility, EPS production, and virulence (Govind et al., 2009; Rabinovich et al., 2012; Nedialkova et al., 2016). In this study, the cytotoxic effects of phi458 were evaluated in DF-1 cells using two different assays: trypan blue and LDH release. The results showed that phi458 was not cytotoxic to cells (Figure 8). Moreover, no genes related to bacterial pathogenicity were found in phi458. Thus, we hypothesized that phi458 affects the virulence of DE458 by regulating genes related to adhesion and conization.

Virulence alterations by prophages were reported previously. After infection by ϕRSM or Rs551, this could lead to decreased virulence, and the exact mechanism consists mainly of regulating the genes related to virulence or motility by phage suppressor proteins (CI or CII) (Addy et al., 2012; Ahmad et al., 2017). The presence of repressor proteins is necessary to inhibit phage lytic genes to maintain a lysogenic state (Gandon, 2016). Compared with the wild-type strain, qRT-PCR revealed that the transcription levels of *fimH* and *csgC* were upregulated 3-fold and 2.8-fold in DE458Δphi458, respectively (Figure 9). FimH is the adhesin of type I fimbriate (Musa et al., 2009) and csgC is involved in the synthesis of curli (Burall et al., 2004). Both of them contribute to virulence and cell adherence in extraintestinal pathogenic *E. coli* (Antao et al., 2009; Krieger and Thumbikat, 2016). Through bioinformatic analysis (Figure 2), we found that phi458 contains two phage repressor proteins (CI and CII). We speculated that the phage repressor protein in phi458 not only inhibited transcription of the phage lysis module but also repressed the expressions of some virulence genes. Therefore, when DE458 was used to infect animals, the downregulated phage repressor resulted in the prophage switching to the lytic cycle and removed the inhibition of virulence genes. Whether *fimH* and *csgC* are regulated by repressor proteins in phi458 needs further study.

In conclusion, this study reveals that deletion of prophage phi458 leads to decreased biofilm formation *in vitro* and increased colonization ability and virulence *in vivo* by upregulating *fimH* and *csgC* expressions. Our research is first toward a better understanding of relationship between spontaneous induction phage and its carrier APEC by determining the role of prophage phi458 on biofilm formation and virulence of its carrier strain DE458.

Data availability statement

The datasets presented in this study can be found in online repositories. The names of the repository/repositories and accession number(s) can be found in the article/Supplementary material.

Author contributions

FT conceived and designed the study. DL was responsible for experimental operation and wrote the manuscript. WL and QH analyzed the data. JR and FX gave experimental help. QL provided valuable suggestions of the manuscript. All authors contributed to the article and approved the submitted version.

Funding

This work was funded by the National Natural Science Foundation of China (32172858) and China Postdoctoral Science Foundation (grant 2021 M692138).

Conflict of interest

The authors declare that the research was conducted in the absence of any commercial or financial relationships that could be construed as a potential conflict of interest.

Publisher's note

Supplementary material

The Supplementary material for this article can be found online at: https://www.frontiersin.org/articles/10.3389/fmicb.2022.1049341/full#supplementary-material

References

Addy, H. S., Askora, A., Kawasaki, T., Fujie, M., and Yamada, T. (2012). Loss of virulence of the phytopathogen *Ralstonia* solanacearum through infection by phiRSM filamentous phages. *Phytopathology* 102, 469–477. doi: 10.1094/PHYTO-11-11-0319-R

Ahmad, A. A., Stulberg, M. J., and Huang, Q. (2017). Prophage Rs551 and its repressor gene orf14 reduce virulence and increase competitive fitness of its *Ralstonia* solanacearum carrier strain UW551. *Front. Microbiol.* 8:2480. doi: 10.3389/fmicb.2017.02480

Antao, E. M., Wieler, L. H., and Ewers, C. (2009). Adhesive threads of extraintestinal pathogenic *Escherichia coli*. *Gut Pathog* 1:22. doi: 10.1186/1757-4749-1-22

Brussow, H., and Hendrix, R. W. (2002). Phage genomics: small is beautiful. *Cells* 108, 13–16. doi: 10.1016/S0092-8674(01)00637-7

Burall, L. S., Harro, J. M., Li, X., Lockatell, C. V., Himpsl, S. D., Hebel, J. R., et al. (2004). Proteus mirabilis genes that contribute to pathogenesis of urinary tract infection: identification of 25 signature-tagged mutants attenuated at least 100-fold. *Infect. Immun.* 72, 2922–2938. doi: 10.1128/IAI.72.5.2922-2938.2004

Canchaya, C., Fournous, G., and Brussow, H. (2004). The impact of prophages on bacterial chromosomes. *Mol. Microbiol.* 53, 9–18. doi: 10.1111/j.1365-2958.2004.04113.x

Casjens, S. (2003). Prophages and bacterial genomics: what have we learned so far? *Mol. Microbiol.* 49, 277–300. doi: 10.1046/j.1365-2958.2003.03580.x

Chung, I. Y., Jang, H. J., Bae, H. W., and Cho, Y. H. (2014). A phage protein that inhibits the bacterial ATPase required for type IV pilus assembly. *Proc. Natl. Acad. Sci. U. S. A.* 111, 11503–11508. doi: 10.1073/pnas.1403537111

Clermont, O., Bonacorsi, S., and Bingen, E. (2000). Rapid and simple determination of the *Escherichia coli* phylogenetic group. *Appl. Environ. Microbiol.* 66, 4555–4558. doi: 10.1128/AEM.66.10.4555-4558.2000

Cordoni, G., Woodward, M. J., Wu, H., Alanazi, M., Wallis, T., and La Ragione, R. M. (2016). Comparative genomics of European avian pathogenic *E. coli* (APEC). *BMC Genomics* 17:960. doi: 10.1186/s12864-016-3289-7

Crowl, R. M., Boyce, R. P., and Echols, H. (1981). Repressor cleavage as a prophage induction mechanism: hypersensitivity of a mutant lambda cI protein to recA-mediated proteolysis. *J. Mol. Biol.* 152, 815–819. doi: 10.1016/0022-2836(81)90128-5

Datsenko, K. A., and Wanner, B. L. (2000). One-step inactivation of chromosomal genes in *Escherichia coli* K-12 using PCR products. *Proc. Natl. Acad. Sci. U. S. A.* 97, 6640–6645. doi: 10.1073/pnas.120163297

DeMarini, D. M., and Lawrence, B. K. (1992). Prophage induction by DNA topoisomerase II poisons and reactive-oxygen species: role of DNA breaks. *Mutat. Res.* 267, 1–17. doi: 10.1016/0027-5107(92)90106-c

Ewers, C., Li, G., Wilking, H., Kiessling, S., Alt, K., Antao, E. M., et al. (2007). Avian pathogenic, uropathogenic, and newborn meningitis-causing *Escherichia coli*: how closely related are they? *Int. J. Med. Microbiol.* 297, 163–176. doi: 10.1016/j.ijmm.2007.01.003

Feiner, R., Argov, T., Rabinovich, L., Sigal, N., Borovok, I., and Herskovits, A. A. (2015). A new perspective on lysogeny: prophages as active regulatory switches of bacteria. *Nat. Rev. Microbiol.* 13, 641–650. doi: 10.1038/nrmicro3527

Fu, D., Shao, Y., Li, J., Wu, J., Wu, X., Song, X., et al. (2022). LuxR family transcriptional repressor YjjQ modulates the biofilm formation and motility of avian pathogenic *Escherichia coli*. *Res. Vet. Sci.* 152, 10–19. doi: 10.1016/j.rvsc.2022.07.011

Gandon, S. (2016). Why be temperate: lessons from bacteriophage lambda. *Trends Microbiol.* 24, 356–365. doi: 10.1016/j.tim.2016.02.008

Gao, Q., Li, X., Su, S., Yang, L., and Gao, S. (2021). Deletion of the c2515 and c2516 genes affects iron uptake and virulence of APEC O1 strain E516. *Front. Vet. Sci.* 8:654721. doi: 10.3389/fvets.2021.654721

Gao, Q., Xia, L., Wang, X., Ye, Z., Liu, J., and Gao, S. (2019). SodA contributes to the virulence of avian pathogenic *Escherichia coli* O2 strain E058 in experimentally infected chickens. *J. Bacteriol.* 201:e00625-18. doi: 10.1128/JB.00625-18

Goshorn, S. C., and Schlievert, P. M. (1989). Bacteriophage association of streptococcal pyrogenic exotoxin type C. *J. Bacteriol.* 171, 3068–3073. doi: 10.1128/jb.171.6.3068-3073.1989

Govind, R., Vediyappan, G., Rolfe, R. D., Dupuy, B., and Fralick, J. A. (2009). Bacteriophage-mediated toxin gene regulation in Clostridium difficile. *J. Virol.* 83, 12037–12045. doi: 10.1128/JVI.01256-09

Hanlon, G. W., Denyer, S. P., Hodges, N. A., Brant, J. A., Lansley, A. B., and Al-Rustamani, W. A. (2004). Biofilm formation and changes in bacterial cell surface hydrophobicity during growth in a CAPD model system. *J. Pharm. Pharmacol.* 56, 847–854. doi: 10.1211/0022357023817

Henein, A. E., Hanlon, G. W., Cooper, C. J., Denyer, S. P., and Maillard, J. Y. (2016). A partially purified *Acinetobacter baumannii* phage preparation exhibits no cytotoxicity in 3'T3 mouse fibroblast cells. *Front. Microbiol.* 7:1198. doi: 10.3389/fmicb.2016.01198

Kathayat, D., Lokesh, D., Ranjit, S., and Rajashekara, G. (2021). Avian pathogenic *Escherichia coli* (APEC): an overview of virulence and pathogenesis factors, zoonotic potential, and control strategies. *Pathogens* 10, 467–498. doi: 10.3390/pathogens10040467

Kim, U., Kim, J. H., and Oh, S. W. (2022). Review of multi-species biofilm formation from foodborne pathogens: multi-species biofilms and removal methodology. *Crit. Rev. Food Sci. Nutr.* 62, 5783–5793. doi: 10.1080/10408398.2021.1892585

Klemm, P., Hancock, V., and Schembri, M. A. (2010). Fimbrial adhesins from extraintestinal *Escherichia coli*. *Environ. Microbiol. Rep.* 2, 628–640. doi: 10.1111/j.1758-2229.2010.00166.x

Krieger, J. N., and Thumbikat, P. (2016). Bacterial prostatitis: bacterial virulence, clinical outcomes, and new directions. *Microbiol Spectr* 4:UTI-0004-2012. doi: 10.1128/microbiolspec.UTI-0004-2012

Li, D., Tang, F., Xue, F., Ren, J., Liu, Y., Yang, D., et al. (2018). Prophage phiv142-3 enhances the colonization and resistance to environmental stresses of avian pathogenic *Escherichia coli*. *Vet. Microbiol.* 218, 70–77. doi: 10.1016/j.vetmic.2018.03.017

Li, Q., Yin, L., Xue, M., Wang, Z., Song, X., Shao, Y., et al. (2020). The transcriptional regulator PhoP mediates the tolC molecular mechanism on APEC biofilm formation and pathogenicity. *Avian Pathol.* 49, 211–220. doi: 10.1080/03079457.2019.1701182

Livny, J., and Friedman, D. I. (2004). Characterizing spontaneous induction of Stx encoding phages using a selectable reporter system. *Mol. Microbiol.* 51, 1691–1704. doi: 10.1111/j.1365-2958.2003.03934.x

Luchnik, A. N. (1979). On the mechanism of SOS-repair and prophage induction: relaxation hypothesis. *J. Theor. Biol.* 77, 229–231. doi: 10.1016/0022-5193(79)90310-2

Lunde, M., Blatny, J. M., Lillehaug, D., Aastveit, A. H., and Nes, I. F. (2003). Use of real-time quantitative PCR for the analysis of phiLC3 prophage stability in *lactococci*. *Appl. Environ. Microbiol.* 69, 41–48. doi: 10.1128/AEM.69.1.41-48.2003

Mitchell, N. M., Johnson, J. R., Johnston, B., Curtiss, R., and Mellata, M. (2015). Zoonotic potential of *Escherichia coli* isolates from retail chicken meat products and eggs. *Appl. Environ. Microbiol.* 81, 1177–1187. doi: 10.1128/AEM.03524-14

Musa, H. H., He, S. F., Wu, S. L., Zhu, C. H., Liu, Z. H., Zhang, Z. N., et al. (2009). Genetic engineering of avian pathogenic *E. coli* to study the functions of FimH adhesin. *Indian J. Exp. Biol.* 47, 916–920. PMID: 20099466

Nanda, A. M., Heyer, A., Kramer, C., Grunberger, A., Kohlheyer, D., and Frunzke, J. (2014). Analysis of SOS-induced spontaneous prophage induction in *Corynebacterium glutamicum* at the single-cell level. *J. Bacteriol.* 196, 180–188. doi: 10.1128/JB.01018-13

Nanda, A. M., Thormann, K., and Frunzke, J. (2015). Impact of spontaneous prophage induction on the fitness of bacterial populations and host-microbe interactions. *J. Bacteriol.* 197, 410–419. doi: 10.1128/JB.02230-14

Nedialkova, L. P., Sidstedt, M., Koeppel, M. B., Spriewald, S., Ring, D., Gerlach, R. G., et al. (2016). Temperate phages promote colicin-dependent fitness of *salmonella* enterica serovar typhimurium. *Environ. Microbiol.* 18, 1591–1603. doi: 10.1111/1462-2920.13077

Nielsen, D. W., Klimavicz, J. S., Cavender, T., Wannemuehler, Y., Barbieri, N. L., Nolan, L. K., et al. (2018). The impact of media, phylogenetic classification, and *E. coli* Pathotypes on biofilm formation in Extraintestinal and Commensal *E. coli* from humans and animals. *Front. Microbiol.* 9:902. doi: 10.3389/fmicb.2018.00902

Rabinovich, L., Sigal, N., Borovok, I., Nir-Paz, R., and Herskovits, A. A. (2012). Prophage excision activates *listeria* competence genes that promote phagosomal escape and virulence. *Cells* 150, 792–802. doi: 10.1016/j.cell.2012.06.036

Robinson, C. M., Sinclair, J. F., Smith, M. J., and O'Brien, A. D. (2006). Shiga toxin of enterohemorrhagic *Escherichia coli* type O157:H7 promotes intestinal colonization. *Proc. Natl. Acad. Sci. U. S. A.* 103, 9667–9672. doi: 10.1073/pnas.0602359103

Sakaguchi, Y., Hayashi, T., Kurokawa, K., Nakayama, K., Oshima, K., Fujinaga, Y., et al. (2005). The genome sequence of clostridium botulinum type C neurotoxin-converting phage and the molecular mechanisms of unstable lysogeny. *Proc. Natl. Acad. Sci. U. S. A.* 102, 17472–17477. doi: 10.1073/pnas.0505503102

Santiviago, C. A., Blondel, C. J., Quezada, C. P., Silva, C. A., Tobar, P. M., Porwollik, S., et al. (2010). Spontaneous excision of the *Salmonella* enterica serovar enteritidis-specific defective prophage-like element phiSE14. *J. Bacteriol.* 192, 2246–2254. doi: 10.1128/JB.00270-09

Shen, M., Yang, Y., Shen, W., Cen, L., McLean, J. S., Shi, W., et al. (2018). A linear plasmid-like prophage of *Actinomyces* odontolyticus promotes biofilm assembly. *Appl. Environ. Microbiol.* 84:e01263-18. doi: 10.1128/AEM.01263-18

Shimizu, T., Ohta, Y., and Noda, M. (2009). Shiga toxin 2 is specifically released from bacterial cells by two different mechanisms. *Infect. Immun.* 77, 2813–2823. doi: 10.1128/IAI.00060-09

Tivendale, K. A., Logue, C. M., Kariyawasam, S., Jordan, D., Hussein, A., Li, G., et al. (2010). Avian-pathogenic *Escherichia coli* strains are similar to neonatal meningitis *E. coli* strains and are able to cause meningitis in the rat model of human disease. *Infect. Immun.* 78, 3412–3419. doi: 10.1128/IAI.00347-10

Wang, X., Kim, Y., Ma, Q., Hong, S. H., Pokusaeva, K., Sturino, J. M., et al. (2010). Cryptic prophages help bacteria cope with adverse environments. *Nat. Commun.* 1:147. doi: 10.1038/ncomms1146

Webb, J. S., Thompson, L. S., James, S., Charlton, T., Tolker-Nielsen, T., Koch, B., et al. (2003). Cell death in *Pseudomonas aeruginosa* biofilm development. *J. Bacteriol.* 185, 4585–4592. doi: 10.1128/JB.185.15.4585-4592.2003

Yamaguchi, T., Hayashi, T., Takami, H., Nakasone, K., Ohnishi, M., Nakayama, K., et al. (2000). Phage conversion of exfoliative toxin a production in *Staphylococcus aureus*. *Mol. Microbiol.* 38, 694–705. doi: 10.1046/j.1365-2958.2000.02169.x

Zegans, M. E., Wagner, J. C., Cady, K. C., Murphy, D. M., Hammond, J. H., and O'Toole, G. A. (2009). Interaction between bacteriophage DMS3 and host CRISPR region inhibits group behaviors of *Pseudomonas aeruginosa*. *J. Bacteriol.* 191, 210–219. doi: 10.1128/JB.00797-08

Zhu Ge, X., Jiang, J., Pan, Z., Hu, L., Wang, S., Wang, H., et al. (2014). Comparative genomic analysis shows that avian pathogenic *Escherichia coli* isolate IMT5155 (O2:K1:H5; ST complex 95, ST140) shares close relationship with ST95 APEC O1:K1 and human ExPEC O18:K1 strains. *PLoS One* 9:e112048. doi: 10.1371/journal.pone.0112048

frontiers | Frontiers in Microbiology

TYPE Original Research
PUBLISHED 15 March 2023
DOI 10.3389/fmicb.2023.1093668

OPEN ACCESS

EDITED BY
Heejoon Myung,
Hankuk University of Foreign Studies,
Republic of Korea

REVIEWED BY
Mikeljon P. Nikolich,
Walter Reed Army Institute of Research,
United States
Alicja Wegrzyn,
Institute of Biochemistry and Biophysics,
Polish Academy of Sciences,
Poland

*CORRESPONDENCE
Qiang Pan
✉ panqiang@phagepharm.com
Huiying Ren
✉ renren0228@sina.com

†These authors have contributed equally to this work

SPECIALTY SECTION
This article was submitted to
Phage Biology,
a section of the journal
Frontiers in Microbiology

RECEIVED 09 November 2022
ACCEPTED 23 February 2023
PUBLISHED 15 March 2023

CITATION
Cui J, Shi X, Wang X, Sun H, Yan Y, Zhao F, Zhang C, Liu W, Zou L, Han L, Pan Q and Ren H (2023) Characterization of a lytic *Pseudomonas aeruginosa* phage vB_PaeP_ASP23 and functional analysis of its lysin LysASP and holin HolASP.
Front. Microbiol. 14:1093668.
doi: 10.3389/fmicb.2023.1093668

Characterization of a lytic *Pseudomonas aeruginosa* phage vB_PaeP_ASP23 and functional analysis of its lysin LysASP and holin HolASP

Jiaqi Cui[1†], Xiaojie Shi[1†], Xinwei Wang[1], Huzhi Sun[2], Yanxin Yan[2], Feiyang Zhao[2], Can Zhang[1], Wenhua Liu[1], Ling Zou[1], Lei Han[3], Qiang Pan[2*] and Huiying Ren[1*]

[1]College of Veterinary Medicine, Qingdao Agricultural University, Qingdao, Shandong, China, [2]Qingdao Phagepharm Bio-Tech Co., Ltd., Qingdao, Shandong, China, [3]College of Chemistry and Pharmaceutical Sciences, Qingdao Agricultural University, Qingdao, Shandong, China

In this study, we isolated a lytic *Pseudomonas aeruginosa* phage (vB_PaeP_ASP23) from the sewage of a mink farm, characterized its complete genome and analyzed the function of its putative *lysin* and *holin*. Morphological characterization and genome annotation showed that phage ASP23 belonged to the *Krylovirinae* family genus *Phikmvvirus*, and it had a latent period of 10min and a burst size of 140 pfu/infected cell. In minks challenged with *P. aeruginosa*, phage ASP23 significantly reduced bacterial counts in the liver, lung, and blood. The whole-genome sequencing showed that its genome was a 42,735-bp linear and double-stranded DNA (dsDNA), with a G+C content of 62.15%. Its genome contained 54 predicted open reading frames (ORFs), 25 of which had known functions. The lysin of phage ASP23 (LysASP), in combination with EDTA, showed high lytic activity against *P. aeruginosa* L64. The holin of phage ASP23 was synthesized by M13 phage display technology, to produce recombinant phages (HolASP). Though HolASP exhibited a narrow lytic spectrum, it was effective against *Staphylococcus aureus* and *Bacillus subtilis*. However, these two bacteria were insensitive to LysASP. The findings highlight the potential of phage ASP23 to be used in the development of new antibacterial agents.

KEYWORDS

***Pseudomonas aeruginosa* phage, genome analysis, *lysin*, *holin*, gene expression, phage display technology**

1. Introduction

Pseudomonas aeruginosa is a Gram-negative opportunistic bacterium that widely exists in soil and water. It is a major pathogen that causes hemorrhagic pneumonia in minks, leading to huge economic losses in the mink farming industry (Qi et al., 2014; Zhao et al., 2018). Minks of all ages are easily affected by bacterial pathogens, especially on hot and humid days from August to November (Zhao et al., 2018). Typical symptoms include cough, nosebleed, and pulmonary hemorrhage (Bai et al., 2019). Antibiotics such as Ceftazidime and Ciprofloxacin are commonly used to treat *P. aeruginosa* infections. However, with the emergence of antibiotic-resistant *P. aeruginosa*, antibiotics has become less effective (Pedersen et al., 2009; Qi et al., 2014). The

resistance mechanisms in *P. aeruginosa* are complicated because its genome carries resistance genes which are capable of producing enzymes that can inactivate β-lactams (Moya et al., 2009). Moreover, the active efflux pump system and biofilms are also considered as primary causes for resistance mechanisms (Ziha-Zarifi et al., 1999). All of these factors and mechanisms increase the difficulty of treatments. As of 2018, about 100 million minks have been farmed in Shandong province, which accounts for a large proportion of farmed minks in China. Qian et al. (2020) reported that 20 strains of *P. aeruginosa* isolated from farmed minks in Shandong, China showed multidrug resistance and cross resistance. Furthermore, many clinical cases of antimicrobial resistance have also been reported in the United States, Denmark, and Canada (Nikolaisen et al., 2017; Cormier et al., 2020). The antimicrobial-resistant bacteria detected from the fecal samples belonged to five antimicrobial classes: macrolide–lincosamide–streptogramin B (MLSB; 100% prevalence), TETs (88.1%), β-lactams (71.4%), aminoglycosides (66.7%), and fluoroquinolones (47.6%) (Agga et al., 2021). So it is necessary to develop new antibacterial agents to control *P. aeruginosa* infections in minks. Recent studies have reported the effectiveness of phage therapy for the treatment of *P. aeruginosa* infections in animals (Forti et al., 2018; Lerdsittikul et al., 2022). However, to the best of our knowledge, only Gu et al. (2016) have evaluated the potential of phage therapy in the treatment of hemorrhagic pneumonia in mink by intranasal administration.

Bacteriophages are viruses that can infect most types of bacteria, and lytic phages have been applied to treat bacterial infections (Cisek et al., 2017). With the increasing threat of multi-resistant bacteria, phage therapy is drawing renewed interest in treating bacterial infections (Ryan et al., 2011). In general, a holin-lysin lysis system exists in double-stranded DNA phages to accomplish host lysis (Labrie et al., 2004). During the reproduction cycle, phage-encoded holin accumulates and forms pores in the membrane, leading to an increased access for lysins to degrade peptidoglycan in bacterial cell walls (Kamilla and Jain, 2016). Due to their high hydrolytic activity and pathogen specificity, lysins are considered as prospective antimicrobial agents for the treatment of multi-resistant bacterial infections (Schmelcher et al., 2012). Many studies have demonstrated the *in vitro* therapeutic efficacy of lysins against Gram-positive pathogens (Roach and Donovan, 2015). However, due to the protective outer membranes (OM), the efficacy of lysins against Gram-negative bacteria is limited (Lood et al., 2015). To increase the permeability of the OM, EDTA has been used as an outer membrane permeabilizer (OMP) to disrupt the structure of lipopolysaccharides by removing divalent cations (Briers et al., 2011). In addition, holins are phage-encoded proteins that can effectively kill Gram-positive bacteria extracellularly, including *Streptococcus suis* and *Staphylococcus aureus* (Song et al., 2016).

Compared to phages, holin proteins are safer and more effective in controlling bacterial infections. To obtain high expression of holin proteins, M13 phage display technology is often used. M13 phage is a filamentous virus (about 6.5 nm in diameter and about 900 nm in length), and it has a circular single-stranded DNA wrapped in an outer protein coat composed of about 2,700 copies of helically arranged major coat proteins (pVIII) and five copies of minor coat proteins (pIII, pVI, pVII, and pIX) at both ends of the phage (Ledsgaard et al., 2018). Phage display is a molecular technique based on genetic modification of phage DNA to enable the expression of a peptide/protein on the phage surface in combination with one of the phage coat proteins (Aghebati-Maleki et al., 2016; Sioud, 2019; Jaroszewicz et al., 2022).

In this study, we characterized a lytic phage vB_PaeP_ASP23 (ASP23) isolated from the sewage of a mink farm. Its genome was also sequenced. To understand the lysin-holin lysis system, we further analyzed the *lysin* and *holin* genes of phage ASP23. The findings highlighted the potential application of phage ASP23 in the development of efficient therapeutic agents in the mink farming industry.

2. Materials and methods

2.1. Ethics statement

Animal experiments performed in this study strictly followed the national guidelines for experimental animal welfare announced by Ministry of Science and Technology of People's Republic of China in 2006 (Guiding Opinions on Kindly Treating Laboratory Animals[1]) and were approved by the Animal Welfare and Research Ethics Committee at Qingdao Agricultural University, Shandong, China.

2.2. Bacterial strains, plasmids, and growth conditions

The bacterial strains and plasmids used in this study are listed in Table 1. All *P. aeruginosa* strains were isolated from minks that died of hemorrhagic pneumonia in Shandong, China. Bacterial strains used for determining antibacterial spectrum were identified by 16S rRNA gene sequencing. In addition, antibiotic susceptibility of *P. aeruginosa* isolates was measured by the Kirby–Bauer disk diffusion method (Forozsh et al., 2012). Bacteria were cultured in Luria Bertani (LB) broth or LB agar (Hopebiol Biotech) at 37°C. The vector pCold TF (N-Trigger factor; Amp^r; His-Tag, Takara) was used for cloning and expression of the *lysin* gene in *Escherichia coli* BL21 (DE3). The plasmid pCANTAB 5E was used for display and expression of the *holin* gene in M13 phages.

2.3. Isolation, purification, and characterization of phage ASP23

Phages were isolated from sewage of a mink farm using a *P. aeruginosa* strain (L64) as the host by the double-layer agar method (Lu et al., 2017). The purification and concentration of phage ASP23 were conducted as described previously (Shi et al., 2020). The purified phages were deposited on copper grids and negatively stained with phosphotungstic acid (2% w/v) for 10 min. After drying, the morphology of single phage particles was observed using an HT7700 transmission electron microscope (TEM, Hitachi, Japan) at 80 kV (Zhang et al., 2013).

1 https://www.most.gov.cn/xxgk/xinxifenlei/fdzdgknr/fgzc/gfxwj/gfxwj2010before/201712/t20171222_137025.html

TABLE 1 Bacterial strains, plasmids, and primers used in this study.

Bacterial strains, plasmids, primers	Characteristics, function, or sequence	Source
Strains		
P. aeruginosa L64	Host for phage ASP23	Our laboratory collection
P. aeruginosa PA1-PA11 (11 strains)	Antibacterial spectrum determination	Our laboratory collection
P. aeruginosa G3-G10 (8 strains)	Antibacterial spectrum determination	Our laboratory collection
P. aeruginosa DL1-DL3 (3 strains)	Antibacterial spectrum determination	Our laboratory collection
Escherichia coli E1	Antibacterial spectrum determination	Our laboratory collection
Salmonella abortus equi S1	Antibacterial spectrum determination	Our laboratory collection
Staphylococcus aureus SA2	Antibacterial spectrum determination	Our laboratory collection
Bacillus subtilis A01	Antibacterial spectrum determination	Our laboratory collection
Proteus mirabilis P1	Antibacterial spectrum determination	Our laboratory collection
Plasmids		
pCold TF	Expression vector; Amp^r; His-Tag	Takara Biotech
pCold TF-LysASP	Recombinant vector	This study
pCANTAB 5E	Phagemids; Amp^r; E-Tag	Detai Biotech
Primers		
LysASP-F	5′-TAGCATATGGTGAACAAGCCCCT-3′	This study
LysASP-R	5′-TTGGAATTCCTACCACAGCAAGGAC-3′	This study
HolASP-F	5′-ATGATGATTGATACCGCCACCG-3′	This study
HolASP-R	5′-TCACTTCTTGAATCTCCGGCG-3′	This study

The one-step growth experiment of phage ASP23 was performed as described previously reported (Shi et al., 2020). The mixtures of phage ASP23 and *P. aeruginosa* strain L64 were collected at different time points, and phage titers were determined immediately using the double-layer agar method. In addition, the host range, thermal stability and pH sensitivity of phage ASP23 were determined as described previously with some modifications (Shi et al., 2020).

2.4. *In vivo* therapeutic effect of phage ASP23 in minks infected with *Pseudomonas aeruginosa*

Minks (American mink, $n = 30$, 40–50 days old, average weight = 600 g) were divided into two groups (15 minks per group), including the control group and treatment group. To determine the therapeutic effect of phage ASP23, minks were challenged with *P. aeruginosa* strain L64 (4×10^8 CFU/mink) by intraperitoneal injection. Two hours after challenge, minks in the treatment group received phages by oral gavage (10^{10} pfu/mink). At the same time, minks in the control group received an equal volume of phosphate buffered saline (PBS). Each group contained 15 minks. At different time points (2 h, 5 h, 9 h, 13 h, and 17 h), 3 minks in each group were humanely euthanized with carbon dioxide (Gu et al., 2016). Tissue samples (liver and lung) were collected, weighed, and homogenized in 2 mL sterilized PBS. Blood samples were collected by venipuncture and stored in tubes containing EDTA. Bacterial counts in blood and tissue homogenates were measured by plating serial dilutions on LB agar plates.

2.5. Sequencing and bioinformatics analysis of the ASP23 genome

Bacteriophage DNA was prepared using a DNA Viral Genome Extraction Kit (Solarbio) after concentration. The genomic DNA was used to construct a 600-bp insert library using a NEBNext® Ultra™ II DNA Library Prep Kit for Illumina according to the manufacturer's instruction. The genomic DNA of ASP23 was subjected to high-throughput sequencing using an Illumina HiSeq 2,500 sequencer (San Diego, United States). The complete genome sequence was assembled using CLC Bio (Aarhus, Denmark). Putative open reading frames (ORFs) were predicted using GeneMarkS[2] and RAST[3] (Besemer et al., 2001; Aziz et al., 2008). The comparative genomic analysis was performed using BRIG (Alikhan et al., 2011). All predicted ORFs were annotated using BLASTp, and the protein domain analysis was conducted using Pfam.[4] Putative tRNA genes were identified using tRNAscan-SE. The structural and functional features of putative proteins were analyzed using TransMembrane prediction using Hidden Markov Models[5] and PredictProtein.[6] The highly conserved amino acid sequences were used to construct neighbor-joining phylogenetic trees using MEGA 7.

2 http://exon.gatech.edu/Genemark/genemarks.cgi
3 http://rast.nmpdr.org
4 http://pfam.xfam.org/
5 http://www.cbs.dtu.dk/services/TMHMM/
6 http://www.predictprotein.org

2.6. Amino acid sequence analysis, synthesis, and purification of LysASP

The deduced amino acid sequence of LysASP was analyzed using BLASTp, and the sequence alignment was generated using ESPript 3.0.[7] The sequences similar to LysASP were searched in the Protein Data Bank (PDB), and the structure of LysASP was predicted using Phyre2.[8]

The *lysin* gene was amplified from ASP23 phage genomic DNA using polymerase chain reaction (PCR) with a pair of specific primers containing *Nde*I and *Eco*RI restriction sites. The primers used are listed in Table 1. The PCR product was purified, digested with *Nde*I and *Eco*RI (Takara), and then cloned into the pCold TF expression vector with an N-terminal His6 tag to generate pCold TF-LysASP. The ligation product was transformed into competent cells (*E. coli* strain DH5α, Takara) using the heat shock method (Froger and Hall, 2007). Restriction enzyme digestions and sequencing were used to confirm the cloned fragment. Then the recombinant plasmid was transformed into *E. coli* BL21 (DE3).

The transformed *E. coli* BL21 cells were grown in LB medium containing ampicillin (50 μg/mL, Solarbio) until the OD_{600} reached 0.6 ~ 0.8. The mixed culture was induced with 0.4 mmol/L isopropyl-β-D-thiogalactopyranoside (IPTG) at 16°C for 12 h. Cells were harvested by centrifugation (10,000 × *g*, 15 min) and resuspended in phosphate-buffered solution (PBS, Solarbio), followed by sonication on ice (22 kHz, 45 W, 3 s work, 2 s pause). After centrifugation and filtration, His-tagged proteins were purified using a His-tag Protein Purification kit (Beyotime Biotech, Shanghai, China). The purified proteins were dialyzed against PBS and separated by 12% SDS-PAGE with a molecular weight marker (15–130 kDa, Solarbio). The protein concentration was determined using a BCA Protein Assay Kit (Solarbio, Beijing, China).

2.7. Lytic activity of recombinant LysASP against *Pseudomonas aeruginosa* L64

Pseudomonas aeruginosa L64 was grown in LB broth to the exponential phase, and 1 mL of culture was pretreated with 2 mM EDTA for 5 min. After centrifugation (10,000 × *g*, 10 min), bacterial cells were washed twice and resuspended in PBS (pH = 7.4). Aliquots (100 μL) of bacterial suspension were added into sterile 96-well plates containing 100 μL of purified LysASP (0.6 mg/mL) per well, followed by incubation at 37°C. The OD_{600} values were measured by a microplate reader at different time points. Simultaneously, the EDTA-pretreated bacterial suspension was added in PBS without LysASP and used as negative control. In the end, the colony-forming units (CFU) were determined. The experiment was performed in triplicate.

2.8. Determination of the lytic range of LysASP

The lytic activity of LysASP against *P. aeruginosa* (PA1-PA11), *E. coli* (E1), *Salmonella abortus equi* (S1) and *S. aureus* (SA2) was determined based on OD_{600} of bacterial culture measured by a microplate reader as mentioned above. *P. aeruginosa* strain L64 and PBS were used as positive and negative controls, respectively. All bacteria strains are listed in Table 1. The experiment was performed in triplicate.

2.9. Expression of *Holin* by M13 phage display technology

The deduced amino acid sequence of *holin* was analyzed by BLASTp, and putative hydrophobic transmembrane domains were predicted using TMHMM 2.0.[9] The *holin* gene was amplified from phage ASP23 genomic DNA using PCR with a pair of specific primers containing *Sfi*I and *Not*I restriction sites. The primers used are listed in Table 1. The PCR product was purified, digested with *Sfi*I/*Not*I (Takara), and cloned into the pCANTAB 5E phagemids to generate pCANTAB 5E-holin, in which a C-terminal E-tag was used. The ligation product was transformed into competent cells (*E. coli* strain TG1) using the heat shock method. Restriction enzyme digestions and sequencing were used to confirm the cloned fragment.

To produce recombinant fusion M13 phages, a single colony of pCANTAB 5E-holin transformed *E. coli* TG1 cells was grown in 2 × YT medium containing 2% glucose and 50 μg/mL ampicillin at 37°C with shaking (220 rpm) until the OD_{600} reached 0.5–0.7. Then, helper phage M13KO7 was added in the medium at a multiplicity of infection of about 1:50, followed by incubation for 35 min. After centrifugation, cells were re-suspended in fresh 2 × YT medium containing 25 μg/mL kanamycin and cultivated for at 37°C with shaking (220 rpm) for 20 h. After centrifugation (13,000 × *g* for 20 min, 4°C), phages were concentrated and precipitated by adding 1/5 (v/v) of PEG/NaCl solution in the supernatant. After incubation on ice for 12 h, the mixture was centrifuged, and the pellet was resuspended in 800 μL PBS (0.01 mM; pH 7.4), followed by incubation at 4°C for 12 h. Finally, after centrifugation, the supernatant containing M13 phages was collected and stored at 4°C (Tanaka et al., 1995). The holin protein of recombinant phages was identified using mass spectrometry (MS)-based shotgun proteomics.

2.10. Determination of the lytic range of HolASP

To determine the lytic range of HolASP (recombinant phages), which was made with M13KO7 displaying *holin* of ASP23, six strains of bacteria were tested (Table 1), including two Gram-positive bacteria (*Staphylococcus aureus* SA2 and *Bacillus subtilis* A01) and four Gram-negative bacteria (*P. aeruginosa* L64, *E. coli* E1, *S. abortus equi* S1, and *Proteus mirabilis* P1). Briefly, qualitative filter papers were placed onto freshly seeded lawns of bacteria, on which 10 μL HolASP (at a final concentration of 10^8 virions/mL) was spotted (Song et al., 2021). After incubation at

7 http://espript.ibcp.fr/ESPript/ESPript/

8 http://www.sbg.bio.ic.ac.uk/phyre2/html/page.cgi?id=index

9 http://www.cbs.dtu.dk/services/TMHMM/

37°C for 12 h, the production of transparent antibacterial rings was assessed. Simultaneously, the mixed solution of PBS and M13KO7 was used as a negative control to exclude the effect of M13KO7 on bacteria.

2.11. Measurement of antimicrobial activity of HolASP

The six strains of bacteria mentioned above were used as indicator strains to determine the antimicrobial activity of recombinant phages (HolASP). Bacterial cells were washed and resuspended with sterile phosphate-buffered saline (PBS) to 5×10^7 CFU/mL (Song et al., 2021). HolASP (at the final concentration of 10^8 virions/mL) was added to the bacterial suspension, and the mixture was incubated at 37°C for 12 h. The antibacterial activity was expressed as CFU reduction following treatment. As a negative control, the bacterial strains were treated with elution buffer (PBS, 0.01 mM; pH 7.4) under the same conditions.

2.12. Genome sequence accession number

The complete genome sequence of phage ASP23 was deposited in GenBank under the accession number MN602045.

2.13. Statistical analyses

The experiments, including the one-step growth curve, temperature sensitivity and pH stability of ASP23, lytic activity of LysASP and antibacterial activity of HolASP, were performed in triplicate. The results were presented as means ± standard deviation (SD). Student's t-test and analysis of variance were used to compare the differences between the numbers of bacteria in different organs using GraphPad Prism 6.0 (GraphPad, CA, United States). Differences were considered statistically significant when $p < 0.05$.

3. Results

3.1. Isolation and characterization of phage ASP23

A *P. aeruginosa* phage was isolated from sewage and named as vB_PaeP_ASP23 (ASP23). The TEM image showed that phage ASP23 had an icosahedral head of 70 nm in diameter and a tail of 40 nm in length (Figure 1A), suggesting that the phage ASP23 belonged to the phiKMV-like phages genus. The one-step growth curve of ASP23 revealed that the latent period and lysis period were 10 and 45 min, respectively, and the average burst size was 140 pfu/infected cell (Figure 1B). The thermal stability test showed that ASP23 was stable

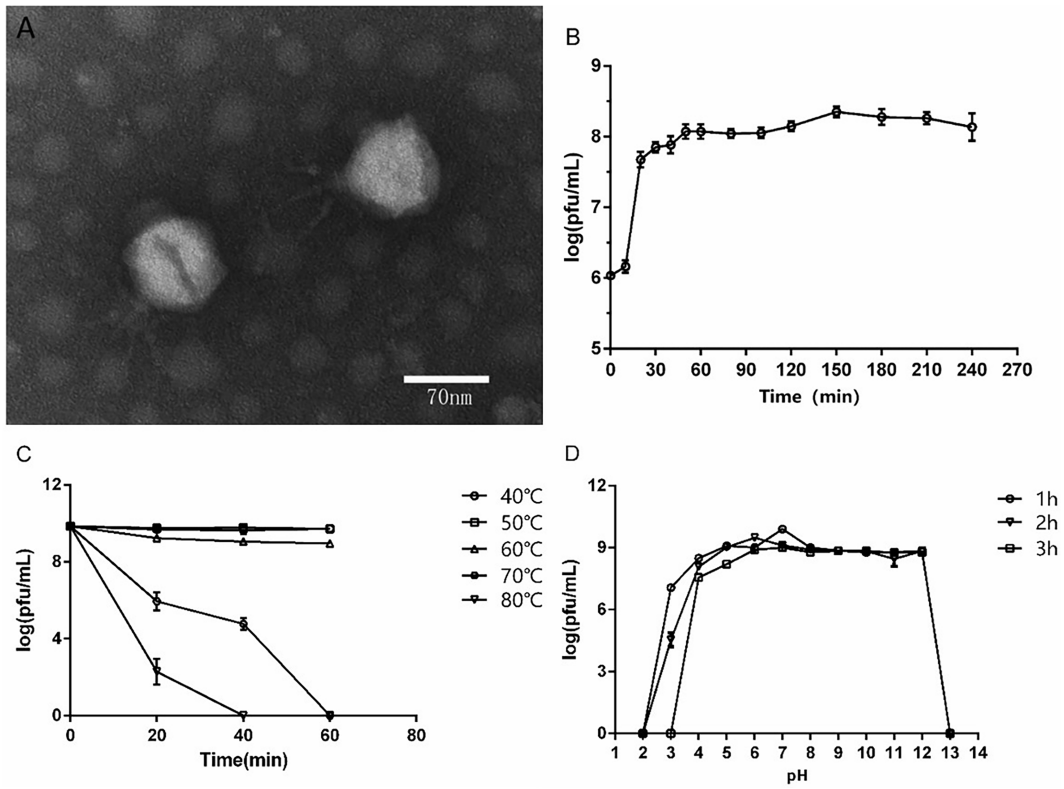

FIGURE 1
Biological characteristics of phage ASP23. **(A)** TEM image of phage ASP23. Phage ASP23 had an icosahedral head of 70nm in diameter and a short tail with 40nm in length. **(B)** One-step growth curve of ASP23. The latent period and burst size were 10min and 140 pfu/infected cell. **(C)** Temperature sensitivity of ASP23. The phage titers were no significant differences at 40°C~60°C. **(D)** pH stability of ASP23. Phage ASP23 was stable over a broad range of pH (5–12). Data are expressed as mean±SD (n=3).

below 60°C, but it was completely inactivated at 80°C after 40 min (Figure 1C). In addition, the titer of ASP23 could be maintained above 10^6 PFU/mL within 20 min at 70°C. ASP23 could maintain high activity (10^9 PFU/mL) over a broad range of pHs (5–12) for at least 3 h (Figure 1D), but it was inactivated at extreme pHs (below pH 4 or above pH 12). ASP23 exhibited lytic activity and lyzed 68% (15/22) of the *P. aeruginosa* strains (Table 2).

3.2. Therapeutic effect of phage ASP23 in minks challenged with *Pseudomonas aeruginosa* L64

To determine the therapeutic effect of phage ASP23 against infection caused by *P. aeruginosa* L64, we treated minks with phage ASP23 after they were challenged with *P. aeruginosa* L64 for 2 h. As shown in Figure 2, phage ASP23 significantly reduced bacterial counts in the liver and blood early at 5 h after treatment, and bacterial count in the lung decreased significantly at 13 h after treatment. The result indicated that phage ASP23 had a therapeutic effect in minks against *P. aeruginosa* L64.

3.3. Complete genome analysis of phage ASP23

The ASP23 genome was 42,735 bp in size and had an overall G + C content of 62.15%, which was similar to lytic phages of the genus *phikmvvirus*, such as Lx18 (100%, GenBank Accession No. MN692672.2), φKMV (98.62%, GenBank Accession No. AJ505558.1) and phiNFS (GenBank Accession No. NC_047852.1). By calculating the average nucleotide identity (ANI) value and the *in silico* DNA–DNA hybridization (*is*DDH) identity, we found that the ANI and *is*DDH values between phage ASP23 and Lx18 were 100%, the ANI

TABLE 2 Antibacterial activities of phage ASP23 and LysASP toward different species of bacteria.

Strain	Antibiotic susceptibility[a]				Lytic activity of ASP23	Lytic activity of LysASP[b]
	PIP	CAZ	OFX	CIP		
Gram-negative strains						
P. aeruginosa L64 (host)	R	R	S	R	+	+
P. aeruginosa PA1	R	I	R	I	+	+
P. aeruginosa PA2	R	R	S	I	+	+
P. aeruginosa PA3	R	R	I	I	+	+
P. aeruginosa PA4	R	R	S	I	–	–
P. aeruginosa PA5	R	R	R	R	–	–
P. aeruginosa PA6	R	R	I	R	+	+
P. aeruginosa PA7	R	I	I	R	+	+
P. aeruginosa PA8	R	R	S	S	+	+
P. aeruginosa PA9	S	R	I	R	+	+
P. aeruginosa PA10	I	R	R	R	+	+
P. aeruginosa PA11	S	R	R	R	+	+
P. aeruginosa G3	R	R	S	I	+	+
P. aeruginosa G4	S	I	R	R	+	+
P. aeruginosa G5	R	R	I	I	+	+
P. aeruginosa G6	R	R	S	R	–	–
P. aeruginosa G8	I	R	R	R	+	+
P. aeruginosa G9	S	R	I	R	+	+
P. aeruginosa G10	R	I	I	R	–	–
P. aeruginosa DL1	S	R	R	R	–	–
P. aeruginosa DL2	R	R	S	I	–	–
P. aeruginosa DL3	I	R	R	S	–	–
E. coli E1	–	–	–	–	–	–
S. abortus equi S1	–	–	–	–	–	–
Gram-positive strain						
S. aureus SA2	–	–	–	–	–	–

[a]S, susceptible; I, intermediate; R, resistant; –, not test; [b]Gram-negative bacteria were pretreated with EDTA. +, lysis; –, no lysis. PIP, Piperacillin; CAZ, Ceftazidime; OFX, Ofloxacin; and CIP, Ciprofloxacin.

and *is*DDH values between ASP23 and phiKMV were 98.08 and 76%, respectively, and the ANI and *is*DDH values between ASP23 and phiNFS were 98.22 and 81.3%, respectively. A total of 54 putative open reading frames (ORFs) longer than 100 bp were predicted, and no ORFs associated with drug resistance or lysogenization were identified (Supplementary Table S1). Among them, 45 ORFs (83.33%) had an ATG start codon, five ORFs had a GTG start codon, and four ORFs carried a TTG start codon. All predicted ORFs were located on the sense strand of the genome. BLASTp analysis revealed that 25 ORFs were annotated to encode proteins of known function. Similar to phage φKMV, the genes of ASP23 could be classified into three clusters: early genes (class I), genes involved in DNA metabolism (class II), and genes encoding structural and lysis proteins (class III) (Figure 3). To investigate the evolutionary relationship between ASP23 and other phages, whole genome sequence, major capsid protein and DNA polymerase were chosen for the construction of phylogenetic trees. As shown in Figure 4, phage ASP23 was clustered with phage φKMV and located near the members of the genus *Phikmvvirus*, confirming their close evolutionary relationship. Thus, phage ASP23 could be classified as a member of the genus *Phikmvvirus* in the family *Krylovirinae*.

Similar to *Phikmvvirus* phages, the early region (ORF1-ORF21) ended after the DNA ligase gene, and these genes included DNA-binding protein (ORF15), DNA primase (ORF18), DNA helicase (ORF19), and DNA ligase (ORF21). The amino acid sequence of DNA ligase showed high identity with φKMV_gp17 and contained a conserved domain (PHA00454). Four ORFs involved in DNA metabolism were identified in the genome of phage ASP23. ORF23 appeared to encode DNA polymerase, and its C-terminal region contained a DNA_pol_A domain (pfam00476). ORF26 and ORF27 were predicted to encode exonuclease and DNA endonuclease VII, respectively. ORF31 was predicted to encode RNA polymerase, and it was not located in the early gene region but at the end of the DNA metabolism region. The structural module of ASP23 was comprised of twelve ORFs, which encoded structural and packaging proteins, capsid proteins, and tail-related proteins. Generally, the terminase is composed of two subunits (big subunit and small subunit) which are involved in DNA packaging (Catalano, 2000). In the ASP23 genome, ORF47 and ORF48 encoded small subunit and big subunit, respectively. For the lysis system of ASP23, ORF49 and ORF50 encoded *holin* and *lysin*, respectively. ORF49 shared sequence homology with a putative *holin* gene in phage phikF77, moreover, its small size and genome location showed that it might encode a *holin*. Furthermore, ORF49 was a membrane protein with a putative hydrophobic transmembrane domain (TMD) and had a hydrophilic C-terminus with several charged amino acids, which should be classified into class II holins.

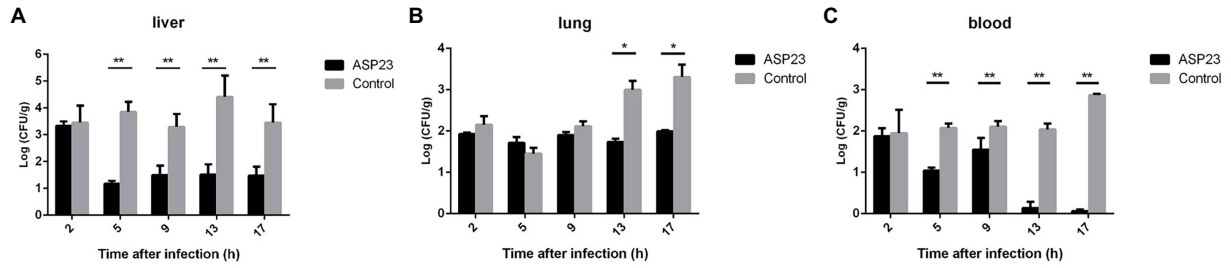

FIGURE 2
Bacterial counts in two tissues and blood of minks treated with phage ASP23 after they were challenged with *P. aeruginosa* L64 for 2h. **(A)** liver, **(B)** lung, and **(C)** blood. Data are expressed as mean±SD (n=3). *p<0.05, **p<0.01.

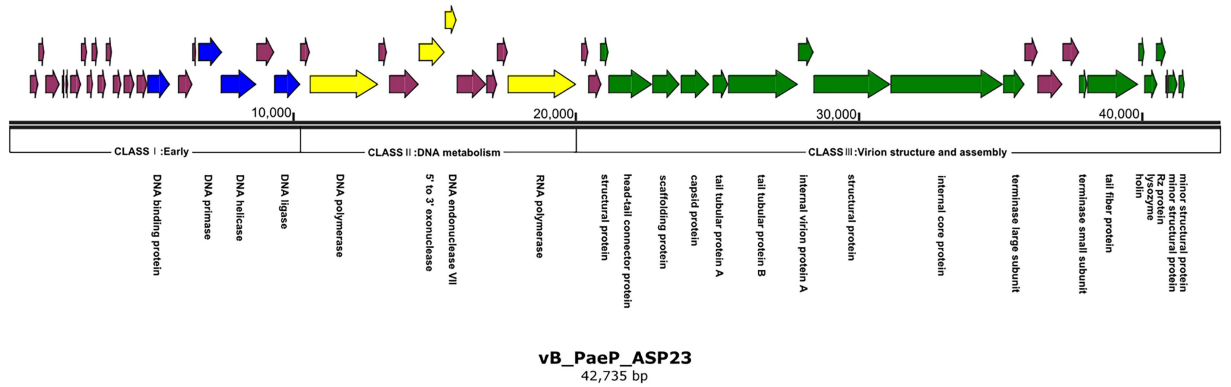

FIGURE 3
Genome map of phage ASP23. Nucleotide sequences were analyzed using SnapGene and predicted open reading frames are denoted by arrows. Genes were classified into different clusters: early genes (blue), genes involved in DNA metabolism (yellow), genes involved in virion structure and assembly (green), genes encoding hypothetical proteins (purple).

10.3389/fmicb.2023.1093668

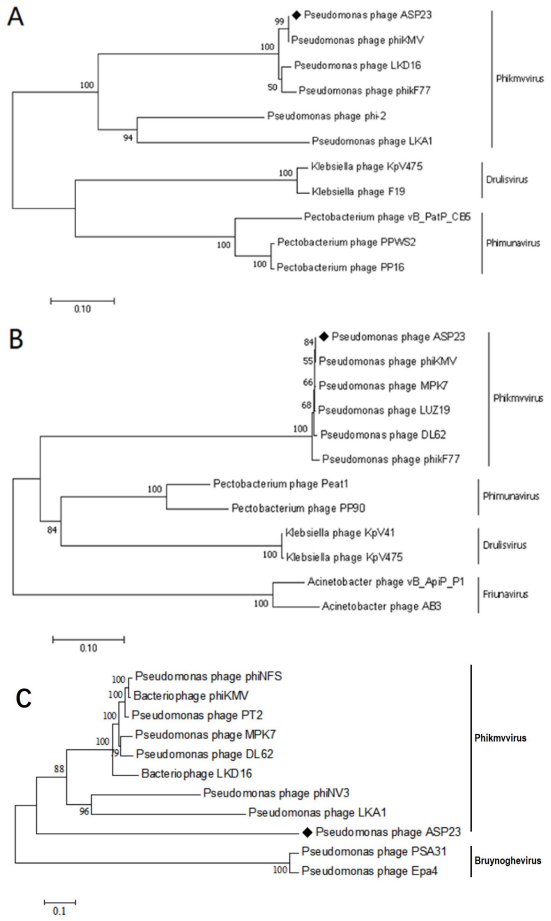

FIGURE 4
Neighbor-joining phylogenetic trees for the amino acid sequences of **(A)** Major capsid protein **(B)** DNA polymerase and **(C)** Whole genome sequence showing the evolutionary relationships between phage ASP23 and other known phages.

3.4. Identification and characterization of LysASP

The 483-bp *lysin* gene of phage ASP23, named as LysASP, contained 160 amino acid residues. Three sequences with high identity to LysASP were selected, and multiple sequence alignments were performed. The Pfam database revealed that it contained a lysozyme-like domain between residues 34 and 141 of LysASP (Supplementary Figure S1A). An alignment of LysASP with three phage lysins showed high similarity in the conserved domain, however, three non-conserved residues (amino acids 61, 64, and 76) were found in the conserved domain (Supplementary Figure S1B). Based on the sequence searches in PDB, LysASP shared the highest identity (30.6%, 59/196) with the Muramidase domain of SpmX (Supplementary Figure S2A; Randich et al., 2019). Furthermore, the structure of LysASP was predicted using Phyre2, and the confidence of the model was 100.0% (Supplementary Figure S2B). Although the predicted backbone structure of the LysASP shared high similarity with SpmX muramidase domain, their surface representations were different (Supplementary Figures S2C,D).

3.5. Synthesis and purification of LysASP

The LysASP gene was successfully amplified from ASP23 genomic DNA and was cloned into the *Nde*I/*Eco*RI sites of the pCold TF expression vector. The recombinant plasmid was confirmed by DNA sequencing. After induction with IPTG, the expression of the fusion protein was detected by SDS-PAGE (Supplementary Figure S3). As expected, the size of LysASP was ~69 kDa and most of the recombinant protein was found to be in the soluble fraction after sonication.

3.6. Lytic activity of LysASP

The lytic activity of LysASP was determined against bacterial cells. As shown in Figure 5, the OD_{600} values of bacterial cells treated with LysASP decreased remarkably from 0.95 to 0.48, whereas the OD_{600} values of bacterial cells in the control group remained constant. Besides, LysASP treatment significantly decreased bacterial counts of *P. aeruginosa* L64 at 2 and 4 h, compared to the control group. These results showed that, in combination with EDTA, LysASP had lytic activity against *P. aeruginosa L16.*

3.7. Antibacterial spectrum of LysASP

To test the lytic range of LysASP, we treated Gram-positive bacteria (*S. aureus* strain SA2) and Gram-negative bacteria (*P. aeruginosa* PA1-PA11, *P. aeruginosa* G3-G10, *P. aeruginosa* DL1-DL3, *E. coli* E1, and *S. abortus equi* S1) with LysASP. The results showed that LysASP exhibited antibacterial activity toward 15 strains

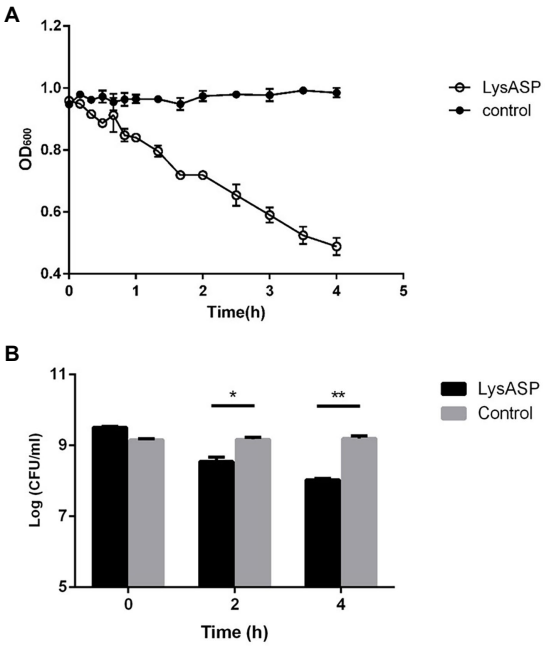

FIGURE 5
Lytic activity of purified LysASP against *P. aeruginosa* L64.
(A) Changes in OD_{600} of bacterial culture following LysASP treatment, **(B)** Bacterial counts at different time points following LysASP treatment. Data are expressed as mean±SD (n=3). *p<0.05, **p<0.01.

of *P. aeruginosa*, but it could not lyse other three bacterial species, which was the same as the antibacterial spectrum of phage ASP23 (Table 2).

3.8. Prediction and expression of *Holin*

TMHMM analysis showed that *holin* of phage ASP23 is a membrane protein with typical *holin* traits (Supplementary Figure S4A), which consisted of 66 amino acids (aa). And disulfide bond, signal peptide and coiled helix were not predicted in *holin*. *Holin* of phage ASP23 had a hydrophobic TMD at the N-terminus and multiple positively charged amino acids at the hydrophilic C-terminus. Since *holin* of phage ASP23 shared structural characteristics with class II holins, it could be considered as a member of the class II family (Reddy and Saier, 2013).

The *holin* gene was successfully amplified from ASP23 genomic DNA and was cloned into the *Sfi*I/*Not*I sites of the pCANTAB 5E phagemids. The recombinant phagemids were confirmed by DNA sequencing. The results of SHOTGUN proteomics indicated that holin protein was successfully displayed on the surface of recombinant phage. The titer of rescued recombinant phage was 6×10^8 virions/mL (Supplementary Figure S4B).

3.9. Antibacterial activity of HolASP

The antibacterial abilities of HolASP are shown in Figure 6. HolASP produced clear rings on bacterial lawns of *Staphylococcus aureus* SA2 and *Bacillus subtilis* A01. However, HolASP had no lytic ability against three of the four Gram-negative bacteria, including *E. coli* E1, *S. abortus equi* S1 and *P. mirabilis* P1. Log-phase cultures of six tested strains were exposed to HolASP (final concentration, 6×10^8 virions/mL) for 12 h. HolASP treatment resulted in $\log_{10}$ CFU reductions of two Gram-positive bacteria (5.3-log10 CFU reduction of *S. aureus* SA2 and 4.48-log10 CFU reduction of *B. subtilis* A01), relative to the controls. Furthermore, HolASP showed slight lytic ability against its host bacterium *P. aeruginosa* L64 (1.6-log10 CFU reduction of L64). The results indicated that HolASP only had efficient lytic ability against Gram-positive bacteria.

4. Discussion

Pseudomonas aeruginosa is a common opportunistic pathogen that can rapidly develop resistance to different types of antibiotics, which makes it difficult to treat *P. aeruginosa* infections (Lu et al., 2013; Qian et al., 2020). In the present study, a new phage ASP23 was isolated from sewage of a mink farm using a mink-derived *P. aeruginosa* strain as host. The biological properties of phage ASP23 were characterized. Due to its short latent period and lack of lysogenesis-related genes, phage ASP23 met the prerequisites for phage therapy. Moreover, phage ASP23 exhibited high resistance to high temperatures and extreme acidic/alkaline environment, which is beneficial to its storage and utilization. More importantly, the therapeutic study showed the ability of phage ASP23 to control *P. aeruginosa* infections in minks. Due to the rapid spread of *P. aeruginosa* after intraperitoneal injection, we did not find significant differences in bacterial counts between phage-treated group and control group at 2 h following treatment. It was reported that a single intranasal dosage of phage YH30 (1×10^8 PFU/mL) can protect 100% minks against hemorrhagic pneumonia 2 h after *P. aeruginosa* challenge (Gu et al., 2016). By contrast, our study demonstrated that phage ASP23 also had an effective therapeutic effect through oral gavage rather than intranasal administration.

The antibiotic resistance in *P. aeruginosa* is rapidly increasing, and it is important to develop therapeutic agents for bacterial infections. In clinical application, quinolones and β-Lactam antibiotics are often used to treat *P. aeruginosa* infections. In our study, all 22 strains of *P. aeruginosa* showed drug resistance to commonly used antibiotics. More importantly, 18 of the 22 isolates (81.81%) showed resistance to Ceftazidime, and 59.09% of the isolates were resistant to Ciprofloxacin. Phage-encoded lysins have high potential to be used as new alternatives to antibiotics. To date, there are many lysins known to target *P. aeruginosa*. In general, due to the presence of the outer membrane in Gram-negative bacteria, exogenous lysins could not

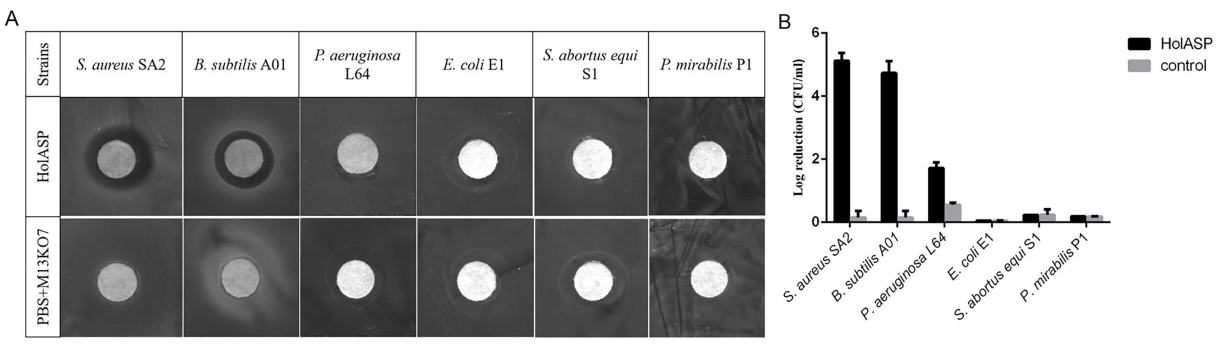

FIGURE 6
The antibacterial activity of recombinant phage HolASP. **(A)** Images of plaques formed on the lawns of different species of bacteria produced by HolASP. Plate lytic assay. The antibacterial activity of HolASP (10^8 virions/mL) against different species of bacteria was tested using plate assays. The mixed solution of PBS and M13KO7 was used as a negative control. **(B)** Antibacterial activity of HolASP against different species of bacteria. The bacterial suspension (5×10^7CFU/mL) were exposed to HolASP (10^8 virions/mL) at 37°C for 12h. Antibacterial activity *in vitro* was expressed as CFU reduction. The bacterial suspension without treatment with HolASP was used as control. Data are represented as mean±SD (n=3). CFU, colony-forming unit; SD, standard deviation.

access the peptidoglycan layer (Fischetti, 2010). On the other hand, outer membranes can be destabilized by many methods, such as outer membrane permeabilizer (EDTA, citric acid, etc.) and high hydrostatic pressure (50 to 200 MPa) (Briers et al., 2008, 2011).

Many studies have shown that lysins can control Gram-negative bacterial infections when the outer membrane is destabilized. Briers et al. (2011) reported that the combination of *lysin* EL188 and EDTA showed antimicrobial activity against *P. aeruginosa* and reduced bacterial count up to 4 log units in 30 min. In this study, we used EDTA to destabilize the outer membrane of host cells, and demonstrated that the recombinant LysASP in combination with EDTA could remarkably inhibit the growth of *P. aeruginosa* L64. Furthermore, the combination of LysASP and EDTA exerted lytic activity against other nine *P. aeruginosa* strains. Similarly, Lai et al. (2011) found that the lysozyme (LysAB2) of phage φAB2 had a lytic effect on EDTA-pretreated bacterial cells. However, LysASP did not exhibit lytic activity against other Gram-negative and Gram-positive bacterial strains. This was consistent with a previous study that lysin possesses specificity at the host level (Loessner, 2005). From a safety point of view, it is expected that phage lysins can specifically kill target pathogens without destroying commensal microflora (Nelson et al., 2012). The result indicated that LysASP had relatively higher specificity for *P. aeruginosa* than other tested bacteria. However, LysASP could not lyse bacterial cells without OMPs.

Holins have been identified in a wide variety of phages. Holins possess some common characteristics. For example, holins have at least one transmembrane α-helical region that has a highly charged hydrophilic C-terminal domain and is crucial for their functionality. A gene close to the *endolysin* gene encodes the majority of holins. During the late infection period, phage-encoded holin proteins can accumulate in the cytoplasmic membrane before triggering; when the concentration of holin proteins reaches a threshold, micronscale holes will be formed, which allow the soluble endolysins to be released from the cytoplasm to reach the peptidoglycan in the cell wall. The function of holins is associated with a collapse of the membrane potential and permeabilization of the membrane (Young, 1992). In this respect, holins have the potential to be used as therapeutic agents in their own right (Donovan, 2007). In this study, we found that HolASP had efficient lytic ability only against Gram-positive bacteria, such as *B. subtilis* A01 and *S. aureus* SA2. Similarly, it has been reported that HolSMP, the holin protein of phage SMP, shows efficient bactericidal ability against Gram-positive bacteria only, such as *S. aureus* and *B. subtilis* (Shi et al., 2012). The holin-like protein from *B. licheniformis* has also been reported to be effective at killing several types of Gram-positive bacteria, such as methicillin-resistant *S. aureus* (MRSA) and *Micrococcus luteus* (Anthony et al., 2010). Compared with *Streptococcus* spp., *P. aeruginosa* and *E. coli*, many *S. aureus* strains have no capsule but a slime layer, so it is possible that it might be easier for holin to target the membrane of *S. aureus*. However, the exact antimicrobial mechanism of holins needs to be elucidated in the future.

Phage display is a powerful method for selecting and engineering polypeptides with desired peptide-binding specificity, and it is achieved by fusing polypeptide libraries to phage coat proteins (Smith and Petrenko, 1997; Sidhu, 2000; Hamzeh-Mivehroud et al., 2013; Hess and Jewell, 2020; Jaroszewicz et al., 2022). This method relies on the fact that if the gene fragment encoding the polypeptide is fused with the M13 coat protein gene, these "fusion genes" can be integrated into phage particles, and the surface of phage particles also shows heterologous proteins (Sidhu, 2001). In this way, a physical linkage is established between phenotype and genotype. Peptides fused to M13 coat proteins will be displayed on the surface of phage particles, given that these fusion proteins can successfully pass through the assembly device and be integrated into assembled phages without affecting their viability. However, the utility of a phage-displayed library depends on the display quality, because a particular library member is only selectable when DNA-encoded polypeptides are efficiently displayed on phage surface. In this study, we integrated the *holin* gene with 66 amino acid residues into the pIII protein of M13 phage, and the concentration of recombinant phage after rescue was 6×10^8 virions/mL. Since the Phagemid display system is univalent phage display and the concentration of the tested strain is 5×10^7 CFU/mL, it can be concluded that 12 protein molecules can lyse one bacterial cell. Therefore, this method can be applied to compare protein lysis ability. In addition, T4 phage is a virulent coliphage that can lyse Gram-negative bacteria. In this case, since HolASP can only lyse Gram-positive bacteria, it is possible for holin to be displayed on T4 phage, which might greatly expanded its lytic spectrum.

5. Conclusion

In this study, we analyzed the complete genome of a lytic *P. aeruginosa* phage isolated from sewage of a mink farm. This phage belonged to the genus *Phikmvvirus* and was named vB_PaeP_ASP23. We performed functional analysis of its putative *lysin* and *holin*. The *lysin* gene was designated as LysASP, functional analysis revealed that LysASP had efficient bactericidal ability against Gram-negative bacteria. Holin protein synthesized by M13 phage display showed efficient lytic activity only against Gram-positive bacteria. Phage ASP23, LysASP and recombinant phage HolASP could be used as potential candidates for the development of therapeutic/antibacterial agents against bacterial infections.

Data availability statement

The datasets presented in this study can be found in online repositories. The names of the repository/repositories and accession number(s) can be found in the article/Supplementary material.

Author contributions

HR designed the study and analyzed the data with QP. JC and XS contributed to the study execution with help from XW, WL, CZ, and LZ on bacteria collection and reagents. HS, YY, and LH conducted animal experiments. JC drafted the manuscript. All authors were responsible for data integrity and accuracy of the analysis and approved the final version of the manuscript.

Funding

This work was funded by grants from the Donkey Industry Innovation Team Program of Modern Agricultural Technology System from Shandong Province, China (SDAIT-27-04) and the Youth Innovation Team Project for Talent Introduction and Cultivation for the universities in Shandong province, China.

Acknowledgments

The authors would like to thank Central Laboratory of Qingdao Agricultural University for the help of electron microscopic observation during this work.

Conflict of interest

HS, YY, FZ, and QP were employed by Qingdao Phagepharm Bio-tech Co., Ltd.

The remaining authors declare that the research was conducted in the absence of any commercial or financial relationships that could be construed as a potential conflict of interest.

Publisher's note

Supplementary material

The Supplementary material for this article can be found online at: https://www.frontiersin.org/articles/10.3389/fmicb.2023.1093668/full#supplementary-material

References

Agga, G. E., Silva, P. J., and Martin, R. S. (2021). Third-generation cephalosporin- and tetracycline-resistant Escherichia coli and antimicrobial resistance genes from metagenomes of mink feces and feed. *Foodborne Pathog. Dis.* 18, 169–178. doi: 10.1089/fpd.2020.2851

Aghebati-Maleki, L., Bakhshinejad, B., Baradaran, B., Motallebnezhad, M., Aghebati-Maleki, A., Nickho, H., et al. (2016). Phage display as a promising approach for vaccine development. *J. Biomed. Sci.* 23:66. doi: 10.1186/s12929-016-0285-9

Alikhan, N. F., Petty, N. K., Ben Zakour, N. L., and Beatson, S. A. (2011). BLAST ring image generator (BRIG): simple prokaryote genome comparisons. *BMC Genomics* 12:402. doi: 10.1186/1471-2164-12-402

Anthony, T., Chellappa, G. S., Rajesh, T., and Gunasekaran, P. (2010). Functional analysis of a putative holin-like peptide-coding gene in the genome of bacillus licheniformis AnBa9. *Arch. Microbiol.* 192, 51–56. doi: 10.1007/s00203-009-0530-7

Aziz, R. K., Bartels, D., Best, A. A., DeJongh, M., Disz, T., Edwards, R. A., et al. (2008). The RAST server: rapid annotations using subsystems technology. *BMC Genomics* 9:75. doi: 10.1186/1471-2164-9-75

Bai, X., Liu, S., Zhao, J., Cheng, Y., Zhang, H., Hu, B., et al. (2019). Epidemiology and molecular characterization of the antimicrobial resistance of *Pseudomonas aeruginosa* in Chinese mink infected by hemorrhagic pneumonia. *Can. J. Vet. Res.* 83, 122–132. PMID: 31097874

Besemer, J., Lomsadze, A., and Borodovsky, M. (2001). GeneMarkS: a self-training method for prediction of gene starts in microbial genomes. Implications for finding sequence motifs in regulatory regions. *Nucleic Acids Res.* 29, 2607–2618. doi: 10.1093/nar/29.12.2607

Briers, Y., Cornelissen, A., Aertsen, A., Hertveldt, K., Michiels, C. W., Volckaert, G., et al. (2008). Analysis of outer membrane permeability of *Pseudomonas aeruginosa* and bactericidal activity of endolysins KZ144 and EL188 under high hydrostatic pressure. *FEMS Microbiol. Lett.* 280, 113–119. doi: 10.1111/j.1574-6968.2007.01051.x

Briers, Y., Walmagh, M., and Lavigne, R. (2011). Use of bacteriophage endolysin EL188 and outer membrane permeabilizers against *Pseudomonas aeruginosa*. *J. Appl. Microbiol.* 110, 778–785. doi: 10.1111/j.1365-2672.2010.04931.x

Catalano, C. E. (2000). The terminase enzyme from bacteriophage lambda: a DNA-packaging machine. *Cell. Mol. Life Sci.* 57, 128–148. doi: 10.1007/s000180050503

Cisek, A. A., Dabrowska, I., Gregorczyk, K. P., and Wyzewski, Z. (2017). Phage therapy in bacterial infections treatment: one hundred years after the discovery of bacteriophages. *Curr. Microbiol.* 74, 277–283. doi: 10.1007/s00284-016-1166-x

Cormier, A. C., Chalmers, G., Cook, S. R., Zaheer, R., Hannon, S. J., Booker, C. W., et al. (2020). Presence and diversity of extended-Spectrum cephalosporin resistance among Escherichia coli from urban wastewater and feedlot cattle in Alberta, Canada. *Microb. Drug Resist.* 26, 300–309. doi: 10.1089/mdr.2019.0112

Donovan, D. M. (2007). Bacteriophage and peptidoglycan degrading enzymes with antimicrobial applications. *Recent Pat. Biotechnol.* 1, 113–122. doi: 10.2174/187220807780809463

Fischetti, V. A. (2010). Bacteriophage endolysins: a novel anti-infective to control gram-positive pathogens. *Int. J. Med. Microbiol.* 300, 357–362. doi: 10.1016/j.ijmm.2010.04.002

Forozsh, F. M., Irajian, G., Moslehi, T. Z., Fazeli, H., Salehi, M., and Rezania, S. (2012). Drug resistance pattern of *Pseudomonas aeruginosa* strains isolated from cystic fibrosis patients at Isfahan AL Zahra hospital, Iran (2009-2010). *Iran J. Microbiol.* 4, 94–97. PMID: 22973476

Forti, F., Roach, D. R., Cafora, M., Pasini, M. E., Horner, D. S., Fiscarelli, E. V., et al. (2018). Design of a broad-range bacteriophage cocktail that reduces *Pseudomonas aeruginosa* biofilms and treats acute infections in two animal models. *Antimicrob. Agents Chemother.* 62:17. doi: 10.1128/AAC.02573-17

Froger, A., and Hall, J. E. (2007). Transformation of plasmid DNA into *E. coli* using the heat shock method. *J. Vis. Exp.* 6:253. doi: 10.3791/253

Gu, J., Li, X., Yang, M., Du, C., Cui, Z., Gong, P., et al. (2016). Therapeutic effect of *Pseudomonas aeruginosa* phage YH30 on mink hemorrhagic pneumonia. *Vet. Microbiol.* 190, 5–11. doi: 10.1016/j.vetmic.2016.03.016

Hamzeh-Mivehroud, M., Alizadeh, A. A., Morris, M. B., Church, W. B., and Dastmalchi, S. (2013). Phage display as a technology delivering on the promise of peptide drug discovery. *Drug Discov. Today* 18, 1144–1157. doi: 10.1016/j.drudis.2013.09.001

Hess, K. L., and Jewell, C. M. (2020). Phage display as a tool for vaccine and immunotherapy development. *Bioeng. Transl. Med.* 5:e10142. doi: 10.1002/btm2.10142

Jaroszewicz, W., Morcinek-Orlowska, J., Pierzynowska, K., Gaffke, L., and Wegrzyn, G. (2022). Phage display and other peptide display technologies. *FEMS Microbiol. Rev.* 46:52. doi: 10.1093/femsre/fuab052

Kamilla, S., and Jain, V. (2016). Mycobacteriophage D29 holin C-terminal region functionally assists in holin aggregation and bacterial cell death. *FEBS J.* 283, 173–190. doi: 10.1111/febs.13565

Labrie, S., Vukov, N., Loessner, M. J., and Moineau, S. (2004). Distribution and composition of the lysis cassette of Lactococcus lactis phages and functional analysis of bacteriophage ul36 holin. *FEMS Microbiol. Lett.* 233, 37–43. doi: 10.1016/j.femsle.2004.01.038

Lai, M. J., Lin, N. T., Hu, A., Soo, P. C., Chen, L. K., Chen, L. H., et al. (2011). Antibacterial activity of Acinetobacter baumannii phage varphiAB2 endolysin (LysAB2) against both gram-positive and gram-negative bacteria. *Appl. Microbiol. Biotechnol.* 90, 529–539. doi: 10.1007/s00253-011-3104-y

Ledsgaard, L., Kilstrup, M., Karatt-Vellatt, A., McCafferty, J., and Laustsen, A. H. (2018). Basics of antibody phage display technology. *Toxins (Basel)* 10:236. doi: 10.3390/toxins10060236

Lerdsittikul, V., Thongdee, M., Chaiwattanarungruengpaisan, S., Atithep, T., Apiratwarrasakul, S., Withatanung, P., et al. (2022). A novel virulent Litunavirus phage possesses therapeutic value against multidrug resistant *Pseudomonas aeruginosa*. *Sci. Rep.* 12:21193. doi: 10.1038/s41598-022-25576-6

Loessner, M. J. (2005). Bacteriophage endolysins--current state of research and applications. *Curr. Opin. Microbiol.* 8, 480–487. doi: 10.1016/j.mib.2005.06.002

Lood, R., Winer, B. Y., Pelzek, A. J., Diez-Martinez, R., Thandar, M., Euler, C. W., et al. (2015). Novel phage lysin capable of killing the multidrug-resistant gram-negative bacterium Acinetobacter baumannii in a mouse bacteremia model. *Antimicrob. Agents Chemother.* 59, 1983–1991. doi: 10.1128/AAC.04641-14

Lu, L., Cai, L., Jiao, N., and Zhang, R. (2017). Isolation and characterization of the first phage infecting ecologically important marine bacteria Erythrobacter. *Virol. J.* 14:104. doi: 10.1186/s12985-017-0773-x

Lu, S., Le, S., Tan, Y., Zhu, J., Li, M., Rao, X., et al. (2013). Genomic and proteomic analyses of the terminally redundant genome of the *Pseudomonas aeruginosa* phage PaP1: establishment of genus PaP1-like phages. *PLoS One* 8:e62933. doi: 10.1371/journal.pone.0062933

Moya, B., Dotsch, A., Juan, C., Blazquez, J., Zamorano, L., Haussler, S., et al. (2009). Beta-lactam resistance response triggered by inactivation of a nonessential penicillin-binding protein. *PLoS Pathog.* 5:e1000353. doi: 10.1371/journal.ppat.1000353

Nelson, D. C., Schmelcher, M., Rodriguez-Rubio, L., Klumpp, J., Pritchard, D. G., Dong, S., et al. (2012). Endolysins as antimicrobials. *Adv. Virus Res.* 83, 299–365. doi: 10.1016/B978-0-12-394438-2.00007-4

Nikolaisen, N. K., Lassen, D. C. K., Chriel, M., Larsen, G., Jensen, V. F., and Pedersen, K. (2017). Antimicrobial resistance among pathogenic bacteria from mink (Neovison vison) in Denmark. *Acta Vet. Scand.* 59:60. doi: 10.1186/s13028-017-0328-6

Pedersen, K., Hammer, A. S., Sorensen, C. M., and Heuer, O. E. (2009). Usage of antimicrobials and occurrence of antimicrobial resistance among bacteria from mink. *Vet. Microbiol.* 133, 115–122. doi: 10.1016/j.vetmic.2008.06.005

Qi, J., Li, L., Du, Y., Wang, S., Wang, J., Luo, Y., et al. (2014). The identification, typing, and antimicrobial susceptibility of *Pseudomonas aeruginosa* isolated from mink with hemorrhagic pneumonia. *Vet. Microbiol.* 170, 456–461. doi: 10.1016/j.vetmic.2014.02.025

Qian, Z., Hui, P., Han, L., Ling-Zhi, Y., Bo-Shun, Z., Jie, Z., et al. (2020). Serotypes and virulence genes of *Pseudomonas aeruginosa* isolated from mink and its pathogenicity in mink. *Microb. Pathog.* 139:103904. doi: 10.1016/j.micpath.2019.103904

Randich, A. M., Kysela, D. T., Morlot, C., and Brun, Y. V. (2019). Origin of a Core bacterial gene via co-option and detoxification of a phage Lysin. *Curr. Biol.* 29, 1634–1646.e6. doi: 10.1016/j.cub.2019.04.032

Reddy, B. L., and Saier, M. H. Jr. (2013). Topological and phylogenetic analyses of bacterial holin families and superfamilies. *Biochim. Biophys. Acta* 1828, 2654–2671. doi: 10.1016/j.bbamem.2013.07.004

Roach, D. R., and Donovan, D. M. (2015). Antimicrobial bacteriophage-derived proteins and therapeutic applications. *Bacteriophage* 5:e1062590. doi: 10.1080/21597081.2015.1062590

Ryan, E. M., Gorman, S. P., Donnelly, R. F., and Gilmore, B. F. (2011). Recent advances in bacteriophage therapy: how delivery routes, formulation, concentration and timing influence the success of phage therapy. *J. Pharm. Pharmacol.* 63, 1253–1264. doi: 10.1111/j.2042-7158.2011.01324.x

Schmelcher, M., Donovan, D. M., and Loessner, M. J. (2012). Bacteriophage endolysins as novel antimicrobials. *Future Microbiol.* 7, 1147–1171. doi: 10.2217/fmb.12.97

Shi, Y., Li, N., Yan, Y., Wang, H., Li, Y., Lu, C., et al. (2012). Combined antibacterial activity of phage lytic proteins holin and lysin from Streptococcus suis bacteriophage SMP. *Curr. Microbiol.* 65, 28–34. doi: 10.1007/s00284-012-0119-2

Shi, X., Zhao, F., Sun, H., Yu, X., Zhang, C., Liu, W., et al. (2020). Characterization and complete genome analysis of *Pseudomonas aeruginosa* bacteriophage vB_PaeP_LP14 belonging to genus Litunavirus. *Curr. Microbiol.* 77, 2465–2474. doi: 10.1007/s00284-020-02011-5

Sidhu, S. S. (2000). Phage display in pharmaceutical biotechnology. *Curr. Opin. Biotechnol.* 11, 610–616. doi: 10.1016/s0958-1669(00)00152-x

Sidhu, S. S. (2001). Engineering M13 for phage display. *Biomol. Eng.* 18, 57–63. doi: 10.1016/s1389-0344(01)00087-9

Sioud, M. (2019). Phage display libraries: from binders to targeted drug delivery and human therapeutics. *Mol. Biotechnol.* 61, 286–303. doi: 10.1007/s12033-019-00156-8

Smith, G. P., and Petrenko, V. A. (1997). Phage display. *Chem. Rev.* 97, 391–410. doi: 10.1021/cr960065d

Song, J., Niu, W., Wu, R., Wang, J., Lei, L., Han, W., et al. (2021). The phage Holin HolGH15 exhibits potential as an antibacterial agent to control listeria monocytogenes. *Foodborne Pathog. Dis.* 18, 574–581. doi: 10.1089/fpd.2020.2833

Song, J., Xia, F., Jiang, H., Li, X., Hu, L., Gong, P., et al. (2016). Identification and characterization of HolGH15: the holin of Staphylococcus aureus bacteriophage GH15. *J. Gen. Virol.* 97, 1272–1281. doi: 10.1099/jgv.0.000428

Tanaka, A. S., Sampaio, C. A., Fritz, H., and Auerswald, E. A. (1995). Functional display and expression of chicken cystatin using a phagemid system. *Biochem. Biophys. Res. Commun.* 214, 389–395. doi: 10.1006/bbrc.1995.2299

Young, R. (1992). Bacteriophage lysis: mechanism and regulation. *Microbiol. Rev.* 56, 430–481. doi: 10.1128/mr.56.3.430-481.1992

Zhang, C., Li, W., Liu, W., Zou, L., Yan, C., Lu, K., et al. (2013). T4-like phage Bp7, a potential antimicrobial agent for controlling drug-resistant Escherichia coli in chickens. *Appl. Environ. Microbiol.* 79, 5559–5565. doi: 10.1128/AEM.01505-13

Zhao, Y., Guo, L., Li, J., Fang, B., and Huang, X. (2018). Molecular epidemiology, antimicrobial susceptibility, and pulsed-field gel electrophoresis genotyping of *Pseudomonas aeruginosa* isolates from mink. *Can. J. Vet. Res.* 82, 256–263. PMID: 30363376

Ziha-Zarifi, I., Llanes, C., Kohler, T., Pechere, J. C., and Plesiat, P. (1999). In vivo emergence of multidrug-resistant mutants of *Pseudomonas aeruginosa* overexpressing the active efflux system MexA-MexB-OprM. *Antimicrob. Agents Chemother.* 43, 287–291. doi: 10.1128/AAC.43.2.287

frontiers | Frontiers in Microbiology

TYPE Original Research
PUBLISHED 23 March 2023
DOI 10.3389/fmicb.2023.1148579

OPEN ACCESS

EDITED BY
Alicja Wegrzyn,
Institute of Biochemistry and Biophysics,
Polish Academy of Sciences,
Poland

REVIEWED BY
Swapnil Ganesh Sanmukh,
University of Leicester,
United Kingdom
Prasanth Manohar,
Center for Phage Technology,
Texas A&M University,
United States

*CORRESPONDENCE
Gajendra P. S. Raghava
✉ raghava@iiitd.ac.in

SPECIALTY SECTION
This article was submitted to
Phage Biology,
a section of the journal
Frontiers in Microbiology

RECEIVED 20 January 2023
ACCEPTED 06 March 2023
PUBLISHED 23 March 2023

CITATION
Aggarwal S, Dhall A, Patiyal S, Choudhury S, Arora A and Raghava GPS (2023) An ensemble method for prediction of phage-based therapy against bacterial infections.
Front. Microbiol. 14:1148579.
doi: 10.3389/fmicb.2023.1148579

An ensemble method for prediction of phage-based therapy against bacterial infections

Suchet Aggarwal[1], Anjali Dhall[2], Sumeet Patiyal[2], Shubham Choudhury[2], Akanksha Arora[2] and Gajendra P. S. Raghava[2]*

[1]Department of Computer Science and Engineering, Indraprastha Institute of Information Technology, New Delhi, India, [2]Department of Computational Biology, Indraprastha Institute of Information Technology, New Delhi, India

Phage therapy is a viable alternative to antibiotics for treating microbial infections, particularly managing drug-resistant strains of bacteria. One of the major challenges in designing phage-based therapy is to identify the most appropriate potential phage candidate to treat bacterial infections. In this study, an attempt has been made to predict phage-host interactions with high accuracy to identify the potential bacteriophage that can be used for treating a bacterial infection. The developed models have been created using a training dataset containing 826 phage- host interactions, and have been evaluated on a validation dataset comprising 1,201 phage-host interactions. Firstly, alignment-based models have been developed using similarity between phage-phage (BLASTPhage), host–host (BLASTHost) and phage-CRISPR (CRISPRPred), where we achieved accuracy between 42.4–66.2% for BLASTPhage, 55–78.4% for BLASTHost, and 43.7–80.2% for CRISPRPred across five taxonomic levels. Secondly, alignment free models have been developed using machine learning techniques. Thirdly, hybrid models have been developed by integrating the alignment-free models and the similarity-scores where we achieved maximum performance of (60.6–93.5%). Finally, an ensemble model has been developed that combines the hybrid and alignment-based models. Our ensemble model achieved highest accuracy of 67.9, 80.6, 85.5, 90, and 93.5% at Genus, Family, Order, Class, and Phylum levels on validation dataset. In order to serve the scientific community, we have also developed a webserver named PhageTB and provided a standalone software package (https://webs.iiitd.edu.in/raghava/phagetb/) for the same.

KEYWORDS

phage-host interaction, taxonomic levels, prediction, ensemble method, bacterial infection

Introduction

Bacterial infections pose a major threat to public health across the globe. According to recent reports around, 1.27 million people died in 2019 of bacterial infections due to antimicrobial-resistance (Antimicrobial Resistance, 2022). In the last few decades, the heavy consumption and misuse of antimicrobial and antibacterial drugs have exacerbated the current crisis (Fair and Tor, 2014; Ventola, 2015). It has been observed in recent studies that several novel

bacterial strains are emerging which are resistant to existing antibiotics (Magiorakos et al., 2012). Therefore, researchers are looking for alternative approaches to tackle this issue. One such approach is "phage therapy" where phages infect and lyse bacterial strains (Sulakvelidze et al., 2001; Lin et al., 2017; Furfaro et al., 2018; Gordillo Altamirano and Barr, 2019). One of the major challenges in designing phage therapy is to identify the most efficient bacteriophage that can lyse a target strain of bacteria (Roucourt and Lavigne, 2009; Yang et al., 2014). Currently, several techniques are available to measure the phage-host interactions such as RNA-sequencing, microfluidic-PCR, PhageFISH, and flow cytometry. In addition, spot test and agar overlay assay are used nowadays to match the phage-bacteria. Though these experimental techniques are highly accurate in identification of phage-bacteria interaction but they are costly and time consuming (Alvarez-Barrientos et al., 2000; Tadmor et al., 2011; Leskinen et al., 2016; Barrero-Canosa and Moraru, 2019; Grainha et al., 2020).

Thus, there is a need to develop computational methods that can predict the correct bacteriophage to treat a bacterial strain. In other words, there is a need to develop a method that can predict phage-host interaction (bacteriophage-bacteria) with high precision. In order to address this problem, a large number of methods have been developed in the past. Broadly, these methods can be classified into three categories - alignment-based, alignment-free and hybrid methods. The following are the brief description of major techniques developed in the past for predicting host-phage interaction. WIsH is an alignment-free tool that predicts prokaryotic hosts of phages using their genomic sequences (Galiez et al., 2017). VirHostMatcher-Net (Wang et al., 2020) is an hybrid method that combine several alignment-free and alignment-based features to construct a two-layered network model. SpacePHARER (Zhang et al., 2021) and VirSorter (Roux et al., 2015) use CRISPRs for predicting phage-host interaction in the prokaryotic genomes. PredPHI (Li et al., 2021) utilizes phage-host protein-based features for predicting phage-host interactions using deep convolutional networks. Despite several methods developed in the past decade for predicting phage-host interaction, their accuracy is far from satisfactory. Moreover, these existing methods do not provide user-friendly webserver facilities (Roux et al., 2015; Galiez et al., 2017; Wang et al., 2020; Li et al., 2021; Zhang et al., 2021). Hence, there is a challenge to develop methods that can predict phage-host interaction with high accuracy. In order to complement the existing methods, we have tried to develop an ensemble method for predicting phage-host interactions. Our proposed ensemble method combines alignment free (machine learning) and alignment-based (BLAST) techniques to predict phage-host interaction across all five taxonomic levels.

To maintain scientific standards and compare our approach with existing methods, we developed and evaluated our models on benchmark datasets used in a recent study (Wang et al., 2020). We have applied several machine learning techniques to develop the prediction models. One of the main objectives of this study is to facilitate researchers working in the field of phage therapy by identifying potential phage candidates that might be suitable to lyse drug-resistant bacterial strains and thus helping in narrowing down the search for suitable phages. Thus, we developed PhageTB (Webserver and Standalone Software) that contain three major modules; (i) host for a phage, (ii) phage-host interaction and (iii) phage for a host. The first module allows the users to predict the bacterial strain (i.e., host) from a phage genome sequence. The second module (Phage-host interaction) allows the user to predict whether a given phage and bacterial strain will interact or not. The third module, phage for a host, allows a user to predict the most appropriate phage that can lyse a given strain of bacteria.

Materials and methods

Dataset collection and pre-processing

In the present study, datasets used for training and validation were obtained from a recent study VirHostMatcher-Net (Wang et al., 2020). The training dataset comprises 826 phages and their corresponding hosts (till the strain level), out of which 817 infect bacteria while nine infect archaea. The chosen dataset is such that each phage has a unique interaction with a bacterial strain. Aggregating the strain to a higher taxonomic level (till Genus, Phylum etc.) allows each phage to have multiple target hosts. Originally, we obtain around 1,462 phage entries and their corresponding hosts as the original testing dataset. However, the original testing dataset has one major issue that it contains phage-host pairs where some of the bacterial hosts belong to a genus that does not fall in the genera of the bacterial hosts of the training phage-host pairs. Evaluation of such phage-host interaction is not prudent as we do not have reference hosts representing such genera in the training phage-host pairs. Ideally, the test dataset should only contain the phage-host interactions, where the host information is available in our reference training data. Hence, we modified the original testing dataset and called it as the testing dataset, by removing the phage-host pairs whose hosts belong to a genus, not represented in the set of hosts from the training phage-host pairs. Out of the 1,462 phage-host pairs, there were 261 phage-host interactions which were not present in the training interactions. Hence, we removed 261 pairs and get 1,201 phage-host interactions in the testing dataset. Finally, our training dataset incorporates 826 phage-host interactions, and the testing dataset has 1,201 phage-host interactions. To make an unbiased comparison with the existing methods, we also evaluate our approach's performance on the original testing dataset (See Supplementary materials). Figure 1 highlights the number of distinct Phylum, Classes, Orders, Families and Genera the bacterial hosts belong to, in at least one inter-action in the training, testing, and original testing datasets.

Outline of the study

In this study, we have developed three alignment-based methods using BLAST called BLASTHost, BLASTPhage and CRISPRPred (See Figure 2C). These alignment-based methods are based on top hits of BLAST search. Alignment based predictions are sometimes inadequate when we do not get any significant hit, in such cases alternative predictions can help. Therefore, we also create machine learning models that we used for predicting the hosts for phages. We also developed a hybrid method that combines a machine-learning based model with similarity scores (bit-scores from BLAST alignments) (See Figure 2B). Finally, an ensemble method has been developed that combines all alignment-based models with the hybrid method in a sequential method (Figure 2A). Predictions from the ensemble model are made in a staged sequential manner. First,

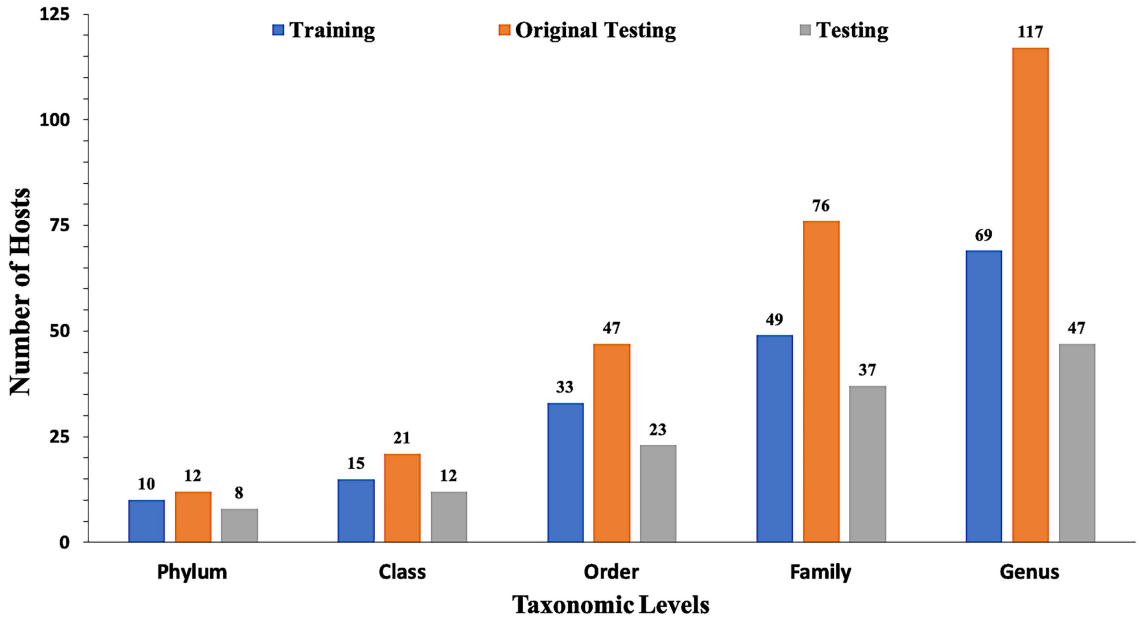

FIGURE 1
Distribution of data in training, testing, and original testing datasets at different taxonomic levels.

predictions for all phages are made using BLASTPhage. We assign hosts corresponding to the top hit for the phages where the e-value of alignment is within a predetermined threshold. Next, for the remaining phages, we make the predictions using BLASTHost. We assign hosts to the phages where the e-value of alignment with the top hit is within a predetermined threshold. Third, for the phages whose hosts have not yet been assigned, we make predictions from the hybrid model and assign hosts for phages where the prediction scores from the model are above a threshold. Finally, for all remaining phages whose host could not be predicted, we assign hosts based on predictions from CRISPRPred.

Alignment-based methods

Most of the alignment-based methods exploit sequence similarity between genomes of phages and their hosts. The most widely used method for searching for similar sequences is BLAST (McGinnis and Madden, 2004). We employed BLAST-based predictions at three levels, i.e., BLASTPhage, BLASTHost, and CRISPRPred. In the case of BLASTPhage, phage's genome sequence is searched against a database of phages whose interacting host is already known. This database is referred to as the reference phage database in our study and it was created using training dataset comprising the information about the phages and their respective interacting hosts. Then, the phage sequences in the testing dataset are searched against the reference phage database using BLAST at different e-values. The host corresponding to the top BLAST hit of a phage is assigned as the predicted host for the query phage. In summary, the BLASTPhage model predicts the host based on similarity in the query and target phage. In the case of BLASTHost, the sequence of a phage is searched in database of 185 host sequences used in the training dataset. The top hit from this alignment task is assigned as the potential host. CRISPR systems play a vital role during the infection process of phages and infection prevention by the hosts. As a prevention strategy, prokaryotes place a fragment of the genome of an infecting phage as a spacer in the CRISPR array, which is a recognizable repeat region in the genome. Such a sequence indicates a recent infection and thus can be used as a potential signal for predicting hosts. CRISPR Recognition Tool (CRT) (Bland et al., 2007) is used to identify CRISPR locus in the bacterial genomes using a reference host database. We extracted CRISPR sequences using the CRT tool and created a reference CRISPR database. The test dataset genomes are aligned with the reference CRISPR database using BLAST, where the host corresponding to the top hit is predicted as the potential host. In the case of CRISPR alignment we have utilized the BLAST short-task parameter as used in a previous study (Biswas et al., 2013). We termed this approach of alignment as the CRISPRPred model.

Generation of features

To develop machine-learning models for prediction, it is necessary to generate fixed-length feature representations for all phage sequences. The phage genome sequences are polymers of four nucleotides (A, T, G, C) and have a wide range of variations in length. One of the commonly used techniques to generate fixed-length feature representation for a sequence is to calculate the frequency of nucleotide sub-sequences or k-mers. For example, one can calculate the frequency of individual nucleotides in a sequence, and the sequence is thus represented by a vector of dimension four. In this case, the total number of k-mer is 4 (4^1), where the subsequence or k-mer length is one. Similarly, the frequency of di-nucleotides (i.e., AA, AC, AG, AT, CA, CC) can be calculated, where the total number of k-mers will be 16 (4^2), with the k-mer length being two. One of the limitations of these frequency-based features is that they are biased by

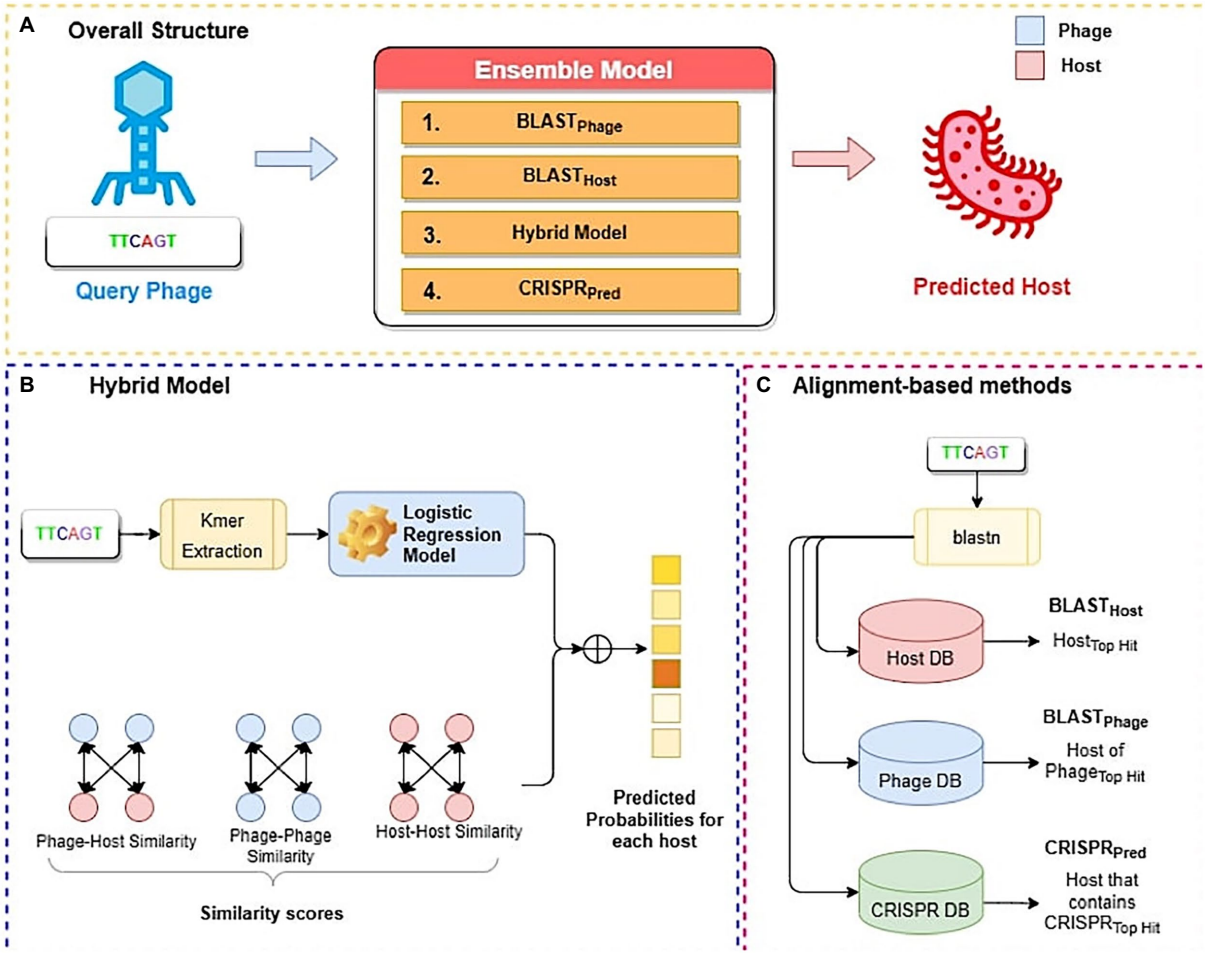

FIGURE 2
Overall structure of algorithms used in this study; **(A)** Ensemble method **(B)** Hybrid model **(C)** Alignment-based method.

the length of the sequence and the noise in the sequence. Thus, we used modified frequency words, subtracting the frequency of k-mers by chance in that sequence (Reinert et al., 2009). The following formulae were used to compute the modified frequency of k-mers, which is used.

$$f_m = f_o - f_c \tag{1}$$

$$f_c = P_w \times \{L - (\mathrm{k} - 1)\} \tag{2}$$

$$P_w = \Pi_{i=1}^{k} p_i \tag{3}$$

Where f_m, f_o, and f_c are modified, the original and chance frequency of a k-mer w, respectively. P_w is the probability of k-mer w, p_i is the probability of a nucleotide i in the k-mer w, L is the sequence length or the number of nucleotides in the sequence, and k is the length of k-mer w.

Machine learning model

Several machine learning classifiers were implemented for predicting the hosts for bacteriophages and compared to develop the best-performing model. We have implemented various techniques including Random Forest (RF), Gaussian Naive Bayes (GNB), Logistic regression (LR), Support vector machine (SVM) with a linear kernel, eXtreme Gradient Boosting (XGBoost), Decision Tree (DT), K-Nearest Neighbor (KNN), and Multi-layer Perceptron (MLP). These classification techniques were implemented using the python-library scikit-learn (Pedregosa et al., 2012).

Hybrid model

We utilize machine learning models at the third level for the remaining phages, i.e., those whose host could not be predicted using the BLASTPhage and BLASTHost method. We term this level of prediction as the hybrid model. Due to the coevolution of phages and their hosts, their genetic compositions are highly similar. Thus, a given phage significantly overlaps with its putative host at the genomic level.

Therefore, similar hosts will likely be infected by the same phage, or similar phages will likely infect the same host. We have used the base machine-learning model prediction probabilities $\mathrm{Pr}_b = \left[\mathrm{Pr}^i \;\; for \;\; i = 1,\ldots M\right]$ for all hosts, where M is the total number of hosts in the reference host database and Pr^i (prediction probability for the ith bacteria) which varies between 0 to 1. In addition, we have added the similarity-scores (SIM) i.e., bit-scores from BLAST alignment tasks between phage-phage, phage-host, and host–host databases using a weighted sum to the prediction probabilities from the base machine-learning model. Further, we have used the Pr_o to calculate the final prediction probabilities for all bacterial hosts.

$$\mathrm{Pr}_o = \mathrm{Pr}_b(1-\gamma) + \left(SIM_{PH}(v_q,H)(1-\alpha) + SIM_{HH}(h_s,\mathrm{H})\alpha\right)\gamma \quad (4)$$

Where, SIM_{PP}, SIM_{PH} *and* SIM_{HH} denote phage-phage, phage-host, and host–host similarity scores, where $SIM_{PH}(v,H)$ gives an M-Dimensional vector that gives the similarity scores of phage v with all hosts in the set $H = [h_1,h_2,\ldots h_M]$ of reference hosts. Similarly, $SIM_{HH}(h,H)$ also gives an M-Dimensional vector denoting the similarity of the host h with all other hosts in set H. v_q corresponds to the input query phage, h_s represents the host of most similar phage in the training dataset based on SIM_{PP} , and Pr_b is the prediction probabilities from the base model. Here, α and γ are the weighting parameters used in the given equation and are determined experimentally during cross-validation using grid search over the value range of 0 to 1 with step size of 0.1. The final predictions from the hybrid model were calculated using Equation 5.

$$Predicted\ Host(v) = argmax_h\ \mathrm{Pr}_o(h) \quad (5)$$

Ensemble model

In order to improve the prediction accuracy, without compromising the coverage we have used an ensembled approach, generating predictions using combinations of different models. Here, we integrate alignment-based, alignment-free models. At first, we calculate predictions from BLASTPhage and assign host against phages where the e-value of alignment is within a threshold. Similarly, this process was repeated for remining phages using BLASTHost. Next, we compute predictions from the hybrid model for phages where final prediction score is above a threshold (See Equation 5). Finally, for the remaining phages, predictions are made using CRISPRPred.

Evaluation parameters

We evaluate the performance of our approach on the original testing dataset, which comprises 1,462 phage samples. Moreover, we have also evaluated the performance of the generated models on the modified testing dataset containing 1,201 phage samples. We also compare our approach with past studies in terms of prediction accuracy for correctly predicting hosts binned by taxonomic levels from Genus to Phylum. The prediction accuracy is defined as the fraction of phages whose hosts were identified correctly out of the total phages at a given taxonomic level.

$$Accuracy = \frac{Number\ of\ Correct\ Predictions}{Total\ number\ of\ test\ samples} \times 100 \quad (6)$$

$$Probability\ of\ correct\ prediction = \frac{Number\ of\ Correct\ Predictions}{Total\ number\ of\ predictions} \times 100 \quad (7)$$

Webserver architecture

A web server named as 'PhageTB'[1] is developed to predict the bacterial hosts, host-phage interactions, and lytic phage for a bacterium. The front end of the web server was developed by using HTML5, JAVA, CSS3 and PHP scripts. It is based on responsive templates which adjust based on the size of the device. It is compatible with almost all modern devices such as mobile, tablet, iMac, and desktop.

Results

Predictions from BLASTPhage, BLASTHost and CRISPRPred

Sequence alignment of phage and host genomes is the primary method for assigning hosts to phages from a set of known hosts. For this purpose, we employed BLAST technique, where first we vary the degree of alignment by changing the threshold on the e-value. For the query phages where we get a sequence match, we observe the prediction accuracies improved when the e-value threshold is reduced, but the overall recall decreases. However, we could not predict hosts using this method for all phages, as shown in Figure 3, the coverage decreases as we decrease the e-value threshold and the sequence match becomes more specific. When aligning the phage genomes in the original testing dataset with the reference phage genome database, and assigning the host based on the top hit, we attained the prediction accuracies of 45.2, 56.2, 62.8, 67.5, and 71.2% at Genus, Family, Order, Class and Phylum levels, respectively (Supplementary Table S1).

Similarly, on aligning the phage genomes with the reference host genome database and assigning the top hit as the predicted host, we obtained accuracies of 34.8, 42.3, 49.7, 57.0, and 62.8% at Genus, Family, Order, Class, and Phylum levels, at e-value 1.00E-02 (Supplementary Table S1). As reported in Table 1, we obtained accuracies of 42.4, 50.5, 57.2, 61.4, and 66.2% across the five taxonomic level using BLASTHost method at e-value 1.00E-02. Similarly, BLASTPhage attained accuracies of 55.0, 66.4, 71.4, 74.9, and 78.4% at Genus, Family, Order, Class, and Phylum levels, respectively on the test dataset. Further predictions were made by aligning phage

1 https://webs.iiitd.edu.in/raghava/phagetb/

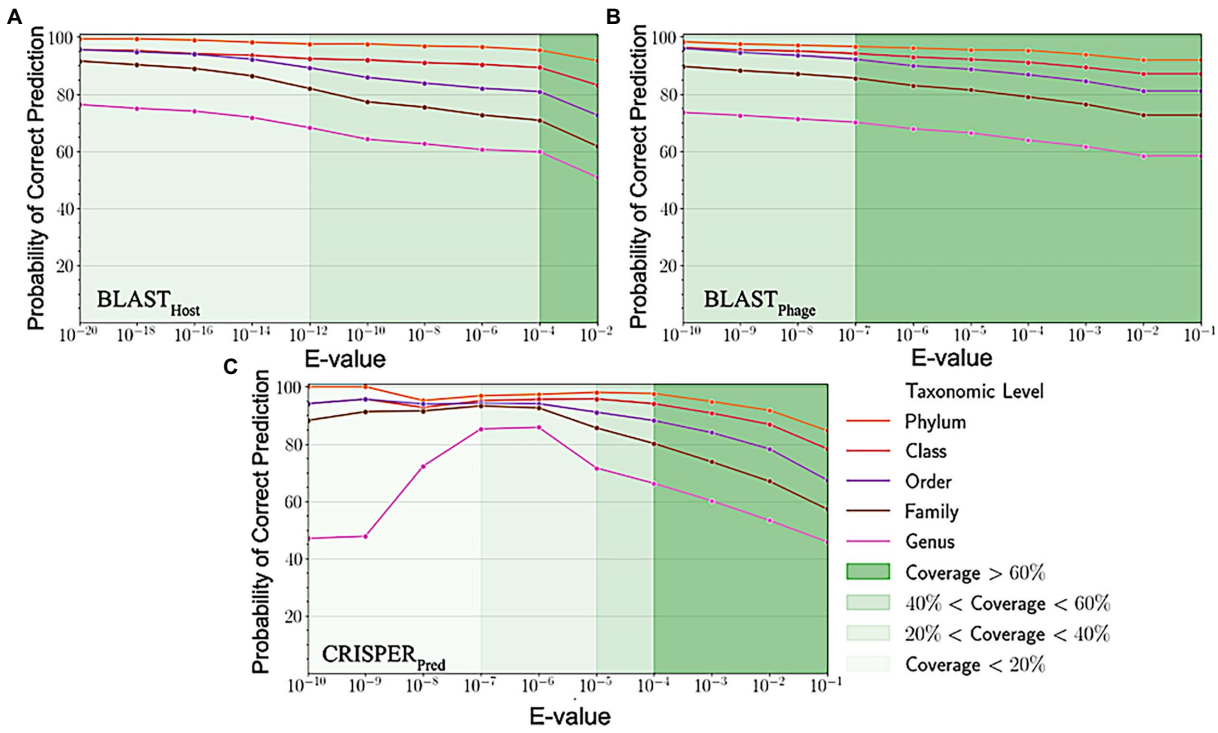

FIGURE 3
Variation in probability of correct prediction **(A)** $BLAST_{Phage}$ **(B)** $BLAST_{Host}$ and **(C)** $CRISPR_{Pred}$ at different e-values.

TABLE 1 Prediction of five taxonomic levels of bacterial host using alignment-based models on validation dataset.

E-value	Method	Cov (%)	Taxonomic Level									
			Genus		Family		Order		Class		Phylum	
			PCP(%)	Acc(%)	PCP(%)	Acc(%)	PCP(%)	Acc(%)	PCP(%)	Acc (%)	PCP (%)	Acc (%)
1.00E-06	$BLAST_{Host}$	50.45	67.00	33.81	79.21	39.97	87.29	44.05	90.43	45.63	96.53	48.71
	$BLAST_{Phage}$	70.77	74.12	52.46	88.24	62.45	93.41	66.11	95.53	67.61	98.24	69.53
	$CRISPR_{Pred}$	21.57	87.64	18.90	92.66	19.98	93.82	20.23	96.14	20.73	97.30	20.98
1.00E-05	$BLAST_{Host}$	53.46	66.98	35.80	78.82	42.13	87.07	46.54	90.34	48.29	96.26	51.46
	$BLAST_{Phage}$	72.11	72.98	52.62	87.07	62.78	92.49	66.69	94.69	68.28	97.58	70.36
	$CRISPR_{Pred}$	38.30	70.22	26.89	85.00	32.56	91.09	34.89	96.30	36.89	98.04	37.55
1.00E-04	$BLAST_{Host}$	58.28	67.14	39.13	78.29	45.63	86.86	50.62	90.00	52.46	96.00	55.95
	$BLAST_{Phage}$	75.52	70.67	53.37	85.12	64.28	90.74	68.53	93.72	70.77	97.35	73.52
	$CRISPR_{Pred}$	51.87	66.45	34.47	81.22	42.13	90.37	46.88	95.83	49.71	97.59	50.62
1.00E-03	$BLAST_{Host}$	64.45	63.31	40.80	74.81	48.21	84.75	54.62	89.41	57.62	95.22	61.37
	$BLAST_{Phage}$	77.10	69.76	53.79	84.23	64.95	89.96	69.36	93.30	71.94	97.19	74.94
	$CRISPR_{Pred}$	62.53	60.59	37.89	74.43	46.54	85.75	53.62	92.01	57.54	94.67	59.20
1.00E-02	$BLAST_{Host}$	71.36	59.51	42.46	70.83	50.54	80.16	57.20	86.11	61.45	92.88	66.28
	$BLAST_{Phage}$	81.77	67.31	55.04	81.57	66.69	87.37	71.44	91.65	74.94	95.93	78.43
	$CRISPR_{Pred}$	73.77	54.40	40.13	68.62	50.62	80.59	59.45	88.94	65.61	92.44	68.19
1.00E-01	$BLAST_{Host}$	71.44	59.44	42.46	70.75	50.54	80.07	57.20	86.01	61.45	92.77	66.28
	$BLAST_{Phage}$	81.77	67.31	55.04	81.57	66.69	87.37	71.44	91.65	74.94	95.93	78.43
	$CRISPR_{Pred}$	90.67	46.83	42.46	58.59	53.12	69.15	62.70	79.89	72.44	85.40	77.44

Cov(%): Coverage in percentage; Acc(%): Accuracy in percentage; PCP(%): Probability of Correct Prediction

TABLE 2 Prediction of five taxonomic levels of bacterial host using machine learning and hybrid models on modified test dataset.

Machine learning methods	Taxonomic levels (Accuracy %)				
	Genus	Family	Order	Class	Phylum
Decision Tree (DT)	22.30	30.50	34.70	45.70	55.90
Gaussian Naive Bayes (GNB)	24.30	32.00	35.20	42.90	45.60
XGBoost (XGB)	37.20	44.20	48.20	53.20	57.80
Random Forest Classifier (RF)	38.80	46.10	51.00	55.70	59.20
Linear SVM (SVM)	51.80	62.10	65.60	71.00	73.50
K-Nearest Neighbor (KNN)	49.20	61.60	67.60	73.20	78.50
Multi-layer perceptron (MLP)	49.20	63.50	69.10	76.10	80.00
Logistic Regression (LR)	54.80	68.10	72.50	77.70	80.80
Hybrid Model (Similarly-scores + LR)	60.60	75.80	82.00	89.70	93.50

genomes with CRISPR sequences extracted from host genomes. The predictions from CRISPRPred were very accurate for smaller e-value thresholds indicating precise predictions up to the Genus level, but at the same time the coverage (fraction of phages for which predictions could be made) was relatively small. This implied that although highly accurate predictions can be made using CRISPR signals but such predictions are not possible for all phages. We observe that in the case of the original test dataset (See Supplementary Table S1) and modified test datasets, the prediction accuracies were improved at the level of class and phylum in comparison with BLASTHost and BLASTPhage methods (refer to Table 1).

Performance of machine learning models

In order to develop various machine learning models, i.e., Decision Tree (DT), Random Forest (RF), Gaussian Naive Bayes (GNB), XGBoost, Logistic Regression (LR), Multi-layer perceptron (MLP), and Support Vector Machine (SVM), we extracted the features f_m using Equation 1 with k = 6, from the phage genomes and using these features, we predicted the bacterial hosts for phages in the testing dataset. As represented in Table 2, on modified test dataset, LR-based models performed best among all other classifiers. In order to improve the performance further, we integrated the prediction score of the best model, i.e., LR with similarity scores, i.e., BLAST bit scores and observed that there is a significant improvement in the predictive accuracies. The parameters for the hybrid model were found by varying the weighting parameters α and γ in Equation 4. We achieved the best performance at $\alpha = 0.9$ and $\gamma = 0.6$. On original test dataset, the prediction accuracies of the hybrid model (LR + similarly score) are 49.7, 64.7, 75.3, 84.8, and 90.6% across the five taxonomic levels, respectively, (Supplementary Table S2). On the other side, the hybrid model evaluated on the modified test dataset, outperformed all other classifiers with an improved accuracies of 60.6, 75.8, 82.0, 89.7, 93.5% at Genus, Family, Order, Class, and Phylum levels, respectively, (See Table 2).

Performance of ensemble models

In order to improve the performance of the models mentioned above, we have used the ensemble approach, where we have generated predictions from combinations of the different models. Here, we have tried combinations of $BLAST_{Phage}$, $BLAST_{Host}$, $CRISPR_{Pred}$ and the Hybrid Model and validated the accuracies at different taxonomic levels on both the testing datasets. We observe improvements across all the taxonomic levels as we progressively add the different prediction methods to the overall framework. Host prediction accuracy was markedly higher than individual components. For higher-order taxonomic levels (Class and Phylum) combination of BLAST and the hybrid model-based predictions also got comparable results. However, for lower and more specific levels, the best-performing approach was the one that combines all prediction methods. Our proposed ensembled model (BLASTPhage + BLASTHost + CRISPRPred + Hybrid Model) outperforms the existing approaches across all taxonomic levels, correctly predicting 61.6, 74.4, 80.5, 85.7, and 91.2%, respectively, for original test dataset (Supplementary Table S3) and 67.9, 80.6, 85.5, 90.0, and 93.5% for test dataset at Genus, Family, Order, Class and Phylum levels. The e-value thresholds for BLASTPhage (1.00E-10), BLASTHost (1.00E-20), CRISPRPred (1.00E-2), and the prediction probability threshold for the hybrid models is 0.6 (Table 3).

Contributions to the scientific community

To serve the scientific community, we integrate our best-performing models in a webserver called "PhageTB." This tool incorporates three major modules (i) Hosts for bacteriophages (ii) Interaction of phage-host pair and (iii) Lytic phage for a bacterial host. The first module "Hosts for bacteriophages" allows users to choose four predictive methods, i.e., BLASTPhage, BLASTHost, CRISPRPred, and Hybrid Model. Users need to provide the query genome sequence and the tool predict the bacterial hosts using the reference host database. The second module "Interaction of phage-host pair" predicts whether a pair of phage and bacteria are likely to interact based on their genome sequences. Users need to provide genome sequences of phage and bacteria in the FASTA format. Our tool predicts the interactions between the query sequences, by first, predicting the host of the query phage using the first module and then using sequence alignment between the predicted and query hosts to determine whether the query pair interact or not. The third module "Lytic phage for a bacterial host" predicts bacteriophages corresponding to query bacterial sequences. The input genome sequence is searched against

TABLE 3 Prediction of five taxonomic levels of bacterial host using ensembled models.

Method	Taxonomic Level (Accuracy %)				
	Genus	Family	Order	Class	Phylum
$BLAST_{Phage}$ + $BLAST_{Host}$	59.40	70.10	73.90	75.50	78.60
$BLAST_{Host}$ + Hybrid Model	65.00	78.10	83.10	89.90	93.90
$BLAST_{Phage}$ + Hybrid Model	62.60	75.80	82.40	89.80	93.60
$CRISPR_{Pred}$ + Hybrid Model	61.10	74.10	80.50	86.40	90.10
$BLAST_{Phage}$ + $BLAST_{Host}$ + Hybrid Model	65.70	78.60	84.30	90.70	94.00
$BLAST_{Host}$ + $CRISPR_{Pred}$ + Hybrid Model	65.50	76.60	81.70	86.80	90.90
$BLAST_{Phage}$ + $CRISPR_{Pred}$ + Hybrid Model	66.70	79.20	84.60	89.80	93.50
$BLAST_{Phage}$ + $BLAST_{Host}$ + $CRISPR_{Pred}$ + Hybrid Model	67.90	80.60	85.50	90.00	93.50

TABLE 4 Lytic phage prediction by phageTB on ESKAPE bacteria.

Bacteria	Predicted phage (GenBank ID)	Evidence (Ref)
Enterococcus faecium	AB746912	Lee et al. (2019)
Staphylococcus aureus	DQ289556	Fish et al. (2016)
Klebsiella pneumoniae	CP000711	Manohar et al. (2018)
Acinetobacter baumannii	AB746912	Badawy et al. (2020)
Pseudomonas aeruginosa	No-Prediction	-
Enterobacter	CP000711	Manohar et al., 2018

the reference database of phage-host interactions, where first we align the query sequence with genome sequences of bacteria that are known hosts for some bacteriophages. The top hit bacteria from the reference database are the most similar bacteria to the query, and thus the query is likely to be infected by the phage associated with the top hit. The webserver "PhageTB" was implemented using HTML, CSS, and PHP and has multi-device compatibility, and provides an easy-to-use and user-friendly interface. The open-source web server is available at https://webs.iiitd.edu.in/raghava/phagetb. The command line standalone can be found on GitHub at https://github.com/raghavagps/phagetb.

Case study: Prediction of lytic phages

Predicting lytic phages that can be used (solely or with other agents) for treatment of multi-drug resistance bacterial infections is a major problem of concern for the scientific community (Lin et al., 2017; Kortright et al., 2019). In this case study we identify suitable phage-based treatments for drug-resistant bacterial infections using our webserver PhageTB to predict the lytic phages corresponding to the six ESKAPE *Enterococcus faecium*, *Staphylococcus aureus*, *Klebsiella pneumoniae*, *Acinetobacter baumannii*, *Pseudomonas aeruginosa*, and *Enterobacter* species (Santajit and Indrawattana, 2016; Mulani et al., 2019) bacteria. ESKAPE comprises six well-known highly virulent antibiotic-resistant bacterial pathogens. Here we have downloaded the genome assemblies of each of the six bacteria from NCBI[2] and predict the specific phage. We utilize the default parameters of the third module, "Lytic phage for a bacterial host" of PhageTB, to predict the phages that are likely to infect a bacterium. Table 4 and Supplementary Table S4 represents the predicted phages with GenBank ID for five out of six ESKAPE bacteria. We could not predict any lytic phage against Pseudomonas aeruginosa bacteria, which could be attributed to the use of strict thresholds for the individual models. We have evaluated the predictions of our tool with existing studies and clinical trials (El Haddad et al., 2019; Mulani et al., 2019). These findings can be extended to other drug-resistant bacterial strains and thus utilized to expedite the process of finding suitable phages for the treatment of drug-resistant bacterial infections where the lytic phages are not known beforehand.

Comparison with other methods

Comparing this newly developed method with the existing tools is crucial to understand the merits and demerits. There are several methods available such as VirHostMatcher-Net, PHP, Phirbo, and PredPHI as shown in Table 5. Therefore, we compare the performance of our method with three existing tools PHP (Lu et al., 2021),

2 https://www.ncbi.nlm.nih.gov/assembly/

TABLE 5 Comparison of PhageTB with the existing phage-host interaction prediction methods.

Tool	PhageTB	PHP	VirHostMatcher-Net	Phirbo	PredPHI
Webserver	Yes	No	No	No	No
Standalone	Yes	Yes	Yes	Yes	Yes
Genus	Yes	Yes	Yes	Yes	No
Family	Yes	Yes	Yes	Yes	No
Order	Yes	Yes	Yes	Yes	No
Class	Yes	Yes	Yes	Yes	No
Phylum	Yes	Yes	Yes	Yes	No
Phage2Host	Yes	Yes	Yes	Yes	Yes
Host2Phage	Yes	No	Yes	No	No
Phage2Phage	Yes	No	Yes	No	No

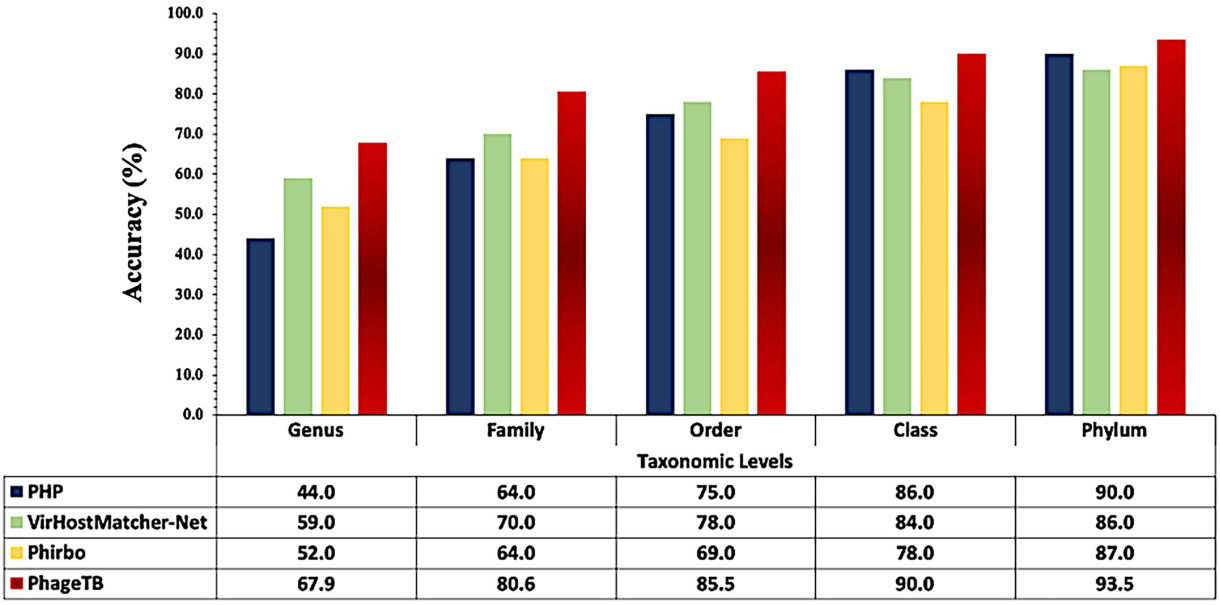

FIGURE 4
Comparison of performance of our method with existing tools at different taxonomic levels.

VirHostMatcher-Net (Wang et al., 2020), and Phirbo (Zielezinski et al., 2021), due to the prediction at all five taxonomic levels is available in only these tools. As shown in Figure 4, PhageTB outperform previous studies at each taxonomic level, with an accuracy of 67.90, 80.60, 85.5, 90.0, and 93.5% at Genus, Family, Order, Class, and Phylum levels. The prediction accuracies of other tools are provided in Figure 4.

Discussion and conclusion

Phage therapy is a leading alternative to antibiotics for the treatment of bacterial infections as most pathogenic strains are now showing resistance to numerous known antibiotics (Topka-Bielecka et al., 2021). The development of phage therapy requires the identification and isolation of a large number of bacteriophages. Phages are generally specific to bacterial species as well as their strains which is an advantage of this therapy as it will only kill the pathogenic bacteria, leaving out the natural bacteria required for the human body. The highly specific nature of bacteriophages necessitates the collection and characterization of their known and potential hosts and the interactions between them (Gorski et al., 2018, 2020). There have been several studies in the past that have tried to identify and predict the hosts of phages and their interactions like WIsH, VirHostMatcher-Net, SpacePHARER, VirSorter, and PredPHI (Roux et al., 2015; Galiez et al., 2017; Wang et al., 2020; Li et al., 2021; Zhang et al., 2021). Despite this, the presently available methods cannot accurately predict the taxonomic classes of the phage and hosts. To bridge this gap and achieve better performance in predicting the phage-host interactions, we developed a method called PhageTB that uses both alignment-based and alignment-free features to predict the hosts from query genomic sequences of bacteriophages.

PhageTB is a hierarchical prediction method that stacks four predictive methods to predict the phage-host interactions across five levels–Genus, Family, Order, Class, and Phylum. These methods include BLASTPhage, BLASTHost, the Hybrid model, and CRISPRPred. BLASTPhage, BLASTHost, employ BLAST alignment-based predictions for query sequences against reference hosts and phages, respectively, and the CRISPRPred approach uses CRISPR based alignment to predict the same. In cases where there is a shortage of phage or bacterial sequence data, traditional alignment-based methods may be unreliable in predicting rare phage-host interactions. However, machine learning models can be used to address this limitation. The Hybrid Model predicts the host based on the machine learning classifier and similarity scores. These four methods combined can accurately predict the host-phage interactions and outperform the previously developed methods to predict phage-host interactions namely PHP, VirHostMatcher-Net, and Phirbo when tested on the dataset containing 1,462 phage-host interactions (Wang et al., 2020; Lu et al., 2021; Zielezinski et al., 2021). We obtained accuracies of 67.9, 80.6, 85.5, 90.0, and 93.5% for Genus, Family, Order, Class, and Phylum, respectively, using the ensemble model which is better than the abovementioned methods. Additionally, it must be noted that the proposed tool has limitations regarding its ability to predict the evolution of bacterial resistance to phages, as it assumes that any phage used in the prediction can infect any bacteria without taking into consideration any developed resistance and does not explicitly identify phage resistance. The approaches combined in PhageTB provide accurate predictions for phage-host interactions making it a valuable tool for the scientific community working in this field worldwide to identify phages that might be suitable to combat the crisis of antibiotic resistance. With the increasing availability of metagenome samples, new methods for identifying phages and determining their hosts are required. We believe that PhageTB will prove to be an effective tool in finding specific hosts for the phages which can be potentially helpful in the development of phage therapy by facilitating as a useful filter to narrow down target phages and hosts, ecology research, viral metagenomics analysis, and human gut microbiocenosis research among others. PhageTB is an easy-to-use method of assigning hosts to bacteriophages, studying their interactions, and narrowing down the search space for candidate phages that can successfully lyse the query bacteria and thus be utilized in phage therapy for treating bacterial infections caused by it. Our tool is freely accessible at https://webs.iiitd.edu.in/raghava/phagetb/, and the Python standalone package is available at GitHub https://github.com/raghavagps/phagetb.

Limitation of the study

In the current study, we have developed an in-silico tool for the prediction of phage-host interactions using ensemble learning approach. Due to the limitation in the available datasets we have not considered phage-host receptors and prophages for developing the prediction models. Moreover, we were not able to discriminate interacting and bacterial resistant strains. In future, we will update this tool by incorporating new features and experimentally validated data, in order to generate a highly accurate and reliable method for designing phage-based therapy.

Data availability statement

The original contributions presented in the study are included in the article/Supplementary material, further inquiries can be directed to the corresponding author.

Author contributions

SA, and GR collected and processed the datasets and implemented the algorithms. SA, AD, and SP created the back end of the web server and front-end user interface. SA developed prediction models. SA, SP, SC, and AD analyzed the results. SA, AD, SC, AA, SP, and GR penned the manuscript. GR conceived and coordinated the project and provided overall supervision to the project. All authors have read and approved the final manuscript.

Funding

This research was funded by Department of Biotechnology (DBT grant BT/PR40158/BTIS/137/24/2021), Government of India, India.

Acknowledgments

Authors are thankful to the Department of Biotechnology (DBT), Department of Science and Technology (DST-INSPIRE) and CSIR for fellowships and the financial support and Department of Computational Biology, IIITD New Delhi for infrastructure and facilities.

Conflict of interest

The authors declare that the research was conducted in the absence of any commercial or financial relationships that could be construed as a potential conflict of interest.

Publisher's note

All claims expressed in this article are solely those of the authors and do not necessarily represent those of their affiliated organizations, or those of the publisher, the editors and the reviewers. Any product that may be evaluated in this article, or claim that may be made by its manufacturer, is not guaranteed or endorsed by the publisher.

Supplementary material

The Supplementary material for this article can be found online at: https://www.frontiersin.org/articles/10.3389/fmicb.2023.1148579/full#supplementary-material

References

Alvarez-Barrientos, A., Arroyo, J., Canton, R., Nombela, C., and Sanchez-Perez, M. (2000). Applications of flow cytometry to clinical microbiology. *Clin. Microbiol. Rev.* 13, 167–195. doi: 10.1128/CMR.13.2.167

Antimicrobial Resistance (2022). Global burden of bacterial antimicrobial resistance in 2019: a systematic analysis. *Lancet* 399, 629–655. doi: 10.1016/S0140-6736(21)02724-0

Badawy, S., Pajunen, M. I., Haiko, J., Baka, Z. A. M., Abou-Dobara, M. I., El-Sayed, A. K. A., et al. (2020). Identification and functional analysis of temperate Siphoviridae bacteriophages of *Acinetobacter baumannii*. *Viruses* 12:604. doi: 10.3390/v12060604

Barrero-Canosa, J., and Moraru, C. (2019). PhageFISH for monitoring phage infections at single cell level. *Methods Mol. Biol.* 1898, 1–26. doi: 10.1007/978-1-4939-8940-9_1

Biswas, A., Gagnon, J. N., Brouns, S. J., Fineran, P. C., and Brown, C. M. (2013). CRISPRTarget: bioinformatic prediction and analysis of crRNA targets. *RNA Biol.* 10, 817–827. doi: 10.4161/rna.24046

Bland, C., Ramsey, T. L., Sabree, F., Lowe, M., Brown, K., Kyrpides, N. C., et al. (2007). CRISPR recognition tool (CRT): a tool for automatic detection of clustered regularly interspaced palindromic repeats. *BMC Bioinformatics* 8:209. doi: 10.1186/1471-2105-8-209

El Haddad, L., Harb, C. P., Gebara, M. A., Stibich, M. A., and Chemaly, R. F. (2019). A systematic and critical review of bacteriophage therapy against multidrug-resistant ESKAPE organisms in humans. *Clin. Infect. Dis.* 69, 167–178. doi: 10.1093/cid/ciy947

Fair, R. J., and Tor, Y. (2014). Antibiotics and bacterial resistance in the 21st century. *Perspect. Med. Chem.* 6, 25–64. doi: 10.4137/PMC.S14459

Fish, R., Kutter, E., Wheat, G., Blasdel, B., Kutateladze, M., and Kuhl, S. (2016). Bacteriophage treatment of intransigent diabetic toe ulcers: a case series. *J. Wound Care* 25, S27–S33. doi: 10.12968/jowc.2016.25.7.S27

Furfaro, L. L., Payne, M. S., and Chang, B. J. (2018). Bacteriophage therapy: clinical trials and regulatory hurdles. *Front. Cell. Infect. Microbiol.* 8:376. doi: 10.3389/fcimb.2018.00376

Galiez, C., Siebert, M., Enault, F., Vincent, J., and Soding, J. (2017). WIsH: who is the host? Predicting prokaryotic hosts from metagenomic phage contigs. *Bioinformatics* 33, 3113–3114. doi: 10.1093/bioinformatics/btx383

Gordillo Altamirano, F. L., and Barr, J. J. (2019). Phage therapy in the Postantibiotic era. *Clin. Microbiol. Rev.* 32:e00066. doi: 10.1128/CMR.00066-18

Gorski, A., Miedzybrodzki, R., Lobocka, M., Glowacka-Rutkowska, A., Bednarek, A., Borysowski, J., et al. (2018). Phage therapy: what have we learned? *Viruses* 10:288. doi: 10.3390/v10060288

Gorski, A., Miedzybrodzki, R., Wegrzyn, G., Jonczyk-Matysiak, E., Borysowski, J., and Weber-Dabrowska, B. (2020). Phage therapy: current status and perspectives. *Med. Res. Rev.* 40, 459–463. doi: 10.1002/med.21593

Grainha, T., Magalhaes, A. P., Melo, L. D. R., and Pereira, M. O. (2020). Pitfalls associated with discriminating mixed-species biofilms by flow cytometry. *Antibiotics (Basel)* 9:741. doi: 10.3390/antibiotics9110741

Kortright, K. E., Chan, B. K., Koff, J. L., and Turner, P. E. (2019). Phage therapy: a renewed approach to combat antibiotic-resistant bacteria. *Cell Host Microbe* 25, 219–232. doi: 10.1016/j.chom.2019.01.014

Lee, D., Im, J., Na, H., Ryu, S., Yun, C. H., and Han, S. H. (2019). The novel enterococcus phage vB_EfaS_HEf13 has broad lytic activity against clinical isolates of enterococcus faecalis. *Front. Microbiol.* 10:2877. doi: 10.3389/fmicb.2019.02877

Leskinen, K., Blasdel, B. G., Lavigne, R., and Skurnik, M. (2016). RNA-sequencing reveals the progression of phage-host interactions between phiR1-37 and Yersinia enterocolitica. *Viruses* 8:111. doi: 10.3390/v8040111

Li, M., Wang, Y., Li, F., Zhao, Y., Liu, M., Zhang, S., et al. (2021). A deep learning-based method for identification of bacteriophage-host interaction. *IEEE/ACM Trans. Comput. Biol. Bioinform.* 18, 1801–1810. doi: 10.1109/TCBB.2020.3017386

Lin, D. M., Koskella, B., and Lin, H. C. (2017). Phage therapy: an alternative to antibiotics in the age of multi-drug resistance. *World J. Gastrointest. Pharmacol. Ther.* 8, 162–173. doi: 10.4292/wjgpt.v8.i3.162

Lu, C., Zhang, Z., Cai, Z., Zhu, Z., Qiu, Y., Wu, A., et al. (2021). Prokaryotic virus host predictor: a Gaussian model for host prediction of prokaryotic viruses in metagenomics. *BMC Biol.* 19:5. doi: 10.1186/s12915-020-00938-6

Magiorakos, A. P., Srinivasan, A., Carey, R. B., Carmeli, Y., Falagas, M. E., Giske, C. G., et al. (2012). Multidrug-resistant, extensively drug-resistant and pandrug-resistant bacteria: an international expert proposal for interim standard definitions for acquired resistance. *Clin. Microbiol. Infect.* 18, 268–281. doi: 10.1111/j.1469-0691.2011.03570.x

Manohar, P., Nachimuthu, R., and Lopes, B. S. (2018). The therapeutic potential of bacteriophages targeting gram-negative bacteria using galleria mellonella infection model. *BMC Microbiol.* 18:97. doi: 10.1186/s12866-018-1234-4

Mcginnis, S., and Madden, T. L. (2004). BLAST: at the core of a powerful and diverse set of sequence analysis tools. *Nucleic Acids Res.* 32, W20–W25. doi: 10.1093/nar/gkh435

Mulani, M. S., Kamble, E. E., Kumkar, S. N., Tawre, M. S., and Pardesi, K. R. (2019). Emerging strategies to combat ESKAPE pathogens in the era of antimicrobial resistance: a review. *Front. Microbiol.* 10:539. doi: 10.3389/fmicb.2019.00539

Pedregosa, F., Varoquaux, G., Gramfort, A., Michel, V., Thirion, B., Grisel, O., et al. (2012). Scikit-learn: machine learning in python. *J. Mach. Learn. Res.* 12, 2825–2830.

Reinert, G., Chew, D., Sun, F., and Waterman, M. S. (2009). Alignment-free sequence comparison (I): statistics and power. *J. Comput. Biol.* 16, 1615–1634. doi: 10.1089/cmb.2009.0198

Roucourt, B., and Lavigne, R. (2009). The role of interactions between phage and bacterial proteins within the infected cell: a diverse and puzzling interactome. *Environ. Microbiol.* 11, 2789–2805. doi: 10.1111/j.1462-2920.2009.02029.x

Roux, S., Enault, F., Hurwitz, B. L., and Sullivan, M. B. (2015). VirSorter: mining viral signal from microbial genomic data. *PeerJ* 3:e985. doi: 10.7717/peerj.985

Santajit, S., and Indrawattana, N. (2016). Mechanisms of antimicrobial resistance in ESKAPE pathogens. *Biomed. Res. Int.* 2016, 1–8. doi: 10.1155/2016/2475067

Sulakvelidze, A., Alavidze, Z., and Morris, J. G. Jr. (2001). Bacteriophage therapy. *Antimicrob. Agents Chemother.* 45, 649–659. doi: 10.1128/AAC.45.3.649-659.2001

Tadmor, A. D., Ottesen, E. A., Leadbetter, J. R., and Phillips, R. (2011). Probing individual environmental bacteria for viruses by using microfluidic digital PCR. *Science* 333, 58–62. doi: 10.1126/science.1200758

Topka-Bielecka, G., Nejman-Falenczyk, B., Bloch, S., Dydecka, A., Necel, A., Wegrzyn, A., et al. (2021). Phage-bacteria interactions in potential applications of bacteriophage vB_EfaS-271 against *Enterococcus faecalis*. *Viruses* 13:318. doi: 10.3390/v13020318

Ventola, C. L. (2015). The antibiotic resistance crisis: part 1: causes and threats. *P T* 40, 277–283. PMID: 25859123

Wang, W., Ren, J., Tang, K., Dart, E., Ignacio-Espinoza, J. C., Fuhrman, J. A., et al. (2020). A network-based integrated framework for predicting virus-prokaryote interactions. *NAR Genom. Bioinform.* 2:lqaa044. doi: 10.1093/nargab/lqaa044

Yang, H., Ma, Y., Wang, Y., Yang, H., Shen, W., and Chen, X. (2014). Transcription regulation mechanisms of bacteriophages: recent advances and future prospects. *Bioengineered* 5, 300–304. doi: 10.4161/bioe.32110

Zhang, R., Mirdita, M., Levy Karin, E., Norroy, C., Galiez, C., and Soding, J. (2021). SpacePHARER: sensitive identification of phages from CRISPR spacers in prokaryotic hosts. *Bioinformatics* 37, 3364–3366. doi: 10.1093/bioinformatics/btab222

Zielezinski, A., Barylski, J., and Karlowski, W. M. (2021). Taxonomy-aware, sequence similarity ranking reliably predicts phage-host relationships. *BMC Biol.* 19:223. doi: 10.1186/s12915-021-01146-6

frontiers | Frontiers in Microbiology

TYPE Original Research
PUBLISHED 25 May 2023
DOI 10.3389/fmicb.2023.1197085

OPEN ACCESS

EDITED BY
Alicja Wegrzyn,
Polish Academy of Sciences, Poland

REVIEWED BY
Karishma Bisht,
Princeton University, United States
Jordi Gómez,
Spanish National Research Council (CSIC), Spain

*CORRESPONDENCE
Ester Lázaro
✉ lazarole@cab.inta-csic.es

RECEIVED 30 March 2023
ACCEPTED 12 May 2023
PUBLISHED 25 May 2023

CITATION
Laguna-Castro M, Rodríguez-Moreno A, Llorente E and Lázaro E (2023) The balance between fitness advantages and costs drives adaptation of bacteriophage Qβ to changes in host density at different temperatures. *Front. Microbiol.* 14:1197085. doi: 10.3389/fmicb.2023.1197085

The balance between fitness advantages and costs drives adaptation of bacteriophage Qβ to changes in host density at different temperatures

Mara Laguna-Castro, Alicia Rodríguez-Moreno, Elena Llorente and Ester Lázaro*

Centro de Astrobiología (CAB), CSIC-INTA, Torrejón de Ardoz, Spain

Introduction: Host density is one of the main factors affecting the infective capacity of viruses. When host density is low, it is more difficult for the virus to find a susceptible cell, which increases its probability of being damaged by the physicochemical agents of the environment. Nevertheless, viruses can adapt to variations in host density through different strategies that depend on the particular characteristics of the life cycle of each virus. In a previous work, using the bacteriophage Qβ as an experimental model, we found that when bacterial density was lower than optimal the virus increased its capacity to penetrate into the bacteria through a mutation in the minor capsid protein (A1) that is not described to interact with the cell receptor.

Results: Here we show that the adaptive pathway followed by Qβ in the face of similar variations in host density depends on environmental temperature. When the value for this parameter is lower than optimal (30°C), the mutation selected is the same as at the optimal temperature (37°C). However, when temperature increases to 43°C, the mutation selected is located in a different protein (A2), which is involved both in the interaction with the cell receptor and in the process of viral progeny release. The new mutation increases the entry of the phage into the bacteria at the three temperatures assayed. However, it also considerably increases the latent period at 30 and 37°C, which is probably the reason why it is not selected at these temperatures.

Conclusion: The conclusion is that the adaptive strategies followed by bacteriophage Qβ, and probably other viruses, in the face of variations in host density depend not only on their advantages at this selective pressure, but also on the fitness costs that particular mutations may present in function of the rest of environmental parameters that influence viral replication and stability.

KEYWORDS

bacteriophage Qβ, host density, experimental evolution, fitness cost, adaptation, molecular evolution, temperature

1. Introduction

The infection cycle of any virus can be divided into two phases, an intracellular one, corresponding to the period of replication inside the cell, and an extracellular one, comprising the time between infections. In the extracellular phase, viruses behave as inert entities –the virions– that are exposed to the physicochemical conditions of the environment, which can damage the virus particles and compromise the ability to initiate new infections. The time that a virus remains in the extracellular environment is strongly conditioned by virus and host concentration. Due to mass action kinetics, host concentration is the most relevant factor influencing the number of infections that can be initiated from a viral population of a given size (Shao and Wang, 2008). Viruses can select strategies to adapt to low host availability, which usually involve modification of some of the parameters that define their infection cycle. In the case of lytic bacteriophages, these parameters are adsorption rate, duration of the latent period, burst size, and stability in the external medium (Hyman and Abedon, 2009; Bull and Gill, 2014; Dennehy and Abedon, 2020a,b). The adsorption rate is the ability of a phage to interact with the cell receptor in order to introduce its genome into the bacterium. The latent period is the time that elapses from the time a phage genome enters the cell until a viral progeny is released. The burst size is the number of phages produced per infected bacterium. Finally, stability in the extracellular medium is other relevant factor influencing the time that a virion remains infective. The optimal combination of values for all these parameters is not fixed, but depends on the environmental conditions to which each particular phage population is exposed (Woody and Cliver, 1995; Chantranupong and Heineman, 2012; Inomata et al., 2012; Yin and Redovich, 2018).

Sometimes, improving one of the parameters described above implies worsening others, that is, it has a fitness cost (Shao and Wang, 2008; Chantranupong and Heineman, 2012; Goldhill and Turner, 2014). An example is the increase in extracellular stability, which is sometimes associated with a decrease in the ability to infect (Elena, 2001; De Paepe and Taddei, 2006; Wasik et al., 2015). Other times, a parameter can only be optimized within a range of values that, when exceeded above or below, has negative consequences. For instance, increasing the adsorption rate may be favorable when there are few bacteria available, but, if these are very scarce, they could be exhausted very quickly, resulting in an infective process of very short duration. Increasing the latent period causes infections to progress more slowly, allowing a fraction of bacteria to continue to reproduce so that they can be infected in subsequent cycles (Abedon et al., 2001, 2003). This strategy has an extra value when conditions in the external environment are very hostile and, therefore, phages would spend less time exposed to them. However, if the latent period is too long, the number of infection rounds in a given period of time will also be lower (Heineman and Bull, 2007), which can reduce the final virus yield. Even it might happen that, when the viral progeny is released, bacteria have reached a state in which they are less susceptible to infection (Abedon, 2016). Finally, variations in burst size are not easy to interpret. Although, in principle, increases in this parameter might seem positive, they usually occur at the cost of increasing the latent period (Abedon et al., 2003), which, as we have indicated, is not always favorable. Habitat structure can also modulate the effect of the increase of the burst size (Dennehy et al., 2007). The conclusion is that the adaptive strategy that a population of bacteriophages will follow when bacteria availability is limited is not easy to predict and will depend on the whole combination of conditions of the extracellular and intracellular environment.

In order to study the changes in the infective cycle of phages in response to host density variation, we used bacteriophage Qβ as an experimental model. Qβ is a lytic phage that infects the bacterium *Escherichia coli* using as receptor the conjugative F pilus. It is a member of the *Leviviridae* family (genus Allolevivirus) (Olsthoorn and Van Duin, 2011). It has a single-stranded, positive-sense RNA genome of 4217 nucleotides that encodes four proteins: A2 or maturation protein, which is present in a single copy and mediates phage binding to the bacterial pili, penetration of the viral genome, and cell lysis; coat protein, which is the major capsid protein; A1 or the minor capsid protein, which is produced occasionally when the stop codon of the capsid protein is read as tryptophan; and the replicase that copies the RNA genome. The precise function of the A1 protein is currently unknown, although it is essential for infection to occur (Hofstetter et al., 1974). It consists of the full-length coat protein connected by a flexible linker to an extension of 196 amino acids at the C-terminal end (Rumnieks and Tars, 2011) that is located on the exterior of the capsid (Vasiljeva et al., 1998). Around 10 copies of A1 are present in the capsid, replacing monomers of the coat protein. Regarding the entry mechanism of Qβ in its host, studies carried out with the related phage MS2, which also infects *E. coli* through the pilus, indicate that, after binding of the phages, continued pilus retraction brings them close to cell surface, where the complex formed by the Mat protein (which interacts with the pilus in MS2) and the virus genomic RNA penetrates inside the central channel that traverse the plasma membrane at the basis of the pilus and is driven into the host cytosol (Dent et al., 2013; Meng et al., 2019). Due to the similarities between MS2 and Qβ (Gorzelnik and Zhang, 2021), a similar mechanism probably is also working in the latter. During the process, a torsional stress is produced that causes the detachment of the pilus and its release to the environment, which has been demonstrated for both phages (Harb et al., 2020).

In a previous work, we studied the adaptation of bacteriophage Qβ to replicate in the presence of different bacterial densities at the optimal replication temperature for the virus (37°C) (Laguna-Castro and Lázaro, 2022). A fraction of the progeny produced after a 2-h incubation was used to initiate a new infection using fresh bacteria at the same concentration as in the previous culture, a process that was repeated for 16 serial transfers. This experimental design prevents evolution of bacteria and permits a reset at each transfer of the selective pressure that we are studying (the bacterial density in this case). The results we obtained showed that in all populations that had evolved at a bacterial density below a given value, a mutation was selected (C2011A), which produces the amino acid change T222N in the A1 protein. The main effect of the mutation was to increase the entry of the virus into the bacterium. The latent period and the stability of the phage in the extracellular medium were not affected, but there did seem to be a decrease in the burst size. These findings suggest that A1 protein could contribute to the initial binding of Qβ to the F-pilus, increasing in this way phage-bacteria interaction.

In the experiments presented in this work, we have studied the effect of varying cell density at the same time that another essential parameter for virus replication, temperature, is also modified. Temperature largely influences the tertiary structure of

proteins. Therefore, it is to be expected that all processes involving interaction between molecules and structures (for instance between phage and bacteria components) or enzymatic catalysis are affected by variations in this parameter. The impact of temperature changes on Qβ replication and evolution has been previously studied in depth in our laboratory, although always at the same bacterial density that we use as a standard. While the decrease in temperature (from 37 to 30°C) does not strongly decrease viral titers, the increase (from 37 to 43°C) produces drastic reductions in the virus yield (Arribas et al., 2014). Nevertheless, the phage is able to adapt to the latter condition through mutations in all its genes (Arribas et al., 2014, 2016; Kashiwagi et al., 2014; Lázaro et al., 2018; Somovilla et al., 2019, 2022; Arribas and Lázaro, 2021). We thought that our experience in Qβ adaptation to 30 and 43°C might be very useful in differentiating the mutations that are selected in response to each of the two main selective pressures that are acting in these new experiments (change in temperature and host density). Therefore, we chose 30 and 43°C to study whether adaptation of Qβ to variations in host density was temperature-dependent.

The new results we have obtained show that, when bacteria availability is reduced, bacteriophage Qβ selects a common adaptive strategy both at 30 and 43°C, which is based in the improvement of its entry into bacteria. However, while at 30°C adaptation is achieved through the same mutation in the A1 protein that was selected at 37°C, at 43°C it does so through a different mutation located in the A2 protein (V256A), which has strong fitness costs at lower temperatures. It appears, therefore, that adaptation of bacteriophage Qβ to low host availability involves different mutational pathways depending on the balance between fitness advantages and costs at each replication temperature.

2. Materials and methods

2.1. Viruses and bacteria. Standard procedures for infection

The plasmid pBRT7Qβ, which contains a cDNA of bacteriophage Qβ cloned in the plasmid pBR322 (Taniguchi et al., 1978; Barrera et al., 1993), was used to transform *Escherichia coli* DH5-α, a strain that permits virus expression, although it cannot be infected because it lacks the virus receptor. The supernatant of an overnight culture, obtained from a transformed colony, was used to infect *E. coli*, strain Hfr (Hayes, 1953), in semisolid agar. The virus progeny contained in a randomly chosen lysis plaque was isolated, and 10^6 plaque forming units (pfu) were used to infect an *E. coli* Hfr culture under standard conditions (37°C, 250 rpm) for 2 h. The supernatant of this culture was used as the ancestor of all the evolutionary lineages analyzed in this work. It was denoted $Q\beta_{Anc}$ and its consensus sequence showed no mutations relative to the Qβ cDNA cloned in pBR322. The virus $Q\beta_{Anc}$ is the same described in our previous work concerning Qβ adaptation to low host density (Laguna-Castro and Lázaro, 2022).

Qβ was propagated in *E. coli* Hfr in NB medium (8 g/l Nutrient Broth from Merck and 5 g/l NaCl). Infections in liquid medium were carried out using fresh log-phase *E. coli* cultures with an OD_{600} of 0.8 that were infected with the amount of pfu indicated in each experiment. Cultures were incubated at the indicated temperature for 2 h with good aeration (250 rpm). To estimate the total virus yield, cultures were treated either with chloroform (1/20 v/v, 28°C, 15 min, shaking 850 rpm in thermoblock) or with egg white lysozyme (Sigma-Aldrich; 0.8 mg/ml, 37°C, 30 min, shaking 850 rpm in thermoblock). Virus supernatants were harvested upon centrifugation at 13000 × *g* and maintained at 4°C for short-term use (less than 15 days) or at −80°C for long-term storage. Virus titers were determined by plaque assay and expressed as the number of pfu per ml of the phage suspension.

2.2. Evolution experiment

The virus $Q\beta_{Anc}$ was used to initiate 8 replicate evolutionary lineages differing in the bacterial density (**Figure 1**). Propagation took place for 16 serial transfers (or until the virus was extinguished) either at 30 or 43°C. At each transfer, bacteria were freshly prepared by growing *E. coli* at 37°C until an OD_{600} of 0.8, which according our estimations corresponds to 6×10^8 colony forming units (cfu) per ml.[1] The culture was serially diluted in NB medium (10^{-1}, 10^{-2}, and 10^{-3} dilutions), and 0.5 ml of either the undiluted culture or the corresponding dilution were placed in 10 ml tubes containing 400 μL of NB. Infections were initiated with 10^7 pfu in 100 μL of phage buffer (25 mM Tris–HCl pH 7.5, 5 mM $MgCl_2$, 0.5 g/l gelatin). After 2 h of incubation under standard conditions either at 30 or 43°C, the virus supernatants were collected upon treatment with chloroform, and a fraction of the phage suspension (10^7 pfu or, when the titers did not allow it, the amount of phage contained in 100 μL of the previous supernatant) was used to infect fresh *E. coli* cultures prepared as described above. Evolutionary lineages were denoted $Q\beta\ (3 \times 10^8)_{30°C}$, $Q\beta\ (3 \times 10^8)_{43°C}$, $Q\beta\ (3 \times 10^7)_{30°C}$, $Q\beta\ (3 \times 10^7)_{43°C}$, $Q\beta\ (3 \times 10^6)_{30°C}$, and $Q\beta\ (3 \times 10^6)_{43°C}$ to indicate the bacterial density (in brackets) and the temperature used in the experiment. Lineages propagated at the bacterial density of 3×10^5 cfu/ml were extinguished before transfer 16 and were not used for further experiments. When necessary, the numbers 1 and 2 were used to distinguish the two replicas performed for each condition.

A negative control in which undiluted bacteria were incubated in culture medium in the absence of virus was set at each transfer. This control was processed and plated exactly the same as the experimental samples. When lysis plaques appeared, the corresponding transfer was discarded and repeated again.

Additional evolution experiments using a similar protocol to that described above were performed with single mutant viruses containing mutation U830C (virus $Q\beta_{U830C}$), and C2011A (virus $Q\beta_{C2011A}$). The replication temperatures and the bacterial densities used are indicated in the text and in the legend of the corresponding figures.

2.3. Determination of the virus replicative ability

The virus yield obtained in replication assays carried out in liquid medium was used as a measure of the virus replicative ability. Triplicate liquid cultures containing the indicated bacterial density

1 https://www.agilent.com/store/biocalculators/calcODBacterial.jsp

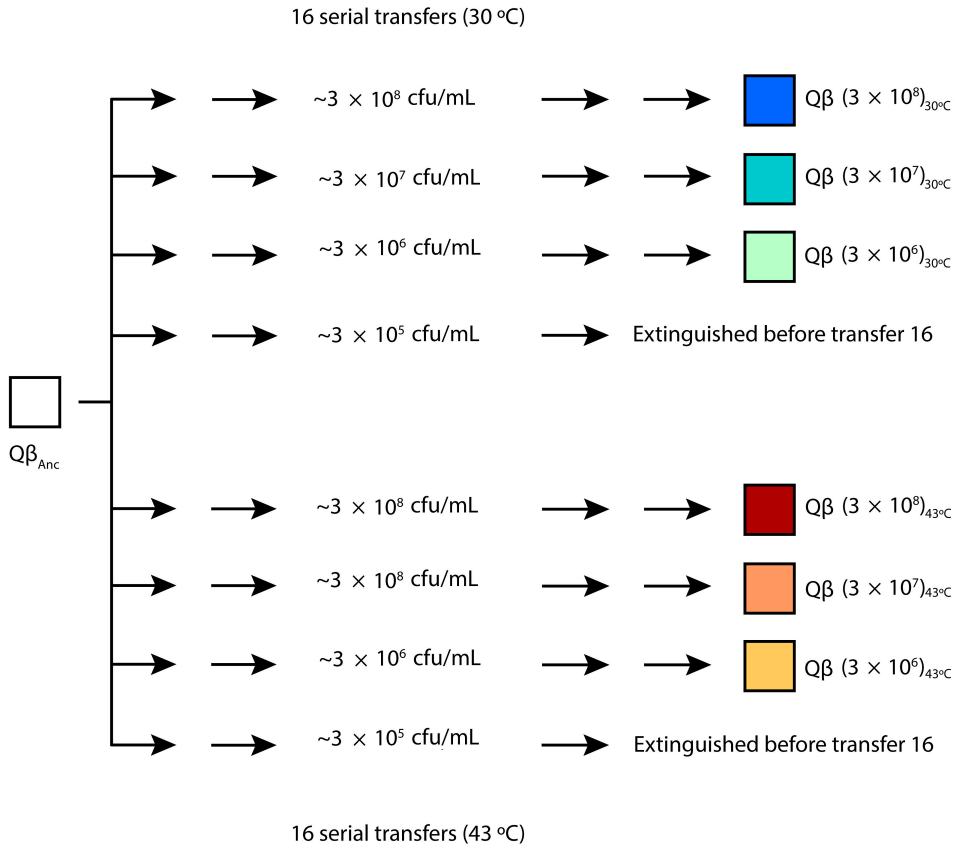

FIGURE 1
Evolution experiment. The virus $Q\beta_{Anc}$ (see section "2.1. Viruses and bacteria. Standard procedures for infection") was propagated for 16 serial transfers (or until the virus was extinguished), carried out at different bacteria densities either at 30 or 43°C. Evolutionary lineages obtained at transfer number 16 were denoted $Q\beta\ (3 \times 10^8)_{30°C}$, $Q\beta\ (3 \times 10^8)_{43°C}$, $Q\beta\ (3 \times 10^7)_{30°C}$, $Q\beta\ (3 \times 10^7)_{43°C}$, $Q\beta\ (3 \times 10^6)_{30°C}$, and $Q\beta\ (3 \times 10^6)_{43°C}$ to indicate the bacterial density (expressed in cfu/ml and shown in brackets) and the temperature used at each transfer. Lineages propagated at the bacterial density of 3×10^5 cfu/ml were extinguished before transfer 16. Two replicas were performed for each condition. When necessary, the numbers 1 and 2 were used to distinguish them. For additional details, see the section "2.2. Evolution experiment".

were inoculated with 10^4 pfu of the virus population assayed, in a final volume of 1 ml. We used this amount of virus to ensure that the replicative capacity of the system was not saturated. After 2 h of incubation at either 30, 37, or 43°C, the total virus produced was estimated through treatment with 0.8 mg/ml of egg white lysozyme (Sigma-Aldrich) for 30 min at 37°C with shaking (850 rpm in thermoblock). Lysozyme was used instead of chloroform because of its higher efficiency to lysate cells, demonstrated in several lysis assays carried out in our lab (data not shown).

2.4. Site-directed mutagenesis

The plasmid pBRT7Qβ was used to engineer two single-mutant viruses containing either mutation U830C (virus $Q\beta_{U830C}$) or C2011A (virus $Q\beta_{C2011A}$). Mutagenesis was carried out using the QuickChange Lightning Site-Directed Mutagenesis Kit (Agilent Technologies) with the primers 5′GACAATCTGTACCCTGCCGCTGCTTACTTTAAACTGAAA3′ (for $Q\beta_{U830C}$) and 5′TGGGATTCTCGGCTTAGTTATAACACGT TCCGCGG3′ (for $Q\beta_{C2011A}$), together with their respective complementary containing the mutations to introduce in the virus genome. The procedures to build and isolate the site-directed mutants were the same as previously described for other Qβ mutants (Arribas et al., 2018). A lytic plaque generated in *E. coli* Hfr by each of the mutants was picked and sequenced to test the presence of the desired mutation and the absence of any other that might have arisen during the mutagenesis process.

2.5. Plaque size assays

Areas of the lysis plaques formed by the viruses $Q\beta_{Anc}$ and the mutants $Q\beta_{U830C}$ and $Q\beta_{C2011A}$ were quantified in the following way. Around 100 pfu of each virus were mixed with $\sim 3 \times 10^8$ bacteria and 3 ml of semisolid agar, and plated in agar plaques that had been prepared using 30 ml of the same preparation of LB-agar (Invitrogen). Plaques were incubated overnight at 37°C. Images of the Petri dishes were taken with ChemiDoc MP Imaging System (Bio-Rad) using a white sample tray and "Coomasie Blue" mode. Images were analyzed with Image Lab Software (Bio-Rad) (RRID:SCR_014210), using the tool "Volume Tool-Round" to manually select 70 lysis plaques of each virus whose areas were calculated. We used the Mann-Whitney test to assess the statistical significance of the differences between different sets of data.

2.6. Determination of virus entry into bacteria

Independent triplicate liquid 1 ml cultures, containing bacteria (3×10^8 cfu/ml) and 10^5 pfu of the indicated virus, were incubated at either 30, 37, or 43°C with low shaking (75 rpm) for 0, 5, 10, 15, and 20 min. At each time, 100 μL of EDTA 100 mM were added to stop virus entry. A control experiment showed that incubation of Qβ with this EDTA concentration completely inhibited its entry into *E. coli*, which agrees with previous results obtained for other phages (Paranchych, 1966). Cultures were centrifuged at 13000 × *g* at 4°C and the supernatant was discarded. The pellet was washed once with 500 μL of cold phage buffer containing EDTA 10 mM and re-suspended in phage buffer without EDTA. The number of infectious centers was estimated by plaque assay. Parallel cultures that were incubated at 4°C in the presence of EDTA 10 mM were used to estimate the virus background. The experimental points were fitted to a model of the form:

$$P = P_0 - P_0 e^{-cNt}$$

where P is the number of infectious centers, P_0 is the number of pfu used in the experiment (10^5 pfu), N is the number of bacteria in the sample (3×10^8 cfu), and t is the incubation time. We defined the parameter k (expressed in ml/min/cell), corresponding to c/N, as the constant of formation of infectious centers at the bacteria density assayed. Fittings were performed using the function NonLinearFit of Mathematica 9.0 (Wolfram Research). Viruses whose k-values were compared were always assayed in the same experiment, using the same cell preparation. Differences were considered statistically significant when the value obtained for a particular virus was outside the confidence interval of the one to which it was compared.

Additional experiments were performed in the same way but with a fixed incubation time (10 min) and using different bacterial concentration (indicated in the corresponding figure). The statistical significance of the differences between the number of infectious centers obtained in different sets of data was assayed by means of the Student's t-test.

2.7. One step growth curves

Duplicate 1 ml liquid cultures containing 3×10^8 bacteria and 10^6 pfu of the viruses $Q\beta_{Anc}$, $Q\beta_{U830C}$, or $Q\beta_{C2011A}$ were incubated for 5 min (curves performed at 30 and 37°C) or 10 min (curves performed at 43°C) in NB medium and 75 rpm. The reason for incubating longer at 43°C was to allow the entry of a greater amount of virus to mitigate the low replication yield at this temperature. In all cases, virus entry was stopped by a 10000-fold dilution of the cultures. Diluted cultures were incubated at the temperature assayed in a static bath, and only mixed by inversion right before taking the samples, to avoid additional encounters between cells and viruses. At different times, 250 μL aliquots were removed and centrifuged to obtain the virus supernatants that were titrated. The duration of the latent period was calculated as the intercept between the regression line of the natural logarithm of the virus titers vs. time during the exponential rise period and the regression line for the points corresponding to the pre-rise period.

2.8. Burst size determination

Triplicate 1 ml liquid cultures containing 3×10^8 bacteria and 10^6 pfu of the virus indicated were incubated for 10 min at either 30, 37, or 43°C in NB medium and 75 rpm to allow virus entry into bacteria. After this time, a 0.3 ml aliquot was removed to determine the number of infectious centers as described above (see section "2.6. Determination of virus entry into bacteria"). Another 0.3 ml were diluted 100000-fold (for the assays carried out at 30 and 37°C) or 10000-fold (for the assays carried out at 43°C, which rendered lower titers), and incubated at the same temperature used for virus entry with shaking (250 rpm). The incubation times were 75, 55, and 75 min for $Q\beta_{Anc}$ and $Q\beta_{C2011A}$ at 30, 37, and 43°C, respectively, and 90, 80, and 75 min for $Q\beta_{U830C}$ at 30, 37, and 43°C, respectively. The times were chosen so that each virus would have reached the plateau as shown in the one step growth curves. After these times, the virus supernatants were collected and titrated to estimate the amount of extracellular virus. The burst size was calculated by dividing the virus titers (multiplied by the initial dilution factor) by the number of infectious centers determined in the aliquot removed after the initial 10 min allowed for virus entry.

2.9. Preservation of Qβ infectivity in cellular lysates

To study the virus interaction with cellular debris, cellular lysates were prepared by transferring 10 ml of a stationary culture of *E. coli* Hfr into a 50 ml flask. The culture was treated with 500 μL of chloroform at 25°C, 250 rpm for 20 min. To completely break the cells, the flask was vortexed at maximum speed for 5 extra minutes. Finally, lysates were centrifuged at 25°C, 12000 rpm for 10 min. A 300 μL fraction of the supernatant was plated on an NB plate to check that there were no live bacteria remaining that could allow virus replication. Triplicates containing 1 ml of lysate supernatant were incubated with 3×10^5 pfu for 16 h at 30, 37, or 43°C. Controls for each temperature were prepared the same way, but using NB instead of lysate supernatant. Test samples and controls were titrated by plaque assay.

2.10. RNA extraction, cDNA synthesis, PCR amplification, and nucleotide sequencing

Viral RNA was prepared following standard procedures to determine the consensus sequence either from biological clones or from complex virus populations. RNAs were used for cDNA synthesis with the avian myeloblastosis virus reverse transcriptase (Promega), followed by PCR amplification using Expand high-fidelity DNA polymerase (Roche). The pairs of oligonucleotide primers used for RT-PCR were the following: P1 forward (5′CTTTAGGGGGTCACCTCACAC3′) with P1 reverse (5′GGATGGGTCACAAGAACCGT3′) to amplify from nucleotide position 10 to 1595, P2 forward (5′GACGT

GACATCCGGCTCAAA3′) with P2 reverse (5′CAACGGAC GGAACATCTCCT3′) to amplify from nucleotide position 1109 to 2787 and P3 forward (5′GTGCCATACCGTTTGACT3′) with P3 reverse (5′GATCCCCCTCTCACTCGT3′) to amplify from nucleotide position 2254 to 4195. PCR products were column purified (Qiagen) and subjected to standard Sanger sequencing using Big Dye Chemistry with an automated sequencer (Applied Biosystems; Perkin Elmer). Sequences were assembled and aligned with Geneious Pro v4.8.5.[2] Mutations relative to the sequence of the virus $Q\beta_{Anc}$ were identified using the same software.

2.11. Statistical analysis

All statistical analyses were performed with the program Mathematica 9.0 (Wolfram Research). When calculating the statistical significance of the differences between two series of data, the Location-Test function was used to choose the most appropriate test for the comparison, which in all cases, except for the comparison of the size of the lysis plaques produced by different viruses, was the *t*-test (Function *T*-Test).

3. Results

3.1. Adaptation of bacteriophage Qβ to low host density and suboptimal temperatures

In our previous publication (Laguna-Castro and Lázaro, 2022), we found that the optimal bacterial density for the growth of bacteriophage Qβ at 37°C under the standard conditions used in our laboratory (2 h incubation with bacteria grown to an optical density at 600 nm of 0.8) was 3×10^8 cfu/ml. To analyze the effect of temperature on phage replication as a function of the host density, the phage was propagated for 16 transfers at either 30 or 43°C. For each temperature, we tested the following concentrations of bacteria: 3×10^8, 3×10^7, 3×10^6, and 3×10^5 cfu/ml, performing two replicas for each (**Figure 1**). Since at 37°C the virus could not be maintained when bacterial density was 3×10^4 cfu/ml, in this new experiment we omitted that condition. In this way, we obtained 8 evolutionary lineages for each temperature that were designated with a nomenclature indicating the bacteria concentration used in the transfers, the replication temperature and the replica number (see section "2.2. Evolution experiment" and **Figure 1**). The growth curve of *E. coli* (not infected with Qβ) as a function of temperature is shown in **Supplementary Figure 1**. It can be seen that, while growth at 37 and 43°C is quite similar, at 30°C it is much slower.

The results obtained in the first transfer, which in all cases was initiated from the same virus sample (virus $Q\beta_{Anc}$), were used to determine whether the optimal bacterial density for Qβ replication depended on temperature. At 30°C, we observed that the curve flattened between 3×10^7 and 3×10^8 cfu/ml, and at 43°C the maximum virus titer was obtained at 3×10^7 cfu/ml (**Figure 2**). It should be noted that, since the optimal bacterial density varies with the number of viruses (Laguna-Castro and Lázaro, 2022), these results are only valid when 10^7 pfu are used in the experiment. The virus was propagated for 16 transfers at all but the lowest bacterial density (3×10^5 cfu/ml). In that case, the virus was extinguished at transfers 9 and 10 for the replicas performed at 30°C, and at transfer 7 for those performed at 43°C. As it happened during the propagation of Qβ at 37°C at lower-than-optimal bacterial densities, the evolutionary lineages (with the only exception of the two replicas propagated at 43°C at 3×10^8 cfu/ml) became progressively enriched in viruses that gave rise to lysis plaques with smaller-than-usual size. In the following sections we will analyze this character quantitatively.

We then determined whether the populations obtained at transfer 16 had increased their replicative ability with respect to the ancestor. To ensure that viral production was not saturated during the assay, this was performed with 10^4 pfu instead of 10^7 pfu (the amount used in the transfers). The results obtained (**Figure 3**) showed that all evolved populations rendered significantly higher titers than the ancestor ($p < 0.05$ for all comparisons between the ancestor and the evolved populations, *t*-test).

3.2. Determination of the consensus sequence of the adapted populations

To determine the genetic changes responsible for adaptation to the assayed conditions, we determined the consensus sequences of all evolutionary lineages obtained at transfer 16 (**Figure 4**). The most remarkable result obtained at 30°C was that all lineages selected the mutation C2011A (T222N in the A1 protein). This mutation was also selected in our previous experiment of evolution at 37°C, although in that case it only appeared in the lineages evolved at lower-than-optimal bacterial density. Other mutations that appeared as polymorphisms at 30°C and lower-than-optimal bacterial densities were C864U and U1044C (both synonymous), which were also detectable in some of the lineages evolved at 37°C (Laguna-Castro and Lázaro, 2022).

The results obtained at 43°C showed interesting differences with those observed at 30 and 37°C. First, mutation C2011A was not selected in any lineage. In contrast, in all those propagated at bacterial densities below 3×10^8 cfu/ml, mutation U830C (V256A in the A2 protein) was present. In addition, other mutations, some of which had previously been identified in other experiments of Qβ adaptation to high temperature and standard bacterial density, were also detected (Arribas et al., 2014; Somovilla et al., 2019, 2022; Arribas and Lázaro, 2021). The presence of these mutations shows that the phage is able to adapt to increased temperature as long as the bacterial density is above 3×10^5 cfu/ml. It is interesting that mutation A1088G (D342G in the A2 protein), which was always selected in our lab when Qβ was adapted to 43°C using bacterial densities around 3×10^8 cfu/ml, was not selected when the amount of available bacteria was lower.

2 https://www.geneious.com

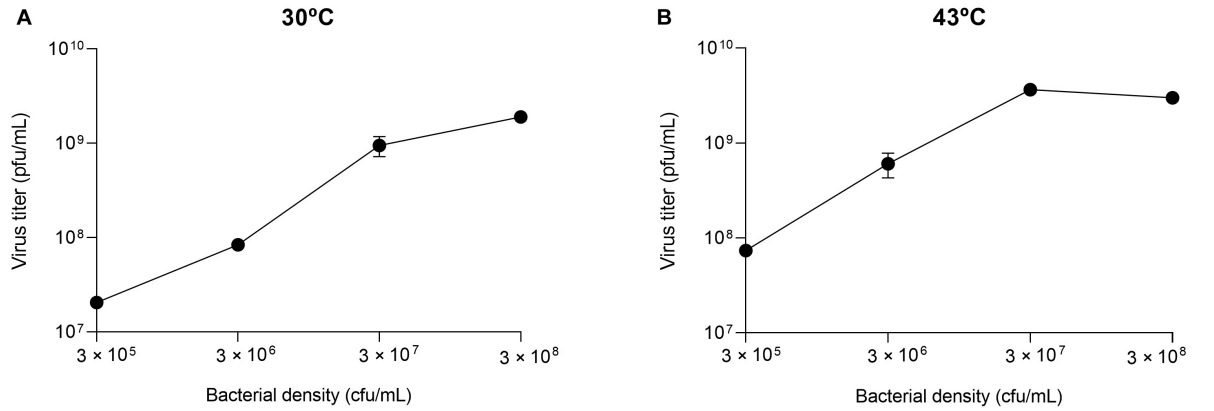

FIGURE 2
Virus titers as a function of the bacterial density. The values represented correspond to the first transfer performed in the evolution experiment (**Figure 1**). They were obtained by infecting independent cultures containing the bacterial densities indicated with 10^7 pfu of the virus $Q\beta_{Anc}$. Error bars represent the standard deviation of the two replicas of the experiment. **(A)** Replication temperature of 30°C. **(B)** Replication temperature of 43°C.

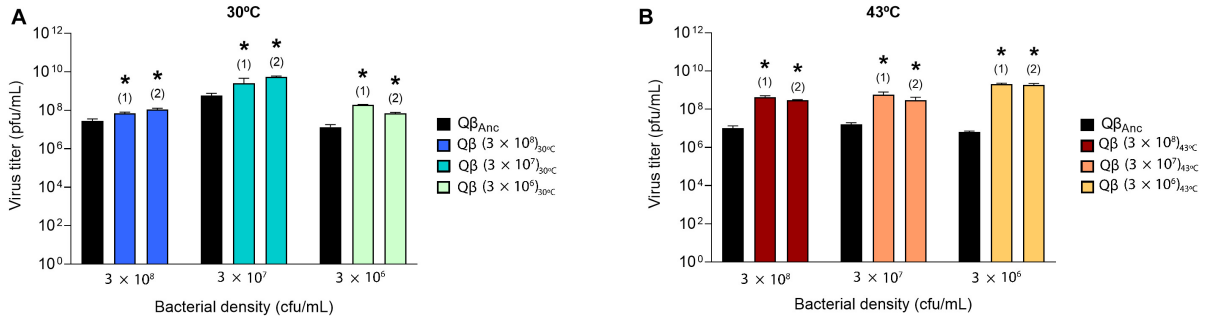

FIGURE 3
Replicative ability of the lineages obtained at transfer number 16 in the evolution experiment (**Figure 1**). The assay was performed as described in section "2.3. Determination of the virus replicative ability". Each evolutionary lineage was assayed at the same bacterial density at which it had evolved (indicated at the bottom of the figure). Each bar represents the average of three replicas. The color code used to distinguish the different lineages is the same shown in **Figure 1**. The virus $Q\beta_{Anc}$, which was assayed at all host densities, is shown in black. **(A)** Replication temperature of 30°C. **(B)** Replication temperature of 43°C. Asterisks above the bars indicate that the result is significantly different from the value obtained for the virus $Q\beta_{Anc}$ ($p < 0.05$) according to a Student's *t*-test. The raw data of the experiment can be found in **Supplementary Tables 1**, **2**.

3.3. Selective value of mutations U830C and C2011A

For a more detailed analysis of the adaptive advantages of mutations U830C and C2011A, we used the Qβ expression vector pBRT7Qβ and specific primers to obtain mutant viruses that only contained mutation U830C (virus $Q\beta_{U830C}$) or C2011A (virus $Q\beta_{C2011A}$). We determined the virus titers obtained in a replication assay carried out with the single mutants at both selective and non-selective temperatures at all the bacteria concentrations compatible with the preservation of the virus population for the 16 transfers of the evolution experiment (**Figures 5**, **6**).

The virus yields obtained at selective temperatures (43°C for $Q\beta_{U830C}$ and 30°C for $Q\beta_{C2011A}$) showed that mutation U830C only increased significantly the virus titers at 43°C at 3×10^7 cfu/ml (**Figure 5**). At other bacterial densities the mutant showed significantly lower titers than the ancestor (3×10^8 cfu/ml) or the difference was non-significant (3×10^6 cfu/ml), suggesting that the presence of this single mutation is not sufficient for the virus to adapt to both selective pressures, high temperature and low host density, simultaneously. Mutation C2011A increased the replicative ability with respect to the virus lacking the mutation at all bacteria densities assayed at 30°C.

In contrast to the results above, at non-selective temperatures (30 and 37°C for $Q\beta_{U830C}$; 43°C for $Q\beta_{C2011A}$), both mutations always rendered lower virus yields than the ancestor (**Figure 6**), suggesting that they probably have a fitness cost under those conditions. Another observation was that the lower the bacterial density assayed the lower the differences between the replicative ability of the ancestor and each of the mutants. In fact, at 43°C and 3×10^6 cfu/ml the differences between the mutant $Q\beta_{C2011A}$ and the ancestor were non-significant. The same happened with the mutant $Q\beta_{U830C}$ when it was compared with the ancestor at a bacterial density of 3×10^5 cfu/ml at 37°C. We included this condition because it was also compatible with the propagation of the virus $Q\beta_{Anc}$.

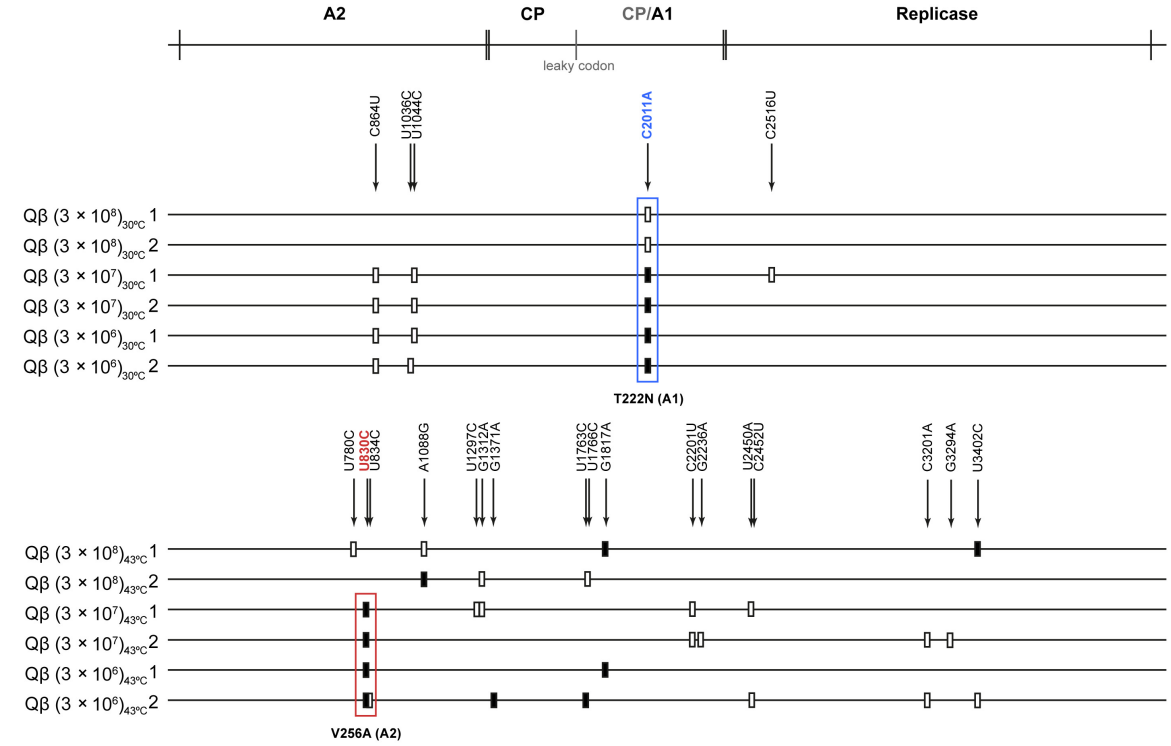

FIGURE 4
Mutations detected in the consensus sequence of the evolutionary lineages at transfer 16. The scheme above the figure represents the Qβ genome with the proteins encoded in it (CP means capsid protein and CP/A1 the additional extension present in the A1 protein). Mutations relative to the sequence of the virus $Q\beta_{Anc}$ are marked with a filled rectangle (fixed mutations) or with a blank rectangle (polymorphic mutations). The exact position of each mutation is indicated by numbers above the lines representing the genomes of populations evolved either at 30 or 43°C (indicated on the left of each line). The most frequently detected mutation during evolution at 30°C, (C2011A, T222N in the A1 protein) is marked with a blue rectangle, whereas the most common mutation during evolution at 43°C (U830C, V256A in the A2 protein) is marked with a red rectangle.

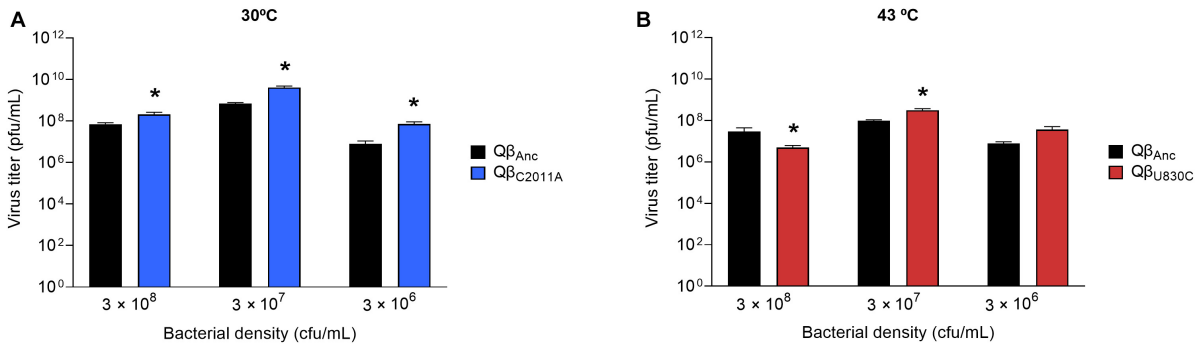

FIGURE 5
Replicative ability of the mutants $Q\beta_{U830C}$ and $Q\beta_{C2011A}$ under selective conditions. The assay was performed as described in section "2.3. Determination of the virus replicative ability". **(A)** Mutant $Q\beta_{C2011A}$ (blue bars) replicating at 30°C and different bacterial densities. **(B)** Mutant $Q\beta_{U830C}$ (red bars) replicating at 43°C and different bacterial densities. In both cases, the virus $Q\beta_{Anc}$ is shown with black bars. Each bar represents the average of three replicas. Asterisks above the bars indicate that the result obtained for the mutant is significantly different from that obtained for the virus $Q\beta_{Anc}$ ($p < 0.05$) according to a Student's *t*-test. The raw data of the experiment can be found in **Supplementary Tables 3**, **4**.

As it happened in the case of mutation C2011A, to confirm whether mutation U830C was also responsible for the smaller size of the plaques observed in most of the evolved lineages at 43°C, we determined the area of 70 lytic plaques produced by each of the viruses $Q\beta_{U830C}$ and $Q\beta_{Anc}$, using the Image Lab Software. The average size of the plaques produced by the ancestor was 3.04 ± 1.31 mm^2, which was significantly higher than that of the plaques produced by $Q\beta_{U830C}$ (0.15 ± 0.09 mm^2) ($p = 3.1 \times 10^{-25}$, Mann-Whitney test). It is remarkable that in all assays carried out to determine the replicative ability of the mutant $Q\beta_{U830C}$ (**Figures 5**, **6**) we always obtained a certain amount of normal-size plaques, which increased with the bacterial density. The only exception was the assay performed at 43°C and 3×10^6 cfu/ml that always rendered small plaques.

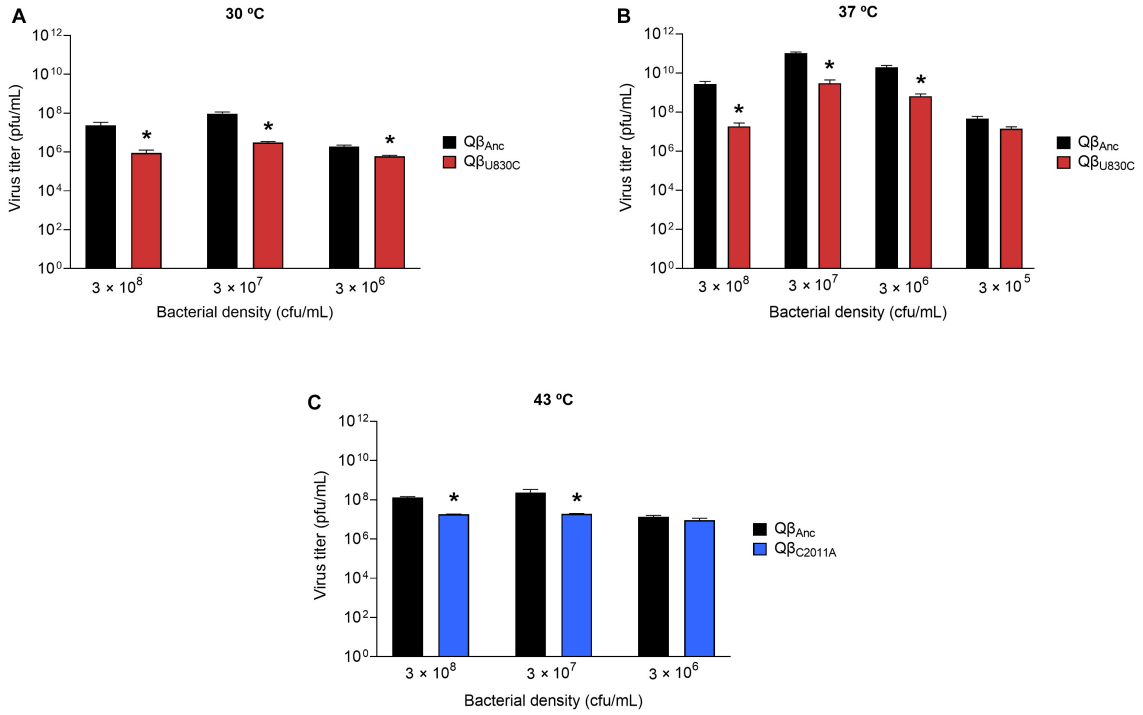

FIGURE 6
Replicative ability of the mutants $Q\beta_{C2011A}$ and $Q\beta_{U830C}$ under restrictive conditions. The assay was performed as described in section "2.3. Determination of the virus replicative ability". **(A)** Mutant $Q\beta_{U830C}$ (red bars) replicating at 30°C. **(B)** Mutant $Q\beta_{U830C}$ (red bars) replicating at 37°C. **(C)** Mutant $Q\beta_{C2011A}$ (blue bars) replicating at 43°C. In all cases, replication took place at different bacterial densities. The virus $Q\beta_{Anc}$ is always shown with black bars. Each bar represents the average of three replicas. Asterisks above the bars indicate that the result obtained for the mutant is significantly different from that obtained for the virus $Q\beta_{Anc}$ ($p < 0.05$) according to a Student's *t*-test. The raw data of the experiment can be found in **Supplementary Tables 5–7**.

In order to find out the reasons of the selective advantages of mutations U830C and C2011A, as well as their possible fitness costs under the conditions that did not promote their selection, we determined several of the parameters that define the viral infection cycle. The results obtained are detailed in the following section.

3.4. Effect of mutations U830C and C2011A on the parameters defining the Qβ infection cycle

To check the effect of mutations U830C and C2011A on the ability of Qβ to infect *E. coli*, we first performed an assay in which we determined the values of the constant of formation of infectious centers (*k*; see section "2.6. Determination of virus entry into bacteria") for the virus $Q\beta_{Anc}$ at 30, 37, and 43°C. We observed that this virus generated infectious centers more rapidly at 43°C than at 37°C, and the lowest value was obtained at 30°C (see the three first rows in **Table 1**). The results are in agreement with a greater capacity for encounters between viruses and bacteria at high temperatures. Note that *k* only indicates how rapidly bacteria are infected without distinguishing between efficiency of adsorption to the pili and efficiency of internalization of the phage genomes.

Then, we compared the value of the constants obtained for the virus $Q\beta_{Anc}$ with those corresponding to the viruses $Q\beta_{U830C}$ and $Q\beta_{C2011A}$ at 30, 37, and 43°C (**Table 1**). Each comparison between a given mutant and the ancestor was performed in the same experiment, to avoid differences due to the state of the bacteria on different days. Differences between constants were considered significant when their confidence intervals did not overlap. The main conclusion was that both mutants increased the velocity of formation of infectious centers at the three temperatures tested. The greatest effect for both mutations was observed at 30°C, which is the temperature at which the virus infected the bacteria worst. The only difference that was non-significant ($Q\beta_{Anc}$ and $Q\beta_{C2011A}$ at 37°C) was probably due to the poorer fit of the experimental points to the function used, resulting in wider confidence intervals.

We also performed a complementary assay in which the viruses $Q\beta_{Anc}$, $Q\beta_{U830C}$, and $Q\beta_{C2011A}$ were incubated for a fixed time (10 min) with different bacterial densities, after which the number of infectious centers formed was determined. The results obtained (**Supplementary Figure 2**) showed that both mutations significantly increased the formation of infectious centers at all cell densities assayed. Altogether, the results suggest that at least a part of the beneficial effect of the mutations U830C and C2011A might be due to a greater entry of Qβ into the bacteria.

Next, we performed one step growth curves to compare the latent period of the ancestor with those of the viruses $Q\beta_{U830C}$ and $Q\beta_{C2011A}$ at 30, 37, and 43°C (**Figure 7**). Curves represented in the same graphic were performed in the same assay, using the same preparation of bacteria. Since these experiments involve the handling of a large number of samples separated by a short period of time, they are subject to some error which is probably the cause of the small differences in the estimated latent period

for the ancestor in different tests. Despite these difficulties, there are some clear results. First, the shortest latent period for the ancestor was obtained at 37°C (between 25 and 30 min). At 30°C it increased to ∼ 35 min, and at 43°C it becomes considerably longer (about 60 min). While mutation C2011A did not produce any appreciable change in the duration of the latent period at any of the temperatures assayed, the same was not true for U830C, which greatly increased it at all temperatures, with the smallest effect being at 43°C. The large increase in the time required for the release of the phage progeny is possibly the reason why this mutation is not selected neither at 30°C nor at 37°C. The lower effect it has at 43°C is probably what makes it an acceptable option at this temperature. It is not clear why mutation C2011A, which does not increase the latent period at 43°C, is not selected at this temperature, especially if it is taken into account that it increases the adsorption rate similarly to U830C.

A remarkable observation is that, at 30°C, the release of progeny produced by the mutant $Q\beta_{U830C}$ took place in two phases. It is intriguing that in the first phase all the lysis plaques were of normal size, while in the second phase all of them had smaller-than-usual size. At 37°C, the same virus produced a mixture of lysis plaques of both sizes, while at 43°C, all plaques were small.

Finally, we determined the burst size produced by the ancestor and the mutant viruses $Q\beta_{U830C}$ and $Q\beta_{C2011A}$ at 30, 37, and 43°C (Table 2). The results show that both mutations produced significant decreases in this parameter, with the only exception of U830C at 43°C that caused a small increase. Given the low viral production at this temperature, it is hard to say if it has any biological significance.

TABLE 1 Values of the constant of formation of infectious centers (k) for the viruses $Q\beta_{Anc}$, $Q\beta_{U830C}$, and $Q\beta_{C2011A}$ at different temperatures.

Virus[1]	Temperature	k (ml/min/cell)[2]	p-value[3]	R^2
$Q\beta_{Anc}$*[4]	30°C	3.7×10^{-11}	0.002	0.99
$Q\beta_{Anc}$*	37°C	$1{,}4 \times 10^{-10}$	0.002	0.98
$Q\beta_{Anc}$*	43°C	3.7×10^{-10}	<0.001	0.99
$Q\beta_{Anc}$	30°C	2.7×10^{-11}	0.001	0.99
$Q\beta_{U830C}$*	30°C	2.0×10^{-10}	<0.001	0.99
$Q\beta_{Anc}$	37°C	1.2×10^{-10}	0.001	0.99
$Q\beta_{U830C}$*	37°C	2×10^{-10}	<0.001	0.99
$Q\beta_{Anc}$	43°C	4.3×10^{-10}	0.001	0.97
$Q\beta_{U830C}$*	43°C	8.3×10^{-10}	0.001	0.99
$Q\beta_{Anc}$	30°C	6.3×10^{-11}	<0.001	0.99
$Q\beta_{C2011A}$*	30°C	5.7×10^{-10}	0.002	0.98
$Q\beta_{Anc}$	37°C	1.3×10^{-10}	0.015	0.96
$Q\beta_{C2011A}$	37°C	3.3×10^{-10}	0.014	0.93
$Q\beta_{Anc}$	43°C	3.2×10^{-10}	0.002	0.97
$Q\beta_{C2011A}$*	43°C	5.3×10^{-10}	<0.001	0.98

[1]Each group of viruses separated by a gray row were tested in the same assay.
[2]k is defined in section "2.6. Determination of virus entry into bacteria".
[3]The p and R^2 values indicate the statistical significance of the fitting of the experimental points to the function indicated in section "2.6. Determination of virus entry into bacteria".
[4]The asterisk indicates whether differences between the k-values for the viruses included in the same group were statistically significant.
The criterion followed was that the k-value for a particular virus was outside the confidence interval of the others to which it was compared.

3.5. Preservation of virus infectivity in different environments

Another feature influencing virus fitness is the time that infectivity can be preserved in the extracellular environment in the period between infections. Previous assays carried out with the virus $Q\beta_{Anc}$ showed that infectivity did not decrease after 2 h of incubation in NB medium in the absence of bacteria at either 37 or 43°C. However, other observations carried out in our lab showed that prolonged incubation of Qβ with bacteria in a replication assay carried out at 43°C resulted in an initial increase in the virus titers (which lasted for about 5–6 h) followed by a sharp decline until almost the total elimination of viral infectivity at 24 h. In contrast to this, different amounts of virus incubated for 24 h in NB medium at 43°C did not show any significant decrease in their titers. The result suggests that Qβ loses infectivity faster when it is replicating in a medium with bacteria than in cell-free NB medium.

The experiment above described can be confounding because, at the same time that a fraction of the virus is losing its infectivity, another fraction is reproducing, and it is not possible to disentangle both processes. To prevent viral replication, we prepared a bacterial lysate artificially (see section "2.9. Preservation of Qβ infectivity in cellular lysates"), and incubated it with about 3×10^5 pfu of the ancestral virus or the mutants $Q\beta_{U830C}$ and $Q\beta_{C2011A}$ for 16 h at 30, 37, and 43°C, after which the virus infectivity in each sample was assayed. The results (Figure 8) showed that whereas all viruses kept most of their infectivity when incubated in NB medium, all they lost a considerable part of it when incubated with the cell lysate. The decay was temperature dependent, showing the largest effect at 43°C. The most interesting result was that the decrease at 43°C was significantly higher for the mutant $Q\beta_{C2011A}$ than for the ancestor or the mutant $Q\beta_{U830C}$. These findings could provide an explanation, which will be exposed in detail in the Discussion, to the question of why mutation C2011A is not selected at 43°C.

3.6. New evolution experiments from viruses $Q\beta_{U830C}$ and $Q\beta_{C2011A}$

To better understand the fitness advantages and costs that determine the preferential selection of particular mutations depending on temperature, we performed two new evolution experiments that were carried out in duplicate. One of them consisted in the propagation of the mutant $Q\beta_{U830C}$ at 37°C (Figure 9A), a temperature at which it causes significant decreases in the growth rate (see Figure 6). The bacterial density was high (3×10^8 cfu/ml) or low (3×10^5 cfu/ml). In both conditions, the

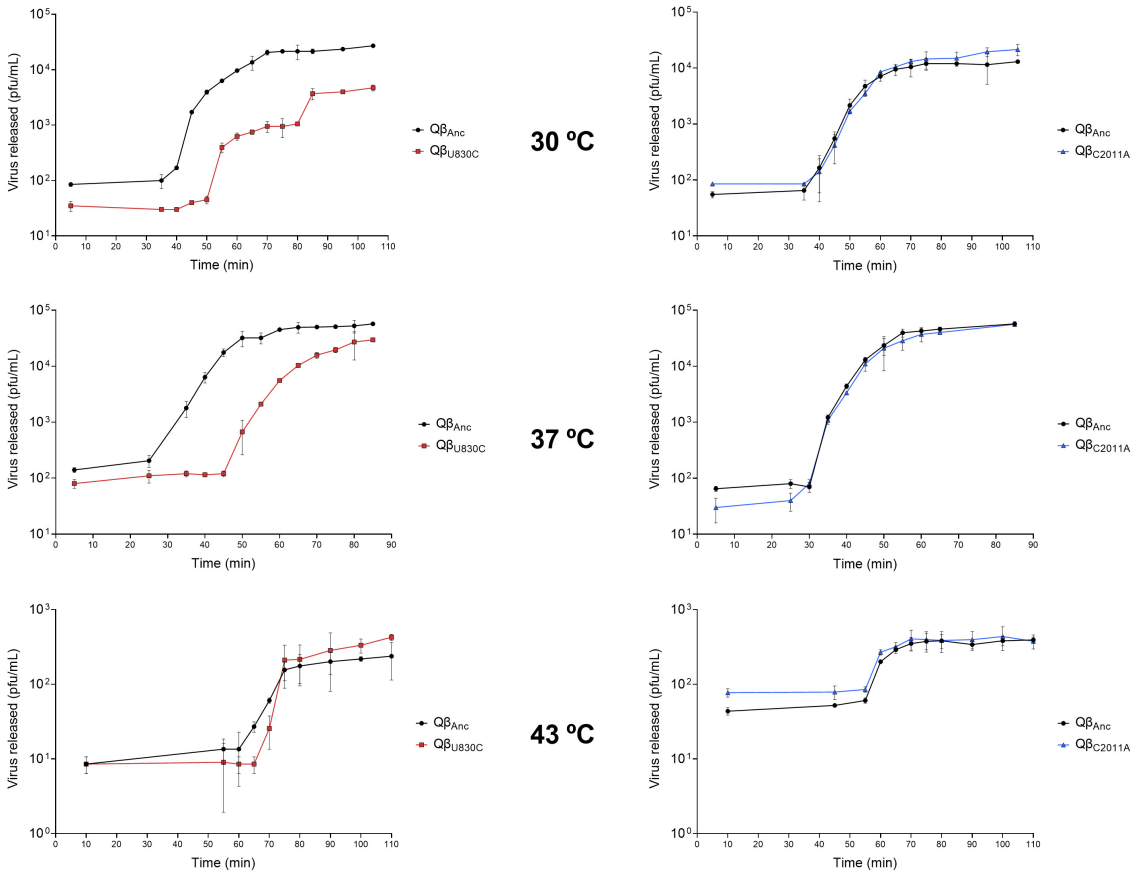

FIGURE 7
One step growth curves obtained for the viruses $Q\beta_{Anc}$, $Q\beta_{U830C}$ and $Q\beta_{C2011A}$ replicating at 30, 37, and 43°C. The details of the experiment are described in section "2.7. One step growth curves".

virus experienced an initial increase in its titers, which was greater at high bacterial density, and remained fairly constant during the rest of transfers. The consensus sequences showed the loss of mutation U830C in the two replicas carried out at high bacterial density and the permanence of the mutation when the bacterial density was low (Table 3). Surprisingly, mutation C2011A did not appear under the latter condition. The results are consistent with the non-significant fitness cost of U830C at 37°C when the bacterial density was 3×10^5 cfu/ml (Figure 6). The initial presence of this mutation seems to confer a sufficient advantage that makes selection of C2011A unnecessary.

The other evolution experiment was initiated with the mutant $Q\beta_{C2011A}$, which was propagated for 10 transfers at 43°C (a temperature at which this mutation is not selected), using a high (3×10^8 cfu/ml) or a low (3×10^6 cfu/ml) bacterial density (Figure 9B). The results showed that, at high bacterial density, the titers decreased until they reached values between 10^4 and 10^6 pfu/ml. However, propagation of the same virus at low bacterial densities produced an early increase in titers (up to approximately 10^8 pfu/ml) that remained constant with some fluctuations throughout the experiment. Determination of the consensus sequences at transfer number 10 showed that, at high bacterial density, mutation C2011A was lost in both replicas, whereas at low bacteria density, the mutation could be preserved, although it was always accompanied by U830C (see Table 3). Therefore, it seems that mutation C2011A can be maintained at 43°C, as long as the bacterial density is low and mutation U830C is selected. The permanence of mutation C2011A agrees with the non-significant fitness cost of this mutation at 43°C when the bacterial density is 3×10^6 cfu/ml (Figure 6).

4. Discussion

In a previous work, we showed that bacteriophage Qβ was able to improve its replicative capacity in the presence of lower bacterial concentrations than the one usually used in our laboratory at the optimal temperature for virus replication (37°C) (Laguna-Castro and Lázaro, 2022). In all cases, adaptation occurred through a mutation in the A1 protein that favored entry of the virus into the bacteria, while at the same time there seemed to be a decrease in burst size. This lower viral production per infected bacterium could be the reason why, when the concentration of bacteria was optimal, the mutation was not selected.

Since both virus entry into bacteria and replication to generate a progeny can be strongly affected by temperature, in this work we wanted to study the adaptive strategies employed by Qβ when the concentration of bacteria was decreased at two temperatures different from the optimum: one lower (30°C) and the other one higher (43°C). It is noteworthy that, in both cases, the curves of

viral yield as a function of bacterial density approached a plateau at about 3×10^7 cfu/ml. From this point on, the increases were low (30°C) or turned into declines (43°C) (**Figure 2**). In this regard, it is necessary to point out that, since the incubation time at each transfer allows more than one infection round, it is difficult to give a precise value for the optimal bacterial density. Depending on the duration of the infection cycle at each temperature, after 2 h there could be a different amount of viruses that have produced a progeny in new infection rounds or are in the eclipse phase, thus being undetectable in a plaque assay.

The first remarkable result we obtained in the evolution experiment was that, at both temperatures, Qβ was able to increase its replicative capacity at all bacterial densities assayed but 3×10^5 cfu/ml. Under this condition, the virus was extinguished in both replicas carried out either at 30 or 43°C, probably due to the low viral production when two selective pressures (suboptimal temperature and low host availability) are operating together. As it happened in the experiment carried out at 37°C, another observable phenotypic feature was that in all lineages evolved at 30 and 43°C [with the only exception of the two replicas of Qβ $(3 \times 10^8)_{43°C}$] as the number of transfers increased the lysis plaques became smaller than usual. There are several theoretical and experimental studies that attempt to relate the changes in the parameters defining the viral infective cycle with the size of the lysis plaques (Abedon and Culler, 2007; Shao and Wang, 2008; Abedon and Yin, 2009; Gallet et al., 2011). Although the results are not easy to interpret and do not always coincide, in some cases the increases in the adsorption rate were related to decreases in plaque size (Shao and Wang, 2008; Gallet et al., 2011).

Sequencing of the evolved populations showed another interesting result, which was that all lineages evolved at 30°C (including those propagated at the highest bacterial density: 3×10^8 cfu/ml) selected mutation C2011A in the A1 protein, similarly to Qβ evolved at 37°C and bacterial densities lower than 3×10^8 cfu/ml (Laguna-Castro and Lázaro, 2022). In contrast to this, all lineages evolved at 43°C and bacterial densities below 3×10^8 cfu/ml did not select mutation C2011A and, instead of it, presented another mutation, U830C, located in the A2 protein. This protein, which is present in a single copy (Gorzelnik et al., 2016), is considered to be the virus component that interacts with the bacterial receptor (Manchak et al., 2002; Toropova et al., 2011; Rumnieks and Tars, 2017), allowing penetration of the virus genome into the cell, as it happens in other levivirus (Kozak and Nathans, 1971; Paranchych et al., 1971; Krahn et al., 1972; Shiba and Miyake, 1975; Reynolds and Paranchych, 1976). All evolutionary lineages presented additional mutations that might represent specific adaptations to the particular temperature assayed, independently of the bacterial density. The fact that most mutations found at 43°C had previously been described in adaptation experiments carried out with Qβ at this temperature agrees with this possibility.

Experiments carried out with single mutant viruses containing either U830C or C2011A showed that both mutations increased the formation of infectious centers at 30, 37, and 43°C, suggesting that the same adaptive mechanism is operating at all temperatures assayed (see **Table 1** and **Supplementary Figure 2**). These findings raise two relevant questions. The first one is: Why is mutation C2011A selected at 30°C at a bacterial density at which it has a fitness cost at 37°C? The second question is: Why are mutations U830C and C2011A selected at different temperatures in an exclusive way?

To answer the first question, we determined the constant of formation of infectious centers for the virus $Q\beta_{Anc}$ at the three temperatures tested, finding that the lowest value was at 30°C, four times lower than at 37°C and ten times lower than at 43°C (**Table 1**). This result suggests that if the constant is low, as it happens at 30°C even when the bacterial density is high, the adaptive strategy employed by the virus is the same as that used when host availability is limited. The slower growth of *E. coli* at 30°C than at 37°C (**Supplementary Figure 1**) may also cause uninfected bacteria to reach lower densities at each transfer, so that the improvement of the interaction with the pilus through mutation C2011A may be an advantage. To investigate the second question, we estimated the replicative ability of the single mutant viruses, which allowed us to verify that mutation U830C had strong fitness costs at 30 and 37°C, while mutation C2011A had similar ones at 43°C (**Figure 6**). Determination of the latent period for both viruses suggested that the fitness cost at 30 and 37°C of mutation U830C was due to a strong increase in its duration at those temperatures (**Figure 7**). At 30°C, the release of the virus $Q\beta_{U830C}$ was biphasic, with a first phase in which all viruses produced normal-size plaques, and a second phase in which all plaques were smaller than usual. Since mutation U830C seemed to be the responsible of the generation of small-size plaques, this result, together with the heterogeneity in the size of the plaques observed in the replicative ability assays performed with the mutant $Q\beta_{U830C}$ (**Figures 5**, **6**), suggests that this mutation can be selected against even in a single replication cycle. In that case, those viruses that lost the mutation earliest would be the first to exit the cell, giving rise to the first phase of the release

TABLE 2 Burst size of viruses $Q\beta_{Anc}$, $Q\beta_{U830C}$, and $Q\beta_{C2011A}$ at different temperatures.

Virus[1]	Temperature	Burst size (pfu)
$Q\beta_{Anc}$	30°C	3530 ± 586
$Q\beta_{U830C}$*[2]	30°C	603 ± 335
$Q\beta_{Anc}$	37°C	761 ± 42
$Q\beta_{U830C}$*	37°C	591 ± 70
$Q\beta_{Anc}$	43°C	2.1 ± 0.1
$Q\beta_{U830C}$*	43°C	6.5 ± 0.6
$Q\beta_{Anc}$	30°C	3180 ± 273
$Q\beta_{C2011A}$*	30°C	948 ± 152
$Q\beta_{Anc}$	37°C	764 ± 75
$Q\beta_{C2011A}$*	37°C	411 ± 27
$Q\beta_{Anc}$	43°C	2.1 ± 0.1
$Q\beta_{C2011A}$	43°C	2.3 ± 0.5

[1]Each group of viruses separated by a gray row were tested in the same assay.
[2]The asterisk indicates that the difference in the burst size of the two viruses included in the same group is statistically significant ($p < 0.05$, Student's *t*-test).

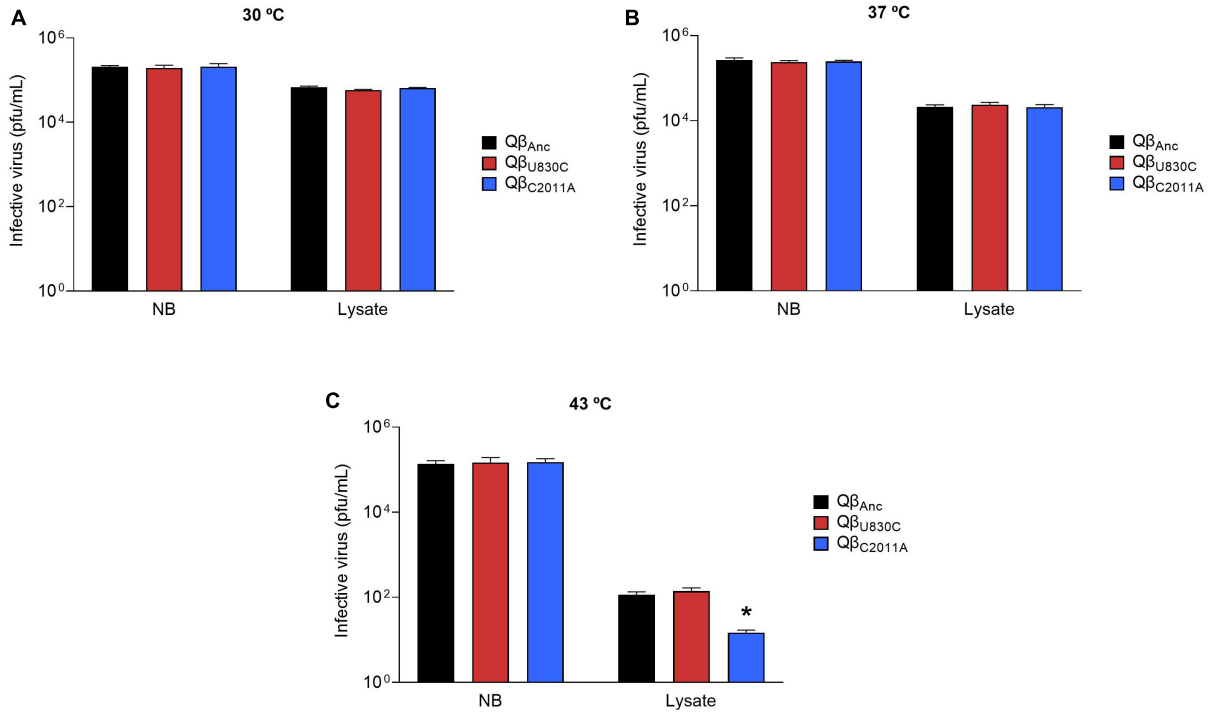

FIGURE 8
Infectivity of viruses $Q\beta_{Anc}$, $Q\beta_{U830C}$, and $Q\beta_{C2011A}$ after incubation in NB medium or a cell lysate in the absence of live bacteria. The assay was performed as described in section "2.9. Preservation of Qβ infectivity in cellular lysates". The virus $Q\beta_{Anc}$ is represented with black bars, $Q\beta_{U830C}$ with red bars and $Q\beta_{C2011A}$ with blue bars. Each bar represents the average of three replicas. **(A)** Incubation temperature of 30°C. **(B)** Incubation temperature of 37°C. **(C)** Incubation temperature of 43°C. The asterisk above the bar corresponding to the virus $Q\beta_{C2011A}$ indicates that the result obtained is significantly different from those obtained for the viruses $Q\beta_{Anc}$ and $Q\beta_{U830C}$ ($p < 0.05$) according to a Student's *t*-test. The raw data of the experiment can be found in **Supplementary Table 8**.

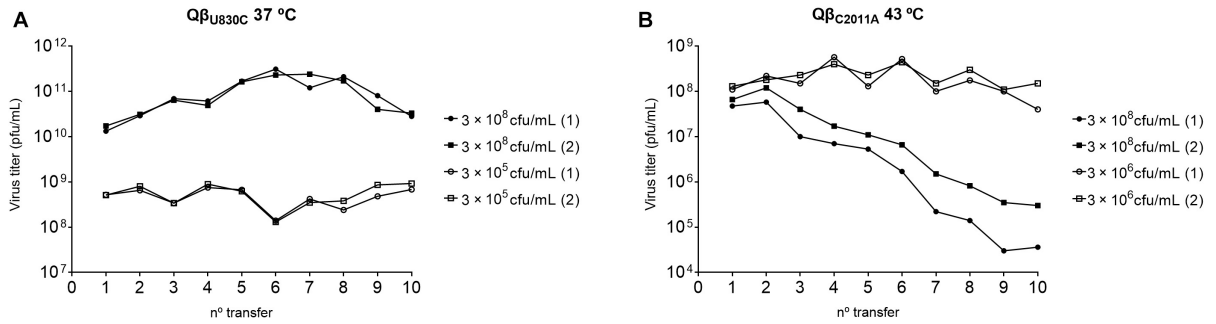

FIGURE 9
Virus titers obtained during the evolution of viruses $Q\beta_{U830C}$ and $Q\beta_{C2011A}$. **(A)** Mutant $Q\beta_{U830C}$ propagated at 37°C at the bacterial densities indicated in the margin of the figure. **(B)** Mutant $Q\beta_{C2011A}$ propagated at 43°C at the bacterial densities indicated in the margin of the figure. In all cases the experiment was initiated with 10^7 pfu. After 2 h of incubation under the conditions indicated, the virus supernatants were collected, and a fraction of the phage suspension (10^7 pfu or, when the titers did not allow it, the amount of phage contained in 100 μL of the previous supernatant) was used to initiate the following transfer and so on. There are two replicas for each condition (indicated with the numbers 1 and 2).

period at 30°C. At 37°C, however, there was a single period of viral release, in which viruses produced a mixture of small and normal-size plaques. This may be due to the fact that, as the latent period at 37°C is shorter, there is no time for a separation into two phases, similar to that observed at 30°C. At 43°C, all viruses released produced small plaques, indicating that the fitness cost of mutation U830C at this temperature and high host density is not sufficient for its selection against in a single infection cycle.

What can be the reason for the increase in the latent period produced by mutation U830C? Its location in the A2 protein, which is multifunctional, offers interesting alternatives. In addition to interacting with the pili, A2 also binds to a cellular protein, MurA, which is involved in the synthesis of peptidoglycan by the bacterium (Brown et al., 1995). When sufficient A2 has been synthesized, its binding to MurA inhibits cell wall synthesis, opening holes, and eventually causing bacterial lysis (Karnik and Billeter, 1983; Winter and Gold, 1983; Bernhardt et al., 2001;

Reed et al., 2012, 2013; Cui et al., 2017). It is possible that the increased latent period produced by mutation U830C is due to a worsening of the interaction of A2 with MurA at 30 and 37°C when the amino acid at position 256 is alanine, instead of valine. At 43°C, the temperature at which the latent period is longer, both amino acids would be almost equally "bad" for the interaction between A2 and MurA, giving rise to only small differences in the latent period. In support of this idea, it has been reported that incubation of Qβ with MurA inhibits infection, suggesting that the pilus and MurA bind to the same region of A2. Thus, improving interaction with the pilus could be at the cost of worsening the interaction with MurA (Reed et al., 2013). Comparison of the complexes generated between wild and mutant A2 with MurA at the three temperatures assayed in this study could explain the molecular mechanisms leading to our results. To this aim, molecular dynamics simulations, combined with microscopy techniques could be of great help (Jana and May, 2020; Bruinsma et al., 2021). In this sense, it is worth mentioning the works carried out with MS2 that have allowed to model not only the viral capsid, but also the gRNA, getting the first complete all-atom model of the virus (Farafonov and Nerukh, 2019; Farafonov et al., 2022).

It is more difficult to interpret why mutation C2011A, which also favors the formation of infectious centers at 43°C without prolonging the latent period, is not selected at this temperature. Our proposal for the mechanism of action of this mutation, located in the A1 protein, is that it provides primary binding sites to the pili (Laguna-Castro and Lázaro, 2022). According to some models, mostly inspired in studies carried out with the related phage MS2 that also uses the bacterial pili as receptor (Toropova et al., 2011; Dent et al., 2013), subsequent retraction of the pili would bring the attached viruses closer to the cell surface, thus facilitating the entry into the cell of the complex formed by Mat (the protein that interacts with the pilus in MS2) and the virus RNA (Meng et al., 2019; Harb et al., 2020). If a similar mechanism is operating in Qβ, it might happen that the empty viral capsids produced after genome internalization would remain in the extracellular environment, and the possibility that they could bind to new susceptible bacteria through the A1 protein cannot be ruled out. Additional studies, carried out with MS2 and Qβ, show that the pili that have undergone the retraction process are detached from the bacteria preventing further infections (Harb et al., 2020). It is quite probable that these free pili are able to bind viruses that otherwise could infect susceptible bacteria, as it has been demonstrated for phages R17 and M12 (Valentine and Strand, 1965; Paranchych et al., 1971). In both situations, the increase in the adsorption rate produced by mutation C2011A would be a disadvantage for the progression of the infection, as it could result in the "sequestration" of susceptible bacteria by empty capsids and of infective viruses by non-functional pili. Both processes would acquire greater relevance at high bacterial density, leading to more negative effects of the mutation. Since mutation U830C is located in the A2 protein, which is introduced into the cell together with the virus genome, it cannot have any effect in the adsorption of empty capsids to bacteria. The presence of A2 in a single copy probably also limits the process of virus binding to detached pili or other bacteria components. Degradation or binding of viruses by some of the bacterial components released after lysis might also contribute to reduce viral infectivity (Rabinovitch et al., 2003; Aviram and Rabinovitch, 2008).

TABLE 3 Mutations present in the consensus sequence of the lineages propagated from viruses $Q\beta_{U830C}$ and $Q\beta_{C2011A}$ for 10 transfers under the conditions indicated.

Virus[1]	Bacterial concentration	Temperature	Mutations[2]
$Q\beta_{U830C}$ (1)	3×10^8	37°C	–
$Q\beta_{U830C}$ (2)	3×10^8	37°C	–
$Q\beta_{U830C}$ (1)	3×10^5	37°C	U830C
$Q\beta_{U830C}$ (2)	3×10^5	37°C	U830C
$Q\beta_{C2011A}$ (1)	3×10^8	43°C	G1820A
$Q\beta_{C2011A}$ (2)	3×10^8	43°C	–
$Q\beta_{C2011A}$ (1)	3×10^6	43°C	U830C C2011A
$Q\beta_{C2011A}$ (2)	3×10^6	43°C	U830C C2011A

[1]The number (1) and (2) indicate the two replicas performed for each evolutionary lineage.
[2]The sign—means that there is no mutations relative to the sequence of the wild-type virus.

Several assays in which $Q\beta_{Anc}$, $Q\beta_{U830C}$, and $Q\beta_{C2011A}$ were incubated with an artificial cell lysate at different temperatures for 16 h showed that the virus titers experienced a decline, which was of greater magnitude at 43°C than at 30 or 37°C (**Figure 8**), perhaps due to the highest value for the constant of formation of infectious centers at that temperature. It was also observed in similar assays that at 43°C (and only at this temperature), the virus containing mutation C2011A reduced its titers much more than the wild-type virus or the mutant containing U830C, which could be due to the mechanisms proposed above, providing in this way an explanation for the fitness costs of C2011A at 43°C. It could be argued that incubation with the lysate lasted longer than the time allowed for virus replication during the transfers in the evolution experiment. In addition, bacteria were lysed in a different way than that occurring during viral infection. We recognize these limitations, which could not be addressed in this study due to the difficulties to separate bacteria that have been lysed by the virus from those that have not been infected or have not completed the lysis process. Nevertheless, the aforementioned detachment of the pili, which might occur at a greater extension during Qβ infections, could increase the non-productive interactions with the virus. This fact would contribute to increase the negative effect of mutation C2011A at 43°C, which could thus be evident in a shorter time. We plan to develop a system to purify bacterial pili that allow us to compare their interaction with Qβ wild type and each of the mutants $Q\beta_{U830C}$ and $Q\beta_{C2011A}$.

Preferential selection of mutation U830C over C2011A at 43°C may also be due to the small increase in burst size it produces at this temperature. In all other conditions tested, both C2011A and U830C mutations produce decreases in burst size (**Table 2**), something for which, with the data we have available, we cannot offer an explanation. However, the increase in burst size would not clarify why mutation U830C is not selected at 43°C at

the higher bacterial density assayed. A possible explanation might be the small increase in the latent period that is also caused by this mutation at 43°C.

Additional evolution experiments have shown that $Q\beta_{U830C}$ propagated at 37°C (non-selective temperature) at high and low bacterial densities could be maintained at this temperature (**Figure 9A**). However, at high bacterial densities mutation U830C was selected against, something that did not happen at low bacterial density. In that case the change U830C could be conserved and mutation C2011A was not selected in 10 transfers, which agrees with the non-significant fitness cost of U830C at 37°C and low bacterial density (3×10^5 cfu/ml) (**Figure 6**). A similar experiment performed with $Q\beta_{C2011A}$ propagated at 43°C (non-selective temperature) at low host density showed an increase in the virus titers as the number of transfers increased (**Figure 9B**). Mutation C2011A was kept, although in the two replicas performed mutation U830C was also selected, indicating that it is a necessary requirement for adaptation to low bacterial density at 43°C. Conversely, lineages propagated at high host density decreased their titers in a progressive way (**Figure 9B**). Sequencing of the populations obtained at transfer number 10 showed that they had lost mutation C2011A. The results suggest that the negative effect of mutation C2011A at 43°C and high host density reduce virus replication so much that the mutations necessary for adaptation to this temperature cannot be selected. Although the mutation is selected against, probably when this happens it is too late for the virus to increase the titers.

The most important conclusion that can be drawn from this work is that adaptation of Qβ to reduced host availability can be addressed by at least two different mutations that increase virus entry into bacteria. The choice of one or other depends on environmental parameters such as temperature that may affect the strength of the virus-cell interaction, the ease of internalizing the virus genome or the ability to generate an infectious progeny. The balance between the advantages and the fitness costs of each mutation under the particular conditions of virus replication is what decides if it is selected or not.

Data availability statement

The original contributions presented in this study are included in the article/**Supplementary material**, further inquiries can be directed to the corresponding author.

Author contributions

EL designed the study and wrote the manuscript. ML-C, AR-M, and ELl performed the experiments. EL and ML-C analyzed the data. All authors interpreted the results and reviewed the manuscript.

Funding

This work has been funded by grant PID2020-113284GB-C22, given by the Spanish Ministry of Science and Innovation/State Agency of Research (MCIN/AEI/10.13039/501100011033), and by "ERDF A way of making Europe".

Acknowledgments

We thank the Instituto Nacional de Técnica Aeroespacial (INTA) for the support received to carry out this work.

Conflict of interest

The authors declare that the research was conducted in the absence of any commercial or financial relationships that could be construed as a potential conflict of interest.

Publisher's note

Supplementary material

The Supplementary Material for this article can be found online at: https://www.frontiersin.org/articles/10.3389/fmicb.2023.1197085/full#supplementary-material

References

Abedon, S., Herschler, T., and Stopar, D. (2001). Bacteriophage latent-period evolution as a response to resource availability. *Appl. Environ. Microbiol.* 67, 4233–4241. doi: 10.1128/AEM.67.9.4233-4241.2001

Abedon, S. T. (2016). Bacteriophage exploitation of bacterial biofilms: phage preference for less mature targets? *FEMS Microbiol. Lett.* 363:fnv246. doi: 10.1093/femsle/fnv246

Abedon, S. T., and Culler, R. R. (2007). Optimizing bacteriophage plaque fecundity. *J. Theor. Biol.* 249, 582–592. doi: 10.1016/j.jtbi.2007.08.006

Abedon, S. T., Hyman, P., and Thomas, C. (2003). Experimental examination of bacteriophage latent-period evolution as a response to bacterial availability. *Appl. Environ. Microbiol.* 69, 7499–7506. doi: 10.1128/AEM.69.12.7499-7506.2003

Abedon, S. T., and Yin, J. (2009). Bacteriophage plaques: theory and analysis. *Methods Mol. Biol.* 501, 161–174. doi: 10.1007/978-1-60327-164-6_17

Arribas, M., Aguirre, J., Manrubia, S., and Lázaro, E. (2018). Differences in adaptive dynamics determine the success of virus variants that propagate together. *Virus Evol.* 4:vex043. doi: 10.1093/ve/vex043

Arribas, M., Cabanillas, L., Kubota, K., and Lázaro, E. (2016). Impact of increased mutagenesis on adaptation to high temperature in bacteriophage Qβ. *Virology* 497, 163–170. doi: 10.1016/j.virol.2016.07.007

Arribas, M., Kubota, K., Cabanillas, L., and Lázaro, E. (2014). Adaptation to fluctuating temperatures in an RNA virus is driven by the most stringent selective pressure. *PLoS One* 9:e100940. doi: 10.1371/journal.pone.0100940

Arribas, M., and Lázaro, E. (2021). Intra-population competition during adaptation to increased temperature in an RNA bacteriophage. *Int. J. Mol. Sci.* 22:6815. doi: 10.3390/ijms22136815

Aviram, I., and Rabinovitch, A. (2008). Dynamical types of bacteria and bacteriophages interaction: shielding by debris. *J. Theor. Biol.* 251, 121–136. doi: 10.1016/j.jtbi.2007.11.003

Barrera, I., Schuppli, D., Sogo, J. M., and Weber, H. (1993). Different mechanisms of recognition of bacteriophage Q beta plus and minus strand RNAs by Q beta replicase. *J. Mol. Biol.* 232, 512–521. doi: 10.1006/jmbi.1993.1407

Bernhardt, T. G., Wang, I. N., Struck, D. K., and Young, R. (2001). A protein antibiotic in the phage Qβ virion: diversity in lysis targets. *Science* 292, 2326–2329. doi: 10.1126/science.1058289

Brown, E. D., Vivas, E. I., Walsh, C. T., and Kolter, R. (1995). MurA (MurZ), the enzyme that catalyzes the first committed step in peptidoglycan biosynthesis, is essential in *Escherichia coli*. *J. Bacteriol.* 177, 4194–4197. doi: 10.1128/jb.177.14.4194-4197.1995

Bruinsma, R. F., Wuite, G. J. L., and Roos, W. H. (2021). Physics of viral dynamics. *Nat. Rev. Phys.* 3, 76–91. doi: 10.1038/s42254-020-00267-1

Bull, J. J., and Gill, J. J. (2014). The habits of highly effective phages: population dynamics as a framework for identifying therapeutic phages. *Front. Microbiol.* 5:618. doi: 10.3389/fmicb.2014.00618

Chantranupong, L., and Heineman, R. H. (2012). A common, non-optimal phenotypic endpoint in experimental adaptations of bacteriophage lysis time. *BMC Evol. Biol.* 12:37. doi: 10.1186/1471-2148-12-37

Cui, Z., Gorzelnik, K. V., Chang, J.-Y., Langlais, C., Jakana, J., Young, R., et al. (2017). Structures of Qβ virions, virus-like particles, and the Qβ-MurA complex reveal internal coat proteins and the mechanism of host lysis. *Proc. Natl. Acad. Sci. U.S.A.* 114, 11697–11702. doi: 10.1073/pnas.1707102114

De Paepe, M., and Taddei, F. (2006). Viruses' life history: towards a mechanistic basis of a trade-off between survival and reproduction among phages. *PLoS Biol.* 4:e193. doi: 10.1371/journal.pbio.0040193

Dennehy, J. J., and Abedon, S. T. (2020a). "Phage infection and lysis," in *Bacteriophages*, eds D. R. Harper, S. T. Abedon, B. H. Burrowes, and M. L. McConville (Norderstedt: BoD – Books on Demand), 1–43. doi: 10.1007/978-3-319-40598-8_53-1

Dennehy, J. J., and Abedon, S. T. (2020b). "Bacteriophage ecology," in *Bacteriophages: biology, technology, therapy*, eds D. R. Harper, S. T. Abedon, B. H. Burrowes, and M. L. McConville (Cham: Springer International Publishing), 1–42. doi: 10.1007/978-3-319-40598-8_8-1

Dennehy, J. J., Abedon, S. T., and Turner, P. E. (2007). Host density impacts relative fitness of bacteriophage Φ6 genotypes in structured habitats. *Evolution* 61, 2516–2527. doi: 10.1111/j.1558-5646.2007.00205.x

Dent, K. C., Thompson, R., Barker, A. M., Hiscox, J. A., Barr, J. N., Stockley, P. G., et al. (2013). The asymmetric structure of an icosahedral virus bound to its receptor suggests a mechanism for genome release. *Structure* 21, 1225–1234. doi: 10.1016/j.str.2013.05.012

Elena, S. F. (2001). Evolutionary history conditions the timing of transmission in vesicular stomatitis virus. *Infect. Genet. Evol.* 1, 151–159. doi: 10.1016/S1567-1348(01)00022-3

Farafonov, V. S., and Nerukh, D. (2019). MS2 bacteriophage capsid studied using all-atom molecular dynamics. *Interface Focus* 9:20180081. doi: 10.1098/rsfs.2018.0081

Farafonov, V. S., Stich, M., and Nerukh, D. (2022). Reconstruction and validation of entire virus model with complete genome from mixed resolution cryo-EM density. *Faraday Discuss.* 240, 152–167. doi: 10.1039/d2fd00053a

Gallet, R., Kannoly, S., and Wang, I.-N. (2011). Effects of bacteriophage traits on plaque formation. *BMC Microbiol.* 11:181. doi: 10.1186/1471-2180-11-181

Goldhill, D. H., and Turner, P. E. (2014). The evolution of life history trade-offs in viruses. *Curr. Opin. Virol.* 8, 79–84. doi: 10.1016/j.coviro.2014.07.005

Gorzelnik, K. V., Cui, Z., Reed, C. A., Jakana, J., Young, R., and Zhang, J. (2016). Asymmetric cryo-EM structure of the canonical Allolevivirus Qβ reveals a single maturation protein and the genomic ssRNA in situ. *Proc. Natl. Acad. Sci. U S A.* 113, 11519–11524. doi: 10.1073/pnas.1609482113

Gorzelnik, K. V., and Zhang, J. (2021). Cryo-EM reveals infection steps of single-stranded RNA bacteriophages. *Prog. Biophys. Mol. Biol.* 160, 76–83. doi: 10.1016/j.pbiomolbio.2020.07.011

Harb, L., Chamakura, K., Khara, P., Christie, P. J., Young, R., and Zeng, L. (2020). ssRNA phage penetration triggers detachment of the F-pilus. *Proc. Natl. Acad. Sci. U.S.A.* 117, 25751–25758. doi: 10.1073/pnas.2011901117

Hayes, W. (1953). The mechanism of genetic recombination in *Escherichia coli*. *Cold Spring Harbor Symposia Q. Biol.* 18, 75–93. doi: 10.1101/SQB.1953.018.01.016

Heineman, R. H., and Bull, J. J. (2007). Testing optimality with experimental evolution: lysis time in a bacteriophage. *Evolution* 61, 1695–1709. doi: 10.1111/j.1558-5646.2007.00132.x

Hofstetter, H., Monstein, H., and Weissmann, C. (1974). The readthrough protein A1 is essential for the formation of viable Qβ particles. *Biochim. Biophys. Acta* 374, 238–251.

Hyman, P., and Abedon, S. T. (2009). "Practical methods for determining phage growth parameters," in *Bacteriophages: Methods in molecular biology™*, Vol. 501, eds M. R. Clokie and A. M. Kropinski (Totowa, NJ: Humana Press), 307. doi: 10.1007/978-1-60327-164-6_18

Inomata, T., Kimura, H., Hayasaka, H., Shiozaki, A., Fujita, Y., and Kashiwagi, A. (2012). Quantitative comparison of the RNA bacteriophage Qβ infection cycle in rich and minimal media. *Arch. Virol.* 157, 2163–2169. doi: 10.1007/s00705-012-1419-3

Jana, A. K., and May, E. R. (2020). Structural and dynamic asymmetry in icosahedrally symmetric virus capsids. *Curr. Opin. Virol.* 45, 8–16. doi: 10.1016/j.coviro.2020.06.002

Karnik, S., and Billeter, M. (1983). The lysis function of RNA bacteriophage Qbeta is mediated by the maturation (A2) protein. *EMBO J.* 2, 1521–1526.

Kashiwagi, A., Sugawara, R., Sano Tsushima, F., Kumagai, T., and Yomo, T. (2014). Contribution of silent mutations to thermal adaptation of RNA bacteriophage Qβ. *J. Virol.* 88, 11459–11468. doi: 10.1128/JVI.01127-14

Kozak, M., and Nathans, D. (1971). Fate of maturation protein during infection by coliphage MS2. *Nat. New Biol.* 234, 209–211. doi: 10.1038/newbio234209a0

Krahn, P. M., O'Callaghan, R. J., and Paranchych, W. (1972). Stages in phage R17 infection. VI. Injection of a protein and RNA into the host cell. *Virology* 47, 628–637. doi: 10.1016/0042-6822(72)90552-1

Laguna-Castro, M., and Lázaro, E. (2022). Propagation of an RNA bacteriophage at low host density leads to a more efficient virus entry. *Front. Virol.* 2:858227. doi: 10.3389/fviro.2022.858227

Lázaro, E., Arribas, M., Cabanillas, L., Román, I., and Acosta, E. (2018). Evolutionary adaptation of an RNA bacteriophage to the simultaneous increase in the within-host and extracellular temperatures. *Sci. Rep.* 8, 1–9. doi: 10.1038/s41598-018-26443-z

Manchak, J., Anthony, K. G., and Frost, L. S. (2002). Mutational analysis of F-pilin reveals domains for pilus assembly, phage infection and DNA transfer. *Mol. Microbiol.* 43, 195–205. doi: 10.1046/j.1365-2958.2002.02731.x

Meng, R., Jiang, M., Cui, Z., Chang, J.-Y., Yang, K., Jakana, J., et al. (2019). Structural basis for the adsorption of a single-stranded RNA bacteriophage. *Nat. Commun.* 10:3130. doi: 10.1038/s41467-019-11126-8

Olsthoorn, R. C. L., and Van Duin, J. (2011). *Leviviridae-Positive Sense RNA Viruses-Positive Sense RNA Viruses*. London: ICTV.

Paranchych, W. (1966). Stages in phage R17 infection: the role of divalent cations. *Virology* 28, 90–99. doi: 10.1016/0042-6822(66)90309-6

Paranchych, W., Ainsworth, S. K., Dick, A. J., and Krahn, P. M. (1971). Stages in phage R17 infection. V. Phage eclipse and the role of F pili. *Virology* 45, 615–628. doi: 10.1016/0042-6822(71)90176-0

Rabinovitch, A., Aviram, I., and Zaritsky, A. (2003). Bacterial debris-an ecological mechanism for coexistence of bacteria and their viruses. *J. Theor. Biol.* 224, 377–383. doi: 10.1016/s0022-5193(03)00174-7

Reed, C. A., Langlais, C., Kuznetsov, V., and Young, R. (2012). Inhibitory mechanism of the Qβ lysis protein A2. *Mol. Microbiol.* 86, 836–844. doi: 10.1111/mmi.12021

Reed, C. A., Langlais, C., Wang, I. N., and Young, R. (2013). A2 expression and assembly regulates lysis in Qβ infections. *Microbiol* 159, 507–514. doi: 10.1099/mic.0.064790-0

Reynolds, S., and Paranchych, W. (1976). The isolation of an infectious A protein RNA complex from coliphage R17. *Can. J. Microbiol.* 22, 1647–1653. doi: 10.1139/m76-242

Rumnieks, J., and Tars, K. (2011). Crystal structure of the read-through domain from bacteriophage Qβ A1 protein. *Protein Sci.* 20, 1707–1712. doi: 10.1002/pro.704

Rumnieks, J., and Tars, K. (2017). Crystal structure of the maturation protein from bacteriophage Qβ. *J. Mol. Biol.* 429, 688–696. doi: 10.1016/j.jmb.2017.01.012

Shao, Y., and Wang, I.-N. (2008). Bacteriophage adsorption rate and optimal lysis time. *Genetics* 180, 471–482. doi: 10.1534/genetics.108.090100

Shiba, T., and Miyake, T. (1975). New type of infectious complex of E. coli RNA phage. *Nature* 254, 157–158. doi: 10.1038/254157a0

Somovilla, P., Manrubia, S., and Lázaro, E. (2019). Evolutionary dynamics in the RNA bacteriophage Qβ depends on the pattern of change in selective pressures. *Pathog* 8:80. doi: 10.3390/pathogens8020080

Somovilla, P., Rodríguez-Moreno, A., Arribas, M., Manrubia, S., and Lázaro, E. (2022). Standing genetic diversity and transmission bottleneck size drive adaptation in bacteriophage Qβ. *Int. J. Mol. Sci.* 23:8876. doi: 10.3390/ijms23168876

Taniguchi, T., Palmieri, M., and Weissmann, C. (1978). QB DNA-containing hybrid plasmids giving rise to QB phage formation in the bacterial host. *Nature* 274, 223–228. doi: 10.1038/274223a0

Toropova, K., Stockley, P. G., and Ranson, N. A. (2011). Visualising a viral RNA genome poised for release from its receptor complex. *J. Mol. Biol.* 408, 408–419. doi: 10.1016/j.jmb.2011.02.040

Valentine, R. C., and Strand, M. (1965). Complexes of F-pili and RNA bacteriophage. *Science* 148, 511–513. doi: 10.1126/science.148.3669.511

Vasiljeva, I., Kozlovska, T., Cielens, I., Strelnikova, A., Kazaks, A., Ose, V., et al. (1998). Mosaic Qbeta coats as a new presentation model. *FEBS Lett.* 431, 7–11. doi: 10.1016/s0014-5793(98)00716-9

Wasik, B. R., Bhushan, A., Ogbunugafor, C. B., and Turner, P. E. (2015). Delayed transmission selects for increased survival of vesicular stomatitis virus. *Evolution* 69, 117–125. doi: 10.1111/evo.12544

Winter, R. B., and Gold, L. (1983). Overproduction of bacteriophage Qβ maturation (A2) protein leads to cell lysis. *Cell* 33, 877–885. doi: 10.1016/0092-8674(83)90030-2

Woody, M. A., and Cliver, D. O. (1995). Effects of temperature and host cell growth phase on replication of F- specific RNA coliphage Qβ. *Appl. Environ. Microbiol.* 61, 1520–1526. doi: 10.1128/aem.61.4.1520-1526.1995

Yin, J., and Redovich, J. (2018). Kinetic modeling of virus growth in cells. *Microbiol. Mol. Biol. Rev.* 82, 1–33. doi: 10.1128/mmbr.00066-17

frontiers | Frontiers in Microbiology

TYPE Original Research
PUBLISHED 16 August 2023
DOI 10.3389/fmicb.2023.1227147

OPEN ACCESS

EDITED BY
Alicja Wegrzyn,
Institute of Biochemistry and Biophysics, Polish Academy of Sciences, Poland

REVIEWED BY
Grazyna Majkowska-Skrobek,
University of Wrocław, Poland
Vijay Singh Gondil,
University of Rochester Medical Center, United States
Prasanth Manohar,
Texas A&M University, United States

*CORRESPONDENCE
Xiaohong Sun
✉ xhsun@shou.edu.cn

RECEIVED 22 May 2023
ACCEPTED 13 July 2023
PUBLISHED 16 August 2023

CITATION
Chen C, Tao Z, Li T, Chen H, Zhao Y and Sun X (2023) Isolation and characterization of novel bacteriophage vB_KpP_HS106 for *Klebsiella pneumonia* K2 and applications in foods.
Front. Microbiol. 14:1227147.
doi: 10.3389/fmicb.2023.1227147

Isolation and characterization of novel bacteriophage vB_KpP_HS106 for *Klebsiella pneumonia* K2 and applications in foods

Changrong Chen[1], Zhenxiang Tao[1], Tengteng Li[1], Hong Chen[1], Yong Zhao[1,2,3] and Xiaohong Sun[1,2,3]*

[1]College of Food Science and Technology, Shanghai Ocean University, Shanghai, China, [2]Shanghai Engineering Research Center of Aquatic-Product Processing and Preservation, Shanghai, China, [3]Laboratory of Quality and Safety Risk Assessment for Aquatic Products on Storage and Preservation (Shanghai), Ministry of Agriculture and Rural Affairs, Shanghai, China

The detection rate of *Klebsiella pneumoniae* in food is increasing, and it has emerged as a food pathogen. Global health is threatened due to the emergence of multidrug-resistant (MDR) and hypervirulent (hv) *K. pneumoniae*. Phages have a promising application as antibacterial agents and have the ability to lyse MDR strains. Hence, phage vB_KpP_HS106 against MDR-hv *K. pneumoniae* strains was isolated from sewage collected from a hospital. It can maintain stable activity at a pH range of 4–12 and a temperature range of 4°C to 50°C. The maximum adsorption rate of phage HS106 was found to be approximately 84.2% at 6 min. One-step growth curve analysis showed that the latent period of HS106 was 10 min and the burst size was approximately 183 PFU/cell. Furthermore, whole genome analysis indicated that the genome of phage HS106 was a double-stranded linear 76,430-bp long DNA molecule with 44% GC content. A total of 95 open reading frames were annotated in the HS106 genome, which did not contain any virulence genes or antibiotic resistance genes. Phage HS106 reduced MDR *K. pneumoniae* in milk by approximately 1.6 $\log_{10}$ CFU/mL at 25°C and in chicken by approximately 2 $\log_{10}$ CFU/cm^3 at 25°C. Therefore, vB_KpP_HS106 is a promising alternative to antibiotics for biocontrol against multidrug-resistant *K. pneumoniae* in foods.

KEYWORDS

antibiotic-resistant, *Klebsiella pneumoniae*, phage, biocontrol, foods

1. Introduction

Klebsiella pneumoniae is a Gram-negative bacterium belonging to the *Enterobacteriaceae* family and has been recognized as the most common nosocomial pathogen (Nazir et al., 2020). It can cause pneumonia, severe infection, sepsis, and other diseases (Guo et al., 2016), which can cause high mortality in immunocompromised humans and newborns (Machado and Bicalho, 2018). In animal husbandry, *K. pneumoniae* causes severe pneumonia, sepsis, meningitis, and mastitis in cattle. Mastitis caused by *Klebsiella* infection is often more severe (Gröhn et al., 2004; Cheng et al., 2018). Studies worldwide have revealed that *K. pneumoniae* can contaminate meat (Veleba et al., 2012) and dairy products (Chen et al., 2009), which contributes to disease and spoilage (Guo et al., 2016). 29 (16%) Carbapenem-resistant *K. pneumoniae* were isolated from 181 chicken samples collected from farms in western Algeria

(Chaalal et al., 2020). Drug sensitivity analysis of 857 milk samples collected from dairy farms in Jiangsu Province and Shandong Province showed that MDR *K. pneumoniae* could be detected in 27.4% of milk samples (Yang et al., 2020), which showed that food is one of the vectors for MDR hypervirulent *K. pneumoniae*. The capsule is one of the most important virulence factors of *K. pneumoniae*. Among more than 80 capsule serotypes, K1, K2, K5, K20, K54, and K57 are closely related to various invasive infections in humans, which are called hypervirulent capsular serotypes of *K. pneumoniae*, of which K1 and K2 are the most virulent (Chuang et al., 2006; Paczosa and Mecsas, 2016). Therefore, effective measures to control hypervirulent *K. pneumoniae* are urgently needed. Bacteriophages (phages) have been studied as valuable antimicrobial alternatives for killing drug-resistant bacteria.

Bacteriophages are viruses that specifically infect bacteria. Phages have been studied as valuable antimicrobial alternatives for killing multidrug-resistant bacteria (Hoang Minh et al., 2016). Compared to antibiotics, phages have the ability to self-proliferate on the infection site with higher host specificity (Wittebole et al., 2014; Xu et al., 2015). In addition, the composition of phages is not toxic to eukaryotic cells (Wittebole et al., 2014). *K. pneumoniae* phages are mainly used in preclinical research and clinical treatment. Cao et al. (2015) have shown that phages can cause *K. pneumoniae* to decline sharply in the lungs of mice within 2 h after lung infection. At present, some commercial bacteriophages have been developed, such as SalmoFresh, Salmonelex, Armament, Listex P100, and ListShield, which have been used to inactivate and control different foodborne pathogens in food substrates and biofilms. Phages are currently marketed to target *Salmonella* spp., *Listeria monocytogenes*, *Shigella* spp., and *Escherichia coli* (García-Anaya et al., 2020). Phage is a good candidate for use as a food additive to control *K. pneumoniae* remaining after pasteurization in dairy products.

MDR *K. pneumoniae* have been detected in fruits, vegetables, dairy products, chicken, seafood, and other foods, which cause increasing harm to human health (Koovapra et al., 2016). In previous studies, phages have not been used to control *K. pneumoniae* in foods. In this study, we focus on the use of bacteriophages as biocontrol agents to control *K. pneumoniae*. A lytic phage against multidrug-resistant *K. pneumoniae* strains (K2 capsular type) was isolated from sewage collected from a hospital, and its characteristic features and genome sequence were determined. Finally, the effectiveness of the application of the phage was determined in milk and chicken meat.

2. Materials and methods

2.1. Bacterial strains and growth conditions

In total, 41 *K. pneumoniae* strains isolated from dairy farms in Shanghai were used in this study. The drug resistance and capsular type of each strain are shown in Table 1 and Supplementary Table 1. The multidrug-resistant (MDR) *K. pneumoniae* 106 (a K2 capsular type) was used as a host bacterium for phage isolation and propagation. All *K. pneumoniae* strains were cultured in 5 mL of LB broth (LB, Land Bridge Technology, Beijing, China) and incubated up to 10^9 CFU/mL at 37°C with shaking for 4 h.

2.2. Isolation and purification of bacteriophage

K. pneumoniae 106 was used as the bacterial host for phage isolation, using the method described previously (Cao et al., 2021). Briefly, sewage (40 mL) collected from Shanghai NO.6 People Hospital was mixed in 40 mL of LB, then 400 µL of 1 M $CaCl_2$ (Sangon Biotech, Shanghai, China) was added to enhance the phage adsorption rate and inoculated with 1 mL of *K. pneumoniae* 106 culture (10^9 CFU/mL). The mixture was incubated at 37°C for 24 h with shaking at 120 rpm. After incubation, the bacteria were removed by centrifugation (8,000× *g* for 10 min at 4°C) (5424, Eppendorf AG 22331, Hamburg, Germany), and the supernatant was filtered through 0.22 µm filters (Millipore, Billerica, MA, USA). The filtrate was collected and used in a spot test to detect the presence of phages. The phages were purified at least three times to obtain a pure phage using a double-layer agar method (Huang et al., 2018). The purified phages were stored at 4°C for further experiments.

2.3. Phage host range determination

As the phage host range is an essential factor for phage therapy and decolonization, we performed spot assays to determine the host range of the phage against 41 MDR *K. pneumoniae* strains using the method described previously (Bao et al., 2019). Briefly, 10 µL of suspension containing phage particles (10^8 PFU/mL) was dropped onto lawn cultures of 41 MDR *K. pneumoniae* strains (Table 1). After overnight incubation at 37°C, the plates were observed for the presence of plaques on the bacterial lawns.

2.4. Transmission electron microscopy of the phage

Cesium chloride density gradient centrifugation was used to purify the enriched phages. Transmission electron microscopy (TEM) was used to observe the morphology of the phage according to Yuan et al. (2015) method. First, 20 µL of phage solution (10^9 PFU/mL) was added dropwise to copper mesh and fixed for 10 min, and the residual liquid was absorbed by filter paper. Then, 2% phosphotungstic acid was added to stain for 2 min. The sample was air-dried and observed by transmission electron microscope (Philips, Eindhoven, The Netherlands).

2.5. Temperature and pH tolerance of the phage

The temperature stability of the phage was tested after treatment in a water bath at 4°C, 25°C, 37°C, 50°C, 60°C,70°C, and 80°C for 1 h using the double-layer agar plate. In order to detect the stability of the phage at different pH values, SM buffer with different pH values (2–13) were prepared using 1 M HCl or 1 M NaOH. At each pH value, 100 µL of the phage and 900 µL SM buffer were mixed. After incubation at 37°C for 1 h, the phage titer was determined using the double-layer agar method.

10.3389/fmicb.2023.1227147

TABLE 1 The host range of phage vB_KpP_HS106.

Strain	ESBL[a]	Capsular type	Lysis[b]
K. pneumoniae 015	–	K62	–
K. pneumoniae 111	–		+++
K. pneumoniae 001	–		–
K. pneumoniae 002	–		++
K. pneumoniae 011	–	K50	–
K. pneumoniae 048	–		–
K. pneumoniae 062	–	K19	++
K. pneumoniae 071	–	K50	–
K. pneumoniae 072	–	K8	+
K. pneumoniae 074	–	K19	+++
K. pneumoniae 308	–		–
K. pneumoniae 106	+	K2	+++
K. pneumoniae 309	+	K62	–
K. pneumoniae 311	+	K27	–
K. pneumoniae 037	–	K3	+++
K. pneumoniae 059	–	K39	+
K. pneumoniae 403	–		+
K. pneumoniae 102	+		+
K. pneumoniae 045	–		+
K. pneumoniae 052	–	K39	+++
K. pneumoniae 112	+	K2	–
K. pneumoniae 206	+		+
K. pneumoniae 313	+	K12	–
K. pneumoniae 061	+	K31	++
K. pneumoniae 211	+	K12	+
K. pneumoniae 031	–		+
K. pneumoniae 042	–		++
K. pneumoniae 204	–		–
K. pneumoniae 023	–	K26	+
K. pneumoniae 405	–	K16	+
K. pneumoniae 036	–	K23	–
K. pneumoniae 077	–		++
K. pneumoniae 304	–		+
K. pneumoniae 058	+		++
K. pneumoniae 103	+	K41	–
K. pneumoniae 411	+		–
K. pneumoniae 413	+		–
K. pneumoniae 006	–	K39	+
K. pneumoniae 021	–	K26	+
K. pneumoniae 060	–	K28	–
K. pneumoniae 208	–	K52	++

[a]ESBL, Extended-Spectrum-β-lactamase.
[b]Lytic, +++, complete lysis; ++, lysis; +, turbid lysis; –, no plaques.

2.6. Optimal multiplicity of infection (MOI) assay

The MOI of the phage was determined according to the method described by Li et al. with some modifications (Li et al., 2020). Briefly, the concentration of the phage was adjusted to 10^9, 10^8, 10^7, 10^6, 10^5, and 10^4 PFU/mL, then the host strain was mixed with MOIs of 100, 10, 1, 0.1, 0.01, 0.001, and 0.0001, respectively. After the mixture was incubated for 4 h at 37°C, the phage titer was determined by the double-layer agar method. The MOI that generated the highest phage titer was considered as the optimal MOI (Feng et al., 2021).

2.7. Phage adsorption rate and one-step growth curve

In order to determine the adsorption rate of phage to host bacteria, phage was mixed with *K. pneumoniae* at the optimal MOI and incubated at 37°C. For a period of 10 min, 100 μL of the mixture was taken at 1 min intervals and then diluted with 0.9 mL LB. The mixture was centrifuged (12,000 × g, 5 min), and the supernatant containing unabsorbed phages was diluted and counted using the double-layer agar plate method. The adsorption rate was expressed by calculating the percentage of free phage in the culture system. The one-step growth curve of the phage was determined using the method described previously with minor modifications (Wang et al., 2019). Briefly, 8 mL of *K. pneumoniae* 106 culture (10^9 CFU/mL) was centrifuged (5,000×*g*, 5 min), the supernatant was discarded, and the precipitate was resuspended in 8 mL of SM buffer. The phage at the optimal MOI was added to the suspension and incubated at 37°C for 6 min. The mixture was then centrifuged at 12,000×*g* for 2 min to remove unabsorbed phages. The pellet was resuspended in 10 mL LB broth and incubated at 37°C. Samples were taken at 10 min intervals during the 100 min period then diluted and counted using the double-layer agar plate method.

2.8. Phage genome extraction and sequencing

Phage DNA was extracted using the phenol/chloroform extraction method (Yuan et al., 2012). Phage DNA libraries were prepared using the Whole Genome Shotgun strategy (WGS) and then sequenced using Illumina NovaSeq. The Sequencing results with the splice sequences removed were first assembled from scratch using A5-miseq v20160825 (Coil et al., 2015) and SPAdesv3.12.0 (Bankevich et al., 2012) to construct contigs. Collinearity analysis was performed on contig, scaffold and the published sequences in GenBank to determine the position of contigs, and fill the gaps between contigs by Mummerv 3.1 (Delcher et al., 2003). The final sequence was assembled by Pilonv1.18 (Walker et al., 2014). The GeneMarkS interface[1] was used to predict open reading frames (ORFs) (Blake and Cohen, 2001). The non-redundant database (NR) of the National Center for Biotechnology Information (NCBI) was used to annotate protein-coding genes functionally. The tRNA genes were predicted using the tRNAscan-SE (Kortright et al., 2019). Antibiotic resistance genes and virulence genes were compared in Antibiotic Resistance Database (ARDB[2]) and Virulence Factor Database (VFDB[3]) (Kleinheinz et al., 2014). GCview server (Stothard and Wishart, 2005) was used to draw the gene map of the phage. The comparison of genome sequences between the phage isolated in this study and its most similar genome was visualized using the EasyFig visualization tool (Sullivan et al., 2011). Phylogenetic trees of the phage based on the major capsid protein and terminase large subunit were also analyzed using MEGA 7 (Kumar et al., 2018) with 1,000 bootstrap replications.

2.9. Inhibition effect of the phage against *Klebsiella pneumonia*

2.9.1. Inhibition effect of the phage against *Klebsiella pneumonia* in LB broth

The inhibition ability of the phage against MDR *K. pneumoniae* 106 in LB broth was detected in 100-well microtiter plates by the method previously described (Alves et al., 2014). Briefly, 100 μL of *K. pneumoniae* 106 was added to 100-well microtiter plates, and the same volume of phage suspension was added to 100-well plates, to which bacteria had been added at 1, 10, and 100 of MOI. As a control, 100 μL of SM buffer was added. The absorbance at 600 nm was measured at 1 h intervals within 12 h by a Bioscreen C Microbiology Reader (Oy Growth Curves Ab Ltd., Helsinki, Finland).

2.9.2. Inhibition effect of the phage against *Klebsiella pneumonia* in milk

To investigate the inhibition effect of the phage on *K.pneumoniae* in milk, sterile skim milk purchased from the Lotus supermarket in Shanghai, China was used as the medium for *K. pneumoniae* according to the method previously described (Noor Mohammadi et al., 2021). Briefly, 50 μL of *K.pneumoniae* 106 was inoculated into 5 mL of skim milk at a final concentration of 10^4 CFU/mL, and 50 μL of the phage (10^5, 10^6 PFU/mL, MOI of 10, 100) was added to the contaminated milk. SM buffer was added instead of phage suspension as the control group. The mixture was incubated at 4°C and 25°C for 24 h. At 0, 3, 6, 12, and 24 h, 100 μL of the mixture was taken for counting.

2.9.3. Inhibition effect of the phage against *Klebsiella pneumonia* in chicken

The inhibition effect of the phage against *K. pneumoniae* in chicken was assessed according to the method with some modifications (Noor Mohammadi et al., 2021). Chicken meat samples were purchased from the Lotus supermarket in Shanghai, China. The chicken meat was cut into pieces (1 cm × 1 cm × 1 cm) and put into a sterile container containing 0.2% NaClO for 30 min then washed three times with sterile water. Each piece of the chicken meat was inoculated with 20 μL of *K. pneumoniae* suspension to approximately 1×10^4 CFU/cm^3. Then, 20 μL of phage solution was added to the final titer of

1 http://exon.gatech.edu/GeneMark/

2 https://card.mcmaster.ca/analyze/rgi

3 http://www.mgc.ac.cn/VFs/

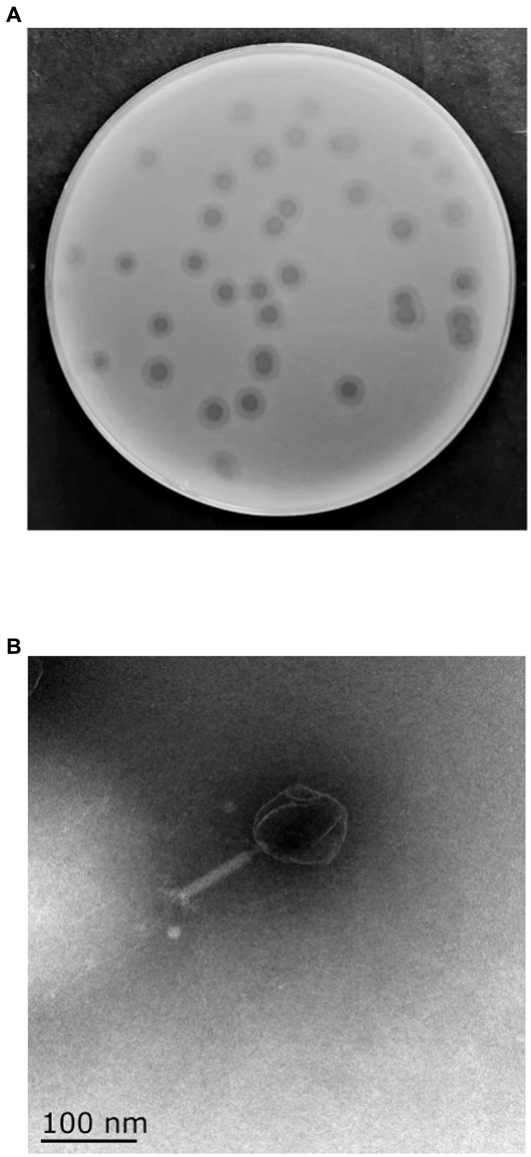

FIGURE 1
Morphology of phage vB_KpP_HS106. **(A)** Phage vB_KpP_HS106 plaques. **(B)** Transmission electron micrograph of phage vB_KpP_HS106.

1×10^5, 1×10^6 PFU/cm^3. SM buffer instead of phage solution was used as the control. Samples were incubated at 4°C and 25°C for 24 h. The treated chicken samples were placed in 5 mL of PBS buffer and shaken at 160 rpm/min for 5 min. The suspension was centrifuged at 8000 rpm/min for 1 min. The precipitate was resuspended with 1 mL of PBS buffer to remove the phage. The viable bacteria were counted by multiplicative dilution of the bacterial suspension.

2.10. Statistical analysis

All experiments in this study were repeated three times. The data were expressed as mean ± standard deviation (SD) and the differences were analyzed with two-way ANOVA using GraphPad Prism 9.0. Differences were considered statistically significant at $p < 0.05$.

3. Results

3.1. Isolation and general features of bacteriophage

One phage was isolated from sewage collected from ShangHai NO.6 People Hospital using MDR *K. pneumoniae* 106 as a host and was designated as vB_KpP_HS106 (phage HS106). The plaque morphology of phage HS106 is shown in Figure 1A. Phage HS106 produced large plaques (diameter, 6.8 mm) with a halo zone (diameter, 5.9 mm) after 12 h. The morphology of phage HS106 observed by TEM is shown in Figure 1B. Phage HS106 had an icosahedral head (diameter about 100 nm) and a long tail (diameter about 100 nm). It can be classified as part of the *Schitoviridae* family according to the demarcation criteria of the International Committee on Taxonomy of Viruses (ICTV) (Adriaenssens et al., 2020).

3.2. Host range and the optimal MOI

The host range of phage HS106 is shown in Table 1. Among the 41 *K.pneumoniae* strains used in this study, 26 could be lysed by phage HS106, which had the ability to lyse multiple capsular serotypes. Phage HS106 could lyse MDR *K.pneumoniae,* including *K.pneumoniae* 211, *K.pneumoniae* 061, and *K.pneumoniae* 102. At an MOI of 0.001, the phage HS106 titer was the highest (Figure 2C). Thus, the optimal MOI of phage HS106 was 0.001.

3.3. Phage temperature and pH stability

To investigate the activity in different environmental conditions, phage HS106 titer was determined at different temperatures and pH values. As shown in Figure 2A, phage titers were stable at approximately 10^9 PFU/ml after 1 h of treatment at 4°C to 50°C. The phage titer decreased to 10^7 PFU/ml and 10^3 PFU/ml after 1 h of exposure at 60°C and 70°C, respectively. When phage HS106 was incubated at 80°C for 1 h, no phage was detectable. As shown in Figure 2B, there was no noticeable reduction after 1 h of incubation at pH 4 to 11. However, when phage HS106 was incubated at pH 3 for 1 h, the titer of the phage decreased to 10^3 PFU/ml. Phage HS106 had no infection ability after exposure to pH 2, pH 12, or pH 13 for 1 h. In brief, phage HS106 had wide tolerance to temperatures and pH.

3.4. Adsorption rate and one-step growth curves

The adsorption rate of phage HS106 is shown in Figure 3A. After phage HS106 was added, the number of unadsorbed phages decreased before 6 min. At 6 min, 84.2% of the phage was adsorbed to the host cells, which was the maximum adsorption rate. To further investigate the proliferative capacity of phage HS106 after infecting the host cell, the one-step growth curve was determined. As shown in Figure 3B, the latent period of phage HS106 was 10 min and the lysis period was 50 min. The burst size was approximately 183 PFU/cell.

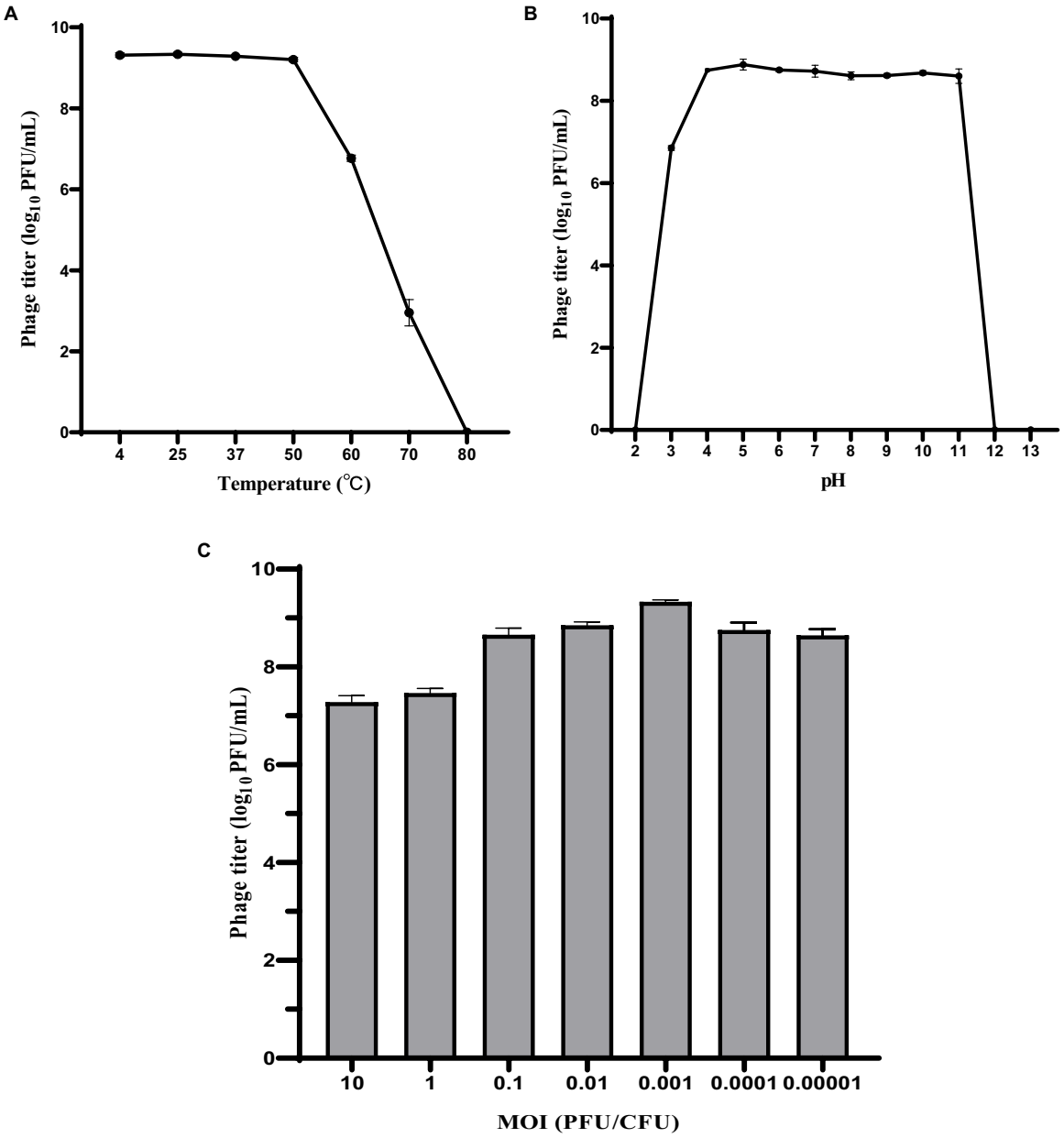

FIGURE 2
Biological characteristics of phage HS106. Stability of phage vB_KpP_HS106 at various **(A)** temperatures and **(B)** pH values. **(C)** Optimal MOI of phage HS106. The data represent the mean ± SD (n = 3).

3.5. Genome characterization of phage HS106

Through assembly and annotation to sequencing data, the phage HS106 genome map is shown in Figure 4. The phage HS106 genome consists of a 76,430 bp linear double-stranded DNA, with a G + C content of 44.0%. The whole genome sequence of phage HS106 was uploaded to the GenBank database with login number OP764672.1. A total of 95 open reading frames (ORFs) were identified with 73 ORFs on the positive strand and 22 ORFs on the negative strand. The 27 ORFs (28.4%) were assigned functions, which were predicted to encode functional proteins associated with DNA replication recombination and regulation, metabolism, phage structure and packaging proteins, and host cell lysis. The DNA replication recombination and regulation module include 7 ORFs: DNA polymerase, RNA polymerase, ATP-dependent DNA helicase, and Holliday junction resolvase. The metabolism module includes 6 ORFs: NTP-PPase-like protein, cell cycle regulatory protein, cytosine-specific methyltransferase, ribonucleoside-diphosphate reductase subunit alpha, and endonuclease. The phage structure and packaging proteins module includes 11 ORFs: major tail protein, putative portal protein, terminase large subunit, and PWWP domain-containing protein. Only 3 ORFs belong to the host lysis module (tail fiber/spick protein, Lysozyme). Sequence analysis showed that phage HS106 did not contain any lysogenic factors, which indicates that it belongs to lytic phages. Genome sequencing and analysis indicated that phage HS106 did not contain virulence factor genes or antibiotic resistance genes.

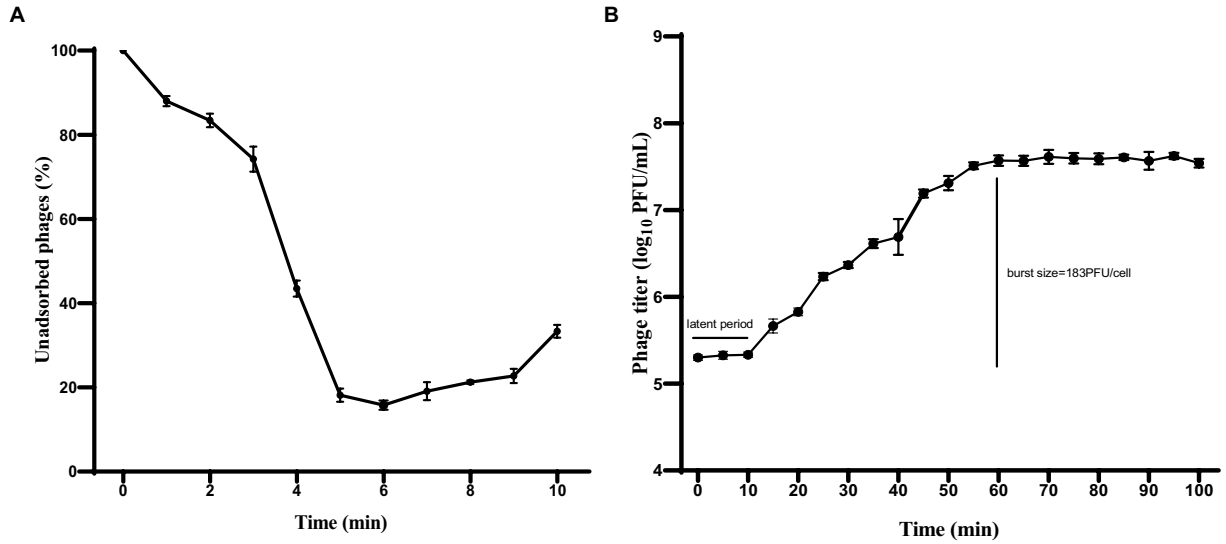

FIGURE 3
Characteristics of phage vB_KpP_HS106. **(A)** Adsorption assay of phage vB_KpP_HS106; **(B)** One-step growth curve of phage vB_KpP_HS106.

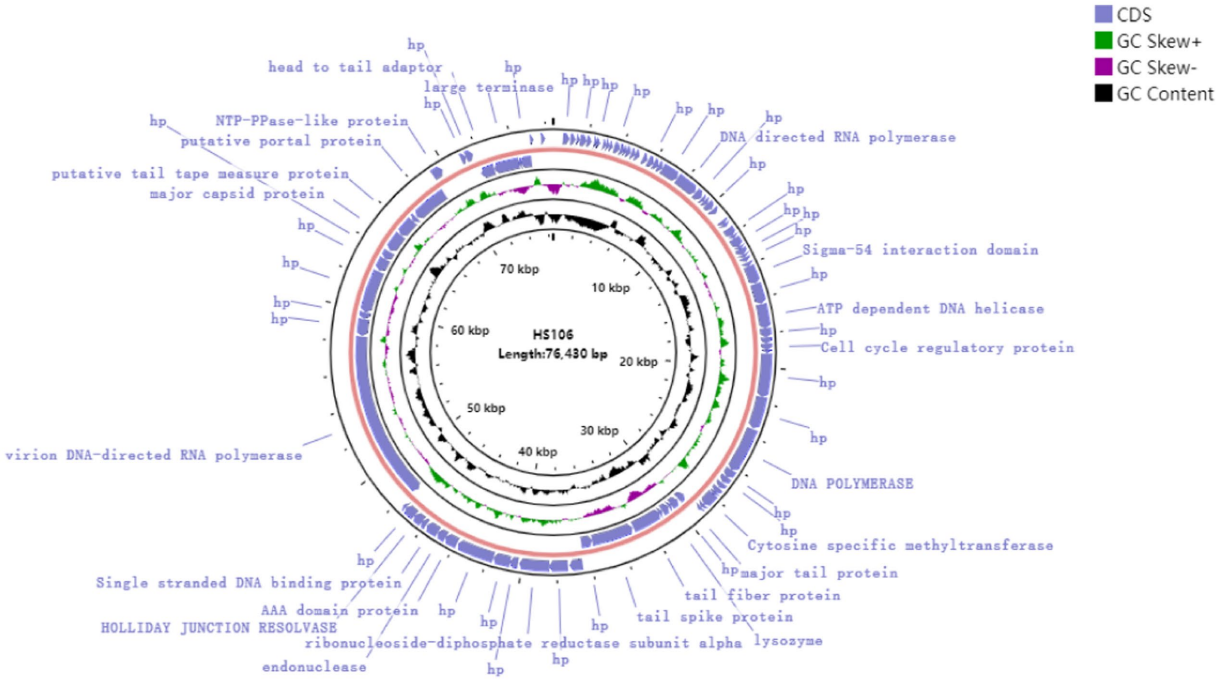

FIGURE 4
Circular genome annotation of phage vB_KpP_HS106. The inner rings show genome location, GC skew + (green) and – (purple) and GC content (black). The most external rings show identified open reading frames.

3.6. Phylogenetic and comparative genomic analysis of phage HS106

Compared with NCBI BLASTn, phage HS106 shared the highest nucleotide identity with *Klebsiella* phage vB_KpnP_P184 (accession:NC_055919.1). The sequence identity between vB_KpP_HS106 and vB_KpnP_P184 was 83.86% (coverage (88.00%) × identity (95.30%) = 83.86%). Comparative genomic analysis using Easyfig software showed that phage HS106 and phage P184 contain similar ORFs. However, there were differences in the tail proteins (ORF60, ORF61), Thymidylate synthase complementing protein (ORF64), and some hypothetical proteins (Supplementary Figure S1). To investigate the relationship between phage HS106 and other phages belonging to the *Schitoviridae* family, a phylogenetic tree based on the major capsid

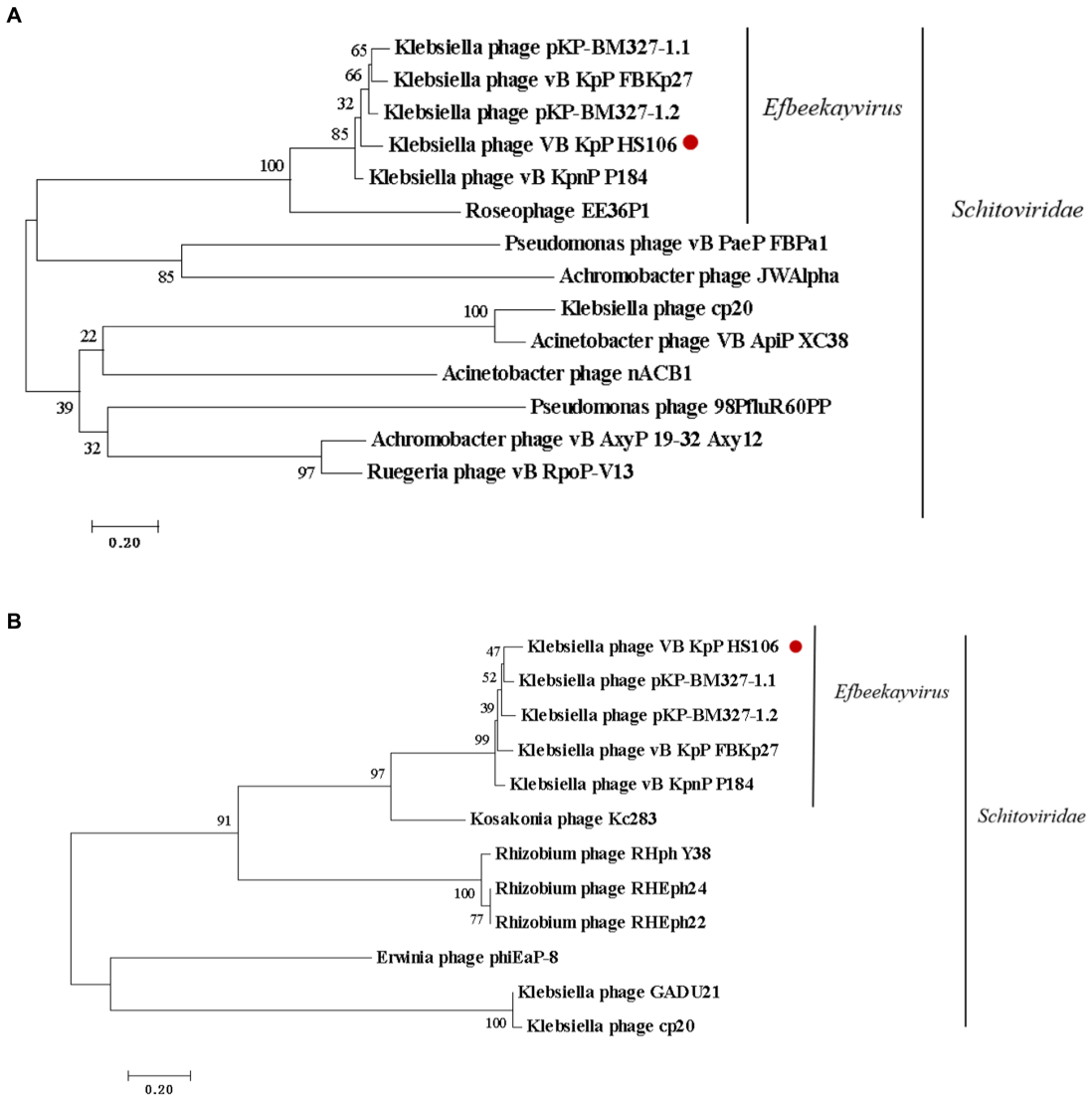

FIGURE 5
Phylogenetic analyses of phage vB_KpP_HS106. Phylogenetic analyses of selected phages and phages of the *Efbeekayvirus* genus based on the protein sequence of **(A)** major capsid protein and **(B)** terminase large subunit.

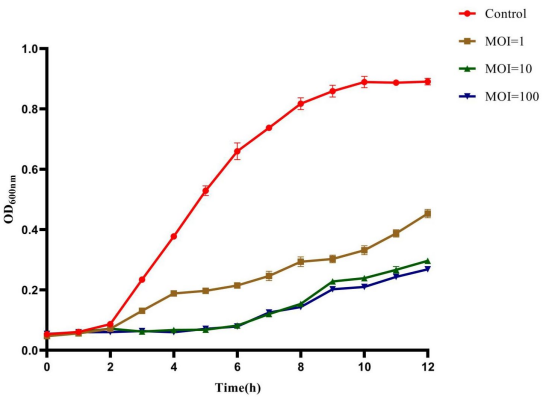

FIGURE 6
Bacteriolytic activity of phage vB_KpP_HS106 at different MOIs against *K. pneumoniae* in LB broth.

protein and terminal enzyme large subunit is shown in Figure 5. Phage HS106 is classified as a member of the *Efbeekayvirus* genus of the *Schitoviridae* family.

3.7. Inhibition effect of phage HS106 against *Klebsiella pneumonia*

3.7.1. Inhibition effect of phage HS106 against *Klebsiella pneumonia* in LB broth

The inhibition effect of phage HS106 on *K. pneumoniae* was evaluated *in vitro*. As shown in Figure 6, during the phage infection for 6 h, the OD_{600} values of phage HS106 treatment groups with MOI of 1, 10, and 100 were less than 0.2. The OD_{600} values of phage HS106 treatment groups with MOI of 10 and 100 were always less than the treatment group with MOI of 1 after incubation for 2 h. After 8 h, the OD_{600} value of the treatment group with high MOI was less than low MOI.

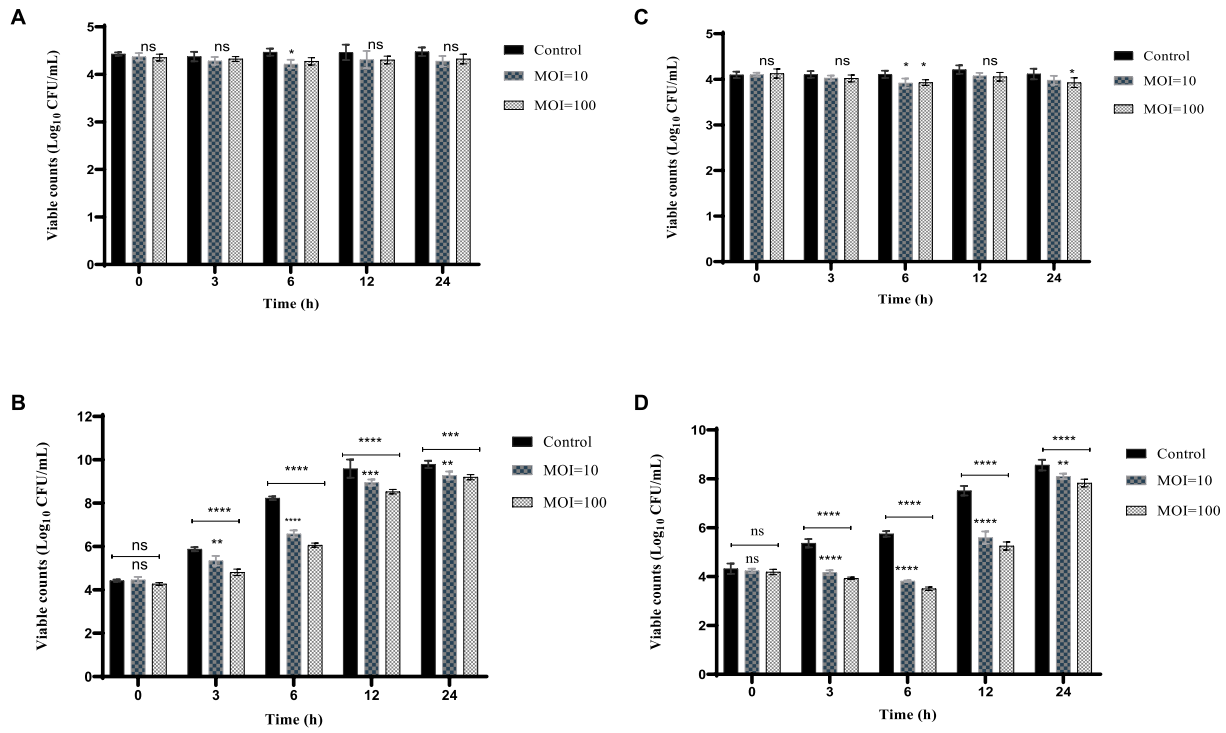

FIGURE 7
Effects of phage vB_KpP_HS106 on the viability of *K. pneumoniae* 106 in foods. Milk at **(A)** 4°C and **(B)** 25°C. Chicken meat at **(C)** 4°C and **(D)** 25°C. All the values were tabulated as mean ± SD and a significant difference between variations was denoted by asterisks using two-way ANOVA. ****Significant at $p < 0.0001$; ***Significant at $p < 0.001$; **Significant at $p < 0.01$; *Significant at $p < 0.05$; ns, not significant at $p > 0.05$.

3.7.2. Inhibition effect of phage HS106 against *Klebsiella pneumonia* in milk

The inhibition effect of phage HS106 on *K. pneumoniae* 106 in milk is shown in Figure 7. At 4°C, the amount of *K. pneumoniae* 106 was not significantly different from the control group within 24 h (Figure 7A). The phage HS106 treated group decreased by 1.6 $\log_{10}$ CFU/mL at 6 h compared with the control group at 25°C (Figure 7B). After 6 h, the bacterial number in the treated group increased by approximately 2 $\log_{10}$ CFU/mL. The results indicated that the antibacterial effect of phage HS106 with high MOI was better than those with low MOI.

3.7.3. Inhibition effect of phage HS106 against *Klebsiella pneumonia* in chicken meat

The inhibition effect of phage HS106 on *K. pneumoniae* 106 in chicken meat is shown in Figure 7. The amount of *K. pneumoniae* 106 was not significantly reduced with phage HS106 treatment for MOI of 10 and 100 compared to the control. At 4°C, the phage did not have a significantly inhibiting effect on *K. pneumoniae* (Figure 7C). At 25°C, the amount of *K. pneumoniae* 106 was reduced by approximately 2 $\log_{10}$ CFU/cm^3 compared with the control group at 6 h. The number of bacteria increased by 4 $\log_{10}$ CFU/cm^3 after 6 h (Figure 7D). The results showed that the antibacterial effect of phage HS106 with high MOI was better than those with low MOI.

4. Discussion

The invention of antibiotics solved the problem of bacterial infections and saved countless lives (Kumar et al., 2012). At present, the drug resistance of *K. pneumoniae* is becoming increasingly serious (Ferreira et al., 2019). Phages have emerged as a viable alternative to antibiotics in the face of MDR *K. pneumoniae* (Domingo-Calap et al., 2016). In this study, a lytic phage, phage HS106, was isolated from sewage.

The host range of a phage is one of the most important criteria for biological control. The wider the host range of a phage, the wider its application prospects (Koovapra et al., 2016). In this study, 63% (26/41) of *K. pneumoniae* could be lysed by phage HS106. The 26 *K. pneumoniae* strains included multiple capsular serotypes. Phage HS106 had a wide host range and good application prospects. Phages with a wide host range may be not only related to tail fiber/spick protein and lysozyme but also to proteins of unknown function. Further exploration is required to confirm the presence of unknown proteins capable of lysing *Klebsiella* strains of other capsule serotypes (Pan et al., 2017). The ability of phages to survive in extreme, harsh environments is also an evaluation criterion for phage applications. In this study, phage HS106 maintained stable activity at pH 4-pH 12 and 4–50°C. Compared with the *Klebsiella* phage reported previously (Peng et al., 2020; Zhang et al., 2021), phage HS106 had better tolerance to an extreme, harsh environment, which indicates that it has better activity as a biocontrol agent for application in food.

It can be less costly to reproduce a large number of bacteriophages with a smaller MOI and a shorter incubation period (Abedon, 1989). In this study, Phage HS106 was determined to have an optimal MOI of 0.001 and an incubation period of 10 min, which was considerably better than other *K. pneumoniae* phages, including vB_KpnP_Bp5 (Zhang et al., 2021), vB_KleS-HSE3 (Peng et al., 2020), and vB_KpP_TUN1 (Eckstein et al., 2021), etc. The burst size of phage HS106 was

larger than phage TUN1 (Eckstein et al., 2021). In brief, phage HS106 has a smaller optimal MOI, a shorter latent period, and a larger burst size, which indicates higher growth efficiency.

The genome size of *K. pneumoniae* phage is in the range of 19,260–346,602 bp (Peng et al., 2020). Phage HS106 has a 76,430 bp linear double-stranded DNA, which is in the range of *K. pneumoniae* phages. Phage HS106 was classified as *Schitoviridae* by genomic comparison. Genome annotation of phage HS106 predicted four modules: DNA replication recombination and regulation, metabolism, phage structure and packaging proteins, and host cell lysis. ORF61 and ORF62 were annotated as tail fiber/spick protein in the HS106 genome, which shared 84.42% identity with the *Klebsiella* phage vB_KpnP_P184 tail fiber/spick protein sequence (GenBank: YP_010114884.1). Tail fiber/spick protein had a pectate domain, which was a depolymerase used to depolymerize bacterial exopolysaccharides. ORF59 was annotated as lysozyme in the HS106 genome, which shared 96.82% identity with the *Caudoviricetes* sp. Lysozyme protein sequence (GenBank: DAQ70617.1). Lysozyme is inhibited from degrading the peptidoglycan by being tethered to the inner membrane and by having its catalytic domain locked in an inactive conformation either covalently or non-covalently (Young, 2014). Pertics confirmed the potential of phages and lysozyme as candidates for antimicrobial agents (Pertics et al., 2021). According to the classification system of the ICTV, the main species classification standard for bacterial and archaeal viruses is 95% genome similarity (Adriaenssens et al., 2020). Phage HS106 has 83.9% DNA sequence identity with vB_KpnP_P184. Therefore, the phage HS106 isolated in this study was a new species of the genus *Efbeekayvirus*. Genome sequencing and analysis indicated that phage HS106 did not contain any virulence factor genes or antibiotic resistance genes. Therefore, phage HS106 could be safely applied in the food hygiene industry.

In recent years, *K. pneumoniae* has been frequently isolated in foods such as fruits, vegetables, dairy products, chicken, and seafood. The risk caused by Extended-Spectrumβ-lactamase (ESBLs) *K.pneumoniae* is increasing (Koovapra et al., 2016). Phages only exclusively search for the corresponding host bacteria, which are harmless to other bacteria in the intestine. Therefore, they do not interfere with the normal flora and metabolism of the body, and the biological body itself can also clear phages in the body through the immune system (Hagens and Loessner, 2007). Phages have been applied to food products to inhibit pathogens, for example, it has been reported that phage ZPAH7 could reduce *A. hydrophila* by 1.2 $\log_{10}$ CFU/m^2 on lettuce (Islam et al., 2021). In this study, we focused on the use of phage HS106 as a biocontrol agent to control *K. pneumoniae* in food (milk and chicken). At 25°C, phage HS106 reduced MDR-*K. pneumoniae* by 1.6 $\log_{10}$ CFU/mL in milk and 2 $\log_{10}$ CFU/cm^3 in chicken. Therefore, phage HS106 is a good candidate for use as a food additive to control *K. pneumoniae* remaining after pasteurization in dairy products. However, in milk and chicken meat, viable counts of *K. pneumoniae* increased after 12 h at 24°C, even in the presence of phage HS106 at an MOI of 100, suggesting that bacteria developed phage resistance (data not shown). The use of a phage cocktail or food additives combined with the phage could be an alternative approach to prevent phage resistance (Soni et al., 2012; Liu et al., 2015).

In conclusion, we isolated a novel lytic phage, vB_KpP_HS106, with high-efficient lysis activity and a wide lysis spectrum. Phage HS106 was found to have a good tolerance to extreme environments. Genome analysis indicated that phage HS106 is a new species of the *Efbeekayvirus* genus of the *Schitoviridae* family. In addition, this phage does not carry any virulence genes or antibiotic resistance genes. It can effectively reduce MDR *K. pneumoniae* in milk and chicken. Therefore, phage HS106 has prospects as a biocontrol agent used to inhibit MDR *K. pneumoniae* in foods.

Data availability statement

The original contributions presented in the study are publicly available. This data can be found here: National Center for Biotechnology Information (NCBI) GenBank, https://www.ncbi.nlm.nih.gov/genbank/, OP764672.1.

Author contributions

XS: methodology. CC: software, data curation and writing—original draft preparation. HC, TL, and ZT: investigation. XS and TL: writing—review and editing. YZ: supervision. XS: project administration. All authors have read and agreed to the published version of the manuscript.

Funding

This work was supported by Shanghai Agriculture Applied Technology Development Program, China (Grant No. 2019-02-08-00-10-F01149).

Acknowledgments

The authors thank the bacteriology staff of Shanghai Agricultural Products Quality and Safety Testing Center for the milk sample collection and *K. pneumoniae* isolation.

Conflict of interest

The authors declare that the research was conducted in the absence of any commercial or financial relationships that could be construed as a potential conflict of interest.

Publisher's note

Supplementary material

The Supplementary material for this article can be found online at: https://www.frontiersin.org/articles/10.3389/fmicb.2023.1227147/full#supplementary-material

References

Abedon, S. T. (1989). Selection for bacteriophage latent period length by bacterial density: a theoretical examination. *Microb. Ecol.* 18, 79–88. doi: 10.1007/BF02030117

Adriaenssens, E. M., Sullivan, M. B., Knezevic, P., van Zyl, L. J., Sarkar, B. L., Dutilh, B. E., et al. (2020). Taxonomy of prokaryotic viruses: 2018-2019 update from the ICTV bacterial and archaeal viruses subcommittee. *Arch. Virol.* 165, 1253–1260. doi: 10.1007/s00705-020-04577-8

Alves, D. R., Gaudion, A., Bean, J. E., Perez Esteban, P., Arnot, T., Harper, D. R., et al. (2014). Combined use of bacteriophage K and a novel bacteriophage to reduce *Staphylococcus aureus* biofilm formation. *Appl. Environ. Microb* 80, 6694–6703. doi: 10.1128/AEM.01789-14

Bankevich, A., Nurk, S., Antipov, D., Gurevich, A. A., Dvorkin, M., Kulikov, A. S., et al. (2012). SPAdes: a new genome assembly algorithm and its applications to single-cell sequencing. *J. Comput. Biol.* 19, 455–477. doi: 10.1089/cmb.2012.0021

Bao, H., Shahin, K., Zhang, Q., Zhang, H., Wang, Z., Zhou, Y., et al. (2019). Morphologic and genomic characterization of a broad host range *Salmonella enterica* serovar Pullorum lytic phage vB_SPuM_SP116. *Microb. Pathog.* 136:103659. doi: 10.1016/j.micpath.2019.103659

Blake, J. D., and Cohen, F. E. (2001). Pairwise sequence alignment below the twilight zone. *J. Mol. Biol.* 307, 721–735. doi: 10.1006/JMBI.2001.4495

Cao, F., Wang, X., Wang, L., Li, Z., Che, J., Wang, L., et al. (2015). Evaluation of the efficacy of a bacteriophage in the treatment of pneumonia induced by multidrug resistance *Klebsiella pneumoniae* in mice. *Biomed. Res. Int.* 2015:752930. doi: 10.1155/2015/752930

Cao, Y., Zhang, Y., Lan, W., and Sun, X. (2021). Characterization of vB_VpaP_MGD2, a newly isolated bacteriophage with biocontrol potential against multidrug-resistant *Vibrio parahaemolyticus*. *Arch. Virol.* 166, 413–426. doi: 10.1007/s00705-020-04887-x

Chaalal, N., Touati, A., Bakour, S., Aissa, M. A., Sotto, A., Lavigne, J., et al. (2020). Spread of OXA-48 and NDM-1-producing *Klebsiella pneumoniae* ST48 and ST101 in chicken meat in Western Algeria. *Microb. Drug Resist.* 27, 492–500. doi: 10.1089/mdr.2019.0419

Chen, J., Su, Z., Liu, Y., Wang, S., Dai, X., and Li, Y. (2009). Identification and characterization of class 1 integrons among *Pseudomonas aeruginosa* isolates from patients in Zhenjiang, China. *Int. J. Infec. Dis.* 13, 717–721. doi: 10.1016/j.ijid.2008.11.014

Cheng, F., Li, Z., Lan, S., Liu, W., Li, X., Zhou, Z., et al. (2018). Characterization of *Klebsiella pneumoniae* associated with cattle infections in Southwest China using multi-locus sequence typing (MLST), antibiotic resistance and virulence associated gene profile analysis. *Braz. J. Microbiol.* 49, 93–100. doi: 10.1016/j.bjm.2018.06.004

Chuang, Y., Fang, C., Lai, S., Chang, S., and Wang, J. (2006). Genetic determinants of capsular serotype K1 of *Klebsiella pneumoniae* causing primary pyogenic liver abscess. *J. Infect. Dis.* 193, 645–654. doi: 10.1086/499968

Coil, D., Jospin, G., and Darling, A. E. (2015). A5-miseq: an updated pipeline to assemble microbial genomes from Illumina MiSeq data. *Bioinformatics* 31, 587–589. doi: 10.1093/bioinformatics/btu661

Delcher, A. L., Salzberg, S. L., and Phillippy, A. M. (2003). Using MUMmer to identify similar regions in large sequence sets. *Curr. Protoc. Bioinformat.* Chapter 10:Unit 10.3. doi: 10.1002/0471250953.bi1003s00

Domingo-Calap, P., Georgel, P., and Bahram, S. (2016). Back to the future: bacteriophages as promising therapeutic tools. *HLA* 87, 133–140. doi: 10.1111/tan.12742

Eckstein, S., Stender, J., Mzoughi, S., Vogele, K., Kühn, J., Friese, D., et al. (2021). Isolation and characterization of lytic phage TUN1 specific for *Klebsiella pneumoniae* K64 clinical isolates from Tunisia. *BMC Microbiol.* 21:186. doi: 10.1186/s12866-021-02251-w

Feng, J., Gao, L., Li, L., Zhang, Z., Wu, C., Li, F., et al. (2021). Characterization and genome analysis of novel Klebsiella phage BUCT556A with lytic activity against carbapenemase-producing *Klebsiella pneumoniae*. *Virus Res.* 303:198506. doi: 10.1016/j.virusres.2021.198506

Ferreira, R. L., da Silva, B. C., Rezende, G. S., Nakamura-Silva, R., Pitondo-Silva, A., Campanini, E. B., et al. (2019). High prevalence of multidrug-resistant *Klebsiella pneumoniae* harboring several virulence and β-lactamase encoding genes in a Brazilian intensive care unit. *Front. Microbiol.* 9:3198. doi: 10.3389/fmicb.2018.03198

García-Anaya, M. C., Sepulveda, D. R., Sáenz-Mendoza, A. I., Rios-Velasco, C., Zamudio-Flores, P. B., and Acosta-Muñiz, C. H. (2020). Phages as biocontrol agents in dairy products. *Trends Food Sci. Tech.* 95, 10–20. doi: 10.1016/j.tifs.2019.10.006

Gröhn, Y. T., Wilson, D. J., González, R. N., Hertl, J. A., Schulte, H., Bennett, G., et al. (2004). Effect of pathogen-specific clinical mastitis on milk yield in dairy cows. *J. Dairy Sci.* 87, 3358–3374. doi: 10.3168/jds.S0022-0302(04)7 3472-4

Guo, Y., Zhou, H., Qin, L., Pang, Z., Qin, T., Ren, H., et al. (2016). Frequency, antimicrobial resistance and genetic diversity of *Klebsiella pneumoniae* in food samples. *PLoS One* 11:e0153561. doi: 10.1371/journal.pone.0153561

Hagens, S., and Loessner, M. J. (2007). Application of bacteriophages for detection and control of foodborne pathogens. *Appl. Microbiol. Biotechnol.* 76, 513–519. doi: 10.1007/s00253-007-1031-8

Hoang Minh, D., Hoang Minh, S., Honjoh, K. I., and Miyamoto, T. (2016). Isolation and biocontrol of Extended Spectrum Beta-Lactamase (ESBL)-producing *Escherichia coli* contamination in raw chicken meat by using lytic bacteriophages. *LWT Food Sci. Technol.* 71, 339–346. doi: 10.1016/j.lwt.2016.04.013

Huang, C., Virk, S. M., Shi, J., Zhou, Y., Willias, S. P., Morsy, M. K., et al. (2018). Isolation, characterization, and application of bacteriophage LPSE1 against *Salmonella enterica* in ready to eat (RTE) foods. *Front. Microbiol.* 9:1046. doi: 10.3389/fmicb.2018.01046

Islam, M. S., Yang, X. W., Euler, C. W., Han, X. Q., Liu, J. H., Hossen, I., et al. (2021). Application of a novel phage ZPAH7 for controlling multidrug-resistant *Aeromonas hydrophila* on lettuce and reducing biofilms. *Food Control* 122:107785. doi: 10.1016/j.foodcont.2020.107785

Kleinheinz, K. A., Joensen, K. G., and Larsen, M. V. (2014). Applying the ResFinder and VirulenceFinder web-services for easy identification of acquired antibiotic resistance and *E. coli* virulence genes in bacteriophage and prophage nucleotide sequences. *Bacteriophage* 4:e27943. doi: 10.4161/bact.27943

Koovapra, S., Bandyopadhyay, S., Das, G. K., Bhattacharyya, D., Banerjee, J., Mahanti, A., et al. (2016). Molecular signature of extended spectrum β-lactamase producing *Klebsiella pneumoniae* isolated from bovine milk in eastern and North-Eastern India. *Infect. Genet. Evol.* 44, 395–402. doi: 10.1016/j.meegid.2016.07.032

Kortright, K. E., Chan, B. K., Koff, J. L., and Turner, P. E. (2019). Phage therapy: a renewed approach to combat antibiotic-resistant bacteria. *Cell Host Microbe* 25, 219–232. doi: 10.1016/j.chom.2019.01.014

Kumar, R. R., Lee, J. T., and Cho, J. (2012). Fate, occurrence, and toxicity of veterinary antibiotics in environment. *J. Korean Soc. Appl. Biol. Chem.* 55, 701–709. doi: 10.1007/s13765-012-2220-4

Kumar, S., Stecher, G., Li, M., Knyaz, C., and Tamura, K. (2018). MEGA X: molecular evolutionary genetics analysis across computing platforms. *Mol. Biol. Evol.* 35, 1547–1549. doi: 10.1093/molbev/msy096

Li, P., Zhang, X., Xie, X., Tu, Z., Gu, J., and Zhang, A. (2020). Characterization and whole-genome sequencing of broad-host-range Salmonella specific bacteriophages for bio-control. *Microb. Pathog.* 143:104119. doi: 10.1016/j.micpath.2020.104119

Liu, H., Niu, Y. D., Meng, R., Wang, J., Li, J., Johnson, R. P., et al. (2015). Control of Escherichia coli O157 on beef at 37, 22 and 4°C by T5-, T1-, T4-and O1-like bacteriophages. *Food Microbiol.* 51, 69–73. doi: 10.1016/j. fm.2015.05.001

Machado, V. S., and Bicalho, R. C. (2018). Prepartum application of internal teat sealant or intramammary amoxicillin on dairy heifers: effect on udder health, survival, and performance. *J. Dairy Sci.* 101, 1388–1402. doi: 10.3168/jds.2017-13415

Nazir, A., Zhao, Y., Li, M., Manzoor, R., Tahir, R. A., Zhang, X., et al. (2020). Structural genomics of repA, repB1-carrying IncFIB family pA1705-qnrS, P911021- tetA, and P1642-tetA, multidrug-resistant plasmids from *Klebsiella pneumoniae*. *Infect. Drug Resist.* 13, 1889–1903. doi: 10.2147/IDR.S228704

Noor Mohammadi, T., Shen, C., Li, Y., Zayda, M. G., Sato, J., Masuda, Y., et al. (2021). Characterization of *Clostridium perfringens* bacteriophages and their application in chicken meat and milk. *Int. J. Food Microbiol.* 361:109446. doi: 10.1016/j.ijfoodmicro.2021.109446

Paczosa, M. K., and Mecsas, J. (2016). *Klebsiella pneumoniae*: going on the offense with a strong defense. *Microbiol. Mol. Biol. Rev.* 80, 629–661. doi: 10.1111/tbed.13787

Pan, Y. J., Lin, T. L., Chen, C. C., Tsai, Y. T., Cheng, Y. H., Chen, Y. Y., et al. (2017). Klebsiella phage ΦK64-1 encodes multiple depolymerases for multiple host capsular types. *J. Virol.* 91:e02457-16. doi: 10.1128/JVI.02457-16

Peng, Q., Fang, M., Liu, X., Zhang, C., Liu, Y., and Yuan, Y. (2020). Isolation and characterization of a novel phage for controlling multidrug-resistant *Klebsiella pneumoniae*. *Microorganisms* 8:542. doi: 10.3390/microorganisms8040542

Pertics, B. Z., Cox, A., Nyúl, A., Szamek, N., Kovács, T., and Schneider, G. (2021). Isolation and characterization of a novel lytic bacteriophage against the K2 capsule-expressing hypervirulent *Klebsiella pneumoniae* strain 52145, and identification of its functional depolymerase. *Microorganisms* 9:650. doi: 10.3390/microorganisms9030650

Soni, K. A., Desai, M., Oladunjoye, A., Skrobot, F., and Nannapaneni, R. (2012). Reduction of *listeria monocytogenes* in queso fresco cheese by a combination of listericidal and listeriostatic GRAS antimicrobials. *Int. J. Food Microbiol.* 155, 82–88. doi: 10.1016/j.ijfoodmicro.2012.01.010

Stothard, P., and Wishart, D. S. (2005). Circular genome visualization and exploration using CGView. *Bioinformatics* 21, 537–539. doi: 10.1093/bioinformatics/bti054

Sullivan, M. J., Petty, N. K., and Beatson, S. A. (2011). Easyfig: a genome comparison visualizer. *Bioinformatics* 27, 1009–1010. doi: 10.1093/bioinformatics/btr039

Veleba, M., Higgins, P. G., Gonzalez, G., Seifert, H., and Schneiders, T. (2012). Characterization of RarA, a novel AraC family multidrug resistance regulator in *Klebsiella pneumoniae*. *Antimicrob. Agents Chemother.* 56, 4450–4458. doi: 10.1128/AAC.00456-12

Walker, B. J., Abeel, T., Shea, T., Priest, M., Abouelliel, A., Sakthikumar, S., et al. (2014). Pilon: an integrated tool for comprehensive microbial variant detection and genome assembly improvement. *PLoS One* 9:e112963. doi: 10.1371/journal.pone.0112963

Wang, R., Cong, Y., Mi, Z., Fan, H., Shi, T., Liu, H., et al. (2019). Characterization and complete genome sequence analysis of phage GP4, a novel lytic Bcep22-like podovirus. *Arch. Virol.* 164, 2339–2343. doi: 10.1007/s00705-019-04309-7

Wittebole, X., De Roock, S., and Opal, S. M. (2014). A historical overview of bacteriophage therapy as an alternative to antibiotics for the treatment of bacterial pathogens. *Virulence* 5, 226–235. doi: 10.4161/viru.25991

Xu, Y., Liu, Y., Liu, Y., Pei, J., Yao, S., and Cheng, C. (2015). Bacteriophage therapy against Enterobacteriaceae. *Virol. Sin.* 30, 11–18. doi: 10.1007/s12250-014-3543-6

Yang, Y., Peng, Y., Jiang, J., Gong, Z., Zhu, H., Wang, K., et al. (2020). Isolation and characterization of multidrug-resistant *Klebsiella pneumoniae* from raw cow milk in Jiangsu and Shandong provinces, China. *Transbound. Emerg. Dis.* 68, 1033–1039. doi: 10.1111/tbed.13787

Young, R. (2014). Phage lysis: three steps, three choices, one outcome. *J. Microbiol.* 52, 243–258. doi: 10.1007/s12275-014-4087-z

Yuan, Y., Gao, M., Wu, D., Liu, P., and Wu, Y. (2012). Genome characteristics of a novel phage from *Bacillus thuringiensis* showing high similarity with phage from *Bacillus cereus*. *PLoS One* 7:e37557. doi: 10.1371/journal.pone.0037557

Yuan, Y., Peng, Q., Wu, D., Kou, Z., Wu, Y., Liu, P., et al. (2015). Effects of actin-like proteins encoded by two *Bacillus pumilus* phages on unstable lysogeny, revealed by genomic analysis. *Appl. Environ. Microbiol.* 81, 339–350. doi: 10.1016/j.micpath.2019.103659

Zhang, C., Yuan, J., Guo, C., Ge, C., Wang, X., Wei, D., et al. (2021). Identification and complete genome of lytic "Kp34likevirus" phage vB_KpnP_Bp5 and therapeutic potency in the treatment of lethal *Klebsiella pneumoniae* infections in mice. *Virus Res.* 297:198348. doi: 10.1016/j.virusres.2021.198348

frontiers | Frontiers in Microbiology

TYPE Original Research
PUBLISHED 14 September 2023
DOI 10.3389/fmicb.2023.1251211

OPEN ACCESS

EDITED BY
Alicja Wegrzyn,
Polish Academy of Sciences, Poland

REVIEWED BY
Steven Batinovic,
Yokohama National University, Japan
Ahmed Askora,
Zagazig University, Egypt

*CORRESPONDENCE
Yunlin Wei
✉ homework18@126.com

RECEIVED 01 July 2023
ACCEPTED 21 August 2023
PUBLISHED 14 September 2023

CITATION
Zou H, Ding Y, Shang J, Ma C, Li J, Yang Y, Cui X, Zhang J, Ji G and Wei Y (2023) Isolation, characterization, and genomic analysis of a novel bacteriophage MA9V-1 infecting *Chryseobacterium indologenes*: a pathogen of *Panax notoginseng* root rot.
Front. Microbiol. 14:1251211.
doi: 10.3389/fmicb.2023.1251211

Isolation, characterization, and genomic analysis of a novel bacteriophage MA9V-1 infecting *Chryseobacterium indologenes*: a pathogen of *Panax notoginseng* root rot

He Zou[1], Yafang Ding[1], Junjie Shang[1], Chunlan Ma[1], Jinhua Li[1], Ye Yang[2], Xiuming Cui[2], Jinhao Zhang[3], Guanghai Ji[3] and Yunlin Wei[1,2]*

[1]Faculty of Life Science and Technology, Kunming University of Science and Technology, Kunming, Yunnan, China, [2]Key Laboratory of Sustainable Development and Utilization of Panax notoginseng Resources in Yunnan Province, Faculty of Life Science and Technology, Kunming University of Science and Technology, Kunming, Yunnan, China, [3]State Key Laboratory for Conservation and Utilization of Bio-resources in Yunnan, Yunnan Agricultural University, Kunming, Yunnan, China

Chryseobacterium indologenes is one of the primary causative agents of root rot of *Panax notoginseng*, which significantly affected plant growth and caused economic losses. With the increasing incidence of antibiotic-resistant bacterial phytopathogens, phage therapy has been garnered renewed attention in treating pathogenic bacteria. However, the therapeutic potential of phage therapy on root rot of *P. notoginseng* has not been evaluated. In this study, we isolated a novel lytic phage MA9V-1 infecting *C. indologenes* MA9 from sewage and monitored the formation of clear and round plaques with a diameter of approximately 0.5–1.5 mm. Phage MA9V-1 exhibited rapid absorption (>75% in 8 min), a latency period of 20 min, and a burst size of 10 particles per cell. Transmission electron microscopy indicated that the phage MA9V-1 is a new myovirus hosting *C. indologenes* MA9. Sequencing of phage genomes revealed that phage MA9V-1 contained a linear double-stranded DNA genome of 213,507 bp with 263 predicted open reading frames, including phage structure, host lysing, and DNA polymerase/helicase but no genes of tRNA, virulence, and antibiotic resistance. Our proteomic tree and genomic analysis revealed that phage MA9V-1 shares identity with *Sphingomonas* phage PAU and *Tenacibaculum* phage PTm1; however, they also showed apparent differences. Further systemic evaluation using phage therapy experiments on *P. notoginseng* suggested that phage MA9V-1 can be a potential candidate for effectively controlling *C. indologenes* MA9 infection. Thus, we have presented a novel approach to solving root rot in *P. notoginseng*.

KEYWORDS

***Panax notoginseng*, *Chryseobacterium indologenes*, root-rot, genome analysis, myovirus, phage therapy**

1. Introduction

Panax notoginseng (Sanqi) is a famous traditional Chinese herb belonging to the family of Acanthopanax and is predominantly grown in Wenshan, Yunnan Province, China (Zhang et al., 2020a). *P. notoginseng* has become one of the most important crops in Yunnan Province owing to its unique medicinal efficacy and economic value and has been cultivated in China for over 400 years (Guo et al., 2010; Fan et al., 2016). The active pharmaceutical ingredients of *P. notoginseng* include saponins, brass, and polysaccharides. This herb has been characterized to have antitumor and antioxidant properties and has traditionally been used in treating cardiovascular diseases such as coronary heart disease (Yang et al., 2014; Xu et al., 2019). Similar to *P. ginseng*, the roots of *P. notoginseng* have been used as the raw material for over 400 medicinal products, such as Xuesaitong capsules, Yunnan Baiyao, and pain relieving powder (Yang et al., 2013). With the increasing demand for *P. notoginseng* products and the rapid development of modern Chinese medicine, there has been increased attention to *P. notoginseng*. However, *P. notoginseng* yield has been severely affected owing to replanting soils, long growth cycles, and various diseases, resulting in a significant reduction in harvest (Tan et al., 2017).

Approximately 70% of medicinal plants have the problem of continuous cropping obstacles, which were caused by varying degrees of phytopathogen infection (Zhao et al., 2016). Among them, root rot disease (RRD) is the most destructive soil-borne disease and is difficult to control using chemical pesticides or field management. One of the primary reasons hindering its eradication is the complexity of interaction between different pathogens, including bacteria, fungi, and parasitic nematodes (Jiang et al., 2011). Continuous cropping for *P. notoginseng* will increase root rot incidence, resulting in a 5%–20% average loss of yield, which may rise to over 70% in unfavorable situations and even with no harvest (Dong et al., 2016). Currently, most research studies on root rot disease have focused on aspects such as screening of antifungal pathogens (Li et al., 2022), the function of endophytic fungi (Zheng et al., 2017), and analysis of fungal community composition in soil (Wang et al., 2021). However, these studies have not yet been able to completely solve or alleviate *P. notoginseng* root rot. Notably, there are very few reports on the bacterial pathogens that infect *P. notoginseng* to date.

Zheng et al. (2022) isolated a bacterium *Stenotrophomonas maltophilia* that is capable of causing *P. notoginseng* root rot from rotten root samples. Similarly, *Chryseobacterium indologenes*, with yellow-orange colony, slightly viscous, and translucent, are aerobic, non-fermenting, catalase-positive gram-negative bacilli. It is known as rare human conditional pathogenic bacteria but rarely reported as a plant pathogen (Aykac et al., 2016). Until 2020, the team of Professor Ji isolated a strain *C. indologenes* MA9 that can also infect and result in *P. notoginseng* root rot, which was the first report indicating *C. indologenes MA9* as a plant pathogen to infect *P. notoginseng* in China (Zhang et al., 2020b). Currently, solutions to bacterial pathogens rely mainly on pesticides (Yang Y. et al., 2022) and antibiotics (Xie et al., 2018), which cause irreversible environmental pollution. Therefore, there is an urgent need for better methods to control these causative agents to improve crop yields and reduce economic losses.

Bacteriophages (phage) are the most abundant biological organisms on the earth and can be classified as lytic and lysogenic phages according to their living habits, which are crucial to maintaining the ecosystem balance (Din et al., 2016). Phages with the ability of high specificity to their hosts are considered an alternative solution to the crisis of antibiotic abuse and thus have been arisen much interests in many industries, especially in the agriculture. For example, RsoM1USA, a strain of *Ralstonia* phage screened from tomato fields in Florida, is a new species of *P2virus*, which can effectively slow down leaf wilting of tomato plants infected with *Ralstonia* when used with a multiplicity of infection (MOI) of 0.01 (Addy et al., 2019). Similarly, phage PHB09 against the plant pathogen *Pseudomonas syringae* pv. *actinidiae* causing kiwifruit bacterial canker exhibited a strong ability to kill host cells both *in vitro* and *in vivo*, which is expected to be a potential biocontrol agent in reduction of crop economic loss (Liu et al., 2021). In addition, a combination of various phages infecting the same host cell was used to prepare a phage cocktail that successfully and effectively suppressed the brown blotch disease of oyster mushrooms by killing the pathogen *Pseudomonas tolaasii* (Yun et al., 2022). However, the applicability of phage therapy on root rot of *P. notoginseng* has not been reported previously in China, and its therapeutic potential on root rot has not been evaluated.

In this study, we isolated and characterized the first *C. indologenes*-infecting phage MA9V-1 from sewage samples. We also compared the whole genome of phage MA9V-1 with others, determined that it is a new virus targeting *C. indologenes*, and evaluated its efficacy in preventing *P. notoginseng* root rot to provide a novel approach to solve this major challenge.

2. Materials and methods

2.1. Bacterial strain and growth conditions

C. indologenes strain MA9 (accession no. CP075170), isolated from rotten roots of *P. notoginseng*, was provided by professor Ji of Yunnan Agricultural University and was used as a host in this study. Samples for screening phages were collected from different regions as follows: (1) The rhizospheric soils of healthy and rotten *P. notoginseng* were collected from Pingyuan Street, Yanshan County, Wenshan Prefecture, Yunnan Province in November 2020; (2) the rotten roots of *P. notoginseng* and *P. notoginseng* root soils were collected from Shilin Yi Autonomous Region, Kunming City, Yunnan Province in January 2021; (3) the soils of different vegetables and fruit trees were collected from the farmland near Kunming University of Science and Technology, Chenggong District, Kunming City, Yunnan Province in January 2021; and (4) tewage samples were collected from the First People's Hospital of Yunnan Province in February 2021. *C. indologenes* MA9 was cultured in an optimized nutrient agar (NA) medium (10 g peptone, 5 g sodium chloride, and 3 g beef extract) at 160 rpm at 28°C.

2.2. Isolation, purification, and propagation of phages

First, we tried to isolate phages from the rhizospheric soil mixtures of healthy and decayed *P. notoginseng* infected with *C. indologenes* MA9; however, we could not find any phage. Subsequently, under the same culture conditions, we attempted to use other samples such as

rotten roots, *P. notoginseng* root soils, and soils of various fruits and vegetables. However, the targeted phage was also not found. Finally, we isolated a *C. indologenes* strain MA9 phage from sewage samples of the First People's Hospital of Yunnan Province, China, using the virus enrichment and double-layer agar plate methods (Pajunen et al., 2000). In brief, samples for phage isolation were filtered through a 0.22-μm filter; then 50 mL filtrate was added to a 250 mL conical flask containing 50 mL SM buffer (100 mM NaCl, 10 mM $MgSO_4$, 50 mM Tris–HCl at pH 7.5, and 0.01% gelatin) and kept static for 12 h. Subsequently, 40 mL suspension, 30 mL of SM buffer, 25 mL of NA liquid medium, and 2 mL of *C. indologenes* MA9 cultures were mixed and incubated overnight on a horizontal rotary shaker (160 rpm) at 28°C. The mixture was transferred to a sterile 50 mL centrifuge tube and centrifuged at 15,000 × g for 15 min at 4°C. Subsequently, the supernatant was filtered with 0.22-μm microporous membranes. In total, 5 mL filtrate was taken and mixed with 50 mL *C. indologenes* MA9 host cell cultures during the period of exponential growth phase [optical density at 600 nm (OD_{600}) =0.6–0.8] and then repeated 2–3 times to enrich phage MA9V-1. Successively, 200 μL of phage stock was serially diluted with SM buffer, and different dilutions were mixed with 300 μL of *C. indologenes* MA9, which were added to 4.5 mL semi-solid NA medium after being incubated at 28°C for 20 min, and finally, the solution was finally poured onto the surface of the NA solid medium. A single clear plaque was picked from NA double-layer agar plate incubated overnight at 28° C, placed into 1 mL of SM buffer, and vortexed vigorously before filtering through a 0.22-μm membrane. The above steps were repeated 2–3 times to obtain pure phage MA9V-1 particles, and the phage MA9V-1 titer was measured to be 10^9 PFU/ml by the double-layer agar plate method. The isolates were stored at 4°C.

2.3. Designing the optimal multiplicity of infection

The optimal multiplicity of infection (MOI) is the ratio of phages to bacteria at the time of infection. The experimental method followed was according to the study mentioned in the reference (Sun et al., 2022). In brief, the CFU/ml of the host cell at the exponential growth phase was counted through the dilution coating method with serial dilutions of 10^{-4}, 10^{-5}, and 10^{-6}. Phage stock of known titer and host cells at the exponential stage were mixed with a gradient of MOI ranging from 0.001 to 10 and cultured in a shaker (180 rpm/min) at 28°C for 12 h. The enrichment was centrifuged at 15,000 × g at 4°C for 15 min and filtered through a 0.22-μm filter membrane, and the phage titer was determined by the double-layer agar plate method with three replicates.

2.4. Phage adsorption assay

Adsorption rate, a value of phage particles adsorbed to the host cell at a particular time, was determined with minor modifications, as previously described (Sasikala and Srinivasan, 2016). In brief, 9 mL of *C. indologenes* MA9 cultures with absorbance of OD_{600} at 0.6–0.8 was infected with 1 mL phage dilution (10^6 PFU/ml) at multiplicity of infection of 0.01 and transferred to a sterile 50 mL conical flask to incubate at 28°C. Approximately 100 μL of culture was taken out at 4-min intervals (0, 4, 8, 12, 16, and 20 min) and added to sterile 2 mL tubes with 1.9 mL of pre-cooled NA medium, vortexed for 10–15 s, and then centrifuged at 15000 × g at 4°C for 15 min, to remove the cell-phage complexes. The titer of free phage in the supernatant was determined by the double-layer overlay method and was repeated three times (Stuer-Lauridsen et al., 2003).

2.5. One-step growth curve

To determine the parameters of the one-step growth curve, the protocol, as described earlier, was adopted (Wu et al., 2007) and modified according to the characteristics of the phage. *C. indologenes* MA9 was cultured up to the exponential growth phase (10^8 CFU/mL), and 10 mL of culture was collected by centrifugation (11,000 × g, 8 min, 4°C) for harvesting, and the precipitate was resuspended with 2 mL of fresh NA liquid medium. Phage was added to the suspension at MOI = 0.01 and incubated at 28°C for 15 min without shaking. The mixture was, then, centrifuged at 11,000 × g for 8 min to remove the free phage particles, and the pellet was suspended with fresh NA medium to culture in a shaker at 180 rpm at 28°C after washed twice with 10 mL nutrient agar medium. In total, 200 μL of culture was taken out every 10 min until 130 min and mixed with 800 μL SM buffer. Finally, the mixture was centrifuged at 15,000 × g for 3 min at 4°C. The titers of the samples were immediately measured by the double-layer agar method. The burst size was calculated according to the following definition: Burst size is the ratio between the number of phage particles at the end of lysis and the number of the host cells at the beginning of the infection (Li et al., 2021). All assays were repeated in three independent experiments.

2.6. Thermal and pH stability

For determining the thermal and pH stability of phage MA9V-1, the experimental protocol was performed as proposed with slight modification (Sasikala and Srinivasan, 2016; Sun et al., 2022). In brief, 1 mL phage MA9V-1 lysate (10^{10} PFU/m) was treated under different temperatures from 30 to75°C at 5°C intervals for 1 h. Then, these treated samples checked the survival rate of phage MA9V-1 using the double-layer agar assay. Similarly, 100 μL of phage stock (10^{10} PFU/ml) was added to 900 μL different buffers of pH ranging from 3 to11 (component of citrate sodium, potassium dihydrogen phosphate, Tris–HCl, and sodium carbonate) for incubation of 1 h at 30°C. After treatment, the titer of phage MA9V-1 was evaluated using the same procedure. All assays were performed in triplicate.

2.7. Phage host range

The host range of *Chryseobacterium* phage MA9V-1 was tested against 11 different bacterial strains using the standard spot testing assay, including *Chryseobacterium indologenes* ($n = 7$), *Bacillus cereus* ($n = 1$), *Pseudomonas syringae* ($n = 1$), and *Escherichia coli* ($n = 1$), of which *Chryseobacterium indologenes* ATCC 29897, *Pseudomonas syringae* CGMCC 1.3070, and *Escherichia coli* ATCC 11303 were type strains purchased from Strain Preservation Center, while the others were isolates. Each 300 μL of bacterial cells was mixed with 200 μL of

10-fold series gradient dilutions (10^{-1}–10^{-7}) of phage MA9V-1 suspension (10^{10} PFU/ml), then adding all mixtures to 4.5 mL semi-solid medium before pouring into the surface of double-layer agar plates, respectively, and incubated at 28°C overnight in triplicate.

2.8. Transmission electron microscopy

The morphology and structure of pure phage particles were visualized using transmission electron microscopy (TEM). The phage particles purified with the density gradient centrifugation method were loaded on a carbon-coated copper grid to adsorb for 10 min, followed by negative staining with 1% phosphotungstic acid. The stained phage MA9V-1 was observed using transmission electron microscopy (Hitachi HT7820) at 120 kV (Johnson et al., 2011).

2.9. Phage DNA extraction, sequencing, and bioinformatics analysis

To improve the purity of the phage genome, 2.5 μL DNase I (1 U/μl) and 0.5 μL RNase A (1 mg/mL) were added to 500 μL phage stock to remove the host cell nucleic acid, and further experimental operation was performed using the phenol–chloroform protocol, as previously described in the study mentioned in the reference (Chen et al., 2019). Nucleic acid concentration of phage was determined by NanoDrop (Shanghai Baoyude Scientific Instruments Co., Ltd., BIO-DL, Shanghai) and imaged by 1% agarose gel electrophoresis. Sequencing of the phage genome was performed by the Illumina_Novaseq_PE150 platform (Shenzhen Huada Intelligent Manufacturing Technology Co., Ltd., Illumina, Shenzhen). First, phage genome was randomly broken into approximately 300–500 bp fragments using the Covaris M220 (Shanghai Tusen Vision Technology Co., Ltd., Shanghai, China) DNA fragmentation instrument, discarding adapters and trimming sequences with a length of less than 50 bp. Then, using the BBMap version 38.51 (Roy and Chanfreau, 2020),[1] comparisons were performed with the existing NCBI database to sift out the corresponding rRNA, host, and other bacterial genome sequences, to purify the phage genome. The assembly of clean reads was performed using the "*De novo* assembly" option of SPAdes v3.5.0 software (Prjibelski et al., 2020).[2] Subsequently, contigs assembled with reads were comparatively analyzed with BLAST (v2.10.0+)[3] (Camacho et al., 2009) to virus-NT, NCBI nt, and viral RefSeq databases to match the most similar gene reference sequences. Finally, the assembled phage MA9V-1 genome was annotated using Proksee (Grant and Stothard, 2008).[4] Functional protein bioinformatic annotation of ORFs was predicted manually using HHpred (Soding et al., 2005).[5] The virulence-associated and antibiotic resistance gene potentially existing in the phage MA9V-1 genome was analyzed through the virulence factor database (Liu et al., 2019)[6] and the comprehensive antimicrobial research database.[7] The presence of transfer RNA genes was assessed using tRNAscan-SE (Lowe and Chan, 2016).[8] The phage MA9V-1 genomic data were aligned by Clustalw v2.1 (Peng et al., 2022)[9] and analyzed using the visualization bioinformatics software Easyfig v2.2 (Peng et al., 2022).[10] MEGA v11 (Tamura et al., 2021)[11] was used to construct a phylogenetic tree for determining phylogenetic relationships between phage MA9V-1 and other strains. Furthermore, phage proteome phylogenetic tree was constructed by viral proteomic tree (ViPTree) server v1.9 (Nishimura et al., 2017).[12]

2.10. Characterization of phage structural proteins

Approximately 7 mL of phage particle suspension with titer of 10^9 PFU/ml purified by the polyethylene glycol (PEG) precipitation method was ultracentrifuged with CsCl density gradient centrifugation (HIMAC CP-100WX Ultracentrifuge, HITACHI, Japan) at 4°C at 150,000 × g for 8 h and extracted the separated layer of phage with a sterilized syringe. Then, 20 μL of ultra-purified phage particles was mixed with 2× SDS loading buffer, heated in boiling water for 15 min, and subjected to SDS-PAGE [12% (w/v) polyacrylamide] (Uchiyama et al., 2014).

2.11. Virulence assay in *P. notoginseng*

The experimental material was the root of a healthy 2-year-old *P. notoginseng* plant collected from Shilin Yi Autonomous Region, Kunming City, Yunnan Province. After a series of pre-treatments, the slices of *P. notoginseng* root were placed onto a plate covered with wetted filter paper. In total, 1 mL of 24-h cultures of *C. indologenes* strain MA9 was transferred to a 50 mL conical flask and grown at 28°C with shaking until the culture reached the OD_{600} of 0.6–0.8. Phage MA9V-1 and *C. indologenes* MA9 were mixed with optimal multiplicity of infection (MOI) of 0.001, 0.01, 0.1, 1, and 10, respectively, and incubated at 28°C for 10 min. In total, 100 μL of different MOI mixtures were was added to the root slices, sealed with tape, and cultured in an incubator at 26°C. This experiment was divided into seven groups with eight parallels in each group. Among them, the negative control was the *C. indologenes* MA9 reaching the exponential stage, whereas the positive control was the inactivated *C. indologenes* MA9 at the log phase after treating with the autoclave sterilization method. Under the same experimental condition, 100 μL of the mixture of different MOI was added to the experimental group at 24-h intervals, the negative control and positive control were added to the equal volume of treatment liquid, and the number of infected and uninfected *P. notoginseng* plants was counted after 7 days. In this study, one condition for determining root rot was the rotting and softening of the root interior. The disease incidence was calculated as

1 https://sourceforge.net/projects/bbmap/
2 https://github.com/ablab/spades
3 https://github.com/enormandeau/ncbi_blast_tutorial
4 https://proksee.ca/
5 https://toolkit.tuebingen.mpg.de/tools/hhpred
6 https://www.mgc.ac.cn/VFs/
7 https://card.mcmaster.ca/
8 https://trna.ucsc.edu/tRNAscan-SE/
9 https://www.clustal.org/download/current/
10 https://mybiosoftware.com/easyfig-genome-comparison-visualizer.html
11 https://www.megasoftware.net/
12 https://www.genome.jp/viptree/

the percentage of rotten roots to the total number of parallel experiments. The experiment was performed in triplicate.

3. Results

3.1. Morphology of phage MA9V-1

To the best of our knowledge, phage MA9V-1 (formal name: vB_CinP_MA9V-1) of the *C. indologenes* strain MA9 is the first phage to have bacteriolytic activity against *C. indologenes* MA9. The results suggested that the phage MA9V-1 can form clear and round plaques with a diameter of approximately 0.5–1.5 mm on lawns of *C. indologenes* MA9 of the double-layered plate (Figure 1A). The morphological characteristics of phage MA9V-1 (Figure 1B) revealed that it has an icositetrahedron-coated protein "head" with a diameter of approximately 121.26 nm and a contractible tail length of approximately 170.34 nm with a width of approximately 44.62 nm. In addition, it also has a relatively short "neck" compared with other myoviruses such as *Ralstonia* phage RsoM1USA, a novel species of *P2virus* (Addy et al., 2019).

3.2. Biological characteristics of phage MA9V-1

As shown in Figure 2A, phage MA9V-1 had the highest titer and was 1.25×10^{10} PFU/ml at an MOI of 0.001. The absorption curve revealed that phage MA9V-1 was capable of rapidly adsorbing onto the surface of the host cell membrane. Within 8 min, >75% of the phage particles had adsorbed, and after 12 min, approximately 90% were adsorbed, indicating that phage MA9V-1 had the ability of high adsorption efficiency (Figure 2B). The latent period, rise period, and burst size are three critical parameters to characterize the phage lifecycle; the results of the one-step growth curve suggested that these values are 20 min, 90 min, and 10 PFU/cell, respectively (Figure 2C). In the thermal stability experiment, Figure 2D shows that the temperature between 30°C and 50°C had no negative effect on phage MA9V-1 after a 1-h incubation. Even at 55°C and 60°C, the phage MA9V-1 also has the ability to infect *C. indologenes* MA9, but its viability is decreased to approximately 85 and 40% at 30°C, respectively. The infectivity of phage MA9V-1 was completely lost at 65°C and subsequent temperature of 70 and 75°C. Meanwhile, phage MA9V-1 had nearly no obvious variation by treating under different pH levels at 5 to 8 but showed strong sensitivity under extreme pH conditions and will be inactivated to no infectivity (Figure 2E). In addition, of 11 different bacterial cells examined, only 3 *C. indologenes* strains were found to be sensitive to the phage MA9V-1, namely *Chryseobacterium indologenes* MA9, *Chryseobacterium indologenes* 02, and *Chryseobacterium indologenes* 06, respectively (Table 1). When *Chryseobacterium indologenes* MA9 was considered as the host strain, phage MA9V-1 had the highest titer approximately two times than others.

3.3. Genomic features of phage MA9V-1

Phage genomic analysis is crucial to determine the specific functional proteins in the genome and the safety of phage application. The results showed that the genome sequence of phage MA9V-1, a linear double-stranded DNA (dsDNA), was 213,507 bp in length and contained 35.99% of G + C content (Figure 3). The phage MA9V-1 genome contained 263 putative open reading frames (ORFs); among them, 257 and 6 ORFs were identified in the forward and reverse strands, respectively (Table 2). The lengths of the longest and shortest ORF gene sequences were 7,122 bp and 90 bp, encoding one hypothetical protein with 2,374 amino acids and one hypothetical protein with 30 amino acids, respectively. According to the BLAST results, 39 ORFs had homologs to genes encoding known functional proteins, and 14 of these clustered into 3 modules related to aspects such as phage structure, host lysing, and DNA replication, and the remaining 25 genes encoded other biofunctional proteins. The absence of integrase in the genome indicated that phage MA9V-1 was a virulent phage targeting *C. indologenes* MA9 not a lysogenic phage. In addition, concerned tRNA gene, lysogenic gene, drug resistance gene, and virulent genes were not found in the phage MA9V-1 genome,

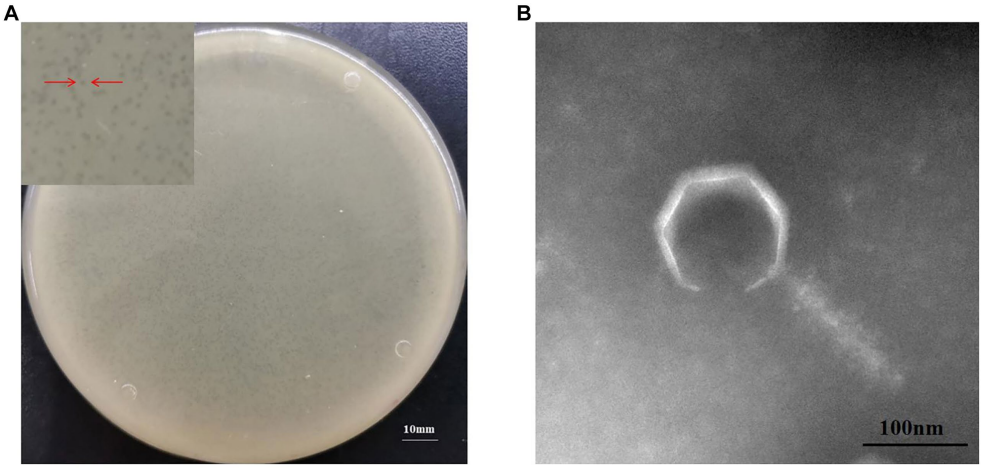

FIGURE 1
Morphological characteristics of *Chryseobacterium indologenes* phage MA9V-1. **(A)** Phage plaque morphology of phage MA9V-1 on an NA double-layer agar plate and **(B)** TEM image of phage MA9V-1.

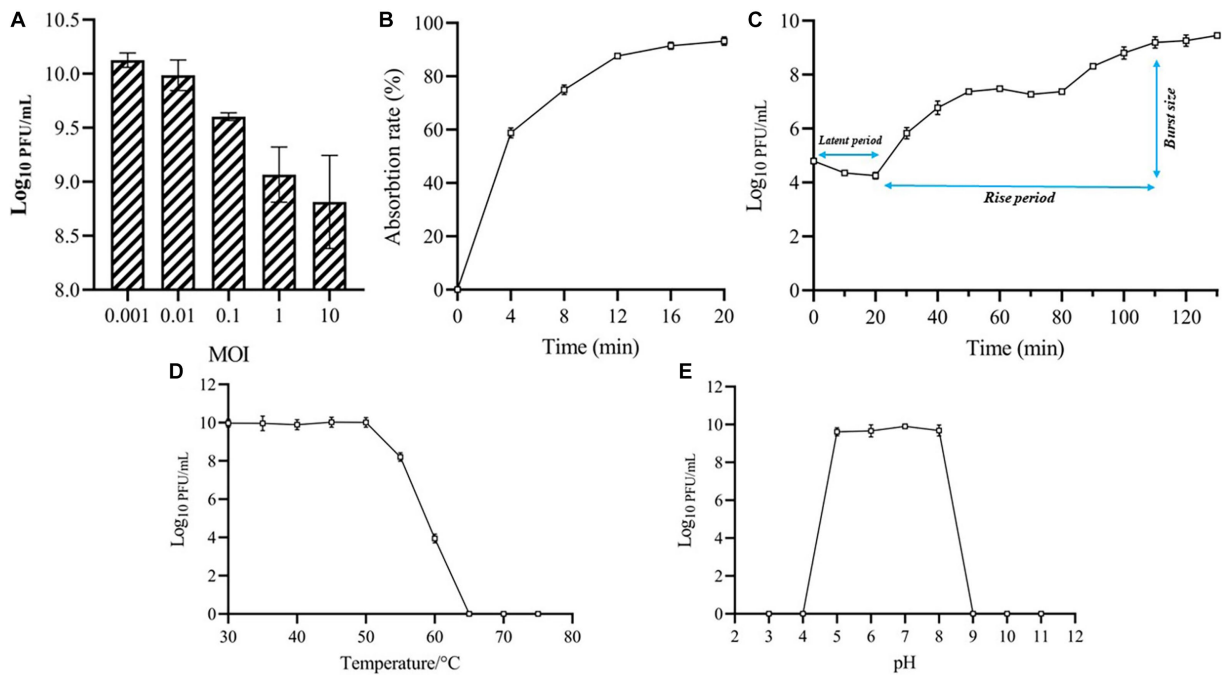

FIGURE 2
Biological features of phage MA9V-1. **(A)** Titers at different MOIs; **(B)** Adsorption curve; **(C)** One-step growth curve; **(D)** Thermal stability analysis; **(E)** pH stability analysis.

TABLE 1 Host ranges of phage MA9V-1.

Strain	Lytic activity
Chryseobacterium indologenes MA9 (primary host)	++
Chryseobacterium indologenes 01	–
Chryseobacterium indologenes 02	+
Chryseobacterium indologenes 03	–
Chryseobacterium indologenes 04	–
Chryseobacterium indologenes 05	–
Chryseobacterium indologenes 06	+
Chryseobacterium indologenes ATCC 29897	–
Bacillus cereus MYB41-22	–
Pseudomonas syringae CGMCC 1.3070	–
Escherichia coli ATCC 11303	–

"++": phage was efficient to infect host; "+": phage was little efficient to infect host; "–": phage was not to infect hot.

indicating that the phage MA9V-1 depended on host translation and satisfied several recommended criteria for safe usage in the prevention and control of *C. indologenes* MA9 (Bruessow, 2012; Han et al., 2017).

3.4. Proteomic tree and comparative genomic analysis

The phage MA9V-1 proteome is comprehensively analyzed through the ViPtree database and selected related genomes, which contain 2,201 virus families and 4,782 host groups. As shown in Figure 4A, a circular proteomic tree of phage MA9V-1 showed that its genome is located in the "others" gray module whatever for "virus family" or "host group." In addition, we constructed a rectangular proteomic tree (Figure 4B), consists of 11 myovirus genomes, which revealed that the phage MA9V-1 was related to *Sphingomonas* phage PAU (accession no.NC_019521) and was branched together with *Tenacibaculum* phage PTm1 (accession no.NC_049340) and *Tenacibaculum* phage PT24 (accession no.NC_049383) (White and Suttle, 2013; Kawato et al., 2020). Moreover, comparative genomic analysis was performed with genome of phage MA9V-1 and other three similar phages to analyze genomic evolutionary relationship (Figure 4C). The result indicated that MA9V-1 was more closely related to PAU than others, showing a similar region between them mainly located in 7,970–40,762 nt and 172,015–200,768 nt region of MA9V-1 genome with a low similarity (< 50% in most regions), whereas other regions share no similarity with PAU (see Figure 4).

3.5. SDS-PAGE analysis of phage MA9V-1

Structural protein expression analysis of purified phage particles by SDS-PAGE gel electrophoresis showed at least 15 bands of protein molecular weight ranging from 20 to 260 kDa. The protein bands were mainly distributed in 75–135, 45–65, and 25–35 kDa regions of SDS-PAGE gel, which were likely related to structural proteins, terminal family proteins, DNA replication proteins, and hypothetical proteins. According to SDS-PAGE results, we only obtained limited knowledge, and whole-genome analysis of phage MA9V-1 was required to better elucidate the role of all proteins (Lu and Breidt, 2015).

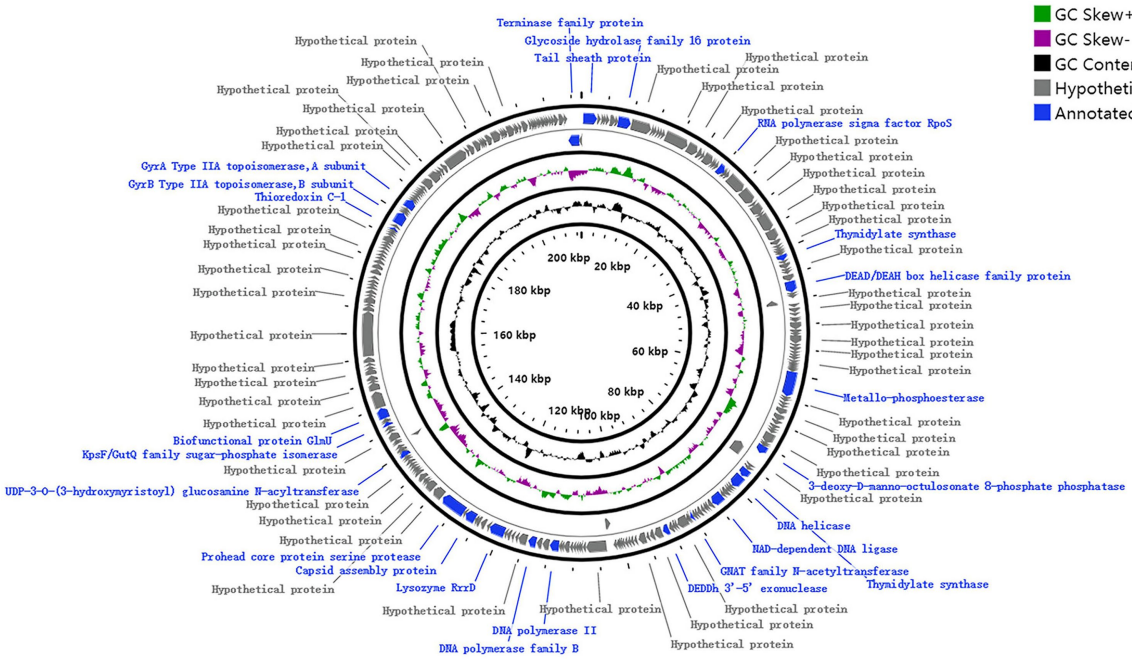

FIGURE 3
Whole-genome map of phage MA9V-1.

3.6. Phylogenetic relationships of phage MA9V-1

Based on the results of the proteomic tree, we constructed a phylogenetic tree analysis with four representative proteins and aimed to accurately validate the taxonomic classification of phage MA9V-1. Phylogenetic relationships were analyzed among phage MA9V-1 and other 15 members based on the amino acid sequences of four highly conserved proteins, namely terminase family protein (ORF262), DNA polymerase II (ORF135), capsid assembly protein (ORF149), and phage tail sheath protein (ORF001), respectively (Figure 6). The results are presented in Figures 6A,B,D. Phage MA9V-1 was more closely related to *Sphingomonas* phage PAU taking as "tree root" than others and grouped into a clade of an independent branch. Similar tree was also obtained using the deduced amino acid sequences of capsid assembly protein ORF149; we can observe that phage MA9V-1 was branched with *Tenacibaculum* phage pT24, which shared the similar results with above three proteins (Figure 6C). Taken together, phage MA9V-1 is similar to *Sphingomonas* phage PAU, *Tenacibaculum* phage PTm1, and *Tenacibaculum* phage pT24, but there is low identity between them, which was consistent with the conclusion of the proteomic tree analysis, indicating that it is a novel phage against *C. indologenes* MA9. According to the latest guidelines of the International Committee on Classification of Viruses (ICTV),[13] in March 2021 (Turner et al., 2021), we only concluded that phage MA9V-1 is a new myovirus.

3.7. Efficiency of MA9V-1 in phage therapy of *P. notoginseng*

To investigate the growth inhibitory effect of phage MA9V-1 on the host strain, *C. indologenes* MA9, we first determined the absorbance value at OD_{600} of *C. indologenes* MA9 with and without phage MA9V-1 for 13 h (Figure 7A). In the absence of phage MA9V-1 (MOI = 0), the bacteria reached a stable phase after 8 h of culture, showing a standard "S" growth curve. After adding different titers of phage MA9V-1 into *C. indologenes* MA9 cultures, as shown in Figure 7A, the curve at MOI of 0.001 and 0.01 was not significantly inhibited, until 5 h; the curve showed a downward trend and then regrew relatively rapidly. While using an MOI of 10, an opposite phenomenon to the earlier situation was observed, wherein the bacterial growth sharply reduced and then regrew slowly for 9 h. Meanwhile, the remaining MOIs inhibited the growth for 10 h. Overall, after treatment with phage MA9V-1 at different MOIs, the growth of *C. indologenes* MA9 could be inhibited. Therefore, we took advantage of phage therapy experiments to roughly estimate the therapeutic effectiveness of phage MA9V-1 on *P. notoginseng* root slice infected with *C. indologenes* MA9 for practical purposes (Figure 7B). Among them, the enlargement picture of second sample of MOI = 0.01 and fifth sample of MOI = 10 more intuitively reflects the difference between healthy and rotten samples (Supplementary Figure S1). According to the results shown in Figure 7C, we can observe that exceeded 85% of the root samples of *P. notoginseng* had been rotted in the negative control, which verified the strong pathogenicity of *C. indologenes* MA9. While all groups treated with phage MA9V-1 at different MOIs had samples with only slight or even no symptoms, especially at MOIs of 0.1 and 1, both of them decreased

13 https://ictv.global/

TABLE 2 Annotated ORFs in the genome of phage MA9V-1.

ORFs	Strand	Start	Stop	Length	Function	Best-match	*E*-values	Per. ident	GenBank accession. no
ORF1	+	276	2,453	2,178	Phage tail sheath protein	*Tenacibaculum phage PTm1*	5e-38	31.95%	YP_009873700.1
ORF8	+	5,806	7,887	2082	Glycoside hydrolase family 16 protein	*Chryseobacterium aquifrigidense*	0.0	80.27%	WP_142018695.1
ORF16	+	17,616	19,355	1840	Short tail fiber protein	*Tenacibaculum phage pT24*	6e-18	25.67%	YP_009876786.1
ORF23	+	23,524	24,687	1,164	RNA polymerase sigma factor RpoS	*Ignavibacteriales bacterium*	3e-11	28.06%	MCF8305946.1
ORF26	+	25,112	25,681	570	CYTH domain-containing protein	*Synechococcus* sp. *A15-127*	9e-08	29.38%	WP_102469181.1
ORF40	+	40,762	41,706	945	Thymidylate synthase	*Flavobacterium stagni*	4e-116	55.95%	WP_129461710.1
ORF46	+	44,076	45,067	990	DEAD/DEAH box helicase family protein	*Tenacibaculum phage PTm1*	3e-28	25.47%	YP_009873724.1
ORF70	+	59,570	63,550	3,981	Metallo-phosphoesterase	*Sphingomonas phage PAU*	1e-66	24.59%	YP_007006895.1
ORF76	+	66,665	67,465	801	Ribonucleoside-diphosphate reductase subunit beta	*Amniculibacterium* sp. *G2-70*	8e-147	64.13%	WP_187477617.1
ORF77	+	67,632	68,348	717	Intron associated endonuclease	*CrAss-like virus* sp.	1e-11	43.52%	DAF35514.1
ORF84	+	72,188	73,558	1,371	3-deoxy-D-manno-octulosonate 8-phosphate phosphatase	*Sphingomonas phage PAU*	6e-10	34.29%	YP_007006823.1
ORF87	+	76,225	76,830	606	Thymidylate kinase	None	N/A	N/A	N/A
ORF88	+	76,818	78,161	1,344	Thymidylate synthase	*Butyrivibrio* sp.	8e-23	33.76%	MBQ7428460.1
ORF89	+	78,229	80,271	2043	DNA helicase	*Tenacibaculum phage PTm1*	4e-59	28.50%	YP_009873805.1
ORF95	+	82,582	84,492	1911	NAD-dependent DNA ligase	*Sphingomonas phage PAU*	7e-44	29.22%	YP_007006813.1
ORF103	+	88,184	88,636	453	GNAT family N-acetyltransferase	*Maritalea porphyrae*	2e-07	35.87%	WP_269392588.1
ORF110	+	92,533	93,522	990	DEDDh 3′-5′ exonuclease	*Citromicrobium phage vB_CbaS-RXM*	7e-15	31.46%	USM11553.1
ORF112	+	94,972	95,745	774	Baseplate protein	*Tenacibaculum phage pT24*	3e-29	33.73%	YP_009876769.1
ORF115	+	97,929	98,273	345	Septal ring lytic transglycosylase RlpA family protein	*Moraxella lacunata*	3e-26	52.73%	WP_115004602.1
ORF124	–	101,658	102,536	879	Neck protein	*Bacteriophage* sp.	1e-23	28.03%	DAV36558.1
ORF135	+	110,343	111,830	1,488	DNA polymerase II	*Ackermannviridae* sp.	2e-51	31.31%	DAM31303.1
ORF138	+	114,019	115,296	1,278	DNA polymerase family B	*Ackermannviridae* sp.	2e-51	31.31%	DAM31303.1
ORF144	+	119,283	121,751	2,469	Lysozyme RrrD	*Synechococcales cyanobacterium M58_A2018_015*	1e-31	45.64%	MBF2003654.1

(Continued)

TABLE 2 (Continued)

ORFs	Strand	Start	Stop	Length	Function	Best-match	*E*-values	Per. ident	GenBank accession. no
ORF145	+	121,762	122,259	498	Head completion protein	*Tenacibaculum phage PTm1*	4e-26	43.87%	YP_009873685.1
ORF147	+	123,439	124,197	759	DNA end protector protein	*Caudoviricetes* sp.	1e-58	40.97%	DAP95445.1
ORF149	+	124,423	126,135	1713	Capsid assembly protein	*Caudoviricetes* sp.	2e-69	30.33%	DAQ63115.1
ORF151	+	126,501	130,544	4,044	Prohead core protein serine protease	*Caudoviricetes sp*	5e-23	39.46%	DAP95449.1
ORF165	+	139,385	140,299	915	UDP-3-O-(3-hydroxymyristoyl) glucosamine N-acyltransferase	*Caudoviricetes* sp.	7e-41	34.26%	DAN50236.1
ORF174	+	144,273	144,869	597	Dihydrofolate reductase	*Comamonadaceae bacterium*	7e-24	42.48%	RYX96028.1
ORF175	+	144,937	145,599	663	KpsF/GutQ family sugar-phosphate isomerase	*Chlamydia poikilotherma*	2e-25	40.99%	WP_117273901.1
ORF178	+	146,220	147,962	1743	Biofunctional protein GlmU	*Caudoviricetes* sp.	1e-46	27.38%	DAP95447.1
ORF206	+	175,015	176,130	1,116	Pyrimidine dimer DNA glycosylase/endonuclease V	*Unclassified Vibrio*	9e-08	29.38%	WP_102469181.1
ORF210	+	177,196	177,474	279	Thioredoxin C-1	*Flavobacterium* sp.	2e-16	39.33%	MCU0351479.1
ORF212	+	178,275	180,254	1980	GyrB Type IIA topoisomerase (DNA gyrase/topo II, topoisomerase IV), B subunit	*Uncultured Caudovirales phage*	1e-117	37.38%	CAB4159554.1
ORF216	+	181,261	182,730	1,470	GyrA Type IIA topoisomerase (DNA gyrase/topo II, topoisomerase IV), A subunit	*Uncultured Caudovirales phage*	2e-94	39.47%	CAB4219051.1
ORF232	+	194,744	195,652	195	CapA family protein	*Bacteroidota bacterium*	4e-18	31.45%	MBU2445609.1
ORF233	+	195,754	196,878	1,125	Hypothetical protein	*Virus NIOZ-UU157*	4e-51	55.70%	QPI16264.1
ORF237	+	197,909	198,853	945	Clamp loader of DNA polymerase	*Sphingomonas phage PAU*	4e-63	36.13%	YP_007006683.1
ORF246	+	203,955	204,944	990	Calcineurin-like phosphoesterase superfamily domain protein	*Uncultured CaudovCirales phage*	1e-126	54.88%	CAB5218431.1
ORF262	–	211,176	213,119	1944	Terminase family protein	*Sphingomonas phage PAU*	1e-77	29.01%	YP_007006694.1

the incidence of disease of *P. notoginseng* root slice up to 50% or more and delayed the occurrence of root rot disease. Preliminary exploratory experiments suggested that the phage MA9V-1 is a good candidate for controlling root rot disease as its inhibition in the development of disease symptoms caused by *C. indologenes* MA9.

4. Discussion

Phage MA9V-1, identified and characterized in this study, is capable for infecting the phytopathogenic bacteria *C. indologenes* MA9 causing *P. notoginseng* root rot (Zhang et al., 2020b). The composition of rhizospheric dominant bacterial and fungal genera significantly differed

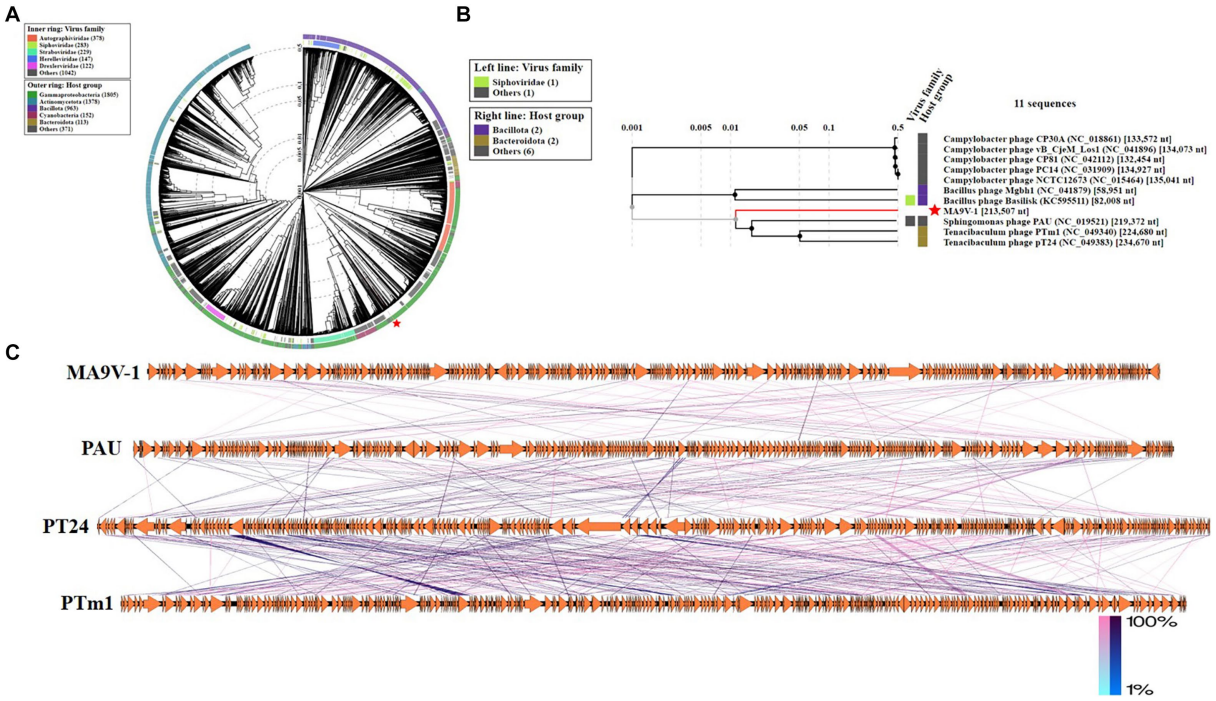

FIGURE 4
Proteomic tree of phage MA9V-1 generated using ViPTree. **(A)** A circular proteomic tree made with phage MA9V-1 and related prokaryotic dsDNA viruses. **(B)** The part of the rectangular proteomic tree of the enlarged part of area MA9V-1 of **(A)**. **(C)** Comparison of the draft genome sequence of *C. indologenes* phage MA9V-1(top) with other six homologous phages using EasyFig v2.2.5. The arrows of different colors indicate predicted ORFs and the direction of transcription. The color intensity from blue to red represents the level of amino acid sequence identity (1%–100%). The position of phage MA9V-1 is marked with a red "pentagram" star.

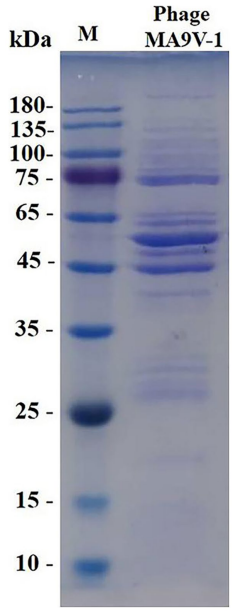

FIGURE 5
SDS-PAGE analysis of purified phage MA9V-1 virion structural proteins. M: protein ladder with its standard molecular weight on the left.

between moderately and severely diseased plants in root rot of *P. notoginseng*, indicating that bacterial pathogens and fungi play critical roles (Dong et al., 2018; Zhang et al., 2020a). However, numerous corresponding studies on this disease rarely focused on bacterial phytopathogens. Furthermore, the rapid development of bacteria resistant to antibiotics and the slow development of new antibiotics greatly stimulated people to seek alternative methods (Kortright et al., 2019). Therefore, applying phage therapy to the bacterial pathogen *C. indologenes* MA9 is expected to provide a potential strategy for solving or alleviating root rot disease of *P. notoginseng*.

MA9V-1 was isolated from sewage like many phages, such as *Clostridium freundii* phage IME-JL8 (Jia et al., 2020), *Vibrio* phage vB_VpaP_FE11P (Yang M. Y. et al., 2022), and *Pseudomonas aeruginosa* phage PPAY (Niu et al., 2022), indicating that sewage is an abundant reservoir of phages. MA9V-1 exhibited as a tiny plaque with a diameter of approximately 0.5–1.5 mm on the lawn of *C. indologenes* MA9, which was smaller than *Enterococcus faecalis* phage EFap02 and *Vibrio parahaemolyticus* phage vB_VpaP_GHSM17 (approximately 2 mm) (Liang et al., 2022; Liu et al., 2022). Morphologically, *C. indologenes* phage MA9V-1, consisted of an icositetrahedron head, a contractible tail, and a relatively short "neck," was similar to *T. maritimum* phages PTm1 and PTm5, according to the size of whole structural portions. Interestingly, though all of them are myoviruses, several flexible fiber-like appendages of length of 50–100 nm appendages at the upper region of the head of phages PTM1 and PTM5 are clearly observed through the imaging of TEM, while phage MA9V-1 is not observed (Kawato et al., 2020). Furthermore, 95% phage MA9V-1 particles were able to rapidly adsorb to the surface of the cell membrane within 12 min that was shorter than 25 min of *T. maritimum* phage PTm1 and 15 min of MDR *A. baumannii* phage vABPW7 and exhibited a brief latent period (20 min), which can make phage MA9V-1 quickly release progeny virus in a life cycle (Kawato

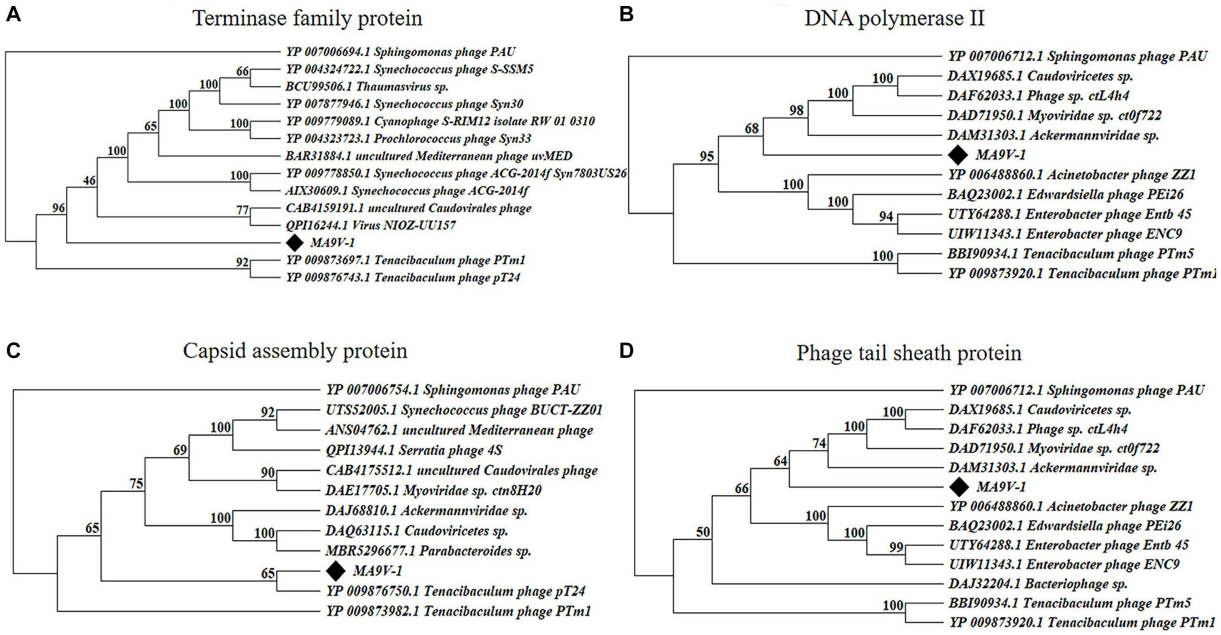

FIGURE 6
Protein phylogenetic tree of the selected *C. indologenes* phage MA9V-1 and 16 other phages based on deduced amino acid sequences of **(A)** terminase family protein; **(B)** DNA polymerase II; **(C)** capsid assembly protein; and **(D)** phage tail sheath protein. The value on the nodes of the branches indicates the credibility of the tree branch (≥50%). The position of phage MA9V-1 in the picture is marked with a black diamond.

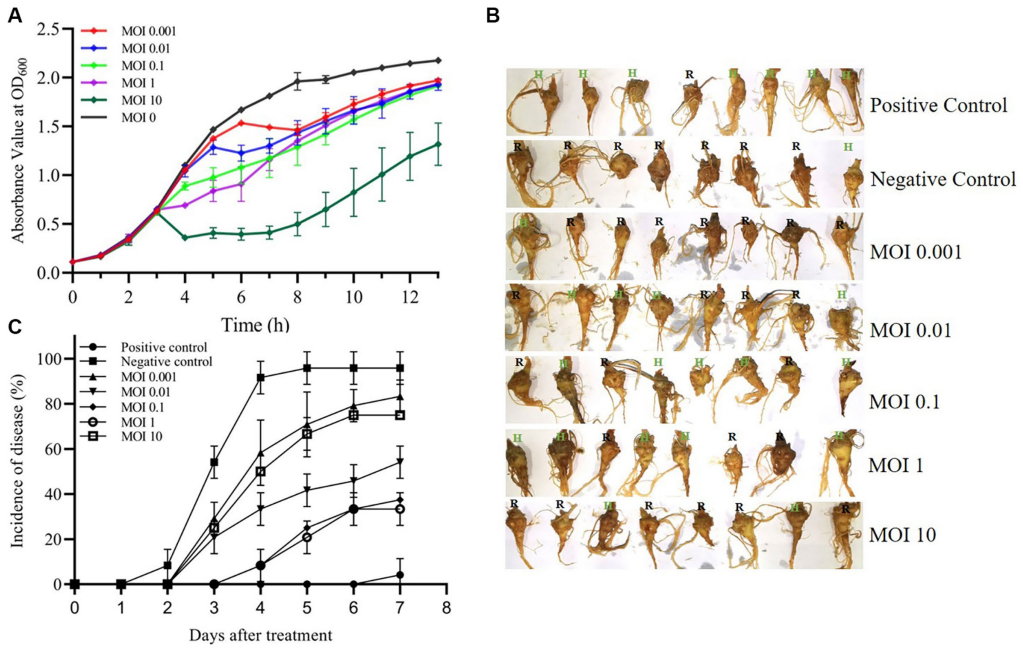

FIGURE 7
Virulence efficiency of phage MA9V-1 on *C. indologenes* strain MA9. **(A)** The growth inhibitory curve of *C. indologenes* MA9 mixed with phage MA9V-1 at various MOIs of 0 (black), 0.001 (red), 0.01 (blue), 0.1 (green), 1 (purple), and 10 (dark green), respectively. The growth curve was graphed with the absorbance of OD_{600} measured every 60min for 13h. **(B)** Representative images of the results after the addition of different mixtures of phage MA9V-1 and *C. indologenes* MA9 to *P. notoginseng* root after treatment for 7days. **(C)** The curve about the incidence of disease at different MOIs, including 0.001 (regular triangle), 0.01 (inverted triangle), 0.1 (diamond-shaped), 1 (hollow circle), and 10 (hollow square). Positive control (solid circle) was treated with inactive *C. indologenes* MA9, and negative control (solid square) was treated with *C. indologenes* MA9 at the exponential phase. The incidence of disease was calculated as the percentage of rotten roots to the total number of parallel experiments. The bars indicate standard errors.

et al., 2020; Wintachai et al., 2022). Moreover, the highly host-specific phage is one of the key factors to phage therapy applied in antibiotic substitutes, medical agents, and agricultural biocontrol (Luong et al., 2020). Due to this unique feature to phage, phage therapy would not directly affect the density, richness, and viability of other microorganisms living in microecology (Wang et al., 2019; Federici et al., 2021). The growth inhibitory curve indicated that the inhibitory ability of MA9V-1 was little weaker than other phages, such as phage *P. syringae* Eisa9 (Korniienko et al., 2022) and *P. aeruginosa* phage PPAY (Niu et al., 2022). We hypothesized a reasonable explanation that phage MA9V-1 required a long time to complete adsorption, invasion, proliferation, maturation, and lysis, since it has a lower burst size value (only 10 PFU/cell), which made it not easy to inhibit the bacterial growth. In addition, comparative genomic and phylogenetic tree analysis showed that phage MA9V-1 has a low similarity with phage *Sphingomonas* PAU and even a lower similarity with other two phages, indicating that phage MA9V-1 is most likely a novel phage infecting *C. indologenes* MA9 (Kwon et al., 2021). Importantly, bacteriophages against *C. indologenes* MA9 have not reported up to present, so further investigation should be needed to explore the characteristics of phage MA9V-1 and its genome sequence.

Lytic phage (also known as virulent phage) can be used for phage therapy of bacterial pathogens because they can continuously complete the life cycle of adsorption, invasion, reproduction, assembling, and release (North and Brown, 2021). Thus, we could derive reasonable inferences about its entire infection process in combination with the predicted functional proteins in the genome. First, to infect, there are proteins relating to tail structure, tail fiber, and others, such as ORF16 short tail fiber protein (Table 2). Then, the tail sheath protein (corresponding to ORF01) of phage MA9V-1 is used like a syringe to inject the genetic content into the host cell, where MA9V-1 utilizes its self-expression protein, including ORF89 DNA helicase, ORF135 DNA polymerase, and ORF95 NAD-dependent DNA ligase to replicate, transcribe, and translate the genetic materials and necessary virion components. Subsequently, recombinase existing in the genome of phage MA9V-1 is used to assemble all the components synthesized in host cells into new progeny phages. Finally, with the function of holin and endolysin proteins (similar to ORF144 Lysozyme RrrD protein), called the lysis system "holin–lysin," new progeny phages are released to complete the whole process of invasion to host cells (Stone et al., 2019). Additionally, in response to the phage infection, the hosts have evolved a restriction–modification system (R-M), which restricts the ability of endonucleases to rapidly degrade unmethylated phage DNA to prevent phage invasion. Phages have evolved the ability to express methylase to protect their DNA from degradation against the R-M system. For example, the *Bacillus* phage SPR encodes a methyltransferase that modifies three base sites to make phage DNA escape from degradation by multiple nucleases (Murphy et al., 2013). Furthermore, mechanisms of preventing adsorption and CRISPR-Cas adaptive immunity are anti-invasion strategies evolved to fight phages (Hampton et al., 2020).Thus, we could assume reasonably that the efficiency of phage therapy depends mainly on whether the phage can release a large number of progeny phages within a brief time and the rate at which the host cell develops resistance to the phage, combined with the understanding of infection strategies and evolutionary mechanisms between bacteria and phages, which is expected to improve the efficiency of phage therapy.

In summary, the phage MA9V-1 is a novel lytic phage specific to *C. indologenes* MA9, which has a potential preventive and biocontrol effect on *P. notoginseng* root rot caused by *C. indologenes* MA9. However, there are some limitations exposed in this study. For example, treating methods and culturing conditions were both conducted under the laboratory environment, which did not really simulate the microecology surroundings in which microorganisms interact with the rhizospheric soils of *P. notoginseng*, leading to deviations in the therapeutic results. When phage therapy applied in the agricultural environment, its functional mechanism is a complicated process. A reasonable insight is that the host undergoes self-evolutionary in response to phage infection, which leads to modification in the cell membrane structure, making it lose the ability to compete with other microbial populations. The weaker ability to compete for survival resources results in a reduction in the abundance of pathogenic bacterium, which enriched bacterial taxa that are highly antagonistic toward the pathogen and achieved the purpose of phage therapy (Wang et al., 2019). Not only that, whether the stability and efficacy of phage therapy will be affected when it is applied under different environmental conditions, and whether it will destroy the pharmacological components contained in *Panax notoginseng* will become the focus of our future research. Similarly, the application of phage therapy in agriculture also brought many challenges and limitations. One is that the large-scale preparation of phage will cost immense manpower and financial resources, which greatly limits the scale of phage therapeutic application. Another one is whether the residual phages remaining in the soil will cause permanent pollution to soil-like pesticides and antibiotics. Therefore, the wide application of phage therapy is a long and difficult process, and there are still many problems waiting for us to explore and solve. We believe that these experimental data would provide a theoretical basis for controlling the root rot disease of *P. notoginseng* and a new idea for preventing the diseases of traditional medicinal plants, such as *P. ginseng*, *P. quinquefolius*, and *P. japonicus*.

Data availability statement

The datasets presented in this study can be found in online repositories. The names of the repository/repositories and accession number(s) can be found in the article/Supplementary material.

Author contributions

HZ wrote the first draft of the manuscript and carried out experiments. YW defined the research theme and revised the manuscript. GJ, JZ, XC and YY provided experimental materials. HZ, YD, JS, JL, and CM designed the methods and experiments and analyzed the results and data. All authors contributed to the article and approved the submitted version.

Funding

This study received support from the National Natural Science Foundation of China (no. 31960232).

Acknowledgments

The authors would like to thank Editage (www.editage.com) for English language editing.

Conflict of interest

The authors declare that the research was conducted in the absence of any commercial or financial relationships that could be construed as a potential conflict of interest.

Publisher's note

All claims expressed in this article are solely those of the authors and do not necessarily represent those of their affiliated organizations, or those of the publisher, the editors and the reviewers. Any product that may be evaluated in this article, or claim that may be made by its manufacturer, is not guaranteed or endorsed by the publisher.

Supplementary material

The Supplementary material for this article can be found online at: https://www.frontiersin.org/articles/10.3389/fmicb.2023.1251211/full#supplementary-material

SUPPLEMENTARY FIGURE S1
The image on the left shows the result of the root of *P. notoginseng* after treatment for five days at MOI of 0.01 (Corresponding to 2nd sample of MOI = 0.01); the picture on the right shows the result of the root of *P. notoginseng* after treatment for seven days under the condition at MOI = 10 (Corresponding to 5th sample of MOI = 10).

References

Addy, H. S., Ahmad, A. A., and Huang, Q. (2019). Molecular and biological characterization of Ralstonia phage RsoM1USA, a new species of P2virus, isolated in the United States. *Front. Microbiol.* 10:267. doi: 10.3389/fmicb.2019.00267

Aykac, K., Ozsurekci, Y., Tuncer, O., Sancak, B., Cengiz, A. B., Kara, A., et al. (2016). Six cases during 2012-2015 and literature review of *Chryseobacterium indologenes* infections in pediatric patients. *Can. J. Microbiol.* 62, 812–819. doi: 10.1139/cjm-2015-0800

Bruessow, H. (2012). What is needed for phage therapy to become a reality in Western medicine? *Virology* 434, 138–142. doi: 10.1016/j.virol.2012.09.015

Camacho, C., Coulouris, G., Avagyan, V., Ma, N., Papadopoulos, J., Bealer, K., et al. (2009). BLAST plus: architecture and applications. *Bmc Bioinformatics* 10:421. doi: 10.1186/1471-2105-10-421

Chen, Y. B., Yang, L., Sun, E. C., Song, J. Y., and Wu, B. (2019). Characterisation of a newly detected bacteriophage infecting *Bordetella bronchiseptica* in swine. *Arch. Virol.* 164, 33–40. doi: 10.1007/s00705-018-4034-0

Din, M. O., Danino, T., Prindle, A., Skalak, M., Selimkhanov, J., Allen, K., et al. (2016). Synchronized cycles of bacterial lysis for in vivo delivery. *Nature* 536:81-+. doi: 10.1038/nature18930

Dong, L. L., Xu, J., Feng, G. Q., Li, X. W., and Chen, S. L. (2016). Soil bacterial and fungal community dynamics in relation to Panax notoginseng death rate in a continuous cropping system. *Sci. Rep.* 6:31802. doi: 10.1038/srep31802

Dong, L. L., Xu, J., Zhang, L. J., Cheng, R. Y., Wei, G. F., Su, H., et al. (2018). Rhizospheric microbial communities are driven by *Panax ginseng* at different growth stages and biocontrol bacteria alleviates replanting mortality. *Acta Pharm. Sin. B* 8, 272–282. doi: 10.1016/j.apsb.2017.12.011

Fan, Z. Y., Miao, C. P., Qiao, X. G., Zheng, Y. K., Chen, H. H., Chen, Y. W., et al. (2016). Diversity, distribution, and antagonistic activities of rhizobacteria of Panax notoginseng. *J. Ginseng Res.* 40, 97–104. doi: 10.1016/j.jgr.2015.05.003

Federici, S., Nobs, S. P., and Elinav, E. (2021). Phages and their potential to modulate the microbiome and immunity. *Cell. Mol. Immunol.* 18, 889–904. doi: 10.1038/s41423-020-00532-4

Grant, J. R., and Stothard, P. (2008). The CGView server: a comparative genomics tool for circular genomes. *Nucleic Acids Res.* 36, W181–W184. doi: 10.1093/nar/gkn179

Guo, H. B., Cui, X. M., An, N., and Cai, G. P. (2010). Sanchi ginseng (Panax notoginseng (Burkill) F. H. Chen) in China: distribution, cultivation and variations. *Genet. Resour. Crop. Evol.* 57, 453–460. doi: 10.1007/s10722-010-9531-2

Hampton, H. G., Watson, B. N. J., and Fineran, P. C. (2020). The arms race between bacteria and their phage foes. *Nature* 577, 327–336. doi: 10.1038/s41586-019-1894-8

Han, H., Li, X. M., Wang, S., Zhang, T. Y., Jang, J. Z., and Wang, R. (2017). Research progress on the safety evaluation of bacteriophages used as antibacterial agents. *Jiangsu Agric. Sci.* 45, 18–23. doi: 10.15889/j.issn.1002-1302.2017.22.005

Jia, K. X., Yang, N., Zhang, X. W., Cai, R. P., Zhang, Y., Tian, J. X., et al. (2020). Genomic, morphological and functional characterization of virulent bacteriophage IME-JL8 targeting *Citrobacter freundii*. *Front. Microbiol.* 11:585261. doi: 10.3389/fmicb.2020.585261

Jiang, N., Qin, L. Y., and Ye, Y. F. (2011). Research advances in diseases of Panax notoginseng. *J. South. Argic.* 42, 1070–1074. doi: 10.1016/j.phymed.2022.154119

Johnson, K. L., Minsavage, G. V., Le, T., Jones, J. B., and Walcott, R. R. (2011). Efficacy of a nonpathogenic *Acidovorax citrulli* strain as a biocontrol seed treatment for bacterial fruit blotch of cucurbits. *Plant Dis.* 95, 697–704. doi: 10.1094/pdis-09-10-0660

Kawato, Y., Istiqomah, I., Gaafar, A. Y., Hanaoka, M., Ishimaru, K., Yasuike, M., et al. (2020). A novel jumbo *Tenacibaculum maritimum* lytic phage with head-fiber-like appendages. *Arch. Virol.* 165, 303–311. doi: 10.1007/s00705-019-04485-6

Korniienko, N., Kharina, A., Zrelovs, N., Jindrichova, B., Moravec, T., Budzanivska, I., et al. (2022). Isolation and characterization of two lytic phages efficient against phytopathogenic bacteria from Pseudomonas and Xanthomonas genera. *Front. Microbiol.* 13:853593. doi: 10.3389/fmicb.2022.853593

Kortright, K. E., Chan, B. K., Koff, J. L., and Turner, P. E. (2019). Phage therapy: a renewed approach to combat antibiotic-resistant bacteria. *Cell Host Microbe* 25, 219–232. doi: 10.1016/j.chom.2019.01.014

Kwon, J., Kim, S. G., Kim, H. J., Giri, S. S., Kim, S. W., Lee, S. B., et al. (2021). Isolation and characterization of Salmonella jumbo-phage pSal-SNUABM-04. *Viruses* 13:27. doi: 10.3390/v13010027

Li, J., Tian, F. J., Hu, Y. J., Lin, W., Liu, Y. J., Zhao, F. Y., et al. (2021). Characterization and genomic analysis of BUCT549, a novel bacteriophage infecting *Vibrio alginolyticus* with flagella as receptor. *Front. Microbiol.* 12:668319. doi: 10.3389/fmicb.2021.668319

Li, T. T., Yang, J., Huo, Y. Y., Zeng, Z. Y., Huang, H. Y., Xu, F. R., et al. (2022). Control of pathogenic fungi on Panax notoginseng by volatile oils from the food ingredients Allium sativum and *Foeniculum vulgare*. *Lett. Appl. Microbiol.* 75, 89–102. doi: 10.1111/lam.13706

Liang, X. R., Wang, Y. H., Hong, B., Li, Y. M., Ma, Y., and Wang, J. F. (2022). Isolation and characterization of a lytic *Vibrio parahaemolyticus* phage vB_VpaP_GHSM17 from sewage samples. *Viruses* 14:8. doi: 10.3390/v14081601

Liu, Y., Liu, M., Hu, R., Bai, J., He, X., and Jin, Y. (2021). Isolation of the novel phage PHB09 and its potential use against the plant pathogen *Pseudomonas syringae* pv. Actinidiae. *Viruses* 13:2275. doi: 10.3390/v13112275

Liu, B., Zheng, D. D., Jin, Q., Chen, L. H., and Yang, J. (2019). VFDB 2019: a comparative pathogenomic platform with an interactive web interface. *Nucleic Acids Res.* 47, D687–D692. doi: 10.1093/nar/gky1080

Liu, J. Z., Zhu, Y. P., Li, Y., Lu, Y. W., Xiong, K., Zhong, Q., et al. (2022). Bacteriophage-resistant mutant of *Enterococcus faecalis* is impaired in biofilm formation. *Front. Microbiol.* 13:913023. doi: 10.3389/fmicb.2022.913023

Lowe, T. M., and Chan, P. P. (2016). tRNAscan-SE on-line: integrating search and context for analysis of transfer RNA genes. *Nucleic Acids Res.* 44, W54–W57. doi: 10.1093/nar/gkw413

Lu, Z. J., and Breidt, F. (2015). *Escherichia coli* O157:H7 bacteriophage phi 241 isolated from an industrial cucumber fermentation at high acidity and salinity. *Front. Microbiol.* 6:67. doi: 10.3389/fmicb.2015.00067

Luong, T., Salabarria, A.-C., Edwards, R. A., and Roach, D. R. (2020). Standardized bacteriophage purification for personalized phage therapy. *Nat. Protoc.* 15, 2867–2890. doi: 10.1038/s41596-020-0346-0

Murphy, J., Mahony, J., Ainsworth, S., Nauta, A., and van Sinderen, D. (2013). Bacteriophage orphan DNA methyltransferases: insights from their bacterial origin, function, and occurrence. *Appl. Environ. Microbiol.* 79, 7547–7555. doi: 10.1128/aem.02229-13

Nishimura, Y., Yoshida, T., Kuronishi, M., Uehara, H., Ogata, H., and Goto, S. (2017). ViPTree: the viral proteomic tree server. *Bioinformatics* 33, 2379–2380. doi: 10.1093/bioinformatics/btx157

Niu, Y. Y., Yang, X. B., Wang, S., Yang, Y. T., Zhou, H. R., Li, C. Y., et al. (2022). Isolation and characterization of two homolog phages infecting *Pseudomonas aeruginosa*. *Front. Microbiol.* 13:946251. doi: 10.3389/fmicb.2022.946251

North, O. I., and Brown, E. D. (2021). Phage-antibiotic combinations: a promising approach to constrain resistance evolution in bacteria. *Ann. N. Y. Acad. Sci.* 1496, 23–34. doi: 10.1111/nyas.14533

Pajunen, M., Kiljunen, S., and Skurnik, M. (2000). Bacteriophage phi YeO3-12, specific for *Yersinia enterocolitica* serotype O: 3, is related to coliphages T3 and T7. *J. Bacteriol.* 182, 5114–5120. doi: 10.1128/jb.182.18.5114-5120.2000

Peng, W. Y., Zeng, F., Wu, Z. Y., Jin, Z. Y., Li, W. X., Zhu, M. Z., et al. (2022). Isolation and genomic analysis of temperate phage 5W targeting multidrug-resistant *Acinetobacter baumannii*. *Arch. Microbiol.* 204:58. doi: 10.1007/s00203-021-02618-7

Prjibelski, A., Antipov, D., Meleshko, D., Lapidus, A., and Korobeynikov, A. (2020). Using SPAdes De novo assembler. *Curr. Protoc. Bioinformatics* 70:e102. doi: 10.1002/cpbi.102

Roy, K. R., and Chanfreau, G. F. (2020). Robust mapping of polyadenylated and non-polyadenylated RNA 3 ' ends at nucleotide resolution by 3 '-end sequencing. *Methods* 176, 4–13. doi: 10.1016/j.ymeth.2019.05.016

Sasikala, D., and Srinivasan, P. (2016). Characterization of potential lytic bacteriophage against Vibrio alginolyticus and its therapeutic implications on biofilm dispersal. *Microb. Pathog.* 101, 24–35. doi: 10.1016/j.micpath.2016.10.017

Soding, J., Biegert, A., and Lupas, A. N. (2005). The HHpred interactive server for protein homology detection and structure prediction. *Nucleic Acids Res.* 33, W244–W248. doi: 10.1093/nar/gki408

Stone, E., Campbell, K., Grant, I., and McAuliffe, O. (2019). Understanding and exploiting phage-host interactions. *Viruses* 11:567. doi: 10.3390/v11060567

Stuer-Lauridsen, B., Janzen, T., Schnabl, J., and Johansen, E. (2003). Identification of the host determinant of two prolate-headed phages infecting *Lactococcus lactis*. *Virology* 309, 10–17. doi: 10.1016/s0042-6822(03)00012-6

Sun, Z. Y., Mandlaa, , Wen, H., Ma, L., and Chen, Z. J. (2022). Isolation, characterization and application of bacteriophage PSDA-2 against *Salmonella Typhimurium* in chilled mutton. *PLoS One* 17:e0262946. doi: 10.1371/journal.pone.0262946

Tamura, K., Stecher, G., and Kumar, S. (2021). MEGA11 molecular evolutionary genetics analysis version 11. *Mol. Biol. Evol.* 38, 3022–3027. doi: 10.1093/molbev/msab120

Tan, Y., Cui, Y. S., Li, H. Y., Kuang, A. X., Li, X. R., Wei, Y. L., et al. (2017). Diversity and composition of rhizospheric soil and root endogenous bacteria in Panax notoginseng during continuous cropping practices. *J. Basic Microbiol.* 57, 337–344. doi: 10.1002/jobm.201600464

Turner, D., Kropinski, A. M., and Adriaenssens, E. M. (2021). A roadmap for genome-based phage taxonomy. *Viruses* 13:3. doi: 10.3390/v13030506

Uchiyama, J., Takemura-Uchiyama, I., Kato, S., Sato, M., Ujihara, T., Matsui, H., et al. (2014). In silico analysis of AHJD-like viruses, *Staphylococcus aureus* phages S24-1 and S13 ', and study of phage S24-1 adsorption. *Microbiology* 3, 257–270. doi: 10.1002/mbo3.166

Wang, X. F., Wei, Z., Yang, K. M., Wang, J. N., Jousset, A., Xu, Y. C., et al. (2019). Phage combination therapies for bacterial wilt disease in tomato. *Nat. Biotechnol.* 37:1513-+. doi: 10.1038/s41587-019-0328-3

Wang, P. P., Yang, L. F., Sun, J. L., Yang, Y., Qu, Y., Wang, C. X., et al. (2021). Structure and function of rhizosphere soil and root endophytic microbial communities associated with root rot of Panax notoginseng. *Front. Plant Sci.* 12:752683. doi: 10.3389/fpls.2021.752683

White, R. A., and Suttle, C. A. (2013). The draft genome sequence of *Sphingomonas paucimobilis* strain HER1398 (Proteobacteria), host to the giant PAU phage, Iindicates that it is a member of the genus Sphingobacterium (Bacteroidetes). *Genome Announc.* 1, 2169–8287. doi: 10.1128/genomeA.00598-13

Wintachai, P., Surachat, K., Chaimaha, G., Septama, A. W., and Smith, D. R. (2022). Isolation and characterization of a phapecoctavirus infecting multidrug-resistant *acinetobacter baumannii* in A549 alveolar epithelial cells. *Viruses* 14:2561. doi: 10.3390/v14112561

Wu, L. T., Chang, S. Y., Yen, M. R., Yang, T. C., and Tseng, Y. H. (2007). Characterization of extended-host-range pseudo-T-even bacteriophage Kpp95 isolated on *Klebsiella pneumoniae*. *Appl. Environ. Microbiol.* 73, 2532–2540. doi: 10.1128/aem.02113-06

Xie, J., Wu, Y. Y., Zhang, T. Y., Zhang, M. Y., Peng, F., Lin, B., et al. (2018). New antimicrobial compounds produced by endophytic Penicillium janthinellum isolated from Panax notoginseng as potential inhibitors of FtsZ. *Fitoterapia* 131, 35–43. doi: 10.1016/j.fitote.2018.10.006

Xu, C. C., Wang, W. W., Wang, B., Zhang, T., Cui, X. M., Pu, Y. Q., et al. (2019). Analytical methods and biological activities of Panax notoginseng saponins: recent trends. *J. Ethnopharmacol.* 236, 443–465. doi: 10.1016/j.jep.2019.02.035

Yang, M. Y., Chen, H. F., Huang, Q. L., Xie, Z. B., Liu, Z. K., Zhang, J. M., et al. (2022). Characterization of the novel phage vB_VpaP_FE11 and its potential role in controlling *Vibrio parahaemolyticus* biofilms. *Viruses* 14:264. doi: 10.3390/v14020264

Yang, W. Z., Hu, Y., Wu, W. Y., Ye, M., and Guo, D. A. (2014). Saponins in the genus Panax L. (Araliaceae): a systematic review of their chemical diversity. *Phytochemistry* 106, 7–24. doi: 10.1016/j.phytochem.2014.07.012

Yang, X., Xiong, X., Wang, H., Yang, G., and Wang, J. (2013). Xuesaitong soft capsule (Chinese patent medicine) for the treatment of unstable angina pectoris: a meta-analysis andsystematic review. *Evid. Based Complement. Alternat. Med.* 2013:948319. doi: 10.1155/2013/948319

Yang, Y., Zheng, K., Guo, L. P., Wang, C. X., Zhong, D. B., Shang, L., et al. (2022). Rapid determination and dietary intake risk assessment of 249 pesticide residues in Panax notoginseng. *Ecotoxicol. Environ. Saf.* 233:113348. doi: 10.1016/j.ecoenv.2022.113348

Yun, Y. B., Um, Y., and Kim, Y. K. (2022). Optimization of the bacteriophage cocktail for the prevention of Brown blotch disease caused by. *Plant Pathol. J.* 38, 472–481. doi: 10.5423/ppj.Oa.03.2022.0026

Zhang, J. H., Wei, L. F., Yang, J., Ahmed, W., Wang, Y. T., Fu, L., et al. (2020a). Probiotic consortia: reshaping the rhizospheric microbiome and its role in suppressing root-rot disease of Panax notoginseng. *Front. Microbiol.* 11:701. doi: 10.3389/fmicb.2020.00701

Zhang, J. H., Yang, J., Ji, G. H., Wang, Y. F., Zhang, R. Q., Dai, Z. L., et al. (2020b). Bacterial pathogen identification of Panax notoginseng root rot in Yunnan Province. *J. South. Agric.* 51, 586–592. doi: 10.3969/j.issn.2095-1191.2020.03.014

Zhao, Y. P., Lin, S., Chu, L. X., Gao, J. T., Azeem, S., and Lin, W. X. (2016). Insight into structure dynamics of soil microbiota mediated by the richness of replanted Pseudostellaria heterophylla. *Sci. Rep.* 6:26175. doi: 10.1038/srep26175

Zheng, Y. K., Miao, C. P., Chen, H. H., Huang, F. F., Xia, Y. M., Chen, Y. W., et al. (2017). Endophytic fungi harbored in Panax notoginseng: diversity and potential as biological control agents against host plant pathogens of root-rot disease. *J. Ginseng Res.* 41, 353–360. doi: 10.1016/j.jgr.2016.07.005

Zheng, K. Y., Su, X. X., Xue, Z., Zhang, L. Z., Chen, Y. D., Wu, K., et al. (2022). First report of *Stenotrophomonas maltophilia* causing root soft rot of Sanqi (Panax notoginseng) in China. *Plant Dis.* 106:755. doi: 10.1094/pdis-07-21-1353-pdn

frontiers | Frontiers in Microbiology

TYPE Original Research
PUBLISHED 28 September 2023
DOI 10.3389/fmicb.2023.1270346

OPEN ACCESS

EDITED BY
Alicja Wegrzyn,
Polish Academy of Sciences, Poland

REVIEWED BY
Sylwia Bloch,
University of Gdansk, Poland
Ewa Brzozowska,
Polish Academy of Sciences, Poland

*CORRESPONDENCE
Claudia Picozzi
✉ claudia.picozzi@unimi.it

RECEIVED 31 July 2023
ACCEPTED 14 September 2023
PUBLISHED 28 September 2023

CITATION
Mangieri N, Vieira RP and Picozzi C (2023) Influence of cheese making process on STEC bacteriophage release.
Front. Microbiol. 14:1270346.
doi: 10.3389/fmicb.2023.1270346

Influence of cheese making process on STEC bacteriophage release

Nicola Mangieri[1], Rui P. Vieira[1,2] and Claudia Picozzi[1]*

[1]DeFENS, Department of Food, Environmental and Nutritional Sciences, Università Degli Studi di Milano, Milano, Italy, [2]Instituto de Medicina Molecular, Faculdade de Medicina, Universidade de Lisboa, Lisboa, Portugal

Shiga toxin-producing *Escherichia coli* (STEC) are foodborne pathogens implicated in diseases including hemolytic uremic syndrome (HUS) and hemorrhagic colitis (HC). The main virulence factor are Shiga toxins; their production and secretion are by-products of the expression of late genes of prophages upon sub-lethal environmental stimuli exposure. Hence, the lysogenic prophage after a stress switch to lytic cycle spreading the Stx phages. In the present study, 35 STEC were screened for the presence and the ability to release Shiga toxin-encoding bacteriophages. Three bacterial strains showed signals of prophage presence both in plate and in PCR. Subsequently, these bacterial strains were subjected to stressors that simulate cheese manufacturing conditions: NaCl (1, 1.5 and 2% w/v), lactic acid (0.5, 1.5 and 3% v/v), anaerobic growth, pasteurization (72°C for 15 s), UV irradiation. The ability to release prophage was evaluated by Real Time qPCR. Induction of the prophages showed that the addition of NaCl at 1.5 and 2% significantly increased viral release compared to control. Conversely, the addition of lactic acid had a significant repressive effect. The other applied stressors had no significant effect in phage release according to the experimental conditions adopted.

KEYWORDS

prophage induction, Shiga toxin-producing *E. coli*, stx-phages, qPCR, cheese production

1. Introduction

Escherichia coli is a commensal bacterium of the gastrointestinal tract of humans and warm-blooded animals, but is also present in water and soil. In most cases these bacteria are harmless to their host, but some strains are characterized by the presence of virulence traits that can cause disease in humans (Croxen et al., 2013). Among the pathogenic strains, Shiga toxin-producing *E. coli* (STEC) is the main group involved in foodborne illness (Castro et al., 2017) causing gastrointestinal symptoms and bloody diarrhea. The disease can potentially progress into hemorrhagic colitis (HC) and hemolytic uremic syndrome (HUS) (Yang et al., 2017).

In 2020 STEC resulted the fourth most frequent bacterial agent detected in foodborne outbreaks in the EU, with 34 outbreaks, 208 cases, 30 hospitalizations and 1 death (The European Union One Health 2020 Zoonoses Report, 2021). The main reservoir of STEC are ruminants, particularly cattle, but also sheep and goats and less frequently other animals such as pigs, horses, domestic poultry, dogs, cats, and other wild animals (Kim et al., 2020). Direct contact with contaminated water or animals is also a relevant route of transmission to humans (Koutsoumanis et al., 2020).

As concern prevalence in food, STEC was most commonly found in meat of different types derived from different animal species (3.4% STEC-positive) and in milk and dairy products (2.1%), while fruits and vegetables were the least contaminated products (0.1%) (The European Union One Health 2020 Zoonoses Report, 2021).

Several virulence factors, including intimin encoded by *eae* gene, are involved in enteropathogenic and enterohaemorrhagic diarrhea. Shiga toxins, for which encoding genes are carried by bacteriophages located in the bacterial chromosome, are the main cause of virulence. Bacteriophages can be divided in lytic and temperate according to their growth potential. Two types of life cycle can occur: lytic and lysogenic. In the lytic cycle, the bacteriophage injects its nucleic acid into the bacterial host and replicates, taking control of the host's molecular machinery. Then, phages lyse the bacterial cell with the production of two types of protein: holins and lysins. The first works to perforate the bacterial cytoplasmic membrane, giving the lysins access to bacterial cell wall (Cisek et al., 2017; Kakasis and Panitsa, 2019). Shiga toxins are expressed during the lytic cycle of bacteriophages that carry the genes for these toxins. During the lysogenic cycle, after the injection phase, the phage nucleic acid integrates into the host bacterial chromosome and replicates along with generations by vertical gene transfer. The expression of the phage genes, including those for Shiga toxins, is repressed during lysogeny. However, when the lysogenic cycle is induced, such as by exposure to stress factors as changes in pH, presence of iron, presence or absence of ions, presence of antibiotics or DNA damage, the phage DNA excises from the host chromosome and enters the lytic cycle (Lin et al., 2017). This results in the production of new phage particles, and the expression of phage genes, including those for Shiga toxins (Rodríguez-Rubio et al., 2021). Therefore, while Shiga toxins are not expressed during the lysogenic cycle, they can be expressed during the lytic cycle of Stx phages. As written before, antibiotics have been reported as prophage inducers. Indeed, in the clinical treatment of STEC infections the use of antibiotics is controversial due to the release of prophages that can infect non-STEC strains and lead to overproduction of toxins (McGannon et al., 2010).

The lysogenic phages involved in the transmission of the Shiga toxin are called Stx phages. Shiga toxin is an exotoxin produced only by STEC and *S. dysenteriae* serotype 1 and is characterized by an AB5 structure containing an A subunit that is not-covalently associated with the five B subunits (Yang et al., 2017). The A subunit plays a role in inhibition of protein synthesis and in cell damage by apoptosis (Yang et al., 2015) and the five B subunits bind the globotriaosylceramide receptor (Gb3) on the surface of susceptible eukaryotic cells. After assimilation by endocytosis, the toxin pass through the trans-Golgi network and endoplasmic reticulum and then hinders ribosomal function by cleavage of adenosine residues from the 28S rRNA of the large subunit (Pacheco and Sperandio, 2012).

STEC strains are a great concern to the dairy industry since they can cause diseases in humans even with a small number of ingested cells (<10) (Etcheverría and Padola, 2013). Furthermore, several psychophysical factors in cheese making process, such as addition of NaCl and changes in temperature and in pH can be considered as potential stressors to induce bacteriophage release and to promote toxin transmission among bacterial cells. Milk pasteurization prevents the possible STEC contamination, but some cheeses are made using raw milk. Besides, STEC can contaminate the product during the different manufacturing and processing steps and persist in the final product (dos Santos Rosario et al., 2021).

The objectives of this work were to characterize temperate bacteriophages from STEC strains used in this work and to evaluate the influence of stress factors related to the cheese-making process, on induction phenomena through a quantitative Real-time PCR (qPCR).

2. Original research

2.1. Materials and methods

2.1.1. Bacterial growth conditions

The STEC strains used (Table 1) are part of Department of Food, Environmental and Nutritional Sciences Collection from Università degli Studi di Milano and were partially characterized in previous works (Picozzi et al., 2016; Mangieri et al., 2020). Strains were streaked on Tryptone Bile X-Glucuronide agar (TBX) (Merck, Darmstadt, Germany) plates and incubated at 37°C for 24 h. A single colony was transferred in a 10 mL LB broth (Alfa Aesar, Karlsruhe, Germany) tube and incubated overnight at 37°C. The overnight culture was centrifuged at 1200 *g* for 15 min (Centrifuge 5,415 D, Eppendorf, Hamburg, Germany), the supernatant was discarded, and the pellet was resuspended in LB broth with 20% (v/v) glycerol and stored at −20°C until further use.

2.2. Bacteriophage DNA extraction and PCR analysis

Strains were subjected to phage induction by adding 0.3 mg/mL of Fosfomycin (Sigma-Aldrich, St. Louis, United States) to cells at exponential phase (OD600nm = 0.2–0.3). After 6 h of incubation at 37°C, the solutions were centrifuged at 4800 *g* for 10 min (Centrifuge 5,415 D, Eppendorf, Hamburg, Germany) and filtered through a 0.45 µm membrane filters (Minisart Syringe filter). The crude filtrates were tested for the presence of phages *via* spot-test in LB agar plates using two sensitive *E. coli* strains CNCTC 6896 and CNCTC 6246 as previously described (Mangieri et al., 2020). Briefly, the exponentially growing CNCTC 6896 and CNCTC6246 cultures (100 µL) were supplemented with $CaCl_2$ to a final concentration of 10 mM and mixed with melted LB soft agar (4 mL) at 48–50°C in sterile test tubes. Each mixture was then poured onto LB bottom agar (1.5%) plates to create a double layer. Phage filtrates (10 µL) were spotted onto agar surface and plates were incubated overnight at 37°C. The presence of infected phage particles was confirmed by the appearance of clear bacterial lysis.

Subsequently, 50 mL of crude bacteriophage filtrate were precipitated by addition of 10% (w/v) of polyethylene glycol (PEG) 6,000 (Merck, Darmstadt, Germany) and 0.5 M NaCl. After 6 h at 4°C, the solution was centrifuged at 4800 *g* for 10 min (Centrifuge 5,415 D) and the supernatant discarded. The pellet was resuspended in 400 µL of SM buffer (100 mM NaCl, 8 mM $MgSO_4$, 50 mM Tris–HCl, pH 7.5, 0.01% gelatin) and incubated overnight at 4°C.

The suspension was subjected to an enzymatic treatment with 5 µL of DNase (20 mg/mL) (Roche, Mannheim, Germany) and 10 µL of RNase (5 mg/mL) (Merck, Darmstadt, Germany) at 37°C for 60 min to remove any non-phage nucleic acids. Subsequently, the enzymes were inactivated by heat treatment at 75°C for 10 min.

A PCR amplification of the 16S rRNA gene was performed to verify the absence of bacterial DNA using the universal primers BSF-8

TABLE 1 List of STEC strains.

Strain	Sample source	Serogroup
214CH	Human stool	O157
214R-ACH	Human stool	O26
214R-MCH-B	Human stool	O157
224SMA-GS	Human stool	ND
225R-A	Human stool	O26
226BB	Human stool	O157
227MCH	Human stool	O157
227Rosa	Human stool	ND
228GS	Human stool	O145
229B-ACH	Human stool	ND
229 M-AS	Human stool	ND
229PRAL-ACH	Human stool	O26
229PRAL-AS	Human stool	ND
229RACH	Human stool	O111
229Rosa-A	Human stool	ND
231PCH-A	Human stool	ND
232AS-B-LUC	Human stool	ND
233P-CH-A	Human stool	ND
239R-A	Human stool	ND
242CH	Human stool	O157
242Rossa	Human stool	O157
243RACH	Human stool	O26
L12-2	Raw Goat Milk	O26
L36-2	Raw Goat Milk	ND
F1-1	Goat's Milking Filter	O26
F10-4	Goat's Milking Filter	O26
F80-1	Goat's Milking Filter	ND
F80-2	Goat's Milking Filter	ND
F80-3	Goat's Milking Filter	ND
F80-4	Goat's Milking Filter	ND
F90-1	Goat's Milking Filter	ND
F90-3	Goat's Milking Filter	ND
F93-3	Goat's Milking Filter	O26
F95-2	Goat's Milking Filter	O26
F95-3	Goat's Milking Filter	O26

(5' AGAGTTTGATCCTGGCTCAG 3′) and BSR-1541 (5'AAGGAGG TGATCCAGCCGCA 3′). The PCR products were processed by electrophoresis and, in case no bacterial DNA was detected, the extraction process continued.

Then, 50 µL of EDTA (0.5 M; pH 8), 50 µL of SDS 10% (w/v) and 2.5 µL of Proteinase K (20 mg/mL) were added to the phage suspensions followed by incubation at 37°C for 1 h. Subsequently, 400 µL of saturated phenol were added, gently mixed, and centrifuged at 13400 *g* for 10 min (Centrifuge 5415 D). The aqueous phase was transferred to a new tube and 200 µL of saturated phenol and 200 µL of chloroform: isoamyl alcohol (24:1) were added and centrifuged at 13400 *g* for 10 min. The liquid phase was transferred in a new tube and added with 200 µL of sodium acetate (3 M; pH 7) and 600 µL of isopropanol, for DNA precipitation. After centrifugation under the same condition, the pellet was resuspended in 200 µL of Ethanol 70% (v/v), followed by centrifugation at 13400 *g* for 4 min. Ethanol was then discarded and pellet dried. After drying at 37°C for 60 min, the pellet was resuspended in 50 µL of TE buffer (Tris–HCl 10 mM, EDTA 1 mM, pH 8) and the DNA was stored at −20°C until further usage.

Phage DNA was tested for the presence of *stx* (*stx1, stx2a, stx2f*) and *eae* genes by PCR, according to EU-RL VTEC_Method_01_Rev 0 (2013) protocol (European Union Reference Laboratory (EURL), 2013). DNA from *Escherichia coli* O157:H7, carrying *stx1*, *stx2* and *eae* genes, was used as positive control in PCR. The previously isolated lytic bacteriophage FM10, not carrying virulence genes, was used as negative control (Mangieri et al., 2020).

2.3. Assessment of bacteriophage inducers by qPCR

STEC strains at the beginning of the exponential phase (OD600nm = 0.2–0.3) were subjected to 0.5, 1.5 and 3% (v/v) lactic acid, 1, 1.5 and 2% (w/v) NaCl, anaerobic growth in LB tubes, pasteurization at 72°C for 15 s, UV irradiation (20 cm distance for 60 s), as stress factors related with cheese production.

After incubation at 37°C for 16 h, the samples were centrifuged at 4800 *g* for 10 min (Centrifuge 5,415 D) and filtered through 0.45 µm filters (Minisart® Sartorius). To remove bacterial DNA, 100 µL aliquots were treated with DNase and RNase (10 mg/mL each) at 37°C for 30 min followed by heat treatment at 70°C for 10 min to inactivate the enzymes.

The assay was designed for 15-µl reactions (QPCR Green Master Mix LRox 1X, Biotechrabbit, Hennigsdorf, Germany) containing 400 nM of primers stx1F (5'ATAAATCGCCATTCGTTGACTAC 3′) and stx1R (5' AGAACGCCCACTGAGATCATC 3′). Real-time qPCR assays were carried out in a MasterCycler® ep Realplex (Eppendorf AG) with an initial denaturation at 95°C for 3 min and 40 cycles as follows: 95°C for 15 s, 60°C for 30 s, 65°C for 30 s. A standard curve was obtained by 5-point interpolation of 10-fold serial dilutions of a bacterial gDNA extracted from STEC strain 225R-A carrying the *stx1* gene (Supplementary Figure S1). The DNA concentration was measured through a spectrophotometric lecture at 260 nm, and the DNA copy number was calculated using a ThermoFisher tool: "DNA Copy Number and Dilution Calculator."

Each experiment was replicated 4 times for each strain. The analysis of variance with post-hoc Tukey HSD (Honestly Significant Difference) was performed using the open-source software: R Core Team (R Core Team, 2017), with the package "agricolae," "ggplot2" package for graphic processing.

2.4. Evaluation of bacterial growth after different stressors

To assess cell growth of STEC subjected to different stressors, 200 µL of each bacterial strain were transferred in a 96-wells plate and incubated at 37°C for 16 h, monitoring the optical density (OD) at 600 nm every 15 min through a plate reader (PowerWave XS2, BioTek, Winooski, VT, USA) using Gen5 software. Only samples submitted to

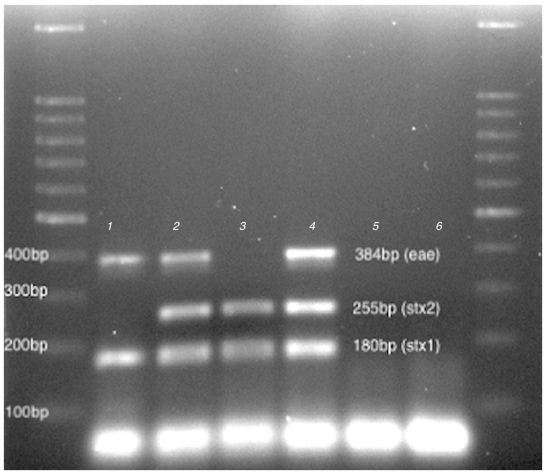

FIGURE 1
Virulence profiling. 100 bp DNA Ladder (LeGene Biosciences, San Diego, United States), 1: vB_Eco225R-A, 2:vB_Eco229R-ACH, 3: vB_EcoF1-1, 4:ATCC 35150 (positive control), 5. FM10 (negative control.), 6: no template and DNA Ladder.

TABLE 2 Summary of SYBR qPCR results organized by stressors.

Stressors	Average Log_{10} copies/mL	std	*n*	groups
2%NaCl	8.19	0.91	12	a
1.5%NaCl	7.97	0.74	12	ab
UV	7.43	0.88	12	abc
1%NaCl	7.15	0.94	12	bcd
Ox	6.69	0.72	12	cd
Sp	6.49	1.00	12	cd
T°	6.29	0.95	12	d
LacAc	5.30	0.32	36	e

Values with different letters are significantly different groups ($p < 0.05$) assigned by One-way ANOVA (Analysis Of Variance) with post-hoc Tukey HSD (Honestly Significant Difference). Ox: oxygen deprivation; Sp: spontaneous release; *T*, heat treatment; LacAc, Lactic acid; std, standard deviation, *n*, number of samples.

oxygen deprivation were transferred into the plate and analyzed at the end of the incubation. Each experiment was performed in triplicate.

3. Results

3.1. Bacteriophages virulence gene assessment

To select the bacterial strains able to release *stx*-phage after a stress, 35 STEC strains were subjected to phage induction using Fosfomycin. Three strains (225R-A, 229RACH and F1-1) showed a sign of bacterial cell lysis in LB double layer agar plates (Supplementary Figure S2) and the presence of *stx* and *eae* genes after PCR amplification of filtrates. In particular, the *stx1* gene was found in all three phages filtrates, the *stx2* was detected only in the 229RACH and F1-1, the *eae* gene in 225R-A and 229RACH (Figure 1). The phage particles were then named vB_Eco225R-A, encoding *stx1* and *eae*, vB_Eco229R-ACH, encoding *stx1*, *stx2* and *eae* and vB_EcoF1-1, encoding *stx1* and *stx2*, based on the nomenclature scheme proposed in Kropinski, Prangishvili, & Lavigne (Kropinski et al., 2009).

3.2. Influence of stressors on bacteriophage induction

The STEC strains that host the bacteriophages have been exposed to various stressors related to the cheese-making process: sodium chloride at three different concentrations (1, 1.5 and 2% w/v), lactic acid (0.5, 1.5 and 3% v/v), pasteurization, UV irradiation and oxygen deprivation.

Evaluation was performed by Real Time qPCR amplification of the *stx1* gene, based on the common presence of this gene in the three lysogenic bacteriophages used in this work. To quantify the amount of DNA contained in the samples, a 5-point standard curve was used: the linear relationship of Ct versus Log (copies/mL) was $Y = -3{,}496x + 43{,}068$, $R2 = 0{,}9{,}983$.

The results, summarized in Table 2, showed that phage induction increased in direct proportion to the NaCl concentration. In fact, the average values were: 8.19, 7.97 and 7.15 Log DNA copies/mL for the addition of 2, 1.5 and 1% of NaCl, respectively, against a spontaneous induction of 6.49 Log DNA copies/mL. Increasing the salinity level to 1.5 and 2% (w/v) significantly boosted the viral content. The effects of heat treatment (72°C for 15 s), irradiation by exposure to UV light and oxygen deprivation were investigated by quantifying phage release after 16 h incubation at 37°C. UV irradiation increased phage induction with a mean value of 7.43 compared to spontaneous induction of 6.49 Log DNA copies/mL. Furthermore, oxygen scarcity improved phage release with a mean value of 6.69 Log DNA copies/mL. In both cases, no significant differences were found ($p < 0.05$) (Table 2). Heat treatment slightly reduced spontaneous release with no significant differences (Table 2). After this treatment, the inoculated bacteria in exponential phase were eliminated. The phenomenon was confirmed by the fact that no colony grew after plating in TBX agar plates after 48 h incubation at 37°C.

To mimic the stressful conditions that protein coagulation can inflict on STEC during the transformation of milk into cheese, caused by the pH-lowering activity of lactic acid bacteria metabolism, the strains were exposed to lactic acid (0.5, 1.5 and 3% v/v). Growth is highly dependent on pH. The data reported in Supplementary Table S1 showed a substantially homogeneous result in the three lactic acid additions (0.5, 1.5 and 3%v/v) performed. Thus, lactic acid addition per strain was reported as lactic acid addition considering the 12 repetitions for each bacterial strain used, regardless the amount of acid added (Table 2).

Noticeably, prophage release was significantly reduced by lactic acid stress, with an average of 5.30 compared to spontaneous release of 6.49 ($p < 0.05$) Log DNA copies/mL.

Considering the single phage behavior under all the stress conditions applied, the average values were 7.35, 6.36 and 6.12 Log DNA copies/mL for the strains 225R-A, F1-1 and 229RACH, respectively. The 225R-A strain was significantly different from the other two ($p < 0.05$) (Table 3).

Results are summarized in Figure 2 where it can be noticed that the median of spontaneous release is lower than the median of 2, 1.5, 1% NaCl, UV irradiation, heat treatment and oxygen deprivation. Hence, these stressors improve phage release.

Significant differences from the control were found for the addition of 2 and 1.5% NaCl with the improvement of phage release and a significant decrease due to the addition of lactic acid (Table 2) ($p < 0.05$). No significant differences were found for the other applied stressors.

3.3. Assessment of bacterial growth

To investigate how different stressors affect bacterial growth, cells were monitored through OD_{600nm} measurements every 15 min. The results are reported in Supplementary Figure S3. The data obtained showed the absence of growth for the bacteria after heat treatment and lactic acid addition. On the contrary, the addition of NaCl at all the concentrations tested and the UV irradiation did not affect the growth curves compared to the control. The oxygen deprivation limited the growth of bacteria.

4. Discussion

Pathogenic bacteria often have multiple temperate bacteriophages within their genome, which can be directed to a lytic cycle in response to a stress. During this work, different stressors related to the cheese making process were analysed to understand the extent of bacteriophage release. To study this phenomenon, 3 out of 35 STEC strains that showed the presence of an inducible prophage, were subjected to stressors.

TABLE 3 Summary of SYBR qPCR organized by different strains.

Bacteria	Average Log copies/mL	std	*n*	groups
225R-A	7.35	1.41	40	a
F1-1	6.36	1.00	40	b
229RACH	6.12	1.02	40	b

Values with different letters are significantly different groups ($p < 0.05$) assigned by One-way ANOVA (Analysis Of Variance) with post-hoc Tukey HSD (Honestly Significant Difference). Copies: Log phage DNA copies/ml; Std, standard deviation; *n*, number of replicates; groups: assigned by Tukey HSD test.

Sodium chloride (NaCl) is added during cheese production to provide texture, consistency, crusting (frequently in ripened cheese varieties); to enhance the flavor, but mainly to inhibit microbial growth (Boisard et al., 2014). Salt content varies between 0.7 and 6.0%, depending on the type of cheese and the method of salting (Bansal and Mishra, 2020). Our findings are in accordance with Harris and colleagues (Harris et al., 2012) that observed increasing frequency in *stx2*+ prophage induction with NaCl concentration up to 2.0%, while 3% NaCl decreased prophage induction significantly.

Commonly, physical methods are used to inactivate pathogenic microorganisms, as well as spoilage microorganisms and their enzymes, ensuring food safety and extending shelf life. As already demonstrated, UV irradiation increased *stx1*-encoding-phage induction (Erill et al., 2007). Oxygen deprivation and pasteurization had no significant effect on induction compared to untreated cultures. Pasteurization treatment causes inactivation of STEC cultures, giving no possibility to any prophage induction event. The presence of phage-derived *stx*-1 genes reported in the samples can be related to a release that took place before treatment, during exponential growth. Given the adaptable metabolism of *E. coli*, oxygen deprivation should not pose substantial stress, favorable to prophage induction.

STEC strains were reported to sustain growth to a minimum of pH 4 for almost 8 h, after which their inherent acid resistance no longer prevented complete loss of viability (Molina et al., 2003). In our study, the bacteria were unable to duplicate under the proposed acidic conditions. Indeed, the pH of the medium after the addition of lactic acid was 3.42, 3.04 and 2.67 for 0.5, 1.5 and 3% of lactic acid (v/v) respectively. The acid-resistant phenotype of STEC is conjectured to be the chief determinant for their low infectious dose (Bernedo-Navarro and Yano, 2016). The reduction in prophage induction by lactic acid exposure was in line with a previous report that showed how stx induction was inhibited at a pH lower than 5.5 (Imamovic and Muniesa,

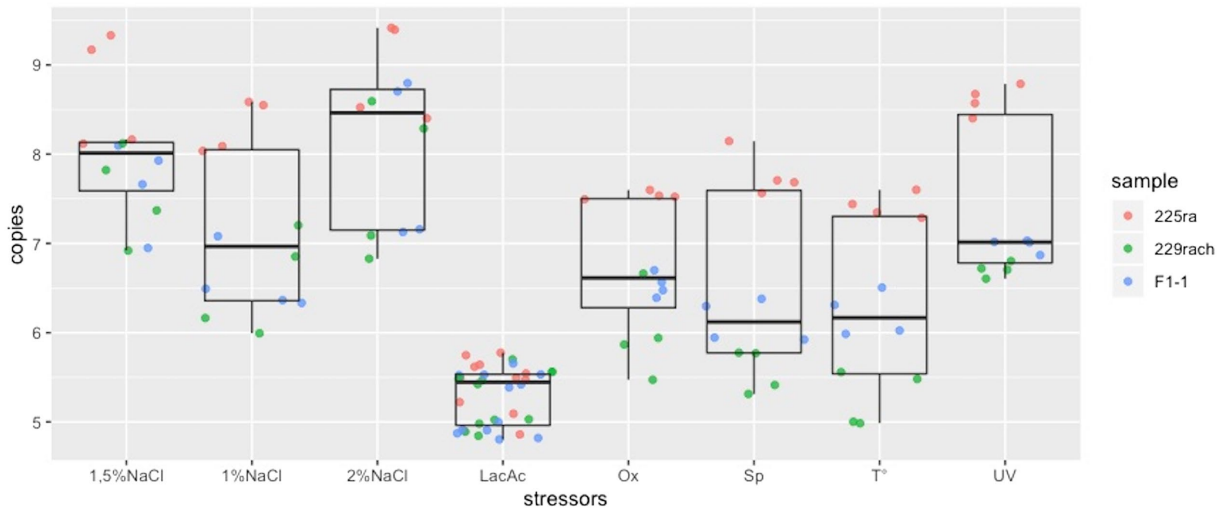

FIGURE 2
Box plots representing the distribution of the phage DNA copies/ml for each stressor. LacAc, Lactic acid; Ox, oxygen deprivation; Sp, spontaneous release; *T*, heat treatment.

2012). Furthermore, in another study in which the phage release was evaluated by adding 1.5 and 3% of lactic acid, temperate phages could not be detected (Bonanno et al., 2017). This may be attributed to the negative effect of weak acids on STEC cellular viability: without significant changes to extracellular pH, assimilation of weak acids disrupts homeostasis by cytoplasmic acidification and anion accumulation, since the conjugate base is unable to diffuse out (Foster, 1999). Albeit significantly decreased, free phage particles in suspension were still detected. However, toxin transmission *via* transduction of viral DNA appears to be unlikely to succeed under acidic conditions. Lowering pH has a halting effect on capsid maturation of virion progeny (Lata et al., 2000), which should disable DNA packaging.

Bacterial growth was monitored through OD measurements after the addition of approximately Log10 6.2 UFC/mL into each tube prior to stress submission. As a result, the values obtained in pasteurization and lactic acid addition did not show any increase over time. However, in the case of NaCl 1.5 and 2%, phage release was significantly different but not observed in bacterial growth, comparing the curves to the control (Supplementary Figure S3).

In conclusion, some stressors related to cheese production can improve or decrease phage release, influencing the safety of the process. As previously reported (Bonanno et al., 2017) free phage particles could infect other *E. coli* both during cheese making process and in the human intestine after ingesting contaminated cheese, increasing the chance of infection. Furthermore, it can be considered that the growth phase of the bacteria influences the spontaneous release of the prophage: the exponential phase is the most favourable. Furthermore, the presence of free *stx*-phage could be a potential cause of false positives in food samples analysed by PCR (Bonanno et al., 2017).

Data availability statement

The original contributions presented in the study are included in the article/supplementary material, further inquiries can be directed to the corresponding author.

Author contributions

NM: Conceptualization, Formal analysis, Methodology, Software, Writing – original draft, Writing – review & editing. RV: Formal Analysis, Investigation. CP: Conceptualization, Data curation, Project administration, Supervision, Writing – review & editing.

Funding

The author(s) declare financial support was received for the research, authorship, and/or publication of this article. They acknowledge the support of the APC central fund of the University of Milan.

Acknowledgments

We would like to thank Roberto Foschino for helpful discussion, funding and resources. We would also like to thank Paula Filomena Martins Lopes for her precious help and support.

Conflict of interest

The authors declare that the research was conducted in the absence of any commercial or financial relationships that could be construed as a potential conflict of interest.

The author(s) declared that they were an editorial board member of Frontiers, at the time of submission. This had no impact on the peer review process and the final decision.

Publisher's note

Supplementary material

The Supplementary material for this article can be found online at: https://www.frontiersin.org/articles/10.3389/fmicb.2023.1270346/full#supplementary-material

References

Bansal, V., and Mishra, S. K. (2020). Reduced-sodium cheeses: implications of reducing sodium chloride on cheese quality and safety. *Compr. Rev. Food Sci. Food Saf.* 19, 733–758. doi: 10.1111/1541-4337.12524

Bernedo-Navarro, R. A., and Yano, T. (2016). Phage display and Shiga toxin neutralizers. *Toxicon* 113, 60–69. doi: 10.1016/j.toxicon.2016.02.009

Boisard, L., Andriot, I., Martin, C., Septier, C., Boissard, V., Salles, C., et al. (2014). The salt and lipid composition of model cheeses modifies in-mouth flavour release and perception related to the free sodium ion content. *Food Chem.* 145, 437–444. doi: 10.1016/j.foodchem.2013.08.049

Bonanno, L., Delubac, B., Michel, V., and Auvray, F. (2017). Influence of stress factors related to cheese-making process and to STEC detection procedure on the induction of Stx phages from STEC O26: H11. *Front. Microbiol.* 8, 296. doi: 10.3389/fmicb.2017.00296

Castro, V. S., Carvalho, R. C. T., Conte-Junior, C. A., and Figueiredo, E. E. S. (2017). Shiga-toxin producing *Escherichia coli*: pathogenicity, Supershedding, diagnostic methods, occurrence, and foodborne outbreaks. *Compr. Rev. Food Sci. Food Saf.* 16, 1269–1280. doi: 10.1111/1541-4337.12302

Cisek, A. A., Dąbrowska, I., Gregorczyk, K. P., and Wyżewski, Z. (2017). Phage therapy in bacterial infections treatment: one hundred years after the discovery of bacteriophages. *Curr. Microbiol.* 74, 277–283. doi: 10.1007/s00284-016-1166-x

Croxen, M. A., Law, R. J., Scholz, R., Keeney, K. M., Wlodarska, M., and Finlay, B. B. (2013). Recent advances in understanding enteric pathogenic *Escherichia coli*. *Clin. Microbiol. Rev.* 26, 822–880. doi: 10.1128/CMR.00022-13

dos Santos Rosario, A. I. L., da Silva Mutz, Y., Castro, V. S., da Silva, M. C. A., Conte-Junior, C. A., and da Costa, M. P. (2021). Everybody loves cheese: crosslink between persistence and virulence of Shiga-toxin *Escherichia coli*. *Crit. Rev. Food Sci. Nutr.* 61, 1877–1899. doi: 10.1080/10408398.2020.1767033

Erill, I., Campoy, S., and Barbé, J. (2007). Aeons of distress: an evolutionary perspective on the bacterial SOS response. *FEMS Microbiol. Rev.* 31, 637–656. doi: 10.1111/j.1574-6976.2007.00082.x

Etcheverría, A. I., and Padola, N. L. (2013). Shiga toxin-producing *Escherichia coli*: factors involved in virulence and cattle colonization. *Virulence* 4, 366–372. doi: 10.4161/viru.24642

European Union Reference Laboratory (EURL) (2013). *Identification and characterization of Verocytotoxin-producing Escherichia coli (VTEC) by real time PCR amplification of the Main virulence genes and the genes associated with the serogroups mainly associated with severe human infections. EU-RL VTEC_Methods*. Available at: www.iss.it/vtec [Accessed July 17, 2020].

Foster, J. W. (1999). When protons attack: microbial strategies of acid adaptation. *Curr. Opin. Microbiol.* 2, 170–174. doi: 10.1016/S1369-5274(99)80030-7

Harris, S. M., Yue, W.-F., Olsen, S. A., Hu, J., Means, W. J., McCormick, R. J., et al. (2012). Salt at concentrations relevant to meat processing enhances Shiga toxin 2 production in *Escherichia coli* O157:H7. *Int. J. Food Microbiol.* 159, 186–192. doi: 10.1016/j.ijfoodmicro.2012.09.007

Imamovic, L., and Muniesa, M. (2012). Characterizing RecA-independent induction of Shiga toxin2-encoding Phages by EDTA treatment. *PLoS One* 7:e32393. doi: 10.1371/journal.pone.0032393

Kakasis, A., and Panitsa, G. (2019). Bacteriophage therapy as an alternative treatment for human infections. A comprehensive review. *Int. J. Antimicrob. Agents* 53, 16–21. doi: 10.1016/j.ijantimicag.2018.09.004

Kim, J.-S., Lee, M.-S., and Kim, J. H. (2020). Recent updates on outbreaks of Shiga toxin-producing Escherichia coli and its potential reservoirs. *Front. Cell. Infect. Microbiol.* 10, 273. doi: 10.3389/fcimb.2020.00273

Koutsoumanis, K., Allende, A., Alvarez-Ordóñez, A., Bover-Cid, S., Chemaly, M., Davies, R., et al. (2020). Pathogenicity assessment of Shiga toxin-producing *Escherichia coli* (STEC) and the public health risk posed by contamination of food with STEC. *EFSA J.* 18, 5967. doi: 10.2903/j.efsa.2020.5967

Kropinski, A. M., Prangishvili, D., and Lavigne, R. (2009). Position paper: the creation of a rational scheme for the nomenclature of viruses of bacteria and archaea. *Environ. Microbiol.* 11, 2775–2777. doi: 10.1111/j.1462-2920.2009.01970.x

Lata, R., Conway, J. F., Cheng, N., Duda, R. L., Hendrix, R. W., Wikoff, W. R., et al. (2000). Maturation dynamics of a viral capsid. *Cells* 100, 253–263. doi: 10.1016/S0092-8674(00)81563-9

Lin, D. M., Koskella, B., and Lin, H. C. (2017). Phage therapy: an alternative to antibiotics in the age of multi-drug resistance. *World J. Gastrointest. Pharmacol. Ther.* 8, 162–173. doi: 10.4292/wjgpt.v8.i3.162

Mangieri, N., Picozzi, C., Cocuzzi, R., and Foschino, R. (2020). Evaluation of a potential bacteriophage cocktail for the control of Shiga-toxin producing *Escherichia coli* in food. *Front. Microbiol.* 11:1801. doi: 10.3389/fmicb.2020.01801

McGannon, C. M., Fuller, C. A., and Weiss, A. A. (2010). Different classes of antibiotics differentially influence Shiga toxin production. *Antimicrob. Agents Chemother.* 54, 3790–3798. doi: 10.1128/AAC.01783-09

Molina, P. M., Parma, A. E., and Sanz, M. E. (2003). Survival in acidic and alcoholic medium of Shiga toxin-producing *Escherichia coli* O157:H7 and non-O157:H7 isolated in Argentina. *BMC Microbiol.* 3, 1–6. doi: 10.1186/1471-2180-3-17

Pacheco, A. R., and Sperandio, V. (2012). Shiga toxin in enterohemorrhagic E.coli: regulation and novel anti-virulence strategies. *Front. Cell. Infect. Microbiol.* 2, 1–12. doi: 10.3389/fcimb.2012.00081

Picozzi, C., Antoniani, D., Vigentini, I., and Foschino, R. (2016). Genotypic characterization and biofilm formation of Shiga-toxin producing *Escherichia coli*. *FEMS Microbiol. Lett.* 364:6971. doi: 10.1093/femsle/fnw291

R Core Team (2017). *R Core team (2017): A language and environment for statistical computing. R found. Stat. Comput. Vienna, Austria. URL http://www.R-project.org/., page R foundation for statistical computing*, Available at: http://www.R-project.org/.

Rodríguez-Rubio, L., Haarmann, N., Schwidder, M., Muniesa, M., and Schmidt, H. (2021). Bacteriophages of Shiga toxin-producing Escherichia coli and their contribution to pathogenicity. *Pathogens* 10:404. doi: 10.3390/pathogens10040404

The European Union One Health 2020 Zoonoses Report (2021). *EFSA J.* 19:6971. doi: 10.2903/J.EFSA.2021.6971

Yang, S. C., Hung, C. F., Aljuffali, I. A., and Fang, J. Y. (2015). The roles of the virulence factor IpaB in Shigella spp. in the escape from immune cells and invasion of epithelial cells. *Microbiol. Res.* 181, 43–51. doi: 10.1016/j.micres.2015.08.006

Yang, S., Lin, C., Aljuffali, I. A., and Fang, J.-y. (2017). Current pathogenic *Escherichia coli* foodborne outbreak cases and therapy development. *Arch. Microbiol.* 199, 811–825. doi: 10.1007/s00203-017-1393-y

frontiers | Frontiers in Microbiology

TYPE Review
PUBLISHED 28 September 2023
DOI 10.3389/fmicb.2023.1268820

OPEN ACCESS

EDITED BY
Alicja Wegrzyn,
Polish Academy of Sciences, Poland

REVIEWED BY
Peter Weigele,
New England Biolabs, United States
Kamil Steczkiewicz,
Polish Academy of Sciences, Poland

*CORRESPONDENCE
Bryan H. Thurtle-Schmidt
✉ brthurtleschmidt@davidson.edu

RECEIVED 28 July 2023
ACCEPTED 14 September 2023
PUBLISHED 28 September 2023

CITATION
Akritidou K and Thurtle-Schmidt BH (2023) OLD family nuclease function across diverse anti-phage defense systems.
Front. Microbiol. 14:1268820.
doi: 10.3389/fmicb.2023.1268820

OLD family nuclease function across diverse anti-phage defense systems

Konstantina Akritidou and Bryan H. Thurtle-Schmidt*

Department of Biology, Davidson College, Davidson, NC, United States

Bacteriophages constitute a ubiquitous threat to bacteria, and bacteria have evolved numerous anti-phage defense systems to protect themselves. These systems include well-studied phenomena such as restriction endonucleases and CRISPR, while emerging studies have identified many new anti-phage defense systems whose mechanisms are unknown or poorly understood. Some of these systems involve overcoming lysogenization defect (OLD) nucleases, a family of proteins comprising an ABC ATPase domain linked to a Toprim nuclease domain. Despite being discovered over 50 years ago, OLD nuclease function remained mysterious until recent biochemical, structural, and bioinformatic studies revealed that OLD nucleases protect bacteria by functioning in diverse anti-phage defense systems including the Gabija system and retrons. In this review we will highlight recent discoveries in OLD protein function and their involvement in multiple discrete anti-phage defense systems.

KEYWORDS

OLD nuclease, overcoming lysogenization defect, Gabija, retrons, Toprim, ABC ATPase, anti-phage defense, abortive infection

1. Introduction

Bacteria are under constant threat from viruses termed bacteriophages, or phages. It is estimated that there are 10^{31} phage particles in nature (Hendrix et al., 1999; Mushegian, 2020), making them the most abundant biological agent on the planet. To protect themselves from this ubiquitous threat, bacteria have evolved numerous systems to ward off phage infections (Hampton et al., 2020; Georjon and Bernheim, 2023). A recurring theme in many of these defense systems is the targeted cleavage of phage nucleic acid. The restriction-modification (R-M) system constitutes a classic example (Loenen et al., 2014), while more recently CRISPR sequences were discovered to generate immunological memory of previous infections and ultimately generate acquired defense (Mojica et al., 2005; Barrangou et al., 2007). Similar to how the R-M system once ushered in the modern era of recombinant DNA technology, the CRISPR/Cas9 system has likewise revolutionized biological and industrial research.

The impact of R-M and CRISPR/Cas9 systems demonstrates the fruitfulness of basic biological research into anti-phage defense mechanisms, and recent years have witnessed the discovery of myriad anti-phage defense systems, many of which remain relatively uncharacterized. Some anti-phage defense systems feature the activity of prokaryotic Argonaute proteins that employ DNA endonuclease activity as the driving mechanism of anti-phage defense (Swarts et al., 2014; Kuzmenko et al., 2020). Others, like BREX (bacteriophage exclusion; Goldfarb et al., 2015), involve methylation to distinguish self from non-self DNA but do not rely on nucleolytic degradation to achieve cell defense (Gordeeva et al., 2019). Other systems do not achieve defense through the preservation of the cell but rather through abortive infection, in

which infected cells effect cell death before the phage can complete its replicative cycle (Lopatina et al., 2020). Systems resulting in abortive infection include CBASS (cyclic oligonucleotide-based antiphage signaling system) and PYCSAR (pyrimidine cyclase system for antiphage resistance) systems, which use cyclic dinucleotides as signaling molecules (Cohen et al., 2019; Tal et al., 2021). Systematic surveys of genomes, in particular focusing on genomic defense islands, continue to uncover new defense systems (Doron et al., 2018; Gao et al., 2020; Millman et al., 2022), most of which remain poorly understood. A close look at several systems, including the Gabija system (Doron et al., 2018; Cheng et al., 2021) and retrons (Millman et al., 2020), illuminate a recurring appearance of overcoming lysogenization defect (OLD) family nucleases. A classification scheme has been proposed in which OLD proteins can be assigned to different classes depending on their surrounding genetic context (Dot et al., 2023). In this review we will focus on the composition, structure, and function of Class 1, Class 2, and Class 3 OLD nucleases across diverse anti-phage defense systems.

2. Class 1 OLD proteins: phage-phage interference and structure overview

Although defense islands have been increasingly observed to harbor anti-phage defense systems (Makarova et al., 2011), Class 1 OLD systems belie this trend as they are instead composed of single genes not found proximal to other candidate defense genes (Figure 1; Schiltz et al., 2019). The archetype for understanding Class 1 OLD proteins, and indeed the original discovery and namesake for the entire OLD family of proteins, arises from early phage genetics experiments. Gianpiero Sironi showed that P2 phage was unable to lysogenize *E. coli* mutants he named *lyd* (lysogenization defective), and subsequently identified P2 mutants that could lysogenize *lyd* mutants (Sironi, 1969). Sironi named this P2 mutant phenotype *old* for overcoming lysogenization defect. Subsequent work determined that lambda phage is unable to lysogenize a wild-type P2 prophage but that this phage interference is eliminated by mutations in *old* (Lindahl et al., 1970). *Lyd* mutants turned out to reside in *recB* and *recC* (Lindahl et al., 1970) components of the RecBCD helicase-nuclease complex that plays critical roles both in homologous recombination and in defense against phages *via* double-stranded DNA degradation (Dillingham and Kowalczykowski, 2008). Expression of the P2 Old protein is sufficient to kill *recBC*$^{-}$ cells (Sironi et al., 1971), a phenotype that continues to be used to assess P2 Old function (Schiltz et al., 2020). P2 Old's interference with lambda phage was an early example of prophage-encoded anti-phage defense, a phenomenon that is now recognized as widespread (Patel and Maxwell, 2023). Indeed, the P2 *old* locus has been observed to encode other anti-phage systems at this position (Rousset et al., 2022; Vassallo et al., 2022).

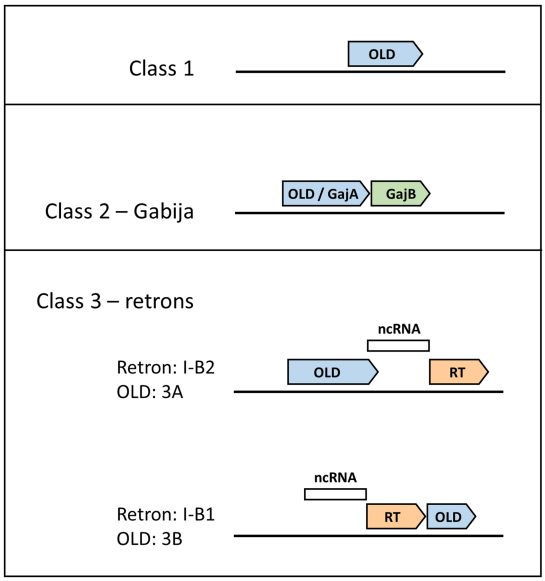

FIGURE 1
Genomic layouts of OLD protein classes. Gene neighborhood organizations for Class 1, 2, and 3 OLD proteins are shown, with OLD proteins in blue. Class 1 OLD proteins appear as single genes. Class 2 OLD proteins are synonymous with GajA, and are found together with GajB (green), which shows homology to UvrD/PcrA/Rep-like helicases. Class 3 OLD proteins are found in retron cassettes and have two possible genomic layouts depending on OLD positioning relative to the reverse transcriptase (RT, orange) and non-coding RNA (ncRNA, white). Class 3A OLD proteins are found in type I-B2 retrons, while Class 3B OLD proteins are found in type I-B1 retrons.

After early phage genetics defined the protein name and function in P2, studies of OLD nucleases mostly disappeared for many years. One notable exception was the purification and characterization of a P2 Old construct fused to maltose-binding protein (MBP; Myung and Calendar, 1995). This study established that P2 Old-MBP displayed 5'to 3′ exonuclease activity on dsDNA. Furthermore, ATP was found to enhance but not be required for DNA cleavage, and the ATPase activity was not stimulated by the addition of DNA. Whether these activities were unique to P2 Old or were common to OLD proteins would remain unknown until recently (Table 1). A few years later, bioinformatic analysis showed that OLD proteins were composed of an N-terminal ATP-binding cassette (ABC)-family ATPase and a C-terminal Toprim domain (Figure 2; Aravind et al., 1998). ABC ATPases are found in diverse proteins ranging from membrane transporters to nuclear structural maintenance of chromosomes (SMC) proteins including condensins and cohesins (Krishnan et al., 2020). The Toprim domain is a divalent metal-binding domain found in topoisomerases, DnaG-type primases, RecR proteins, and OLD family nucleases (Aravind et al., 1998). Toprim domains possess a conserved acidic motif that binds to divalent cations which promote phosphoryl transfer reactions (Keck et al., 2000; Kato et al., 2003; Schmidt et al., 2010), suggesting that DNA cleavage by OLD proteins may follow canonical two-metal DNA cleavage mechanisms (Steitz and Steitz, 1993).

Decades would pass until the field of OLD nuclease research was reignited recently with detailed studies of OLD nuclease structure and function, as well as bioinformatic and genetic analyses of their function in anti-phage defense systems. A critical breakthrough was the first structural determination of a full-length OLD protein, the Class 1 OLD in *Thermus scotoductus* (TsOLD; Figure 2; Schiltz et al., 2020). The structure revealed the protein to adopt a homodimeric structure in which dimerization was mediated through a dimerization domain inserted into the ABC ATPases. Although the ATPases are docked in a conformation not competent to achieve ATP hydrolysis, the structure confirmed that the ATPase domain has structural homology with the ATP-binding cassette (ABC) family of ATPases.

TABLE 1 Functional properties of OLD protein classes.

OLD class	Surrounding genetic context	Select examples	Targeted phages	Structural data	DNA cleavage activities	Nucleotide effect on DNA cleavage	ATP hydrolysis activity?
Class 1	Single genes	P2 Old (UniProt: P13520)	Lambda	None	Nonspecific 5′ to 3′ exonuclease	Higher [ATP] causes slight increase in DNA cleavage	Yes
		T. scotoductus OLD (UniProt: E8PLM2)	Unknown	Homodimeric assembly (PDB: 6P74)	Nonspecific 5′ to 3′ exonuclease; linearizes circular DNA	Negligible	Yes
Class 2 Gabija	Adjacent to UvrD/PcrA/Rep-like helicase	*B. cereus* VD045 GajA (UniProt: J8H9C1)	SBSphiC, SPβ, Φ105, rho14, Φ29	Octamer with 4:4 ratio of GajA:GajB (PDB: 8SM3)	Site-specific nicking Activity	Higher [ATP] strongly inhibits DNA cleavage	No
		B. pseudomallei OLD (UniProt: A3NFC3)	Unknown	Isolated Toprim domain (PDB: 6NK8)	nonspecific 5′ to 3′ exonuclease; linearizes circular DNA	Negligible	Yes
Class 3 retrons	Upstream (3A) or downstream (3B) from reverse transcriptase and non-coding RNA	*E. coli* 200,499 Retron-Eco8 (UniProt: P0DV58)	T4, T7, SECΦ4, SECΦ6, SECΦ18	None	Unknown	Unknown	Unknown

Further structural studies will be required to determine whether Class 1 OLD proteins may exist in higher multimeric complexes or associate with other proteins. Biochemical characterization of TsOLD showed that, like P2 Old, TsOLD displays robust 5'to 3′ exonuclease activity on linear dsDNA, as well as the ability to linearize circular plasmid DNA substrates. However, TsOLD is unlike P2 OLD in that the addition of ATP has essentially no effect on DNA cleavage by TsOLD (Table 1; Schiltz et al., 2020).

Mutagenesis studies in P2 Old showed that the conserved acidic metal-binding residues of the Toprim domain, as well as the conserved Walker A lysine critical for ATP binding, were all required for killing *recBC*$^{-}$ cells, implicating both the ATPase and Toprim domains as essential for at least some *in vivo* activities (Schiltz et al., 2020). However, although the structural determination of TsOLD was a watershed moment propelling OLD protein research forward, the only Class 1 OLD protein established to provide defense against a phage remains P2 Old's defense of prophages against lambda. The anti-phage defense functions of OLD proteins are better understood from studies of multicomponent systems featuring Class 2 or Class 3 OLD proteins.

3. Class 2 OLD proteins: the Gabija system

Recent discoveries of diverse anti-phage defense systems show that OLD proteins not only function on their own as Class 1 proteins but also are found in multicomponent anti-phage defense systems such as Class 2 OLDs found in the Gabija system (Doron et al., 2018). The genetic organization of the Gabija system was discovered independently by two groups. In the first instance, as part of a systematic discovery of anti-phage defense systems, the Sorek group identified a system composed of an OLD protein (GajA), and a UvrD/PcrA/Rep-like helicase (GajB), a system they would name Gabija after the Lithuanian mythology goddess of fire (Figure 1; Doron et al., 2018). They estimated the Gabija system is present in 8.5% of a set of 38,167 microbial genomes, while more recent bioinformatic tools designed to identify anti-phage defense systems place Gabija frequency closer to 15% (Payne et al., 2022; Tesson et al., 2022). The second Gabija system discovery came from the Chappie group which was studying OLD nucleases and termed them as Class 1 or Class 2 depending on whether they were found alone (Class 1) or in tandem with a UvrD/PcrA/Rep-like helicase (Class 2; Schiltz et al., 2019).

The first structural work on Class 2 OLD nucleases was performed on isolated Toprim domains from *Burkholderia pseudomallei* (BpOLD) and *Xanthomonas campestris* p.v. *campestris* (XccOLD; Schiltz et al., 2019). Their Toprim domains contain an extra helical domain insert that differentiates them from Class 1 OLD proteins and makes Class 2 OLD proteins about 50 amino acids longer on average (Figure 2). Structural analysis of the BpOLD Toprim domain shows its conserved acidic motif binds two Mg^{2+} ions and suggests a canonical two-metal mechanism for DNA cleavage. Biochemical assays with full-length BpOLD and XccOLD show nonspecific endonuclease and exonuclease activity on lambda phage DNA which is unaffected by ATP concentration (Table 1). The authors proposed that the BpOLD ATPase domain, which is competent to hydrolyze ATP (Cheng et al., 2021), plays a regulatory role in the cleavage of substrates by the Toprim domain (Schiltz et al., 2019).

The most studied Gabija system is from *Bacillus cereus* VD045 and is found to offer protection against phages of the *Siphoviridae* family including the SPβ, Φ105, and rho14, as well as phages from the *Podoviridae* family such as Φ29 (Table 1; Doron et al., 2018). Although initial biochemical characterization described the *B. cereus* GajA (BcGajA) as functionally distinct from OLD nucleases (Cheng et al., 2021), structural superposition of full-length monomers from *T. scotoductus* OLD and BcGajA reveals an RMSD of 4.4 Å despite a sequence identity of only 22.2% (Figure 2; Schiltz et al., 2020; Antine

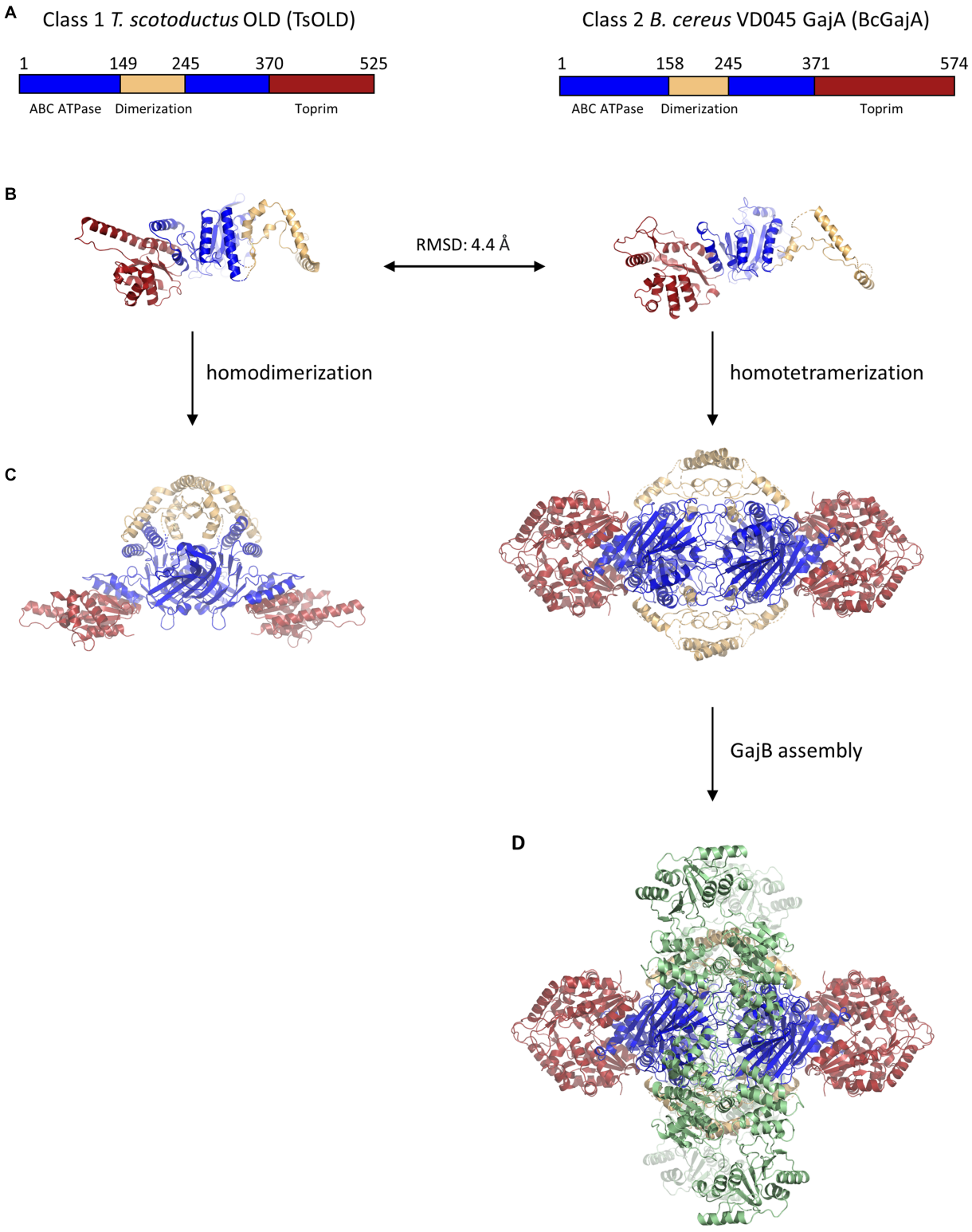

FIGURE 2
Structural similarity and multimeric assembly of Class 1 and Class 2 OLD proteins. **(A)** Schematics showing domain organization within Class 1 *T. scotoductus* OLD and Class 2 *B. cereus* GajA OLD proteins. A dimerization domain (tan) is inserted into each ABC ATPase domain (blue). The larger size of BcGajA arises from a helical insert into the Toprim domain (red) that is conserved among Class 2 OLD proteins and makes them larger than Class 1 OLD proteins by about 50 amino acids on average. **(B)** Structural superposition of TsOLD (PDB: 6P74) and BcGajA (PDB: 8SM3) full-length monomers shows structural similarity (RMSD = 4.4 Å) despite only 22.2% sequence identity. **(C)** TsOLD dimerizes and BcGajA tetramerizes in crystal structures, but in neither structure are the ATPases poised for ATP hydrolysis. **(D)** Two separate GajB dimers (green) bind to a GajA homotetramer to assemble an octameric GajAB complex.

et al., 2023). On the basis of their structural similarity and their shared genomic proximity to UvrD/PcrA/Rep-like helicases, we suggest that all GajA proteins are Class 2 OLD proteins, and vice versa.

Like all Class 2 OLD proteins, BcGajA comprises an N-terminal ABC ATPase domain and a C-terminal Toprim domain. BcGajA is currently the only OLD protein known to cleave DNA with sequence specificity (Table 1), as it nicks DNA at a site found both in lambda and T7 phage dsDNA (Cheng et al., 2021). Interestingly, in lambda DNA the two cut sites overlap, resulting in apparent dsDNA cleavage activity. It is worth noting that BcGajA resides in a gram-positive bacteria that is not infected by lambda or T7 phages, and thus the significance of this cut site being found in lambda and T7 phage DNA is not clear. BcGajA endonuclease activity is robust under low ATP concentrations, while high nucleotide concentrations inhibit BcGajA DNA binding and cleavage (Cheng et al., 2021, 2023). Interestingly, BcGajA is the first OLD protein shown to lack ATP hydrolysis activity (Table 1). These results led the authors to propose that the ATPase domains regulate the Toprim domain by inhibiting its DNA cleavage activity in the presence of high nucleotide concentrations and that GajA becomes activated upon nucleotide depletion resulting from phage invasion, replication, and transcription. Recent studies have reported nucleotide depletion mechanisms in other anti-phage defense systems (Hsueh et al., 2022; Tal et al., 2022), supporting the idea that nucleotide depletion may be common in abortive infection mechanisms.

The second component of the Gabija system, GajB, is predicted to be a UvrD/PcrA/Rep-like helicase (Doron et al., 2018). UvrD helicases translocate along ssDNA in the 3′ to 5′ direction and couple the binding and hydrolysis of one ATP with the unwinding of one base-pair of duplex DNA (Matson, 1986; Lee and Yang, 2006). Recent structural and biochemical data have shed light on the function of GajB and its interactions with GajA. Structural studies show that BcGajB binds to a pre-formed BcGajA tetramer to assemble a 4:4 octameric complex in which with two sets of GajB dimers flank a centralized GajA tetramer (Figure 2; Antine et al., 2023). Although BcGajA purified in the absence of BcGajB displays robust endonuclease nicking activity (Cheng et al., 2021), BcGajB is required for anti-phage defense via an abortive infection mechanism (Doron et al., 2018; Cheng et al., 2023). A recent study shows that BcGajB, surprisingly, does not exhibit any helicase activity but instead functions as a (d)ATP/(d)GTPase (Cheng et al., 2023). Furthermore, the addition of either ssDNA or dsDNA stimulates nucleotide hydrolysis by GajB. The authors propose that BcGajB senses 3′ termini, possibly originating from BcGajA DNA cleavage, which activates its (d)ATP/(d)GTPase hydrolytic activity, thereby driving nucleotide depletion and contributing to cell death (Cheng et al., 2023). Further studies will be required to see whether these results, including a lack of GajB helicase activity, are generalizable to other Gabija systems.

4. Class 3 OLD proteins: retron-driven anti-phage defense

Retrons are genetic elements found in bacteria comprising a reverse transcriptase and an adjacent non-coding RNA. Their discovery stems from a 1984 study identifying a small multi-copy, single-stranded DNA (msDNA; Yee et al., 1984), which subsequent studies determined was composed of a ssDNA covalently linked to a non-coding RNA used as a template by the reverse transcriptase (Dhundale et al., 1987; Lampson et al., 1989). Retron function remained mysterious until a recent breakthrough study that demonstrated retrons belong to anti-phage defense systems triggering cell death through abortive infection (Millman et al., 2020). These defense systems contain three components: the aforementioned reverse transcriptase and non-coding RNA, as well as an effector protein (Figure 1). Effector proteins vary tremendously and include cold shock proteins, zinc finger nucleases, and proteases. Out of 4,802 genomes analyzed, the retron effector protein was an OLD nuclease 4% of the time (Millman et al., 2020). OLD nucleases found as effector proteins in retron defense systems have been classified as Class 3 OLD enzymes, with further subdivision depending on whether the *old* gene lies upstream (Class 3A) or downstream (Class 3B) of the reverse transcriptase (Dot et al., 2023). Within the retron naming system, these genomic organizations have been described as type I-B2 or type I-B1, respectively (Mestre et al., 2020).

Class 3 OLD enzymes have not yet been characterized through biochemical and structural means like either Class 1 or Class 2 OLD enzymes, but AlphaFold models show that, like their Class I and Class 2 counterparts, they comprise an N-terminal ABC ATPase and a C-terminal Toprim domain. Most of what is known about Class 3 OLD proteins arises from genetic studies of anti-phage defense. The best characterized Class 3 OLD protein belongs to Retron-Eco8, which provides defense against T4, T7, SECΦ4, SECΦ6, and SECΦ18 through an abortive infection mechanism (Table 1; Millman et al., 2020). Mutational analysis shows that mutations in the conserved aspartates in the YADD motif of the reverse transcriptase, or in the conserved guanosine branching point in the non-coding RNA, or in the Walker A lysine of the OLD nuclease each eliminate anti-phage defense activity (Millman et al., 2020). These data demonstrate that all three retron components are necessary for anti-phage defense by Retron-Eco8.

The mechanisms by which retrons in general and Class 3 OLD enzymes in particular lead to either phage recognition or abortive infection remain elusive. A recent study shows that T7, SECΦ4, SECΦ6, and SECΦ18 phages were all able to escape anti-phage defense by Retron-Eco8 through mutations in phage single-stranded binding (SSB) protein (Stokar-Avihail et al., 2023). This study showed that expressing the phage SSB in cells that express Retron-Eco8 was sufficient to drive cell toxicity and that mutations in the SSB were sufficient to alleviate that toxicity. Furthermore, pull-down experiments showed that wild-type but not mutant phage SSB was pulled down with Retron-Eco8 msDNA. While these data demonstrate a direct association between retron msDNA and phage SSB, they do not explain the role of the Class 3 OLD enzyme, which was already established to be essential for anti-phage defense (Millman et al., 2020). Further studies of Class 3 OLD enzymes will be required to understand their role in mediating retron-dependent anti-phage defense.

5. Future considerations

The last several years have seen a marked increase in studies examining the structure, biochemistry, and *in vivo* function of OLD proteins. The results of these studies reveal a complicated landscape in which the biochemical properties and functions of OLD proteins can vary from one another and depend heavily on the surrounding genetic, cellular, and chemical context. Many outstanding questions in the field remain, and below we highlight just a few of them:

Do Class 1 OLD proteins provide broad-spectrum anti-phage defense on their own? The only known example of a Class 1 OLD

protein offering protection against a phage is the idiosyncratic example of P2 prophages providing Old-dependent defense only against lambda phage. Although the broad-spectrum anti-phage defense by Class 2 (Gabija) and Class 3 (retron) OLD proteins has been definitively established, there remains no known example of a bacterial or archaeal Class 1 OLD protein sufficient to drive broad-spectrum anti-phage defense. Multicomponent systems like Gabija and retrons have shown that each genetic component is necessary for anti-phage defense, and so it would be valuable to learn of cellular systems where an OLD protein alone is sufficient to drive anti-phage defense.

What are the regulatory relationships between OLD ATPases, Toprim domains, and DNA engagement? It may be that the answer depends on the specific OLD protein in question. For example, ATP has been reported to increase DNA cleavage for P2 Old, have minimal effect on DNA cleavage in TsOLD, and strongly inhibit DNA cleavage activity in BcGajA (Table 1). More work will be required to understand the regulatory relationships between the ATPase and Toprim domains. Moreover, although structural studies of OLD proteins have been critical breakthroughs, there remains a paucity of structural data of OLD proteins bound to DNA. Such studies will be required to understand how the protein engages with DNA, the physical basis for any sequence- or structural specificity OLD proteins may have, and what regulatory mechanisms might prevent DNA binding or cleavage depending on the surrounding biochemical context.

How do phages escape these defense systems? While bacteria have evolved complex mechanisms to impede viral infection, phages continually develop mechanisms to overcome them (Gao and Feng, 2023). One such mechanism involves the release of the Gabija anti-defense 1 (Gad1) protein by phage Φ3T to thwart the Gabija system of *B. cereus* VD045 (Yirmiya et al., 2023). To resist anti-phage defense, Gad1 binds to the GajA dimerization domain of the GajAB complex and prevents DNA binding and cleavage (Antine et al., 2023). Similar phage proteins called Thoeris anti-defense 1 and 2 (Tad1 and Tad2) have been recently discovered in the Thoeris system, another widely distributed bacterial anti-phage defense system (Leavitt et al., 2022). Future studies will no doubt illuminate other escape mechanisms, the understanding of which may be critical for the development of successful phage therapy (Kortright et al., 2019).

How many classes of OLD proteins exist, and in how many different systems? Class 4 OLD proteins have been proposed to contribute to the function of the PARIS system (Rousset et al., 2022; Dot et al., 2023). Unlike the other three classes, in the PARIS system the ATPase and Toprim domains are encoded on separate genes (designated ariA and ariB, respectively; Rousset et al., 2022). However, the authors noted that sometimes AriAB is encoded as a single-gene fusion, in which case it is not clear whether the system comprises a separate OLD class, or whether the system operates differently from Class 1 OLD proteins. Further studies will be required to determine whether the PARIS system constitutes a separate OLD class. Another recent study noted that a component of the anti-plasmid Wadjet system (Doron et al., 2018), jetD, has homology with the Toprim domain of OLD nucleases, while the jetABC components include an ABC ATPase with homology to the bacterial condensin complex MukBEF (Deep et al., 2022). These studies suggest we have much to learn about the myriad systems in which an ABC ATPase and a Toprim domain work in concert in defense systems. Future studies will surely uncover in more detail how OLD proteins have been leveraged by organisms to defend themselves.

Author contributions

KA: Writing – original draft, Writing – review and editing. BT-S: Conceptualization, Visualization, Writing – original draft, Writing – review and editing.

Funding

The author(s) declare financial support was received for the research, authorship, and/or publication of this article. This work was supported by Davidson College.

Acknowledgments

We thank Joshua Chappie and Philip Kranzusch for helpful discussions.

Conflict of interest

The authors declare that the research was conducted in the absence of any commercial or financial relationships that could be construed as a potential conflict of interest.

Publisher's note

References

Antine, S. P., Johnson, A. G., Mooney, S. E., Leavitt, A., Mayer, M. L., Yirmiya, E., et al. (2023). Structural basis of Gabija anti-phage defense and viral immune evasion. *bioRxiv*:2023.05.01.538945. doi: 10.1101/2023.05.01.538945

Aravind, L., Leipe, D. D., and Koonin, E. V. (1998). Toprim--a conserved catalytic domain in type IA and II topoisomerases, DnaG-type primases, OLD family nucleases and RecR proteins. *Nucleic Acids Res.* 26, 4205–4213. doi: 10.1093/nar/26.18.4205

Barrangou, R., Fremaux, C., Deveau, H., Richards, M., Boyaval, P., Moineau, S., et al. (2007). CRISPR provides acquired resistance against viruses in prokaryotes. *Science* 315, 1709–1712. doi: 10.1126/science.1138140

Cheng, R., Huang, F., Lu, X., Yan, Y., Yu, B., Wang, X., et al. (2023). Prokaryotic Gabija complex senses and executes nucleotide depletion and DNA cleavage for antiviral defense. *Cell Host Microbe* 31, 1331–1344.e5. doi: 10.1016/j.chom.2023.06.014

Cheng, R., Huang, F., Wu, H., Lu, X., Yan, Y., Yu, B., et al. (2021). A nucleotide-sensing endonuclease from the Gabija bacterial defense system. *Nucleic Acids Res.* 49, 5216–5229. doi: 10.1093/nar/gkab277

Cohen, D., Melamed, S., Millman, A., Shulman, G., Oppenheimer-Shaanan, Y., Kacen, A., et al. (2019). Cyclic GMP-AMP signalling protects bacteria against viral infection. *Nature* 574, 691–695. doi: 10.1038/s41586-019-1605-5

Deep, A., Gu, Y., Gao, Y.-Q., Ego, K. M., Herzik, M. A. J., Zhou, H., et al. (2022). The SMC-family Wadjet complex protects bacteria from plasmid transformation by recognition and cleavage of closed-circular DNA. *Mol. Cell* 82, 4145–4159.e7. doi: 10.1016/j.molcel.2022.09.008

Dhundale, A., Lampson, B., Furuichi, T., Inouye, M., and Inouye, S. (1987). Structure of msDNA from *Myxococcus xanthus*: evidence for a long, self-annealing RNA precursor for the covalently linked, branched RNA. *Cells* 51, 1105–1112. doi: 10.1016/0092-8674(87)90596-4

Dillingham, M. S., and Kowalczykowski, S. C. (2008). RecBCD enzyme and the repair of double-stranded DNA breaks. *Microbiol. Mol. Biol. Rev.* 72, 642–671. doi: 10.1128/MMBR.00020-08

Doron, S., Melamed, S., Ofir, G., Leavitt, A., Lopatina, A., Keren, M., et al. (2018). Systematic discovery of antiphage defense systems in the microbial pangenome. *Science* 359:eaar4120. doi: 10.1126/science.aar4120

Dot, E. W., Thomason, L. C., and Chappie, J. S. (2023). Everything OLD is new again: how structural, functional, and bioinformatic advances have redefined a neglected nuclease family. *Mol. Microbiol.* 120, 122–140. doi: 10.1111/mmi.15074

Gao, L., Altae-Tran, H., Böhning, F., Makarova, K. S., Segel, M., Schmid-Burgk, J. L., et al. (2020). Diverse enzymatic activities mediate antiviral immunity in prokaryotes. *Science* 369, 1077–1084. doi: 10.1126/science.aba0372

Gao, Z., and Feng, Y. (2023). Bacteriophage strategies for overcoming host antiviral immunity. *Front. Microbiol.* 14:1211793. doi: 10.3389/fmicb.2023.1211793

Georjon, H., and Bernheim, A. (2023). The highly diverse antiphage defence systems of bacteria. *Nat. Rev. Microbiol.* 21, 686–700. doi: 10.1038/s41579-023-00934-x

Goldfarb, T., Sberro, H., Weinstock, E., Cohen, O., Doron, S., Charpak-Amikam, Y., et al. (2015). BREX is a novel phage resistance system widespread in microbial genomes. *EMBO J.* 34, 169–183. doi: 10.15252/embj.201489455

Gordeeva, J., Morozova, N., Sierro, N., Isaev, A., Sinkunas, T., Tsvetkova, K., et al. (2019). BREX system of *Escherichia coli* distinguishes self from non-self by methylation of a specific DNA site. *Nucleic Acids Res.* 47, 253–265. doi: 10.1093/nar/gky1125

Hampton, H. G., Watson, B. N. J., and Fineran, P. C. (2020). The arms race between bacteria and their phage foes. *Nature* 577, 327–336. doi: 10.1038/s41586-019-1894-8

Hendrix, R. W., Smith, M. C. M., Burns, R. N., Ford, M. E., and Hatfull, G. F. (1999). Evolutionary relationships among diverse bacteriophages and prophages: all the world's a phage. *Proc. Natl. Acad. Sci.* 96, 2192–2197. doi: 10.1073/pnas.96.5.2192

Hsueh, B. Y., Severin, G. B., Elg, C. A., Waldron, E. J., Kant, A., Wessel, A. J., et al. (2022). Phage defence by deaminase-mediated depletion of deoxynucleotides in bacteria. *Nat. Microbiol.* 7, 1210–1220. doi: 10.1038/s41564-022-01162-4

Kato, M., Ito, T., Wagner, G., Richardson, C. C., and Ellenberger, T. (2003). Modular architecture of the bacteriophage T7 primase couples RNA primer synthesis to DNA synthesis. *Mol. Cell* 11, 1349–1360. doi: 10.1016/s1097-2765(03)00195-3

Keck, J. L., Roche, D. D., Lynch, A. S., and Berger, J. M. (2000). Structure of the RNA polymerase domain of *E. coli* primase. *Science* 287, 2482–2486. doi: 10.1126/science.287.5462.2482

Kortright, K. E., Chan, B. K., Koff, J. L., and Turner, P. E. (2019). Phage therapy: a renewed approach to combat antibiotic-resistant bacteria. *Cell Host Microbe* 25, 219–232. doi: 10.1016/j.chom.2019.01.014

Krishnan, A., Burroughs, A. M., Iyer, L. M., and Aravind, L. (2020). Comprehensive classification of ABC ATPases and their functional radiation in nucleoprotein dynamics and biological conflict systems. *Nucleic Acids Res.* 48, 10045–10075. doi: 10.1093/nar/gkaa726

Kuzmenko, A., Oguienko, A., Esyunina, D., Yudin, D., Petrova, M., Kudinova, A., et al. (2020). DNA targeting and interference by a bacterial Argonaute nuclease. *Nature* 587, 632–637. doi: 10.1038/s41586-020-2605-1

Lampson, B. C., Inouye, M., and Inouye, S. (1989). Reverse transcriptase with concomitant ribonuclease H activity in the cell-free synthesis of branched RNA-linked msDNA of *Myxococcus xanthus*. *Cells* 56, 701–707. doi: 10.1016/0092-8674(89)90592-8

Leavitt, A., Yirmiya, E., Amitai, G., Lu, A., Garb, J., Herbst, E., et al. (2022). Viruses inhibit TIR gc ADPR signalling to overcome bacterial defence. *Nature* 611, 326–331. doi: 10.1038/s41586-022-05375-9

Lee, J. Y., and Yang, W. (2006). UvrD helicase unwinds DNA one base pair at a time by a two-part power stroke. *Cells* 127, 1349–1360. doi: 10.1016/j.cell.2006.10.049

Lindahl, G., Sironi, G., Bialy, H., and Calendar, R. (1970). Bacteriophage lambda; abortive infection of bacteria lysogenic for phage P2. *Proc. Natl. Acad. Sci. U. S. A.* 66, 587–594. doi: 10.1073/pnas.66.3.587

Loenen, W. A. M., Dryden, D. T. F., Raleigh, E. A., Wilson, G. G., and Murray, N. E. (2014). Highlights of the DNA cutters: a short history of the restriction enzymes. *Nucleic Acids Res.* 42, 3–19. doi: 10.1093/nar/gkt990

Lopatina, A., Tal, N., and Sorek, R. (2020). Abortive infection: bacterial suicide as an antiviral immune strategy. *Annu. Rev. Virol.* 7, 371–384. doi: 10.1146/annurev-virology-011620-040628

Makarova, K. S., Wolf, Y. I., Snir, S., and Koonin, E. V. (2011). Defense islands in bacterial and archaeal genomes and prediction of novel defense systems. *J. Bacteriol.* 193, 6039–6056. doi: 10.1128/JB.05535-11

Matson, S. W. (1986). *Escherichia coli* helicase II (urvD gene product) translocates unidirectionally in a 3′ to 5′ direction. *J. Biol. Chem.* 261, 10169–10175. doi: 10.1016/S0021-9258(18)67506-4

Mestre, M. R., González-Delgado, A., Gutiérrez-Rus, L. I., Martínez-Abarca, F., and Toro, N. (2020). Systematic prediction of genes functionally associated with bacterial retrons and classification of the encoded tripartite systems. *Nucleic Acids Res.* 48, 12632–12647. doi: 10.1093/nar/gkaa1149

Millman, A., Bernheim, A., Stokar-Avihail, A., Fedorenko, T., Voichek, M., Leavitt, A., et al. (2020). Bacterial retrons function in anti-phage defense. *Cells* 183, 1551–1561.e12. doi: 10.1016/j.cell.2020.09.065

Millman, A., Melamed, S., Leavitt, A., Doron, S., Bernheim, A., Hör, J., et al. (2022). An expanded arsenal of immune systems that protect bacteria from phages. *Cell Host Microbe* 30, 1556–1569.e5. doi: 10.1016/j.chom.2022.09.017

Mojica, F. J. M., Díez-Villaseñor, C., García-Martínez, J., and Soria, E. (2005). Intervening sequences of regularly spaced prokaryotic repeats derive from foreign genetic elements. *J. Mol. Evol.* 60, 174–182. doi: 10.1007/s00239-004-0046-3

Mushegian, A. R. (2020). Are there 10^{31} virus particles on earth, or more, or fewer? *J. Bacteriol.* 202:e00052-20. doi: 10.1128/JB.00052-20

Myung, H., and Calendar, R. (1995). The old exonuclease of bacteriophage P2. *J. Bacteriol.* 177, 497–501. doi: 10.1128/jb.177.3.497-501.1995

Patel, P. H., and Maxwell, K. L. (2023). Prophages provide a rich source of antiphage defense systems. *Curr. Opin. Microbiol.* 73:102321. doi: 10.1016/j.mib.2023.102321

Payne, L. J., Meaden, S., Mestre, M. R., Palmer, C., Toro, N., Fineran, P. C., et al. (2022). PADLOC: a web server for the identification of antiviral defence systems in microbial genomes. *Nucleic Acids Res.* 50, W541–W550. doi: 10.1093/nar/gkac400

Rousset, F., Depardieu, F., Miele, S., Dowding, J., Laval, A.-L., Lieberman, E., et al. (2022). Phages and their satellites encode hotspots of antiviral systems. *Cell Host Microbe* 30, 740–753.e5. doi: 10.1016/j.chom.2022.02.018

Schiltz, C. J., Adams, M. C., and Chappie, J. S. (2020). The full-length structure of *Thermus scotoductus* OLD defines the ATP hydrolysis properties and catalytic mechanism of class 1 OLD family nucleases. *Nucleic Acids Res.* 48, 2762–2776. doi: 10.1093/nar/gkaa059

Schiltz, C. J., Lee, A., Partlow, E. A., Hosford, C. J., and Chappie, J. S. (2019). Structural characterization of class 2 OLD family nucleases supports a two-metal catalysis mechanism for cleavage. *Nucleic Acids Res.* 47, 9448–9463. doi: 10.1093/nar/gkz703

Schmidt, B. H., Burgin, A. B., Deweese, J. E., Osheroff, N., and Berger, J. M. (2010). A novel and unified two-metal mechanism for DNA cleavage by type II and IA topoisomerases. *Nature* 465, 641–644. doi: 10.1038/nature08974

Sironi, G. (1969). Mutants of *Escherichia coli* unable to be lysogenized by the temperate bacteriophage P2. *Virology* 37, 163–176. doi: 10.1016/0042-6822(69)90196-2

Sironi, G., Bialy, H., Lozeron, H. A., and Calendar, R. (1971). Bacteriophage P2: interaction with phage lambda and with recombination-deficient bacteria. *Virology* 46, 387–396. doi: 10.1016/0042-6822(71)90040-7

Steitz, T. A., and Steitz, J. A. (1993). A general two-metal-ion mechanism for catalytic RNA. *Proc. Natl. Acad. Sci. U. S. A.* 90, 6498–6502. doi: 10.1073/pnas.90.14.6498

Stokar-Avihail, A., Fedorenko, T., Hör, J., Garb, J., Leavitt, A., Millman, A., et al. (2023). Discovery of phage determinants that confer sensitivity to bacterial immune systems. *Cells* 186, 1863–1876.e16. doi: 10.1016/j.cell.2023.02.029

Swarts, D. C., Jore, M. M., Westra, E. R., Zhu, Y., Janssen, J. H., Snijders, A. P., et al. (2014). DNA-guided DNA interference by a prokaryotic Argonaute. *Nature* 507, 258–261. doi: 10.1038/nature12971

Tal, N., Millman, A., Stokar-Avihail, A., Fedorenko, T., Leavitt, A., Melamed, S., et al. (2022). Bacteria deplete deoxynucleotides to defend against bacteriophage infection. *Nat. Microbiol.* 7, 1200–1209. doi: 10.1038/s41564-022-01158-0

Tal, N., Morehouse, B. R., Millman, A., Stokar-Avihail, A., Avraham, C., Fedorenko, T., et al. (2021). Cyclic CMP and cyclic UMP mediate bacterial immunity against phages. *Cells* 184, 5728–5739.e16. doi: 10.1016/j.cell.2021.09.031

Tesson, F., Hervé, A., Mordret, E., Touchon, M., d'Humières, C., Cury, J., et al. (2022). Systematic and quantitative view of the antiviral arsenal of prokaryotes. *Nat. Commun.* 13:2561. doi: 10.1038/s41467-022-30269-9

Vassallo, C. N., Doering, C. R., Littlehale, M. L., Teodoro, G. I. C., and Laub, M. T. (2022). A functional selection reveals previously undetected anti-phage defence systems in the *E. coli* pangenome. *Nat. Microbiol.* 7, 1568–1579. doi: 10.1038/s41564-022-01219-4

Yee, T., Furuichi, T., Inouye, S., and Inouye, M. (1984). Multicopy single-stranded DNA isolated from a gram-negative bacterium, *Myxococcus xanthus*. *Cells* 38, 203–209. doi: 10.1016/0092-8674(84)90541-5

Yirmiya, E., Leavitt, A., Lu, A., Avraham, C., Osterman, I., Garb, J., et al. (2023). Phages overcome bacterial immunity via diverse anti-defense proteins. *bioRxiv*:2023.05.01.538930. doi: 10.1101/2023.05.01.538930

frontiers | Frontiers in Microbiology

TYPE Original Research
PUBLISHED 11 October 2023
DOI 10.3389/fmicb.2023.1286046

OPEN ACCESS

EDITED BY
Alicja Wegrzyn,
Polish Academy of Sciences, Poland

REVIEWED BY
Guangtao Huang,
Shenzhen Second People's Hospital, China
Prasanth Manohar,
Texas A&M University, United States

*CORRESPONDENCE
María Tomás
✉ MA.del.Mar.Tomas.Carmona@sergas.es

RECEIVED 30 August 2023
ACCEPTED 26 September 2023
PUBLISHED 11 October 2023

CITATION
Pacios O, Blasco L, Ortiz Cartagena C, Bleriot I, Fernández-García L, López M, Barrio-Pujante A, Cuenca FF, Aracil B, Oteo-Iglesias J and Tomás M (2023) Molecular studies of phages-*Klebsiella pneumoniae* in mucoid environment: innovative use of mucolytic agents prior to the administration of lytic phages.
Front. Microbiol. 14:1286046.
doi: 10.3389/fmicb.2023.1286046

Molecular studies of phages-*Klebsiella pneumoniae* in mucoid environment: innovative use of mucolytic agents prior to the administration of lytic phages

Olga Pacios[1,2], Lucía Blasco[1,2], Concha Ortiz Cartagena[1,2], Inés Bleriot[1,2], Laura Fernández-García[1,2], María López[1,2], Antonio Barrio-Pujante[1,2], Felipe Fernández Cuenca[2,3,4], Belén Aracil[4,5,6], Jesús Oteo-Iglesias[2,4,5,6] and María Tomás[1,2,4]*

[1]Grupo de Microbiología Traslacional y Multidisciplinar (MicroTM)-Servicio de Microbiología Instituto de Investigación Biomédica A Coruña (INIBIC), Hospital A Coruña (CHUAC), Universidad de A Coruña (UDC), A Coruña, Spain, [2]Grupo de Estudio de los Mecanismos de Resistencia Antimicrobiana (GEMARA) formando parte de la Sociedad Española de Enfermedades Infecciosas y Microbiología Clínica (SEIMC), Madrid, Spain, [3]Unidad Clínica de Enfermedades Infecciosas y Microbiología Clínica, Hospital Universitario Virgen Macarena, Instituto de Biomedicina de Sevilla (Hospital Universitario Virgen Macarena/CSIC/Universidad de Sevilla), Sevilla, Spain, [4]MePRAM, Proyecto de Medicina de Precisión contra las resistencias Antimicrobianas, Madrid, Spain, [5]Laboratorio de Referencia e Investigación de Resistencias a Antibióticos e Infecciones Sanitarias, Centro Nacional de Microbiología, Instituto de Salud Carlos III, Madrid, Spain, [6]CIBER de Enfermedades Infecciosas (CIBERINFEC), Instituto de Salud Carlos III, Madrid, Spain

Mucins are important glycoproteins that form a protective layer throughout the gastrointestinal and respiratory tracts. There is scientific evidence of increase in phage-resistance in the presence of mucin for some bacterial pathogens. Manipulation in mucin composition may ultimately influence the effectiveness of phage therapy. In this work, two clinical strains of *K. pneumoniae* (K3574 and K3325), were exposed to the lytic bacteriophage vB_KpnS-VAC35 in the presence and absence of mucin on a long-term co-evolution assay, in an attempt to mimic *in vitro* the exposure to mucins that bacteria and their phages face *in vivo*. Enumerations of the bacterial and phage counts at regular time intervals were conducted, and extraction of the genomic DNA of co-evolved bacteria to the phage, the mucin and both was performed. We determined the frequency of phage-resistant mutants in the presence and absence of mucin and including a mucolytic agent (N-acetyl L-cysteine, NAC), and sequenced them using Nanopore. We phenotypically demonstrated that the presence of mucin induces the emergence of bacterial resistance against lytic phages, effectively decreased in the presence of NAC. In addition, the genomic analysis revealed some of the genes relevant to the development of phage resistance in long-term co-evolution, with a special focus on the mucoid environment. Genes involved in the metabolism of carbohydrates were mutated in the presence of mucin. In conclusion, the use of mucolytic agents prior to the administration of lytic phages could be an interesting therapeutic option when addressing *K. pneumoniae* infections in environments where mucin is overproduced.

KEYWORDS

***Klebsiella pneumoniae*, lytic bacteriophages, phage resistance, co-evolution, mucin, n-acetyl cysteine**

1. Introduction

Klebsiella pneumoniae is a Gram-negative opportunistic pathogen that causes urinary tract, wound and soft tissue infections, pneumonia, and even life-threatening sepsis (Kamruzzaman and Iredell, 2019; Mackow et al., 2019). Moreover, the recent increase of carbapenemase-producing strains of *K. pneumoniae* worldwide, together with its ability to grow in biofilm and to acquire plasmids conferring antibiotic (multi)resistance, underlie the importance of developing innovative and effective strategies against *K. pneumoniae* infections (Majkowska-Skrobek et al., 2021; Pacios et al., 2021).

In this context, the use of bacteriophages (or phages), viruses that specifically target bacteria in a highly effective and safe manner, is being evaluated as a therapeutic approach against bacterial infections, especially antibiotic-resistant ones (Pacios et al., 2020; Majkowska-Skrobek et al., 2021). Nevertheless, just as it happens with antibiotics, the emergence of phage-resistant mutants is a major hurdle to the establishment of phage therapy (Majkowska-Skrobek et al., 2021; Uyttebroek et al., 2022). Indeed, to counter phage infection, bacteria display several defence mechanisms: mutation of the receptor recognized by a particular phage to inhibit adsorption (surface mutation) (Denes et al., 2015), induction of programmed cell death, known as abortive infection (Abi) (Lopatina et al., 2020), translation of nucleases that specifically degrade the phage DNA [CRISPR-Cas, restriction-modification… (Castillo et al., 2020; Ambroa et al., 2021)], etc. Despite the inconvenience of resistant bacteria against phages, their compassionate use in clinics has been approved in many countries and has already saved many life-threatening infections in patients (Schooley et al., 2017; Dedrick et al., 2019; Law et al., 2019).

Cystic Fibrosis (CF), an autosomal recessive genetic disorder that produces mutations in the cystic fibrosis transmembrane conductance regulator (CFTR) protein, is characterized by an overproduction of viscous mucins, since lack of CFTR function reduces airway mucus fluidity and influences hydration and mucin viscosity in the airways (Riquelme et al., 2018). This allows the trapping of inhaled bacteria in the lungs and explains why CF patients often become colonized by pathogens from an early age, which can lead to chronic infections (Pletzer et al., 2017). Even if a few typical bacteria are traditionally involved in CF lung infections, such as *Staphylococcus aureus* and *Pseudomonas aeruginosa*, CF patients are susceptible to infection by other opportunistic pathogens, including *K. pneumoniae* (Leão et al., 2011; Delfino et al., 2015). Especially relevant are the hypervirulent *K. pneumoniae* strains, in which hypermucoviscosity plays a key role in their pathogenesis and immune evasion, as shown in human and animal serum survival assays (Xu et al., 2021).

To improve therapeutic outcomes in phage therapy, the arising of phage-resistant bacteria in the complex *in vivo* context needs to be exploited. Furthermore, not many studies address the efficiency of phage in long-term evolutionary experiments, nor look at phage co-evolution during phage treatments, as reviewed by Moulton-Brown and Friman (2018).

One of the main components of the gastrointestinal and respiratory tracts are mucins. Mucins are high-molecular-weight proteins that are glycosylated and can be transmembrane (forming a protective "brush" border on the epithelium) or gel-forming (providing hydration and protection from shear stress) (Hansson, 2019; Paone and Cani, 2020). They protect the intestinal mucosa from physical contact with commensal bacteria, as well as from invasion of intruders and pathogens (Carroll-Portillo and Lin, 2021). Changes in mucin expression are relevant in inflammatory and neoplastic disorders of the gastrointestinal tract, being important in the etiology of some infectious diseases, such as *Helicobacter pylori* gastritis (Jass and Walsh, 2001).

In the present work, we have used two bacteriemia-causing clinical isolates of *K. pneumoniae*, named K3574 and K3325, and exposed them to the lytic bacteriophage vB_KpnS-VAC35 [previously characterized by our group (Bleriot et al., 2023)] in the presence and absence of mucin on a long-term co-evolution assay, intending to study the phage resistance in a mucoid environment. We determined the relationship between mucin and the difficulties in applying phage therapy, and we included the mucolytic agent N-acetyl cysteine (NAC) to improve the use of phages by avoiding the emergence of resistance.

2. Materials and methods

2.1. Bacterial strains and growth conditions

K. pneumoniae clinical strains K3574 and K3325 were isolated from patient's blood and stored at the National Centre for Microbiology (Carlos III Health Institute, Spain), the former being the one of choice for the phenotypic characterization of the lytic bacteriophage vB_KpnS-VAC35 (Bleriot et al., 2023). All the bacterial strains were cultivated using Luria-Bertani broth (LB, 1% tryptone, 0.5% yeast extract and 0.5% NaCl). When required, purified mucin from porcine stomach (SigmaAldrich®), previously diluted in distilled water and autoclave-sterilized, was added at a final concentration of 1 mg/mL. NAC was also purchased from SigmaAldrich®, diluted with nuclease-free water, filter-sterilized and added (when corresponded) to a final concentration of 10 mM. The absence of interaction between NAC and the bacteriophage was confirmed with a growth curve of the clinical isolate K3574 (Supplementary Figure S1).

2.2. Establishment of the infectivity of the phage

2.2.1. Efficiency of plating

The EOP assay was done as previously described (Kutter, 2009), calculated as the ratio between the phage titre (plaque forming units, PFU/mL) in the test strain and the titre in the isolation host (*K. pneumoniae* K3574). For both assays, TA-soft medium (1% tryptone, 0.5% NaCl and 0.4% agar) was used to make plates by the top-agar method (Abedon and Yin, 2009). Strains exhibiting susceptibility to phage infection in the spot test performed by Bleriot et al. in a previous work from our group were selected for the EOP assay (Bleriot et al., 2023).

2.2.2. Infection curves

To assess the lytic capacity of vB_KpnS-VAC35, infection curves at different multiplicities of infection (MOI) were performed. Overnight cultures of the clinical isolates of *K. pneumoniae* K3574 and K3325 were diluted 1:100 in LB broth and then incubated at 37°C at 180 rpm until an early exponential phase (OD_{600nm} = 0.3–0.4) was reached. Then, vB_KpnS-VAC35 was added to the cultures at MOI of 0.1 and 1, and OD_{600nm} was measured during 6 h at 1 h intervals.

2.3. Co-evolution between vB_KpnS-VAC35 and *Klebsiella pneumoniae* strains K3574 and K3325

The bacterial strains were incubated in 20 mL LB-containing flasks at 37°C and 180 rpm for 6 (K3325) or 15 days (K3574), re-inoculated daily into fresh LB medium (1:100 dilution). The flasks were infected with vB_KpnS-VAC35 at a MOI = 1 in the presence and absence of porcine mucin at a final concentration of 1 mg/mL, and a non-infected control of the bacterial isolate growing in presence of 1 mg/mL mucin was included. The infections with the phage were performed at OD ≈ of 0.4. From this moment and every 24 h, each condition was 1:100 diluted in fresh LB medium, containing 1 mg/mL mucin when required, and enumeration of colony forming units (CFU) and PFU was performed. For the CFU enumeration, 1 mL aliquots of bacterial cultures were serially diluted in the saline buffer then platted on LB-agar plates (100 µL) and incubated overnight. For the PFU assessment, 1 mL aliquots were centrifuged 5 min at maximum speed (14,000 rpm) for the collection of phage particles in the supernatant. Serial dilutions of these PFU were performed in SM buffer (100 mM NaCl, 10 mM MgSO4, 20 mM Tris-HCl, pH 7.5), then 10 µL of the pertinent dilutions were plated by the double-layer method and enumerated after overnight incubation (Abedon and Yin, 2009). Two flasks per condition were considered as biological duplicates.

2.4. Assessment of phage resistance

2.4.1. Spot test

The spot test assay was undertaken as described by Raya and H'bert (2009). We used vB_KpnS-VAC35 WT, vB_KpnS-VAC35_ad15 and vB_KpnS-VAC35_ad15_m phages, that is prior to co-evolution, and adapted to K3574 during 15 days in the absence and presence of mucin, respectively.

2.4.2. Calculation of the frequency of phage-resistant mutants

The frequency of resistant mutants was calculated as previously described by Lopes et al., (2018). Overnight cultures of the strains K3574 and K3325 at the different conditions evaluated were diluted 1:100 in LB and grown to an OD_{600nm} of 0.7. An aliquot of 1 mL of the culture containing 10^8 CFU/mL was serially diluted, and the corresponding dilutions were mixed with 100 µL of vB_KpnS-VAC35 at 10^9 PFU/mL, then plated by the double-layer method in TA medium. The plates were incubated at 37°C for 24 h, then the colonies of resistant mutants were enumerated. The mutation rate was calculated by dividing the number of resistant bacteria (growing in the presence of the phage) by the total number of bacteria plated in conventional LB-agar (100 µL).

2.5. Genomic DNA extraction and whole-genome sequencing

The DNeasy Blood & Tissue Kit (Qiagen®) was used for extracting the genomic DNA of bacterial cultures co-evolved 15 dpi with the vB_KpnS-VAC35 alone (K3574_ad15_P), in the presence of mucin (K3574_ad15_P + M) and exposed 15 days to mucin (K3574_ad15_M), following the manufacturer's instructions. Samples were quantified with a Qubit 3.0 fluorometer using a Qubit dsDNA HS Assay Kit and with a Nanodrop spectrophotometer to evaluate the DNA purity.

The Oxford Nanopore MinION MK1C platform with the Rapid Barcoding Kit (SQK-RBK004) were employed to obtain the long reads. A Nanopore sequencing library was made, and the pooled samples were loaded onto the FLO-MIN106 R9 (v.9.4.1) flowcell, following the manufacturer's instructions. A 48 h run was conducted without real time basecalling since this step was performed afterwards (see below).

2.6. Bioinformatic analysis

Basecalling was performed using GUPPY (Version 5.0.7 Super-accuracy model (SUP)) to generate fastQ sequencing reads from electrical data (the fast5 files generated by MinION). Quality control of the generated fastQ reads was performed using the FastQC[1] and NanoPlot[2] tools. The reads were then further subsampled according to their barcodes and *de novo* assembled using Unicycler (v1.0+). Draft assemblies were corrected by iterative rounds of polishing with the error correction software Racon. Subsequently, the Bandage tool was used in order to assess the quality of assemblies quickly and visually. Annotations were performed using Prokka (Seemann, 2014), and insertions, deletions and other SNPs were called using the structural variant caller Snippy (v1.0.11). The presence and absence of intact genetic sequences were analyzed using Roary and Orthovenn2.[3] OrthoVenn2 was used to compare the proteins of the four complete genomes using the files generated by Prokka analysis. Fasta files obtained after annotation were surveilled for indels using the blastn and blastp tools from the NCBI and compared to the reference genome (for K3574_WT, BioSample code SAMEA3649560 included in the European BioProject PRJEB10018). The workflow taken from Nanopore sequencing to the genomic analysis is summarized in Figure 1A.

3. Results

3.1. Infectivity of phage vB_KpnS-VAC35

The two strains exhibiting the highest EOP values (K3574 and K3325) were chosen for further assays (Figure 2A). Optical density growth curves showed good lytic activity of vB_KpnS-VAC35 in these strains at MOI of 0.1 (purple line) and 1 (orange line) (Figures 2B,C, respectively). The isolate K3325 was less susceptible to the lytic phage vB_KpnS-VAC35 than the isolation host, K3574.

3.2. Co-evolution of K3574 and K3325 with the phage vB_KpnS-VAC35 in a mucoid environment

For the co-evolution experiment, the initial bacterial inoculum was 2×10^8 CFU/mL for K3574 and 10^8 CFU/mL for K3325 (Figure 3).

1 https://github.com/s-andrews/FastQC
2 https://github.com/wdecoster/NanoPlot
3 https://orthovenn2.bioinfotoolkits.net/home

10.3389/fmicb.2023.1286046

A

Strain	EOP	Biological origin	Capsular type
K3574	1	Blood	KL30
K3325	0.478	Blood	KL64
ST437-OXA245	0.435	Rectal	KL36
K2783	0.309	Blood	KL134
ST11-VIM1	0.007	Respiratory	KL24

EOP values: 1 0.45-0.5 0.1-0.45 <0.1

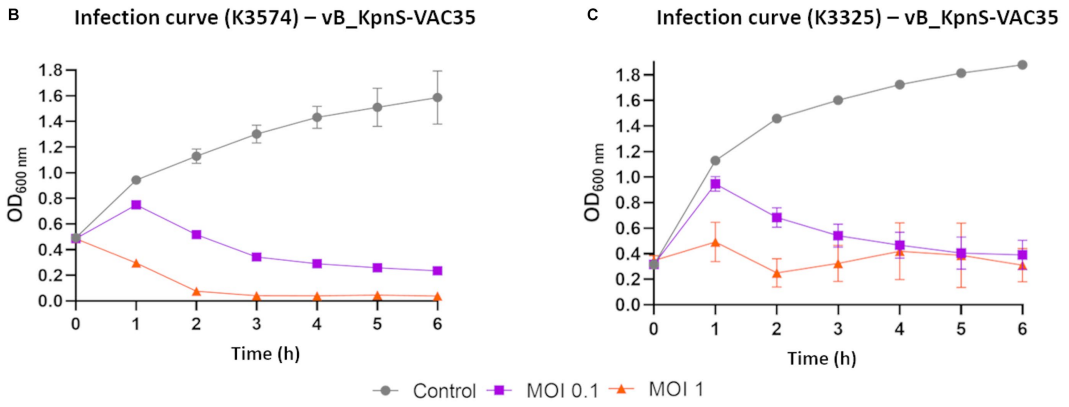

FIGURE 1
(A) EOP of vB_KpnS-VAC35 on the clinical isolates of *K. pneumoniae* that exhibited a positive spot test. **(B)** and **(C)** Infection curves of clinical isolates K3574 and K3325, respectively, by the lytic phage vB_KpnS-VAC35, prior to co-evolution, at MOI 0.1 and 1.

As we infected both cultures in the exponential growth phase at a MOI = 1, the initial phage concentration was 2×10^8 PFU/mL and 10^8 PFU/mL, respectively (Figure 3). The CFU counts remained stable at around 10^{10} CFU/mL for both strains at every condition tested, whereas the PFUs fluctuated slightly more: in what concerns the isolate K3574 co-adapted to the phage, PFU counts ranged from 10^9 PFU/mL at 1 day post-infection (dpi) to 10^7 PFU/mL at 15 dpi, whereas in the presence of mucin these counts reached 10^8 PFU/mL at 9 dpi, then slightly decreased till 10^7 PFU/mL at 15 dpi (Figure 3A), which corresponds to the 1:100 dilution performed every day along the experiment. Regarding the isolate K3325, co-evolution lasted 6 days as the PFU numbers dropped to 0 in the absence of mucin (Figure 3B). Nonetheless, in the presence of this compound, 10^3 PFU/mL of vB_KpnS-VAC35 were assessed at 6 dpi.

3.3. Assessment of phage-resistance

3.3.1. Spot test

In order to evaluate how the presence of mucin will affect the bacterial susceptibility to the adapted phages a spot test of *K. pneumoniae* K3574 and K3325 prior to the co-evolution (named as "WT" in Figure 4), but also co-evolved in the presence of mucin, the phage, and both during 15 and 6 days, respectively, was conducted. The only conditions in which phage-susceptibility was kept was for WT and mucin-adapted cells (K3574_ad15_m and K3325_ad6_m), in which no phage-infection was established (Figure 4). However, we observed differences when comparing the infection established by the non-adapted phage (vB_KpnS-VAC35_WT) and the adapted ones (vB_KpnS-VAC35_ad15 and vB_KpnS-VAC35_ad15_m), which were isolated after 15 days of co-evolution with K3574 and produced more turbid spots (Figure 4, middle and right columns). The presence of more colonies growing inside the lytic halos of vB_KpnS-VAC35_ad15_m compared to the infection established by vB_KpnS-VAC35_ad15 suggested that mucin either affected the phage-infection capacity, or it enhanced the bacterial defence to the phage [as it has already been documented in the literature for different microorganisms (Green et al., 2021; de Freitas Almeida et al., 2022)].

3.3.2. Frequency of arising of resistant mutants in the presence of the mucolytic N-acetyl L-cysteine

To quantitatively assess the effect that the presence of mucin had during bacteria and phage co-evolution, we determined the frequency of phage-resistant mutants to vB_KpnS-VAC35 in 6 different conditions, depicted in Figure 5: (i) WT (orange bar); (ii) exposed to mucin alone (blue bar); (iii) mucin and its inhibitor, NAC (red bar); (iv) phage alone (green bar); (v) phage and mucin (pink bar); and, finally, (vi) phage, mucin and the NAC inhibitor (black bar). Thus, the condition in which *K. pneumoniae* clinical isolates K3574 and K3325 were incubated in presence of mucin and NAC for 15 and 6 days, respectively, was included. Consistently with the infection curves of vB_KpnS-VAC35 in these two strains, we obtained a higher frequency for K3325 than K3574 (Figure 5, orange bar). In the case of phage-exposed bacteria, either in the presence of mucin alone, mucin and NAC, or in the absence of these compounds, no statistical difference

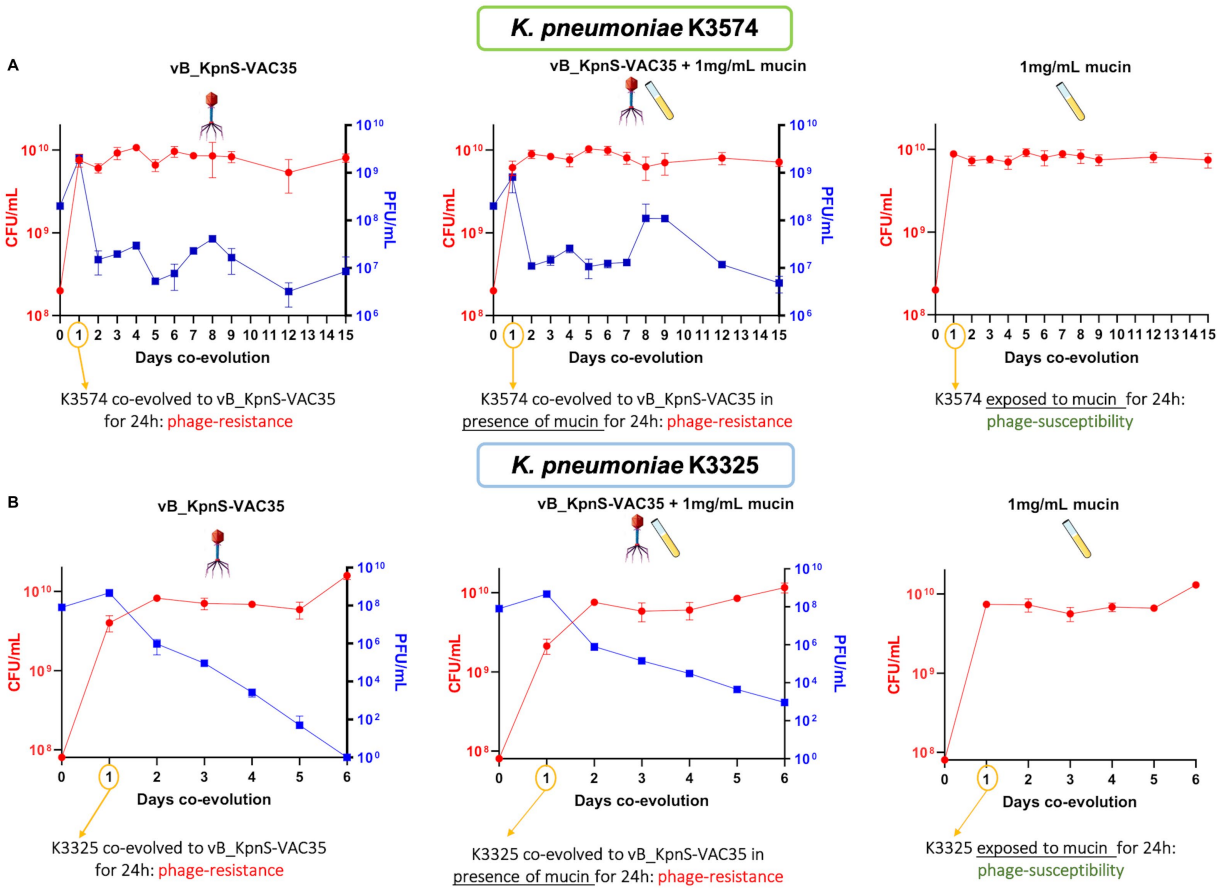

FIGURE 2
Titration of the colony forming units (CFU, left *Y*-axis) and plaque forming units (PFU, right *Y*-axis) per mL during the co-evolution experiments between clinical isolates K3574 **(A)** and K3325 **(B)** and the lytic bacteriophage vB_KpnS-VAC35, in the absence and presence of mucin (1 mg/mL).

was observed (Figure 5). Importantly, cells pre-exposed to mucin and NAC exhibited a statistically significant reduction in the phage-resistance frequency (Figure 5, red bar) compared to the cells exposed exclusively to mucin (Figure 5, blue bar, *p*-values <0.001).

3.4. Genomic analysis of *Klebsiella pneumoniae* strains before and after the co-evolution in the presence of mucin

Genomic analysis of the clinical strain K3574 adapted to mucin, to the phage alone or to both agents, were performed. We exclusively chose this strain, considered the "isolation host," as previously said, because its co-evolution with the bacteriophage vB_KpnS-VAC35 lasted 15 days (instead of 6) and showed a higher susceptibility to the infection (Figure 2).

The reference genome of this strain (BioSample code SAMEA3649560, European BioProject PRJEB10018) possesses 5,635,279 bp (5,561 coding sequences) with a GC content of 57.1%, a sequence-type ST3647 and a capsular type KL30. We extracted the bacterial DNA at 15 dpi of this isolate co-evolved to the phage (K3574_ad15_P, deposited into GenBank under the BioSample code SAMN37179281 and the Genome Accession JAVLVI000000000), to mucin (K3574_ad15_M, deposited into GenBank under the BioSample code SAMN37179282 and the Genome Accession JAVLVH010000001) and to both (K3574_ad15_P + M, deposited into GenBank under the BioSample code SAMN37179283 and the Genome Accession JAVLVG000000000). These three sequences belong to the BioProject PRJNA1010120.

A Venn diagram was used to visualize the different and overlapping protein clusters displayed by the four complete genomes taken into consideration (Figure 1B). In total, 5,000 common protein clusters were found between the strain prior to co-evolution and bacteria co-evolved to the phage (K3574_ad15_P), whereas 4,938 were found between K3574_WT and the mucin-adapted cells (K3574_ad15_M), and 4,947 common protein clusters between K3574_WT and cells co-evolved to the phage in the presence of mucin (K3574_ad15_P + M). No specific protein clusters were found for the strain adapted only to mucin (K3574_ad15_M) and to phage and mucin together (K3574_ad15_P + M), while 3 unique protein clusters were found in the isolate co-evolved to the phage alone (K3574_ad15_P) (Figure 1B).

Comparison of the genomes revealed important mutations (Figure 6 and Table 1). Among the genes in which nucleotide changes were found, we highlight several interesting ones grouped into different categories: concerning the bacterial defense mechanisms to phage infection, a tRNA-guanosine (18)-2'-O-methyltransferase carrying a nucleotide deletion in the position 362 was found in the case of K3574_ad15_P and K3574_ad15_P + M, whereas the non-infected isolate (K3574_ad15_M) had the intact locus compared to the K3574_WT. This change (c.-362G) leads to

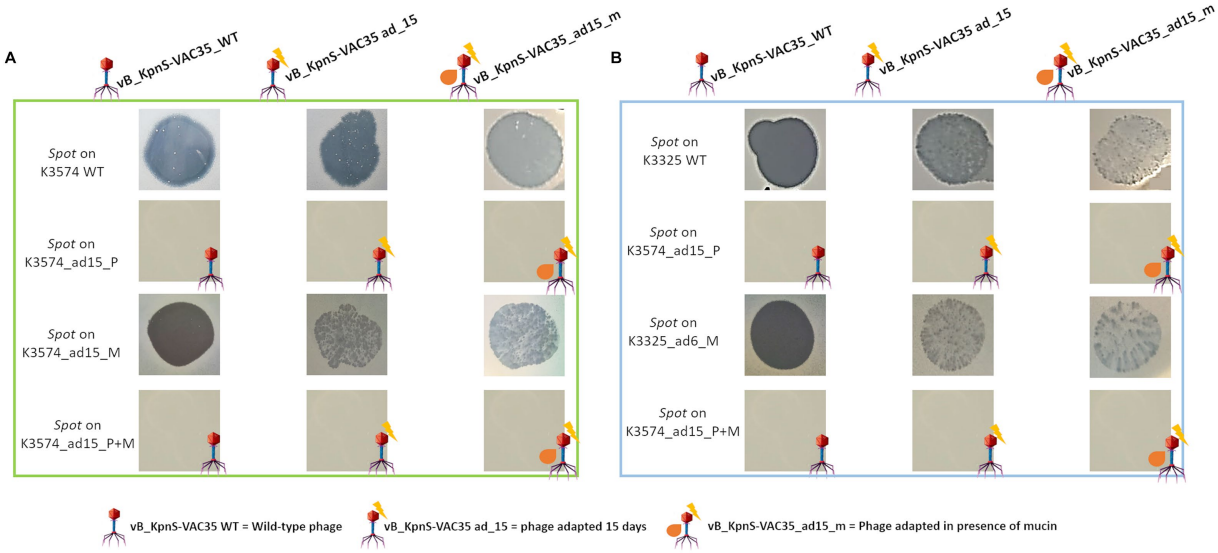

FIGURE 3
Spot tests of phages prior to co-evolution (vB_KpnS-VAC35 WT), co-evolved to K3574 in the absence and in the presence of mucin (vB_KpnS-VAC35_ad15 and vB_KpnS-VAC35_ad15_m, respectively). **(A)** Spot test using the clinical isolate *K. pneumoniae* K3574 WT, adapted 15 days to the phage, to mucin and to both. **(B)** Spot test using the clinical isolate *K. pneumoniae* K3325 WT, adapted 6 days to the phage, to mucin and to both.

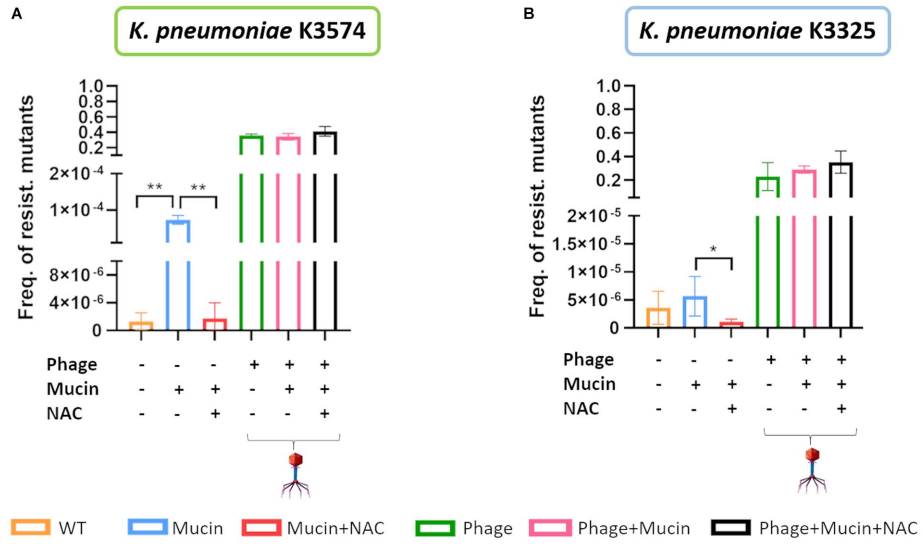

FIGURE 4
Frequency of occurrence of resistant mutants for *K. pneumoniae* K3574 **(A)** and *K. pneumoniae* K3325 **(B)**. The statistical analysis (*t*-test) was performed with GraphPad Prism v.9. **value of p <0.001 and *value of p 0.042. Absence of asterisk corresponds with no statistical significance.

a frameshift mutation translated into two truncated versions of the methyltransferase. Furthermore, the antitoxin HigA displayed mutations in the phage-infected cultures (K3574_ad15_P and K3574_ad15_P+M) that led to two different truncated proteins, whereas the non-infected strain had fewer changes that led to a shorter, unique version. Furthermore, the autoinducer 2-binding protein LsrB presented the same nucleotide deletion in the strains that co-evolved to the phage, also corresponding to a frameshift mutation (therefore a truncated protein lacking 11 amino acids); this was absent in the isolate exposed only to mucin.

Mutations in the core gene involved in Type VI secretion system, *vgrG*, were found in these same two strains but absent in the strain adapted only to mucin (K3674_ad15_M). Similarly, the same changes were found in the coding sequence of the outer membrane protein Ail (*attachment invasion locus*) of K3574_ad15_P and K3574_ad15_P+M, being intact in the isolate K3574_ad15_M. Interestingly, *fhuA*, the gene encoding a ferrichrome transporter protein, showed a frameshift mutation that led to two truncated versions of this protein in K3574_ad15_P+M, whereas this mutation was absent in K3574_ad15_P and K3574_ad15_M.

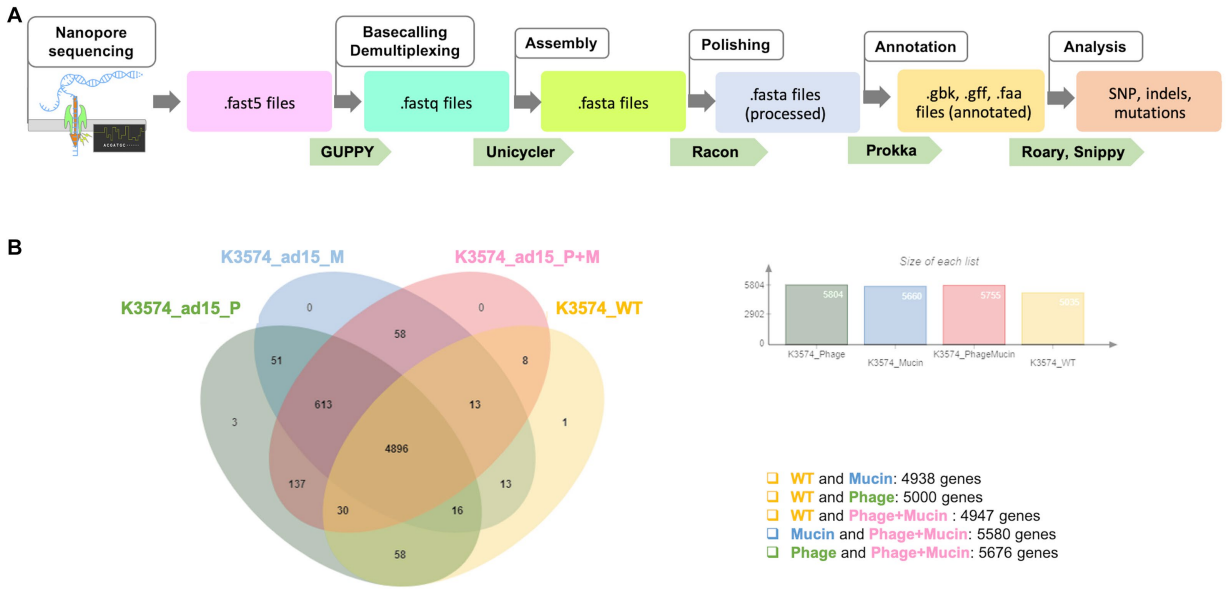

FIGURE 5
(A) Schematic representation of the workflow followed from the whole-genome sequencing with Nanopore till the analyse of the genomic sequences. **(B)** Venn diagram performed with OrthoVenn2 to visualize the overlapped and unique protein clusters in the four complete genomes analysed.

Mutations were found in genes involved in the metabolism of carbohydrates only for the strains adapted 15 days to mucin alone and to the phage in presence of mucin. For instance, nucleotide changes were observed in the gene *licC*, involved in the phosphoenolpyruvate-dependent sugar phosphotransferase system (PTS), in *rbsA*, *rbsB*, and *fruK*, encoding the ribose and fructose import ATP-binding proteins RbsA/RbsB and FruK, respectively, or in *malI*, encoding a maltose regulon regulatory protein. More nucleotide changes in other relevant genes are reported in Table 1.

4. Discussion

Most of the works studying the interactions between pathogenic bacteria and their phages are generally carried out in well-defined laboratory conditions. However, these microbes in a natural environment develop complex interactions on mucosal surfaces of the vertebrate host (de Freitas Almeida et al., 2022). In 2022, de Freitas et al. demonstrated that co-evolution of *Flavobacterium columnare* to its virulent phage V156 in presence of mucin dramatically increased the acquisition of spacers in the CRISPR arrays of *F. columnare*, thus increasing immunity to this phage (de Freitas Almeida et al., 2022). This work highlights the need to consider both biotic and abiotic variables if bacteriophages are to be used therapeutically. It is thus essential to take a close look at the study of how mucins and other mucosal components influence the acquisition of bacterial resistance towards lytic phages, so that the therapeutic potential of these could be better understood in the *in vivo* system.

Throughout the co-evolution, we observed that phage-resistant mutants arose at the first day post-infection (Figure 3), similar to what has been claimed in previous co-evolution works (Oechslin, 2018). Interestingly, both phage production (from 1 dpi onwards) and evolved *K. pneumoniae* populations seemed to stabilize over the days, consistently with other studies (Rendueles et al., 2023). This is likely due to the fact that vB_KpnS-VAC35 selects for resistant bacterial mutants. Due to its gelatinous nature, mucin limits the diffusion of bacteria through this space and facilitates the interaction of phages with bacteria, a less well-studied function but already documented in literature (Barr et al., 2013; de Freitas Almeida et al., 2022). In 2013, Barr et al. proposed a model in which bacteriophages would bind to mucins using the Ig-like domains present in many structural proteins, concentrate there, and protect humans and other metazoans against bacterial invaders (Barr et al., 2013; Almeida et al., 2019). Taken together, these two reasons could explain why the phage counts were higher in the presence of mucin than in the absence of this compound (Figure 3).

Interestingly, when the lytic phage was co-evolved to K3574 in the mucoid environment (vB_KpnS-VAC35_ad15_m), it showed an impaired infection ability compared to the adapted phage in the absence of mucin (vB_KpnS-VAC35_ad15) (Figure 4). As expected, no spot was visible for the cells exposed to the phage either in the presence or the absence of mucin, leading to the conclusion that resistance arose as a result of co-evolution. We phenotypically confirmed that mucin increased the frequency of resistant mutants for *K. pneumoniae* K3574 and K3325 strains (Figure 5). This resistant phenotype could be due to the modification of the phage receptor; however, as this strategy represents an important fitness cost for bacteria, these have developed other strategies to avoid phage attachment (Wright et al., 2019). For instance, receptors can be masked, preventing recognition while retaining function. Capsules or exopolysaccharides provide phage resistance in *Pseudomonas* spp. and *K. pneumoniae* (Hao et al., 2021), and these bacterial structures can be favorized in the presence of mucosal components such as mucins. Furthermore, NAC effectively reduced this frequency in the case of the cells incubated with this mucolytic (Figure 5). Numerous reports have claimed the absence of toxicity of NAC, an FDA-approved drug that has been in clinical practice for several decades, widely used in the case of acetaminophen intoxication (Bunchorntavakul and Reddy, 2018) and in several dermatologic conditions (such as trichotillomania, ichthyoses,

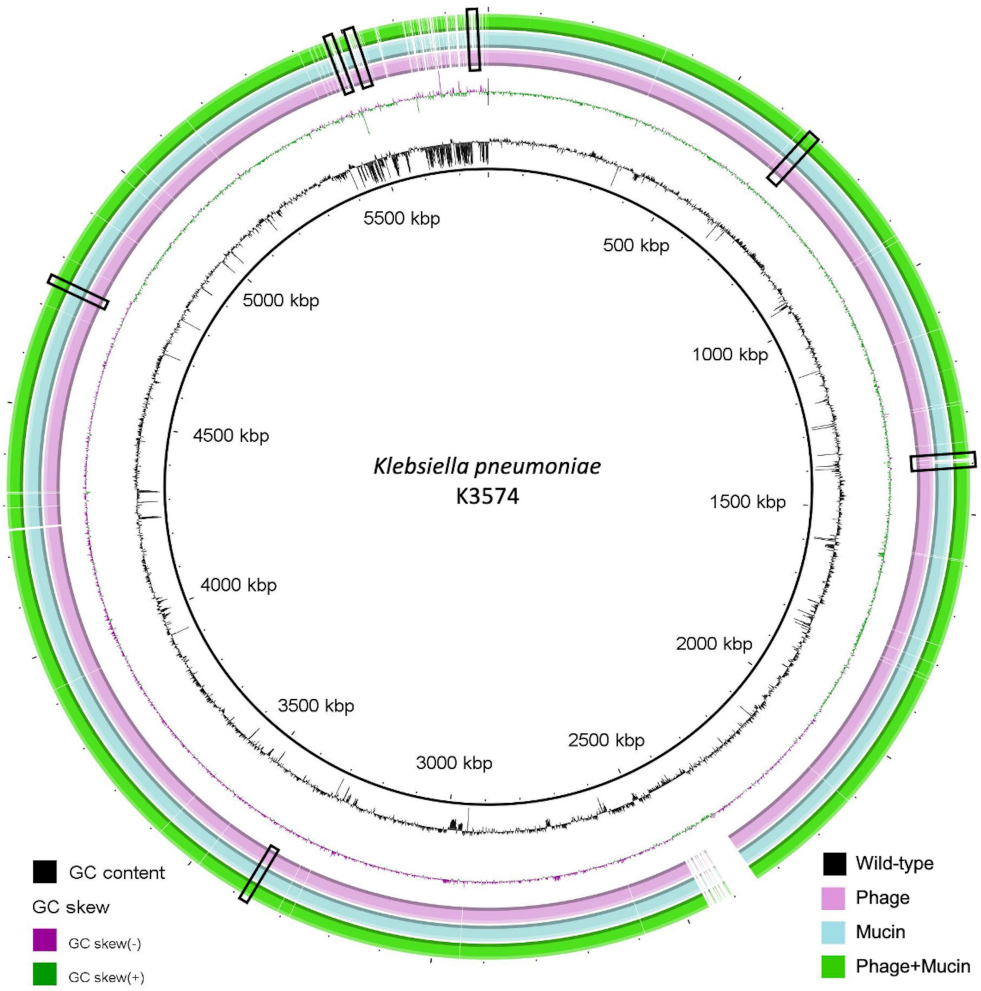

FIGURE 6
Comparative genomic analysis of *K. pneumoniae* K3574 co-evolved to phage alone (pink ring), mucin alone (blue ring) and both (green ring) constructed with the BLAST Ring Image Generator (BRIG). The sequence corresponding to K3574_WT is located on the innermost side (black ring). The double ring adjacent to the reference sequence represents the GC content (black) and the GC skew (dark purple and dark green). The white parts of the rings represent absent or divergent content and are squared in black.

dermatitis, melasma or pseudoporphyria) (Adil et al., 2018). NAC is a cheap, hydrophilic molecule, exhibiting an optimal toxicity profile (Mant et al., 1984; Mahmoudi et al., 2015). These properties make NAC an interesting compound for other therapeutic purposes, even a suitable adjuvant (De Flora et al., 2020; Biswas and Tk, 2022).

We wanted to have a better comprehension of the bacterial mutations in the co-evolution context, so we conducted an exhaustive genomic study (Figures 1, 6). The analysis of protein clusters suggested that the presence of the phage in this long-term co-evolution experiment was the main driver in the acquisition of mutations. The genomic analysis of *K. pneumoniae* K3574 adapted to the phage alone and in presence of mucin revealed mutations in some proteins involved in the bacterial defense to phages, such as methyltransferases, the HigA antitoxin, the *quorum sensing* autoinducer LsrB or the type 6 secretion system VgrG, as reported in other works (Liu et al., 2022; Blasco et al., 2023) (Figure 6). In the presence of mucin, mutations were observed in the genes encoding proteins that were involved in the carbohydrates metabolism, such as in the PTS system, which is a major carbohydrate active-transport system that catalyzes the phosphorylation of incoming sugar substrates concomitant with their translocation across the cell membrane (Deutscher et al., 2006).

Since changes concerning the synthesis, secretion or structure of mucins have been linked to gastrointestinal and respiratory disorders, manipulation of mucin may ultimately influence the microbiota and the effectiveness of phage therapy for bacterial imbalances (Carroll-Portillo and Lin, 2021), and the use of a mucolytic agent as an adjuvant of lytic phages could be an interesting therapeutic option to take into consideration. It has been shown that the presence of bacteria upregulates mucin production and enhances their encapsulation by mucin in the colon, so this could be even more important in CF patients in which overproduction of mucins leads to lung chronic infections (Bergstrom et al., 2020). Importantly, the trade-off costs that phage pressure and co-evolution represent for bacteria might render them less virulent in case of mutations in surface virulence factors, so maximizing the fitness costs that come with co-evolution may ultimately enhance the long-term efficacy of phage therapy. Optimization of these fitness costs could be a relevant factor to enhance the patient's prognosis (Mangalea and Duerkop, 2020).

Among the limitations of this work, it is of highlight the fact that we performed an *in vitro* co-evolution between *K. pneumoniae* strains and a lytic bacteriophage, so the time of phage-resistance arising might be really different in the *in vivo* setting. Moreover, most of the infections

10.3389/fmicb.2023.1286046

TABLE 1 Mutations found in the four complete genomes analyzed, grouped into different categories by function.

	K3574_ad15_P (co-evolved with the phage)	K3574_ad15_M (non-infected, exposed to mucin)	K3574_ad15_P + M (co-evolved with the phage in presence of mucin)
Anti-phage bacterial defense			
Anti-toxin HigA	c.T66-, c.T114-, c.A152- c.C199T, c.C201A. 2 truncated proteins	c.T66-, c.T105-, c.T106-. 1 protein FDNEPAPDTPEGDF>LIMNLRRTRRKG-I	c.T66-, c.T114-, c.A152- c.C199T, c. C201A. 2 truncated proteins
CRISPR-associated endonuclease/helicase Cas3	None	None	c.A2130-, c.A1236-, p. ALLAEVGVGTLDQLL>RYSLKL-VSVLSISF
tRNA (guanosine(18)-2'-O)-methyltransferase	c.A362-	None	c.A362-
Quorum sensing			
Autoinducer 2-binding protein LsrB	c.G341-, truncated protein (11 aa less)	None	c.G341-, truncated protein (11 aa less)
PG synthesis			
Murein DD-endopeptidase MepS/Murein LD-carboxypeptidase	Truncated version (lack 28 aas)	None	Truncated version (lack 28 aas)
FtsI Peptidoglycan D-transpeptidase	c.A1495- p.W501V	None	c.A1495- p.W501V
LPS biosynthesis			
undecaprenyl phosphate-alpha-4-amino-4-deoxy-L-arabinose arabinosyl transferase	None	None	c.G664-, 2 truncated proteins (263 and 251 aas)
lipopolysaccharide assembly protein LptD	Truncated version c.G1861-; p.*	None	None
Efflux			
BepE (efflux)	Shorter protein	Deletions in positions 370,371,381,1,641 (truncated protein, p.G125W, p.v126R, p. v127S)	Deletions in positions 370,371,381,1,641 (truncated protein, p.G125W, p.v126R, p.v127S)
BepG (efflux)	Deletion c.2867 (truncated protein)	Truncated version c.C1937T, Truncated protein	Deletion c.2867 (truncated protein)
Multidrug efflux transporter transcriptional repressor AcrR	Mutations p.K53R, p.K55N, p. K80N, p.N54I, p.N60T	Shorter version	Mutations p.K53R, p.K55N, p.K80N, p.N54I, p.N60T
Multidrug resistance protein MdtM	LGVLRDFRNVFRNRIF>WACC AIFATSFATASF	c.202 GILH>PRCRM	Lack 83 aa
Secretion systems			
T2SS protein F	Truncated version	Truncated version	Truncated version
T6SS VgrG1	c.G2182-, Truncated protein(p. N768*)	None	c.G2182-, Truncated protein (p.N768*)
Fimbrial proteins			
Fimbrial chaperone YadV	c.C624-; Truncated protein p. P210L	Truncated protein	Truncated protein
Putative hydrolase YxeP (active on CN bonds)	Truncated version	None	Truncated version
Outer membrane usher protein HtrE	Deletion 2,205 (truncated protein)	c.C2202-. Shorter sequence	Deletion 2,205 (truncated protein)
Xylose import ATP-binding protein XylG	Truncated version	Truncated version	Truncated version
Putative receptors			
Outer membrane channel OprM	Insertion in position 177 (1 truncated protein, lacking 18 aa)	c.G539-	Insertion in position 177 (1 truncated protein, lacking 18 aa)
Ail/Lom family outer membrane protein	Truncated version (65 aa)	None	Truncated version (65 aa)

(Continued)

TABLE 1 (Continued)

	K3574_ad15_P (co-evolved with the phage)	K3574_ad15_M (non-infected, exposed to mucin)	K3574_ad15_P + M (co-evolved with the phage in presence of mucin)
Receptor vitamin B12 BtuB	Truncated version; truncated protein	None	Truncated version deletion 1,234, truncated protein p.S414P, p.L415S
Ferrichrome FhuA	None	None	2 truncated versions
Ferrienterobactin receptor (FepA)	3 truncated versions*	2 truncated versions	3 truncated versions*
Virulence factors			
Ail/Lom family outer membrane protein	Deletion c.193- (truncated protein)	None	Deletion c.193- (truncated protein)

"c." corresponds to the nucleotide changes found in the coding sequences, with "-" representing a deletion, while "p." stands for protein sequences, with asterisks representing a stop codon. The symbol "†" indicates that mutations are the same between the studied conditions.

in patients are indeed polymicrobial (Peters et al., 2012; Filkins and O'Toole, 2015). All in all, this study sheds some light in the phage resistance behavior that might be expected for some clinical strains of *K. pneumoniae* in a mucoid environment, and takes a deeper look at the rise in the phage-resistance that mucins impose to bacteria, already reported in literature (de Freitas Almeida et al., 2022). Evolutionary dynamics between bacterial pathogens and their natural predators in *in vivo* environments where mucin overproduction occurs deserve further investigation, which could help clinicians to predict the success of a particular phage administered to counteract infections. Finally, our results showed that an innovative option could be the application of mucolytic agents prior to the administration of lytic phages against *K. pneumoniae* infections, especially in environments where mucins are overproduced, as in cystic fibrosis disease. However, it would be necessary to carry out more studies that include a broader number of clinical isolates to confirm this innovative therapeutic option.

Data availability statement

The datasets presented in this study can be found in online repositories. The names of the repository/repositories and accession number(s) can be found in the article/Supplementary Material.

Author contributions

OP: Investigation, Methodology, Writing – original draft. LB: Investigation, Supervision, Writing – review & editing. CO: Investigation, Visualization, Writing – review & editing. IB: Investigation, Visualization, Writing – review & editing. LF-G: Writing – review & editing. ML: Investigation, Supervision, Visualization, Writing – review & editing. AB-P: Visualization, Writing – review & editing. FC: Visualization, Methodology, Writing – review & editing. BA: Visualization, Investigation, Writing – review & editing. JO-I: Visualization, Methodology, Writing – review & editing. MT: Writing – review & editing, Formal analysis, Funding acquisition, Investigation, Supervision, Validation.

Funding

The author(s) declare financial support was received for the research, authorship, and/or publication of this article. This study has been funded by Instituto de Salud Carlos III (ISCIII) through the projects PI19/00878 and PI22/00323 and co-funded by the European Union, and by the Study Group on Mechanisms of Action and Resistance to Antimicrobials, GEMARA (SEIMC). (SEIMC, http://www.seimc.org/). This research was also supported by CIBERINFEC (CIBER21/13/00095) and by Personalized and precision medicine grant from the Instituto de Salud Carlos III (MePRAM Project, PMP22/00092). MT was financially supported by the Miguel Servet Research Programme (SERGAS and ISCIII). OP, LF-G, and ML were financially supported by the grants IN606A-2020/035, IN606B-2021/013, and IN606C-2022/002, respectively (GAIN, Xunta de Galicia). IB was financially supported by the pFIS program (ISCIII, FI20/00302). Finally, to thank to PIRASOA laboratory which is the reference laboratory for molecular typing of nosocomial pathogens and detection of mechanisms of resistance to antimicrobials of health interest in Andalusia, Virgen Macarena Hospital, Seville, to send us the clinical isolates. Thanks to Alvaro Pascual and Luis Martínez-Martínez from Virgen Macarena Hospital, Seville and Reina Sofia Hospital, Cordoba.

Conflict of interest

The authors declare that the research was conducted in the absence of any commercial or financial relationships that could be construed as a potential conflict of interest.

Publisher's note

Supplementary material

The Supplementary material for this article can be found online at: https://www.frontiersin.org/articles/10.3389/fmicb.2023.1286046/full#supplementary-material

References

Abedon, S. T., and Yin, J. (2009). Bacteriophage plaques: theory and analysis. *Methods Mol. Biol.* 501, 161–174. doi: 10.1007/978-1-60327-164-6_17

Adil, M., Amin, S. S., and Mohtashim, M. (2018). N-acetylcysteine in dermatology. *Indian J. Dermatol. Venereol. Leprol.* 84, 652–659. doi: 10.4103/ijdvl.IJDVL_33_18

Almeida, G. M. F., Laanto, E., Ashrafi, R., and Sundberg, L. R. (2019). Bacteriophage adherence to mucus mediates preventive protection against pathogenic bacteria. *MBio* 10:19. doi: 10.1128/mBio.01984-19

Ambroa, A., Blasco, L., Lopez, M., Pacios, O., Bleriot, I., Fernandez-Garcia, L., et al. (2021). Genomic analysis of molecular bacterial mechanisms of resistance to phage infection. *Front. Microbiol.* 12:784949. doi: 10.3389/fmicb.2021.784949

Barr, J. J., Auro, R., Furlan, M., Whiteson, K. L., Erb, M. L., Pogliano, J., et al. (2013). Bacteriophage adhering to mucus provide a non-host-derived immunity. *Proc. Natl. Acad. Sci. U. S. A.* 110, 10771–10776. doi: 10.1073/pnas.1305923110

Bergstrom, K., Shan, X., Casero, D., Batushansky, A., Lagishetty, V., Jacobs, J. P., et al. (2020). Proximal colon-derived O-glycosylated mucus encapsulates and modulates the microbiota. *Science* 370, 467–472. doi: 10.1126/science.aay7367

Biswas, D. P., and Tk, D. S. (2022). The efficacy of adjuvant N acetyl cysteine for the eradication of H pylori infections: a systematic review and meta-analysis of randomized clinical trials. *Clin. Res. Hepatol. Gastroenterol.* 46:101832. doi: 10.1016/j.clinre.2021.101832

Blasco, L., López-Hernández, I., Rodríguez-Fernández, M., Pérez-Florido, J., Casimiro-Soriguer, C. S., Djebara, S., et al. (2023). Case report: analysis of phage therapy failure in a patient with a Pseudomonas aeruginosa prosthetic vascular graft infection. *Front. Med.* 10:1199657. doi: 10.3389/fmed.2023.1199657

Bleriot, I., Blasco, L., Pacios, O., Fernández-García, L., López, M., Ortiz-Cartagena, C., et al. (2023). Proteomic study of the interactions between phages and the bacterial host. *Microbiol Spectr* 11:e0397422. doi: 10.1128/spectrum.03974-22

Bunchorntavakul, C., and Reddy, K. R. (2018). Acetaminophen (APAP or N-acetyl-p-aminophenol) and acute liver failure. *Clin. Liver Dis.* 22, 325–346. doi: 10.1016/j.cld.2018.01.007

Carroll-Portillo, A., and Lin, H. C. (2021). Exploring mucin as adjunct to phage therapy. *Microorganisms* 9:509. doi: 10.3390/microorganisms9030509

Castillo, J. A., Secaira-Morocho, H., Maldonado, S., and Sarmiento, K. N. (2020). Diversity and evolutionary dynamics of Antiphage defense Systems in Ralstonia solanacearum species complex. *Front. Microbiol.* 11:961. doi: 10.3389/fmicb.2020.00961

De Flora, S., Balansky, R., and La Maestra, S. (2020). Rationale for the use of N-acetylcysteine in both prevention and adjuvant therapy of COVID-19. *FASEB J.* 34, 13185–13193. doi: 10.1096/fj.202001807

de Freitas Almeida, G. M., Hoikkala, V., Ravantti, J., Rantanen, N., and Sundberg, L. R. (2022). Mucin induces CRISPR-Cas defense in an opportunistic pathogen. *Nat. Commun.* 13:3653. doi: 10.1038/s41467-022-31330-3

Dedrick, R. M., Guerrero-Bustamante, C. A., Garlena, R. A., Russell, D. A., Ford, K., Harris, K., et al. (2019). Engineered bacteriophages for treatment of a patient with a disseminated drug-resistant Mycobacterium abscessus. *Nat. Med.* 25, 730–733. doi: 10.1038/s41591-019-0437-z

Delfino, E., Giacobbe, D. R., Del Bono, V., Coppo, E., Marchese, A., Manno, G., et al. (2015). First report of chronic pulmonary infection by KPC-3-producing and colistin-resistant Klebsiella pneumoniae sequence type 258 (ST258) in an adult patient with cystic fibrosis. *J. Clin. Microbiol.* 53, 1442–1444. doi: 10.1128/JCM.03199-14

Denes, T., den Bakker, H. C., Tokman, J. I., Guldimann, C., and Wiedmann, M. (2015). Selection and characterization of phage-resistant mutant strains of Listeria monocytogenes reveal host genes linked to phage adsorption. *Appl. Environ. Microbiol.* 81, 4295–4305. doi: 10.1128/AEM.00087-15

Deutscher, J., Francke, C., and Postma, P. W. (2006). How phosphotransferase system-related protein phosphorylation regulates carbohydrate metabolism in bacteria. *Microbiol. Mol. Biol. Rev.* 70, 939–1031. doi: 10.1128/MMBR.00024-06

Filkins, L. M., and O'Toole, G. A. (2015). Cystic fibrosis lung infections: polymicrobial, complex, and hard to treat. *PLoS Pathog.* 11:e1005258. doi: 10.1371/journal.ppat.1005258

Green, S. I., Liu, C. G., Yu, X., Gibson, S., Salmen, W., Rajan, A., et al. (2021). Targeting of mammalian Glycans enhances phage predation in the gastrointestinal tract. *MBio* 12:20. doi: 10.1128/mBio.03474-20

Hansson, G. C. (2019). Mucus and mucins in diseases of the intestinal and respiratory tracts. *J. Intern. Med.* 285, 479–490. doi: 10.1111/joim.12910

Hao, G., Shu, R., Ding, L., Chen, X., Miao, Y., Wu, J., et al. (2021). Bacteriophage SRD2021 recognizing capsular polysaccharide shows therapeutic potential in serotype K47 Klebsiella pneumoniae infections. *Antibiotics* 10:894. doi: 10.3390/antibiotics10080894

Jass, J. R., and Walsh, M. D. (2001). Altered mucin expression in the gastrointestinal tract: a review. *J. Cell. Mol. Med.* 5, 327–351. doi: 10.1111/j.1582-4934.2001.tb00169.x

Kamruzzaman, M., and Iredell, J. R. (2019). CRISPR-Cas system in antibiotic resistance plasmids in Klebsiella pneumoniae. *Front. Microbiol.* 10:2934. doi: 10.3389/fmicb.2019.02934

Kutter, E. (2009). Phage host range and efficiency of plating. *Methods Mol. Biol.* 501, 141–149. doi: 10.1007/978-1-60327-164-6_14

Law, N., Logan, C., Yung, G., Furr, C. L., Lehman, S. M., Morales, S., et al. (2019). Successful adjunctive use of bacteriophage therapy for treatment of multidrug-resistant Pseudomonas aeruginosa infection in a cystic fibrosis patient. *Infection* 47, 665–668. doi: 10.1007/s15010-019-01319-0

Leão, R. S., Pereira, R. H., Folescu, T. W., Albano, R. M., Santos, E. A., Junior, L. G., et al. (2011). KPC-2 carbapenemase-producing Klebsiella pneumoniae isolates from patients with cystic fibrosis. *J. Cyst. Fibros.* 10, 140–142. doi: 10.1016/j.jcf.2010.12.003

Liu, M., Hernandez-Morales, A., Clark, J., Le, T., Biswas, B., Bishop-Lilly, K. A., et al. (2022). Comparative genomics of Acinetobacter baumannii and therapeutic bacteriophages from a patient undergoing phage therapy. *Nat. Commun.* 13:3776. doi: 10.1038/s41467-022-31455-5

Lopatina, A., Tal, N., and Sorek, R. (2020). Abortive infection: bacterial suicide as an antiviral immune strategy. *Annu Rev Virol* 7, 371–384. doi: 10.1146/annurev-virology-011620-040628

Lopes, A., Pereira, C., and Almeida, A. (2018). Sequential combined effect of phages and antibiotics on the inactivation of Escherichia coli. *Microorganisms* 6:125. doi: 10.3390/microorganisms6040125

Mackow, N. A., Shen, J., Adnan, M., Khan, A. S., Fries, B. C., and Diago-Navarro, E. (2019). CRISPR-Cas influences the acquisition of antibiotic resistance in Klebsiella pneumoniae. *PLoS One* 14:e0225131. doi: 10.1371/journal.pone.0225131

Mahmoudi, G. A., Astaraki, P., Mohtashami, A. Z., and Ahadi, M. (2015). N-acetylcysteine overdose after acetaminophen poisoning. *Int Med Case Rep J* 8, 65–69. doi: 10.2147/IMCRJ.S74563

Majkowska-Skrobek, G., Markwitz, P., Sosnowska, E., Lood, C., Lavigne, R., and Drulis-Kawa, Z. (2021). The evolutionary trade-offs in phage-resistant Klebsiella pneumoniae entail cross-phage sensitization and loss of multidrug resistance. *Environ. Microbiol.* 23, 7723–7740. doi: 10.1111/1462-2920.15476

Mangalea, M. R., and Duerkop, B. A. (2020). Fitness trade-offs resulting from bacteriophage resistance potentiate synergistic antibacterial strategies. *Infect. Immun.* 88:19. doi: 10.1128/IAI.00926-19

Mant, T. G., Tempowski, J. H., Volans, G. N., and Talbot, J. C. (1984). Adverse reactions to acetylcysteine and effects of overdose. *Br. Med. J. (Clin. Res. Ed.)* 289, 217–219. doi: 10.1136/bmj.289.6439.217

Moulton-Brown, C. E., and Friman, V. P. (2018). Rapid evolution of generalized resistance mechanisms can constrain the efficacy of phage-antibiotic treatments. *Evol. Appl.* 11, 1630–1641. doi: 10.1111/eva.12653

Oechslin, F. (2018). Resistance development to bacteriophages occurring during bacteriophage therapy. *Viruses* 10:351. doi: 10.3390/v10070351

Pacios, O., Blasco, L., Bleriot, I., Fernandez-Garcia, L., Gonzalez Bardanca, M., Ambroa, A., et al. (2020). Strategies to combat multidrug-resistant and persistent infectious diseases. *Antibiotics* 9:65. doi: 10.3390/antibiotics9020065

Pacios, O., Fernández-García, L., Bleriot, I., Blasco, L., González-Bardanca, M., López, M., et al. (2021). Enhanced antibacterial activity of repurposed Mitomycin C and Imipenem in combination with the lytic phage vB_KpnM-VAC13 against clinical isolates of Klebsiella pneumoniae. *Antimicrob. Agents Chemother.* 65:e0090021. doi: 10.1128/AAC.00900-21

Paone, P., and Cani, P. D. (2020). Mucus barrier, mucins and gut microbiota: the expected slimy partners? *Gut* 69, 2232–2243. doi: 10.1136/gutjnl-2020-322260

Peters, B. M., Jabra-Rizk, M. A., O'May, G. A., Costerton, J. W., and Shirtliff, M. E. (2012). Polymicrobial interactions: impact on pathogenesis and human disease. *Clin. Microbiol. Rev.* 25, 193–213. doi: 10.1128/CMR.00013-11

Pletzer, D., Mansour, S. C., Wuerth, K., Rahanjam, N., and Hancock, R. E. (2017). New mouse model for chronic infections by gram-negative bacteria enabling the study of anti-infective efficacy and host-microbe interactions. *MBio* 8:17. doi: 10.1128/mBio.00140-17

Raya, R. R., and H'bert, E. M. (2009). Isolation of phage via induction of Lysogens. *Methods Mol. Biol.* 501, 23–32. doi: 10.1007/978-1-60327-164-6_3

Rendueles, O., de Sousa, J. A. M., and Rocha, E. P. C. (2023). Competition between lysogenic and sensitive bacteria is determined by the fitness costs of the different emerging phage-resistance strategies. *elife* 12:83479. doi: 10.7554/eLife.83479

Riquelme, S. A., Ahn, D., and Prince, A. (2018). Pseudomonas aeruginosa and Klebsiella pneumoniae adaptation to innate immune clearance mechanisms in the lung. *J. Innate Immun.* 10, 442–454. doi: 10.1159/000487515

Schooley, R. T., Biswas, B., Gill, J. J., Hernandez-Morales, A., Lancaster, J., Lessor, L., et al. (2017). Development and use of personalized bacteriophage-based therapeutic cocktails to treat a patient with a disseminated resistant Acinetobacter baumannii infection. *Antimicrob. Agents Chemother.* 61:17. doi: 10.1128/AAC.00954-17

Seemann, T. (2014). Prokka: rapid prokaryotic genome annotation. *Bioinformatics* 30, 2068–2069. doi: 10.1093/bioinformatics/btu153

Uyttebroek, S., Chen, B., Onsea, J., Ruythooren, F., Debaveye, Y., Devolder, D., et al. (2022). Safety and efficacy of phage therapy in difficult-to-treat infections: a systematic review. *Lancet Infect. Dis.* 22, e208–e220. doi: 10.1016/S1473-3099(21)00612-5

Wright, R. C. T., Friman, V. P., Smith, M. C. M., and Brockhurst, M. A. (2019). Resistance evolution against phage combinations depends on the timing and order of exposure. *MBio* 10:19. doi: 10.1128/mBio.01652-19

Xu, Q., Yang, X., Chan, E. W. C., and Chen, S. (2021). The hypermucoviscosity of hypervirulent K. pneumoniae confers the ability to evade neutrophil-mediated phagocytosis. *Virulence* 12, 2050–2059. doi: 10.1080/21505594.2021.1960101

frontiers | Frontiers in Microbiology

TYPE Original Research
PUBLISHED 31 October 2023
DOI 10.3389/fmicb.2023.1278791

OPEN ACCESS

EDITED BY
Alicja Wegrzyn,
Polish Academy of Sciences, Poland

REVIEWED BY
Malgorzata Barbara Lobocka,
Polish Academy of Sciences, Poland
Thomas Klose,
Purdue University, United States
Joel Bozue,
United States Army Medical Research Institute of Infectious Diseases (USAMRIID), United States

*CORRESPONDENCE
Sarah L. Grady
✉ sarah.grady@jhuapl.edu
Shanmuga Sozhamannan
✉ shanmuga.sozhamannan.ctr@army.mil

RECEIVED 16 August 2023
ACCEPTED 11 October 2023
PUBLISHED 31 October 2023

CITATION
Forrest S, Ton S, Sholes SL, Harrison S, Plaut RD, Verratti K, Wittekind M, Ettehadieh E, Necciai B, Sozhamannan S and Grady SL (2023) Genetic evidence for the interaction between *Bacillus anthracis*-encoded phage receptors and their cognate phage-encoded receptor binding proteins.
Front. Microbiol. 14:1278791.
doi: 10.3389/fmicb.2023.1278791

Genetic evidence for the interaction between *Bacillus anthracis*-encoded phage receptors and their cognate phage-encoded receptor binding proteins

Samantha Forrest[1], Sarah Ton[1], Samantha L. Sholes[1], Sarah Harrison[1], Roger D. Plaut[2], Kathleen Verratti[1], Michael Wittekind[3], Elham Ettehadieh[3], Bryan Necciai[4], Shanmuga Sozhamannan[4,5]* and Sarah L. Grady[1]*

[1]Johns Hopkins University Applied Physics Laboratory, Laurel, MD, United States, [2]Division of Bacterial, Parasitic, and Allergenic Products, Center for Biologics Evaluation and Research, Food and Drug Administration, Silver Spring, MD, United States, [3]Olympic Protein Technologies, Seattle, WA, United States, [4]Joint Program Executive Office for Chemical, Biological, Radiological and Nuclear Defense (JPEO-CBRND), Joint Project Lead for CBRND Enabling Biotechnologies, Frederick, MD, United States, [5]Joint Research and Development, Inc., Stafford, VA, United States

Bacteriophages such as γ and AP50c have been shown to infect strains of *Bacillus anthracis* with high specificity, and this feature has been exploited in the development of bacterial detection assays. To better understand the emergence of phage resistance, and thus the potential failure of such assays, it is important to identify the host and phage receptors necessary for attachment and entry. Using genetic approaches, the bacterial receptors of AP50c and γ have been identified as *sap* and GamR, respectively. A second AP50c-like phage, Wip1, also appears to use *sap* as a receptor. In parallel with this work, the cognate phage-encoded receptor binding proteins (RBPs) have also been identified (Gp14 for γ, P28 for AP50c, and P23 for Wip1); however, the strength of evidence supporting these protein–protein interactions varies, necessitating additional investigation. Here, we present genetic evidence further supporting the interaction between *sap* and the RBPs of AP50c and Wip1 using fluorescently tagged proteins and a panel of B. anthracis mutants. These results showed that the deletion of the *sap* gene, as well as the deletion of *csaB*, whose encoded protein anchors *sap* to the bacterial S-layer, resulted in the loss of RBP binding. Binding could then be rescued by expressing these genes in *trans*. We also found that the RBP of the γ-like prophage λBa03 relied on csaB activity for binding, possibly by a different mechanism. $RBP_{\lambda Ba03}$ binding to *B. anthracis* cells was also unique in that it was not ablated by heat inactivation of vegetative cells, suggesting that its receptor is still functional following incubation at 98°C. These results extend our understanding of the diverse attachment and entry strategies used by *B. anthracis* phages, enabling future assay development.

KEYWORDS

***Bacillus anthracis*, phages, phage resistance, receptor binding proteins, bacterial receptors, S-layer, fluorescence detection**

1. Introduction

Bacillus anthracis, the causative agent of anthrax, is a spore-forming, Gram-positive bacterium that qualifies as a CDC Tier 1 select agent due to its potential use as a bioterrorism agent (Darling et al., 2002). Due to its impact on national biodefense, it is vital to have surveillance strategies in place that are rapid, reliable, and can be performed with limited equipment. (Bacterio)phages that specifically infect *B. anthracis* represent an appealing set of tools towards this end (Abshire et al., 2005; Sozhamannan et al., 2008; Schuch et al., 2010). Indeed, an engineered *lux* fusion reporter phage has been developed and tested for rapid detection of viable *B. anthracis* spores in environmental samples (Sharp et al., 2016). In addition to their potential utility in bacterial identification, there has also been a recent resurgence in use of phages as therapeutics due to the growing threat of multi-drug resistant bacteria (Aranaga et al., 2022). With all of these potential applications, it is critical to understand the genetic mechanisms driving phage resistance, allowing for the intelligent design of both therapeutic phage cocktails and diagnostic/surveillance tools.

An important step towards deciphering these resistance mechanisms is identifying phage receptor binding proteins (RBP) and their cognate bacterial surface receptor(s). The specificity of a phage for its target bacteria is attributed, at least in part, to the strength of this interaction, and receptors can be any of a diverse set of molecules, including proteins, (lipo)polysaccharides, and carbohydrate moieties (Rakhuba et al., 2010; Bertozzi Silva et al., 2016; Hyman and van Raaij, 2018). With respect to *B. anthracis*-specific phages, the bacterial protein GamR was identified as the bacterial receptor of phage γ almost two decades ago using genetic approaches (Davison et al., 2005). Identification of the bacterial receptors of other phages, including AP50c and Wip1, came later. These efforts started with whole genome sequence analysis of spontaneous AP50c-resistant *B. anthracis* mutants. Here, mutations in the *csaB* gene were found to result in phage resistance (Bishop-Lilly et al., 2012). As *csaB* is known to anchor the surface-array protein (*sap*) to the bacterial S-layer present on the *B. anthracis* vegetative cell surface (Mignot et al., 2002), it was postulated that *sap*, more appropriately the S-layer, could be the receptor for AP50c (Bishop-Lilly et al., 2012). S-layer, which itself provides structural integrity and stability to the cell wall (Fioravanti et al., 2022), was also hypothesized to be the bacterial receptor of Wip1 due to its genetic similarity to AP50c (Kan et al., 2013). More direct evidence in support of the AP50c-*sap* binding hypothesis was produced when incubation of purified *sap* protein with intact AP50c phage particles reduced the titer of free phage (Plaut et al., 2014). Ultimately, analysis of various transposon insertions and targeted mutants revealed that not only *sap* and *csaB,* but also the sporulation genes *spo0A*, *spo0B,* and *spo0F* all had roles in productive AP50c infection of *B. anthracis* cells (Plaut et al., 2014). While the direct roles of *sap* and *csaB* in the formation of the S-layer are clear, whether the sporulation genes play a direct or indirect role in either S-layer formation or phage attachment and infection is not clear at this time.

As the potential bacterial receptors of these phage were put forth, research was also conducted to identify their respective phage receptors. The RBP of Wip1 was identified as P23 (henceforth referred to as RBP_{Wip1}) based on phage adsorption tests and immunofluorescence assays (Kan et al., 2013). The activity of P23 was found to require the translation of the downstream *p24* gene (Kan et al., 2013), which shares extensive sequence similarity to *p29* gene of AP50c (Braun et al., 2020). Based on its location immediately upstream of *p29*, along with a short amino acid sequence identity to the Wip1 P23 protein, the AP50c protein P28 (RBP_{AP50c}) was then posited as its RBP (Braun et al., 2020). When the Wip1 *p23* and AP50c *p28* genes were then cloned into expression vectors with fluorescent protein genes, the resulting fusion proteins were shown to bind to *B. anthracis* cell surfaces (Braun et al., 2020). Together, this work supported the role of P23 and P28 in phage binding but did not establish their interaction with *sap*. Here, we describe a set of genetic and molecular experiments to further probe these phage-bacterial interactions and provide evidence that presence of *sap*, *csaB*, and the sporulation proteins Spo0A, Spo0B, and Spo0F are likely required for RBP_{Wip1} and RBP_{AP50c} binding to *sap* on *B. anthracis* cell surface.

In addition to prototypical phages, there have also been prophages identified in the chromosome of *B. anthracis*, including the γ-like prophage λBa03 (Sozhamannan et al., 2006). The genome of λBa03 encodes the hypothetical protein BA4079 (henceforth referred to as $RBP_{\lambda Ba03}$) that shares significant amino acid sequence homology to γ phage encoded RBP Gp14, making it an ideal candidate for λBa03 RBP (Braun et al., 2020). Like RBP_{AP50c} and RBP_{Wip1}, a domain of $RBP_{\lambda Ba03}$ lacking the first 120 amino acids (designated as $RBP_{\lambda 03\Delta 1\text{-}120}$) has been shown to bind to the cell surface of vegetative *B. anthracis* bacterium, but little else is known about its bacterial target for binding. Here, we find that λBa03 represents a different paradigm than Wip1 and AP50c in that it requires *csaB* activity for binding, but that this phenotype appears to be unrelated to its role in anchoring *sap* to the S-layer. Intriguingly, $RBP_{\lambda 03\Delta 1\text{-}120}$ binding to *B. anthracis* also is maintained following heat treatment, meaning its receptor is not heat labile or protected from heat inactivation. These results underscore the significant diversity in strategies adopted by these phages and corresponding genetic requirements for attachment and entry during infection of their host bacteria.

2. Materials and methods

2.1. Bacterial strains and plasmids

B. anthracis and *Escherichia coli* strains, plasmid vectors and recombinant plasmids used in this study are listed in Table 1. Construction of the in-frame mutant *B. anthracis* strains used in this study is originally described in Plaut et al. (2014).

2.2. Culturing of *Bacillus anthracis* strains and heat inactivation

Glycerol stocks of bacteria were used to inoculate 50 mL of tryptic soy broth (TSB). The cultures were grown overnight at 37°C in 250 mL flasks at 150 rotations per minute (rpm). In experiments using heat-killed cells, a 1 mL aliquot was taken from these cultures, diluted to an optical density (OD_{600}) of 1.0 and incubated at 98°C for 30 min. Serial dilutions of cells were plated on tryptic soy agar (TSA) to verify non-viability.

2.3. Spore preparation

Spores were produced as described in Braun et al. (2020). Briefly, a colony from a fresh overnight TSA plate was inoculated in 50 mL of

TABLE 1 *E. coli*, *B. anthracis* strains and plasmids used in this study.

Strain	Description	Source/ reference
E. coli		
Arctic Express (DE3) (230192)	*E. coli* B F$^-$ *ompT hsdS* ($r_B^- m_B^-$) *dcm*$^+$ Tet^r *gal* λ(DE3) *endA* Hte [*cpn10 cpn60* Gent^r]	Agilent
C2925H	*ara-14 leuB6 fhuA31 lacY1 tsx78 glnV44 galK2 galT22 mcrA dcm-6 hisG4 rfbD1 R(zgb210::Tn10)* Tet^S *endA1 rspL136* (Str^R) *dam13::Tn9* (Cam^R) *xylA-5 mtl-1 thi-1 mcrB1 hsdR2*	NEB
TOP10 (C404010)	F- *mcrA* Δ(*mrr-hsd*RMS-*mcr*BC) Φ80*lacZ*ΔM15 Δ *lac*X74 *rec*A1 *ara*D139 Δ(*araleu*)7697 *gal*U *gal*K *rps*L (StrR) *end*A1 *nup*G	Thermo Fisher
B. anthracis		
7702	Sterne/pXO1+/pXO2−	Plaut et al. (2014)
BA749	7702 Δ*BAS0566*	Plaut et al. (2014)
BA750	7702 Δ*sap*	Plaut et al. (2014)
BA751	7702 Δ*eag*	Plaut et al. (2014)
BA752	7702 Δ*BAS1792*	Plaut et al. (2014)
BA754	7702 Δ*spo0A*	Plaut et al. (2014)
BA755	7702 Δ*spo0F*	Plaut et al. (2014)
BAP350	7702 Δ*csaB*	Plaut et al. (2014)
DP-B-5747	JB220 Δ*spoB*	Plaut et al. (2014)
Plasmids		
pSW4	*E. coli-B. anthracis* shuttle vector	Pomerantsev et al. (2003)
pSW4-*csaB*	*pSW4::csaB*	This study
pSW4-*spo0A*	*pSW4::spo0A*	This study
pSW4-*spo0B*	*pSW4::spo0B*	This study
pSW4-*spo0F*	*pSW4::spo0F*	This study
pSW4-*sap*	*pSW4::sap*	This study

sporulation medium containing 0.8% nutrient broth supplemented with 0.05 mM $MnCl_2$, 0.7 mM $CaCl_2$, and 1 mM $MgCl_2$ in a 250 mL flask. After cultivation for 72 h at 37°C with shaking at 150 rpm, 3% Tween-80 was added to each flask and incubated for an additional 24 h under the same conditions. Samples were harvested in a 50 mL conical tube by centrifugation at 2000 × g for 10 min. The supernatant was discarded and the pellet was washed twice with 3% Tween-80. Samples were resuspended in 25 mL of 3% Tween-80 and incubated at 37°C for 24 h with shaking at 150 rpm. Phase contrast microscopy was used to approximate the percentage of spores versus vegetative cells in each suspension. When the spore percentage reached >95%, they were harvested by centrifugation at 2000 × g for 10 min, the supernatant was discarded, and the pellet was resuspended in 3 mL of ice-cold ultrapure water and stored at 4°C. The final purity of a given spore preparation was determined by (i) documenting the size and light refractivity by microscopy and (ii) measuring viability following the heating process described above.

2.4. DNA isolation

Isolation of DNA from bacterial cultures was performed using the GeneJET Plasmid Miniprep kit (ThermoFisher Scientific) K0502 or the Nanobind High Molecular Weight Extraction kit (Circulomics 102-762-700) according to manufacturer's recommendations. Extracted nucleic acids were quantified using either the Qubit dsDNA HS Assay (ThermoFisher Scientific Q32851) or the High Sensitivity DNA ScreenTape (Agilent 5,067–5,584).

2.5. Whole genome sequencing and variation detection

Whole genome sequencing on the Oxford Nanopore and Illumina platforms and downstream assembly and alignment, were performed as described in Sholes et al. (2023). Single nucleotide polymorphisms (SNPs) and small insertions or deletions were called and filtered as described in Forde et al. (2022). In brief, VarScan v2.4.4 was used with a minimum read depth of 4x, a minimum base quality of 20, and a variant allele frequency ≥ 0.95 (Koboldt et al., 2012). Large structural variations were inspected using sniffles v2.0 (Sedlazeck et al., 2018). All variants were visually validated using IGV (Thorvaldsdóttir et al., 2013).

2.6. Cloning of *rbp-gfp* gene fusions

The pASG-105-TST-eGFP-RBP plasmids expressing the receptor binding proteins of phages Wip1 and AP50C and the soluble domain of prophage λBa03 described in Braun et al. (2020) were used as the basis for construction of the new expression constructs used herein. The sequences for the RBPs and corresponding chaperone proteins (when applicable) and for eGFP were provided kindly by Gregor Grass. Insert sequence synthesis, cloning, and sequence validation were performed by Azenta (Burlington, MA). Briefly, an oligonucleotide encoding a start codon and N-terminal HISTAG-thrombin site-Twin-Strep tag was synthesized upstream of the eGFP sequence. A short -CTCGAG- linker sequence was added, followed immediately by the phage RBP sequence. For those RBPs requiring the co-expression of a second protein (RBP_{AP50c} and RBP_{Wip1}), the linker sequence -AAGGAGGGAACTAT- was added, followed by the full coding sequence of respective gene. These inserts were cloned into plasmid pET22 using *Nde*I and *Hind*III restriction sites.

2.7. Expression and purification of RBP fusion proteins

Protein expression and purification were performed by Olympic Protein Technologies (Seattle, WA). The pET22-eGFP-RBP expression vectors were used to transform (i) *E. coli* Arctic Express

DE3 cells (Agilent 230,192) for protein production and (ii) *E. coli* TOP10 (Thermo Fisher C404010) cells for plasmid stock production. Cultures were grown on LB-carbenicillin (100 μg/mL) plates at 37°C overnight prior to single colony selection, outgrowth in liquid culture, and sequence verification using the pET22 entry primers T7 (TAATACGACTCACTATAGGG) and T7 term (GCTAGTTATTGCTCAGCGG).

For protein production, colonies were grown in 25 mL Terrific Broth (TB) with 20 μg/mL gentamicin overnight at 30°C (250 rpm). One liter of autoinduction medium (MagicMedia™ Thermo K6803) was inoculated with 20 mL of the overnight culture and grown at 30°C for 4 hrs before the temperature of the shaken cultures was shifted to 12°C and allowed to proceed overnight. To test for expression, cell pellets were harvested by centrifugation at 10,000 rpm for 10 min at 4°C and lysed using an equal volume of BugbusterHT+ (Millipore Sigma 70,922) and fractionated into soluble and insoluble material. Insoluble fractions were taken up in equal volume as the original culture. All samples were run on a 4–20% Tris-glycine reducing SDS-PAGE gel to ascertain the presence of the tagged protein in the soluble fraction.

For purification, separate cell pellets were resuspended in IMAC breaking buffer (25 mM Tris–HCl, pH 7.9, 500 mM NaCl, 2 mM imidazole, with a complete protease inhibitor tablet and benzonase). The suspensions were lysed via three passages through a microfluidizer. Lysates were centrifuged as above, and, the cleared supernatants were passed through a 0.45 μm filter, and frozen at −80°C.

Thawed lysates were loaded on to a 5 mL Nickel Excel IMAC column (Cytiva) previously equilibrated with IMAC running buffer (50 mM Tris–HCl, pH 8.0, 300 mM NaCl, 2 mM imidazole) using an AKTA instrument. The immobilized proteins were then washed with IMAC running buffer followed by running buffer containing 12 mM imidazole. Once baseline Abs_{280} readings were reached, the bound proteins were eluted using IMAC elution buffer (50 mM Tris–HCl, pH 8.0, 300 mM NaCl, 250 mM imidazole), and peak protein fractions were collected and pooled by Abs_{280} measurements.

Pooled IMAC fractions were adjusted to 10 mM $CaCl_2$, and thrombin (Sigma 69,671) was added to a final concentration of 0.24 U/mg of protein. Thrombin reactions were carried out at room temperature for 3 h under conditions of slow rotation. The reaction products were loaded at 3 mL/min on to a 5 mL Strep-Tactin XL Superflow high-capacity column (IBA) previously equilibrated with buffer W (100 mM Tris, pH 8.0, 150 mM NaCl, 1 mM EDTA). Bound samples were washed with buffer W until Abs_{280} measurements reached a steady baseline value. Proteins were eluted using buffer BXT (100 mM Tris, pH 8.0, 150 mM NaCl, 1 mM EDTA, 50 mM biotin). As above, protein peaks were measured by Abs_{280} values and pooled. Overall sample purities were quantified by running a 15 μL aliquot run on an HPLC-SEC column (Tosoh G3000SW) in SEC running buffer (1X PBS) at 200 μL/min. Eluents were run on 4–20% Tris-glycine SDS-PAGE gels (ThermoFisher).

2.8. Fluorescence microscopy experiments to assess RBP binding to bacterial cells

A 100 μL aliquot of living or heat-killed vegetative cells ($OD_{600} = 1$) was added to a 1.5 mL microcentrifuge tube and centrifuged at 5000 × g for 2 min. For spore preparations, 2×10^6 spores were added to 10 mL of Ringer-HEPES buffer (50 mM HEPES, 1.5 mM $CaCl_2$, 1.5 mM KCl, 100 mM NaCl, 0.6 mM $NaHCO_3$, pH 7.4) and centrifuged at 5000 × g for 2 min. After the supernatant was removed, the pellet was resuspended in 1 mL of Ringer-HEPES buffer then transferred to a 1.5 mL microcentrifuge tube and centrifuged again under the same conditions. The supernatant was removed and the pellet was resuspended in 100 μL of Ringer-HEPES buffer and 5 μg of purified RBP fusion protein was added to the sample. Samples were incubated at room temperature for 5 min then centrifuged and resuspended in 100 μL of Ringer-HEPES buffer. A 3 μL aliquot of the sample was added to a glass microscope slide and imaged by both brightfield and FITC filter. All fluorescence images of samples containing the same phage protein were processed in the same way, with contrast, brightness, and exposure times kept constant. All microscopy images in this manuscript were taken at 100X under oil immersion.

2.9. Construction of genetic complementation plasmids

The starting plasmid for the cloning of *B. anthracis* genes was the *E. coli-B. anthracis* shuttle vector, pSW4, the construction of which was previously described (Pomerantsev et al., 2003). The coding sequences of the bacterial genes of interest were individually synthesized, inserted into pSW4 linearized using *Bgl*II and *Blp*I, and sequence verified by Azenta Life Sciences (Burlington, MA). Constructs were then transformed into competent *dam*$^-$/*dcm*$^-$ *E. coli* cells (NEB C2925H) and purified to yield unmethylated plasmid stocks.

2.10. Electroporation of plasmids into *Bacillus anthracis* strains

To make electrocompetent cells, *B. anthracis* wild type or mutant strains were grown overnight on LB plates containing 1% w/v glucose (LBG agar). Colonies were inoculated into 1 mL of LBG medium and incubated for 10 min at 37°C and 225 rpm before being spiked into a larger 25 mL LBG culture. The culture was incubated and shaken until the OD_{600} reached 0.15–0.25. Cells were centrifuged at 4000 × g for 5 min and washed three times with electroporation buffer (10% sucrose, 15% glycerol, 2 mM potassium phosphate buffer, pH 8.0–8.4). Cells were resuspended in 200 μL of electroporation buffer and transferred to a 0.2 cm electroporation cuvette. After incubation on ice for 10 min, approximately 0.5 μg of unmethylated plasmid was added into the cuvette and mixed gently with the cells. Cells were pulsed once at 1.77 kV with a mean time constant between 3.5–5 msec, then 1 mL of S.O.C medium was added to the cells. Cells were transferred to a FALCON 14 mL tube and incubated at 37°C for 1 h. A 200 μL aliquot was plated on LBG-kanamycin plates and incubated for 16 h at 37°C.

3. Results

3.1. Whole genome sequencing of *Bacillus anthracis* Sterne mutants verifies gene deletions

A transposon insertion screen previously identified several genes in *B. anthracis* Sterne 7702 that appeared to be necessary for AP50c

10.3389/fmicb.2023.1278791

phage adsorption (Plaut et al., 2014). These included *sap*, *spo0A*, and *spo0F* (discussed in the Introduction section), as well genes encoding the transcriptional regulator BAS0566 and the branched amino-acid ABC transporter BAS1792. Each of these genes, as well as two genes in the same operon as *sap*, (*csaB* and *eag*, the latter of which is an alternate S-layer protein), were then individually deleted using markerless allelic exchange, and a final mutant strain was created that lacked the additional sporulation gene *spo0B* (Plaut et al., 2014). Recently, the full sequences of the genomes of these strains were published (Sholes et al., 2023). We found that each of these mutant strains contained the expected deletions of the targeted genes (Figure 1), in addition to individual SNPs or deletions present

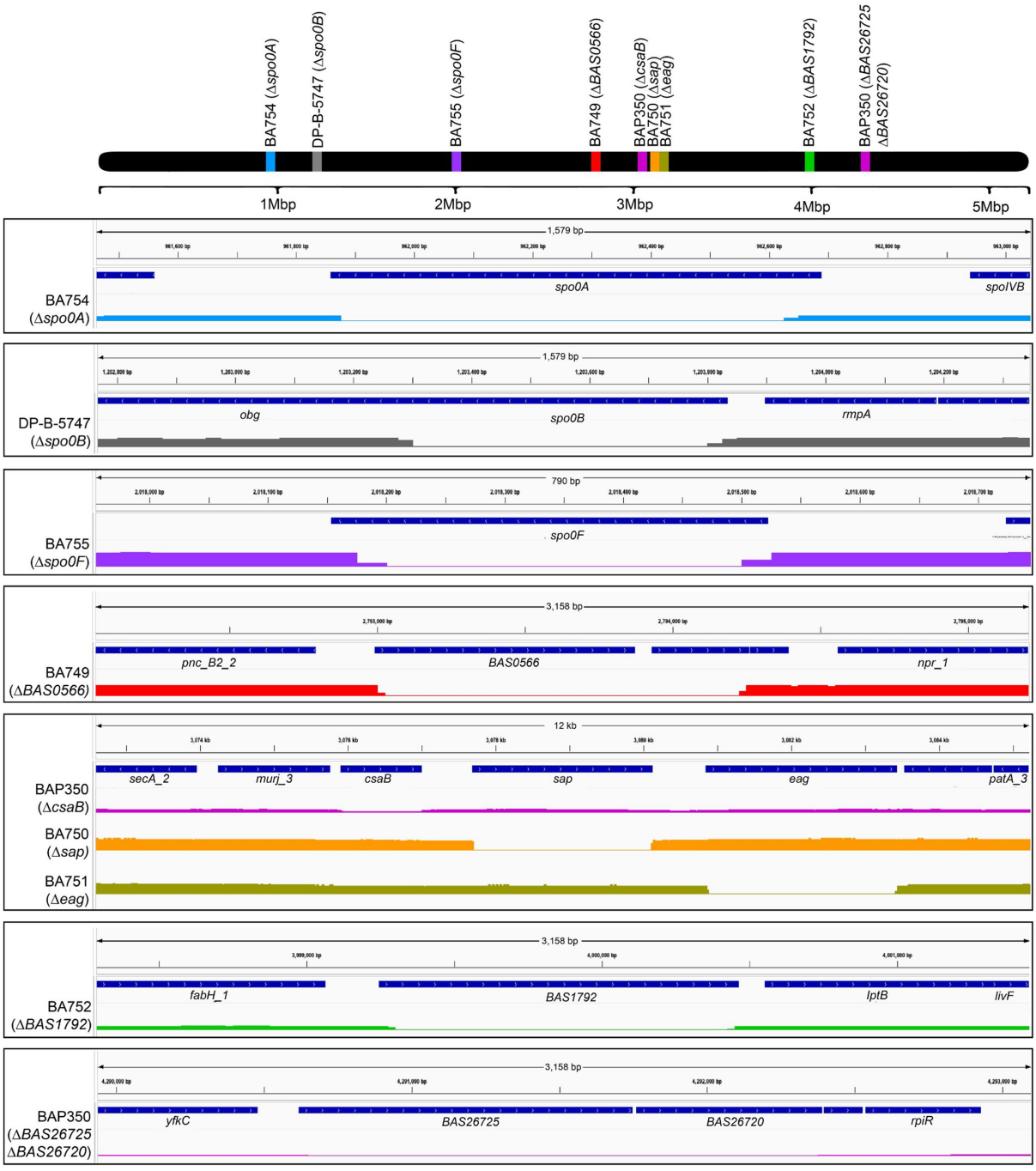

FIGURE 1
Genomic maps of wild type and mutant strains of *B. anthracis* Sterne 7702 indicating the presence of deletions in different locations. The top black bar represents the bacterial chromosome with the relative locations of the genes targeted for deletion in the mutants. The bottom blocks zoom in on the individual regions of each deletion with genome positions provided on top, relevant open reading frames in the middle, and sequence coverage of respective locus with flanking regions on the bottom. The mutant bars are color coded to match with the genes indicated on the whole chromosome map on top. Black boxes are to aid in visual differentiation of different strains. The secondary, off-target hitch-hiker deletions in the BAP350 strain (ORFs *BAS26725* and *BAS26720*) are indicated in the bottom-most box.

elsewhere in the genome (Supplementary Table S1). The BAP350 mutant (Δ*csaB*) also contained two additional deletions in genes *BAS26725* and *BAS26720* (Figure 1, bottom block). All these "hitch-hiker" mutations were taken into consideration when examining the results of RBP binding experiments described below.

3.2. Expression and purification of phage receptor binding proteins

Earlier work by Braun et al. described the identification, cloning, expression, and purification of the putative receptor binding proteins (RBPs) of phages Wip1 (P23), AP50c (P28), γ (Gp14) and a soluble domain of λBa03 (BA4079 Δ1-120) (Braun et al., 2020). Here, we expanded on this work and developed a plasmid system in which each RBP could be expressed with GFP fused to the N-terminus. These constructs additionally contained a His-thrombin site and *Twin-Strep-tag* epitope to aid in purification. For the plasmids expressing the Wip1 or AP50c RBP-GFP fusion proteins, a second protein encoded immediately downstream in the phage genome was co-expressed based on previous results suggesting these secondary proteins were required for RBP function (Braun et al., 2020). Proteins were produced in Arctic Express *E. coli* cells and following autoinduction, lysates were separated into soluble and insoluble fractions. As all proteins of interest were soluble, these samples were fractionated using immobilized nickel affinity chromatography columns. The purity of each fraction was measured by Abs_{280} and size exclusion chromatography. Final preparations were visualized on a 4–20% Tris-glycine gel (Figure 2). These proteins are henceforth referred to as RBP_{Wip1}-GFP, RBP_{AP50c}-GFP, and $RBP_{\lambda03\Delta1\text{-}120}$-GFP.

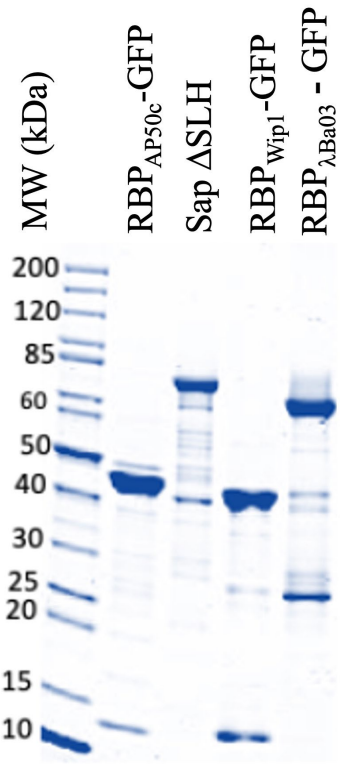

FIGURE 2
Production and purification of the three GFP-tagged phage receptor binding proteins and the untagged *sap*ΔSLH domain (not used in current study). Five microgram aliquots of the final preparations of each purified product were run on a denaturing 4–20% Tris-glycine gel and imaged using a LI-COR instrument (LI-COR Biosciences). The <15 kDa bands in the RBP_{AP50c}-GFP (P28) and RBP_{Wip1}-GFP (P23) lanes represent the co-expressed chaperone proteins P29 and P24, respectively.

3.3. Binding of phage RBPs to *Bacillus anthracis* mutants

The protein preparations containing the recombinant, tagged phage RBPs were next tested for binding against the panel of sequence-verified mutant strains described in Figure 1. As previous work suggested that phage RBP binding (i) is dependent on the growth phase of the bacteria and (ii) is strong for RBP_{Wip1}, RBP_{AP50c}, and $RBP_{\lambda03\Delta1\text{-}120}$ during logarithmic growth (Braun et al., 2020), all experiments were performed using cells harvested during this period. Cells were not otherwise synchronized. As expected, all three phage RBPs bound to wild type Sterne strain 7702, as well as to mutants lacking expression of *BAS0566* (BA749), *eag* (BA751), and *BAS1792* (BA752) (Figure 3). In support of earlier work with whole phage AP50c (Plaut et al., 2014), the deletion of *sap*, *csaB*, or any one of the three sporulation genes *spo0A*, *spo0B*, or *spo0F* also resulted in the loss of RBP_{AP50c}-GFP binding. The same binding profile was observed with the RBP_{Wip1}-GFP. Interestingly, the putative $RBP_{\lambda03\Delta1\text{-}120}$-GFP bound to all mutant strains with the exception of BAP350, which lacks *csaB*.

We next looked to determine whether the binding of the phage RBPs would be affected by heating of the bacterial culture. Aliquots of mid-log cultures were heated for 30 min at 98°C and plated to verify inactivation prior to incubation with each tagged phage RBP. This process resulted in the loss of RBP_{AP50c}-GFP and RBP_{Wip1}-GFP binding to all strains (Supplementary Figure S1). The binding of $RBP_{\lambda03\Delta1\text{-}120}$-GFP to bacterial cells was not affected by heating, with the exception of the *csaB* mutant.

As *B. anthracis* cells show significant changes in surface protein expression following sporulation when compared to vegetative cells (Chateau et al., 2020), we were interested to determine whether the bacterial receptors for the RBPs were present on spore surfaces. To this end, tagged RBPs were incubated with spores prepared from each mutant strain. Of those strains that successfully sporulated, no phage RBP binding was observed (Supplementary Figure S2). A summary of the binding profiles for each RBP to each mutant strain under all three conditions can be seen in Table 2.

3.4. Expression of *csaB* in *trans* restores wild-type phage RBP binding profiles

The only mutant strain that resulted in the loss of binding for all three phage RBPs with live vegetative cells was BAP350 (Δ*csaB*). To ensure that this phenotype was due only to this mutation and not to the two hitch-hiker mutations and/or SNPs present in this strain, we expressed *csaB* in *trans* from a complementation plasmid.

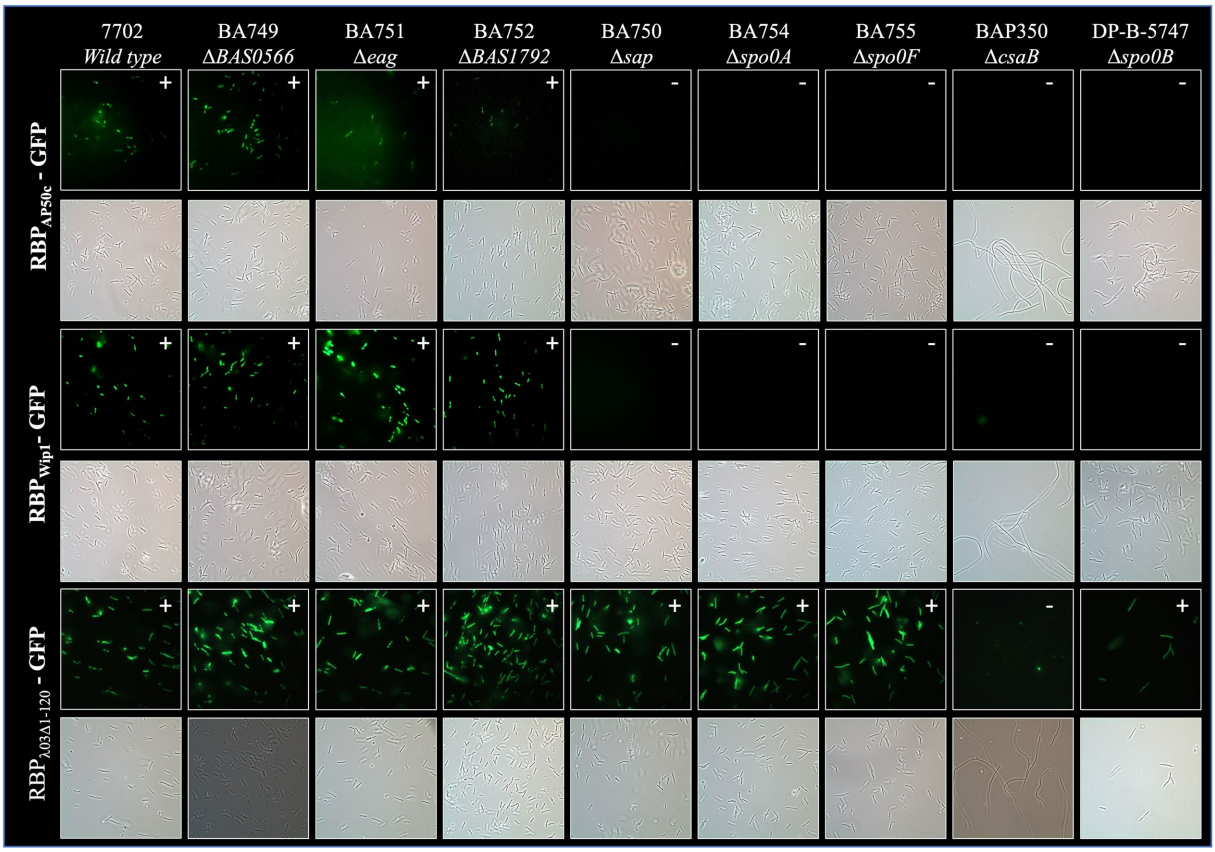

FIGURE 3
Representative fluorescence and brightfield images showing binding of RBP$_{AP50c}$-GFP, RBP$_{Wip1}$-GFP, and RBP$_{λ03Δ1-120}$-GFP to cultures of vegetative *B. anthracis* Sterne mutants. All slides were prepared using cultures harvested at OD_{600} = 1.0 following a five-minute incubation with 5 µg of purified phage proteins. Note the filamentous morphology of the BAP350 strain lacking *csaB*.

The coding sequence for *csaB* was cloned into the pSW4 shuttle expression vector as described in the Materials and Methods (Figure 4A) and introduced into BAP350 (*ΔcsaB*) or the wild type 7702 strain by electroporation. The presence of the plasmid in electroporated cells was verified by PCR (Figure 4B), and binding studies were repeated as described above. Supplying *csaB* protein in *trans* in BAP350 indeed rescued wild-type binding profiles of all three RBPs (Figures 4C,D), suggesting that the phenotype seen with the *csaB* mutant strain in earlier experiments was due to the lack of *csaB* expression alone. It should additionally be noted that expression of *csaB* in *trans* also reversed the mucoid/filamentous morphology phenotype observed in BAP350. It appears that the presence of pSW4 vector by itself, is somewhat partially reverting the mucoid phenotype as observed by the fluffy nature of the culture in the tube (Supplementary Figure S3).

3.5. Expression of *sap* and *spo0* genes in *trans* rescues RBP$_{Wip1}$-GFP, RBP$_{AP50c}$-GFP binding

In addition to the role of *csaB* in the binding of all 3 phage RBPs, the RBP$_{Wip1}$-GFP and RBP$_{AP50c}$-GFP proteins also required the expression of *sap* and the sporulation genes *spo0A*, *spo0B*, and *spo0F* for successful binding (Figure 3). This had been observed previously with whole phage particles (Plaut et al., 2014). A similar set of complementation experiments was carried out for all of these mutant strains, each of which were electroporated with either the empty pSW4 vector or the appropriate complementation construct. The successful electroporation of each plasmid was verified both by PCR (Supplementary Figure S4) and by the restoration of sporulation in mutant strains (Supplementary Figure S5). In the bacteria containing the complementation plasmids expressing *sap* (complementation in strain BA750) (Figure 5), *spo0A* (BA754, Figure 6), and spo0B (DP-B-5747, Figure 7), the wild-type binding profile was restored. In experiments with the *spo0F* mutant (BA755), however, complementation rescued RBP$_{AP50c}$-GFP binding to live vegetative cells but did not rescue the binding of the RBP$_{Wip1}$-GFP (Figure 8). RBP$_{λ03Δ1-120}$-GFP binding was unaffected in these mutants or the corresponding complemented strains.

4. Discussion

In this study, we have investigated the genetic requirements for the binding of bacteria and phage in a *B. anthracis* model system. We assessed the binding of three different phage RBPs with a collection

10.3389/fmicb.2023.1278791

TABLE 2 Binding phenotypes observed for each of the *B. anthracis* Sterne mutant cultures when incubated with RBPs-GFP fusion proteins.

Strain	Phenotype	Live vegetative cells			Heat-killed vegetative cells			Spores		
		RBP_{AP50c}	RBP_{Wip1}	$RBP_{\lambda03\Delta1-120}$	RBP_{AP50c}	RBP_{Wip1}	$RBP_{\lambda03\Delta1-120}$	RBP_{AP50c}	RBP_{Wip1}	$RBP_{\lambda03\Delta1-120}$
7702	Wild-Type	+	+	+	–	–	+	–	–	–
BA749	*ΔBAS0566*	+	+	+	–	–	+	–	–	–
BA751	*Δeag*	+	+	+	–	–	+	–	–	–
BA752	*ΔBAS1792*	+	+	+	–	–	+	–	–	–
BA750	*Δsap*	–	–	+	–	–	+	–	–	–
BA754	*Δspo0A*	–	–	+	–	–	+	N/A	N/A	N/A
BA755	*Δspo0F*	–	–	+	–	–	+	N/A	N/A	N/A
BAP350	*ΔcsaB*	–	–	–	–	–	–	–	–	–
DP-B-5747	*Δspo0B*	–	–	+	–	–	+	N/A	N/A	N/A

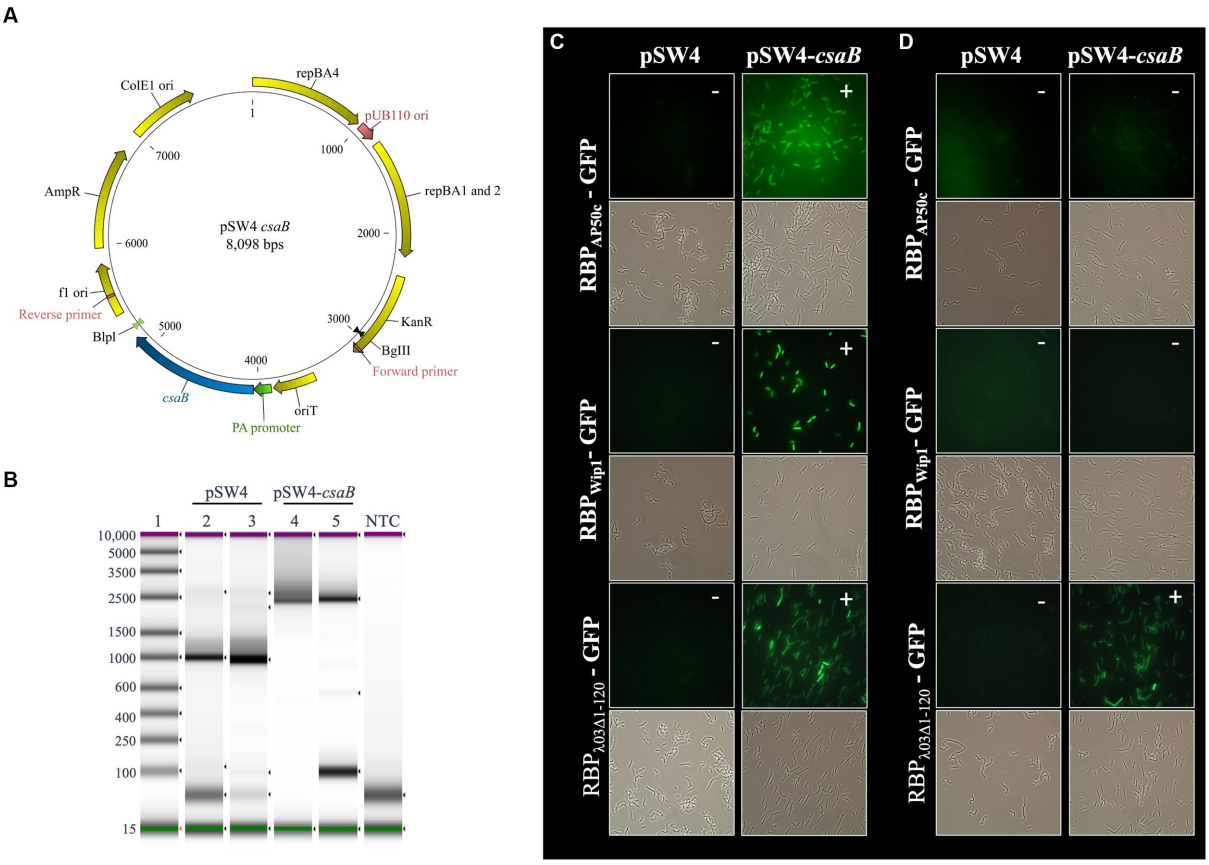

FIGURE 4
Expression of *csaB* in *trans* rescues (i) RBP_{AP50c}-GFP and RBP_{Wip1}-GFP binding to live cultures of Δ*csaB* mutant strain BAP350 and (ii) $RBP_{\lambda03\Delta1-120}$-GFP binding to heat-killed cultures. **(A)** Plasmid map for pSW4-*csaB*. **(B)** PCR amplicon products show the presence of the expression vector/complementation plasmid in strain BAP350. Lane 1: base pair ladder. Lanes 2 and 4: Stock plasmid preparations. Lane 3 and 5: Plasmids isolated from electroporated BAP350 cultures. NTC indicates no template control. Representative fluorescent microcopy images show binding patterns of tagged phage RBPs to **(C)** vegetative, or **(D)** heat-killed preparations of BAP350 with and without *csaB* complementation. Small white notations in upper right-hand corner of each image indicate the presence (+) or absence (–) of binding.

10.3389/fmicb.2023.1278791

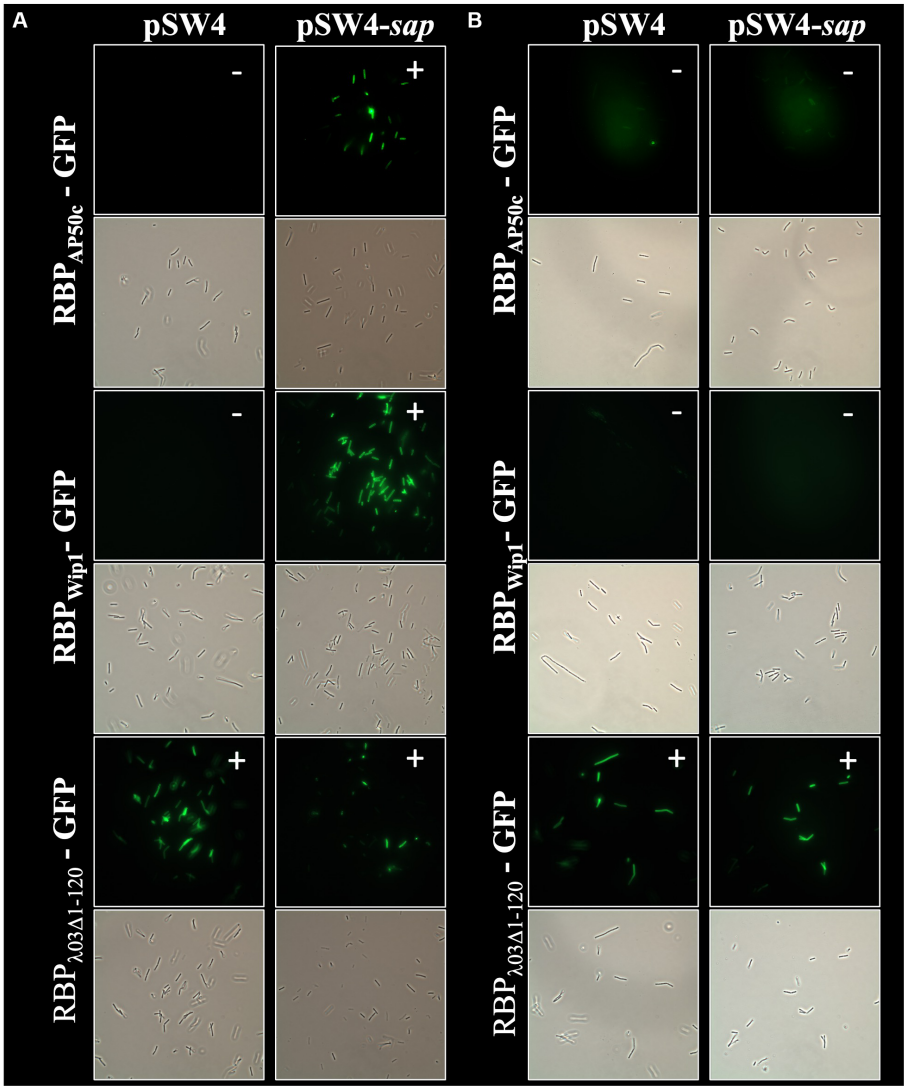

FIGURE 5
Expression of *sap* in *trans* rescues RBP$_{AP50c}$-GFP and RBP$_{Wip1}$-GFP binding to Δ*sap* mutant strain BA750. Representative fluorescent microcopy images show binding patterns of tagged phage RBPs to **(A)** vegetative, or **(B)** heat-killed preparations of BA750 with and without *sap* complementation. Small white notations in upper right-hand corner of each image indicate the presence (+) or absence (–) of binding.

of *B. anthracis* mutant strains with the goal of better understanding the underlying biology driving these interactions. While there has been previous work on the binding of these 3 phage RBPs to wild type bacteria (Braun et al., 2020), two questions remained unanswered; namely, (i) is there genetic evidence for these binding pairs? and (ii) is this binding affected by mutations in a specific set of bacterial genes? These questions are critical as they relate directly to the potential for development of phage resistance and the failure of assays that rely on this binding. Here we provide experimental evidence that answers these questions.

Using a set of GFP-tagged recombinant proteins, we recapitulated earlier results derived from whole phage particle experiments. These results indicated that: (i) the RBP$_{AP50c}$ likely binds the bacterial receptor *sap*, (ii) this binding interaction requires the expression of *csaB* and the sporulation genes *spo0A*, *spo0B*, and *spo0F*, and (iii) the binding is ablated following heat inactivation. While the putative RBP$_{Wip1}$-GFP does not share extensive sequence similarity to that of RBP$_{AP50c}$-GFP, it does contain a small region of identical amino acids at its C-terminal, and there does exist a striking similarity in the product of genes immediately downstream of the RBPs in both phage genomes (Braun et al., 2020). Our study here suggests that Wip1 likely uses the same bacterial protein, *sap*, as its receptor, and that *csaB* and the same three sporulation genes are necessary for this interaction. The role of *csaB* in this binding interaction is not surprising, as it has a known role in anchoring *sap* to the S-layer (Mesnage et al., 2000). The role of the sporulation genes, however, is less intuitive. We hypothesize that the activity of Spo0A, a major transcriptional

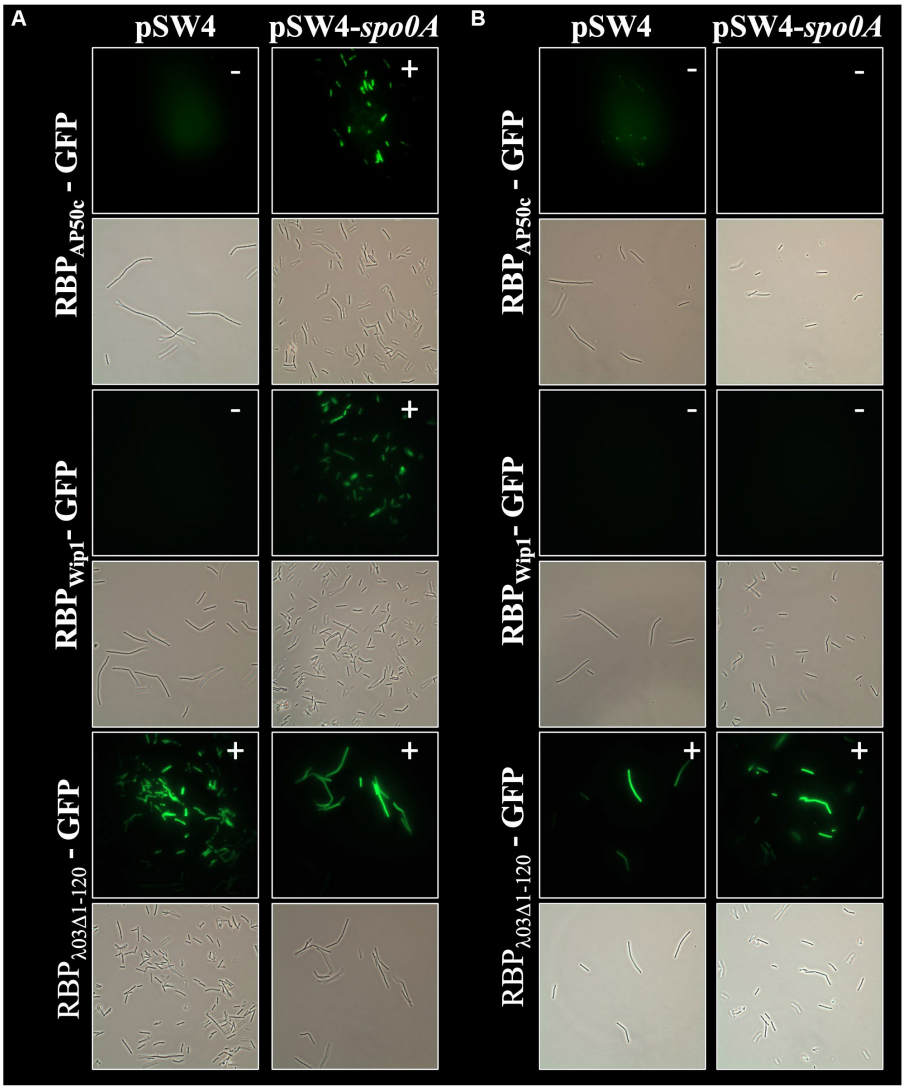

FIGURE 6
Expression of *spo0A* in *trans* rescues RBP$_{AP50c}$-GFP and RBP$_{Wip1}$-GFP binding to Δ*spo0A* mutant strain BA754. Representative fluorescent microcopy images show binding patterns of tagged phage RBPs to **(A)** vegetative, or **(B)** heat-killed preparations of BA754 with and without *spo0A* complementation. Small white notations in upper right-hand corner of each image indicate the presence (+) or absence (–) of binding.

regulator (Burbulys et al., 1991), has a role in the expression or stability of *sap* or the S-layer in general. This concept has been introduced in previous work (Plaut et al., 2014), and our results support an expansive role for the sporulation phosphorelay in overall cell state. The successful rescue of wild-type binding profiles, except *spo0F* with RBP$_{Wip1}$-GFP, upon complementation with the protein absent in a given mutant strain suggests that the minor additional "hitch-hiker" mutations play no role in the phenotypes seen in each of these strains. Additionally, we could find no evidence in the literature supporting the potential involvement of these genetic loci in phage binding, S-layer function, or sporulation. The anomaly with the failure of rescue of *spo0F* complementation with RBP$_{Wip1}$-GFP binding is not clear at this time.

Our results showing a lack of binding of RBP$_{AP50c}$-GFP and RBP$_{Wip1}$-GFP to heat-inactivated vegetative cells is somewhat unexpected based on earlier published results (Braun et al., 2020). We hypothesize that this difference could be attributed to strain- and experiment-specific differences. Even in the previously published studies, binding of each RBP to heat-inactivated cells was somewhat diminished compared to wild type cells, and it varied based both on the method of inactivation and the RBP in question (Braun et al., 2020).

Similar to previous works, and unlike the results observed with RBP$_{AP50c}$-GFP and RBP$_{Wip1}$-GFP, we found that prophage RBP$_{\lambda03\Delta1\text{-}120}$-GFPbinding was not affected by heat inactivation. However, while earlier work also indicated that *csaB* was *not* involved in the growth of phage γ, which shows high sequence homology to λBa03

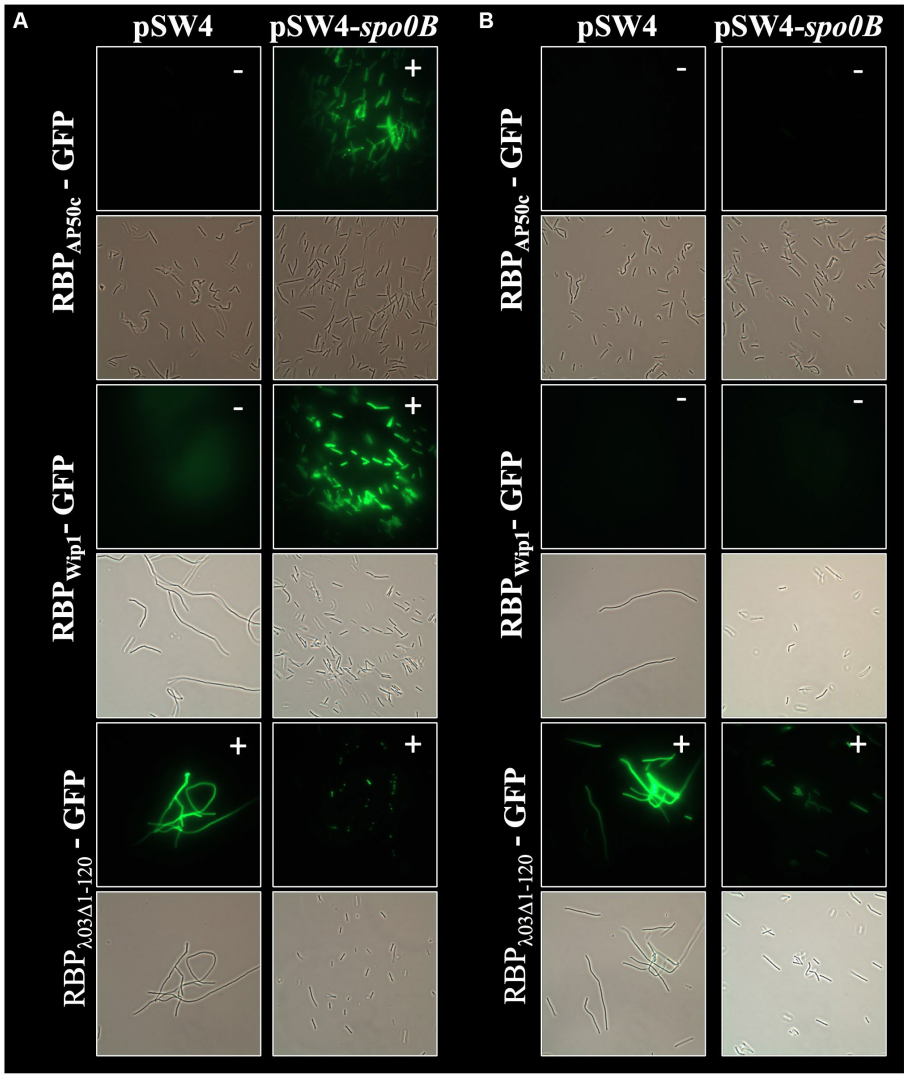

FIGURE 7
Expression of *spo0B* in *trans* rescues RBP$_{AP50c}$-GFP and RBP$_{Wip1}$-GFP binding to Δ*spo0B* mutant strain DP-B-5747. Representative fluorescent microcopy images show binding patterns of tagged phage RBPs to **(A)** vegetative, or **(B)** heat-killed preparations of DP-B-5747with and without *spo0B* complementation. Small white notations in upper right-hand corner of each image indicate the presence (+) or absence (–) of binding.

(Davison et al., 2005), we find here that the absence of *csaB* ablated RBP$_{\lambda03\Delta1\text{-}120}$-GFP binding. The sequence similarity between phage γ and prophage λBa03 suggests that λBa03 shared the same bacterial host receptor as gamma (GamR). Our results, however, suggest that either (i) GamR is not accessible to the RBP$_{\lambda03\Delta1\text{-}120}$-GFP in the absence of *csaB* (but it is accessible to the whole γ phage particle). The *csaB* mutants are known to secrete an extracellular flocculent material and in fact, scanning electron microscopic analysis of this mutant revealed the presence of a thin coating of an extracellular material on the outer cell surface (Sozhamannan et al., 2008); it is possible that this layer prevents access of RBP$_{\lambda03\Delta1\text{-}120}$-GFP to the bacterial receptor, or (ii) GamR is not the bacterial receptor for λBa03. If the former is true, GamR may be somehow shielded from heat denaturation, while if the latter is true, it may be that the receptor for RBP$_{\lambda03\Delta1\text{-}120}$-GFP is not proteinaceous in nature, as most proteins lose secondary structure following high temperature exposure. Recent work has in fact suggested that other γ-like phages utilize sugar moieties as part of their binding process (Nakonieczna et al., 2022) and we postulate that this may be the case for λBa03. Our future studies will examine this possibility, and further probe direct protein–protein interactions between phage RBPs and bacterial receptor proteins.

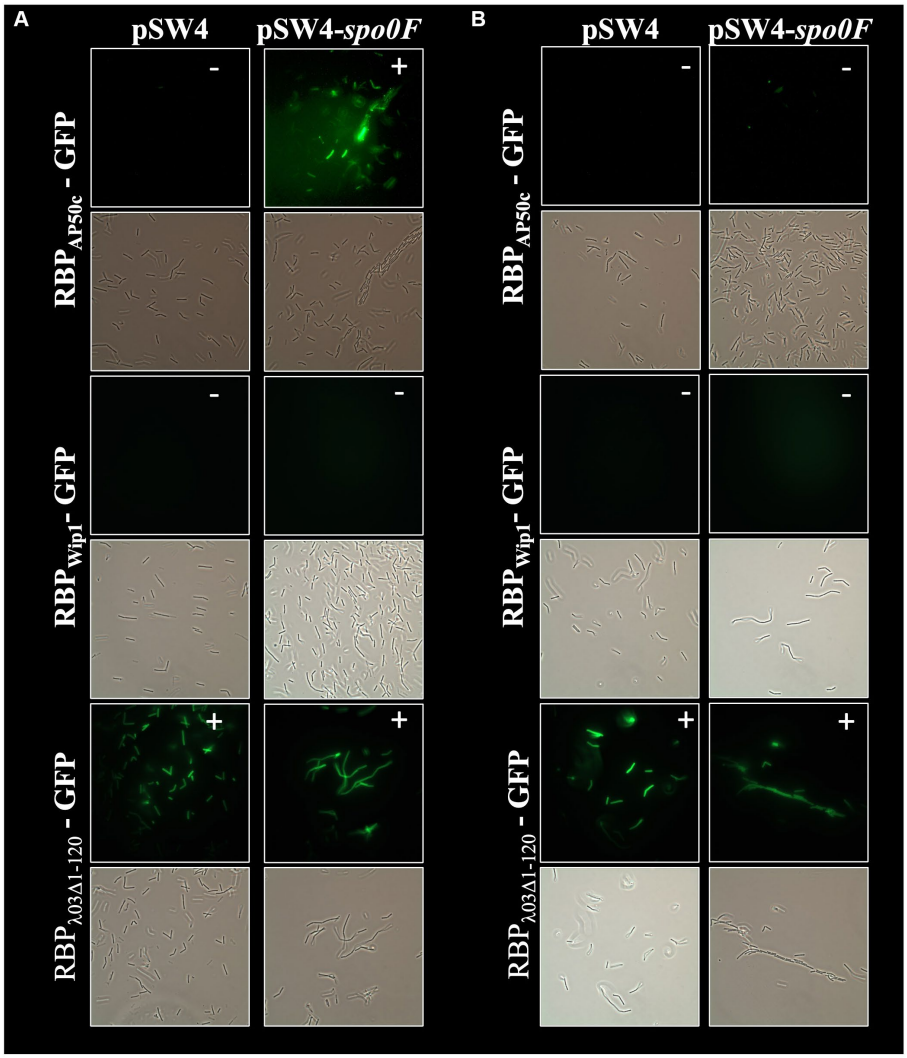

FIGURE 8
Expression of *spo0F* in *trans* does rescue RBP$_{AP50c}$-GFP binding and does not rescue RBP$_{Wip1}$-GFP binding to Δ*spo0F* mutant strain BA755. Representative fluorescent microcopy images show binding patterns of tagged phage RBPs to **(A)** vegetative, or **(B)** heat-killed preparations of BA755 with and without *spo0F* complementation small white notations in upper right-hand corner of each image indicate the presence (+) or absence (–) of binding.

Data availability statement

The data presented in the study are deposited in GenBank, accession numbers CP110279, JAOZJJ000000000, CP110281, JAOZJK000000000, JAOZJL000000000, JAOZJM000000000, CP110283, CP110285, and CP110287.

Author contributions

SF: Conceptualization, Formal analysis, Investigation, Writing – review & editing. ST: Conceptualization, Formal analysis, Investigation, Writing – review & editing. SaS: Conceptualization, Formal analysis, Investigation, Writing – review & editing. SH: Conceptualization, Formal analysis, Investigation, Writing – review & editing. RP: Investigation, Writing – review & editing. KV: Project administration, Writing – review & editing. MW: Investigation, Writing – review & editing. EE: Investigation, Writing – review & editing. BN: Funding acquisition, Writing – review & editing. ShS: Conceptualization, Data curation, Formal analysis, Funding acquisition, Project administration, Writing – original draft, Writing – review & editing. SG: Conceptualization, Formal analysis, Investigation, Writing – original draft, Writing – review & editing.

Funding

The author(s) declare financial support was received for the research, authorship, and/or publication of this article. Funding for this work was provided by the Department of Defense (DoD) Joint Program Executive Office for Chemical, Biological, Radiological and Nuclear Defense (JPEO-CBRND) under NAVSEA contract number

N00024-13-D-6400. The views expressed in this article are those of the authors and do not necessarily reflect the official policy or position of the JPEO-CBRND, the Departments of the Army, Navy, or Defense, nor the U.S. Government. References to non-federal entities do not constitute or imply Department of Defense or Army endorsement of any company or organization.

Acknowledgments

The authors would like to acknowledge Andrei Pomerantsev, Steve Leppla, and Gregor Grass for their kind provision of plasmids, sequences, reagents, and expertise. We also appreciate the many useful comments provided by the reviewers.

Conflict of interest

ShS was employed by Joint Research and Development, Inc. MW and EE were employed by Olympic Protein Technologies.

The remaining authors declare that the research was conducted in the absence of any commercial or financial relationships that could be construed as a potential conflict of interest.

Publisher's note

All claims expressed in this article are solely those of the authors and do not necessarily represent those of their affiliated organizations, or those of the publisher, the editors and the reviewers. Any product that may be evaluated in this article, or claim that may be made by its manufacturer, is not guaranteed or endorsed by the publisher.

Supplementary material

The Supplementary material for this article can be found online at: https://www.frontiersin.org/articles/10.3389/fmicb.2023.1278791/full#supplementary-material

References

Abshire, T. G., Brown, J. E., and Ezzell, J. W. (2005). Production and validation of the use of gamma phage for identification of *Bacillus anthracis*. *J. Clin. Microbiol.* 43, 4780–4788. doi: 10.1128/JCM.43.9.4780-4788.2005

Aranaga, C., Pantoja, L. D., Martínez, E. A., and Falco, A. (2022). Phage therapy in the era of multidrug resistance in bacteria: a systematic review. *Int. J. Mol. Sci.* 23:4577. doi: 10.3390/ijms23094577

Bertozzi Silva, J., Storms, Z., and Sauvageau, D. (2016). Host receptors for bacteriophage adsorption. *FEMS Microbiol. Lett.* 363:fnw002. doi: 10.1093/femsle/fnw002

Bishop-Lilly, K. A., Plaut, R. D., Chen, P. E., Akmal, A., Willner, K. M., Butani, A., et al. (2012). Whole genome sequencing of phage resistant *Bacillus anthracis* mutants reveals an essential role for cell surface anchoring protein CsaB in phage AP50c adsorption. *Virol. J.* 9:246. doi: 10.1186/1743-422X-9-246

Braun, P., Wolfschläger, I., Reetz, L., Bachstein, L., Jacinto, A. C., Tocantins, C., et al. (2020). Rapid microscopic detection of *Bacillus anthracis* by fluorescent receptor binding proteins of bacteriophages. *Microorganisms* 8:934. doi: 10.3390/microorganisms8060934

Burbulys, D., Trach, K. A., and Hoch, J. A. (1991). Initiation of sporulation in *B. subtilis* is controlled by a multicomponent phosphorelay. *Cells* 64, 545–552. doi: 10.1016/0092-8674(91)90238-t

Chateau, A., Van der Verren, S. E., Remaut, H., and Fioravanti, A. (2020). The *Bacillus anthracis* cell envelope: composition, physiological role, and clinical relevance. *Microorganisms* 8:1864. doi: 10.3390/microorganisms8121864

Darling, R. G., Catlett, C. L., Huebner, K. D., and Jarrett, D. G. (2002). Threats in bioterrorism. I: CDC category a agents. *Emerg. Med. Clin. North Am.* 20, 273–309. doi: 10.1016/s0733-8627(02)00005-6

Davison, S., Couture-Tosi, E., Candela, T., Mock, M., and Fouet, A. (2005). Identification of the *Bacillus anthracis* (gamma) phage receptor. *J. Bacteriol.* 187, 6742–6749. doi: 10.1128/JB.187.19.6742-6749.2005

Fioravanti, A., Mathelie-Guinlet, M., Dufrêne, Y. F., and Remaut, H. (2022). The *Bacillus anthracis* S-layer is an exoskeleton-like structure that imparts mechanical and osmotic stabilization to the cell wall. *PNAS Nexus* 1:pgac121. doi: 10.1093/pnasnexus/pgac121

Forde, T. L., Dennis, T. P. W., Aminu, O. R., Harvey, W. T., Hassim, A., Kiwelu, I., et al. (2022). Population genomics of *Bacillus anthracis* from an anthrax hyperendemic area reveals transmission processes across spatial scales and unexpected within-host diversity. *Microb Genom* 8:000759. doi: 10.1099/mgen.0.000759

Hyman, P., and van Raaij, M. (2018). Bacteriophage T4 long tail fiber domains. *Biophys. Rev.* 10, 463–471. doi: 10.1007/s12551-017-0348-5

Kan, S., Fornelos, N., Schuch, R., and Fischetti, V. A. (2013). Identification of a ligand on the Wip1 bacteriophage highly specific for a receptor on *Bacillus anthracis*. *J. Bacteriol.* 195, 4355–4364. doi: 10.1128/JB.00655-13

Koboldt, D. C., Zhang, Q., Larson, D. E., Shen, D., McLellan, M. D., Lin, L., et al. (2012). VarScan 2: somatic mutation and copy number alteration discovery in cancer by exome sequencing. *Genome Res.* 22, 568–576. doi: 10.1101/gr.129684.111

Mesnage, S., Fontaine, T., Mignot, T., Delepierre, M., Mock, M., and Fouet, A. (2000). Bacterial SLH domain proteins are non-covalently anchored to the cell surface via a conserved mechanism involving wall polysaccharide pyruvylation. *EMBO J.* 19, 4473–4484. doi: 10.1093/emboj/19.17.4473

Mignot, T., Mesnage, S., Couture-Tosi, E., Mock, M., and Fouet, A. (2002). Developmental switch of S-layer protein synthesis in *Bacillus anthracis*. *Mol. Microbiol.* 43, 1615–1627. doi: 10.1046/j.1365-2958.2002.02852.x

Nakonieczna, A., Rutyna, P., Fedorowicz, M., Kwiatek, M., Mizak, L., and Łobocka, M. (2022). Three novel bacteriophages, J5a, F16Ba, and z1a, specific for Bacillus anthracis, define a new clade of historical Wbeta phage relatives. *Viruses* 14:213. doi: 10.3390/v14020213

Plaut, R. D., Beaber, J. W., Zemansky, J., Kaur, A. P., George, M., Biswas, B., et al. (2014). Genetic evidence for the involvement of the S-layer protein gene sap and the sporulation genes spo0A, spo0B, and spo0F in phage AP50c infection of *Bacillus anthracis*. *J. Bacteriol.* 196, 1143–1154. doi: 10.1128/JB.00739-13

Pomerantsev, A. P., Kalnin, K. V., Osorio, M., and Leppla, S. H. (2003). Phosphatidylcholine-specific phospholipase C and sphingomyelinase activities in bacteria of the *Bacillus cereus* group. *Infect. Immun.* 71, 6591–6606. doi: 10.1128/IAI.71.11.6591-6606.2003

Rakhuba, D. V., Kolomiets, E. I., Dey, E. S., and Novik, G. I. (2010). Bacteriophage receptors, mechanisms of phage adsorption and penetration into host cell. *Pol. J. Microbiol.* 59, 145–155. doi: 10.33073/pjm-2010-023

Schuch, R., Pelzek, A. J., Kan, S., and Fischetti, V. A. (2010). Prevalence of *Bacillus anthracis*-like organisms and bacteriophages in the intestinal tract of the earthworm *Eisenia fetida*. *Appl. Environ. Microbiol.* 76, 2286–2294. doi: 10.1128/AEM.02518-09

Sedlazeck, F. J., Rescheneder, P., Smolka, M., Fang, H., Nattestad, M., von Haeseler, A., et al. (2018). Accurate detection of complex structural variations using single-molecule sequencing. *Nat. Methods* 15, 461–468. doi: 10.1038/s41592-018-0001-7

Sharp, N. J., Molineux, I. J., Page, M. A., and Schofield, D. A. (2016). Rapid detection of viable *Bacillus anthracis* spores in environmental samples by using engineered reporter phages. *Appl. Environ. Microbiol.* 82, 2380–2387. doi: 10.1128/AEM.03772-15

Sholes, S. L., Harrison, S., Forrest, S., Ton, S., Grady, S. L., Verratti, K., et al. (2023). Draft genome assemblies of phage AP50c-resistant derivatives of *Bacillus anthracis* Sterne strain 7702 lacking plasmid pXO2. *Microbiol Resour Announc* 12:e0131322. doi: 10.1128/mra.01313-22

Sozhamannan, S., Chute, M. D., McAfee, F. D., Fouts, D. E., Akmal, A., Galloway, D. R., et al. (2006). The *Bacillus anthracis* chromosome contains four conserved, excision-proficient, putative prophages. *BMC Microbiol.* 6:34. doi: 10.1186/1471-2180-6-34

Sozhamannan, S., McKinstry, M., Lentz, S. M., Jalasvuori, M., McAfee, F., Smith, A., et al. (2008). Molecular characterization of a variant of *Bacillus anthracis*-specific phage AP50 with improved bacteriolytic activity. *Appl. Environ. Microbiol.* 74, 6792–6796. doi: 10.1128/AEM.01124-08

Thorvaldsdóttir, H., Robinson, J. T., and Mesirov, J. P. (2013). Integrative genomics viewer (IGV): high-performance genomics data visualization and exploration. *Brief. Bioinform.* 14, 178–192. doi: 10.1093/bib/bbs017

frontiers | Frontiers in Microbiology

TYPE Original Research
PUBLISHED 30 November 2023
DOI 10.3389/fmicb.2023.1307349

OPEN ACCESS

EDITED BY
Alicja Wegrzyn,
Polish Academy of Sciences, Poland

REVIEWED BY
Bartłomiej Grygorcewicz,
Pomeranian Medical University, Poland
Ravikumar Patel,
Connecticut Agricultural Experiment Station, United States
Agata Jurczak-Kurek,
University of Gdansk, Poland

*CORRESPONDENCE
Robert Czajkowski
robert.czajkowski@ug.edu.pl

RECEIVED 04 October 2023
ACCEPTED 14 November 2023
PUBLISHED 30 November 2023

CITATION
Borowicz M, Krzyżanowska DM, Narajczyk M, Sobolewska M, Rajewska M, Czaplewska P, Węgrzyn K and Czajkowski R (2023) Soft rot pathogen *Dickeya dadantii* 3937 produces tailocins resembling the tails of *Peduovirus* P2. *Front. Microbiol.* 14:1307349. doi: 10.3389/fmicb.2023.1307349

Soft rot pathogen *Dickeya dadantii* 3937 produces tailocins resembling the tails of *Peduovirus* P2

Marcin Borowicz[1], Dorota M. Krzyżanowska[1], Magdalena Narajczyk[2], Marta Sobolewska[1], Magdalena Rajewska[3], Paulina Czaplewska[4], Katarzyna Węgrzyn[5] and Robert Czajkowski[1]*

[1]Laboratory of Biologically Active Compounds, Intercollegiate Faculty of Biotechnology of UG and MUG, University of Gdańsk, Gdańsk, Poland, [2]Bioimaging Laboratory, Faculty of Biology, University of Gdańsk, Gdańsk, Poland, [3]Laboratory of Plant Microbiology, Intercollegiate Faculty of Biotechnology of UG and MUG, University of Gdańsk, Gdańsk, Poland, [4]Laboratory of Mass Spectrometry-Core Facility Laboratories, Intercollegiate Faculty of Biotechnology of UG and MUG, University of Gdańsk, Gdańsk, Poland, [5]Laboratory of Molecular Biology, Intercollegiate Faculty of Biotechnology of UG and MUG, University of Gdańsk, Gdańsk, Poland

Tailocins are nanomolecular machines with bactericidal activity. They are produced by bacteria to contribute to fitness in mixed communities, and hence, they play a critical role in their ecology in a variety of habitats. Here, we characterized the new tailocin produced by *Dickeya dadantii* strain 3937, a well-characterized member of plant pathogenic Soft Rot *Pectobacteriaceae* (SRP). Tailocins induced in *D. dadantii* were *ca.* 166 nm long tubes surrounded by contractive sheaths with baseplates having tail fibers at one end. A 22-kb genomic cluster involved in their synthesis and having high homology to the cluster coding for the tail of the Peduovirus P2 was identified. The *D. dadantii* tailocins, termed dickeyocins P2D1 (phage P2-like dickeyocin 1), were resistant to inactivation by pH (3.5–12), temperature (4–50°C), and elevated osmolarity (NaCl concentration: 0.01–1 M). P2D1 could kill a variety of different *Dickeya* spp. but not any strain of *Pectobacterium* spp. tested and were not toxic to *Caenorhabditis elegans*.

KEYWORDS

bacteriophage, phage tail, tailocin, *Erwinia chrysanthemi*, bacteriocin, bacteria-bacteria interactions, *Caenorhabditis elegans*

Introduction

Under natural conditions, bacterial species inhabit shared environments, developing spatial and temporal interspecies associations and communities having complex networks of interactions (Little et al., 2008; Gorter et al., 2020). In such communities, a particular member needs to continuously compete for limited resources (i.e., scarce nutrients and limited space) with most other members of the community to gain a competitive edge (Bauer et al., 2018; Wagner, 2022). Given such challenging conditions, bacteria have evolved diverse strategies to successfully coexist with both closely and distantly related microbes (Granato et al., 2019). Such strategies, although employing a broad range of mechanisms, can be distinguished as either (1) indirect, exploitative competition that occurs through the

consumption of resources and (2) direct, interference competition, where individual cells directly kill one another, limiting their lifespan (Ghoul and Mitri, 2016). Whereas exploitative competition depends primarily on the utilization of limited resources by a strain, thereby restricting it from the competitor, interference competition relies on producing various antimicrobial agents that aim to kill other cells (Hibbing et al., 2010). These antimicrobials include, but are not limited to, broad-spectrum antibiotics, toxins, contact-dependent inhibition, effectors transported via type VI secretion system (T6SS effectors), low molecular weight bacteriocins, and tailocins (Stubbendieck and Straight, 2016; Granato et al., 2019). A given bacterial cell may often use several such systems to gain fitness advantages in the environment (Hibbing et al., 2010). Among the systems bacteria exploit to fight competitive microbes, tailocins are now receiving increasing attention (Scholl, 2017; Patz et al., 2019).

Tailocins are syringe-like nanomolecular entities that are evolutionary and morphologically related to bacteriophage tails, type VI secretion systems, and extracellular contractile injection systems (Scholl, 2017). These particles, also known as high molecular weight bacteriocins or phage tail-like particles, are chromosomally encoded and ribosomally synthesized toxins that usually express a narrow killing range, interacting only with closely-related bacterial species that typically would occupy the same niche (Patz et al., 2019). These agents adsorp to the surface of susceptible cells, thereby puncturing the cell envelope, leading to depolymerization of the cell membrane and, ultimately, the death of the attacked cell (Ge et al., 2015).

Tailocins are classified into two distinct families: rigid and contractile (R-type) and noncontractile but flexible particles (F-type; Ghequire and De Mot, 2015). The R-type tailocins have features of tails of *Peduovirus* P2 or T-even bacteriophages infecting *Escherichia coli*. In contrast, the F-type tailocins resemble the flexible tails of bacteriophage lambda (λ). Although tailocins exhibit remarkable morphological similarity to bacteriophage tails of the viruses mentioned above, it is now believed that they have evolved independently from bacteriophages and should not be considered exclusively as domesticated prophages or phage remnants that bacteria harness for their advantage (Scholl, 2017).

The production of tailocins has been demonstrated both in Gram-negative and Gram-positive bacterial species. Producing strains include both human, animal, and plant pathogens and saprophytic bacteria residing in various environments (Morales-Soto et al., 2012; Liu et al., 2013; Ghequire and De Mot, 2014; Gebhart et al., 2015). Until recently, tailocins have been best characterized in *Pseudomonas* species (Michel-Briand and Baysse, 2002; Fischer et al., 2012). There are, however, reports of tailocins isolated from *Clostridioides* spp., *Serratia* spp., *Xenorhabdus* spp., *Burkholderia* spp., *Kosakonia* spp., *Budvicia* spp., *Pragia* spp., *Pectobacterium* spp. as well as from other bacteria (Smarda et al., 2005; Becker et al., 2022).

The omnipresence of tailocins in phylogenetically unrelated bacterial genera suggests that these particles are important for fitness in various habitats (Scholl, 2017). However, the ecological role of tailocins in the natural environment of the producing strains has received little attention, especially for plant-pathogenic bacteria residing in agricultural locations. This issue is important given the diversity of conditions such bacteria encounter in such natural settings. No comprehensive studies have addressed tailocins produced by Soft Rot *Pectobacteriaceae* (SRP) bacteria (Van Gijsegem et al., 2021), which, due to their complex lifestyle, have a variety of spatial and temporal interactions in varied environments (Perombelon, 2002; Charkowski, 2007, 2018).

Plant pathogenic SRP (consisting of *Pectobacterium* spp., *Dickeya* spp., and *Musicola* spp., formerly characterized as pectinolytic *Erwinia* spp.) are a useful model for studying the environmental role of tailocins. SRP bacteria are widespread in various ecological niches, including rain and surface water, natural and agricultural bulk and rhizosphere soils, sewage, the exterior and interior of host and non-host plants as well as the surface and interior of insects (Van Gijsegem et al., 2021). Because of the diverse environments in which SRP bacteria may be found, these pathogens may encounter various other bacteria with whom they must effectively compete.

This study aimed to assess the presence and activity of tailocins induced and isolated from pectinolytic *Dickeya dadantii* strain 3937 (Kotoujansky et al., 1982). This strain (formerly *Erwinia chrysanthemi* and *Pectobacterium chrysanthemi*; Samson et al., 2005) is a well-known necrotrophic plant pathogen that causes soft rot disease in a variety of crop, ornamental, and other nonfood plants worldwide, causing losses in agriculture (Kotoujansky, 1987). Strain 3937 has been widely used as a potent model system for research on the molecular biology and pathogenicity of bacteria belonging to Soft Rot *Pectobacteriaceae* for several decades (Reverchon and Nasser, 2013; Reverchon et al., 2016). While this strain continues to be the most studied strain of all *Dickeya* species its production of tailocins has not been previously described. Here, we characterize for the first time the tailocin produced by *D. dadantii* strain 3937.

Results

Dickeya dadantii 3937 produces tailocins

Cells of *D. dadantii* 3937 treated with mitomycin C produced syringe-like macromolecular structures resembling bacteriophage tails. Following convention, the tailocins produced by *D. dadantii* were named dickeyocins. Imaging using TEM and AFM revealed that these structures consist of a central rod-shaped core (tube) wrapped in a contractable sheath (Figure 1). Both the tube and the sheath were built of multiple protein subunits, with a clearly visible helical arrangement of the subunits in the sheath. The average length of the dickeyocins produced by strain 3937 was 166 ± 7 nm. When the sheath entirely covered the tube (in the extended, "loaded" form), the individual dickeyocin has a diameter of 23 ± 2 nm. Fibers were visible at the distal end of the sheath. When the sheath contracts, it revealed an internal tube of a length of 92 ± 7 nm with an attached spike at the distal end (Figure 1).

The yield of tailocins purified from mitomycin-induced cells of *D. dadantii* 3937 equaled approx. 10^{11} particles mL^{-1} of culture. The particles could also be isolated from non-treated cells, indicating a low basal production level. However, induction with mitomycin C increased the yield approx. 10–100-fold. We employed three different methods to estimate the concentration of phage-tail-like particles in the tested preparations. The results were consistent for the independently obtained batches of purified dickeyocins (Supplementary Table S2). The average concentration from three independently obtained samples was 10^6 relative units (AU) mL^{-1}, 10^{11} killing particles mL^{-1}, and 10^{11} particles mL^{-1}, according to the spot test, the

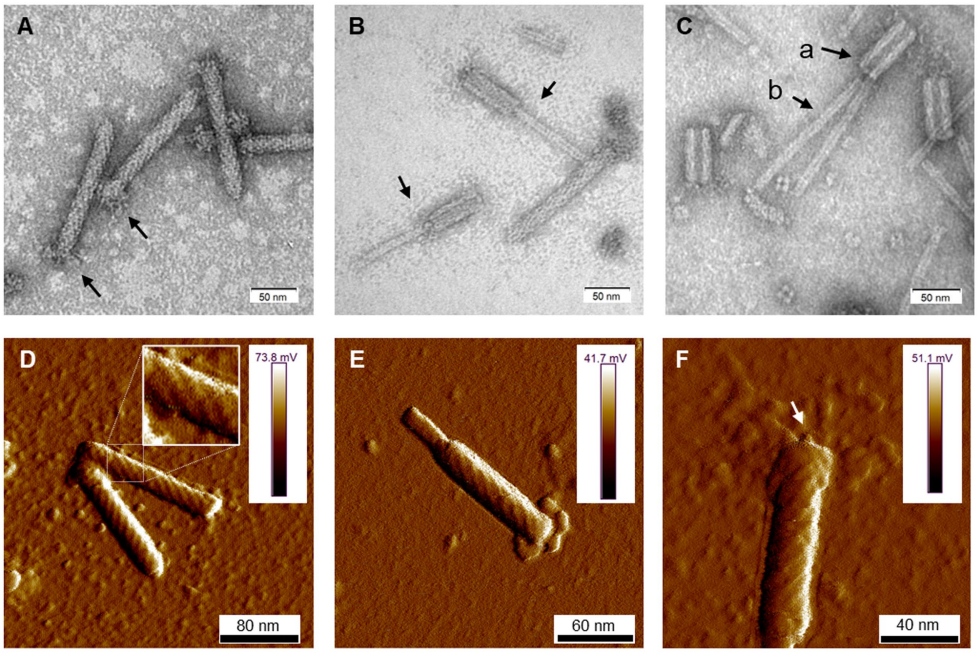

FIGURE 1
The morphology of tailocins from *Dickeya dadantii* 3937. Images were obtained using TEM **(A–C)** and AFM **(D–F)**. The individual panels show: **(A)** particles in an extended (active) form. Arrows indicate the positioning of fibers; **(B)** contracted particles indicated by arrows; **(C)** tailocins disintegrated by heat treatment (50°C); Arrows indicate: **(a)** empty sheath with a hollow inner channel and **(b)** tube (core) separated from the sheath; **(D)** two extended particles. A fragment of the photo was magnified to display the helical arrangement of protein subunits in the sheath; **(E)** a contracted molecule in an AFM image; and **(F)** an extended particle with an arrow pointing at the presumed tube-attached spike.

Poisson distribution killing method, and the NanoSight measurements, respectively. Furthermore, comparing the results from the activity-based Poisson method and the direct particle count indicated that most phage-like particles purified from the cultures of *D. dadantii* strain 3937 were undamaged and in the extended ("loaded") form. This was in line with the microscopic observations done with TEM and AFM.

Dickeyocins from *Dickeya dadantii* strain 3937 are phylogenetically related to the tail of *Peduovirus* P2

Proteins in the dickeyocins were separated by SDS-PAGE and sequenced. Eight cleary distinguishable bands were excised from the gel, and the digested peptides were analyzed by MS. The peptides could be readily mapped to six *D. dadantii* proteins with annotations implying their phage relationship: phage baseplate assembly protein (encoded in locus Dda3937_00029/DDA3937_RS12055), baseplate assembly protein J (Dda3937_00030/DDA3937_RS12060), tail fiber protein (Dda3937_04606/DDA3937_RS12070), putative side tail fiber protein (Dda3937_03808/DDA3937_RS12100), major sheath protein (Dda3937_03810/DDA3937_RS12110), and major tail tube protein (Dda3937_03811/DDA3937_RS12115; Figure 2). Genes encoding these six proteins were mapped to a single *ca.* 22-kb region in the genome of *D. dadantii* strain 3937 (GenBank accession number: NC_014500.1: genome location: 2,734,508–2,757,061; Figure 2C). This genomic region contained 28 genes, from which 16 genes encoded various bacteriophage structural proteins.

The nucleotide sequence of the 22-kb putative dickeyocin-encoding fragment in *D. dadantii* strain 3937 showed the highest similarity to a prophage region in *D. dadantii* strain XJ12 [100% query coverage (qc), 99.35% identity]. Highly similar regions were also found in the genomes of several other strains of *D. dadantii*, as well as *D. solani*, *D. dianthicola*, and *D. fangzhongdai* (Supplementary Data S1). Strains of *D. zeae* showed lower similarity, with query coverage between 54 and 76% and identity of 83–84%. A much lower score was observed for the next best hit—*Musicola paradisiaca* (formerly *Dickeya paradisiaca*). Other non-*Dickeya* microorganisms with regions showing some degree of homology included *Serratia* sp. ATCC 39006 (Supplementary Data S1; with 10% query coverage and 81.45% identity).

Importantly, at the nucleotide level, the dickeyocin region of *D. dadantii* strain 3937 showed no significant similarity to the known carotovorocin Er cluster of *P. carotovorum* Er (Genbank accession: AB045036; Yamada et al., 2006). Moreover, the amino acid sequence of the sheath protein of tailocin from strain 3937 showed only a 34% identity to that of carotovorocin Er, with a query coverage of 83%.

The *ca.* 22-kb cluster encoding dickeyocin from *D. dadantii* strain 3937 was also surveyed against the collection of viral sequences (NCBI taxid: 10239), yielding only low similarity scores (7% query coverage, 78% identity for the best hit).

Furthermore, in an attempt to find undomesticated phages related to dickeyocin we searched the viral protein database, using three structural proteins of dickeyocin as queries: sheath protein (WP_013318223), tail tube protein (WP_013318224), and baseplate assembly protein J (WP_013318212). Based on this search, proteins in dickeyocin exhibited homology to proteins of *Salmonella* phages

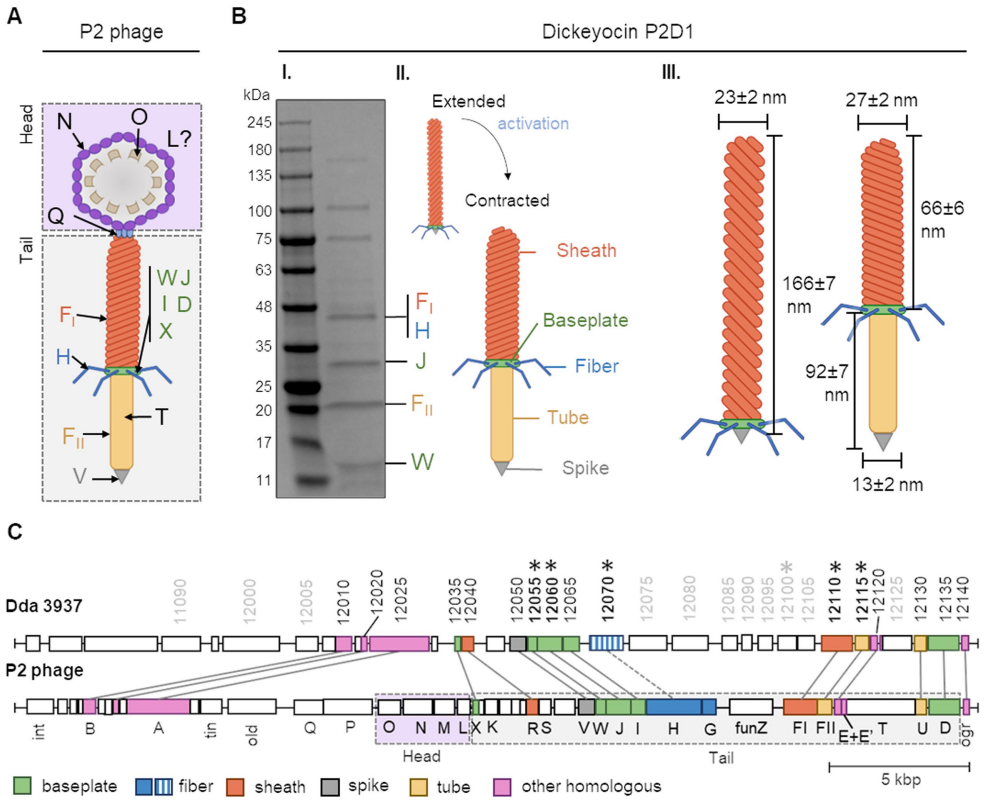

FIGURE 2
The building blocks of tailocins of *Dickeya dadantii* strain 3937 and their encoding genes in relation to those of the *Peudovirus* P2. Panel **(A)** shows a schematic representation of the structure of the P2 phage, together with the nomenclature of the building proteins. The graph was prepared based on Christie and Calendar (2016) (PMID: 27144088, https://pubmed.ncbi.nlm.nih.gov/27144088/). WJIDX—baseplate proteins, F_I—sheath, H—fiber, F_{II}—tube, V—spike, T—tape measure protein, Q—portal protein, N—major capsid protein, O—capsid scaffold, and L—head completion protein. Panel **(B)** shows: **(I)** an SDS-PAGE separation of proteins from mitomycin-induced cultures of *D. dadantii* 3937. Bands containing proteins homologous to those of the P2 phage are provided with the respective protein designations; **(II)** schematic representation of extended and contracted forms of dickeyocin P2D1; and **(III)** dimensions of extended and contracted forms of dickeyocin P2D1. Panel **(C)** shows the alignment between the complete genome sequence of the P2 phage (NC_001895; 33,593 bp) and a region of the same length in the genome of *D. dadantii* 3937 (NC_014500.1; range: 2,723,487–2,757,061). The numbering of genes in *D. dadantii* corresponds to the numbering of loci in the genome (locus tag prefix DDA3937_RS). Homologous proteins are marked with the same color.

SW9 and PSP3, *Erwinia* phage Etg, *Enterobacteria* phage fiAA91-ss, *Peduovirus* P2, several *Escherichia* and *Yersinia* phages, as well as to multiple poorly-characterized phages of bacteria in class *Caudoviricetes*, derived from the human metagenome (Supplementary Data S1). The best-characterized phage having a high homology to dickeyocin was *Peduovirus* P2—a phage that infects *Escherichia coli* and other hosts, including *Salmonella* and *Klebsiella* (Bertani, 1951; Christie and Calendar, 2016). For the three investigated dickeyocin proteins, their amino acid identity toward their P2 homologs ranged from 70 to 79%, with 100% query coverage (Supplementary Data S2). Therefore, we used the *Peduovirus* P2 bacteriophage as a reference to assign functions to proteins in dickeyocin, as well as to investigate the genetic rearrangements in the dickeyocin cluster in relation to the fully-functional phage P2 (Figure 2C). The dickeyocin cluster in the genome of *D. dadantii* strain 3937 lacked sequences associated with the phage head (proteins O, M, N, L), as well as the tape measure protein. There was also a difference in the genetic content of the intergenic region of the tail, as well as low homology of proteins building the tail fibers (31% query coverage, 54% identity). Following the present naming convention, we named the newly characterized tailocins from *D. dadantii* 3937 dickeyocin P2D1 (P2-like Dickeyocin 1).

Dickeyocin P2D1 expresses bactericidal activity exclusively against members of soft rot *Pectobacteriaceae*

Fifty-two bacterial strains were surveyed for their sensitivity to tailocins induced from *D. dadantii* strain 3937. These included 41 strains of different species and subspecies of *Dickeya* and *Pectobacterium*, as well as six other bacterial strains belonging to the *Enterobacteriaceae* family, a single strain of *Serratia marcescens* (family *Yersiniaceae*), three *Pseudomonas* spp., and a single strain of *Staphylococcus aureus* representing Gram-positive bacteria (Supplementary Table S1). Bactericidal activity was observed against eight strains [*D. dadantii* subsp. *dieffenbachie* strain NCPPB 2976, *D. dianthicola* strains NCPPB 3534 and IPO 980, *D. undicola* CFBP 8650, *D. zeae* strains NCPPB 3532 and 3531, *D. oryzae* strain CSL RW192, and *Musicola paradisiaca* strain NCPPB 2511 (old name:

Dickeya paradisiaca strain NCPPB 2511)], but not against any of the *Pectobacterium* spp. tested (Supplementary Table S1; Figure 3). Likewise, dickeyocin P2D1 was inactive against any of the non-SRP strains included in the screening assay: six *Enterobacteriaceae* strains (*Citrobacter freundii* ATCC 8090, *Escherichia coli* ATCC 8739, *Escherichia coli* ATCC 25922, *Escherichia coli* OP50, *Klebsiella quasipneumoniae* ATCC 700603, and *Klebsiella aerogenes* ATCC 51697), three *Pseudomonas* spp.: (*Pseudomonas aeruginosa* PA14, *Pseudomonas aeruginosa* PAO1, and *Pseudomonas donghuensis* P482), *Serratia marcescens* ATCC 14756 and *S. aureus* ATCC 25923 indicating their limited range of bactericidal activity (Figure 3).

P2D1 killing efficiency is bacterial species-dependent

We determined the kinetics of killing of eight susceptible strains treated with P2D1. The share of intact cells at two time points: 20 and 120 min post treatment is shown in Supplementary Figure S1. In all the cases, the killing of the susceptible cells was fast; in the first 20 min, the most killing effect was observed for *D. dianthicola* strain IPO 980 (*ca.* 60% reduction of cell numbers). In contrast, the slowest killing caused by dickeyocin P2D1 was observed for *D. dianthicola* strain NCPP 3534 (*ca.* 22% reduction of cell numbers). For the other six strains tested, on average, a 45–60% reduction in cell numbers was observed after this same time (20 min.). About 50–60% killing of all strains by dickeyocin P2D1 was seen after 120 min-incubation (Supplementary Figure S1).

P2D1 dickeyocin directly punctures the cell envelope of susceptible bacterial strains

We assessed the interaction of dickeyocin P2D1 on cells of the susceptible *M. paradisiaca* strain at the single-cell level using transmission electron microscopy (TEM). Images clearly showed that

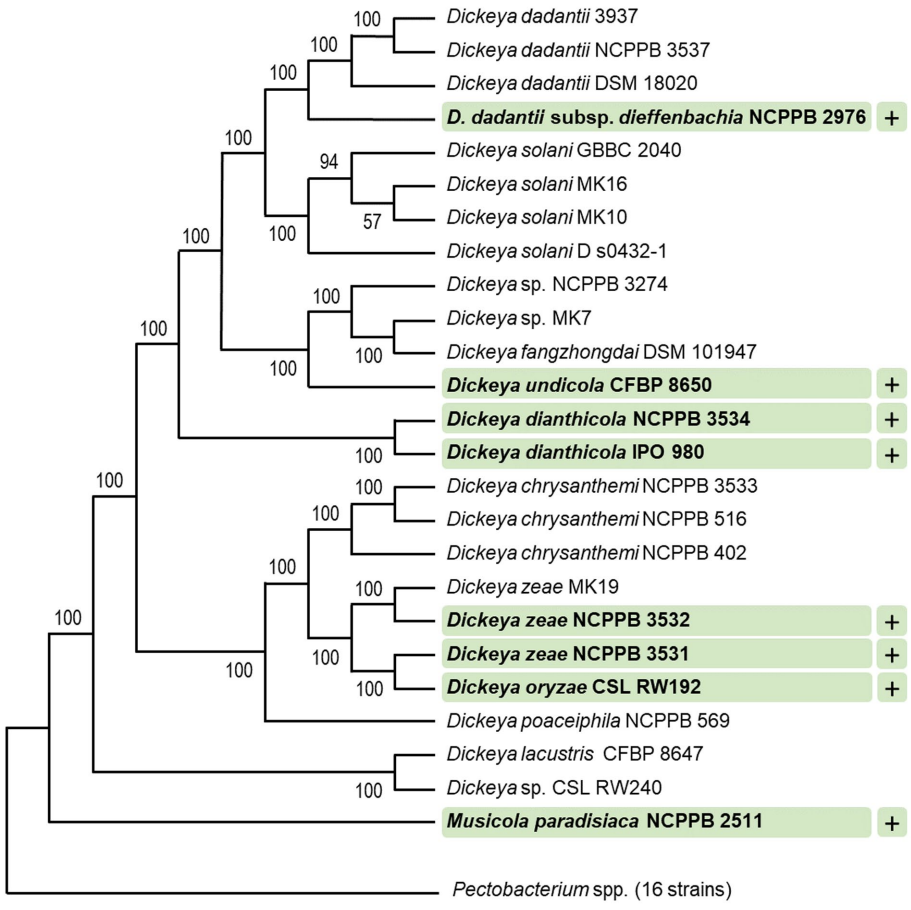

FIGURE 3
Target range of tailocins from *Dickeya dadantii* 3937. Strains susceptible to P2D1 dickeyocin were marked with a plus (+). A phylogenetic tree for 41 SRP strains was obtained using EDGAR 3.2 Fasttree 2.1 algorithm. The tree was built out of a core of 1,616 genes per genome (nucleotide sequences), 66,256 genes in total. The core had 1,560,951 bp per genome, 63,998,991 in total. The lengths of the branches do not reflect the phylogenetic distance. All analyzed *Pectobacterium* spp. were collapsed. This included 16 strains: *Pectobacterium cacticida* CFBP 3628, *Pectobacterium fontis* CFBP 8629, *Pectobacterium betavasculorum* CFBP 2122, *Pectobacterium peruviense* CFBP 5834, *Pectobacterium atrosepticum* SCRI1043, *Pectobacterium atrosepticum* NCPPB 549, *Pectobacterium parmentieri* CFBP 8475, *Pectobacterium parmentieri* SCC3193, *Pectobacterium polonicum* DPMP 315, *Pectobacterium punjabense* CFBP 8604, *Pectobacterium actinidiae* LMG 26003, *Pectobacterium brasiliense* LMG21371, *Pectobacterium polaris* NCPPB 4611, *Pectobacterium versatile* CFBP 6051, *Pectobacterium carotovorum* CFBP 2046, and *Pectobacterium aroidearum* NCPPB 929. The numbers at the tree branches represent Shimodaira-Hasegawa (SH) branch support values (Shimodaira, 2002).

dickeyocin P2D1 adsorbed to the bacterial cell envelope (Figures 4A,B), followed by puncturing the outer cell membrane (resulting from the conformational change of dickeyocin P2D1 from an extended "loaded" to a contracted form; Figures 4C,D), creating a pore connecting the cytoplasm of the cell with the external environment and leading eventually to the death of the attacked cell.

Dickeyocin P2D1 is able to bind to nonviable (dead) bacterial cells

A cell adsorption assay was employed to investigate whether the dickeyocin P2D1 can adsorb to nonviable (dead) and viable bacterial cells of the susceptible or resistant bacterial species. Dickeyocin P2D1 was incubated either with viable or chloramphenicol-killed cells of susceptible *M. paradisiaca* or with viable or antibiotic-killed cells of resistant *D. dadantii* for 40 min and the remaining dickeyocin P2D1 in the medium was measured. Incubation of dickeyocin P2D1 both with the dead and viable cells of *M. paradisiaca* resulted in the total loss of the tailocin activity, indicating that it bound equally efficiently to viable as well as nonviable cells of the susceptible bacterium. No adsorption of dickeyocin P2D1 to either dead or alive cells of the resistant *D. dadantii* cells was observed (Supplementary Figure S2).

Production of dickeyocin P2D1 is not associated with T6SS

To determine whether dickeyocin P2D1 production in *D. dadantii* depends on the type VI secretion system (T6SS), dickeyocin P2D1 production was induced in *D. dadantii* mutant A5587 (Golanowska, 2015) that carries an insertional mutation in the *tssK* gene (type VI secretion system baseplate subunit TssK)—an essential subunit of the type VI secretion apparatus (Nguyen et al., 2017). The tailocins obtained from the *D. dadantii* T6SS mutant using standard mitomycin induction methods were morphologically indistinguishable and similarly abundant compared to dickeyocin P2D1 induced in the wild-type *D. dadantii* strain 3937 (Supplementary Figure S3). These results suggest that at least *tssK* gene, essential for the proper function of T6SS, does not affect dickeyocin P2D1 production, morphology, or release from the cell.

Activity of P2D1 dickeyocins is modulated by environmental conditions and enzyme treatments

Dickeyocin P2D1 was stable at temperatures between 4 and 42°C, showing no significant loss in activity following 24 h incubation at these temperatures. Temperatures above 50°C, however, led to a 32-fold loss in activity while incubation at 65 and 80°C (Figure 5A) led to a complete loss of activity. Likewise, a single freeze–thaw cycle negatively affected the stability of dickeyocin P2D1. Freezing at −20°C resulted in a 128-fold reduction in activity, while no bactericidal effect remained after freezing at −80°C (Figure 5A). We tested the stability of P2D1 under seven different pH conditions (2, 3.5, 5, 7, 9, 10.5, and 12). The particles remained active after 24 h incubation in pHs ranging from 3.5 to 12. However, their bactericidal properties were lost at pH 2 (Figure 5B). To determine whether dickeyocin P2D1 that was inactivated at low pH could be restored to an active (extended, "loaded") form, we diluted the pH 2-treated, inactive dickeyocin P2D1 in PBS buffered to pH 12 to achieve a neutral pH environment. Dickeyocin P2D1 did not regain bactericidal activity at pH 7. Osmotic

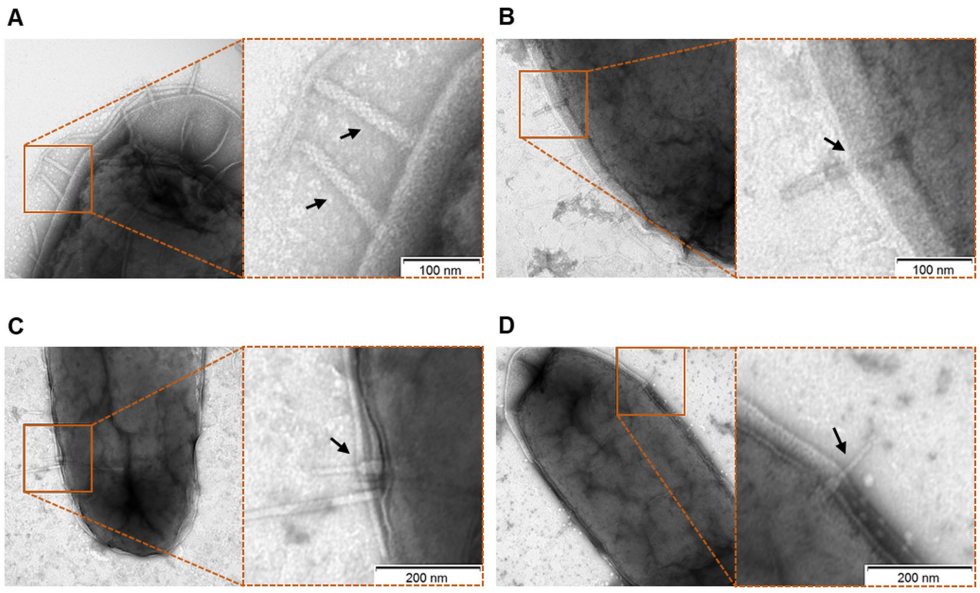

FIGURE 4
Interaction of P2D1 dickeyocins with the cells of a susceptible strain *Musicola paradisiaca* NCPPB strain 2511, evaluated using transmission electron microscopy (TEM). Bacterial cells of *M. paradisiaca* NCPPB 2511 from overnight culture in TSB were harvested and washed with PBS. Such prepared cells were incubated with PEG-purified dickeyocins (approximate concentration in bacterial suspension 10^6 particles mL^{-1}) for 20 min, followed by obtaining images with TEM. For all panels, the TEM images on the right are the enlarged sections of the original micrographs on the left. Arrows indicate P2D1 attached to the surface of bacterial cells, either in extended **(A,B)** or contracted **(C,D)** form.

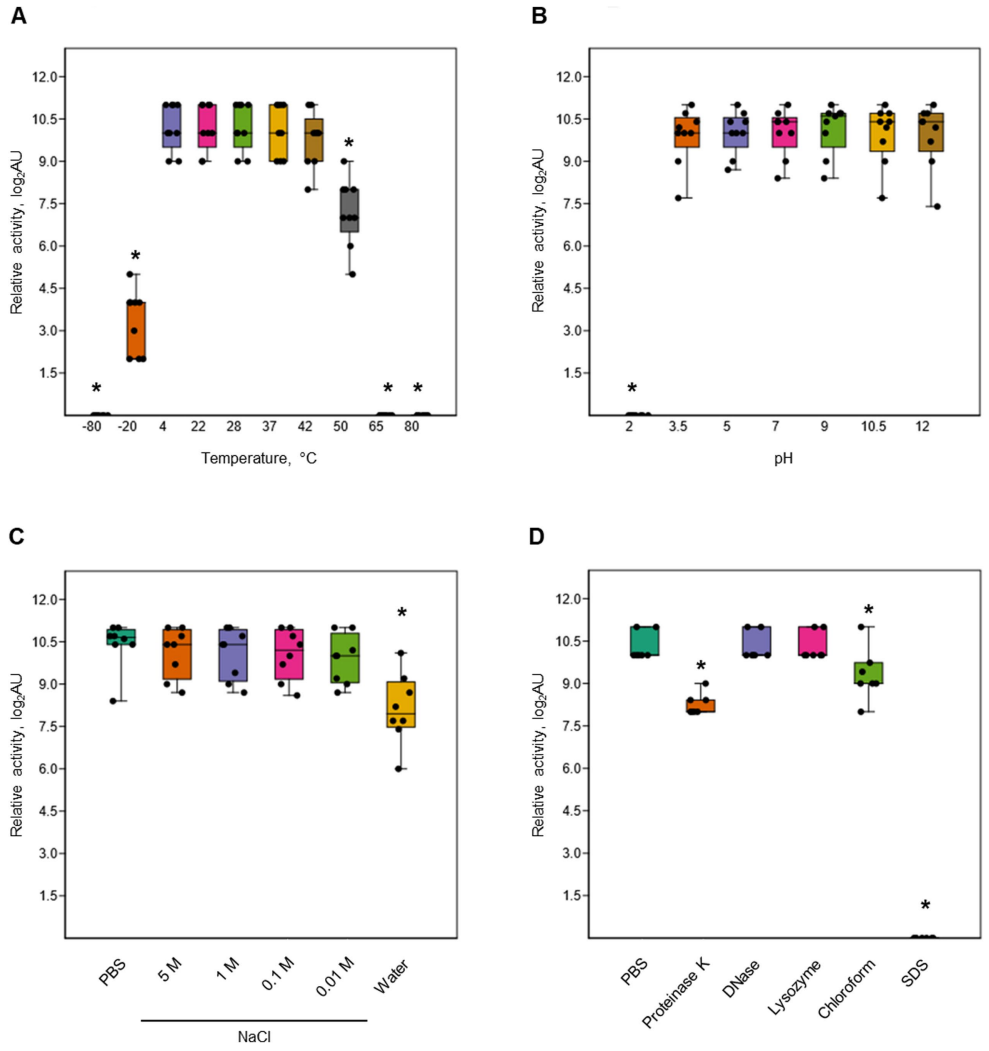

FIGURE 5
Stability of P2D1 dickeyocins from *Dickeya dadantii* strain 3937 upon different treatments. The graphs show the influence of temperature **(A)**, pH **(B)**, salinity **(C)**, as well as enzymatic digestion (proteinase K, DNase, and lysozyme), chloroform treatment, and SDS detergent **(D)** on bactericidal activity of P2D1 against *Musicola paradisiaca* NCPPB 2511. For temperature, pH/osmolarity, and enzyme/detergent/organic solvent treatments, dickeyocins stored in PBS pH 7, were used as a control. The results are shown as a box plot; whiskers reflect the maximum and minimum, box sides reflect the first and third quartile, and the bars reflect medians. Points indicate particular measurements ($n = 9$). The asterisks (*) represent statistically significant differences ($p < 0.05$) between the treatment and the control using the Mann–Whitney test.

conditions generated by NaCl added to water at concentrations between 0.01 and 5 M had no adverse effect on the activity of dickeyocin P2D1 within 24 h when compared to controls (dickeyocin P2D1 in PBS containing 0.137 M NaCl and 0.0027 mM KCl). In contrast, incubation of dickeyocin P2D1 in deionized water led to a 4-fold loss in activity (Figure 5C). Dickeyocin P2D1 activity was significantly ($p < 0.05$) reduced by treatment with proteinase K and chloroform for 1 h (4-fold and 2-fold loss of activity, respectively). Complete loss of activity was seen after incubation in 1% SDS. In contrast, neither lysozyme nor DNase influenced dickeyocin P2D1 activity (Figure 5D).

Dickeyocin P2D1 is nontoxic for *Caenorhabditis elegans*

No inhibition of the survival of *C. elegans* was seen after its exposure to high concentrations of purified dickeyocin P2D1 (Supplementary Figure S4). The average survival rate of *C. elegans* cultivated in the presence of P2D1 dickeyocins was *ca.* 98–99% and was not significantly statistically different from that of nematodes grown without dickeyocin P2D1. The survival of *C. elegans* was not dickeyocin P2D1-concentration-dependent, as similar survival rates were recorded for all dickeyocin concentrations tested (Supplementary Figure S4). Furthermore, dickeyocin P2D1 did not exhibit bactericidal activity against *E. coli* OP50—the food source for *C. elegans*.

Discussion

Our understanding of the mechanisms underlying bacterial competitive behaviors remains limited. Although numerous bacterial species are known to produce and exploit tailocins for their competitive advantage, little is known of how commonly such

entities are employed by plant-pathogenic bacteria, including pectinolytic, necrotrophic SRP pathogens, to enable their environmental fitness (Scholl, 2017; Patz et al., 2019). This study revealed the presence of tailocins in one of the broadest characterized and economically important member of the Soft Rot *Pectobacteriaceae* family—strain *D. dadantii* 3937. We identified and characterized in detail a novel phage tail-like particle—dickeyocin P2D1, produced by this strain not only upon mitomycin C treatment but also constitutively in culture. Although tailocins were initially noted in a limited number of *Dickeya* spp. (strains of *Erwinia chrysanthemi* dissimilar from strain 3937) isolated from several crop and ornamental plants in the past (1960 and 1970s; Echandi, 1979), these particles were not characterized in detail, probably due to the lack of appropriate molecular techniques at that time.

Dickeyocin P2D1 has a typical morphology and expresses features similar to those of other R-type tailocins described so far for a large group of bacteria, including *Escherichia coli* (Mennigmann, 1965), *Burkholderia cenocepacia* (Yao et al., 2017), *Pseudomonas aeruginosa* (Scholl, 2017), *Proteus vulgaris* (Coetzee et al., 1968), and *Yersinia enterocolitica* (Strauch et al., 2001). Likewise, tailocins were also identified in *Pectobacterium* spp. (Kamimiya et al., 1977; Choi and Kim, 1988; Yamada et al., 2006)—plant pathogens closely related to *Dickeya* spp. The tailocin of SRP bacteria best characterized to date is carotovorocin Er isolated from *P. carotovorum* Er (Kamimiya et al., 1977; Nguyen et al., 2002). Interestingly, as shown in this study, despite the morphological similarities of dickeyocin P2D1 and carotovorocin Er and the rather close phylogenetic relationship and the lifestyle shared by the producer strains, these tailocins show little sequence homology. This suggests that dickeyocin P2D1 and carotovorocin Er originated from different phage ancestors and that the ability to produce tailocins was acquired several times and independently by various members of the SRP family.

The cluster encoding dickeyocin P2D1 exhibits high homology with that encoding the tail of phage *Peduovirus* P2, indicating that these two probably had a common ancestor. Phage P2 is a temperate bacteriophage commonly found in genomes of strains belonging to the *Pseudomonadota* phylum (Christie and Calendar, 2016). Its presence has been noted in at least 127 genera in 32 *Pseudomonadota* families (Casjens and Grose, 2016), indicating its extreme ubiquitousness in the bacterial world. Accordingly, R-type tailocins resembling the tail of phage P2 have been extensively studied and are now the best characterized to date (Scholl, 2017; Granato et al., 2019). To explore the occurrence of R-type tailocins in SRP, we searched available *Dickeya* spp. and *Pectobacterium* spp. genomes for regions carrying phage tail-like genes homologous to those encoding dickeyocin P2D1 and having organizational similarity. Our analysis revealed the presence of P2D1-like clusters in several *Dickeya* spp. strains, including *D. solani*, *D. dianthicola*, *D. zeae*, and *D. fangzhongdai*. The P2D1-like clusters were, however, absent in all *Pectobacterium* spp. genomes as well as in genomes of the other bacterial species unrelated to SRP analyzed in our study. The lack of the dickeyocin P2D1 cluster both in *Pectobacterium* spp. and in bacteria phylogenetically distant to SRP may indicate a strong and sustained phylogenetic association between dickeyocin P2D1and *Dickeya* spp. This is somewhat unexpected given that various *Dickeya* and *Pectobacterium* are often present in the same environment (e.g., soil, water, and plant surface; Van Gijsegem et al., 2021). Under such conditions, horizontal gene transfer would frequently occur between these phylogenetically related SRP species (Toth et al., 2021).

The restricted occurrence of genes encoding dickeyocin P2D1 in the genomes of *Dickeya* spp. aligns with its narrow bactericidal activity. In our study, dickeyocin P2D1 exclusively targeted *Dickeya* species as well as *Musicola paradisiaca* (former *Dickeya paradisiaca*) but not any other bacteria tested. It is noteworthy, however, that these *Dickeya* strains differed somewhat in the susceptibility to dickeyocin P2D1 while these differences were unrelated to the phylogenetical distance between them. This is in line with other studies (Chopra et al., 2015; Fagundes et al., 2016; Principe et al., 2018) that showed that the host range of pyocins, tailocins produced by *Pseudomonas* spp., is usually restricted to kin strains (Patz et al., 2019). Likewise the tailocins of *Escherichia coli* (Tantoso et al., 2022) and *Yersinia enterocolitica* (Strauch et al., 2001) also killed only related taxa. Contrarily, some recent reports have revealed tailocins that target different species of the same genus and/or even different genera. For example, *Burkholderia cenocepacia* tailocins were active against other *Burkholderia* species (Yao et al., 2017) and those of *P. fluorescens* were active against *Xanthomonas vesicatoria* (Principe et al., 2018). The quite narrow target range of dickeyocin P2D1 is somewhat surprising given that multiple species of SRP bacteria are often found together in the same infected plant (Perombelon, 1988; Pérombelon, 1992; Ge et al., 2021). In such a setting, these various species would be expected to experience intense competition and would be expected to benefit from a promiscuous tailocin (Shyntum et al., 2019). It thus appears that in such mixed infections, *Dickeya* spp. and *Pectobacterium* spp. compete using mechanisms unrelated to phage-tail-like particles, as reported previously (Ma et al., 2007; Czajkowski et al., 2013), but this conjecture requires more experimental support. Similarly, the presumed bacterial receptor for P2D1 remains unidentified. A number of tailocins that engage with *Pseudomonas* spp. bacteria rely on lipopolysaccharide (LPS) components as their receptors (Scholl, 2017). It is plausible to consider that P2D1 may also engage with the bacterial LPS of susceptible hosts, but further research is required to investigate this interaction on a molecular level.

Our study revealed that dickeyocin P2D1 is produced even without induction with mitomycin C, although such induction boosts the tailocin production 10 to 100-fold. To precisely estimate the concentration of P2D1 particles, we used a well-established Poisson distribution killing method (Kageyama et al., 1964; Williams et al., 2008) as well as a new approach we developed. The Poisson distribution killing method is an indirect enumeration method as it employs the number of survivors in tailocin-treated bacterial suspensions. Advantage of indirect methods is that they provide the number of active ("loaded") tailocin particles in a sample. In this study, we have complemented the indirect counting approach by direct enumeration of tailocin particles with NanoSight NS300. Direct particle counts avoid the need for culturing and, when combined with killing-based methods, enables an estimation of the fraction of active tailocins in preparation. This appears to be a novel application of NanoSight to evaluate the quality and the active fraction of tailocin preparations.

One of the immediate applications of dickeyocin P2D1 would be in controlling SRP infections in crops (Becker et al., 2022). A major practical limitation of tailocins as therapeutic agents is their narrow bactericidal range. This can, however, be at least partially overcome by using cocktails of tailocins having different bactericidal ranges,

similarly as in the use of bacteriophages (Abedon et al., 2021). Despite this limitation, tailocins have shown to be effective antibacterial agents in various applications (Scholl and Martin, 2008; Behrens et al., 2017). They have several benefits compared to other biological control agents evaluated to date (Becker et al., 2022). One of the biggest advantages of tailocins is their incapacity to proliferate on-site after application. Likewise, tailocins themselves cannot spread via transduction or transformation mechanisms because only the protein products and not the encoding nucleic acids are employed. The high target selectivity of tailocins also prevents disruption of other, often beneficial bacteria present in the same niche. Likewise, since dickeyocin P2D1 was nontoxic to *C. elegans*, a model eukaryotic organism, such tailocins are unlikely to impact other eukaryotic organisms present in soil and/or on plants (Balciunas et al., 2013). Additional studies are needed to fully explore the potential of dickeyocin P2D1 to achieve plant disease control, such as targeting production, the long-term effectiveness, and consistency of control under field conditions, including stability, formulation, and eco-toxicological risks. Studies of the *in planta* expression of dickeyocin P2D1 should provide great insight into the interactions of *Dickeya* species with each other and with other bacteria under natural and agricultural conditions.

Materials and methods

Bacterial strains and culture conditions

All bacterial strains included in this study are listed in Supplementary Table S1. Bacteria were routinely propagated in liquid Trypticase Soy Broth (TSB, Oxoid) or on solid Trypticase Soy Agar (TSA, Oxoid) at 28°C for 24 h. Liquid cultures were agitated during incubation (120 rpm). When required, bacterial cultures were supplemented with kanamycin (Sigma-Aldrich) to a final concentration of 50 μg mL^{-1}.

Induction, purification, and concentration of tailocins from *Dickeya dadantii* 3937 culture

Dickeya dadantii strain 3937 was grown overnight (*ca.* 16 h) in TSB at 28°C with shaking (120 rpm). The cultures were then rejuvenated by diluting them 1: 40 in 250 mL of fresh TSB medium. The diluted culture grew for 2.5 h under the same conditions. Such prepared 3937 cultures were then supplemented with mitomycin C (Abcam, Poland) to a final concentration of 0.1 μg mL^{-1} to induce the production of tailocins. Following mitomycin C treatment, the cultures were incubated for another 24 h at 28°C with shaking (120 rpm). Bacterial cells were then removed by centrifugation (10 min, 8,000 RCF), and the supernatant containing putative particles was collected and filtered through a sterile 0.2 μm PES (polyether sulfone) membrane filter using the Nalgene Rapid-Flow Sterile Disposable Filter Units (Thermo Fisher Scientific). Finally, to precipitate tailocins, PEG-8000 (Promega) was added to the filtrate to a final concentration of 10%, and the sample was incubated at 4°C on a magnetic stirrer for the next 16–24 h. The tailocins were collected by centrifugation (1 h, 16,000 RCF, 4°C) and resuspended in 5 mL of Phosphate Buffered Saline (PBS, pH 7.2, Sigma-Aldrich). The resulting pellet was resuspended in 1/50 of the initial volume of the initial sample. The purified particles were stored at 4°C for future use.

Initial qualitative screen of tailocins for the bactericidal activity

The activity of the purified and concentrated particles was initially tested qualitatively on a limited panel of bacterial strains (=17 strains, Supplementary Table S1) using a spot test assay as described before (Hockett and Baltrus, 2017; Yao et al., 2017).

Microscopic imaging

Tailocins were imaged using both transmission electron microscopy (TEM) and atomic force microscopy (AFM), as described earlier (Vacheron et al., 2021). TEM analyses were done at the Laboratory of Electron Microscopy (Faculty of Biology, University of Gdansk, Poland). For TEM analysis, particles obtained as described above were adsorbed onto carbon-coated grids (GF Microsystems), stained with 1.5% uranyl acetate (Sigma-Aldrich), and directly visualized with an electron microscope (Tecnai Spirit BioTWIN, FEI) using a previously described protocol (Bartnik et al., 2022). At least 10 images were taken for each preparation to estimate the diameters of the particles. For the AFM analysis, purified and PEG-concentrated particles were used directly without further preparations. AFM imaging was conducted in air mode using the Bioscope Resolve microscope (Bruker), in ScanAsyst (Peak Force Tapping) mode, employing the SCANASYST-AIR probes (f0 7.0 kHz, diameter < 12 nm, k: 0.4 N/m) as described earlier (Sokolova et al., 2023). Similarly, as described for TEM analysis, for AFM, at least 10 images were taken for each preparation to estimate the diameters of the particles.

Determination of the concentration of tailocins

To estimate the concentration of tailocins, three independent methods were applied.

Direct particle count with NanoSight NS300

NanoSight NS300 instrument (Malvern Panalytical), equipped with an sCMOS camera and a Blue488 laser, was used to directly assess the concentration and size distribution of particles obtained after induction and purification, as described above. The tailocin samples were diluted 1,000 times in sterile PBS buffer pH 7.2 (Sigma-Aldrich) to achieve the optimal concentration for observation. The camera gain was set to 14, the number of captures per sample equaled 5, each lasting 60 s, and the detection threshold was set to 5 as suggested by the manufacturer. Measurements were conducted at room temperature (*ca.* 22–23°C). Three biological replicates were used to determine the concentration and size distribution of the obtained tailocins, and the results were averaged for further analysis.

Semiquantitative estimation by a spot test

Samples interrogated for tailocins were serially 2-fold diluted in PBS pH 7.2 (Sigma-Aldrich; Yao et al., 2017). Two μL of each dilution

were spotted onto TSA plates overlayed with 15 mL of soft top agar [Nutrient Broth (NB, Oxoid) with 7 g L^{-1} agar]. Before pouring, the soft top agar was cooled to 45°C and inoculated with 250 µL of an overnight culture of a tailocin indicator strain (susceptible strain *M. paradisiaca*). Plates were incubated overnight at 28°C. The highest dilutions of particles capable of cell lysis, visible as plaques (halos) in the bacterial lawn in soft top agar, were determined. Each tailocin dilution was tested in triplicates and the entire experiment was repeated two times with the same setup. The reciprocal of the highest dilution causing a visible plaque was defined as the value of the relative activity in arbitrary units (=1 AU).

Poisson distribution killing method

Tailocins were also quantified using the Poisson distribution killing method based on the protocol described by Yao et al. (2017) and initially introduced by Kageyama et al. (1964) and Williams et al. (2008). This method is based on the number of bactericidal events, determined from the number of bacterial survivors in a population with a known number of initial viable cells (Yao et al., 2017). To determine this, 10 µL of undiluted and 10-fold diluted samples of tailocins were added to 100 µL of an overnight TSB (Oxoid) culture of a susceptible strain *Musicola paradisiaca* NCPPB 2511 (10^8 CFU mL^{-1}) and incubated for 40 min at 28°C with shaking (120 rpm). As a negative control, PBS pH 7.2 was used instead of the tailocins suspension. Each combination was tested in triplicates. After incubation, the suspensions were serially diluted up to 10^{-7} in PBS and plated in triplicate on TSA plates. The colonies that emerged following overnight incubation at 28°C were enumerated to calculate the bacterial survival ratio (S) in the treated samples compared to the negative control. S was calculated as the number of viable bacteria in a sample incubated with tailocins divided by the number of viable bacteria in the negative control. The number of lethal events per bacterial cell (m) was calculated as $m = -\ln(S)$. The total number of active killing particles per milliliter (based on the assumption that tailocins adsorption to bacterial cells in each sample was quantitative within the first 40 min incubation period) was calculated by multiplying m by the initial number of bacterial cells per milliliter (CFU mL^{-1}).

Target range of the tailocins isolated from *Dickeya dadantii* 3937

Overnight cultures of the investigated strains were prepared in 1 mL aliquots of TSB in 2 mL microcentrifuge tubes (Eppendorf) which were incubated horizontally with shaking (120 rpm) at 28°C for 16–24 h. The overnight cultures were used as an inoculum in a spot test carried out on 48-well plates (Greiner). Briefly, 10 µL of the inoculum was transferred to each well of the plate and mixed with 500 µL of liquified soft top agar [Nutrient Broth, NB, (Oxoid) with 7 g L^{-1} agar], precooled to 45°C in a water bath. Plates were gently stirred (20 rpm) to ensure an even distribution of bacterial cells in the inoculated wells. After the agar had solidified, plates were left to dry for 10 min. in a laminar flow hood. 2 µL of 10-fold diluted tailocins (approximately 10^{10} particles mL^{-1}) purified from mitomycin-induced cultures of *D. dadantii* 3937 were spotted on the surface of the inoculated soft-top agar in the wells of the multitier plate. Inoculated plates were incubated for 24 h at 28°C and then inspected for the presence of a growth inhibition. A spot of lack of growth was interpreted as the susceptibility of the given strain to the tailocins (positive reaction). 2 µL of sterile PBS was spotted on a lawn of a susceptible strain as a negative control. The susceptibility of each bacterial strain was tested in triplicate, and the entire experiment was repeated twice.

Determination of the bacterial killing rate

The rapidity by which tailocins killed bacteria was measured in 96-well plates (Nest) using an Epoch 2 microplate reader (BioTek). 25 µL of a suspension containing tailocins (approximately 10^{11} particles mL^{-1}) in PBS pH 7.2 were added to 100 µL of 5 McF (approximately 10^8 CFU mL^{-1}) bacterial suspension in PBS. An overnight culture of a tested strain in TSB were harvested by centrifugation (5 min, 8,000 RCF). The OD_{600} of the PBS suspensions was measured each minute for 2 h. The plate was incubated at 28°C with shaking. The susceptible strain *M. paradisiaca* strain NCPPB 2511 was used as a positive control, and sterile PBS pH 7.2 without tailocins was used as a negative control. The log-transformed values of OD_{600} at each time point were normalized to the log-transformed starting OD_{600} and regressed against time. The regression coefficient [$\Delta Log_{10}(OD_{600})min^{-1}$] was calculated for each of the obtained curves. The killing proportion was estimated at two representative time points (20 and 120 min) as the average % of the initial OD_{600} of the selected bacterial culture compared to controls ($n = 10$).

Analysis of the tailocins with SDS-PAGE and ESI LC–MS/MS

Proteins within tailocins were separated using a 4–20% sodium dodecyl sulfate-polyacrylamide gradient gel (Mini-PROTEAN TGX Stain-Free Precast, Bio-Rad Hercules, United States) electrophoresis (SDS-PAGE) using previous methods (Sambrook et al., 1989). Protein bands were excised from the gel using a sterile scalpel, and the excised gel pieces were placed in separate 1.5 mL Eppendorf tubes for amino acid sequencing. In-gel digestion was performed according to a standard protocol consisting of gel de-coloration and removal of Coomassie staining, reduction/alkylation with dithiothreitol (DTT), and iodoacetamide (IAA), respectively (Golebiowski et al., 2022). First, digestion was carried out overnight with trypsin (Promega Mass Spectrometry Grade Gold) at 37°C. The tryptic peptides were then eluted from the gel with sequential washing of gel pieces with 50 mM ammonium bicarbonate buffer, 5% formic acid in 50% acetonitrile, and 100% acetonitrile (Goldman et al., 2019). All samples were then concentrated (SpeedVac), and the final cleanup was carried out using the StageTips method on the C18 phase to a 50% acetonitrile solution with 1% acetic acid (Schmidt and Sinz, 2017). After concentrating the samples to 30 mL using the SpeedVac, fragmentation mass spectra were recorded for analysis. ESI LC–MS/MS analysis was performed on Triple Tof 5600+ mass spectrometer with DuoSpray Ion Source (AB SCIEX, Framingham, MA, United States) connected to the Eksigent microLC (Ekspert MicroLC 200 PLus System, Eksigent, Redwood City, CA, United States) equipped

with the ChromXP C18CL column (3 µm, 120 Å, 150 mm × 0.5 mm). The microLC−MS/MS system was controlled by the AB SCIEX Analyst TF 1.6 software. Chromatographic separation was carried out for 30 min in a gradient program: (1) 0–1 min—20% solvent B, (2) 1–26 min—20 − 60% solvent B, (3) 26–28 min—98% solvent B, and (4) 29–30 min—20% solvent B, where solvent A was 0.1% formic acid in water and solvent B 0.1% formic acid in acetonitrile. The identification of proteins present in the examined gel bands was carried out based on the obtained fragmentation spectra using the ProteinPilot software (v 4.5) or Peaks Studio and the appropriate protein database (UniProt *Dickeya dadantii 15.02.2023, unreviewed*) with an automated false discovery rate (1% FDR).

Bioinformatic analyses

Prediction of prophage regions in the genome of *D. dadantii* 3937 (Genbank accession: NC_014500.1) was conducted using PHASTER (Arndt et al., 2016). The tailocin cluster and individual proteins it encodes were analyzed against NCBI databases using BLASTn and BLASTp (Altschul et al., 1990). The topology of the tailocin cluster in *D. dadantii* 3937 was investigated using BioCyc (Karp et al., 2019). Phylogenomic analysis of the Soft Rot *Pectobacteriaceae* (SRP) genomes was based on core genome sequences and was performed using EDGAR ver. 3.0 (Dieckmann et al., 2021) accessed via https://edgar3.computational.bio.uni-giessen.de.

Stability of tailocins

Tailocins were incubated for 24 h at several different temperatures (−80, −20, 4, 22, 28, 37, 42, 50, 65, and 80°C), pH values (2, 5, 3.5, 7, 9, 10.5, and 12), and NaCl concentrations (0.01, 0.1, 1, and 5 M), after which their bacterial growth inhibitory activity was assessed by a spot test using *M. paradisiaca* as described above. All tested samples had a total volume of 200 µL, and the initial concentration of PEG-purified tailocin of approximately 10^{10} particles mL^{-1}. To obtain the test samples, tailocins were diluted by mixing a volume of 20 µL of PEG-purified samples with 180 µL of either PBS (temperature stability), PBS with pH modified by addition of either HCl or NaOH to the desired values (pH stability), or in water containing different concentrations of NaCl. The experiments were repeated three times, each with three technical replications per tested condition.

Effect of enzyme/detergent/organic solvent treatment on the activity of tailocins

Tailocins were incubated for 1 h at 37°C with the following enzymes: proteinase K (Sigma-Aldrich, final concentration: 0.5 mg mL^{-1}), DNase (Sigma-Aldrich, final concentration: 10 U mL^{-1}), or lysozyme (Sigma-Aldrich, final concentration: 0.5 mg mL^{-1}), and at room temperature (22°C) with sodium dodecyl sulfate (SDS, Sigma Aldrich, final concentration: 1%), or chloroform (POCH, 50% v/v). The remaining activity of treated tailocins was then assessed in a spot test as described above. The processed samples had a total volume of 200 µL, and a tailocin concentration of approximately 10^{10} particles mL^{-1}. The samples were prepared by mixing 20 µL of PEG-purified samples (about 10^{11} particles mL^{-1}) with the appropriate volume of the factor stock to a final volume of 200 µL with PBS. The exception were the chloroform-treated samples where 200 µL of sample were mixed on a shaker with 200 µL of chloroform. Prior to testing, the chloroform-treated sample was centrifuged (5 min at 4000 RCF), and the aqueous phase was removed for assay. The experiments were repeated three times, each with three technical repetitions per tested condition.

Binding of tailocins to nonviable bacterial cells

Overnight bacterial cultures of *M. paradisiaca* NCPPB 2511 and *D. dadantii* strain 3937 grown in TSB were washed twice with PBS buffer and then killed by incubation with 5 mg mL^{-1} chloramphenicol (Sigma-Aldrich) for 60 min, with shaking (120 rpm, 28°C; Gonzalez and Kunka, 1987). The killing of the cells after 1 h was confirmed by plating 4 aliquots (10 µL) of treated culture on TSA plates, incubating at 28°C for 24 h, and verifying last of bacterial growth. After killing, the nonviable bacterial cells were again washed three times with PBS to remove the remaining antibiotic. The PEG-purified tailocin samples were then added to suspension of viable and nonviable susceptible and nonsusceptible bacteria to a final concentration of approximately 10^{10} particles mL^{-1} and incubated for 40 min with shaking at 120 rpm at 28°C. After incubation, samples were filtered through a 0.2 µm PES (polyether sulfone) membrane filter, and the remaining tailocins was assessed by a spot test using *M. paradisiaca*. The experiments were repeated three times, each with three technical replication per tested condition.

Testing the influence of pH on the bactericidal activity of tailocins

The PEG-purified tailocins (approximately 10^{11} particles mL^{-1}) were diluted 10-fold in PBS buffered to pH 2, 7, and 12 and incubated for 24 h at room temperature. The pH of each sample was then adjusted to neutral pH (pH 7) using an equal volume of the buffered PBS. The solutions were then incubated for 4 h at room temperature and tested for growth inhibitory activity using a spot test in three replicates as described above.

Caenorhabditis elegans toxicity assay

Sensitivity of *Caenorhabditis elegans* to tailocins produced by *D. dadantii* was tested as described before (Kirienko et al., 2014) with slight modifications. Briefly, wild-type Bristol N2 strain of *C. elegans* nematode obtained from the *Caenorhabditis* Genetic Center (CGC, University of Minnesota, Minneapolis, United States) was maintained as described before (Stiernagle, 2006; Krzyzanowska et al., 2019) on Nematode Growth Medium (NGM) plates with *Escherichia coli* strain OP50 as a food source. The toxicity of the tailocins was tested on nematode cultures synchronized as described earlier (Porta-de-la-Riva et al., 2012). Briefly, nematode eggs were harvested from cultures treated with a mixture of 5 M NaOH and 5.25% NaOCl (1,

3, v:v)—a treatment that eliminates adult worms. Recovered eggs were hatched in an S-complete medium, and the nematodes were grown to the L4 stage using *E. coli* OP50 as a food source. The synchronized cultures were then transferred into wells of a 96-well plate. The worms were counted under the microscope (Leica MZ10f stereomicroscope, Leica) and *ca.* 30 worms placed in each well supplemented with PEG-purified and ultracentrifugation concentrated (1 h, 26,000 RCF, 4°C) tailocin in an S-complete medium at a concentration of 10^{12} particles mL^{-1}. Nematode cultures grown without tailocins were used as control. The plates were incubated for 24 h in the dark at 25°C. The survival of nematodes in tailocin-supplemented cultures was compared to the control. The experiment was repeated twice with the same setup, and the results were averaged for analysis.

Statistical analysis

All statistical tests were conducted using either Past 4.13 software (Hammer et al., 2001) or Microsoft Office Excel.[1] The Shapiro–Wilk (Shapiro and Wilk, 1965) and F-tests (Shen and Faraway, 2004) were used to test for normality and variance equality of data, respectively. For pairwise testing, the *t*-test (Semenick, 1990) was applied for data having a normal distribution and equal variances, the Welch test (Welch, 1947) was used for samples with a normal distribution but unequal variances, while the U Mann–Whitney test (Mann and Whitney, 1947) was applied for data that were not normally distributed. One-way ANOVA (Ross and Willson, 2017) was used to compare more than two data groups. Levene's test (Schultz, 1985) was used to test the homogeneity of variance, and the normality of the residuals was conducted using the Shapiro–Wilk test. Welch's one-way ANOVA, followed by the Games-Howell *post hoc* test (Mégevand, 2022), was used for the data groups with non-homogeneous variance and normally distributed residuals. For groups with a non-homogeneous variance and without normally distributed residuals Kruscal-Wallis's one-way ANOVA (McKight and Najab, 2010) followed by Dunn's *post hoc* test (Ruxton and Beauchamp, 2008) was applied.

Data availability statement

The datasets presented in this study can be found in online repositories. The names of the repository/repositories and accession number(s) can be found in the article/Supplementary material.

Author contributions

MB: Conceptualization, Investigation, Methodology, Visualization, Writing – original draft, Writing – review & editing. DK: Conceptualization, Investigation, Supervision, Visualization, Writing – original draft, Writing – review & editing. MN: Investigation, Methodology, Visualization, Writing – original draft. MS: Investigation, Methodology, Writing – original draft. MR: Investigation, Methodology, Writing – original draft. PC: Methodology, Writing – original draft. KW: Investigation, Methodology, Writing – original draft. RC: Conceptualization, Data curation, Funding acquisition, Resources, Supervision, Writing – original draft, Writing – review & editing.

Funding

The author(s) declare financial support was received for the research, authorship, and/or publication of this article. This research was financially supported by the National Science Center, Poland (Narodowe Centrum Nauki, Polska) via a research grant SONATA BIS 10 (2020/38/E/NZ9/00007) to RC.

Acknowledgments

The authors would like to express their gratitude to Nicole Hugouvieux-Cotte-Pattat [Laboratory of Microbiology Adaptation and Pathogenesis (UMR 5240) CNRS, Université Lyon 1 & INSA de Lyon, France] for providing strain A5587 (*D. dadantii* strain 3937 *tssK*::*uidA* kanR) for this study, Alfonso Jaramillo and Cristina Ramos [*De novo* Synthetic Biology Lab, Institute for Integrative Systems Biology (I2SysBio-CSIC)], for providing valuable information on the P2 phage, Jochen Blom (Justus Liebig University, Giessen, Germany) for helpful discussion on phylogenomic analysis, and Steven E. Lindow (University of California-Berkeley, Berkeley, CA, United States) for his comments on the manuscript and his editorial work.

Conflict of interest

The authors declare that the research was conducted in the absence of any commercial or financial relationships that could be construed as a potential conflict of interest.

The reviewer AJ-K declared a shared affiliation with the authors to the handling editor at the time of review.

The author(s) declared that they were an editorial board member of Frontiers, at the time of submission. This had no impact on the peer review process and the final decision.

Publisher's note

Supplementary material

The Supplementary material for this article can be found online at: https://www.frontiersin.org/articles/10.3389/fmicb.2023.1307349/full#supplementary-material

1 www.office.com

References

Abedon, S. T., Danis-Wlodarczyk, K. M., and Wozniak, D. J. (2021). Phage cocktail development for bacteriophage therapy: toward improving Spectrum of activity breadth and depth. *Pharmaceuticals (Basel)* 14, 1–25. doi: 10.3390/ph14101019

Altschul, S. F., Gish, W., Miller, W., Myers, E. W., and Lipman, D. J. (1990). Basic local alignment search tool. *J. Mol. Biol.* 215, 403–410. doi: 10.1016/S0022-2836(05)80360-2

Arndt, D., Grant, J. R., Marcu, A., Sajed, T., Pon, A., Liang, Y., et al. (2016). PHASTER: a better, faster version of the PHAST phage search tool. *Nucleic Acids Res.* 44, W16–W21. doi: 10.1093/nar/gkw387

Balciunas, E. M., Martinez, F. A. C., Todorov, S. D., De Melo Franco, B. D. G., Converti, A., and De Souza Oliveira, R. P. (2013). Novel biotechnological applications of bacteriocins: a review. *Food Control* 32, 134–142. doi: 10.1016/j.foodcont.2012.11.025

Bartnik, P., Lewtak, K., Fiolka, M., Czaplewska, P., Narajczyk, M., and Czajkowski, R. (2022). Resistance of Dickeya solani strain IPO 2222 to lytic bacteriophage PhiD5 results in fitness tradeoffs for the bacterium during infection. *Sci. Rep.* 12:10725. doi: 10.1038/s41598-022-14956-7

Bauer, M. A., Kainz, K., Carmona-Gutierrez, D., and Madeo, F. (2018). Microbial wars: competition in ecological niches and within the microbiome. *Microb. Cell* 5, 215–219. doi: 10.15698/mic2018.05.628

Becker, Y., Patz, S., Werner, S., Hoppe, B., Feltgen, S., Berger, B., et al. (2022). Bacteria producing contractile phage tail-like particles (CPTPs) are promising alternatives to conventional pesticides. *J. Kult.* 74, 85–93. doi: 10.5073/JfK.2022.03-04.06

Behrens, H. M., Six, A., Walker, D., and Kleanthous, C. (2017). The therapeutic potential of bacteriocins as protein antibiotics. *Emerg. Top Life Sci.* 1, 65–74. doi: 10.1042/ETLS20160016

Bertani, G. (1951). Studies on lysogenesis. I. The mode of phage liberation by lysogenic *Escherichia coli*. *J. Bacteriol.* 62, 293–300. doi: 10.1128/jb.62.3.293-300.1951

Casjens, S. R., and Grose, J. H. (2016). Contributions of P2-and P22-like prophages to understanding the enormous diversity and abundance of tailed bacteriophages. *Virology* 496, 255–276. doi: 10.1016/j.virol.2016.05.022

Charkowski, A. O. (2007). "The soft rot Erwinia," in *Plant-Associated Bacteria*. ed. S. S. Gnanamanickam (Dordrecht: Springer).

Charkowski, A. O. (2018). The changing face of bacterial soft-rot diseases. *Annu. Rev. Phytopathol.* 56, 269–288. doi: 10.1146/annurev-phyto-080417-045906

Choi, J. K., and Kim, I. O. (1988). Properties of carotovoricin H, a bacteriocin from *Erwinia carotovora* subsp. carotovora. *Plant Pathol. J.* 4, 33–39.

Chopra, L., Singh, G., Kumar Jena, K., and Sahoo, D. K. (2015). Sonorensin: a new bacteriocin with potential of an anti-biofilm agent and a food biopreservative. *Sci. Rep.* 5:13412. doi: 10.1038/srep13412

Christie, G. E., and Calendar, R. (2016). Bacteriophage P2. *Bacteriophage* 6:e1145782. doi: 10.1080/21597081.2016.1145782

Coetzee, H. L., De Klerk, H. C., Coetzee, J. N., and Smit, J. A. (1968). Bacteriophage-tail-like particles associated with intra-species killing of *Proteus vulgaris*. *J. Gen. Virol.* 2, 29–36. doi: 10.1099/0022-1317-2-1-29

Czajkowski, R., De Boer, W. J., Van Der Zouwen, P. S., Kastelein, P., Jafra, S., De Haan, E. G., et al. (2013). Virulence of 'Dickeya solani' And*dickeya dianthicola*biovar-1 and-7 strains on potato (*Solanum tuberosum*). *Plant Pathol.* 62, 597–610. doi: 10.1111/j.1365-3059.2012.02664.x

Dieckmann, M. A., Beyvers, S., Nkouamedjo-Fankep, R. C., Hanel, P. H. G., Jelonek, L., Blom, J., et al. (2021). EDGAR3.0: comparative genomics and phylogenomics on a scalable infrastructure. *Nucleic Acids Res.* 49, W185–W192. doi: 10.1093/nar/gkab341

Echandi, E. (1979). Production, properties, and morphology of Bacteriocins from *Erwinia chrysanthemi*. *Phytopathology* 69, 1204–1207. doi: 10.1094/Phyto-69-1204

Fagundes, P. C., Farias, F. M., Santos, O. C. S., De Oliveira, N. E. M., Da Paz, J. A. S., Ceotto-Vigoder, H., et al. (2016). The antimicrobial peptide aureocin A53 as an alternative agent for biopreservation of dairy products. *J. Appl. Microbiol.* 121, 435–444. doi: 10.1111/jam.13189

Fischer, S., Godino, A., Quesada, J. M., Cordero, P., Jofre, E., Mori, G., et al. (2012). Characterization of a phage-like pyocin from the plant growth-promoting rhizobacterium *Pseudomonas fluorescens* SF4c. *Microbiology* 158, 1493–1503. doi: 10.1099/mic.0.056002-0

Ge, T., Ekbataniamiri, F., Johnson, S. B., Larkin, R. P., and Hao, J. (2021). Interaction between Dickeya dianthicola and Pectobacterium parmentieri in potato infection under field conditions. *Microorganisms* 9:316. doi: 10.3390/microorganisms9020316

Ge, P., Scholl, D., Leiman, P. G., Yu, X., Miller, J. F., and Zhou, Z. H. (2015). Atomic structures of a bactericidal contractile nanotube in its pre-and postcontraction states. *Nat. Struct. Mol. Biol.* 22, 377–382. doi: 10.1038/nsmb.2995

Gebhart, D., Lok, S., Clare, S., Tomas, M., Stares, M., Scholl, D., et al. (2015). A modified R-type Bacteriocin specifically targeting *Clostridium difficile* prevents colonization of mice without affecting gut microbiota diversity. *MBio* 6:6. doi: 10.1128/mbio.02368-02314

Ghequire, M. G. K., and De Mot, R. (2014). Ribosomally encoded antibacterial proteins and peptides from Pseudomonas. *FEMS Microbiol. Rev.* 38, 523–568. doi: 10.1111/1574-6976.12079

Ghequire, M. G. K., and De Mot, R. (2015). The Tailocin tale: peeling off phage tails. *Trends Microbiol.* 23, 587–590. doi: 10.1016/j.tim.2015.07.011

Ghoul, M., and Mitri, S. (2016). The ecology and evolution of microbial competition. *Trends Microbiol.* 24, 833–845. doi: 10.1016/j.tim.2016.06.011

Golanowska, M. (2015). Characterization of Dickeya solani strains and identification of bacterial and plant signals involved in the induction of virulence. Doctor of philosophy, CNRS, Université Lyon 1 & INSA de Lyon, France, University of Gdansk, Gdansk, Poland.

Goldman, A. R., Beer, L. A., Tang, H. Y., Hembach, P., Zayas-Bazan, D., and Speicher, D. W. (2019). Proteome analysis using gel-LC-MS/MS. *Curr. Protoc. Protein Sci.* 96:e93. doi: 10.1002/cpps.93

Golebiowski, A., Pomastowski, P., Rafinska, K., Zuvela, P., Wong, M. W., Pryshchepa, O., et al. (2022). Functionalization of alpha-Lactalbumin by zinc ions. *ACS Omega* 7, 38459–38474. doi: 10.1021/acsomega.2c03674

Gonzalez, C. F., and Kunka, B. S. (1987). Plasmid-associated Bacteriocin production and sucrose fermentation in *Pediococcus acidilactici*. *Appl. Environ. Microbiol.* 53, 2534–2538. doi: 10.1128/aem.53.10.2534-2538.1987

Gorter, F. A., Manhart, M., and Ackermann, M. (2020). Understanding the evolution of interspecies interactions in microbial communities. *Philos. Trans. R. Soc. Lond. Ser. B Biol. Sci.* 375:20190256. doi: 10.1098/rstb.2019.0256

Granato, E. T., Meiller-Legrand, T. A., and Foster, K. R. (2019). The evolution and ecology of bacterial warfare. *Curr. Biol.* 29, R521–R537. doi: 10.1016/j.cub.2019.04.024

Hammer, Ø., Harper, D. A. T., and Ryan, P. D. (2001). PAST: paleontological statistics software package for education and data analysis. *Palaeontol. Electron.* 4:9.

Hibbing, M. E., Fuqua, C., Parsek, M. R., and Peterson, S. B. (2010). Bacterial competition: surviving and thriving in the microbial jungle. *Nat. Rev. Microbiol.* 8, 15–25. doi: 10.1038/nrmicro2259

Hockett, K. L., and Baltrus, D. A. (2017). Use of the soft-agar overlay technique to screen for bacterially produced inhibitory compounds. *J. Vis. Exp.* (119), e55064. doi: 10.3791/55064

Kageyama, M., Ikeda, K., and Egami, F. (1964). Studies of a Pyocin. Iii. Biological properties of the Pyocin. *J. Biochem.* 55, 59–64. doi: 10.1093/oxfordjournals.jbchem.a127841

Kamimiya, S., Izaki, K., and Takahashi, H. (1977). Bacteriocins in Erwinia-Aroideae with tail like structure of bacteriophages. *Agric. Biol. Chem.* 41, 911–912.

Karp, P. D., Billington, R., Caspi, R., Fulcher, C. A., Latendresse, M., Kothari, A., et al. (2019). The bio Cyc collection of microbial genomes and metabolic pathways. *Brief. Bioinform.* 20, 1085–1093. doi: 10.1093/bib/bbx085

Kirienko, N. V., Cezairliyan, B. O., Ausubel, F. M., and Powell, J. R. (2014). "*Pseudomonas aeruginosa* PA14 pathogenesis in *Caenorhabditis elegans*" in *Pseudomonas methods and protocols*. eds. A. Filloux and J.-L. Ramos (New York, NY: Springer New York), 653–669.

Kotoujansky, A. (1987). Molecular genetics of pathogenesis by soft-rot Erwinias. *Annu. Rev. Phytopathol.* 25, 405–430. doi: 10.1146/annurev.py.25.090187.002201

Kotoujansky, A., Lemattre, M., and Boistard, P. (1982). Utilization of a thermosensitive episome bearing transposon TN10 to isolate Hfr donor strains of *Erwinia carotovora* subsp. chrysanthemi. *J. Bacteriol.* 150, 122–131. doi: 10.1128/jb.150.1.122-131.1982

Krzyzanowska, D. M., Maciag, T., Siwinska, J., Krychowiak, M., Jafra, S., and Czajkowski, R. (2019). Compatible mixture of bacterial antagonists developed to protect potato tubers from soft rot caused by Pectobacterium spp. and Dickeya spp. *Plant Dis.* 103, 1374–1382. doi: 10.1094/PDIS-10-18-1866-RE

Little, A. E., Robinson, C. J., Peterson, S. B., Raffa, K. F., and Handelsman, J. (2008). Rules of engagement: interspecies interactions that regulate microbial communities. *Annu. Rev. Microbiol.* 62, 375–401. doi: 10.1146/annurev.micro.030608.101423

Liu, J., Chen, P., Zheng, C., and Huang, Y. P. (2013). Characterization of maltocin P28, a novel phage tail-like bacteriocin from *Stenotrophomonas maltophilia*. *Appl. Environ. Microbiol.* 79, 5593–5600. doi: 10.1128/AEM.01648-13

Ma, B., Hibbing, M. E., Kim, H. S., Reedy, R. M., Yedidia, I., Breuer, J., et al. (2007). Host range and molecular phylogenies of the soft rot enterobacterial genera pectobacterium and dickeya. *Phytopathology* 97, 1150–1163. doi: 10.1094/PHYTO-97-9-1150

Mann, H. B., and Whitney, D. R. (1947). On a test of whether one of two random variables is stochastically larger than the other. *Ann. Math. Stat.* 18, 50–60. doi: 10.1214/aoms/1177730491

Mckight, P. E., and Najab, J. (2010). "Kruskal-wallis test" in *The Corsini Encyclopedia of Psychology*. eds. I. B. Weiner, and W. Edward Craighead (Wiley) 1.

Mégevand, P. (2022). "Games-Howell post-hoc test for one-way ANOVA."

Mennigmann, H. (1965). Electronmicroscopy of the anti-bacterial agent produced by *Escherichia coli* 15. *Microbiology* 41, 151–154.

Michel-Briand, Y., and Baysse, C. (2002). The pyocins of *Pseudomonas aeruginosa*. *Biochimie* 84, 499–510. doi: 10.1016/S0300-9084(02)01422-0

Morales-Soto, N., Gaudriault, S., Ogier, J.-C., Thappeta, K. R. V., and Forst, S. (2012). Comparative analysis of P2-type remnant prophage loci in Xenorhabdus bovienii and *Xenorhabdus nematophila* required for xenorhabdicin production. *FEMS Microbiol. Lett.* 333, 69–76. doi: 10.1111/j.1574-6968.2012.02600.x

Nguyen, H. A., Kaneko, J., and Kamio, Y. (2002). Temperature-dependent production of carotovoricin Er and pectin lyase in phytopathogenic *Erwinia carotovora* subsp. carotovora Er. *Biosci. Biotechnol. Biochem.* 66, 444–447. doi: 10.1271/bbb.66.444

Nguyen, V. S., Logger, L., Spinelli, S., Legrand, P., Huyen Pham, T. T., Nhung Trinh, T. T., et al. (2017). Type VI secretion TssK baseplate protein exhibits structural similarity with phage receptor-binding proteins and evolved to bind the membrane complex. *Nat. Microbiol.* 2:17103. doi: 10.1038/nmicrobiol.2017.103

Patz, S., Becker, Y., Richert-Poggeler, K. R., Berger, B., Ruppel, S., Huson, D. H., et al. (2019). Phage tail-like particles are versatile bacterial nanomachines—a mini-review. *J. Adv. Res.* 19, 75–84. doi: 10.1016/j.jare.2019.04.003

Perombelon, M.C.M. (1988). "Ecology of Erwinias causing stem and tuber diseases" in Bacterial disease of potato: Report of the planning conference on bacterial diseases of potato).

Pérombelon, M. C. M. (1992). Potato blackleg: epidemiology, host-pathogen interaction and control. *Neth. J. Plant Pathol.* 98, 135–146. doi: 10.1007/BF01974480

Perombelon, M. C. M. (2002). Potato diseases caused by soft rot erwinias: an overview of pathogenesis. *Plant Pathol.* 51, 1–12. doi: 10.1046/j.0032-0862.2001.Shorttitle.doc.x

Porta-De-La-Riva, M., Fontrodona, L., Villanueva, A., and Ceron, J. (2012). Basic *Caenorhabditis elegans* methods: synchronization and observation. *J. Vis. Exp.* 64:e4019. doi: 10.3791/4019-v

Principe, A., Fernandez, M., Torasso, M., Godino, A., and Fischer, S. (2018). Effectiveness of tailocins produced by *Pseudomonas fluorescens* SF4c in controlling the bacterial-spot disease in tomatoes caused by *Xanthomonas vesicatoria*. *Microbiol. Res.* 212-213, 94–102. doi: 10.1016/j.micres.2018.05.010

Reverchon, S., Muskhelisvili, G., and Nasser, W. (2016). "Chapter three-virulence program of a bacterial plant pathogen: the Dickeya model" in *Progress in Molecular Biology and Translational Science*. ed. D. B. Teplow (San Francisco: Academic Press), 51–92.

Reverchon, S., and Nasser, W. (2013). Dickeya ecology, environment sensing and regulation of virulence programme. *Environ. Microbiol. Rep.* 5, 622–636. doi: 10.1111/1758-2229.12073

Ross, A., and Willson, V. L. (2017). "One-way ANOVA" in *Basic and Advanced Statistical Tests* (SensePublishers), 21–24.

Ruxton, G. D., and Beauchamp, G. (2008). Time for some a priori thinking about post hoc testing. *Behav. Ecol.* 19, 690–693. doi: 10.1093/beheco/arn020

Sambrook, J., Fritsch, E.F., and Maniatis, T. (1989). *Molecular Cloning: A Laboratory Manual*. Cold Spring Harbor, NY, USA: Cold Spring Harbor Laboratory Press.

Samson, R., Legendre, J. B., Christen, R., Fischer-Le Saux, M., Achouak, W., and Gardan, L. (2005). Transfer of *Pectobacterium chrysanthemi* (Burkholder et al. 1953) Brenner et al. 1973 and *Brenneria paradisiaca* to the genus Dickeya gen. Nov. as *Dickeya chrysanthemi* comb. nov. and *Dickeya paradisiaca* comb. nov. and delineation of four novel species, *Dickeya dadantii* sp. nov., *Dickeya dianthicola* sp. nov., *Dickeya dieffenbachiae* sp. nov. and *Dickeya zeae* sp. nov. *Int. J. Syst. Evol. Microbiol.* 55, 1415–1427. doi: 10.1099/ijs.0.02791-0

Schmidt, R., and Sinz, A. (2017). Improved single-step enrichment methods of cross-linked products for protein structure analysis and protein interaction mapping. *Anal. Bioanal. Chem.* 409, 2393–2400. doi: 10.1007/s00216-017-0185-1

Scholl, D. (2017). Phage tail–like bacteriocins. *Annu. Rev. Virol.* 4, 453–467. doi: 10.1146/annurev-virology-101416-041632

Scholl, D., and Martin, D. W. Jr. (2008). Antibacterial efficacy of R-type pyocins towards *Pseudomonas aeruginosa* in a murine peritonitis model. *Antimicrob. Agents Chemother.* 52, 1647–1652. doi: 10.1128/AAC.01479-07

Schultz, B. B. (1985). Levene's test for relative variation. *Syst. Zool.* 34, 449–456. doi: 10.2307/2413207

Semenick, D. (1990). Tests and measurements: the T-test. *Strength Condition. J.* 12, 36–37.

Shapiro, S. S., and Wilk, M. B. (1965). An analysis of variance test for normality (complete samples). *Biometrika* 52, 591–611. doi: 10.1093/biomet/52.3-4.591

Shen, Q., and Faraway, J. (2004). An F test for linear models with functional responses. *Stat. Sin.* 14, 1239–1257.

Shimodaira, H. (2002). An approximately unbiased test of phylogenetic tree selection. *Syst. Biol.* 51, 492–508. doi: 10.1080/10635150290069913

Shyntum, D. Y., Nkomo, N. P., Shingange, N. L., Gricia, A. R., Bellieny-Rabelo, D., and Moleleki, L. N. (2019). The impact of type VI secretion system, Bacteriocins and antibiotics on bacterial competition of *Pectobacterium carotovorum* subsp. brasiliense and the regulation of Carbapenem biosynthesis by Iron and the ferric-uptake regulator. *Front. Microbiol.* 10:2379. doi: 10.3389/fmicb.2019.02379

Smarda, J., and Benada, O. (2005). Phage tail-like (high-molecular-weight) bacteriocins of Budvicia aquatica and *Pragia fontium* (Enterobacteriaceae). *Appl. Environ. Microbiol.* 71, 8970–8973. doi: 10.1128/AEM.71.12.8970-8973.2005

Sokolova, D., Smolarska, A., Bartnik, P., Rabalski, L., Kosinski, M., Narajczyk, M., et al. (2023). Spontaneous mutations in hlyD and tuf genes result in resistance of Dickeya solani IPO 2222 to phage varphiD5 but cause decreased bacterial fitness and virulence in planta. *Sci. Rep.* 13:7534. doi: 10.1038/s41598-023-34803-7

Stiernagle, T. (2006). *Maintenance of C. elegans*. Available at: https://www.ncbi.nlm.nih.gov/books/NBK19649/

Strauch, E., Kaspar, H., Schaudinn, C., Dersch, P., Madela, K., Gewinner, C., et al. (2001). Characterization of enterocoliticin, a phage tail-like bacteriocin, and its effect on pathogenic *Yersinia enterocolitica* strains. *Appl. Environ. Microbiol.* 67, 5634–5642. doi: 10.1128/AEM.67.12.5634-5642.2001

Stubbendieck, R. M., and Straight, P. D. (2016). Multifaceted interfaces of bacterial competition. *J. Bacteriol.* 198, 2145–2155. doi: 10.1128/JB.00275-16

Tantoso, E., Eisenhaber, B., Kirsch, M., Shitov, V., Zhao, Z. Y., and Eisenhaber, F. (2022). To kill or to be killed: pangenome analysis of *Escherichia coli* strains reveals a tailocin specific for pandemic ST131. *BMC Biol.* 20, 1–26. doi: 10.1186/s12915-022-01347-7

Toth, I.K., Barny, M.-A., Czajkowski, R., Elphinstone, J.G., Li, X., Pédron, J., et al. (2021). "Pectobacterium and Dickeya: taxonomy and evolution" in *Plant Diseases Caused by Dickeya and Pectobacterium Species*. (eds.) GijsegemF. Van, WolfJ.M. Van Der and I.K. Toth (Cham: Springer International Publishing), 13–37

Vacheron, J., Heiman, C. M., and Keel, C. (2021). Live cell dynamics of production, explosive release and killing activity of phage tail-like weapons for Pseudomonas kin exclusion. *Commun. Biol.* 4:87. doi: 10.1038/s42003-020-01581-1

Van Gijsegem, F., Van Der Wolf, J. M., and Toth, I. K. (2021). *Plant Diseases Caused by Dickeya and Pectobacterium Species*. Springer Nature Switzerland.

Wagner, A. (2022). Competition for nutrients increases invasion resistance during assembly of microbial communities. *Mol. Ecol.* 31, 4188–4203. doi: 10.1111/mec.16565

Welch, B. L. (1947). The generalisation of student's problems when several different population variances are involved. *Biometrika* 34, 28–35.

Williams, S. R., Gebhart, D., Martin, D. W., and Scholl, D. (2008). Retargeting R-type pyocins to generate novel bactericidal protein complexes. *Appl. Environ. Microbiol.* 74, 3868–3876. doi: 10.1128/AEM.00141-08

Yamada, K., Hirota, M., Niimi, Y., Nguyen, H. A., Takahara, Y., Kamio, Y., et al. (2006). Nucleotide sequences and organization of the genes for carotovoricin (Ctv) from *Erwinia carotovora* indicate that Ctv evolved from the same ancestor as *Salmonella typhi* prophage. *Biosci. Biotechnol. Biochem.* 70, 2236–2247. doi: 10.1271/bbb.60177

Yao, G. W., Duarte, I., Le, T. T., Carmody, L., Lipuma, J. J., Young, R., et al. (2017). A broad-host-range Tailocin from *Burkholderia cenocepacia*. *Appl. Environ. Microbiol.* 83, 1–17. doi: 10.1128/AEM.03414-16

frontiers | Frontiers in Microbiology

TYPE Original Research
PUBLISHED 06 December 2023
DOI 10.3389/fmicb.2023.1282372

OPEN ACCESS

EDITED BY
Sylwia Bloch,
University of Gdansk, Poland

REVIEWED BY
Jhonatan Hernandez-Valdes,
Expert Capability Center Deventer, Netherlands
Magdalena Plotka,
University of Gdansk, Poland
Anna Wanecka,
Wroclaw University of Environmental and Life Sciences, Poland

*CORRESPONDENCE
Satoshi Tsuneda
✉ stsuneda@waseda.jp
Naohiro Noda
✉ noda-naohiro@aist.go.jp

RECEIVED 24 August 2023
ACCEPTED 14 November 2023
PUBLISHED 06 December 2023

CITATION
Hoshino M, Ota Y, Suyama T, Morishita Y, Tsuneda S and Noda N (2023) Water-in-oil droplet-mediated method for detecting and isolating infectious bacteriophage particles via fluorescent staining.
Front. Microbiol. 14:1282372.
doi: 10.3389/fmicb.2023.1282372

Water-in-oil droplet-mediated method for detecting and isolating infectious bacteriophage particles via fluorescent staining

Miu Hoshino[1,2], Yuri Ota[2,3], Tetsushi Suyama[2], Yuji Morishita[3], Satoshi Tsuneda[4]* and Naohiro Noda[1,2,4]*

[1]Department of Computational Biology and Medical Sciences, Graduate School of Frontier Sciences, The University of Tokyo, Chiba, Japan, [2]Biomedical Research Institute, National Institute of Advanced Industrial Science and Technology (AIST), Ibaraki, Japan, [3]On-chip Biotechnologies Co., Ltd., Tokyo, Japan, [4]Department of Life Science and Medical Bioscience, School of Advanced Science and Engineering, Waseda University, Tokyo, Japan

Bacteriophages are the most abundant entities on Earth. In contrast with the number of phages considered to be in existence, current phage isolation and screening methods lack throughput. Droplet microfluidic technology has been established as a platform for high-throughput screening of biological and biochemical components. In this study, we developed a proof-of-concept method for isolating phages using water-in-oil droplets (droplets) as individual chambers for phage propagation and co-cultivating T2 phage and their host cell *Escherichia coli* within droplets. Liquid cultivation of microbes will facilitate the use of microbes that cannot grow on or degrade agar as host cells, ultimately resulting in the acquisition of phages that infect less known bacterial cells. The compartmentalizing characteristic of droplets and the use of a fluorescent dye to stain phages simultaneously enabled the enumeration and isolation of viable phage particles. We successfully recultivated the phages after simultaneously segregating single phage particles into droplets and inoculating them with their host cells within droplets. By recovering individual droplets into 96-well plates, we were able to isolate phage clones derived from single phage particles. The success rate for phage recovery was 35.7%. This study lays the building foundations for techniques yet to be developed that will involve the isolation and rupturing of droplets and provides a robust method for phage enumeration and isolation.

KEYWORDS

bacteriophage, water-in-oil droplets, droplet isolation, plaque assay, bacteriophage screening

1 Introduction

Bacteriophages (phages) are viruses that need to infect bacterial cells to propagate, which results in the lysis or slowed reproduction rate of host cells. This parasitic life cycle and the resulting deceleration in host cell growth coupled with the species-specificity establish phages as a next-generation antimicrobial agent with a focused area of action (Harada et al., 2018). As such, phages have begun to reattract attention for use as microbial control agents in fields such as medicine (Febvre et al., 2019; Rasmussen et al., 2020), agriculture (Zhou et al., 2013; Wang et al., 2019), and food safety (Goodridge et al., 1999a; Tian et al., 2022). With the progress of

phage research, many interactions between phages and host cells were uncovered, such as the numerous phage resistance mechanisms of bacterial cells and phage-phage interactions (Erez et al., 2017; Borges et al., 2018). In this era of phage research, a high-throughput method of isolating phages from the environment would be of monumental value. Here, we propose a novel method to isolate viable phages from the environment, using model phages as a proof-of-concept.

Phages are thought to have been discovered independently by Twort (Twort, 1915) in 1915 and D'Herelle (D'Herelle, 2007) in 1917). Plaque assay has remained the gold standard for isolation and enumeration of phages since it was introduced over a century ago. This method and the phages obtained using this method have provided mankind with a fundamental understanding of molecular biology (Salmond and Fineran, 2015). However, the plaque assay has limitations such as the requirement of an even lawn of host cells. This limits the range of host cells to those that can grow on agar plates, preferably with limited mobility. In addition, various types of bacteria that have the ability to degrade agar (Chi et al., 2012), which may be problematic for their use as host cells in plaque assays. To overcome such limitations, we employed water-in-oil droplets (droplets) as a platform for segregating and cultivating phage particles.

In the last decade, droplet technology has emerged as a powerful high-throughput platform for screening micro-sized particles (Kaminski et al., 2016). Some uses for this technology in the field of microbiology include screening for microbial and fungal cells (Samlali et al., 2022) and enzymes (van Loo et al., 2019; Yanakieva et al., 2020), cultivation of rare or hard-to-culture microbes (Ota et al., 2019; Saito et al., 2021), and single-cell analyses (Terekhov et al., 2017; Pryszlak et al., 2022). This technology is typically used in combination with fluorescence to distinguish droplets containing target cells or enzymes from others. As such, technologies for differentiating droplets are also being developed, Woronoff et al. (2011), Ota et al. (2019), Nakamura et al. (2022) as are technologies to exchange the solution within droplets (Abate et al., 2010; Huang et al., 2021). Droplet-based technologies are based on the precondition that absolute compartmentalization of particles can be achieved upon generation of droplets. Similarly, our proposed method compartmentalizes phage particles into individual droplets upon generation, thereby effectively isolating phage particles. We employed a fluorescent dye to stain bacteriophage particles and differentiate droplets in which phage propagation occurred via fluorescence intensity. We selected YOYO-1 for this purpose, because its cell-impermeant characteristic prevents active staining of host cells, while its property as an intercalating dye actively promoted the staining of phage nucleic acid (Goodridge et al., 1999b), as shown in Figure 1 Step 2. In addition, YOYO-1 is a stable homo-dimer complex available for use which have numerous similar intercalators with differing excitation/emission wavelengths, such as TOTO-1 (Fürstenberg et al., 2006).

In this study, we demonstrated the ability to isolate viable phage particles via droplet technology. By co-encapsulating phages, host cells, and fluorescent dye within droplets, we could observe propagation of single phage particles in droplets through monitoring droplet fluorescence intensities. We successfully targeted and isolated individual droplets into 96-well plates for upscaled cultivation of isolated phages. Using YOYO-1, fluorescent staining of the general phage population in a sample is enabled without the use of any genetic recombination, making this a highly applicable method. This method is capable of yielding previously undiscovered phages for known host cells when applied to environmental samples. In addition, this method may enable tractable screening of phage even when using microbes that grow slowly or are difficult to handle on agar plates as host cells.

2 Materials and methods

2.1 Bacteriophage, host cell, and culture medium

Escherichia coli B (NBRC 13168) and T2 phage (NBRC 20002) were obtained from NITE Biological Resource Center (NBRC) culture Cells were cultured following NBRC's recommended protocol in 802 culture medium and frozen at −80°C as glycerol stocks. Glycerol stocks of these cells grown in M9 culture medium were also created and stored at −80°C.

Prior to compartmentalization into droplets, *E. coli* cells were inoculated from the glycerol stocks (grown in M9 medium) into 2 mL of M9 culture broth and shaken overnight at 30°C for preculturing. Cell were then diluted (1,100) into fresh M9 medium and cultured for one more day. Resulting cells were washed 3 times and resuspended into fresh M9 medium at a concentration of 10^9 cells/mL. This concentration was calculated based on optical density of the cell suspension at 600 nm (OD_{600}), which was measured with GeneQuant 1,300 (Biochrom Ltd., United Kingdom). Phages were propagated by co-cultivation with their host cells in liquid 802 medium. Prior to co-cultivation with phage, *E. coli* host cells were inoculated into 2 mL of 802 medium from glycerol stocks and shaken overnight. This preculture was resuspended into two flasks containing 20 mL of 802 medium each and shaken for 1–2 h (30°C, 120 rpm), after which 200 µL of phage suspension was added to one of the flasks. Both flasks were shaken for an additional 3–4 h, and the contents of both flasks were combined. Following another 3–4 h of shaking, the contents of both flasks were centrifuged (4°C, 8,000 ×*g*, 15 min) to remove remaining host cells. PEG 6000 (4 g) and sodium chloride (1.6 g) were added to the supernatant and vigorously vortexed. This mixture was cooled down by placement in a − 20°C freezer for 1 h prior to centrifugation (4°C, 10,000 × *g*, 60 min) to pellet phage. Supernatant was discarded, and the resulting phage pellet was resuspended in 6 mL of sodium magnesium (SM) buffer, which was subsequently washed three times with chloroform to remove debris. The resulting phage particles suspended in SM buffer were used as concentrated phage suspension.

2.2 Droplet generation and optical signal intensity assessment

Monodisperse droplets with diameters of approximately 30 µm were generated using 2D chip-800DG (On-chip Biotechnologies, Japan) attached to an On-chip Droplet Generator (On-chip Biotechnologies, Japan). After both the oil (200 µL/sample) and sample (40 µL/sample) phases were loaded into their respective reservoirs, both phases were simultaneously pressurized for 20 min to

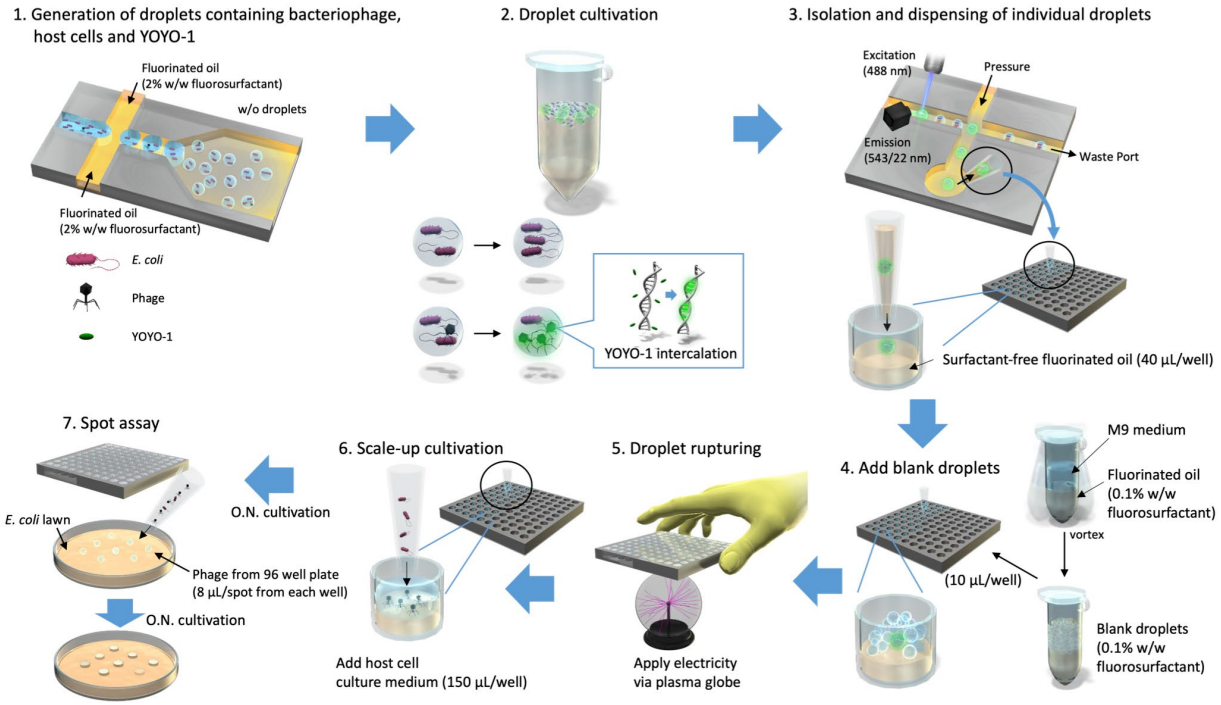

FIGURE 1
Isolation of droplets in which bacteriophage propagation occurred. Droplets containing T2 phage, *Escherichia coli*, and YOYO-1 were generated using On-chip Droplet Generator (Step1) and placed in a 30°C incubator to allow for bacteriophage infection to occur within droplets (Step 2). Following incubation, On-chip Droplet Selector was used to assess fluorescence intensities of individual droplets and isolate those which met a particular criterion regarding droplet size and fluorescence intensity. Droplets in this target range were isolated into individual wells of 96-well plates containing 40 µL/well of surfactant-free fluorinated oil along with an additional 10 µL of fluorinated oil (Step 3). Following isolation, droplets produced by emulsifying culture medium and fluorinated oil containing 0.1% (w/w) surfactant (referred to as "blank droplets") were added to the 96-well plates (Step 4). These 96-well plates, containing a single target droplet, 10 µL of blank droplets, and 50 µL of fluorinated oil per well, were pressed onto an active plasma globe to induce a chain reaction of droplet rupturing (Step 5). This was conducted approximately 5 s per well. Subsequently, 150 µL of *E. coli* overnight culture was added to each well (Step 6) and incubated overnight (O.N.). The contents of each well were used to conduct a round of spot assay to monitor bacteriophage propagation within the well (Step 7).

generate droplets (Figure 1 Step 1). The pressure applied to the oil phase was 27 kPa, and the pressure applied to the sample (aqueous) phase was 25 kPa. Following generation, droplets were collected into 0.6 mL sample tubes and incubated at 30°C (Figure 1 Step 2). Sample phases were prepared shortly before application to 2D chip-800 DG and droplet generation. The sample phase comprised 160 nM YOYO-1 (ThermoFisher Scientific, USA), T2 phage and *E. coli* in M9 medium, or YOYO-1 and *E. coli*. The oil phase used was HFE-7500 Novec Engineered fluid (3 M) with 008-FluoroSurfactant (Ran Biotechnologies, USA) mixed at 2% (w/w). On-chip Sort (On-chip Biotechnologies, Japan) and Chip-Z1001 (On-chip Biotechnologies, Japan) were used for measuring fluorescence intensities of droplet samples. For sheath oil, 0.1% (w/w) 008-FluoroSurfactant in HFE-7500 was used. A 488 nm wavelength laser was used as an excitation light source, and fluorescence intensities in the range of 543/22 nm and forward-scatter intensities were measured. For each droplet sample whose optical intensities were measured, optical intensities of approximately 20,000 droplets were measured and recorded to test YOYO-1 resolution. Similarly, approximately 40,000 droplets were measured and recorded to visualize changes in fluorescence intensity distribution of droplets generated with YOYO-1, phage, and host cells over time. In our experiments, we used On-chip Droplet Generator to generate approximately 1.0×10^6 droplets in 20 min, and On-chip Sort to measure droplet fluorescence intensities at a rate of approximately 180 droplets/s.

2.3 Isolation of individual droplets

Fluorescence intensities of a few thousand droplets were measured using On-chip Droplet Selector (On-chip Biotechnologies, Japan) to produce plots showing the distributions of fluorescence intensity. Then fluorescence intensity boundaries of target droplets were chosen based on the graphs obtained from the measurements. For fluorescence intensity measurement, droplets were loaded into the sample port of 2D Chip-SD1000 (On-chip Biotechnologies, Japan), which was then set into the On-chip Droplet Selector. After setting the fluorescence intensity boundaries, fluorescence intensities of droplets were measured once more, and those with fluorescence intensities within the chosen threshold were sorted and isolated (Figure 1 Step 3). On-chip Droplet Selector works by pushing out droplets within the chosen threshold into a chamber for isolation and can isolate up to 96 droplets in 10 min. The isolated droplets are then automatically dispensed into a 96-well plate. Single droplet isolation was conducted into individual wells of 96-well plates pre-filled with 40 µL of HFE-7500. A 488 nm wavelength laser was used as an excitation light

source, and fluorescence intensities in the range of 543/22 nm and forward-scatter intensities were measured.

2.4 Optical intensity signal analyses and data visualization

Fluorescence intensities of droplets were analyzed by importing the data of fluorescence intensities and forward-scatter intensities of droplet samples as csv files into Rstudio (ver. 4.1.0). Packages tidyverse (ver. 1.3.1), ggplot2 (ver. 3.3.5), ggridges (ver. 0.5.3), and ggExtra (ver. 0.9) were used for data manipulation and visualization. Forward-scatter intensities were used to filter out the measurements of droplets with abnormal sizes (see Supplementary Tables S1–S3 for details). To account for variations in forward-scatter intensity means across different time points, measurements of droplets with forward-scatter intensities deviating by more than one standard deviation from the mean intensity of their corresponding time point were removed.

2.5 Image analyses

Microscopic photos of droplet samples were taken with a Nikon Ti2 Eclipse microscope (Nikon, Japan) and NIS-Elements Basic Research software ver. 5.20.00 (Nikon). The photos were imported into WinRoof 2018 software ver. 4.8.0 (Mitani Corporation, Japan) to analyze the diameters of droplets. These measurements were used to calculate the volumes of droplets as required.

2.6 Droplet rupturing using static electricity

Equal volumes of M9 medium and HFE-7500 with 0.1% (w/w) 008-FluoroSurfactant were added to a 15-mL Falcon tube, or a 2-mL tube and emulsified by thorough mixing with a vortex. We termed the resulting emulsion "blank droplets." Blank droplets were added to 96-well plates following droplet isolation, 10 µL/well, as shown in step four of Figure 1. As emulsions are prone to breaking when placed in an electric field (Karbaschi et al., 2017; Mizoguchi and Muto, 2019), an active plasma globe was used to generate an electric field while rupturing the droplets. To rupture isolated droplets, the bottom of the 96-well plate was pressed onto an active plasma globe to trigger a chain reaction of droplet rupturing using the added blank droplets (Figure 1 Step 5). During this step, the plate was slowly repositioned to allow all wells to be evenly stimulated by the plasma globe.

2.7 Digitization of phage existence within isolated droplets via spot assay

Overnight culture suspension of *E. coli* was added to the droplet solution (Figure 1 Step 6), which was obtained via isolation and rupturing in 96-well plates (150 µL/well). This was then incubated at 30°C overnight to promote further propagation of phages. To assess the existence of phage within the solution, spot assays were conducted using an agar plate made of 802 medium and a lawn of *E. coli*. This lawn was created by mixing 100 µL of *E. coli* suspension into molten 802 medium (0.7% w/v Lonza SeaPlaque Agarose) and pouring the entire mixture onto the original plate. After the lawn solidified, 8 µL of the solution was taken from each well of the 96-well plate containing isolated droplets and gently spotted on the lawn (Figure 1 Step 7). Plates were inverted and incubated overnight after the spots dried. Wells were counted as phage-positive if the solution used for spotting resulted in a difference on the *E. coli* lawn after incubation.

2.8 Plaque assay using phages within droplets

A fixed volume (8 µL) of droplets containing phage and *E. coli* was taken into 0.6-mL tubes containing 50 µL of HFE-7500 and 45 µL of M9 medium and vortexed. The sides of the tube containing this mixture were pressed onto a plasma globe for rupturing by slowly rolling it around to stimulate the emulsion as evenly as possible. The resulting sample was serially diluted with M9 medium to be used in plaque assays. Plaque assays were done in triplicate for each dilution, and one dilution for each timepoint was selected to calculate the average titer. The plaque assays were conducted using a modified version of the protocol by Kropinski et al. (2009).

3 Results

We developed a droplet-based approach for isolating bacteriophage particles which we evaluated using a spot assay. As shown in Figure 1, this method starts by co-encapsulating T2 phage particles with their host cell *E. coli* into micro-sized droplets with YOYO-1 iodide (Step 1). These droplet samples are placed in an incubator to allow for the occurrence of in-droplet phage infection and propagation (Step 2). When phage infection and subsequent propagation occurs, YOYO-1 intercalates into DNA of progeny phage, thereby distinguishing droplets with phages from those without by fluorescence intensity. The droplets in which phage propagation occurred are then isolated into individual wells of 96-well plates pre-filled with 40 µL/well of HFE-7500 (Step 3). The isolated droplets are then ruptured and subjected to scale-up cultivation. The first of these steps involves the creation of "blank droplets" by emulsifying culture medium and fluorinated oil containing 0.1% (w/w) fluorosurfactant. These "blank droplets" are added to 96-well plates (10 µL/well), into which droplet isolation was conducted (Step 4). Following the addition of "blank droplets," the 96-well plate is pressed on the top of an active plasma globe (Step 5). This electrical stimulation is used to induce a chain reaction of droplet rupturing. Host cell culture is added to each well (150 µL/well) for scale-up cultivation of phage, which were within isolated droplets (Step 6). To evaluate the success rate of our method, we checked whether the whole process, from the generation of droplets to the isolation and scale-up cultivation of phages, yielded phage in 96-well plates. This was done by conducting a spot test with the sample phase of the 96-well plate (Step 7).

3.1 Fluorescence intensities of droplets containing bacteriophage suspension and YOYO-1 iodide

To evaluate the resolution of YOYO-1 iodide, the fluorescence intensities of droplets generated with 160 nM YOYO-1 and bacteriophage suspension at various final concentrations were

measured. Fluorescence intensities of droplets generated with bacteriophage suspensions at final concentrations of 0, 2.3×10^4, 2.3×10^5, 2.3×10^6, 2.3×10^7, and 2.3×10^8 plaque forming units (PFU) per mL are shown in Figure 2. Fluorescence intensities of droplet samples increased concurrently with phage concentration, with medians of 11.0, 5.0, 9.0, 116, 400, and 485 starting from the sample containing the lowest concentration of phage suspension. The sample without phage, which contained deionized water instead of phage suspension, had a slightly higher fluorescence intensity medium compared to the other samples containing low concentrations of phage.

The number of phage particles within individual droplets is given as "λ_{phg}" which can be calculated from the concentration of phage suspension (Supplementary Equation S1). Here, the λ_{phg} depends on the phage concentration of the solution used to generate droplets. Samples with higher λ_{phg} generally had a broader distribution of fluorescence intensity, whereas samples with lower λ_{phg} had narrower distributions. The rightmost sample in Figure 2 had a λ_{phg} of approximately 800. This was calculated based on results obtained from a standard plaque assay protocol using the same phage suspension used to create the droplet sample. Fluorescence intensities of the sample generated with 2.3×10^5 PFU/mL and the sample generated with 2.3×10^4 PFU/mL were similar. However, fluorescence intensities of these samples and the sample generated with 2.3×10^6 PFU/mL were different. These results show that droplets generated with 160 nM YOYO-1 iodide have fluorescence intensities dependent on the concentration of phage within droplets. In other words, the fluorescence intensity of a droplet, in comparison with other droplets, can be used to determine its phage content in comparison to other droplets.

3.2 Transition of droplet fluorescence intensity and titer

To assess the correlation between droplet fluorescence intensities and the corresponding phage content, we tracked the changes in fluorescence intensities of droplets generated with YOYO-1, phage, and host cells, and measured the titer of phage suspension within the droplets via plaque assay. Droplet samples containing T2 phage, *E. coli*, and YOYO-1 were generated and incubated at 30°C, as were droplets containing only *E. coli* and YOYO-1. For both samples, YOYO-1 was used at a final concentration of 160 nM. At the 0, 1, 3, 5, 7, 9, and 24-h time points, fluorescence intensities of approximately 40,000 droplets were measured. These measurements were used to plot the transformation of density distribution in droplet fluorescence intensity over time (Figures 3A,B). In the sample containing phage (Figure 3A), a subgroup of droplets with a strong fluorescence intensity could be observed. This subgroup was not observed in the sample generated without phage (Figure 3B). This subgroup, which appeared during the first hour of incubation, increased in both proportion and fluorescence intensity as incubation progressed. During the first 9 h of incubation, the two groups of droplets with high and low fluorescence intensities in Figure 3A were clearly distinguishable from each other. Conversely, while the two groups of droplets could be divided into fluorescent and non-fluorescent droplets even after 24 h of incubation, a trace proportion of measurements fell mid-way between the two groups. This group of droplets with medium fluorescence intensities could also be clearly seen in the sample generated without phage, incubated for 24 h. Similarly, droplets with medium fluorescence intensities were also observed in the samples generated without phage, incubated for 7 and 9 h. The percentage of droplets with fluorescence intensities stronger than 130 were calculated and plotted as Figure 3C. As less than 0.5% of droplets without phage measured at the 5-h time point had fluorescence intensities higher than 130, this was chosen as the fluorescence intensity differentiating fluorescent droplets and non-fluorescent droplets. In the sample containing phage, a sharp increase in the percentage of fluorescent droplets could be observed until 5 h of incubation. After 5 h, a sharp decrease in the differential of fluorescent droplets to cultivation time was observed. In contrast with the phage-containing sample, the proportion of fluorescent droplets in the sample prepared without phage remained relatively low throughout the whole 24 h.

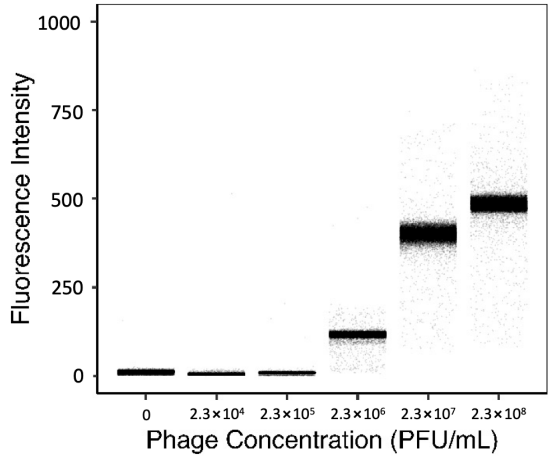

FIGURE 2
Fluorescence intensities of droplets containing 160nM YOYO-1 and various concentrations of phage suspension. The average number of PFU within individual droplets for each sample shown were 0, 0.08, 0.8, 8, 80, and 800 PFU/droplet respectively, from the leftmost sample.

Alongside the measurements of droplet fluorescence intensities, the phage titers within the droplets were also measured. To do this, 8 µL of emulsion from the droplet sample generate with phage was sampled to use in plaque assays at each timepoint. The results of these plaque assay are plotted in Figure 3D. The initial hour of incubation resulted in an over 17-fold increase in the phage titer within droplets. After the first hour, phage titer within 8 µL of emulsion continued to increase steadily, albeit at a lowered rate, until 9 h of incubation. Contrary to the surge in phage population during the first few hours of incubation, phage titer within 8 µL of emulsion measured after 9 h and 24 h were comparable. Together these results show that phage infection and propagation are indeed occurring within droplets, and that this increase in phage population causes droplet fluorescence intensity to increase as well.

3.3 Visualization of temporal changes within droplets

To document visible temporal changes in droplets, we captured sequential photographs of droplet samples. Microscopic photos of both the droplets generated with (Figure 4 left side) and without phage (Figure 4 right side) were taken. These photos were taken at 0, 3, and 5 h after incubation, following generation. Bright field and fluorescent

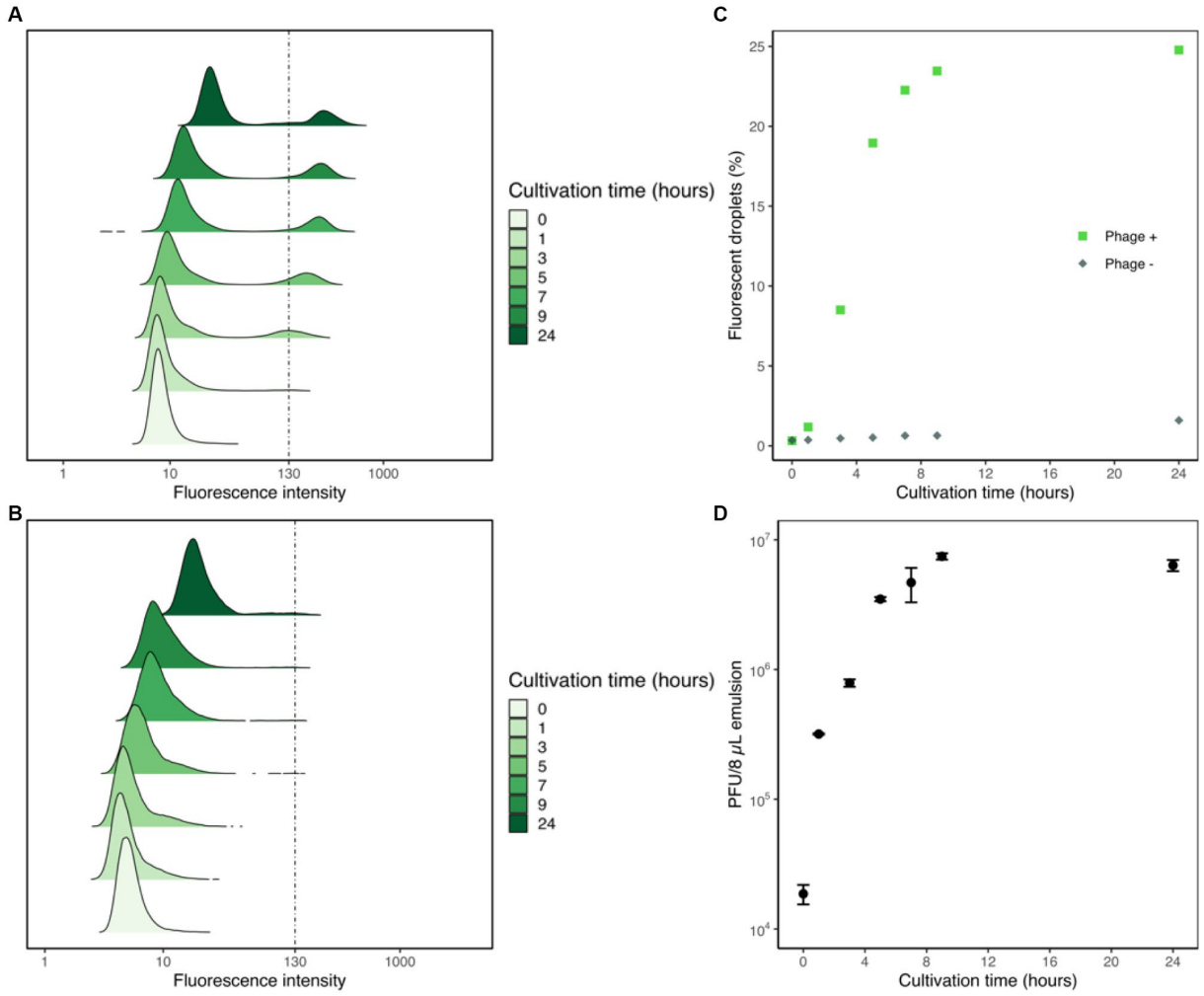

FIGURE 3
Flow cytometric analyses of droplet samples with and without phage. Fluorescence intensities of droplet samples containing phage, *E. coli*, and YOYO-1 **(A)** and samples with *E. coli* and YOYO-1 **(B)** were measured to create density ridgeline plots. These measurements were used to plot the percentages of droplets with fluorescence intensities higher than 130 **(C)**. Concurrent with fluorescence intensity measurements, a fixed volume (8 μL) of droplets was sampled and ruptured from the phage containing droplet samples to perform a titer check via plaque assay **(D)**.

field microscopic photos of droplets were taken. Comparison of these images revealed a difference in overall fluorescence intensity, which amplified over time. Figure 4F shows bright green spots as well as hazy circular droplets around them, which were not visible in 4 L. Fluorescent droplets can be observed in Figure 4E, demonstrating that fluorescence intensifies enough to enable differentiation via microscopic observation by the third hour of incubation. Furthermore, the number of *E. coli* cells that could be observed microscopically within droplets varied between the two samples, and this difference was seen as intensifying over time.

3.4 Isolation of individual droplets and upscaled cultivation of phage

To test the effectiveness of our phage isolation method, we employed our model to obtain phages from individual droplets. To do this, droplets containing T2 phage, *E. coli,* and YOYO-1 were generated and incubated for 5 h. After 5 h, On-chip Droplet Selector was used to dispense droplets within the target range of fluorescence intensity and forward scatter intensities. Two target ranges were chosen here, with one being droplets with high fluorescence intensities, and the other being droplets with low fluorescence intensities. For each target range, droplet isolation into 96-well plates was conducted into at least 184 wells. Following isolation, droplets were ruptured using static electricity. Subsequently, fresh *E. coli* cultured in M9 medium was added to the wells and incubated overnight to promote further propagation of phage. These upscaled culture solutions in 96-well plates were used to conduct spot assay to determine the existence of phage. Spot assay results of wells containing droplets with high fluorescence intensities showed that 82/230 (35.7%) wells were phage-positive. In contrast, for wells containing droplets with low fluorescence intensities, 0/184 (0%) were phage-positive. Supplementary Figure S1 displays spot assay results from 32 of wells containing droplets with high and low fluorescence intensities. These results show that droplets with low fluorescence intensities did not contain phage, demonstrating that droplets containing viable phage will have a high fluorescence intensity.

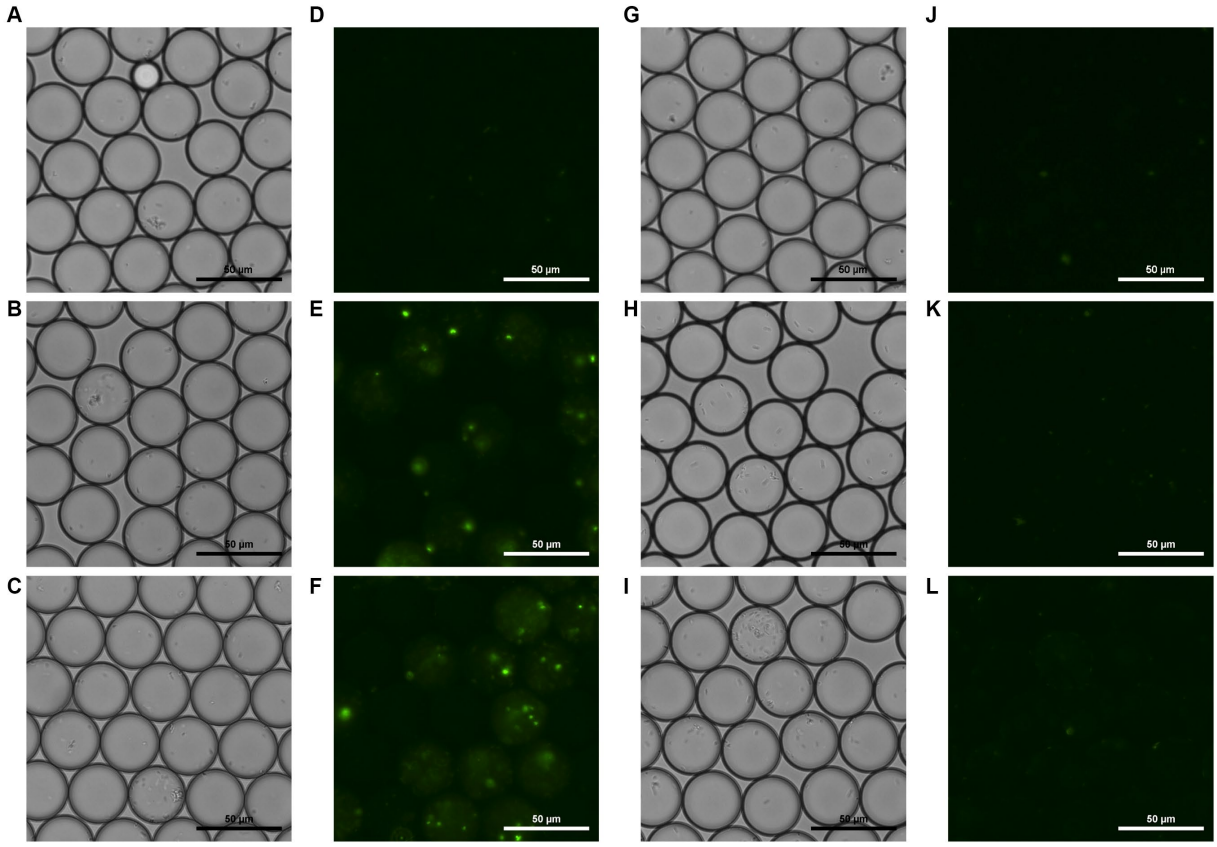

FIGURE 4
Bright field and fluorescent field microscopic photos of droplets containing phage, *E. coli*, and YOYO-1 **(A–F)**, and droplets containing *E. coli* and YOYO-1 **(G–L)**. **(A,D,G,J)**, were taken right after droplet generation. **(B,E,H,K)**, were taken after 3 h of static incubation at 30°C, and **(C,F,I,L)** were taken after approximately 5 h of static incubation at 30°C.

4 Discussion

There have been studies reporting the rapid enumeration of phage using droplets, both by means of propagation and without. These propagation-based studies include the use of LacZ phage (Tjhung et al., 2014), and indirect observation of phage via analysis of light scattering (Yu et al., 2014). Phage enumeration without propagation was conducted by droplet digital PCR of phage genome sequences (Morella et al., 2018). In our method we used YOYO-1 to fluorescently stain progeny phage, and successfully differentiated droplets in which phage propagation occurred. Isolation and rupturing of fluorescent droplets, followed by upscaled recultivation of phage resulted in successful recovery of phage from individual droplets. To the best of our knowledge, this is the first study to propose an approach to isolate target droplets and test the success rate of the isolation and recultivation of single phage particles.

4.1 Probability calculations using the Poisson distribution

The number of particles encapsulated into droplets follow the Poisson distribution, meaning that the λ_{phg} is the mean number of phage particles in a droplet sample, and does not indicate the number of particles in each droplet. This difference in the number of phage particles confined in each droplet can be seen in Figure 2, where the droplet samples generated with a higher concentration of phage suspension had broader distributions of fluorescence intensity.

The probability of a droplet containing a specific number of phage particles can be calculated from the λ_{phg} value, and the numerical range of phage particles enclosed within individual droplets increases as the λ_{phg} increases. This increase in numerical range likely resulted in a broadening of fluorescence intensity range, as can be observed in the droplet samples generated with 2.3×10^7 PFU/mL and 2.3×10^8 PFU/mL phage suspension. However, when λ_{phg} was sufficiently small, as was the case with the droplet sample containing 2.3×10^4 PFU/mL phage suspension, the vast majority of droplets generated were likely devoid of phage particles. With the λ_{phg} of this sample estimated to be 0.08, 92.3% of droplets in this sample are expected to lack phages following the Poisson distribution, and 96.0% of phage-containing droplets are expected to contain a single phage particle. Thus, we can conclude that in samples with a sufficiently small λ_{phg}, droplets likely contain no, or a very small number of phage particles, resulting in a narrow range of fluorescence intensity. This pattern can be observed in the droplet sample containing 2.3×10^5 PFU/mL phage suspension, which had a λ_{phg} of 0.8, and similarly had a narrow distribution of droplet fluorescence intensity.

Contrary to the similarities between the samples whose λ_{phg} were 0.08 and 0.8, the sample with λ_{phg} of 8.0 (sample containing 2.3×10^6 PFU/mL phage suspension) had a distinctly different distribution of droplet fluorescence intensity. This difference in fluorescence intensity implies that the resolution limit of this method ranges between 1 and 8 phage particles.

There are two ways to calculate $\lambda_{phg.}$ The first way is to calculate $\lambda_{phg.}$ Based on droplet size and titer of phage solution and the λ_{phg} of this sample calculated from phage titer was 0.4. The second way is to calculate it from the fraction of non-fluorescent droplets using the Poisson distribution. From the results in section 4.4, we concluded that droplets containing viable phage will have elevated fluorescence intensities after cultivation. In other words, droplets with low fluorescence intensities even after cultivation do not contain viable phage. This indicates that the fraction of non-fluorescent droplets in the sample generated with phage is the fraction of droplets devoid of phage, and the Poisson distribution can be used to calculate the λ_{phg} of the droplet sample before cultivation (Supplementary Equation S2). Using the fractions of non-fluorescent droplets measured after 5 h of cultivation, the λ_{phg} value of the droplet sample generated with phage in Figure 3 was approximately 0.2.

4.2 Phage-host interaction within droplets

Given that YOYO-1 is cell-impermeant, live *E. coli* cells are not expected to exhibit a strong fluorescence. Therefore, the increase in fluorescence intensity observed in droplets containing YOYO-1, phage and host cells can be attributed primarily to the intercalation of YOYO-1 into the nucleic acid of phage. Together with the observation that the subgroups of droplets with strong fluorescence intensities observed in Figure 3A appeared only after cultivation, we can deduce that phage infection and propagation occurred in these droplets, and that these droplets contain a substantial amount of phage. This phage propagation resulted in an increase in phage nucleic acid, into which YOYO-1 intercalation occurred, consequentially raising the fluorescence intensity of the droplet. A sharp increase in percentage of fluorescent droplets seen until 5 h of cultivation can be observed (Figure 3A), which continued to increase at a slower pace after this time point. This slowdown in the increase of fluorescent droplet percentage implies that the phage infection and release of progeny phage occurred at least once within the first 5 h of cultivation in most droplets that contained phage. Notably, approximately 5 h of incubation produced only miniscule plaques in plaque assay experiments conducted using T2 phage and *E. coli* B (Supplementary Figure S2), while it was enough time for phages to propagate enough within droplets to allow for clear differentiation from non-fluorescent droplets.

When the changes in percentage of fluorescent droplets are compared to the changes of phage titer within droplets, the first hour of cultivation resulted in an intense increase of phage titer, but not in the percentage of fluorescent droplets. From these results, it can be inferred that the number of phages after 1 h of cultivation was not sufficient to significantly increase fluorescence intensities. Comparison of these two parameters between the 9 and 24-h time points reveal a small increase in the ratio of fluorescent droplets, and a small decrease in phage titer. The lack of increase in phage titer indicates additional infection and propagation of phage did not occur within this 15-h time period, which contradicts the slight increase in proportion of fluorescent droplets. The increase in fluorescence may be attributed to host cell DNA and cell debris derived from lysed cells. Possible factors constraining phage population growth may include the host cells' developing a resistance to phage, and the obliteration of the host cell population confined with the phage.

The aforementioned contradiction between fluorescent droplet percentages and phage titer indicates that other factors affected fluorescence intensities. These other factors may include the deterioration of *E. coli* cells during the stationary growth phase. Starvation of *E. coli* cells result in a loss of membrane integrity, which allows for nutrients to leak out of the cells (Schink et al., 2019). This weakness of cell membrane could allow for YOYO-1 to enter the cell, or nucleic acids to leak out, along with other cell debris resulting in elevated fluorescence not attributed to phage. This phenomenon could justify the presence of droplets with slightly elevated fluorescence intensities in both the sample generated with and without phage. We hypothesize that such droplets were generated with a higher-than-average number of *E. coli* cells by chance, resulting in accelerated depletion of nutrients, hence starvation.

4.3 Recovery of phages derived from single droplets

The results of droplet isolation and upscaled cultivation of phage in our research had a success rate of 35.7%, while previous studies on single droplet isolation and recultivation of *E. coli* inside reported a minimum of 80% recovery rate when upscaling on solid media (Weber et al., 2022). Although the latter study produced high recovery rates on solid medium, the recovery rates when liquid medium was used was 31%, which was similar to our phage recovery results. Note that our results are the recovery rate of phage, which require the additional steps of phage propagation following droplet isolation and rupturing. Some reasons for these relatively low recovery rates may include the loss of the target droplet, and the fluorescence of the droplet being unrelated to phage propagation, as mentioned in section 5.2. Target droplets may be lost due to the On-chip Droplet Selector accidentally isolating a droplet different than the target one, the droplet rupturing being unsuccessful, which prevents the upscaling of phages, or the target droplet becoming lost due to its small size. Individual droplets have a volume of approximately 18.8 pL which is very small relative to the wells of a 96-well plate and could be easily lost during steps subsequent to isolation, for example by adsorption onto pipette tips. These steps include but are not limited to the additions of blank droplets (Figure 1 Step 4) and culture medium (Figure 1 Step 6).

Despite the chance of droplet loss during the isolation and upscaled cultivation steps, we believe our proposed method's throughput and ability to compartmentalize particles can compensate for this. Our method requires only a small phage concentration upon droplet generation to enable the isolation of individual phage particles and simultaneous differentiation of viable phage from non-viable ones. This method is capable of determining phage concentration of the original phage solution post-segregation and cultivation with host cells and can be applied to screen viable phage particles from environmental samples. The compartmentalizing characteristic of this method eliminates the need to conduct numerous rounds of plaque assay to completely isolate phage particles, as long as the initial phage concentration is set sufficiently low. This can drastically shorten the process of phage screening, which may be useful in scenes such as

phage therapy. Since phages isolated using our method require further upscaling and purification for use in scenes such as phage therapy, the YOYO-1 that was within the single isolated droplet should become diluted enough to lose relevance.

In conclusion, we developed a method to simultaneously enumerate and isolate viable phage particles by co-cultivation inside droplets. This method of phage detection is expected to enable easy and high-throughput screening of lytic phages that infect a particular host cell. In addition, the liquid-based cultivation of this method may enable the use of bacteria with slow growth and growth restricted by agar as host cells. By establishing a method to isolate, rupture, and recultivate target droplets into liquid medium, we have successfully laid the foundations for future droplet-based high-throughput bacteriophage screening experiments.

Data availability statement

The raw data supporting the conclusions of this article will be made available by the authors, without undue reservation.

Author contributions

MH: Conceptualization, Data curation, Formal analysis, Investigation, Methodology, Software, Validation, Visualization, Writing – original draft, Writing – review & editing. YO: Conceptualization, Data curation, Investigation, Methodology, Writing – review & editing. TS: Conceptualization, Data curation, Methodology, Writing – review & editing. YM: Conceptualization, Data curation, Investigation, Methodology, Writing – review & editing. ST: Conceptualization, Data curation, Project administration, Supervision, Writing – review & editing. NN: Conceptualization, Data curation, Funding acquisition, Methodology, Project administration, Resources, Supervision, Writing – review & editing.

Funding

The author(s) declare financial support was received for the research, authorship, and/or publication of this article. This work is based on results obtained from a project, JPNP20011, commissioned by the New Energy and Industrial Technology Development Organization (NEDO). This work was supported by JST SPRING, Grant Number JPMJSP2108.

Conflict of interest

YO and YM were employed by On-chip Biotechnologies Co., Ltd.

The remaining authors declare that the research was conducted in the absence of any commercial or financial relationships that could be construed as a potential conflict of interest.

The author(s) declared that they were an editorial board member of Frontiers, at the time of submission. This had no impact on the peer review process and the final decision.

Publisher's note

All claims expressed in this article are solely those of the authors and do not necessarily represent those of their affiliated organizations, or those of the publisher, the editors and the reviewers. Any product that may be evaluated in this article, or claim that may be made by its manufacturer, is not guaranteed or endorsed by the publisher.

Supplementary material

The Supplementary material for this article can be found online at: https://www.frontiersin.org/articles/10.3389/fmicb.2023.1282372/full#supplementary-material

References

Abate, A. R., Hung, T., Mary, P., Agresti, J. J., and Weitz, D. A. (2010). High-throughput injection with microfluidics using picoinjectors. *Proc. Natl. Acad. Sci. U. S. A.* 107, 19163–19166. doi: 10.1073/pnas.1006888107

Borges, A. L., Zhang, J. Y., Rollins, M. F., Osuna, B. A., Wiedenheft, B., and Bondy-Denomy, J. (2018). Bacteriophage cooperation suppresses CRISPR-Cas3 and Cas9 immunity. *Cells* 174, 917–925.e10. doi: 10.1016/j.cell.2018.06.013

Chi, W., Chang, Y., and Hong, S. (2012). Agar degradation by microorganisms and agar-degrading enzymes. *Appl. Microbiol. Biotechnol.* 94, 917–930. doi: 10.1007/s00253-012-4023-2

D'Herelle, F. (2007). On an invisible microbe antagonistic toward dysenteric bacilli: brief note by Mr. F. D'Herelle, presented by Mr. roux. 1917. *Res. Microbiol.* 158, 553–554. doi: 10.1016/j.resmic.2007.07.005

Erez, Z., Steinberger-Levy, I., Shamir, M., Doron, S., Stokar-Avihail, A., Peleg, Y., et al. (2017). Communication between viruses guides lysis-lysogeny decisions. *Nature* 541, 488–493. doi: 10.1038/nature21049

Febvre, H. P., Rao, S., Gindin, M., Goodwin, N. D. M., Finer, E., Vivanco, J. S., et al. (2019). PHAGE study: effects of supplemental bacteriophage intake on inflammation and gut microbiota in healthy adults. *Nutrients* 11:666. doi: 10.3390/nu11030666

Fürstenberg, A., Julliard, M. D., Deligeorgiev, T. G., Gadjev, N. I., Vasilev, A., and Vauthey, E. (2006). Ultrafast excited-state dynamics of DNA fluorescent intercalators: new insight into the fluorescence enhancement mechanism. *Am. Chem. Soc.* 128, 7661–7669. doi: 10.1021/ja0609001

Goodridge, L., Chen, J., and Griffiths, M. (1999a). Development and characterization of a fluorescent-bacteriophage assay for detection of *Escherichia coli* O157:H7. *Appl. Environ. Microbiol.* 65, 1397–1404. doi: 10.1128/AEM.65.4.1397-1404.1999

Goodridge, L., Chen, J., and Griffiths, M. (1999b). The use of a fluorescent bacteriophage assay for detection of *Escherichia coli* O157:H7 in inoculated ground beef and raw milk. *Int. J. Food Microbiol.* 47, 43–50. doi: 10.1016/s0168-1605(99)00010-0

Harada, L. K., Silva, E. C., Campos, W. F., Del Fiol, F. S., Vila, M., Dabrowska, K., et al. (2018). Biotechnological applications of bacteriophage: state of the art. *Microbiol. Res.* 212-213, 38–58. doi: 10.1016/j.micres.2018.04.007

Huang, C., Zhang, H., Han, S., and Han, A. (2021). Cell washing and solution exchange in droplet microfluidic systems. *Anal. Chem.* 93, 8622–8630. doi: 10.1021/acs.analchem.1c01558

Kaminski, T. S., Scheler, O., and Garstecki, P. (2016). Droplet microfluidics for microbiology: techniques, applications and challenges. *Lab Chip* 16, 2168–2187. doi: 10.1039/c6lc00367b

Karbaschi, M., Shahi, P., and Abate, A. R. (2017). Rapid, chemical-free breaking of microfluidic emulsions with a hand-held antistatic gun. *Biomicrofluidics* 11:044107. doi: 10.1063/1.4995479

Kropinski, A. M., Mazzocco, A., Waddell, T. E., Lingohr, E., and Johnson, R. P. (2009). "Enumeration of bacteriophages by double agar overlay plaque assay" in *Bacteriophages. Methods in molecular biology*. eds. M. R. Clokie and A. M. Kropinski, vol. *501* (Totowa: Humana Press)

Mizoguchi, Y., and Muto, A. (2019). Demulsification of oil-in-water emulsions by application of an electric field: relationship between droplet size distribution and demulsification efficiency. *J. Chem. Eng. Jpn* 52, 799–804. doi: 10.1252/jcej.19we022

Morella, N. M., Yang, S. C., Hernandez, C. A., and Koskella, B. (2018). Rapid quantification of bacteriophages and their bacterial hosts in vitro and in vivo using

droplet digital PCR. *J. Virol. Methods* 259, 18–24. doi: 10.1016/j.jviromet.2018.05.007

Nakamura, A., Honma, N., Tanaka, Y., Suzuki, Y., Shida, Y., Tsuda, Y., et al. (2022). 7-Aminocoumarin-4-acetic acid as a fluorescent probe for detecting bacterial dipeptidyl peptidase activities in water-in-oil droplets and in bulk. *Anal. Chem.* 94, 2416–2424. doi: 10.1021/acs.analchem.1c04108

Ota, Y., Saito, K., Takagi, T., Matsukura, S., Morita, M., Tsuneda, S., et al. (2019). Fluorescent nucleic acid probe in droplets for bacterial sorting (FNAP-sort) as a high-throughput screening method for environmental bacteria with various growth rates. *PLoS One* 14:e0214533. doi: 10.1371/journal.pone.0214533

Pryszlak, A., Wenzel, T., Seitz, K. W., Hildebrand, F., Kartal, E., Cosenza, M. R., et al. (2022). Enrichment of gut microbiome strains for cultivation-free genome sequencing using droplet microfluidics. *Cell. Rep. Methods* 2:100137. doi: 10.1016/j.crmeth.2021.100137

Rasmussen, T. S., Koefoed, A. K., Jakobsen, R. R., Deng, L., Castro-Mejía, J. L., Brunse, A., et al. (2020). Bacteriophage-mediated manipulation of the gut microbiome-promises and presents limitations. *FEMS Microbiol. Rev.* 44, 507–521. doi: 10.1093/femsre/fuaa020

Saito, K., Ota, Y., Tourlousse, D. M., Matsukura, S., Fujitani, H., Morita, M., et al. (2021). Microdroplet-based system for culturing of environmental microorganisms using FNAP-sort. *Sci. Rep.* 11:9506. doi: 10.1038/s41598-021-88974-2

Salmond, G. P. C., and Fineran, P. C. (2015). A century of the phage: past, present and future. *Nat. Rev. Microbiol.* 13, 777–786. doi: 10.1038/nrmicro3564

Samlali, K., Alves, C. L., Jezernik, M., and Shih, S. C. C. (2022). Droplet digital microfluidic system for screening filamentous fungi based on enzymatic activity. *Microsyst. Nanoeng.* 8:123. doi: 10.1038/s41378-022-00456-1

Schink, S. J., Biselli, E., Ammar, C., and Gerland, U. (2019). Death rate of *E. coli* during starvation is set by maintenance cost and biomass recycling. *Cell syst.* 9:64–73. e3. doi: 10.1016/j.cels.2019.06.003

Terekhov, S. S., Smirnov, I. V., Stepanova, A. V., Bobik, T. V., Mokrushina, Y. A., Ponomarenko, N. A., et al. (2017). Microfluidic droplet platform for ultrahigh-throughput single-cell screening of biodiversity. *Proc. Natl. Acad. Sci. U. S. A.* 114, 2550–2555. doi: 10.1073/pnas.1621226114

Tian, L., He, L., Jackson, K., Saif, A., Khan, S., Wan, Z., et al. (2022). Self-assembling nanofibrous bacteriophage microgels as sprayable antimicrobials targeting multidrug-resistant bacteria. *Nat. Commun.* 13:7158. doi: 10.1038/s41467-022-34803-7

Tjhung, K. F., Burnham, S., Anany, H., Griffiths, M. W., and Derda, R. (2014). Rapid enumeration of phage in monodisperse emulsions. *Anal. Chem.* 86, 5642–5648. doi: 10.1021/ac500244g

Twort, F. W. (1915). An investigation on the nature of ultra-microscopic viruses. *Lancet* 186, 1241–1243. doi: 10.1016/s0140-6736(01)20383-3

van Loo, B., Heberlein, M., Mair, P., Zinchenko, A., Schüürmann, J., Eenink, B. D. G., et al. (2019). High-throughput, lysis-free screening for sulfatase activity using *Escherichia coli* autodisplay in microdroplets. *ACS Synth. Biol.* 8, 2690–2700. doi: 10.1021/acssynbio.9b00274

Wang, X., Wei, Z., Yang, K., Wang, J., Jousset, A., Xu, Y., et al. (2019). Phage combination therapies for bacterial wilt disease in tomato. *Nat. Biotechnol.* 37, 1513–1520. doi: 10.1038/s41587-019-0328-3

Weber, T., Hengoju, S., Samimi, A., Roth, M., Tovar, M., and Rosenbaum, M. A. (2022). Recovery and isolation of individual microfluidic picoliter droplets by triggered deposition. *Sens. Actuat. B Chem.* 369:132289. doi: 10.1016/j.snb.2022.132289

Woronoff, G., El Harrak, A., Mayot, E., Schicke, O., Miller, O. J., Soumillion, P., et al. (2011). New generation of amino coumarin methyl sulfonate-based fluorogenic substrates for amidase assays in droplet-based microfluidic applications. *Anal. Chem.* 83, 2852–2857. doi: 10.1021/ac200373n

Yanakieva, D., Elter, A., Bratsch, J., Friedrich, K., Becker, S., and Kolmar, H. (2020). FACS-based functional protein screening via microfluidic co-encapsulation of yeast secretor and mammalian reporter cells. *Sci. Rep.* 10:10182. doi: 10.1038/s41598-020-66927-5

Yu, J. Q., Huang, W., Chin, L. K., Lei, L., Lin, Z. P., Ser, W., et al. (2014). Droplet optofluidic imaging for λ-bacteriophage detection via co-culture with host cell *Escherichia coli*. *Lab Chip* 14, 3519–3524. doi: 10.1039/c4lc00042k

Zhou, L., Powell, C. A., Li, W., Irey, M., and Duan, Y. (2013). Prophage-mediated dynamics of 'Candidatus Liberibacter asiaticus' populations, the destructive bacterial pathogens of citrus huanglongbing. *PLoS One* 8:e82248. doi: 10.1371/journal.pone.0082248

frontiers | Frontiers in Microbiology

TYPE Review
PUBLISHED 05 January 2024
DOI 10.3389/fmicb.2023.1320345

OPEN ACCESS

EDITED BY
Sylwia Bloch,
University of Gdansk, Poland

REVIEWED BY
Bozena Nejman-Falenczyk,
University of Gdansk, Poland
Krzysztof Hinc,
Medical University of Gdansk, Poland
Aneta Skaradzinska,
Wroclaw University of Environmental and Life Sciences, Poland

*CORRESPONDENCE
Marta Gliźniewicz
✉ marta.glizniewicz@pum.edu.pl
Bartłomiej Grygorcewicz
✉ bartlomiej.grygorcewicz@pum.edu.pl;
✉ b.grygorcewicz@gmail.com

RECEIVED 12 October 2023
ACCEPTED 04 December 2023
PUBLISHED 05 January 2024

CITATION
Gliźniewicz M, Miłek D, Olszewska P, Czajkowski A, Serwin N, Cecerska-Heryć E, Dołęgowska B and Grygorcewicz B (2024) Advances in bacteriophage-mediated strategies for combating polymicrobial biofilms.
Front. Microbiol. 14:1320345.
doi: 10.3389/fmicb.2023.1320345

Advances in bacteriophage-mediated strategies for combating polymicrobial biofilms

Marta Gliźniewicz[1]*, Dominika Miłek[1], Patrycja Olszewska[1], Artur Czajkowski[1], Natalia Serwin[1], Elżbieta Cecerska-Heryć[1], Barbara Dołęgowska[1] and Bartłomiej Grygorcewicz[1,2]*

[1]Faculty of Pharmacy, Medical Biotechnology and Laboratory Medicine, Pomeranian Medical University in Szczecin, Szczecin, Poland, [2]Department of Chemical Technology and Engineering, Institute of Chemical Engineering and Environmental Protection Processes, West Pomeranian University of Technology, Szczecin, Poland

Bacteria and fungi tend to coexist within biofilms instead of in planktonic states. Usually, such communities include cross-kingdom microorganisms, which make them harder to remove from abiotic surfaces or infection sites. Additionally, the produced biofilm matrix protects embedded microorganisms from antibiotics, disinfectants, or the host immune system. Therefore, classic therapies based on antibiotics might be ineffective, especially when multidrug-resistant bacteria are causative factors. The complexities surrounding the eradication of biofilms from diverse surfaces and the human body have spurred the exploration of alternative therapeutic modalities. Among these options, bacteriophages and their enzymatic counterparts have emerged as promising candidates, either employed independently or in synergy with antibiotics and other agents. Phages are natural bacteria killers because of mechanisms of action that differ from antibiotics, phages might answer worldwide problems with bacterial infections. In this review, we report the attempts to use bacteriophages in combating polymicrobial biofilms in *in vitro* studies, using different models, including the therapeutical use of phages. In addition, we sum up the advantages, disadvantages, and perspectives of phage therapy.

KEYWORDS

phage therapy, depolymerases, multi-species biofilm, phage-antibiotic synergy, polymicrobial infections

Introduction—biofilm

A biofilm is a structure composed of bacteria and other microorganisms (fungi, viruses) anchored in an extracellular matrix composed of organic substances produced by these microorganisms. Approximately 2–35% of the biofilm's volume comprises microorganisms, while the matrix constitutes the remaining portion. Biofilm matrix primarily consists of proteins, lipids, polysaccharides, extracellular RNA and DNA, minerals, and ions suspended in water (Vu et al., 2009). Biofilm adheres to the biotic or abiotic surface. The biofilm's structure may vary on homogeneous, composed of one species, or heterogeneous, consisting of many different strains of microorganisms. Biofilm

is more challenging to eradicate than planktonic forms of microorganisms due to the protective properties of the matrix (Augustyniak et al., 2021). The properties of the biofilm enable pathogens to escape from the immune system, antibiotics, disinfectants, and other chemical substances (Jamal et al., 2018; Roy et al., 2018). Microorganisms regulate biofilm formation by expressing genes responsible for synthesizing and modifying extracellular components and communicating with each other by sending biochemical signals. This signaling network includes two-component systems (TCS), which regulate signal transduction via phosphorylation of cyclic di-GMP (c-di-GMP), diguanylate cyclase (DGC) systems which cooperate with TCS and coordinate the transition of bacteria from planktonic to biofilm growth mode, and quorum sensing (QS), mechanism that involves autoinducers which are small signal molecules and receptors (Guła et al., 2018). The signaling occurs interkingdom between microorganisms (bacteria, fungi) and host cells.

Biofilm formation

The main stages of biofilm formation are initial contact with a surface, irreversible contact with a surface, formation of microcolonies—expansion, maturation of the biofilm, and cell detachment of the individual cells from the matrix. Surfaces susceptible to bacterial adhesion encompass a variety of substrates such as sewage system pipes, soil particles, living tissues, and medical equipment (e.g., urological catheters, venous catheters, artificial heart valves, intrauterine coils, dental units, and contact lenses) (Vu et al., 2009; Stickler, 2014; Augustyniak et al., 2021). Additional cellular structures, such as fimbriae and flagella, bacterial proteins—adhesins, and physical forces, are responsible for the colonization. Environmental factors, such as the amount of available energy, surface structure, pressure, temperature, and orientation of bacterial cells, influence the possibility of adhesion to the substrate. The main physical forces involved in biofilm formation are van der Waals, steric, or electrostatic interactions associated with the cell membrane double layer (Delcaru et al., 2016).

Following the adhesion stage, there is a phase of microbial multiplication, leading to an expansion in the biofilm volume and the formation of a three-dimensional structure regulated by quorum sensing (QS). This mechanism relies on the secretion of proteins and autoinducers of the expression of genes coding for surface proteins, such as porins. This facilitates more effective nutrient absorption within the biofilm. The secretion of exopolysaccharides (EPSs), which stabilize the biofilm structure, also increases. Special channels are created in the entire biofilm volume to facilitate the removal of unnecessary metabolites and provide an appropriate gas environment and nutrients. Due to the static growth, the development of additional membrane structures responsible for the movement of bacteria is inhibited. In addition, a reduction in protease and phospholipase C synthesis, a decrease in the synthesis and release of toxins, and the production of rough and sometimes mucus-like polysaccharides to better adapt cells to specific conditions of the biofilm microenvironment are observed (Jamal et al., 2018; Narayanan et al., 2018; Amankwah et al., 2022).

The final phase of biofilm life occurs when the ratio of newly formed cells equals the number of dead ones. Environmental conditions such as oxygen depletion and nutrient unavailability result in the switching of bacterial metabolism. Enzymes (e.g., hydrolases and endonucleases) that break down the extracellular matrix, allowing individual bacteria to be released into the environment, are produced. In addition, the expression of genes leading to the formation of flagella returns, restoring the ability of bacteria to move and find a new location for biofilm expansion (Garrett et al., 2008).

Biofilm bacteria virulence and eradication methods

Biofilm production by bacteria is related to their virulence and may imply the occurrence of chronic diseases in the host organism. This is related to many factors, e.g., the production of endotoxins or the protection of bacteria living in the biofilm against the mechanisms of the host immune system, such as phagocytosis or coating with antibodies (Roy et al., 2018). In addition, higher resistance to antibiotics is observed, which is associated with the problematic penetration of active drug ingredients through the biofilm, alternation in biofilm bacteria metabolic activity and presence of cells with a reduced metabolic activity called persister cells, multi-species biofilm, and facilitation of horizontal gene transfer (HGT) among bacteria (Ehrlich et al., 2010; Lehman and Donlan, 2015; Koo et al., 2017).

Biofilm eradication is an enlarging problem in medicine, agriculture, and the food industry. The Center for Disease Control and Prevention (CDC) estimates that even more than 65% of all chronic bacterial infections are caused by biofilm forms of pathogens (Amankwah et al., 2022). One of the novel antimicrobials is lactoferrin, mammalian transferrin with antimicrobial activity, which binds iron, preventing bacteria from using this metal. Another strategy is using molecules that inhibit the mechanisms of the QS system by suppressing signal generation, distribution or blocking signal receptors, and signal responses (Myszka and Czaczyk, 2010). The potential use of substances that influence the structure and work of efflux pumps, which are responsible for removing antibiotics from the bacterial cell, e.g., peptidomimetics, has also been investigated.

The possibility of using phages and phage-derived enzymes to combat bacteria in biofilm structures is also being explored. Furthermore, combination therapy using phages and/or phage-derived products with other antimicrobial agents, including antibiotics, nanoparticles, and antimicrobial peptides, is auspicious. Such a solution could be widely used in medicine to treat severe cases and the broadly understood industry (Herce-Ros et al., 2021; Srinivasan et al., 2021; Tanaka et al., 2021; Amankwah et al., 2022).

Polymicrobial biofilm

Mixed biofilms occur in many natural environments, e.g., the oral cavity, where many microorganisms form dental plaques, intestines, or vaginas. Certain multi-species biofilm-related diseases can arise when a single pathogen is introduced into an existing microbiome, leading to dysbiosis or when opportunistic pathogens become virulent due to environmental imbalances. Dysbiosis can develop gradually or rapidly and often leads to chronic destructive inflammation. Other situations occur when one pathogen first adheres to the infection site as first and prepares the environment for another. The initial pathogen

that adheres to the surface may influence the subsequent bacterial cell selection and, consequently, the final composition of biofilm. It is called coaggregation and may occur when the secondary colonizer binds to specific molecules on the surface of a first one or several bacteria coordinate among themselves and favor some phenotypic changes that lead to the coaggregation on biofilms (Rickard et al., 2003; Peters et al., 2012; Szafrański et al., 2017). Moreover, due to the recruitment of a new species, the gene pool is broadened, and it helps control and regulate the survival mechanisms of individual members, such as adhesion, stimulation of host cellular senescence mechanisms to prevent the shedding of bacteria, and the production of plasma exudate for nutrition through local inflammation (Anju et al., 2022).

The interactions between microbes are complex and involve competition for space and nutrients. The biofilm community's physiology and function often change and are regulated by various interspecies interactions. Bacterial species are organized into different spatial forms based on their type: interspecific segregation, coaggregation, and stratification (Liu et al., 2016; Anju et al., 2022). Microorganisms grouped in one community may act synergistically, antagonistically, or be indifferent to each other. Cooperation between bacteria facilitates their adhesion and growth of, resistance to antimicrobial agents, virulence, exopolysaccharide production, and protective properties of the whole biofilm.

Moreover, the exchange of nutrients and metabolic products may occur in some species' relationships. For example, *Fusobacterium nucleatum* and *Prevotella intermedia* produce ammonia, which increases the pH and creates an environment suitable for the growth of *Porphyromonas gingivalis*. Another example is *Pseudomonas aeruginosa*, which produces substances that protect *Staphylococcus aureus* from aminoglycosides (Wolcott et al., 2013; Anju et al., 2022). The opposite behavior is observed when antagonistic interaction occurs. Then, one microorganism inhibits or kills the competing species, ensuring itself to avail available space, energy sources, and nutrients. Competition can be exploitative and involves the superiority of energy utilization or interference that produces compounds preventing other species' growth (Mgomi et al., 2022).

Multi-species biofilms can also be characterized by the distribution of microorganisms within the matrix. Microorganisms may coexist in separate microcolonies, with limited interactions, in one style of organization. Another style is characterized by a thoroughly mixed arrangement where cells from different species randomly coexist throughout the biofilm. One species forms the bottom layer in the third organizational structure, while the second species places on top (Mgomi et al., 2022). Another scheme is frequently observed in bacteria–fungi biofilms where hyphae form a scaffold that carries bacteria cells (Bernard et al., 2020; Roszak et al., 2022). Different structures of biofilms generate different interactions between species and mechanisms of cellular responses for therapies.

Biofilm-related chronic infection is frequently polymicrobial. Coexisting in multi-species communities increases genetic material exchange between cells, metabolic cooperation, development of antibiotic resistance, niche optimization, host immune system modulation, and virulence induction (Kifelew et al., 2019; Mgomi et al., 2022). Creating a standard matrix on tissues or medical devices is a characteristic of population virulence, making the behavior of polymicrobial societies distinct from mono-species. These societies can alter their physical properties in response to the environment and evolve through mutation to better adapt to their surroundings (Ehrlich et al., 2010). Moreover, additional pathogens can be integrated into the biofilm, and the primary ones can mutate to improve the interaction with other resident species, producing a more stable and productive community. All these properties cause more severe disease symptoms than mono-species infections.

One of the biggest problems associated with polymicrobial infection is increased resistance to antimicrobial agents, which might be higher than in mono-species biofilm. It is caused by the extensive diversity of EPSs produced by heterogeneously distributed bacteria that disturb drug penetration (Topka-bielecka et al., 2021). Moreover, some bacteria and fungi can produce polysaccharides or other substances that protect themselves or cells of partner species from antibiotics and antifungal agents. Another threat is interspecies HGT, which results in gene exchange between evolutionarily distant species. This may create bacteria and fungi with different phenotypes with new features that may increase their virulence and drug resistance.

Biofilm-associated polymicrobial communities are responsible for many diseases, e.g., bone infections and osteomyelitis, gall bladder disease, various chronic middle-ear disease processes, and chronic rhinosinusitis, chronic infections of the urogenital systems, e.g., bacterial vaginosis, dental infections, tonsillitis, surgical site infections, chronic non-healing wounds such as venous and diabetic ulcers, pressure sores, and burn injuries, respiratory infections, e.g., cystic fibrosis and medical device-related infection (Ehrlich et al., 2010; Peters et al., 2012; Szafrański et al., 2017; Iszatt et al., 2021; Uyttebroek et al., 2021). Some of these diseases were subjected to phage therapy. In addition, many scientists investigated various possibilities for phage treatment in *in vitro* research.

Bacteriophages and mechanisms of biofilm combating

Bacteriophages (phages) are viruses that infect bacteria and cannot multiply outside their host cells. Phages were discovered independently by Frederick Twort and Felix d'Hèrelle over 100 years ago and are the most diverse and numerous life forms on the earth. They show high host specificity, recognizing their host at the species and even strain level due to presence of characteristic receptors on the surface of the bacterial cell (Drulis-Kawa et al., 2015; Atshan et al., 2023). The use of bacteriophages is extensive. It covers many areas of life, e.g., medicine and veterinary (phage therapy), food industry (disinfectants of surfaces), agriculture (plant growth promoters), biotechnology and pharmacy (nanocarriers of drugs, biosensors, or diagnostic molecules), and diagnostic (phage typing) (Cowley et al., 2015; Drulis-Kawa et al., 2015). Currently, phages are classified by the European Union (EU) as medical products and by the Food and Drug Administration (FDA) as drugs. Good manufacturing practice (GMP) must be implemented during phage particle production. Nevertheless, all clinical trials are conducted as a therapy of a last chance according to Article 37 of the Declaration of Helsinki and need the permission of the ethical commission. The preparation of consistent legislation regarding the usage of phages in medicine is still ongoing (Patey et al., 2019).

The rate at which bacteria acquire antibiotic resistance is alarming, and the current epidemiological situation requires the search for alternative methods of combating bacterial infections. One of the options is to use bacteriophages (Iszatt et al., 2021). The usage

of phages has many advantages, e.g., rapid clearance from organisms, self-propagation in the site of infection, host specificity, opportunity to make a genetic modification, easy isolation, stability, and relatively low-cost production (Łubowska et al., 2019; Mgomi et al., 2022). The right phage must be selected carefully because not all have good therapeutic results. When choosing phages, some rules should be followed: specificity to target bacteria, lytic activity, and the lack of genes encoding bacterial virulence factors, antibiotic resistance products, and toxins. Only fully sequenced bacteriophages can be used for treatment in medicine. Another concern about phage therapy is to optimize the dosage of virions and the method of administration to provide good delivery to the site of infection (Morrisette et al., 2019). The pharmacokinetics of phages are complicated due to their ability to self-replicate. After killing all pathogenic bacteria, the phages are removed from the body as they cannot multiply in eukaryotic cells. In addition, if selected carefully, phages are safe for the human microbiome (Sartini et al., 2021). On the other hand, they may be neutralized by the host's immune system, removed from the body too quickly, and bring no profit. Another issue from the immune system might be an allergic reaction that may limit the scope of possible use of bacteriophages. Unfortunately, bacteria have developed multiple resistance mechanisms to phages (e.g., modification and blockage phage receptors on the bacterial surface), and even though phages have an equally impressive assortment of tools to overcome this resistance, it is better to use a cocktail of phages (Chegini et al., 2021). Notably, phage resistance observed *in vitro* may not necessarily translate to *in vivo* conditions. This discrepancy arises from the fact that the most prevalent resistance mechanisms often involve alterations in the cell surface that untenable host infection by the phage (Park et al., 2014; Iszatt et al., 2021). Another issue is that phage therapy could release bacterial endotoxins during bacterial cell lysis, which occurs as an effect of phage infection.

Next, to phages themselves, lytic enzymes that they produce are also considered as treatment factors. Bacteriophages synthesize enzymes such as peptidoglycan hydrolases, holins, and endolysins, which allow to release progeny virions by destroying bacterial cells walls (Sousa et al., 2023). Based on their mechanism of action, we can divide them into hydrolases and lyases. Both groups can degrade polysaccharides, including capsular polysaccharides (CPSs), lipopolysaccharides (LPSs), O-polysaccharides, or exopolysaccharides (EPSs), and sometimes polypeptides and lipids (Topka-bielecka et al., 2021). Endolysin can induce lysis from within as an antimicrobial agent active against pathogens. This refers mainly to Gram-negative bacteria, which need to treat with additional factors, e.g., holins that allow the endolysin to move through the cytoplasmic outer membrane and reach the peptidoglycan layer (Mgomi et al., 2022). Other phage enzymes—depolimerases, can be tail-spike proteins with the enzymatic domain or occurring as free molecules. Phage-delivered enzymes are usually unique and species-specific. However, sometimes enzymes can show activity across a broad spectrum between strains and species (Chegini et al., 2021). Treatment of polymicrobial communities usually requires several different enzymes or combined therapy. Bacteria rarely evolve resistance to lysins because they attack sites on the peptidoglycan cell wall critical to bacterial viability. Nevertheless, combining phage lysins and antibiotics, phages and other agents, or the production of genetically engineered enzymes may be more effective in infection elimination.

Lytic phage can be an effective weapon in the fight against biofilm, both in the context of preventing its formation and its eradication. The attempts to use phages as prevention factors include coating urinary catheters and disinfectants in hospital or industry environments (Curtin and Donlan, 2006; Lehman and Donlan, 2015; Melo et al., 2016; Santiago and Donlan, 2020). The activity of phages in mature biofilm depends on the bacteria growth phase, placement, coaggregation with other cells, nutrient availability, access to receptors, and diffusion capacity. Phages can be used not only in biofilms of multi-bacteria species but also in bacteria–yeast ones. *P. aeruginosa* infecting phage Pf4 can inhibit *Candida albicans* biofilm formation, possibly by sequestrating iron (Nazik et al., 2017; Pohl, 2022). Phages act differently from antibiotics. They produce enzymes, e.g., depolymerases (DP), that can destroy biofilm matrices made of polysaccharides, including EPS or alginase, breaking down the alginate matrix produced by *P. aeruginosa* (Peters et al., 2012; Santiago and Donlan, 2020). Moreover, phages can stimulate the host bacteria to produce EPS-degrading enzymes and proteases that degrade bacterial capsules. Phages oppositely to antibiotics can degrade bacteria that manifest low metabolic activity due to nutrient depletion. Another mechanism that helps overcome the matrix is to diffuse through water channels or to adsorb to motile bacteria and "have a ride" to the target site (Kifelew et al., 2019; Amankwah et al., 2022; Atshan et al., 2023). These actions collectively enhance the effectiveness of phages in combating biofilms. Initially, they facilitate the penetration of phages, allowing entry into the biofilm for subsequent replication within bacterial cells. The elevated bacterial density within biofilms significantly amplifies phage infection, leading to the release of new virions. Even when targeting cells with reduced metabolic activity, lytic phages prove effective by releasing intracellular materials. This release stimulates bacterial metabolism, ensuring sustained efficacy (Amankwah et al., 2022). Basting an expanded host range, polyvalent phages emerge as valuable assets in disrupting polymicrobial biofilms.

Phages also exhibit adaptability during isolation, potentially enriched by employing multiple bacterial hosts rather than a singular one. Additionally, an alternative strategy involves leveraging phages as quorum quenchers. Some phages eliminate bacteria conventionally and produce enzymes that disrupt bacterial signal molecules, providing a multifaceted approach to biofilm intervention (Kifelew et al., 2019; Santiago and Donlan, 2020).

Microbial communities have mechanisms of protection from phages that affect phage ability to adsorb, penetrate, diffuse, and proliferate in biofilm. The ability of biofilm to resist phage invasion depends on its age, shape, structure, and morphology. Bacteria can evolve to be insensitive to phage by changing their phenotypes in response to heterogeneous environments. *P. aeruginosa* may transform into a pili-defective variant to avoid infection of phages that use these structures as their receptors (Yamamoto et al., 2021). Biofilm matrix comprises many bacterial enzymes, e.g., amidases and peptidases, that may inactivate phages. Moreover, in deeper biofilm layers, more dead cells occur, and phages may adsorb to them without any benefits for therapy. Molecules can also catch virions in the matrix (Pires et al., n.d.). One of the ways of bacteria defense is the production of systems that interfere with phage nucleic acids, e.g., clustered regularly interspaced short palindromic repeats (CRISPR)–Cas9 (Yang et al., 2020). Bacteria may also prevent phage DNA integration by a superinfection exclusion system or use an abortive infection system

to block the synthesis of phage particle compounds (Pires et al., n.d.). Another protection is related to hiding binding phage receptors by the production of curli polymer (CsgA) as extracellular fibers that curtain bacterial cells (Vidakovic et al., 2017; Santiago and Donlan, 2020).

To intensify the action of phages, they can also be used with various groups of antibiotics (phage-antibiotic synergy (PAS) phenomenon). However, not every drug acts synergistically with selected phages and every combination should be checked in *in vitro* studies. For example, the synergistic effect may arise from the stimulation of lytic phage development in the presence of beta-lactam antibiotics. Bacteria under beta-lactam stress change their morphology, facilitating phage assembly and increasing bacterial sensitivity to phage lysins (Comeau et al., 2007; Chegini et al., 2021). Another mode of action of phages is to interfere with bacterial efflux pumps, which increases the sensitivity to various drugs (Chan et al., 2016). Bacteriophages can also be combined with disinfectants such as chloride, hypochlorite, or quaternary ammonium compounds and enzymes, e.g., polysaccharides depolymerases. In addition, in the case of a biofilm with a heterogeneous structure, it is possible to use a phage cocktail composed of several bacteriophages showing bacteriolytic activity against various bacterial pathogens (Comeau et al., 2007). Another alternative to enhance phage penetration through the matrix is debriding biofilm mechanically before phage treatment (Pires et al., n.d.).

Another way to improve phage performance is to modify their genome or synthesize novel ones (Javed et al., 2019). Modified phages may have inserted gene coding for additional exopolysaccharide-degrading enzymes for better biofilm penetration. Bacteriostatic phages can be changed to suppress the DNA repair mechanism, or overexpression of sensitizing proteins, and to disrupt the cell–cell communication between the bacteria in the biofilm. Another target for phage engineering is to use phages as a modulators of antibiotic resistance or to make it possible to reach intracellularly bacteria present in eukaryotic cells (Hagens et al., 2004; Lu and Collins, 2007, 2009; Edgar et al., 2012; Pei and Lamas-Samanamud, 2014). Since sometimes bacterial lysis leads to release toxins and pro-inflammatory products, phages can be engineered to be toxic for bacteria but not lytic for their host (Szafrański et al., 2017). The possibilities of degrading polymicrobial biofilm using phage-mediated methods are presented in Figure 1.

Bacteriophages as a component of multi-species communities

Bacteriophages should be recognized as a potent tool against pathogenic bacteria and integral components of healthy microbiomes, including those in the oral, intestinal, or vaginal environments. Phages interact with commensal bacteria, fungi, and chemical compounds and contribute to microbial communities assembly, stability, and function. They contribute to biofilm formation as extracellular DNA release through phage-mediated cell lysis may induce mobile genetic element transfer between microbes which, in turn, triggers a response of stabilizing the biofilm matrix (Amankwah et al., 2022). Some phages and their hosts developed reciprocal predator–prey relationships, e.g., in the intestine, phages may promote the evolution of bacterial resistance to phages in response to infection (Duerkop, 2018). Furthermore, phages may bind to mucin glycoproteins, providing phage-mediated antibacterial protection of animal mucosal surfaces (Barr et al., 2013).

Bacterial and phage composition in the intestine depends on diet and may drastically change during infection or other diseases. Increased or changed phage dsDNA levels were noticed during inflammatory bowel disease and type 1 diabetes in children (Zhao et al., 2017; Duerkop, 2018). Phages may stably multiplicate in their host for weeks but not lead to the elimination of pathogens. For example, enteroaggregative *Escherichia coli* (EAEC) and its phages may coexist without resolution, linked to persistent colonization and prolonged diarrhea (Maura et al., 2012). Beyond the intestine, in different niches, the phageome (bacteriophage community in the niche) of the bacterially infected site may be distinct from the healthy one, e.g., during cystic fibrosis (*CF*) (Reece et al., 2021). Phages, as a component of the polymicrobial community, may cooperate with the mammalian immune system and actively eliminate bacteria from the lungs during infection. Oppositely, *P. aeruginosa* prophages can stabilize biofilm in the lungs by promoting attachment to lung mucus and restricting the dispersal of cells from the biofilm. Moreover, phages may decrease the pro-inflammatory response of the immune system and lead to chronic infection (Duerkop, 2018). In another niche, lysogenic phages may modulate the number of vaginal lactobacilli during bacterial vaginosis (Jung et al., 2017). In addition, the taxonomic composition of phages may change during infection, e.g., chronic wound virome is more diverse than contralateral skin, which may influence microbial community and impact healing outcomes (Verbanic et al., 2022).

Elimination of pathogens from polymicrobial biofilm by phages

Numerous researchers explore phage therapy as a potential solution in the era of limited options for treating antibiotic-resistant bacterial infections. Various approaches are investigated, for example, using phages to eradicate mono-and multi-species biofilm, prevent biofilm formation, or change the composition of multi-species biofilm by removing only the harmful species. The *in vitro* studies implementing phage therapy and the research results employing various models are summed up in Table 1.

Mixed therapies based on phages or phage-delivered enzymes

Even though phages occurred to be effective to some point in biofilm-forming prevention and eradication of mature polymicrobial biofilm, some limitation of phage therapy must be overcome to achieve fully effectiveness. The main problems are acquiring phage resistance by bacteria in polymicrobial biofilm, reaching target bacteria in this complex structure, or selecting phages for all pathogens in biofilm. The solution might be combined therapy based on phages mixed with antibiotics, nanoparticles, other substances, or using phage-delivered enzymes with different properties than phages.

Different approaches to using phage-antibiotic synergy (PAS) therapy are listed in Table 2. The selection of good phage-antibiotic pair is strictly individual to the bacterial strain and case (Grygorcewicz et al., 2023). However, the effort is worth it and brings better results

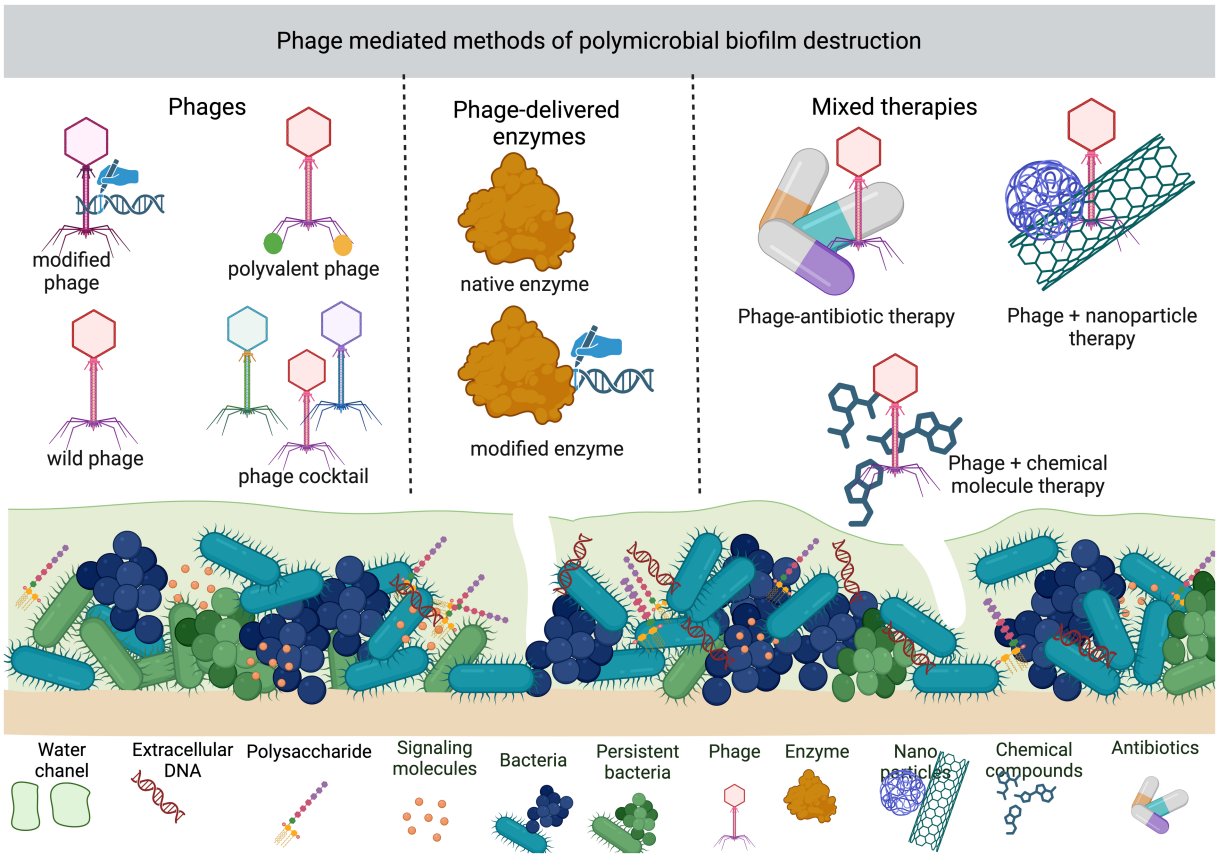

FIGURE 1
Methods of disturbing polymicrobial biofilm by phage-mediated methods.

than monotherapy. Phage may prevent the development of antibiotic-resistant minority bacterial populations, and conversely, antibiotics may stimulate phage infection, changing the phenotype of the target host, and phages may interfere with drug-resistant mechanisms, making bacteria more vulnerable (Comeau et al., 2007; Chan et al., 2016; Dickey and Perrot, 2019; Chegini et al., 2021). In many cases, PAS is necessary for successful therapy due to its better ability to degrade biofilm complex. At the same time, more than one factor is applied and all of them present different mechanisms of action (Roszak et al., 2022). Phages are considered more effective against biofilm due to the production of polysaccharide depolymerases which loosen matrix structure and help antibiotics reach the bacteria cell surface. Another mode of action is the lysis of cell from exterior parts of biofilm which results in uncovering the deeper layers of cells, and giving them access to nutrients and oxygen. This makes bacteria more metabolically active and more susceptible to an antibiotic (Park et al., 2017). The effectiveness of such therapy also depends on the dosage of antibiotics and phages, time and order of administration, adsorption rate, burst size, latent period, and external physical factors such as pH and temperature (Morrisette et al., 2019).

Another approach is to combine phages with nanoparticles. That solution may enhance phage penetration through biofilm. Moreover, nanoparticle migration in matrix might be modulated by a magnetic field in *ex vivo* models. Li et al. (2017) investigated how polyvalent phages (PEL1) immobilized onto Fe_3O_4-based magnetic colloidal nanoparticle clusters (CNC) coated with chitosan (PEL1-CS-Fe3O4) penetrate *P. aeruginosa/E. coli* dual-species biofilm. The complex penetration was facilitated under a small magnetic field (660 gauss), leading to better plaque formation capability of PEL1 and removal of 88.7 ± 2.8% of the biofilm formed on a glass surface after 6 h of treatment. The usage of such a particle complex physically disrupts the biofilm and mitigates phage dilution, which, in turn, allow to keep a high concentration of phages and facilitate phage tail fibers exposition to the hosts (Li et al., 2017). Another study where phages were covalently conjugated with magnetic CNCs shows that this approach is noteworthy. Yu et al. (2019) used phages PEB1 or PEB2 conjugated with CNCs of different sizes to combat *P. aeruginosa/ E. coli* dual-species biofilm and *P. aeruginosa/E. coli/B. subtilis* and *Shewanella oneidensis* multi-species biofilm. Smaller complexes disrupted the biofilm bottom layer and detached the biofilm within 6 h with efficiency of 98.3 ± 1.4% for dual-species biofilm and 92.2 ± 3.1% for multi-species biofilm. Larger complexes were less effective, implying that the size of nano-phage complex matters (Yu et al., 2019). It was reported that magnetic field might influence bacteriophage development. Phages T4 for *E. coli* and vB_SauM_A for *S. aureus* exposed to a rotating magnetic field enhance their adsorption and propagation rate (Struk et al., 2017; Konopacki et al., 2020; Grygorcewicz et al., 2022). In addition, a magnetic field might modulate the metabolism of bacteria and other microorganisms (Jabłońska et al., 2022).

In addition to antibiotics and nanoparticles, other chemical compounds or groups of compounds might be combined with phages

TABLE 1 Examples of phage treatment of polymicrobial biofilms in *in vitro* and *in vivo* studies with models.

No.	Pathogens	Aim of the study	Phages used	Experimental model	Outcome	References
1.	*S. aureus* IPLA16/*Lactobacillus plantarum* 55-1 or *Lactobacillus pentosus* A1 and B1 or *Enterococcus faecium* MMRA	Elimination of *S. aureus* from dual-species biofilm	Phage phiIPLA-RODI against *S. aureus*	biofilm formation in 96-well plates for 5 or 24 h at 32°C or 37°C, then phage treatment: 10^7, 10^8, or 10^9 PFU/well for 4 h in nutrient limitation conditions; BIOFILM formation for 5 h, then phage treatment 10^6 or 10^9 PFU/well for 18 h in nutrient-rich conditions	• 5-h treatment with 10^9 PFU/Well Preparation: o Decreased the biomass of *S. aureus-L. plantarum* and *S. aureus-E. faecium* biofilms by 31 and 67%, respectively o In nutrient limitation conditions, *S. aureus* cell counts were reduced by 0.8 and 0.7 $\log_{10}$ units • 24-h treatment with 10^9 PFU/Well Preparation: o Resulted in an 18 and 63% decrease in the biomass of *S. aureus-L. plantarum* and *S. aureus-E. faecium* biofilms, respectively o In nutrient limitation conditions, 0.4 and 0.6 $\log_{10}$ units reduced *S. aureus* cell counts • Effects on *S. aureus-L. plantarum* Biofilm Biomass: o After treatment with a 10^9 PFU/well preparation, the biomass increased by 120% o Viable cell counts for *S. aureus* decreased by 2.0 $\log_{10}$ units, while counts for *L. plantarum* increased by about 2.3 $\log_{10}$ units in nutrient-rich conditions • Effects on *S. aureus-L. pentosus* A1 and *S. aureus-L. pentosus* B1 Biofilms: o The biomass of *S. aureus-L. pentosus* A1 biofilm decreased by 86% o Cell counts of *S. aureus* decreased by 2.9 and 1.8 $\log_{10}$ units after treatment with 10^9 and 10^6 PFU/well preparations, respectively o No significant difference in *S. aureus-L. pentosus* B1 biofilm biomass, but cell counts of *S. aureus* decreased by 1.7 and 0.7 $\log_{10}$ units after treatment with 10^9 and 10^6 PFU/well preparations, respectively, in nutrient-rich conditions • Phage Treatment Observations: o In all biofilms treated with a 10^6 PFU/well preparation, there were increases in phage particles, signifying phage multiplication o Conversely, those treated with a 10^9 PFU/well preparation exhibited no alterations in the number of viable phages	González et al. (2017)
2.	*S. aureus* IPLA1-rifR/*Staphylococcus epidermidis* LO5081	Dual-species biofilm eradication	Phage (phiIPLA-RODI) against *S. aureus* and phage (phiIPLA-C1C) against *S. epidermidis*	biofilm formation in 96-well plates for 24 h at 37°C, then phage treatment: 10^9 PFU/well separately or together for 4 h	• phiIPLA-RODI Treatment: o Reduced *S. aureus* by 4.27 $\log_{10}$ units o Reduced *S. epidermidis* by 2.66 $\log_{10}$ units • phiIPLA-C1C Treatment: o Reduced *S. aureus* by 3.23 $\log_{10}$ units o Reduced *S. epidermidis* by 2.64 $\log_{10}$ units • Mixture of Phages: o The combined use of phages did not enhance the bacterial count reduction compared to individual phages o Application of both phages resulted in higher reduction in biofilm biomass compared to individual phage treatments	Gutiérrez et al. (2015)

(Continued)

10.3389/fmicb.2023.1320345

TABLE 1 (Continued)

3.	*E. coli* MG1655/*P. aeruginosa* PAO1	Dual-species biofilm eradication	Phage λW60 (ATCC 97537) against *E. coli* and phage PB-1 (ATCC 15692-B3) against *P. aeruginosa*	biofilm formation on silicone rubber disks placed in flasks with LB medium and inoculated with *E. coli* and *P. aeruginosa* 10^6/mL for 2 days at 37°C with shaking, then phage treatment (MOI = 10) for 5 days with daily media refreshment	• *E. coli* and *P. aeruginosa* Levels in Biofilm: o Regardless of the presence of one or both phages, levels of *E. coli* and *P. aeruginosa* in the biofilm remained relatively constant • Phage Resistance Development: o *E. coli* demonstrated less resistance to its corresponding phage compared to *P. aeruginosa*	Kay et al. (2011)
4.	*S. aureus* KUB7/*P. aeruginosa* PAO1	Dual-species biofilm eradication	Phage cocktail AB-SA01 (J-Sa-36, Sa-83, Sa-87) against *S. aureus*; Phage cocktail AB-PA01 (Pa-193, Pa-204, Pa-222, Pa-223) against *P. aeruginosa*	biofilm formation in 96-well plates for 48 h at 37°C with shaking, then phage treatment: AB-SA01 9.1 $\log_{10}$ PFU/mL and AB-PA01 10.3 $\log_{10}$ PFU/mL	• Cell Reduction in Biofilm: o Treatment resulted in a similar reduction in cell numbers for both *S. aureus* and *P. aeruginosa* compared to individual phage cocktails • Specific Reduction Levels: o When only AB-SA01 was applied: 1.6 $\log_{10}$ PFU/mL o When AB-SA01 + AB-PA01 were applied together: 1.2 $\log_{10}$ PFU/mL o When only AB-PA01 was applied: 2.5 $\log_{10}$ PFU/mL o When AB-SA01 + AB-PA01 were applied together: 2.1 $\log_{10}$ PFU/mL	Kifelew et al. (2020)
5.	*P. aeruginosa* clinical isolates/ *Proteus mirabilis* clinical isolates	biofilm formation prevention on urinary catheter	Phage cocktail (φPaer4, φPaer14, M4, 109, φE2005-A, φE2005-C,) against *P. aeruginosa*; phage cocktail (φPmir1, φPmir32, φPmir34, φPmir37) against *P. mirabilis*	Flowing catheter reactor model. Hydrogel-coated Foley catheters were pretreated with one or both cocktails (*P. aeruginosa* phages 10^9 PFU/mL; *P. mirabilis* phages 3×10^8 PFU/mL) for 1 h and challenged with 10^3 CFU/mL of bacteria pumped through the catheters at 1 mL/ min for 2 h in artificial urine medium, then sterile medium was pumped through the catheters at 0.5 mL/min for up to 4 days	• Effects of phage pretreatment on *P. aeruginosa* biofilm counts: o Phage pretreatment resulted in a reduction of *P. aeruginosa* biofilm counts by 4 $\log_{10}$CFU/cm^2 over 24 h and 48 h o The population was eliminated by 72 h, irrespective of the continued presence of phages • Effects of phage pretreatment on *P. mirabilis* biofilm counts o Phage pretreatment led to a reduction of *P. mirabilis* biofilm counts by 2 $\log_{10}$ CFU/cm^2 over 24 h and 48 h o The population continued to decline by 72 h, regardless of the presence of phages	Lehman and Donlan (2015)

(Continued)

10.3389/fmicb.2023.1320345

TABLE 1 (Continued)

6.	*E. coli* HU2117/*P. aeruginosa* EAMS2005-A	biofilm formation prevention on urinary catheter by *P. aeruginosa*	Phage φE2005-A against *P. aeruginosa*	Silicone catheter segments were exposed to *E. coli* 10^5 CFU/mL and phage 10^8 PFU/mL for 24 h at 37°C with shaking, then inoculated with *P. aeruginosa* 10^5 CFU/mL for 30 min and transferred to new flask with human urine for 24, 48, or 72 h at 37°C with shaking	• Adherence Reduction in 24 h Experiments: o *P. aeruginosa* adherence to catheters was almost 4 $\log_{10}$ units lower when pretreated with *E. coli* and phage compared to no pretreatment • Adherence Reduction in 72 h Experiments: o *P. aeruginosa* adherence to catheters was more than 3 $\log_{10}$ units lower with pretreatment compared to no pretreatment • Isolated *P. aeruginosa* Counts from Pretreated Catheters: o *P. aeruginosa* isolated from *E. coli* and phage-pretreated catheters was 3.1 $\log_{10}$ units lower at 24 h, 4.8 $\log_{10}$ units lower at 48 h, and 4.5 $\log_{10}$ units lower at 72 h compared to untreated catheters o *P. aeruginosa* was completely eradicated from catheters in eight out of 27 (30%) experiments when catheters had been pretreated with *E. coli* and phage	Liao et al. (2012)
7.	*S. aureus* Rumba – bovine mastitis isolate/*E. coli* KKH 001 – clinical isolate	Dual-species biofilm dispersal	Phage φ44AHJD against *S. aureus* and phage ϕX174 against *E. coli*	biofilm formation on glass covers for 96 h with daily media refreshment at 37°C with shaking, bacteria inoculum 10^8 CFU/mL; then phages treatment 10^8 PFU/mL (one or both phages) for 96 h at 37°C with shaking	• Untreated Control: o The biofilm intensity of the untreated control consistently decreased over a period of 192 h • Phage ϕ44AHJD Treatment: Initially, no visual difference in biofilm intensity was observed until 72 h o Subsequently, an increase of 26% in biofilm intensity was noticed after 96 h • Phage ϕX174 Treatment: o No visual difference in biofilm intensity was seen until 48 h o An increase of 28 and 39% in biofilm intensity was noticed after 72 h and 96 h, respectively • Combined Phage Treatment (ϕX174 and ϕ44AHJD): o No visual difference in biofilm intensity was observed o Biofilm intensity decreased to 6% after 96 h	Manoharadas et al. (2021)
8.	*E. coli* CECT 434 and CECT 515/*Salmonella Enteritidis* Ex2 and 269	Dual-species biofilm formation control	Phage Daica against *E. coli;* phage ϕ135 against *Salmonella*	biofilm formation in 96-well plates for 24 h at 37°C with shaking, then phage treatment: MOI = 1 for 24 h at 37°C with shaking	• *E. coli* 434 + *Salmonella Enteritidis* Ex2 Biofilm: o Reached the lowest numbers of viable cells at 8 h of treatment o *E. coli* 434 reduction: 1.15 Log_{10} o *Salmonella Enteritidis* Ex2 reduction: 0.88 Log_{10} • *E. coli* 515 + *Salmonella Enteritidis* 269 Biofilm: Reached the lowest numbers of viable cells at 4 h of treatment o *E. coli* 515 reduction: 1.07 Log_{10} o *Salmonella Enteritidis* 269 reduction: 2.42 Log_{10} at 8 h	Milho et al. (2019)
9.	*P. aeruginosa* PAO1/*E. coli* BL21 and TG1	biofilm formation prevention	Engineered T7 phage incorporating the acyl homoserine lactones AHL aiiA gene from *Bacillus anthracis* degraded AHLs	biofilm formation in 96-well plates, inoculated total number of CFU for the mixture of *P. aeruginosa* PAO1, *E. coli* TG1, and *E. coli* BL21 was 5×10^7, with phage (T7wt or T7aiiA) 10^4 PFU/mL for 24 h at 37°C	• Reductions in Biofilm: o T7aiiA phage caused reductions of the biofilm by 74.9 and 65.9% at 4 and 8 h post-plating, respectively o T7wt phage caused reductions of 23.8 and 31.7% at 4 and 8 h, respectively, compared to the no-phage control • Cell Counts at 8 h: o At 8 h, the control biofilm reached an average cell count per well of 8.5×10^8 CFU o T7wt-treated biofilm had an average cell count of 4.1×10^7 CFU o T7aiiA-treated biofilm had an average cell count of 1.2×10^7 CFU • PFU Counts in Biofilm: o PFU counts for T7wt and T7aiiA in the biofilm were 4.6×10^5 and 4.8×10^5 PFU, respectively	Pei and Lamas-Samanamud (2014)

(Continued)

10.3389/fmicb.2023.1320345

TABLE 1 (Continued)

10.	*P. aeruginosa* ATCC 10145 and *P. aeruginosa* PA01/*C. albicans* CECT 1472	Elimination of *P. aeruginosa* from dual-species biofilm	Phage ϕ IBB-PAA2 and phage ϕ BB-PAP21 against *P. aeruginosa*	biofilm formation in 24-well plates, inoculation 1.9×10^9 CFU/mL for *P. aeruginosa* ATCC 10145 or 1.1×10^9 CFU/mL for *P. aeruginosa* PAO1 and 1.1×10^7 CFU/mL for *C. albicans* for 24 h with media refreshment every 12 h at 37°C with shaking, then phage treatment (MOI = 1) for 24 h at 37°C with shaking	• *P. aeruginosa* Inhibition of *C. albicans*: o *P. aeruginosa* caused inhibition of the proliferation of *C. albicans* in mixed biofilm without phage • Phage Treatment on *P. aeruginosa*: o Both phiIBB-PAA2 and phiIBB-PAP21 phages achieved a 2.0 and 1.5 $\log_{10}$ reduction, respectively, in the number of viable cells of *P. aeruginosa* 6 h post-infection • *P. aeruginosa* Viability at 24 h post-infection: o At 24 h post-infection, an increase in the number of viable cells of *P. aeruginosa* was noticed o The increase was 1.5 $\log_{10}$ for *P. aeruginosa* ATCC 10145 strain and 1 $\log_{10}$ for *P. aeruginosa* PAO1 compared to the CFU numbers 6 h post-infection • *C. albicans* CFU Increase: o An increase of 0.5 and 1 $\log_{10}$ in the CFU of *C. albicans* was observed in the presence of *P. aeruginosa* PAO1 and ATCC 10145, respectively, at the 24 h time point	Pires et al. (2013)
11.	*Pseudomonas fluorescens* PF7 and/*Staphylococcus lentus* SL58	Dual-species biofilm eradication	Polyvalent phage ϕ IBB-SL58B against *S. lentus*, T7-like phage (phage ϕ IBB-PF7A) against *Pseudomonas*	biofilm formation on stainless steel slide for 72 h at 30°C with media refreshment every 12 h with or without shaking, then phage treatment of both or only phage ϕIBB-PF7A (both: 10^7 PFU/ mL)	• Dynamic Conditions: o The phage cocktail significantly reduced the 72-h-old biofilm by 4 orders of magnitude o Phages demonstrated high efficiency in disrupting biofilm structure under dynamic conditions • Static Conditions: o Phages showed less efficiency in destroying biofilm under static conditions, with only a 10-fold decrease observed after 4 h of phage treatment • Viable Cell Release: o Phage application to the biofilm induced the release of viable cells (103 CFU/mL) into the planktonic phase • Phage Replication in Dual Species Biofilm: o Both phages, fIBB-SL58B and fIBB-PF7A, replicated well in the dual-species biofilm o Infection with the *Pseudomonas* phage alone resulted in a 100-fold increase in the number of *S. lentus* cells in the planktonic phase compared to biofilm treatments with a cocktail of phages	Sillankorva et al. (2010)
12.	*Enterobacter cloacae* NCTC 5920/*Enterobacter agglomerans* industrial surface isolate *(Ent)*	Dual-species biofilm eradication	Phage ϕ1.15, 11,229 and Blackburn against *Enterobacter cloacae* NCTC 5920 and Philipstown phage against *Enterobacter agglomerans* strain *Ent*	biofilm formation on glass coverslips for 16 h at 30°C, then phage treatment of one or various phage cocktails (MOI = 0.1, 0.01, and 0.001) for 24 h	• When Phage ϕ 1.15 was added, there was a reduction of the susceptible strain by 4.0, 3.7, and 4.75 $\log_{10}$ CFU/cm^2 when MOI = 0.1, 0.01, and 0.001 were applied, respectively. The reduction of the unsusceptible strain was 3.2, 3.7, and 0.75 $\log_{10}$ CFU/cm^2 when MOI = 0.1, 0.01, and 0.001 were applied, respectively • When Phage Philipstown was added, the reduction of the susceptible strain was 2.9, 2.3, and 3.1 $\log_{10}$ CFU/cm2 when MOI = 0.1, 0.01, and 0.001 were applied, respectively. The reduction of the unsusceptible strain was 3.0, 0.4, and 0.5 $\log_{10}$ CFU/cm^2 for MOI = 0.1, 0.01, and 0.001 applied, respectively • When Phages ϕ 1.15 and 11,229 were added, there was a reduction of the susceptible strain by 5.0 $\log_{10}$ CFU/cm^2 when MOI = 0.01 was applied, and the reduction of the unsusceptible strain was 2.2 $\log_{10}$ CFU/cm^2 when MOI = 0.01 was applied • When Phages ϕ 1.15, 11,229, and Blackburn were added, there was a reduction of the susceptible strain by 5.7 log10 CFU/cm2 when MOI = 0.01 was applied, and the reduction of the unsusceptible strain was 2.1 $\log_{10}$ CFU/cm^2 when MOI = 0.01 was applied (all data read from the original figures)	Tait et al. (2002)

(Continued)

10.3389/fmicb.2023.1320345

TABLE 1 (Continued)

13.	*P. aeruginosa* PAO1/*P. aeruginosa* PA14	Elimination by the phage of the sensitive strain from dual-species biofilm	Phage 352 against PAO1,	biofilm was formed as colony onto agar on membrane filter for 12 h at 37°C (PAO1 10^4 CFU/mL and PA14 10^5 or 10^6 CFU/mL) then filter was transferred to new plate with drop of phage 10^6 or 10^9 PFU/mL then incubated for 36 h at 37°C	• PAO1 population size was reduced in the phage treated mixed colonies. Microscopy revealed the absence of PAO1 cells from the edges of the colonies treated with phages, suggests that cell lysis occurred at the actively growing edges and not in the middle of the colony • Coculture colonies contained a lower infectious load (fewer phage per sensitive bacteria) compared to mono-culture colonies at the end of the experiment; phage could replicate less in the presence of PA14 • Phage resistance was much less likely to emerge in mixed colonies	Testa et al. (2019)
14.	*Cupriavidus metallidurans* 101480065–2, *Chryseobacterium gleum* 113330055–2, *Ralstonia insidiosa* 130770013–1, *Methylorubrum populi* 122620021–1, *Sphingomonas paucimobilis* 121220007–2, *Ralstonia pickettii* 113330051–2	Prevention of *S. paucimobilis* presence in multi-species biofilm; elimination of *S. paucimobilis* from multi-species biofilm	Phage ϕ Scott against *S. paucimobilis*	biofilm formation in 96-well plates for 24-96 h at 30°C, no shaking, then phage treatment with 2×10^4 PFU/mL either at 0 h, or 24 h post-inoculation	• The application of bacteriophage ϕScott at the beginning resulted in the absence of *S. paucimobilis* at 24 h of biofilm formation in mixed cultures • Phage treatment of pre-existing BIOFILM resulted in no substantial biofilm removal – 20–50 CFU reduction for *S. paucimobilis*	Thompson et al. (2020)
15.	*E. coli* AR3110/*Vibrio cholerae* N16961 (serogroup O1 El Tor)	Elimination of *E. coli* from dual-species biofilm	Recombinant T7 phages against *E. coli*	biofilm formation of *V. cholerae* and *E. coli* into the microfluidic chambers bonded to glass coverslips at a ratio of 2:1 for 48 h and then treated with phages 5×10^6 PFU/μL for 16 – 96 h	• After phage introduction, most *E. coli* cells lysed. Over the next 16 h, *E. coli* cells embedded on the bottom layers of *V. cholerae*-dominated cell groups largely survived phage exposure. Persisted *E. coli* was observed up to 144 h but did not appear to be active • After 16 h in the dual species biofilm, T7 infection could be seen proceeding partially into groups of *E. coli* embedded within *V. cholerae* biofilm, but a fraction of *E. coli* survived	Winans et al. (2022)
16.	*E. faecalis* Efa1/*E. faecium* C410	Dual-species biofilm eradication	Phage vB_EfaS-Zip against *E. faecium* and vB_EfaP-Max against *E. faecalis*	biofilm formation on collagen wound model (CWM) in 24-well plates for 48 h at 37°C with shaking, with daily media refreshment; then phage treatment 10^8 PFU/mL of each phage for 24 h	o Cell concentration was reduced by approx. 2.5 log CFU/mL after 3 h of infection, however phage resistance occurred and after 24 h of phage infection the reduction was only of 1.0 $\log_{10}$ CFU/mL	Melo et al. (2019)

(Continued)

10.3389/fmicb.2023.1320345

TABLE 1 (Continued)

17.	*S. typhimurium* ATCC 14028 and *E. coli* O157: H7	Dual-species biofilm eradication; biofilm formation prevention	Polyvalent phage STP55 against multiple serotypes of *Salmonella* and *E. coli*	biofilm formation in 96-well plate (for prevention): both bacteria inoculum 10^9 CFU/mL, phage concentration 10^8 PFU/mL, incubation for 6, 12, and 24 h at 37°C; (for eradication): both bacteria inoculum 10^9 CFU/mL, incubation at 37°C for 24 h, then phage treatment 10^8 PFU/mL, incubation at 37°C for 2, 6, and 8 h Spiked lettuce model: lettuce pieces were submerged in bacterial suspension (10^9 CFU/mL) for 2 min then dried and incubated for 24 h at 37°C, then phage treatment 10^8 PFU/mL for 10 min, dried and incubated for 2 h at 37°C	• Prevention: o the increase in the biomass of biofilm was suppressed in the presence of phage. After 6 h it was 48.6% lower and after 24 h it was 52.8% lower than in the control; cells count was lower than those of the control by 1.7, 1.1, and 1.3 $\log_{10}$CFU/well, respectively, at 6, 12, and 24 h • Eradication: o More than 46.2% of the biofilm was removed after 8 h of phage treatment • Spiked lettuce model: o After phage treatment, the structure of the biofilm changed: net-like matrix had a much flatter and looser structure, the dense structures were dispersed, and the matrix richness of the mixed cells was reduced, the dense structures were dispersed, and the matrix richness of the mixed cells was reduced	Zhu et al. (2022).
18.	*E. coli* K-12 (ATCC 700926)/*Pseudomonas. putida* F1 (ATCC 700007)/*Bacillus subtilis* 168 (ATCC 23857)	Elimination of *E. coli* from the multi-species biofilm	Polyvalent phage Pef1 against *E. coli* and *P. putida* or coliphage T4 against *E. coli*	biofilm formation in glass vials filled with quartz sand, each bacteria inoculum 10^5 CFU/mL, incubation for 24 h at 30°C with shaking, then media refreshment with bacteria and phage T4 or Pef1 at 10^6 PFU/mL, incubation for 5 days with daily media refreshment	o Pef1 was 20-fold more effective than T4 in suppressing *E. coli*, *E. coli* concentration was 1.3 orders of magnitude lower (4.7 $\log_{10}$CFU/mL) than in microcosms with T4 after 3 days in the presence of Pef1; Pef1 proliferated better than T4 o After Pef1 amendment, the density of the attached 5-day-old *E. coli* biofilm decreased by 93% to 4.51 $\log_{10}$ CFU/mg sand, with T4 it increased by 44% to 5.80 $\log_{10}$ CFU/mg sand	Yu et al. (2017)

(Continued)

10.3389/fmicb.2023.1320345

TABLE 1 (Continued)

19.	KPC+ *Klebsiella pneumoniae* (CAV1016)/*P. aeruginosa*, *Micrococcus luteus*, *Stenotrophomonas. Maltophilia*, *Elizabethkingia nopheles*, *Cupriavidus metallidurans*, and *Methylobacterium fujisawaense*	*K. pneumoniae* elimination from multi-species biofilm	Phage cocktail (SNP1_2017, SNP2_2017, SNP3_2017, RLS1_2017) against *K. pneumoniae*	biofilm formation on CDC biofilm reactor (CBR) p-trap model for 28 days; phage treatment for 2h at either 25°C or 37°C with the phage cocktail (10^9 PFU/mL) at 7, 14, and 21 day post-inoculation	o Phage treatment reduced *K. pneumoniae* viability by 1 $\log_{10}$ CFU/cm2 at 7 and 14 days (37°C) and 1.4 $\log_{10}$ and 1.6 log10 CFU/cm2 at 7 and 14 days, respectively (25°C), no significant reduction was observed at 21 day post-inoculation. Phage treatment had no significant effect on the biofilm heterotrophic plate counts at any time point or temperature. Supplementation with a non-ionic surfactant appears to enhance phage association within biofilm	Santiago et al. (2020)

to minimize formation and eradicate polymicrobial biofilm. Chhibber et al. (2015) tested how bacteriophages combined with xylitol will eradicate *K. pneumoniae/P. aeruginosa* dual-species biofilm formed on polycarbonate disks. *K. pneumoniae*-specific depolymerase-producing phage KPO1K2 and *P. aeruginosa* specific non-depolymerase-producing phage Pa29 led to 2.13 and 1.27 $\log_{10}$ CFU/mL reduction of *K. pneumoniae* and *P. aeruginosa* cell counts, respectively in 1-day-old biofilm. They obtained slightly worse results for 2-day-old biofilm. The authors emphasize that depolymerase-producing phage was crucial for matrix disruption. The addition of xylitol to the system significantly enhanced the antibiofilm activity of phages and caused complete elimination of *K. pneumoniae* both in 1- and 2-day-old biofilms and also 3.5 and 3.02 $\log_{10}$ CFU/mL reduction of *P. aeruginosa* in 1- and 2-day-old biofilm, respectively. Xylitol may diffuse into the biofilm and accumulate as a toxic, non-metabolizable sugar alcohol phosphate, thus inhibiting bacterial growth, or it can hinder stress proteins that arise in the biofilm (Ichikawa et al., 2008; Chhibber et al., 2015). An interesting approach was presented by Oliveira et al. (2018), who used chestnut honey bacteriophages (vB_EcoS_CEB_EC3a and vB_PaeP_PAO1-D) against *P. aeruginosa/E. coli* dual-species biofilm formed on polystyrene and porcine skin. Honey has antimicrobial properties associated with high osmolarity, low availability of water, hydrogen peroxide production, acidic pH level, and the presence of methylglyoxal. The results of using different combinations of phage and honey showed that *E. coli* cell number reduction in biofilm depends on the applied treatment time and honey concentration. In the case of *P. aeruginosa,* combined treatment brought better results than phage or honey alone, however, without presenting a synergy effect on the polystyrene model. *E. coli* elimination from dual-species biofilm formed on porcine skin model was the most effective using phage and 50% honey and led to 1.4 log reduction at 24h post-treatment. The combination of phage and honey acts synergistically in *P. aeruginosa* cell elimination at both concentrations (25 and 50%), leading to 2.2 $\log_{10}$ and 2.3 $\log_{10}$ higher cell reduction than the sum of phage and honey alone (Oliveira et al., 2018).

Phage-delivered enzymes are the next option to eliminate polymicrobial biofilm. Their main advantages are host specificity and easy matrix penetration and removal. Skillman and Sutherland (1999) proposed the usage of polysaccharide depolymerases isolated from a bacteriophage infecting *E. agglomerans* to degrade EPS in a dual-species biofilm formed with *K. pneumoniae*. Such treatment caused limited adhesion of *E. agglomerans* to *K. pneumoniae*, degradation of EPS, and effective removal of both species from the surface, even though the used enzyme was specific toward *E. agglomerans* only. This effect might have been caused by the proximity of both species or the larger contribution of *E. agglomerans* EPS in the mixed biofilm. Schuch et al. (2017) used bacteriophage lysin *CF*-301 and combined it with lysostaphin to target *S. aureus* and *S. epidermidis* in mixed biofilm formed on various surfaces (polystyrene, surgical mesh, and catheters). Dual-species biofilm was susceptible to disruption by *CF*-301 applied at concentrations down to 0.032 mg/L over 24h. The reduction of both species on catheter and surgical mesh reached over 90% and over 80% on 24-well polystyrene plates. The good enzymatic activity against both species is reasonable because they belong to the same genus. However, more than one protein should be used when more phylogenetically distant species form a mixed biofilm. This approach was investigated by Manoharadas et al. (2023), who used two engineered enzybiotics (BP404 5 mg/L and P16-17/100 5 mg/L)

TABLE 2 Examples of phage-antibiotic synergy therapy in combating polymicrobial biofilm in *in vitro* studies.

No.	Pathogens	Aim of the study	Phages used	Antibiotic used	Experimental model	Outcome	References
1.	*P. aeruginosa* PAO1/ *S. aureus* ATCC 25923	Dual-species biofilm eradication	Phage (EPA1) against *P. aeruginosa*	Gentamicin	biofilm formation in 24-well plates for 48 h at 37°C with shaking, Both bacteria 10^8 CFU/mL. Then one of the antibiotic concentrations (MIC or 8xMIC) and phage at MOI = 1 were added simultaneously for 24 h treatment or the second agent was added after 6 h	• In the control, *P. aeruginosa* and *S. aureus* cells, concentration was 1.4×10^9 CFU/mL and 2.3×10^5 CFU/mL, respectively • Gentamicin only (1 × MIC (4 mg/L) and 8 × MIC) reduced 3.3 orders-of-magnitude and 4.6 orders-of-magnitude of *P. aeruginosa* cells, respectively. Phage treatment reduced by 0.7 orders of magnitude of *P. aeruginosa* cells. None of the individual treatments showed an impact on the *S. aureus* population • The simultaneous treatments: phage-gentamicin 1 × MIC resulted in 4.1-orders-of-magnitude reduction of *P. aeruginosa* and 0.4 of *S. aureus*, phage-gentamicin 8 × MIC resulted in 4.6-orders-of-magnitude reduction of *P. aeruginosa* and 0.8 of *S. aureus* • Preliminary phage treatment (6 h) before gentamicin 1 × MIC reduced 6.3 orders-of-magnitude the *P. aeruginosa* population and had no impact on the *S. aureus* population. Phage-gentamicin 8 × MIC almost eradicated *P. aeruginosa* cells (approx. 7 orders-of-magnitude reduction) and reduced 2-orders-of-magnitude *S. aureus* population	Akturk et al. (2019)
2.	*P. aeruginosa* PAO1/*S. aureus* ATCC 25923	Dual-species biofilm eradication	Phage SAFA against *S. aureus* and phage EPA1 against *P. aeruginosa*	Gentamicin	biofilm formation in 24-well plates for 48 h at 37°C, with shaking Both bacteria inoculum 10^8 CFU/mL. Then treatment (various combinations of phages and gentamicin) biofilm formation on wound model - biofilm was treated with the antimicrobials (GEN 4 mg/L, phages MOI = 1); alone, in simultaneous (EPA1 + SAFA+GEN) or sequential combinations (first EPA1 + SAFA and then GEN with 6 h delay), then incubation at 37°C for 24 h	• Single-dose, wound model • 6 h treatment: Phage EPA1 treatment reduced the *P. aeruginosa* population by 1.5 log, phage SAFA did not reduce the *S. aureus* population, treatment with GEN reduced the *P. aeruginosa* population by 1.0 log and *S. aureus* by 0.9 log • 24 h treatment: Phage EPA1 treatment reduced the *P. aeruginosa* population by 1.5 log, phage SAFA did not reduce the *S. aureus* population, treatment with GEN reduced the *P. aeruginosa* population by 3.4 log and *S. aureus* by 1.7 log • When EPA1 + SAFA, followed by GEN 6 h later were applied, biofilm reductions of 4.8 and 2.3 log were observed for *P. aeruginosa* and *S. aureus*, respectively • Multiple doses, 24 well plate • A single dose of phages and GEN, phages alone, and GEN alone for 8 h resulted in a reduction of *P. aeruginosa* population by 0.8, 1.1, and 1.3 log, and *S. aureus* populations by 0.2, 0.8, and 1.0 log. The second dose led to biofilm reductions ranging from 1.1 to 5.0 log for *P. aeruginosa* and 1.6 to 6.8 log for *S. aureus* • The most effective reduction was obtained following multiple doses of EPA1 + SAFA+GEN, with a 6.2 log reduction for *P. aeruginosa* and 5.7 log for *S. aureus*	Akturk et al. (2023)

(Continued)

10.3389/fmicb.2023.1320345

TABLE 2 (Continued)

3.	*S. aureus* MRSA ATCC 37741/*S. epidermidis* ATCC 12228	Dual-species biofilm eradication	Phage type 92 (ATCC 33741-B) against *S. aureus*	Teicoplanin	biofilm formation in 96-well plates for 48 h at 37°C with shaking, then phage at MOI = 10 or teicoplanin (10 mg/L) or both agents treatment for 12 h	• In untreated mixed-culture biofilms, MRSA outcompeted *S. epidermidis* • The most effective treatment was phage alone: *S. aureus* reduction approx. 1.5 Log_{10} CFU/cm^2, *S. epidermidis* approx. 0.25 Log_{10} CFU/cm^2; teicoplanin alone: *S. aureus* reduction approx. 0.4 Log_{10} CFU/cm^2, *S. epidermidis* no reduction; combined therapy: *S. aureus* reduction approx. 1.05 Log_{10} CFU/cm^2, *S. epidermidis* no reduction (data read from the original figure) • *S. epidermidis* acquired increased tolerance to teicoplanin	Infect et al. (2016)
4.	*P. aeruginosa* PA01/*C. albicans* C11	Dual-species biofilm eradication	Phage Motto (NCBI accession number ON843697) against *P. aeruginosa*	Fluconazole, cefotaxime, ciprofloxacin, gentamicin, meropenem and tetracycline	biofilm formation in 96-well plates for 6 or 24 h at 37°C both microorganisms (10^5 CFU/mL), then phage (10^2 to 10^9 or 10^{12} PFU/mL) and fluconazole (2 to 128 mg/L) or cefotaxime, ciprofloxacin, gentamicin, meropenem, and tetracycline (0.5 to 128 mg/L) were added, incubation for 16 h	• The eradication of biofilm was impossible in the presence of phage alone or antibiotics alone • High phage and fluconazole concentrations reduced biofilm up to 30%, with 6 and 24 h biofilm samples, but full eradication was not observed • Phage had a positive impact on the removal of the dual-species biofilm in combination with the exposure to fluconazole • Even at the highest concentration of cefotaxime, ciprofloxacin, gentamicin, meropenem or tetracycline and highest phage titer tested, biofilms remained unaltered	Manohar et al. (2022)
5.	*S. aureus* ATCC 6538/*C. albicans* ATCC 10231	Elimination of *S. aureus* from dual-species biofilm	Phages vB_SauM-A and vB_SauM-D against *S. aureus*	Ciprofloxacin	biofilm formation in 96-well plates for 24 h at 37°C, then phages (10^7 PFU/mL) and ciprofloxacin (1 to 32 mg/L) were added separately or together	• The individual treatments with phage A or D or both lead to 50% reduction of biofilm specific activity and 67% reduction of *S. aureus* population; individual treatment with ciprofloxacin lead to 83–23% reduction of biofilm specific activity depending on concentration (32–1 mg/L) and 55% reduction of *S. aureus* population (ciprofloxacin 1 mg/L) • The combined treatment: the reduction of biofilm specific activity was 82 to 69% depending on ciprofloxacin concentration (32–1 mg/L) and 95% reduction of *S. aureus* population (ciprofloxacin 1 mg/L) • Presence of *C. albicans* lead to less *S. aureus* reduction in comparison to mono-species biofilm	Roszak et al. (2022)

(Continued)

10.3389/fmicb.2023.1320345

TABLE 2 (Continued)

6.	*P. aeruginosa* ATCC 27853/*S. aureus* (MRSA) ATCC 43300	Dual-species biofilm eradication	Phages Sb-1 and PYO	Ciprofloxacin	biofilm formation on porous sintered glass bead for 24 h at 37°C, 5×10^6 CFU/mL *S. aureus*, 5×10^3 CFU/mL *P. aeruginosa*; then phage treatment: simultaneously addition of PYO or Sb-1 + PYO or Sb-1 + PYO + sub-inhibitory concentration of ciprofloxacin; staggered exposure to PYO or PYO + Sb-1 for 3, 6, 12, or 24 h followed by a 24 h-exposure to sub-inhibitory concentrations of ciprofloxacin	• Delay on the heat production was observed when PYO was applied, and it was enhanced when Sb1 was added, no complete inhibition of the biofilm was observed • A reduction of more than 2 $\log_{10}$ of MRSA and 1 $\log_{10}$ of *P. aeruginosa* cells was observed after exposure to PYO • The combination of PYO + Sb-1 showed a complete eradication of MRSA cells and no substantial reduction of *P. aeruginosa* cells • PYO+ ciprofloxacin 16–64 mg/L decreased heat flow production reduced over 90% • PYO + Sb-1 + ciprofloxacin 4 mg/L reduce over a 90% of the heat flow production • The highest anti-biofilm activity was observed when the antibiotic (2 mg/L or 1 mg/L) was added after 12 h of pre-exposure to either PYO or PYO + Sb-1, no presence of bacteria on the beads was observed	Tkhilaishvili et al. (2020)

against a dual-species biofilm formed by *S. aureus* and *E. faecalis* in an inert glass surface. The chimeric protein P16-17/100 was constructed, linking domains from endolysin P16 and minor tail protein P17 from phage φ44AHJD. Protein cocktail usage resulted in significant biofilm dispersal (absorbance OD575 reduction from 0.7 to less than 0.1) and more than 90% reduction of both species cells embedded in the matrix after 16 h of treatment.

Bacterial vaginosis (BV) is a common vaginal infection caused by anaerobic pathogens such as *Gardnerella vaginalis*, *Fannyhessea vaginae*, and *Prevotella bivia*, usually forming a polymicrobial biofilm. Therapy of BV usually relies on metronidazole and clindamycin treatment. However, sometimes, these antibiotics do not lead to the complete eradication of pathogens. The curation of biofilm-associated BV is challenging. Therefore, Landlinger et al. (2021) generated engineered endolysin Pm-477 encoded on *Gardnerella* prophages as an alternative treatment. The endolysin actively killed *G. vaginalis* in mono- and dual-species communities with *Lactobacillus crispatus*. Moreover, the efficacy of PM-477 was tested by fluorescence *in situ* hybridization on vaginal samples of 15 women with BV. Endolysin eliminated *Gardnerella* bacteria in 13 cases and physically dissolved the biofilm matrix. The remaining vaginal microbiome remained unaltered. Castro et al. (2022) also tested previously synthesized engineered phage endolysin PM-477 to disrupt dual-species biofilms composed of *G. vaginalis/F. vaginae* or *G. vaginalis/P. bivia* in *in vitro* study. In all dual-species biofilms, endolysin prevented biomass accumulation (from 24 to 48 h) but did not reduce existing ones. In *G. vaginalis/F. vaginae,* biofilm cell viability reduction was not obtained, but in *G. vaginalis/P. bivia,* biofilm reduction reached a 3 $\log_{10}$ CFU. The phage endolysin had high anti-*G. vaginalis* and slightly anti-*P. bivia* but no anti-*F. vaginae* activity.

Johnston et al. (2023) also investigated how endolysin therapy against *G. vaginalis* biofilm works *in vitro.* In their study, a four-species biofilm made of *G. vaginalis, F. vaginae, P. bivia*, and *Mobiluncus curtisii* was treated using an anti-*Gardnerella* endolysin (CCB7.1) as this species is the most abundant in polymicrobial community. The reduction of live cells of *G. vaginalis* reached 1–2 $\log_{10}$ after 24 h of endolysin treatment in all tested concentrations (128, 256, and 512 μg/mL) and a slight reduction of *M. curtisii* when the highest concentration of endolysin was applied. Worth mentioning is that CCB7.1 was ineffective against commensal lactobacilli. Novel endolysins against *G. vaginalis* are still being searched. Arroyo-Moreno et al. (2022) identified 84 diverse anti-*Gardnerella* endolysins and selected 5 (CCB2M94_8, CCB7.1, CCB8.1, CCB2.2, and CCB4.1) with the best properties. All of them could disturb *G. vaginalis/Atopobium vaginae* dual-species biofilm in the concentration of 200 μg/mL and had no activity against commensal lactobacilli.

Bacteriophages in the fight against chronic infections

In vitro studies provide valuable data about phage therapy efficiency against polymicrobial biofilms. Research shows that phages themselves or in combination with antibiotics or other substances can reduce biofilm formed on various surfaces, e.g., polystyrene, glass, stainless steel, or silicone (urine catheters) (Curtin and Donlan, 2006; Carson et al., 2010; Kaźmierczak et al., 2022). Promising results from *in vitro* studies allowed to start more comprehensive clinical trials

using bacteriophages. Even though in some countries (Georgia, Russia, Poland) phage therapy has been used for many years, the Western world has only recently started the first attempts to treat patients with phages. Reported cases when phages or their enzymes were included in therapy refer to wound infections, bone infections, surgical site infections, etc.

Bone and joint infections are the hardest to cure and are usually related to post-traumatic or implant infections. Bacteria quickly form polymicrobial biofilm and can persist in osteoblasts or synovial cells, implicated in chronicity and recurrence, usually requiring heavy surgery with implant exchange. Bacteria mainly isolated from bone infections are *S. aureus*, coagulase-negative staphylococci, *Cutibacterium acnes*, *Streptococcus* spp., *Enterobacteriaceae*, and *P. aeruginosa* (Ferry et al., 2021). When antibiotics fail, phage therapy is proposed to patients.

Nir-Paz et al. (2019) successfully treated a 42-year-old male patient with a trauma-related left tibial infection caused by extensively drug-resistant *Acinetobacter baumannii* and multidrug-resistant *K. pneumoniae.* Patient with trauma was first treated with external fixation, irrigation, and debridement, plus left leg fasciotomies and a prolonged course of antibiotics: 6 weeks of piperacillin/tazobactam, initially followed by an 8-week course of meropenem and colistin. After 7 months of unsuccessful therapy, phages were included. The patient received a phage cocktail (ϕAbKT21phi3 and ϕKpKT21phi1 in concentration 5×10^7 PFU/ml each), colistin (4.5×10^6 units/bid), and meropenem intravenously. The first effect of curation was visible after a few days, and 8 months post-treatment, no bacteria were detected. Phage-antibiotic therapy saved the patient's leg from amputation. Onsea et al. (2019) provide further instances of successful phage therapy. The group developed a protocol for intraoperative phage application and postoperative use of a draining system. They reported three successful curation of patients with polymicrobial bone infection: Patient 1 (infection: the trauma of pelvis; bacteria: *P. aeruginosa, S. epidermidis*; antibiotics used beside phages: for 3 months, vancomycin, rifampicin, moxifloxacin; phage therapy: for 7 days, BFC1 phage cocktail contains phages against *S. aureus* and *P. aeruginosa* 10^7 PFU/mL); patient 2 (infection: the trauma of femur; bacteria: *P. aeruginosa, S. epidermidis*; antibiotics used in addition to phages: for 6 weeks, vancomycin, colistin, fosfomycin; phage therapy: for 10 days, BFC1 phage cocktail); patient 3 (infection: trauma of femur; bacteria: *S. agalactiae, S. aureus*; antibiotics used in addition to phages: for 3 months, vancomycin, clindamycin, moxifloxacin; phage therapy: for 9 days, BFC1 phage cocktail). After 8 or 16 months, no signs of infection were observed (patients 1 and 3), and patient 2 needed further treatment. Van Nieuwenhuyse et al. (2021) report the case of a 13-year-old patient who developed chronic polymicrobial biofilm infection of a pelvic bone allograft. *Clostridium hathewayi*, *P. mirabilis*, *Finegoldia magna,* and methicillin-susceptible *S. aureus* were isolated from the infectious site. Conventional therapy (intravenous antibiotics and surgical debridement) with anti-*S. aureus* phage treatment (BFC1 phage cocktail) *in situ* was implemented. At first, therapy led to marked clinical and microbiological improvement, but it failed to prevent a recurrence of infection later.

Difficult to treat and chronic bacterial infections can occur at different sites of infection. They are born by various bacteria that cannot be eliminated with antibiotic therapy due to the formation of polymicrobial biofilm and the possibility of cell survival (Morozova et al., 2018). Phage therapy was proposed in many cases, referring to polymicrobial infections. Püschel et al. (2022) reported a case of successful treatment of drive line infection acquired after left ventricular assist device (LVAD) implantation with a combination of antibiotics, debridement, and local bacteriophage treatment. *P. mirabilis* and *S. aureus* were isolated due to unsuccessfully treated surgically for a driveline phage therapy was used. Phage cocktail containing phages against *E. coli, S. aureus, P. aeruginosa, S. pyogenes, P. vulgaris,* and *P. mirabilis* (10^7 PFU) was applied to the site of infection. The wound was healing well; the patient received cotrimoxazole for 20 days. Afterward, only *S. aureus* was detected in the infection site, and further flucloxacillin treatment was applied. In a follow-up examination 8 months later, the primary site of infection was free from bacteria.

Another example might be considered a success. However, the patient died long after phage therapy. Rubalskii et al. (2020). present a case of 52-year-old patients with a prosthetic infection after aortic arch replacement. Implant drainage and bronchial lavage were infected with *S. aureus, E. faecium. P. aeruginosa,* and *E. faecium*. Following the ineffectiveness of antibiotic therapy, a combination of phages (10^8 PFU/mL of *Staphylococcus* phage CH1, *Enterococcus* phage Enf1, *Pseudomonas* phage PA5, and *Pseudomonas* phage PA10), was applied in combination with two applications of gentamicin and daptomycin locally during the intraoperative phase, and a long-term intravenous application of cefepime, daptomycin, linezolid, and tobramycin was employed. After the intervention, *S. aureus, E. faecium*, and *P. aeruginosa* were undetected. However, the patient died after 2 months due to a new bacterial infection.

A research group from Eliava Phage Therapy Center, Tbilisi, Georgia (Nadareishvili et al., 2020) presents cases of successful phage treatment of polymicrobial infection related to biofilm (Nadareishvili et al., 2020). Patient 1, a 69-year-old male patient with a diabetic foot ulcer, was infected with following bacteria: *Burkholderia cepacia, S. aureus,* and *E. faecalis.* The staphylococcus phage and Intesti bacteriophage cocktail (consisting of *Shigella* spp., *Salmonella* spp., *E. coli, Proteus* spp., *S. aureus*, *P. aeruginosa,* and *E. faecalis* phages) were applied daily in the site of infection and orally for 40 days. The size of the wound was reduced after a few weeks; in addition, there was no recurrence after 1 year of treatment. Patient 2, a 68-year-old male patient with a postsurgical infection (after skin graft surgery), had two infections: the first infection was mono-species, and the second one was caused by *S. aureus* and *Serratia marcescens*. After the application of staphylococcus phage daily at the site of infection and orally for 3 months, the infection was resolved, and the tissue healed completely. Another example is reported in cooperation with Johri et al. (2021) group. Patient with chronic bacterial prostatitis (CBP) infected by methicillin-resistant *S. aureus* (MRSA), *Staphylococcus haemolyticus, E. faecalis, and Streptococcus mitis* was first unsuccessfully treated with antibiotics. Then, Pyo (a cocktail of phages against *Streptococcus* spp., *Staphylococcus* spp., *E. coli*, *P. aeruginosa*, and *Proteus* spp.) and Intesti bacteriophage cocktail, combined with additional *Staphylococcal* phage, was introduced in three forms: oral liquid, rectal suppositories, and urethral installations. After 5 days of therapy, the patient's body temperature normalized. The therapy was prolonged, and isolated from patient bacteriophage against *S. mitis* was included. After almost a year, in a follow-up examination, semen and expressed prostatic secretion were free from bacteria, and the prostate was small and firm by rectal palpation.

Conclusion and perspectives

In conclusion, bacteria and other microorganisms prefer to organize themselves in multi-species communities. Such biofilms are difficult to cure using antibiotic therapy and to remove from abiotic surfaces. Due to the persistence of multi-species biofilms, alternative methods of their eradication are being developed. Bacteriophages are one of the solutions. Studies have been conducted using both wild-type and genetically modified or polyvalent phages. In addition, they can be successfully used in combination with antibiotics or other chemical molecules. A separate group consists of enzymes and modified enzymes produced by phages. All these methods allow for better penetration of the biofilm matrix and reaching the surface of the target bacterial strains. The use of phage therapy is also increasingly used in medicine in the treatment of severe multi-species infections. However, the routine use of bacteriophages in medicine still requires a lot of research, including optimization and legislative work. However, despite further work required, bacteriophages and therapies using them to any extent are the future in treating bacterial infections. These viruses are and will be increasingly used to prevent bacteria in the hospital environment and other cases, e.g., in the food industry, veterinary medicine, or agriculture.

Author contributions

MG: Conceptualization, Data curation, Funding acquisition, Methodology, Project administration, Validation, Visualization, Writing – original draft, Writing – review & editing. DM: Writing – original draft. PO: Writing – original draft. AC: Writing – original draft. NS: Writing – original draft. EC-H: Writing – original draft. BD: Writing – original draft. BG: Conceptualization, Formal analysis, Funding acquisition, Resources, Supervision, Validation, Visualization, Writing – original draft, Writing – review & editing.

Funding

The author(s) declare financial support was received for the research, authorship, and/or publication of this article. This study was supported by the National Science Centre, Poland (PRELUDIUM 19, Project No. 2020/37/N/NZ9/02947).

Conflict of interest

The authors declare that the research was conducted in the absence of any commercial or financial relationships that could be construed as a potential conflict of interest.

Publisher's note

All claims expressed in this article are solely those of the authors and do not necessarily represent those of their affiliated organizations, or those of the publisher, the editors and the reviewers. Any product that may be evaluated in this article, or claim that may be made by its manufacturer, is not guaranteed or endorsed by the publisher.

References

Akturk, E., Melo, L. D. R., Oliveira, H., Crabbé, A., and Coenye, T. (2023). *Biofilms* 6. doi: 10.1016/j.bioflm.2023.100147

Akturk, E., Oliveira, H., Santos, S. B., Costa, S., Kuyumcu, S., Melo, L. D. R., et al. (2019). Synergistic action of phage and antibiotics: parameters to enhance the killing efficacy against mono and dual-species biofilms. *Antibiotics* 8:103. doi: 10.3390/antibiotics8030103

Amankwah, S., Abdella, K., Kassa, T., and Amankwah, S. (2022). Bacterial biofilm destruction: A focused review on the recent use of phage-based strategies with other Antibiofilm agents. *Nanotechnol. Sci. Appl.* 14, 161–177. doi: 10.2147/NSA.S325594

Anju, V. T., Busi, S., Imchen, M., Kumavath, R., Mohan, M. S., Salim, S. A., et al. (2022). Polymicrobial infections and biofilms: Clinical significance and eradication strategies. *Antibiotics (Basel)* 11:1731. doi: 10.3390/antibiotics11121731

Arroyo-Moreno, S., Cummings, M., Corcoran, D. B., Coffey, A., and McCarthy, R. R. (2022). Identification and characterization of novel endolysins targeting *Gardnerella vaginalis* biofilms to treat bacterial vaginosis. *NPJ Biofilms Microbiom.* 8, 29–12. doi: 10.1038/s41522-022-00285-0

Atshan, S. S., Hamat, R. A., Aljaberi, M. A., Chen, J., Huang, S., Lin, C., et al. (2023). Phage therapy as an alternative treatment modality for resistant *Staphylococcus aureus* infections. *Antibiotics (Basel)* 12:286. doi: 10.3390/antibiotics12020286

Augustyniak, A., Sikora, P., Grygorcewicz, B., Despot, D., Braun, B., Rakoczy, R., et al. (2021). Biofilms in the gravity sewer interfaces: making a friend from a foe. *Rev. Environ. Sci. Biotechnol.* 20, 795–813. doi: 10.1007/S11157-021-09582-0

Barr, J. J., Auro, R., Furlan, M., Whiteson, K. L., Erb, M. L., Pogliano, J., et al. (2013). Bacteriophage adhering to mucus provide a non-host-derived immunity. *Proc. Natl. Acad. Sci. U. S. A.* 110, 10771–10776. doi: 10.1073/pnas.1305923110

Bernard, C., Girardot, M., and Imbert, C. (2020). *Candida albicans* interaction with gram-positive bacteria within interkingdom biofilms. *J Mycol Med* 30:100909. doi: 10.1016/j.mycmed.2019.100909

Carson, L., Gorman, S. P., and Gilmore, B. F. (2010). The use of lytic bacteriophages in the prevention and eradication of biofilms of Proteus mirabilis and *Escherichia coli*. *FEMS Immunol. Med. Microbiol.* 59, 447–455. doi: 10.1111/j.1574-695X.2010.00696.x

Castro, J., Sousa, L. G. V., França, Â., Tisakova, L. P., Corsini, L., and Cerca, N. (2022). Exploiting the anti-biofilm effect of the engineered phage Endolysin PM-477 to disrupt *in vitro* single-and dual-species biofilms of vaginal pathogens associated with bacterial vaginosis. *Antibiotics* 11:558. doi: 10.3390/antibiotics11050558

Chan, B. K., Sistrom, M., Wertz, J. E., Kortright, K. E., Narayan, D., and Turner, P. E. (2016). Phage selection restores antibiotic sensitivity in MDR *Pseudomonas aeruginosa*. *Sci. Rep.* 6, 1–8. doi: 10.1038/srep26717

Chegini, Z., Khoshbayan, A., Vesal, S., Moradabadi, A., Hashemi, A., and Shariati, A. (2021). Bacteriophage therapy for inhibition of multi drug-resistant uropathogenic bacteria: a narrative review. *Ann. Clin. Microbiol. Antimicrob.* 20, 1–13. doi: 10.1186/s12941-021-00433-y

Chhibber, S., Bansal, S., and Kaur, S. (2015). Disrupting the mixed-species biofilm of *klebsiella pneumoniae* B5055 and *pseudomonas aeruginosa* PAO using bacteriophages alone or in combination with xylitol. *Microbiology (United Kingdom)* 161, 1369–1377. doi: 10.1099/mic.0.000104

Comeau, A. M., Tétart, F., Trojet, S. N., Prère, M. F., and Krisch, H. M. (2007). Phage-antibiotic synergy (PAS): β-lactam and quinolone antibiotics stimulate virulent phage growth. *PLoS One* 2, 8–11. doi: 10.1371/journal.pone.0000799

Cowley, L. A., Beckett, S. J., Chase-Topping, M., Perry, N., Dallman, T. J., Gally, D. L., et al. (2015). Analysis of whole genome sequencing for the *Escherichia coli* O157: H7 typing phages. *BMC Genomics* 16, 1–13. doi: 10.1186/s12864-015-1470-z

Curtin, J. J., and Donlan, R. M. (2006). Using bacteriophages to reduce formation of catheter-associated biofilms by *Staphylococcus epidermidis*. *Antimicrob. Agents Chemother.* 50, 1268–1275. doi: 10.1128/AAC.50.4.1268

Delcaru, C., Alexandru, I., Podgoreanu, P., Grosu, M., Stavropoulos, E., Chifiriuc, M., et al. (2016). Microbial biofilms in urinary tract infections and prostatitis: etiology, pathogenicity, and combating strategies. *Pathogens* 5:65. doi: 10.3390/pathogens5040065

Dickey, J., and Perrot, V. (2019). Adjunct phage treatment enhances the effectiveness of low antibiotic concentration against *Staphylococcus aureus* biofilms *in vitro*. *PLoS One* 14, e0209390–e0209317. doi: 10.1371/journal.pone.0209390

Drulis-Kawa, Z., Majkowska-Skrobek, G., and Maciejewska, B. (2015). Bacteriophages and phage-derived proteins–application approaches. *Curr. Med. Chem.* 22, 1757–1773. doi: 10.2174/0929867322666150209152851

Duerkop, B. A. (2018). Bacteriophages shift the focus of the mammalian microbiota. *PLoS Pathog.* 14, e1007310–e1007316. doi: 10.1371/journal.ppat.1007310

Edgar, R., Friedman, N., Shahar, M. M., and Qimron, U. (2012). Reversing bacterial resistance to antibiotics by phage-mediated delivery of dominant sensitive genes. *Appl. Environ. Microbiol.* 78, 744–751. doi: 10.1128/AEM.05741-11

Ehrlich, G. D., Ahmed, A., Earl, J., Hiller, N. L., Costerton, J. W., Stoodley, P., et al. (2010). The distributed genome hypothesis as a rubric for understanding evolution in situ during chronic bacterial biofilm infectious processes. *FEMS Immunol. Med. Microbiol.* 59, 269–279. doi: 10.1111/j.1574-695X.2010.00704.x

Ferry, T., Kolenda, C., Briot, T., Souche, A., Lustig, S., Josse, J., et al. (2021). Past and future of phage therapy and phage-derived proteins in patients with bone and joint infection. *Viruses* 13, 1–20. doi: 10.3390/v13122414

Garrett, T. R., Bhakoo, M., and Zhang, Z. (2008). Bacterial adhesion and biofilms on surfaces. *Prog. Nat. Sci.* 18, 1049–1056. doi: 10.1016/j.pnsc.2008.04.001

González, S., Fernández, L., Campelo, A. B., Gutiérrez, D., Martínez, B., Rodríguez, A., et al. (2017). The behavior of *Staphylococcus aureus* dual-species biofilms treated with bacteriophage phiIPLA-RODI depends on the accompanying microorganism. *Appl. Environ. Microbiol.* 83:e02821-16. doi: 10.1128/AEM.02821-16

Grygorcewicz, B., Gliźniewicz, M., Olszewska, P., Miłek, D., Czajkowski, A., Serwin, N., et al. (2023). Response surface methodology application for bacteriophage–antibiotic Antibiofilm activity optimization. *Microorganisms* 11:2352. doi: 10.3390/MICROORGANISMS11092352

Grygorcewicz, B., Rakoczy, R., Roszak, M., Konopacki, M., Kordas, M., Piegat, A., et al. (2022). Rotating magnetic field-assisted reactor enhances mechanisms of phage adsorption on bacterial cell surface. *Curr. Issues Mol. Biol* 44, 1316–1325. doi: 10.3390/cimb44030088

Guła, G., Dorotkiewicz-Jach, A., Korzekwa, K., Valvano, M. A., and Drulis-Kawa, Z. (2018). Complex signaling networks controlling dynamic molecular changes in *Pseudomonas aeruginosa* biofilm. *Curr. Med. Chem.* 26, 1979–1993. doi: 10.2174/0929867325666180912110151

Gutiérrez, D., Vandenheuvel, D., Martínez, B., Rodríguez, A., Lavigne, R., and García, P. (2015). Two phages, phiIPLA-RODI and phiIPLA-C1C, lyse mono-and dual-species staphylococcal biofilms. *Appl. Environ. Microbiol.* 81, 3336–3348. doi: 10.1128/AEM.03560-14

Hagens, S., Habel, A., Von Ahsen, U., Von Gabain, A., and Bläsi, U. (2004). Therapy of experimental Pseudomonas infections with a nonreplicating genetically modified phage. *Antimicrob. Agents Chemother.* 48, 3817–3822. doi: 10.1128/AAC.48.10.3817-3822.2004

Herce-Ros, N., Álvarez-Sagües, A., Álvarez-Losa, L., Nistal-Villan, E., Amador, U., Presa, J., et al. (2021). Antibacterial ability of sodium hypochlorite activated with PUI vs. XPF file against Bacteria growth on *Enterococcus faecalis* mature biofilm. *Dent J (Basel)* 9:9. doi: 10.3390/dj9060067

Ichikawa, T., Yano, Y., Fujita, Y., Kashiwabara, T., and Nagao, K. (2008). The enhancement effect of three sugar alcohols on the fungicidal effect of benzethonium chloride toward *Candida albicans*. *J. Dent.* 36, 965–968. doi: 10.1016/j.jdent.2008.07.013

Infect, J., Epidemiol, D., Riggs, J. M., Mclean, R. J. C., Rohde, R. E., and Aron, G. M. (2016). Development of teicoplanin tolerance by staphylococcus epidermidis and increased susceptibility to bacteriophage type 92 by methicillin-resistant *Staphylococcus aureus* in polymicrobial biofilms. *J. Infect. Dis. Epidemiol.* 2:009. doi: 10.23937/2474-3658/1510009

Iszatt, J. J., Larcombe, A. N., Chan, H., Stick, S. M., Garratt, L. W., and Kicic, A. (2021). *Tract infections*, 1–14.

Jabłońska, J., Dubrowska, K., Augustyniak, A., Kordas, M., and Rakoczy, R. (2022). Application of magnetically assisted reactors for modulation of growth and Pyocyanin production by *Pseudomonas aeruginosa*. *Front. Bioeng. Biotechnol.* 10, 1–7. doi: 10.3389/fbioe.2022.795871

Jamal, M., Ahmad, W., Andleeb, S., Jalil, F., Imran, M., Nawaz, M. A., et al. (2018). Bacterial biofilm and associated infections. *J. Chin. Med. Assoc.* 81, 7–11. doi: 10.1016/j.jcma.2017.07.012

Javed, A., Parvaiz, F., and Manzoor, S. (2019). Bacterial vaginosis: an insight into the prevalence, alternative regimen treatments and it's associated resistance patterns. *Microb. Pathog.* 127, 21–30. doi: 10.1016/j.micpath.2018.11.046

Johnston, W., Ware, A., Frederique, W., Delaney, C., Lee, J., Hagen, S., et al. (2023). Biofilm *in vitro* bacterial vaginosis biofilm community manipulation using endolysin therapy. *Biofilms* 5:100101. doi: 10.1016/j.bioflm.2022.100101

Johri, A. V., Johri, P., Hoyle, N., Pipia, L., Nadareishvili, L., and Nizharadze, D. (2021). Case report: chronic bacterial prostatitis treated with phage therapy after multiple failed antibiotic treatments. *Front. Pharmacol.* 12, 1–8. doi: 10.3389/fphar.2021.692614

Jung, H., Ehlers, M. M., Lombaard, H., Redelinghuys, M. J., and Kock, M. M. (2017). Etiology of bacterial vaginosis and polymicrobial biofilm formation. *Crit. Rev. Microbiol.* 43, 651–667. doi: 10.1080/1040841X.2017.1291579

Kay, M. K., Erwin, T. C., McLean, R. J. C., and Aron, G. M. (2011). Bacteriophage ecology in *Escherichia coli* and *pseudomonas aeruginosa* mixed-biofilm communities. *Appl. Environ. Microbiol.* 77, 821–829. doi: 10.1128/AEM.01797-10

Kaźmierczak, N., Grygorcewicz, B., Roszak, M., Bochentyn, B., and Piechowicz, L. (2022). Comparative assessment of bacteriophage and antibiotic activity against multidrug-resistant *Staphylococcus aureus* biofilms. *Int. J. Mol. Sci.* 23:1274. doi: 10.3390/IJMS23031274

Kifelew, L. G., Mitchell, J. G., and Speck, P. (2019). Mini-review: efficacy of lytic bacteriophages on multispecies biofilms Mini-review: efficacy of lytic bacteriophages on multispecies biofilms. *Biofouling* 35, 472–481. doi: 10.1080/08927014.2019.1613525

Kifelew, L. G., Warner, M. S., Morales, S., Thomas, N., Gordon, D. L., Mitchell, J. G., et al. (2020). Efficacy of lytic phage cocktails on staphylococcus aureus and *pseudomonas aeruginosa* in mixed-species planktonic cultures and biofilms. *Viruses* 12:559. doi: 10.3390/v12050559

Konopacki, M., Grygorcewicz, B., Kordas, M., Dołęgowska, B., and Rakoczy, R. (2020). Methods of bacteriophages production with application of alternate magnetic field. PAIC 2019: Practical Aspects of Chemical Engineering, 171–182.

Koo, H., Allan, R. N., Howlin, R. P., Stoodley, P., and Hall-Stoodley, L. (2017). Targeting microbial biofilms: current and prospective therapeutic strategies. *Nat. Rev. Microbiol.* 15, 740–755. doi: 10.1038/nrmicro.2017.99

Landlinger, C., Tisakova, L., Oberbauer, V., Schwebs, T., Muhammad, A., Latka, A., et al. (2021). Engineered phage endolysin eliminates gardnerella biofilm without damaging beneficial bacteria in bacterial vaginosis ex vivo. *Pathogens* 10, 1–19. doi: 10.3390/pathogens10010054

Lehman, S. M., and Donlan, R. M. (2015). Bacteriophage-mediated control of a two-species biofilm formed by microorganisms causing catheter-associated urinary tract infections in an *in vitro* urinary catheter model. *Antimicrob. Agents Chemother.* 59, 1127–1137. doi: 10.1128/AAC.03786-14

Li, L. L., Yu, P., Wang, X., Yu, S. S., Mathieu, J., Yu, H. Q., et al. (2017). Enhanced biofilm penetration for microbial control by polyvalent phages conjugated with magnetic colloidal nanoparticle clusters (CNCs). *Environ. Sci. Nano* 4, 1817–1826. doi: 10.1039/c7en00414a

Liao, K. S., Lehman, S. M., Tweardy, D. J., Donlan, R. M., and Trautner, B. W. (2012). Bacteriophages are synergistic with bacterial interference for the prevention of *Pseudomonas aeruginosa* biofilm formation on urinary catheters. *J. Appl. Microbiol.* 113, 1530–1539. doi: 10.1111/j.1365-2672.2012.05432.x

Liu, W., Røder, H. L., Madsen, J. S., Bjarnsholt, T., Sørensen, S. J., and Burmølle, M. (2016). Interspecific bacterial interactions are reflected in multispecies biofilm spatial organization. *Front. Microbiol.* 7, 1–8. doi: 10.3389/fmicb.2016.01366

Lu, T. K., and Collins, J. J. (2007). Dispersing biofilms with engineered enzymatic bacteriophage. *Proc. Natl. Acad. Sci. U. S. A.* 104, 11197–11202. doi: 10.1073/pnas.0704624104

Lu, T. K., and Collins, J. J. (2009). Engineered bacteriophage targeting gene networks as adjuvants for antibiotic therapy. *Proc. Natl. Acad. Sci. U. S. A.* 106, 4629–4634. doi: 10.1073/pnas.0800442106

Łubowska, N., Grygorcewicz, B., Kosznik-Kwaśnicka, K., Zauszkiewicz-Pawlak, A., Węgrzyn, A., Dołęgowska, B., et al. (2019). Characterization of the three new Kayviruses and their lytic activity against multidrug-resistant *Staphylococcus aureus*. *Microorganisms* 7:471. doi: 10.3390/microorganisms7100471

Manohar, P., Loh, B., Nachimuthu, R., Leptihn, S., and Nachimuthu Assistant Professor, R. (2022). Phage-antibiotic combinations to control *Pseudomonas aeruginosa*-Candida two-species biofilms. *bio Rxiv 2022.08.18.504394* Available at: https://www.biorxiv.org/content/10.1101/2022.08.18.504394v1%0Ahttps://www.biorxiv.org/content/10.1101/2022.08.18.504394v1.abstract

Manoharadas, S., Ahmad, N., Altaf, M., Alrefaei, A. F., and Al-Rayes, B. F. (2023). An Enzybiotic cocktail effectively disrupts preformed dual biofilm of *Staphylococcus aureus* and *Enterococcus faecalis*. *Pharmaceuticals* 16:564. doi: 10.3390/ph16040564

Manoharadas, S., Altaf, M., Alrefaei, A. F., Hussain, S. A., Devasia, R. M., Badjah Hadj, A. Y. M., et al. (2021). Microscopic analysis of the inhibition of staphylococcal biofilm formation by Escherichia coli and the disruption of preformed staphylococcal biofilm by bacteriophage. *Microsc. Res. Tech.* 84, 1513–1521. doi: 10.1002/jemt.23707

Maura, D., Morello, E., du Merle, L., Bomme, P., Le Bouguénec, C., and Debarbieux, L. (2012). Intestinal colonization by enteroaggregative *Escherichia coli* supports long-term bacteriophage replication in mice. *Environ. Microbiol.* 14, 1844–1854. doi: 10.1111/j.1462-2920.2011.02644.x

Melo, L. D. R., Ferreira, R., Costa, A. R., Oliveira, H., and Azeredo, J. (2019). Efficacy and safety assessment of two enterococci phages in an *in vitro* biofilm wound model. *Sci. Rep.* 9, 6643–6612. doi: 10.1038/s41598-019-43115-8

Melo, L. D. R., Veiga, P., Cerca, N., Kropinski, A. M., Almeida, C., Azeredo, J., et al. (2016). Development of a phage cocktail to control *Proteus mirabilis* catheter-associated urinary tract infections. *Front. Microbiol.* 7:1024. doi: 10.3389/fmicb.2016.01024

Mgomi, F. C., Yuan, L., Chen, C., Zhang, Y. S., and Yang, Z. Q. (2022). Bacteriophages: a weapon against mixed-species biofilms in the food processing environment. *J. Appl. Microbiol.* 133, 2107–2121. doi: 10.1111/jam.15421

Milho, C., Silva, M. D., Alves, D., Oliveira, H., Sousa, C., Pastrana, L. M., et al. (2019). Escherichia coli and *Salmonella Enteritidis* dual-species biofilms: interspecies interactions and antibiofilm efficacy of phages. *Sci. Rep.* 9, 18183–18115. doi: 10.1038/s41598-019-54847-y

Morozova, V. V., Kozlova, Y. N., Ganichev, D. A., and Tikunova, N. V. (2018). Bacteriophage treatment of infected diabetic foot ulcers. *Methods Mol. Biol.* 1693, 151–158. doi: 10.1007/978-1-4939-7395-8_13

Morrisette, T., Kebriaei, R., Lev, K. L., Morales, S., and Rybak, M. J. (2019). Bacteriophage therapeutics: a primer for clinicians on phage-antibiotic combinations. *Pharmacotherapy* 40, 153–168. doi: 10.1002/phar.2358

Myszka, K., and Czaczyk, K. (2010). Quorum sensing mechanism as a factor regulating virulence of gram-negative bacteria. *Postepy Hig. Med. Dosw.* 64, 582–589.

Nadareishvili, L., Hoyle, N., Nakaidze, N., Nizharadze, D., Kutateladze, M., Balarjishvili, N., et al. (2020). Bacteriophage therapy as a potential management option for surgical wound infections. *PHAGE: Ther. Appl. Res.* 1, 158–165. doi: 10.1089/phage.2020.0010

Narayanan, A., Nair, M. S., Muyyarikkandy, M. S., and Amalaradjou, M. A. (2018). Inhibition and inactivation of uropathogenic *escherichia coli* biofilms on urinary catheters by sodium selenite. *Int. J. Mol. Sci.* 19:1703. doi: 10.3390/ijms19061703

Nazik, H., Joubert, L. M., Secor, P. R., Sweere, J. M., Bollyky, P. L., Sass, G., et al. (2017). Pseudomonas phage inhibition of *Candida albicans*. *Microbiology (United Kingdom)* 163, 1568–1577. doi: 10.1099/mic.0.000539

Nir-paz, R., Gelman, D., Khouri, A., Sisson, B. M., Yerushalmy, O., Bader, R., et al. (2019). Successful treatment of antibiotic-resistant poly-microbial bone infection with bacteriophages and antibiotics combination. *Clin. Infect. Dis.* 69, 2015–2018. doi: 10.1093/cid/ciz222

Oliveira, A., Sousa, J. C., Silva, A. C., Melo, L. D. R., and Sillankorva, S. (2018). Chestnut honey and bacteriophage application to control pseudomonas aeruginosa and *escherichia coli* biofilms: evaluation in an ex vivo wound model. *Front. Microbiol.* 9, 1–13. doi: 10.3389/fmicb.2018.01725

Onsea, J., Soentjens, P., Djebara, S., Merabishvili, M., Depypere, M., Spriet, I., et al. (2019). Bacteriophage application for difficult-to-treat musculoskeletal infections: development of a standardized multidisciplinary treatment protocol. *Viruses* 11:891. doi: 10.3390/v11100891

Park, K., Cha, K. E., and Myung, H. (2014). Observation of inflammatory responses in mice orally fed with bacteriophage T7. *J. Appl. Microbiol.* 117, 627–633. doi: 10.1111/jam.12565

Park, T., Chaudhry, W. N., Concepcio, J., Andleeb, S., Bull, J. J., and Levin, B. R. (2017). Synergy and order effects of antibiotics and phages in killing *Pseudomonas aeruginosa* biofilms. *PLoS One* 12:e0168615. doi: 10.1371/journal.pone.0168615

Patey, O., McCallin, S., Mazure, H., Liddle, M., Smithyman, A., and Dublanchet, A. (2019). Clinical indications and compassionate use of phage therapy: personal experience and literature review with a focus on osteoarticular infections. *Viruses* 11, 1–21. doi: 10.3390/v11010018

Pei, R., and Lamas-Samanamud, G. R. (2014). Inhibition of biofilm formation by T7 bacteriophages producing quorum-quenching enzymes. *Appl. Environ. Microbiol.* 80, 5340–5348. doi: 10.1128/AEM.01434-14

Peters, B. M., Jabra-Rizk, M. A., O'May, G. A., William Costerton, J., and Shirtliff, M. E. (2012). Polymicrobial interactions: impact on pathogenesis and human disease. *Clin. Microbiol. Rev.* 25, 193–213. doi: 10.1128/CMR.00013-11

Pires, D. P., Melo, L. D. R., Boas, D. V., and Sillankorva, S. (n.d.). Science direct phage therapy as an alternative or complementary strategy to prevent and control biofilm-related infections. *Curr. Opin. Microbiol.* 39, 48–56. doi: 10.1016/j.mib.2017.09.004

Pires, D. P., Silva, S., Almeida, C., Henriques, M., Anderson, E. M., Lam, J. S., et al. (2013). Evaluation of the ability of *C. albicans* to form biofilm in the presence of phage-resistant phenotypes of *P. aeruginosa*. *Biofouling* 29, 1169–1180. doi: 10.1080/08927014.2013.831842

Pohl, C. H. (2022). Recent advances and opportunities in the Study of *Candida albicans* Polymicrobial biofilms. *Front. Cell. Infect. Microbiol.* 12, 1–17. doi: 10.3389/fcimb.2022.836379

Püschel, A., Skusa, R., Bollensdorf, A., and Gross, J. (2022). Local treatment of driveline infection with bacteriophages. *Antibiotics* 11, 1–6. doi: 10.3390/antibiotics11101310

Reece, E., de Almeida Bettio, P. H., and Renwick, J. (2021). Polymicrobial interactions in the cystic fibrosis airway microbiome impact the antimicrobial susceptibility of *pseudomonas aeruginosa*. *Antibiotics* 10:827. doi: 10.3390/antibiotics10070827

Rickard, A. H., Gilbert, P., High, N. J., Kolenbrander, P. E., and Handley, P. S. (2003). Bacterial coaggregation: an integral process in the development of multi-species biofilms. *Trends Microbiol.* 11, 94–100. doi: 10.1016/S0966-842X(02)00034-3

Roszak, M., Dołęgowska, B., Cecerska-Heryć, E., Serwin, N., Jabłońska, J., and Grygorcewicz, B. (2022). Bacteriophage-ciprofloxacin combination effectiveness depends on *Staphylococcus aureus-Candida albicans* dual-species communities' growth model. *Microb. Drug Resist.* 28, 613–622. doi: 10.1089/mdr.2021.0324

Roy, R., Tiwari, M., Donelli, G., and Tiwari, V. (2018). Strategies for combating bacterial biofilms: a focus on anti-biofilm agents and their mechanisms of action. *Virulence* 9, 522–554. doi: 10.1080/21505594.2017.1313372

Rubalskii, E., Ruemke, S., Salmoukas, C., Boyle, E. C., Warnecke, G., Tudorache, I., et al. (2020). Bacteriophage therapy for critical infections related to cardiothoracic surgery. *Antibiotics* 9, 1–12. doi: 10.3390/antibiotics9050232

Santiago, A. J., Burgos-Garay, M. L., Kartforosh, L., Mazher, M., and Donlan, R. M. (2020). Bacteriophage treatment of carbapenemase-producing *Klebsiella pneumoniae* in a multispecies biofilm: a potential biocontrol strategy for healthcare facilities. *AIMS Microbiol.* 6, 43–63. doi: 10.3934/microbiol.2020003

Santiago, A. J., and Donlan, R. M. (2020). *Bacteriophage infections of biofilms of health care-associated pathogens: Klebsiella pneumoniae*. *9*, 1–12. doi:10.1128/ecosalplus.ESP-0029-2019

Sartini, S., Permana, A. D., Mitra, S., Tareq, A. M., Salim, E., Ahmad, I., et al. (2021). Current state and promising opportunities on pharmaceutical approaches in the treatment of Polymicrobial diseases. *Pathogens* 10:245. doi: 10.3390/pathogens10020245

Schuch, R., Khan, B. K., Raz, A., Rotolo, J. A., and Wittekind, M. (2017). Bacteriophage lysin CF-301, a potent antistaphylococcal biofilm agent. Antimicrob Agents Chemother 61:e02666–16. doi: 10.1128/AAC.02666-16

Sillankorva, S., Neubauer, P., and Azeredo, J. (2010). Phage control of dual species biofilms of Pseudomonas fluorescens and *Staphylococcus lentus*. *Biofouling* 26, 567–575. doi: 10.1080/08927014.2010.494251

Skillman, L. C., and Sutherland, I. W. (1999). *The role*, vol. 21, 13–18.

Sousa, L. G. V., Pereira, S. A., and Cerca, N. (2023). Fighting polymicrobial biofilms in bacterial vaginosis. *Microb. Biotechnol.* 16, 1423–1437. doi: 10.1111/1751-7915.14261

Srinivasan, R., Santhakumari, S., Poonguzhali, P., Geetha, M., Dyavaiah, M., and Xiangmin, L. (2021). Bacterial biofilm inhibition: a focused review on recent therapeutic strategies for combating the biofilm mediated infections. *Front. Microbiol.* 12, 1–19. doi: 10.3389/fmicb.2021.676458

Stickler, D. J. (2014). Clinical complications of urinary catheters caused by crystalline biofilms: something needs to be done. *J. Intern. Med.* 276, 120–129. doi: 10.1111/joim.12220

Struk, M., Grygorcewicz, B., Nawrotek, P., Augustyniak, A., Konopacki, M., Kordas, M., et al. (2017). Enhancing effect of 50 Hz rotating magnetic field on induction of Shiga toxin-converting lambdoid prophages. *Microb. Pathog.* 109, 4–7. doi: 10.1016/j.micpath.2017.05.018

Szafrański, S. P., Winkel, A., and Stiesch, M. (2017). The use of bacteriophages to biocontrol oral biofilms. *J. Biotechnol.* 250, 29–44. doi: 10.1016/j.jbiotec.2017.01.002

Tait, K., Skillman, L. C., and Sutherland, I. W. (2002). The efficacy of bacteriophage as a method of biofilm eradication. *Biofouling* 18, 305–311. doi: 10.1080/0892701021000034418

Tanaka, T., Yahata, Y., Handa, K., Venkataiah, S. V., Njuguna, M. M., Kanehira, M., et al. (2021). An experimental intraradicular biofilm model in the pig for evaluating irrigation techniques. *BMC Oral Health* 21, 177–112. doi: 10.1186/s12903-021-01536-w

Testa, S., Berger, S., Piccardi, P., Oechslin, F., Resch, G., and Mitri, S. (2019). Spatial structure affects phage efficacy in infecting dual-strain biofilms of *Pseudomonas aeruginosa*. *Commun. Biol.* 2, 405–412. doi: 10.1038/s42003-019-0633-x

Thompson, A. F., English, E. L., Nock, A. M., Willsey, G. G., Eckstrom, K., Cairns, B., et al. (2020). Characterizing species interactions that contribute to biofilm formation in a multispecies model of a potable water bacterial community. *Microbiology (United Kingdom)* 166, 34–43. doi: 10.1099/mic.0.000849

Tkhilaishvili, T., Wang, L., Perka, C., Trampuz, A., and Gonzalez Moreno, M. (2020). Using bacteriophages as a Trojan horse to the killing of dual-species biofilm formed by Pseudomonas aeruginosa and methicillin resistant *Staphylococcus aureus*. *Front. Microbiol.* 11:695. doi: 10.3389/fmicb.2020.00695

Topka-bielecka, G., Dydecka, A., Necel, A., and Bloch, S. (2021). Bacteriophage-derived Depolymerases against bacterial biofilm. *Antibiotics (Basel)* 10:175. doi: 10.3390/antibiotics10020175

Uyttebroek, S., Onsea, J., Metsemakers, W. J., Dupont, L., Devolder, D., Wagemans, J., et al. (2021). The potential role of bacteriophages in the treatment of recalcitrant chronic rhinosinusitis. *Antibiotics* 10, 1–13. doi: 10.3390/antibiotics10060675

Van Nieuwenhuyse, B., Galant, C., Brichard, B., Docquier, P. L., Djebara, S., Pirnay, J. P., et al. (2021). A case of in situ phage therapy against *staphylococcus aureus* in a bone allograft polymicrobial biofilm infection: outcomes and phage-antibiotic interactions. *Viruses* 13, 1–12. doi: 10.3390/v13101898

Verbanic, S., Deacon, J. M., Chen, I. A. (2022). The chronic wound Phageome: Phage diversity and associations with wounds and healing outcomes. *Microbiol Spectr*. 10:e0277721. doi: 10.1128/spectrum.02777-21

Vidakovic, L., Singh, P. K., Hartmann, R., Nadell, C. D., and Drescher, K. (2017). Dynamic biofilm architecture confers individual and collective mechanisms of viral protection. *Nat. Microbiol.* 3, 26–31. doi: 10.1038/s41564-017-0050-1

Vu, B., Chen, M., Crawford, R. J., and Ivanova, E. P. (2009). Bacterial extracellular polysaccharides involved in biofilm formation. *Molecules* 14, 2535–2554. doi: 10.3390/molecules14072535

Winans, J. B., Wucher, B. R., and Nadell, C. D. (2022). Multispecies biofilm architecture determines bacterial exposure to phages. *PLoS Biol.* 20, e3001913–e3001924. doi: 10.1371/journal.pbio.3001913

Wolcott, R., Costerton, J. W., Raoult, D., and Cutler, S. J. (2013). The polymicrobial nature of biofilm infection. *Clin. Microbiol. Infect.* 19, 107–112. doi: 10.1111/j.1469-0691.2012.04001.x

Yamamoto, K., Kusada, H., Kamagata, Y., and Tamaki, H. (2021). Parallel evolution of enhanced biofilm formation and phage-resistance in *Pseudomonas aeruginosa* during adaptation process in spatially heterogeneous environments. *Microorganisms* 9:569. doi: 10.3390/microorganisms9030569

Yang, D., Wang, Z., Ma, J., Fu, Q., Wu, L., Wang, H., et al. (2020). Glycine Cleavage System and cAMP Receptor Protein Co-Regulate CRISPR/cas3 Expression to Resist bacteriophage. *Viruses* 12:90. doi: 10.3390/v12010090

Yu, P., Mathieu, J., Yang, Y., and Alvarez, P. J. J. (2017). Suppression of enteric Bacteria by bacteriophages: importance of phage polyvalence in the presence of soil Bacteria. *Environ. Sci. Technol.* 51, 5270–5278. doi: 10.1021/acs.est.7b00529

Yu, P., Wang, Z., Marcos-Hernandez, M., Zuo, P., Zhang, D., Powell, C., et al. (2019). Bottom-up biofilm eradication using bacteriophage-loaded magnetic nanocomposites: a computational and experimental study. *Environ. Sci. Nano* 6, 3539–3550. doi: 10.1039/c9en00827f

Zhao, G., Vatanen, T., Droit, L., Park, A., Kostic, A. D., Poon, T. W., et al. (2017). Intestinal virome changes precede autoimmunity in type I diabetes-susceptible children. *Proc. Natl. Acad. Sci. U. S. A.* 114, E6166–E6175. doi: 10.1073/pnas.1706359114

Zhu, W., Ding, Y., Huang, C., Wang, J., Wang, J., and Wang, X. (2022). Genomic characterization of a novel bacteriophage STP55 revealed its prominent capacity in disrupting the dual-species biofilm formed by Salmonella typhimurium and *Escherichia coli* O157: H7 strains. *Arch. Microbiol.* 204, 1–17. doi: 10.1007/s00203-022-03208-x

frontiers | Frontiers in Microbiology

TYPE Original Research
PUBLISHED 25 March 2024
DOI 10.3389/fmicb.2024.1356206

OPEN ACCESS

EDITED BY
Alicja Wegrzyn,
University of Gdansk, Poland

REVIEWED BY
Aline Maria Da Silva,
University of São Paulo, Brazil
Miguel Angel Cevallos,
Universidad Nacional Autónoma de México, Centro de Ciencias Genómicas, Mexico

*CORRESPONDENCE
Małgorzata Łobocka
✉ lobocka@ibb.waw.pl

RECEIVED 15 December 2023
ACCEPTED 21 February 2024
PUBLISHED 25 March 2024

CITATION
Giermasińska-Buczek K, Gawor J, Stefańczyk E, Gągała U, Żuchniewicz K, Rekosz-Burlaga H, Gromadka R and Łobocka M (2024) Interaction of bacteriophage P1 with an epiphytic *Pantoea agglomerans* strain—the role of the interplay between various mobilome elements. *Front. Microbiol.* 15:1356206. doi: 10.3389/fmicb.2024.1356206

Interaction of bacteriophage P1 with an epiphytic *Pantoea agglomerans* strain—the role of the interplay between various mobilome elements

Katarzyna Giermasińska-Buczek[1,2], Jan Gawor[2], Emil Stefańczyk[2], Urszula Gągała[1], Karolina Żuchniewicz[2], Hanna Rekosz-Burlaga[1], Robert Gromadka[2] and Małgorzata Łobocka[2]*

[1]Department of Biochemistry and Microbiology, Institute of Biology, Warsaw University of Life Sciences (SGGW-WULS), Warsaw, Poland, [2]Institute of Biochemistry and Biophysics of the Polish Academy of Sciences, Warsaw, Poland

P1 is a model, temperate bacteriophage of the 94 kb genome. It can lysogenize representatives of the *Enterobacterales* order. In lysogens, it is maintained as a plasmid. We tested P1 interactions with the biocontrol *P. agglomerans* L15 strain to explore the utility of P1 in *P. agglomerans* genome engineering. A P1 derivative carrying the Tn*9* (cm^R) transposon could transfer a plasmid from *Escherichia coli* to the L15 cells. The L15 cells infected with this derivative formed chloramphenicol-resistant colonies. They could grow in a liquid medium with chloramphenicol after adaptation and did not contain prophage P1 but the chromosomally inserted cm^R marker of P1 Tn*9* (*cat*). The insertions were accompanied by various rearrangements upstream of the Tn*9 cat* gene promoter and the loss of IS*1* (IS*1*L) from the corresponding region. Sequence analysis of the L15 strain genome revealed a chromosome and three plasmids of 0.58, 0.18, and 0.07 Mb. The largest and the smallest plasmid appeared to encode partition and replication incompatibility determinants similar to those of prophage P1, respectively. In the L15 derivatives cured of the largest plasmid, P1 with Tn*9* could not replace the smallest plasmid even if selected. However, it could replace the smallest and the largest plasmid of L15 if its Tn*9* IS*1*L sequence driving the Tn*9* mobility was inactivated or if it was enriched with an immobile kanamycin resistance marker. Moreover, it could develop lytically in the L15 derivatives cured of both these plasmids. Clearly, under conditions of selection for P1, the mobility of the P1 selective marker determines whether or not the incoming P1 can outcompete the incompatible L15 resident plasmids. Our results demonstrate that *P. agglomerans* can serve as a host for bacteriophage P1 and can be engineered with the help of this phage. They also provide an example of how antibiotics can modify the outcome of horizontal gene transfer in natural environments. Numerous plasmids of *Pantoea* strains appear to contain determinants of replication or partition incompatibility with P1. Therefore, P1 with an immobile selective marker may be a tool of choice in curing these strains from the respective plasmids to facilitate their functional analysis.

KEYWORDS

bacteriophage P1, *Pantoea agglomerans* complete genome sequence, lysogeny, Tn*9* and mobile antibiotic resistance marker, plasmid curing, transduction, plasmid-prophage, replication and partition incompatibility

1 Introduction

Environmental bacteria offer a plethora of genes whose product, either by themselves or as parts of metabolic pathways, could find practical use in various fields of economics. The possibility of studying them in an isolated form, cloned in laboratory bacterial strains, is limited, often due to the association of their function with other functions or certain intracellular environments. Thus, the ability to knock out or modify the genes of interest directly in the cells of their natural hosts is important for elucidating their functions. This depends on the availability of genetic engineering tools that could be easily introduced to cells of environmental bacterial isolates, serving as sources of donor DNA for genetic exchanges or as platforms for expressing introduced genes. While plasmids are common tools in genetic manipulations of laboratory bacteria, their introduction to cells of environmental bacterial isolates is problematic mostly due to barriers from foreign DNA that are formed by the restriction-modification systems in addition to problems related to transformation (Dubnau, 1999; Ershova et al., 2015; Ren et al., 2019). Thus, there is a growing interest in the universal possibilities of foreign DNA introduction to environmental bacteria cells using wild-type or engineered bacteriophages (Westwater et al., 2002; Kittleson et al., 2012). One such bacteriophage is P1, which can productively infect or lysogenize various strains of *Enterobacterales* order and could even introduce heterologous DNA to bacterial cells that cannot be productively infected (Kaiser and Dworkin, 1975; Yarmolinsky and Sternberg, 1988; Łobocka and Gągała, 2021 and references therein; Giermasińska and Łobocka, 2016; Keller et al., 2021).

P1 is a temperate, tailed bacteriophage of myovirus morphology and 94 kb genome (Łobocka et al., 2004). It was isolated in 1951 by Giuseppe Bertani from the lysogenic *E. coli* strain Li and could infect a *Shigella desynteriae* strain (Bertani, 1951). Its transducing potential, discovered soon thereafter, became a basis for the wide use of P1 in the genetic mapping of *E. coli* chromosomes and the transfer of chromosomal genes between various *E. coli* strains (Lennox, 1955; Yarmolinsky and Sternberg, 1988). After infection, P1 can be maintained in a cell as a unit copy-number plasmid, and its mutants carrying antibiotic resistance markers facilitate the selection of lysogens (Konddo and Mitsuhashi, 1964; Goldberg et al., 1974). The plasmidial form of prophage P1 allows one to combine the high efficiency of heterologous DNA introduction to bacteria through infection with the possibility of studying the expression of cloned genes. The P1 head can accommodate ~112% of the P1 genomic DNA. This 12% of redundant information can be potentially replaced by heterologous DNA, even by a whole plasmid, without interfering with phage and prophage functions if inserted in a non-essential genome region. Another possibility is the construction of P1-based phagemids—plasmids that additionally contain the P1 lytic replicon and P1 *pac* site to initiate their packaging to P1 phage heads if other required functions are provided from the P1 helper phage (Westwater et al., 2002). Therefore, P1 has practical use in transferring heterologous plasmids to bacterial cells and is a vector for heterologous DNA expression by itself. The latter possibility has been facilitated by the recent development of simple and traceless methods of targeted P1 DNA mutagenesis, including the introduction of foreign genes of unknown phenotypes to P1 (Bednarek et al., 2023).

The entering and maintenance of P1 lysogeny is controlled by the P1-encoded C1 protein—a repressor of lytic functions (reviewed in Yarmolinsky, 2004). The introduction to a common use of P1 *c1-100*, a P1 mutant which encodes a temperature-sensitive C1 protein, allows the synchronous induction of P1 lytic development in lysogens by a shift in the growth temperature of the lysogen culture (Rosner, 1972). The stable inheritance of the P1 plasmid-prophage in a population depends on the synchronization of plasmid replication with the cell cycle, on the tight control of the P1 plasmid copy number, on the resolution of plasmid multimers to monomers, and on the active segregation (partition) of newly replicated plasmid copies to the centers of future daughter cells before cell division (Łobocka et al., 2004). The replicon of P1 plasmid-prophage belongs to the IncY replicons (Yarmolinsky and Sternberg, 1988). Its replication initiator protein, RepA, controls the replication initiation and copy number of the P1 plasmid-prophage by binding to two groups of 19 bp sequences (iterons) upstream and downstream of the *repA* gene (Chattoraj and Schneider, 1997). The iterons also determine the replication incompatibility of plasmid-prophage P1. The active partition of P1 depends on an operon of two genes, *parAB,* which ends with the *parS* site—an analog of eukaryotic centromere serving as an anchor for partitioning machinery through binding of ParB protein (Surtees and Funnell, 2003). Plasmids with similar partition systems and conserved ParB-*parS* interaction sites are incompatible with prophage P1.

P1 was shown to infect and lysogenize certain Gram-negative bacteria representing mainly *Enterobacteriaceae* and *Rhizobiaceae* families (Yarmolinsky and Sternberg, 1988; Łobocka et al., 2004; Giermasińska and Łobocka, 2016; Łobocka and Gągała, 2021; Bednarek et al., 2022). It indicates its natural adaptation to taxonomically different hosts. Certain P1 properties contributing to its wide host range have been identified. P1 adsorption to bacteria depends on six kinked tail fibers. The invertible C-segment of P1 DNA encodes two alternative variants of the C-terminal parts of tail fibers with different specificities. The variant, which is predominantly expressed in *E. coli* K-12 cells, has been suggested to adsorb to the terminal glucose of the LPS outer core oligosaccharide. The phages with the oppositely oriented C-segment could adsorb to *Shigella flexneri* 2a 2457O, *S. flexneri* 5a M90T, and *E. coli* O3 strain cells (Huan et al., 2022). The injected phage DNA is protected from degradation by restrictases of different subsets of enterobacterial type I restriction-modification systems by two P1 head proteins, DarA and DarB (Walker and Walker, 1981; Iida et al., 1987; Streiff et al., 1987). The multimer resolution system composed of recombinase Cre and its site of action, *loxP,* was functional in different cellular environments, including eukaryotic cells (reviewed by Yarmolinsky and Hoess, 2015). The lysis of taxonomically different host cells by P1 at the release of phage progeny is ensured by an unusually complex system of P1 cell lysis genes (Bednarek et al., 2022).

Pantoea agglomerans, a motile, yellow-pigmented rod of the *Enterobacteriaceae* family, is widely distributed in nature (reviewed by Walterson and Stavrinides, 2015). Its name was assigned in 1989 to bacteria known formerly as *Enterobacter agglomerans*, *Erwinia*

herbicola, and *Erwinia millatiae. P. agglomerans* strains have been isolated from various aquatic and terrestrial environments, humans, animals, and plants. They can often be found among plant endophytes or epiphytes, playing a beneficial bioprotective role, but some of them are plant pathogens causing galls, wilting, soft rot, and necrosis in a variety of agriculturally relevant plants (Lindow et al., 1998; Walterson and Stavrinides, 2015). Certain strains of *P. agglomerans* inhibit the growth of bacteria or fungi pathogenic to plants by competition, production of antibiotics, cell wall-degrading enzymes, siderophores, hydrogen cyanide, and by the induction of systemic resistance (Wilson and Lindow, 1994; Thissera et al., 2020; Carobbi et al., 2022; Xu et al., 2022; Matilla et al., 2023; reviewed by Lorenzi et al., 2022). Phylogenetic analysis based on the sequences of 16S rDNA and *fusA, gyrB, leuS, pyrG, rplB,* and *rpoB* genes revealed a high similarity between *P. agglomerans* and *E. coli*—a hallmark of common ancestry of these two bacterial species (Delétoile et al., 2009). This prompted us to test whether bacteriophage P1 could be used as a molecular biology tool in studies on *P. agglomerans* L15 (an environmental epiphytic isolate of *P. agglomerans*), which has shown to be antagonistic to certain fungal plant pathogens (Rekosz-Burlaga et al., 2014).

2 Materials and methods

2.1 Bacterial strains, plasmids, bacteriophages, and oligonucleotides

E. coli strains N99 (*galK2 strA*; Cole and Guest, 1980), C600 (*F- supE44 hsdR17 thi-1 thr-1 leuB6 lacY1 tonA21*; Sambrook et al., 1989), and DJ125 (*recA*$^-$ derivative of C600; Łobocka and Yarmolinsky, 1996) were used for phage propagation, lysogenization, transformation, cloning and plasmid isolation experiments, where indicated. *Pantoea agglomerans* L15 is an epiphytic strain with biocontrol properties isolated from *Hypericum perforatum* leaves (Rekosz-Burlaga et al., 2014). Its derivatives deprived of one or two plasmids were constructed in this work, as described further in the text. P1 *c1-100* Tn*9* (Łobocka et al., 2004), a mutant of P1 bacteriophage, was used to study the interaction with *P. agglomerans* L15. It carries the Tn*9* transposon conferring the chloramphenicol resistance to its lysogens. Additionally, the *c1-100* mutation makes the repressor of its lytic functions thermosensitive, enabling the synchronous thermal induction of P1 lytic development in lysogens. The P1 *c1-100* Tn*9* derivatives, with the IS*1* sequence, inactivated by the insertion of kanamycin resistance cassette (P1 *c1-100* IS*1*::km^R) or the *ccdA* gene of pPagL15_3 plasmid (P1 *c1-100* IS*1*::*ccdA*$_{pPagL15\_3}$), were constructed by replacing wild-type IS*1* with inactivated IS*1* using homologous recombination and plasmid pKGI10 and pKGI12, respectively, as donors of the inactivated IS*1*. The replacement method has been described previously (Bednarek et al., 2023). Plasmids that were used in this study are listed in Supplementary Table 1. The sequence correctness of DNA fragments obtained by PCR amplification and cloned in plasmids was verified by DNA sequencing with appropriate primers. The oligonucleotides used for the DNA amplification, construction of plasmids, or verification of plasmid sequence correctness are listed in Supplementary Table 2. DNA sequencing and oligonucleotide synthesis were performed at the Laboratory of DNA Sequencing and Oligonucleotides Synthesis of the Institute of Biochemistry and Biophysics of the Polish Academy of Sciences.

2.2 Media and bacterial growth conditions

Bacteria were grown in LB liquid medium with aeration or on LA solid medium (LB with 1.5% agar) at 30, 33, 35, 37, or 42°C, where indicated (Miller, 1972). Solid minimal M9 medium supplemented with glucose (0.2%) with or without thiamine (1 μg/mL) was used in certain experiments (Miller, 1972). Antibiotics were added to liquid or solid media, when appropriate, at the following final concentrations: ampicillin −50 or 100 μg/mL, chloramphenicol −12.5 μg/mL, kanamycin −12.5 or 25 μg/mL, and tetracycline (10 μg/mL). Bacterial growth was monitored by measuring the optical density of cultures at 600 nm (OD_{600}). Media used for phage adsorption or infection experiments were supplemented with $CaCl_2$ and $MgSO_4$ (to the final concentration of 5 mM each).

2.3 Induction of phage lytic development in lysogens, and phage propagation

Overnight cultures of lysogens grown at 30°C in LB medium supplemented with chloramphenicol or kanamycin (12.5 μg/mL each), where indicated, were diluted 50 times in a similar medium supplemented with glucose (0.2%) and grown with shaking (200 RPM/min) until the optical density OD_{600} of about 0.4 (*E. coli* lysogens) or 0.5 (*P. agglomerans* lysogens). Prophage induction was initiated by the rapid heating of cultures to 43°C. The warmed-up cultures were incubated at 42°C with shaking for 30 min (*E. coli*) or 15 min (*P. agglomerans*), transferred to 37°C (*E. coli*) or 33°C (*P. agglomerans*), and incubated with shaking until the signs of lysis could be seen (clearing *E. coli* culture or slightly visible flocculation of *P. agglomerans* culture). In the case of *E. coli,* lysis typically occurred in about 50 min from induction, while in the case of *P. agglomerans*, the signs of flocculation were visible in about 90 min from induction.

Bacteriophages were propagated upon thermal induction of lysogens, as described previously (Bednarek et al., 2022). Briefly, *E. coli* cells lysogenized with P1 *c1-100* IS*1*::Tn*9* or its mutant derivatives were grown overnight in LB supplemented with chloramphenicol (12.5 μg/mL) at 30°C. The overnight cultures were diluted 50 times in fresh LB with 0.2% glucose and chloramphenicol or kanamycin, where indicated, and grown at 30°C until the optical density (OD_{600}) reached 0.3–0.4. Prophages were thermally induced by rapid heating of cultures to 42°C. Then, the cultures were returned to 42°C and grown with shaking for about 45–60 min until the signs of lysis were manifested. When the OD600 of lysed cultures fell to 0.15 they were centrifuged at 29,030 × g for 40 min at 4°C to pellet bacteria. The remaining cell remnants were removed from the lysates by filtration through a 0.22 μm syringe filter (Filtropur, Sarstedt, Nümbrecht, Germany). The titer of phages in the lysates was assayed using the standard double-layer agar method, according to Adams (1959).

2.4 Lysogenization

Portions (100 μL) of overnight cultures of *E. coli* N99 or *P. agglomerans* L15 grown in LB medium at 30°C with aeration, supplemented with $CaCl_2$ and $MgSO_4$, were gently mixed with 100 μL of appropriately diluted lysate containing phages to MOI ≤ 1, and incubated for 25–30 min at room temperature without shaking. Following that, free calcium ions were removed from the mixtures by adding 200 μL 0.5 M sodium citrate to block the adsorption of the remaining phages. The mixtures were supplemented with 1 mL of LB medium, incubated for 1 h at 30°C to express the antibiotic resistance gene, and plated on LA medium containing chloramphenicol (12.5 μg/mL) or kanamycin (25 μg/mL), where indicated. Plates were incubated for ~36 h at 30°C. Each experiment was repeated three times.

2.5 Plasmid transduction

Overnight cultures of *E. coli* C600 cells grown at 30°C in LB medium were refreshed by 50 times dilution in a similar medium and grown with shaking (200 RPM/min) until the optical density (OD_{600}) of about 0.3 or 1.4, where indicated. Samples (0.1 mL) withdrawn from the cultures were supplemented with 0.1 mL of lysate with phages (10^5-10^8 pfu/mL, where indicated), 0.1 mL of $CaCl_2$ and 0.1 mL $MgSO_4$ (20 mM each), gently mixed and incubated at room temperature without shaking for 25–30 min. Next, 0.2 mL of 0.5 M sodium citrate was added to each mixture to stop phage adsorption. The mixtures were supplemented with 0.5 mL LB medium and incubated at 30°C with shaking for 1 h to express the plasmid antibiotic resistance marker. Equal aliquots of each mixture were plated on an LA medium with chloramphenicol, tetracycline, or chloramphenicol and tetracycline. The transduction procedure of *P. agglomerans* L15 cells was performed using 10 times increased volumes of all components of the transduction mixture. After adding the LB medium to the mixture, the mixtures were incubated overnight at room temperature, centrifuged to pellet the bacteria, and resuspended in 300 μL of LB medium. Equal aliquots of the suspensions were plated on the LA medium with chloramphenicol, tetracycline or chloramphenicol, and tetracycline. The plated bacteria were incubated for about 36 h at 30°C. The acquisition of P1 transducing phages and optimization of P1 mediated plasmid transduction procedure are described in detail in the Supplementary material.

2.6 Testing the stability of chloramphenicol resistance carrier

The stability of the chloramphenicol resistance carrier was tested as described previously by Grigoriev and Lobocka (2001). Briefly, the colonies of *P. agglomerans* L15 that were obtained after infection with P1 *c1-100* Tn*9* as grown on LA medium with chloramphenicol were purified once by restreaking on the same medium and restreaked again on LA medium without chloramphenicol. Three colonies of each clone were cut out with a portion of underlying agar, resuspended in 1 mL of LB, and vortexed vigorously. One hundred μL portions of serially diluted cell suspensions were plated on LB plates without chloramphenicol and incubated for ~36 h at 30°C. Grown colonies were replica plated on fresh LA medium with and without chloramphenicol. The comparisons of colony counts on plates with and without chloramphenicol were used to calculate the fraction of the cell population that retained the chloramphenicol resistance marker. Calculations were based on colony counts from the progeny of verified carriers of the chloramphenicol resistance marker. Verification was based on chloramphenicol-resistant colony-forming units in undiluted cell suspensions.

2.7 Mapping of the Tn*9* transposon insertion sites

The DNA of bacteriophage P1 *c1-100* Tn*9* or the total genomic DNA *P. agglomerans* cells obtained as stable chloramphenicol-resistant clones following the infection with P1 *c1-100* Tn*9* were digested with restriction endonuclease Taq1, which recognizes three sites within the Tn*9* transposon, between the IS*1* sequences of Tn*9*. One of these sites is between the left IS*1* (IS*1*L) and the beginning of the *cat* gene. The two other sites are between the end of the *cat* gene and the right IS*1* (IS*1*R) of Tn*9* (Figure 1). The digested DNA was diluted 20 times to increase the probability of preferential encounters of ends of the same fragment. The fragments were circularized by ligation with the T4 phage DNA ligase. To identify the borders between the *P. agglomerans* L15 DNA and the left end of Tn*9* in the Tn*9* insertion sites, we used the ligation mixture as a source of templates in PCR amplification with primers OMLO738 and OMLO739 specific for the Tn*9* sequence between the IS*1*L and the leftmost TaqI recognition site and oriented outwards. The products of the PCR amplification were separated electrophoretically in 1.0% agarose gel, cut out of the gel, and purified using the Gel Out kit (A&A Biotechnology, Gdańsk, Poland). The purified DNA fragments were amplified again with OMLO738 and OMLO739 primers, separated again in 1.0% agarose gel, purified from the gel as described above, and sequenced with the use of the same primers. In the case of too short sequence reads, they were sequenced additionally with OMLO763 primer.

2.8 DNA isolation and manipulation

Total DNA was isolated from bacteria using a Genomic Mini kit (A&A Biotechnology, Gdansk, Poland) according to the manufacturer's recommendations. Plasmid DNA was isolated from cells with the use of Qiagen Plasmid Midi kit (Qiagen, Inc., Chatsworth, Calif.) or Plasmid Mini kit (A&A Biotechnology, Gdańsk, Poland) as recommended by the kit providers. Restriction digestions, ligations, and DNA amplifications were performed according to the standard protocols (Sambrook et al., 1989) or as recommended by enzyme suppliers. DNA was analyzed by electrophoresis in agarose gels as described previously (Sambrook et al., 1989).

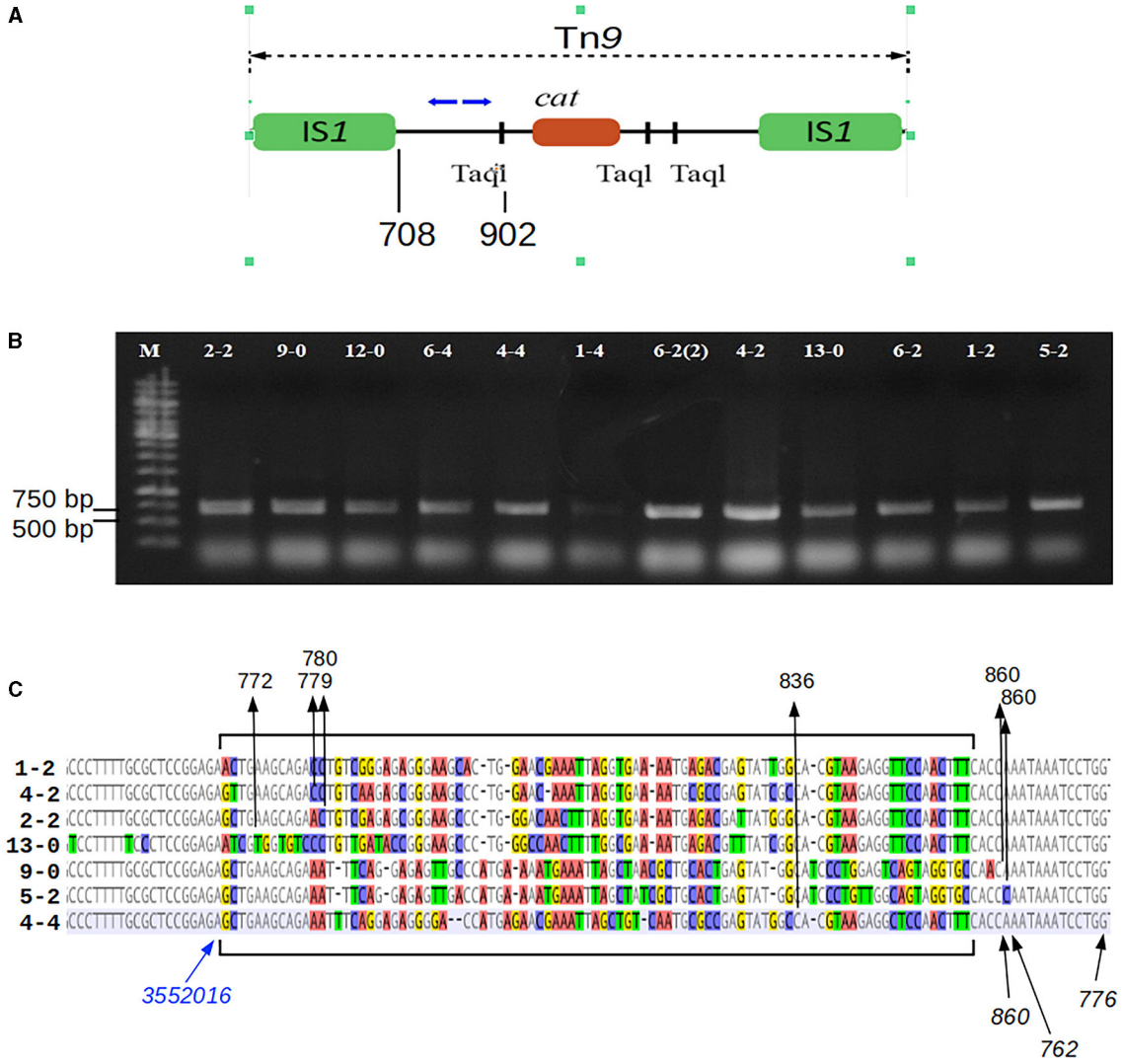

FIGURE 1
Mapping of the Tn*9* insertion sites in the P1-infected *P. agglomerans* L15 clones that acquired the resistance to chloramphenicol. **(A)** The mapping was performed by sequencing circular ligation products obtained after the digestion of the total DNA of the cmR-resistant L15 clones with TaqI. Blue arrows above the scheme of Tn*9* show the upper (OMLO739) and lower (OMLO738 or OMLO763) primers used for amplification and sequencing. Positions of the right end of left IS*1* and the leftmost TaqI site are indicated below the scheme. **(B)** Amplicons of 12 independently isolated cm^R clones. **(C)** Alignment of the border regions between the sequence of the L15 chromosome and the Tn*9*-derived DNA at the insertion sites of Tn*9* with different insertion sites. The differentiated fragments of the border regions are bracketed. The black arrows with numbers at the top of the alignment indicate the junctions between L15- and Tn9-derived DNA. The numbers represent the coordinates of Tn*9*-derived DNA in the complete sequence of Tn*9*. The blue arrow indicates the leftmost coordinate of the L15 genomic sequence that is common to all clones (see GenBank acc. no. CP034148).

2.9 *P. agglomerans* L15 genomic DNA sequencing and sequence assembly

The determination of the total *P. agglomerans* L15 DNA sequence was performed at the Laboratory of DNA Sequencing and Oligonucleotide Synthesis of the Institute of Biochemistry and Biophysics, Polish Academy of Sciences (Warsaw, Poland), by whole genome sequencing (WGS). Bacterial total genomic DNA was isolated using the CTAB/lysozyme method (Wilson, 2001). DNA quality was checked on standard 0.8% agarose gel, and 1% PFGE gel on Biorad CHEF-III apparatus (BioRad, Hercules, USA). The template quantity was measured using a Qubit fluorimeter (Thermo Fisher Scientific, Waltham, USA). The genomic bacterial DNA was mechanically sheared to the appropriate size and used for Paired-End TruSeq-like library construction using the KAPA Library preparation kit (KAPA/Roche, Basel, Switzerland) following the manufacturer's instructions. The bacterial genome was sequenced in paired-end mode (v3, 600 cycle chemistry kit) using the MiSeq instrument (Illumina, San Diego, CA). Illumina sequencing yielded 804,080 reads and 1,053,625,110 nucleotides of sequence data. The obtained sequence reads were filtered by quality using the FastX toolkit (http://hannonlab.cshl.edu/fastx_toolkit/), and residual Illumina adapters were removed using Cutadapt (https://github.com/marcelm/cutadapt). Quality-filtered Illumina data (1,204,850 paired reads and 357,606,583 nucleotides of sequence data) were assembled using Spades v3.8.0 (http://

cab.spbu.ru/software/spades/) to estimate the approximate size of the draft bacterial genome. In the next stage, long reads were generated using the MinION nanopore sequencing instrument (Oxford Nanopore Technologies, Oxford, UK). Bacterial DNA was sheared into ~10 kb fragments using Covaris gTube (Covaris, Ltd., Brighton, United Kingdom), and the library was constructed using the ONT 1D ligation sequencing kit (SQK-LSK108) with the native barcoding expansion kit (EXP-NBD103). Nanopore sequencing was performed using the NC_48 h_Sequencing_Run_FLO-MIN106_SQK-LSK108 protocol and R9.4 MinION flowcell. Raw nanopore data were basecalled using Albacore v2.1.7 (Oxford Nanopore Technologies, Oxford, UK). After quality filtering and sequencing adapter removal using Porechop (https://github.com/rrwick/Porechop), 20,701 barcoded reads remained. The obtained dataset was quality-checked using NanoPlot (De Coster et al., 2018). The median read length of the obtained dataset was 7,736 nucleotides and 164,707,659 of total bases. Long nanopore reads were assembled in a hybrid mode with Illumina data using Spades v3.8.0. Genome hybrid assembly resulted in four circular replicons: a 4 Mb size chromosome and three plasmids. The remaining sequence errors in the genome assembly were verified by the PCR amplification of DNA fragments, followed by Sanger sequencing with an ABI3730xl Genetic Analyzer (Life Technologies, USA) using BigDye Terminator Mix v. 3.1 chemistry (Life Technologies, USA). All sequence errors and misassemblies were further corrected using the Seqman software (DNAStar, USA) to obtain the complete nucleotide sequence of the bacterial genome.

2.10 DNA sequence analysis and annotations

Protein coding genes in the assembled DNA sequences were annotated automatically with the use of NCBI Prokaryotic Genome Annotation Pipeline (released 2013) https://www.ncbi.nlm.nih.gov/genome/annotation_prok/ (Tatusova et al., 2016; Haft et al., 2018). Additional protein-coding genes were identified with the help of the RAST annotation server (Aziz et al., 2008; Overbeek et al., 2014; Brettin et al., 2015). The annotations were corrected manually, using the results of the comparative analysis of predicted proteins with proteins in the NCBI database of non-redundant protein sequences (NR) with Blastp (Altschul et al., 1997). A search for conserved sequence motifs in selected proteins was done by comparing each protein sequence with motifs in the InterProScan [http://www.ebi.ac.uk/Tools/pfa/iprscan5/] (Jones et al., 2014) protein sequence motifs library. BLASTn (https://blast.ncbi.nlm.nih.gov/Blast.cgi, accessed on 29 June 2023) was used to find the closest relatives of the tested *P. agglomerans* strains and its plasmids among *Pantoea* strains and plasmids of completely sequenced genomes deposited in GenBank. A scheme of the plasmid genome organization was made using the Proksee package (Grant et al., 2023). A search for the presence of homologs of essential *E. coli* K-12 substr. MG1655 proteins among the predicted proteins of *P. agglomerans* L15 was performed using tblastx and the database of essential *E. coli* K-12 substr. MG1655 proteins at https://shigen.nig.ac.jp/ecoli/pec/ (Hashimoto et al., 2005; Kato and Hashimoto, 2007; Yamazaki et al., 2008).

To detect potential anti-phage systems in the *P. agglomerans* chromosome (NZ_CP034148) and plasmids (NZ_CP034149, NZ_CP034150, and NZ_CP034151), the DefenseFinder tool was used with the database version 1.2.2 and default settings (Abby et al., 2014; Tesson et al., 2022). Additionally, the predicted products of sequenced DNA molecules were searched manually for the presence of proteins similar to those of known anti-phage defense systems of confirmed activity against bacteriophage P1.

3 Results

3.1 Bacteriophage P1 *c1-100* Tn*9*-mediated plasmid transfer from *E. coli* to cells of an epiphytic *Pantoea agglomerans* isolate

We tested whether the commonly used P1 *c1-100* Tn*9* mutant, which is thermo-inducible and carries the chloramphenicol resistance marker in the Tn*9* transposon, could be used as a convenient vector in foreign DNA transfer by transduction to epiphytic *Pantoea agglomerans* strain L15 isolated from *Hypericum perforatum* leaves (Rekosz-Burlaga et al., 2014). The adsorption of P1 *c1-100* IS*1*::Tn*9* to cells of the L15 strain was indistinguishable from that to cells of the *E. coli* N99 strain, which served as a phage propagation host (Supplementary Figure 1), suggesting the sensitivity of *P. agglomerans* L15 to infection with P1. To verify whether P1 *c1-100* Tn*9* can transfer foreign plasmid DNA to *P. agglomerans* L15 cells, we used it to infect *E. coli* cells carrying the wide-host-range pRK2 (tc^R) plasmid derivatives with cloned fragments of the P1 genome to provide the regions of homology with prophage P1 (see Supplementary Table 1). Colonies of infected cells that could grow on chloramphenicol and tetracycline were used to induce P1 lytic development and to obtain plasmid-transducing phages (see subchapter 1.2 of Supplementary material). Of the tested plasmids, the pKGI5 plasmid containing the cloned fragment of P1 *phd doc* operon could be transferred by P1 *c1-100* Tn*9* between *E. coli* cells (Supplementary Table 3, Supplementary Figure 2), and also from *E. coli* to *P. agglomerans* L15 cells, albeit less efficiently (Supplementary Table 4, Supplementary Figures 3, 4). This shows that P1 can be a vector in DNA transfer between these two bacterial species.

3.2 Bacteriophage P1 *c1-100* Tn*9*-mediated transfer of chloramphenicol resistance gene to cells of *P. agglomerans* L15

When the L15 cells were treated with P1 *c1-100* IS*1*::Tn*9* to obtain lysogens and plated on LA medium with chloramphenicol, colonies appeared on this medium after overnight incubation at 30°C. They could be restreaked on a similar medium with chloramphenicol, where also they formed colonies. However, when these colonies were used to inoculate liquid medium with chloramphenicol, most of their overnight cultures did not reach

the optical density (OD_{600}) of over 0.05. The refreshment of such cultures (1:50) in a fresh medium with chloramphenicol and their prolonged incubation in 19 of 40 cases resulted in growth improvement, suggesting the stabilization of the chloramphenicol resistance phenotype. Besides, when these cultures were diluted and plated on media with and without chloramphenicol, the number of single colonies obtained was similar on both kinds of media. However, our attempts to thermally induce lytic development of P1 *c1-100* Tn*9* in these potential lysogens failed. Further, while the total DNA isolated from them could serve as a template to obtain the amplicons with a primer pair specific for the *cat* gene of Tn*9* transposon, we did not obtain any amplicons with a primer pair specific for a region of P1 DNA outside of the Tn*9* insertion (Supplementary Figure 5). This suggested that P1 infected cells were not lysogenized with P1 but only acquired the chloramphenicol resistance marker of P1 Tn*9*.

3.3 Mapping of the Tn*9* insertion in the chloramphenicol-resistant derivatives of P1 *c1-100* Tn*9*-treated *P. agglomerans* L15 cells

To identify the sites of Tn*9* transposition from the DNA of phage P1 *c1-100* Tn*9* to the *P. agglomerans* L15 genome, we mapped the insertion of Tn*9* in nine independently selected stable chloramphenicol-resistant L15 clones obtained after infection with P1 *c1-100* Tn*9* (Figure 1, see Materials and methods section). The *Pantoea*-derived sequences at the border of Tn*9* in all clones represented the regulatory and 5′ region of a gene encoding a DUF1471 domain-containing protein of unknown function (WP_013359194.1, see further in this manuscript). However, the insertion sites were not the same, varying up to 82 nucleotide residues downstream from the last L15 chromosome coordinate common to all clones (Figure 1C). Further, the Tn*9*-derived sequences at the border differed between the clones by up to 79 nucleotide residues. Moreover, most represented the rearranged fragments of the region between the leftmost TaqI site and IS*1*L, but none included IS*1*L. Clearly, the insertion of Tn*9* in its target site was associated with the deletion of IS*1*L and the accompanying rearrangements and deletions in the Tn*9* sequences to the right of IS*1*L (Figure 1C). The deletion was most likely associated with IS*1*L transposition to a different genomic region. Positive results of PCR amplification with primers complementary to the internal region of IS*1* (OMLO759 and OML760) and the DNA of the tested clones indicate that they contain at least one IS*1* sequence (data not shown). The loss of IS*1*L of Tn*9* in the L15 clones must have occurred during or after the transfer of Tn*9* from the genome of P1 *c1-100* Tn*9* to the genome of L15. The sequence analysis of circularized amplicons of TaqI-cleaved P1 *c1-100* Tn*9* DNA with the primers that were used for Tn*9* mapping in the L15 chromosome confirmed the results of De Bruijn and Bukhari (1978) showing that Tn*9* in P1 *c1-100* Tn*9* is inserted in the native IS*1* sequence of P1 and contains IS*1*L (data not shown).

3.4 Identification of the *P. agglomerans* L15 traits that could be potentially responsible for the inability of P1 *c1-100* Tn*9* to stably lysogenize this strain

Genus *Pantoea* was not so long ago separated from the genus *Enterobacter*, whose strains representing different species can be infected and lysogenized with P1 (Goldberg et al., 1974; Murooka and Harada, 1979; Tominaga and Enomoto, 1986; Bednarek et al., 2022). Moreover, circular sequences resembling the D6-like prophages, distantly related to P1, have been identified in a few *Pantoea* sp. strains (Gilcrease and Casjens, 2018, and references therein). Therefore, the inability of *P. agglomerans* L15 to be lysogenized with P1 *c1-100* Tn*9* was an unexpected feature of this strain. Additionally, the transfer of the Tn*9* *cat* gene from the genome of P1 *c1-100* Tn*9* to the genome of L15 suggested that the mechanisms preventing the lysogeny act relatively late, leaving enough time for the interactions between the incoming DNA of P1 and the L15 chromosome. To identify these mechanisms we isolated the total DNA of *P. agglomerans* L15 and determined its complete genomic sequence using a hybrid approach (Illumina and MinIon; see Materials and methods). The assembly of sequence reads revealed four circular DNA molecules representing a chromosome (4,029,228 bp) and three plasmids of 583,567, 179,590, and 66,484 bp, that were designated by us as pPagL15_1, pPagL15_2, and pPagL15_3, respectively. The overall features of all determined sequences are summarized in Table 1 and Figure 2. The sequence of the L15 chromosome and the two largest plasmids appeared to be highly similar to the previously described chromosomal and plasmid sequences of other *P. agglomerans* strains isolated from different plants or soil (Table 1 and references therein). The sequence of the smallest plasmid was only up to 24% identical to the sequences of its most closely related plasmids from the GenBank database. The detailed description of the L15 chromosome and plasmidome coding potential, especially the identification of features that may be associated with the biocontrol properties of the L15 strain, will be described elsewhere. Here, we searched for genetic determinants of this strain and its plasmids that could be responsible for the inability of L15 to support the lysogeny by phage P1 *c1-100* Tn*9*.

Bacteria encode numerous anti-phage defense systems that act at the post-infection step to destroy the incoming phage DNA or to cause a suicide of the infected cell, preventing the infection from spreading. Our search revealed that the L15 chromosome encodes five predicted defense systems: Mokosh type II and Shango (Millman et al., 2022), RloC (Davidov and Kaufmann, 2008), and MazEF (Hazan and Engelberg-Kulka, 2004) and restriction-modification system of type I (Supplementary Table 5). Two other systems, the R-M system of type II and the Gao-ppl system (Gao et al., 2020), are encoded by the pPagL15_1 and pPagL15_3 plasmid, respectively. The Makosh, Shango, and Gao_ppl systems did not exhibit anti-phage activity against the P1 bacteriophage (Gao et al., 2020; Millman et al., 2022). RloC is an anticodon nuclease that targets the $tRNA^{Lys}$ of the host cell to inhibit translation during the T4 infection (Klaiman et al., 2012). Yet, its influence on P1 infection has not been studied. The MazEF is a toxin-antitoxin system that significantly decreased the rate

TABLE 1 General features of the *P. agglomerans* L15 chromosome and plasmids.

Genome part	Size (bp)	% GC	Number of predicted protein coding genes	*rrn* operons (tRNA genes)	Closest relatives	Size (bp)	GenBank Acc. No. (reference)	% coverage/ % identity
Chromosome	4,029,228	55.6	3,698	7 (75)	*P. agglomerans* ASB05	4,022,781	CP046722 (Lee et al., 2021)	95/99
					P. agglomerans C410P1	4,182,028	CP016889	94/98
					P. agglomerans TH81	4,128,817	CP031649 (Humphrey et al., 2019)	94/99
pPagL15_1	583,567	53.0	614	0 (6)	*P. agglomerans* C410P1 plasmid, unnamed1	543,504	CP016890	73/96
					P. vegans C9-1 plasmid pPag3	529,676	CP001895 (Smits et al., 2010)	63/87
pPagL15_2	179,590	53.0	163	0 (0)	*P. agglomerans* ASB05 plasmid pASB05p2	207,454	CP046724 (Lee et al., 2021)	99/99
					P. agglomerans PSV1-7, plasmid, unnamed2	179,440	CP091191	99/99
					P. agglomerans CHTF15 plasmid, unnamed2	180,424	CP103403	99/99
					Pantoea vegans C9-1 plasmid pPag1	167,983	CP001893 (Smits et al., 2010)	75/89
pPagL15_3	66,484	50.4	79	0 (0)	*P. agglomerans* DAPP-PG734 plasmid P2	174,327	OW970317	22/96
					P. agglomerans ASB05 plasmid pASB05p2	64,606	CP046725 (Lee et al., 2021)	16/97
					P. agglomerans C410P1 plasmid, unnamed2	216,117	CP016891	26/91
					Pantoea vegans C9-1 plasmid pPag2	165,693c	CP001894 (Smits et al., 2010)	13/90
					P. agglomerans TH81 plasmid unnamed3	152,523	CP031652 (Humphrey et al., 2019)	18/92

of P1 lysogen formation in *E. coli* (Hazan and Engelberg-Kulka, 2004). However, the action of the MazEF system caused the premature death of infected cells, but fewer stable lysogens could still be formed. A search for the CRISPR-Cas regions in the L15 chromosome and its plasmids revealed some positive incomplete matches. However, their predicted spacer regions did not have similarities to any P1-derived sequence fragment (data not shown).

Several genes of P1 that are present in lysogens encode proteins, preventing the superinfection of lysogens with P1 or related phages. To find possible homologs of such proteins, we searched predicted sequences of proteins encoded by the chromosome of L15 and its plasmids using BlastP and tBlastN programs and sequences of bacteriophage P1 proteins (Supplementary Table 6). Our search revealed that both the L15 chromosome and its plasmids encode proteins highly similar to the proteins of P1.

Chromosomally encoded homologs of P1 proteins include mainly proteins associated with replication. Homologs of these proteins are also encoded by the *E. coli* chromosome, and they support replication from the P1 plasmid or phage replication origin (Łobocka et al., 2004).

Surprisingly, two plasmids of the L15 strain appeared to encode homologs of P1 proteins that could potentially contribute to interactions with P1 responsible for the difficulties in establishing P1 lysogeny. The pPagL15_1 plasmid encodes proteins highly similar to the partition proteins of P1, ParA, and ParB (Supplementary Table 6, Figure 3). In the genome of P1, immediately downstream of the *parB* gene, there is a ParB binding site, *parS*, which acts as an analog of the eukaryotic centromere (Abeles et al., 1985). The binding of ParB to *par*S is essential for active plasmid segregation. Immediately downstream of the *parB* gene of pPagL15_1, there is a sequence nearly identical to the *parS* site of prophage P1 (designated here as $parS_{pPagL15\_1}$; Figure 3A). In P1 *parS* there are two ParB binding sites—heptameric sites designated as BoxA and hexameric sites designated as BoxB. They are organized in two clusters (BA and AABA) and separated by the site that binds a host factor, IHF protein. Only A2-A3 and B2 boxes (forming the so-called *parS* small) are required to bind ParB. The BoxB sequences are discriminatory elements that are responsible for the specific interaction of ParB with the *parS* site of P1 but not with the related *parS* sequences of other

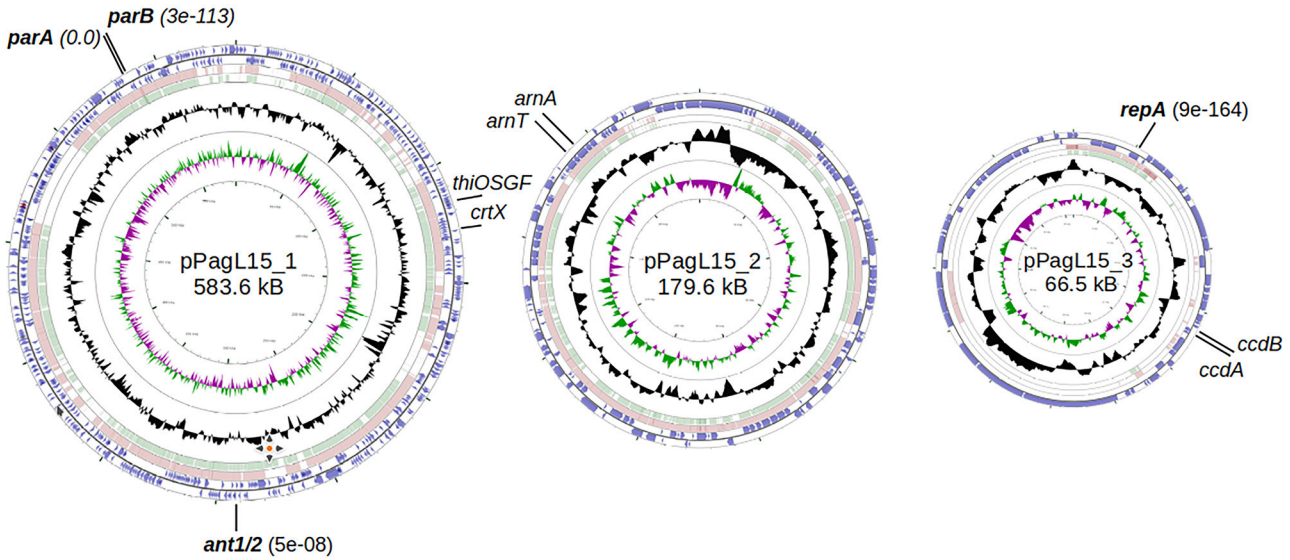

FIGURE 2
Genome maps of *P. agglomerans* L15 plasmids: pPagL15_1, pPAGL15_2, and pPagL15_3 (GenBank acc. no. CP034149, CP034150, and CP034151). The two outermost circles in each map represent genes transcribed in clockwise and counterclockwise directions, respectively. The two innermost circles show GC content and G-C skew. Circles in between show regions similar in sequence to those of the two closest representatives of each plasmid in the GenBank: CP016890 and CP001895, CP016892 and CP001893, and CP016891 and CP001894 in the case of pPagL15_1, pPAGL15_2, and pPagL15_3, respectively. Plasmid genes whose products encode close homologs of P1 proteins that may be responsible for the inability of P1 to stably lysogenize the L15 strain are in bold. Other genes indicated were used in curing the L15 strain from its plasmids.

plasmids (Dabrazhynetskaya et al., 2005, 2009; Sergueev et al., 2005). The $parS_{pPagL15\_1}$ site appears to be organized similarly. It contains all A and B boxes shown to be essential for P1 partitioning and the specific binding of P1 ParB. Box B2, which was shown to be the only B box essential for determining the P1 specific partition incompatibility (Dabrazhynetskaya et al., 2005), is identical in P1 *parS* and pPagL15_1 *parS*. Moreover, the amino acid residues of P1 ParB, which are essential for binding to *parS* and are involved in discriminating *parS* of P1 from the related *parS* sites of other plasmids (Łobocka and Yarmolinsky, 1996; Radnedge et al., 1998; Dabrazhynetskaya et al., 2005, 2009), are conserved in the ParB of pPagL15_1 (Figure 3B). Taken together this indicates that prophage P1 and plasmid pPagL15_1 are partitionally incompatible and cannot stably coexist in one cell.

The predicted replication initiator protein of pPagL15_3 plasmid, designated here as $RepA_{pPagL15\_3}$, is 73% identical over 97% of its length to the RepA replication initiator protein of phage P1 (Figure 4). Additionally, the so-called iteron sequences that, by prediction, bind this protein by analogy to other plasmids replicating in the theta mode, are nearly identical to the iteron sequences binding the RepA protein of P1 (Figure 4). The aforementioned similarities indicate that the pPagL15_3 plasmid and prophage P1 belong to the same replication incompatibility group (IncY) and cannot be stably maintained in the same cell. Certain other RepA proteins of IncY group plasmids of experimentally proven incompatibility with P1 are also identical 72–73% to P1 RepA at the protein sequence level and recognize iterons similar to those of P1 (Fu et al., 1997).

3.5 Curing of *P. agglomerans* L15 strain from the pPagL15_1 plasmid which is partitionally incompatible with prophage P1

To test whether the presence of the L15 strain of the two plasmids incompatible with prophage P1 could be responsible for the inability of P1 to stably lysogenize this strain, we first attempted to cure the L15 strain from the pPagL15_1 plasmid, which was partitionally incompatible with P1. This plasmid encodes at least two phenotypic markers, namely the synthesis pathway of pigment zeaxanthin, which is responsible for the yellow coloring of the L15 colonies, and the thiamine biosynthesis pathway (Figure 2). Thus, to cure the L15 cells from this plasmid, we incubated them at 35°C (the highest temperature tolerated by L15) and plated them on an LA medium to obtain single colonies. Of over 9,000 single colonies inspected, six did not show yellow coloring. Additionally, when tested for the ability to grow on a minimal solid M9 medium with glucose and with or without thiamine, they could only grow on the medium with thiamine, contrary to the wild-type L15 cells that could grow on both these media (Figure 5). Shotgun WGS sequencing of the DNA of one of the obtained strains confirmed the absence of DNA fragments representing the pPagL15_1 plasmid in its cells (Supplementary Table 7). We designated the obtained L15 derivative cured of pPagL15_1 plasmid as IPAG312.

Our attempts to obtain stable P1 *c1-100* Tn*9* lysogens of the IPAG312 strain appeared unsuccessful. As in previous attempts, we could obtain colonies grown on LA medium with chloramphenicol. However, testing them for the presence of P1 *c1-100* Tn*9* and the pPagL15_3 plasmid after several generations of growth in

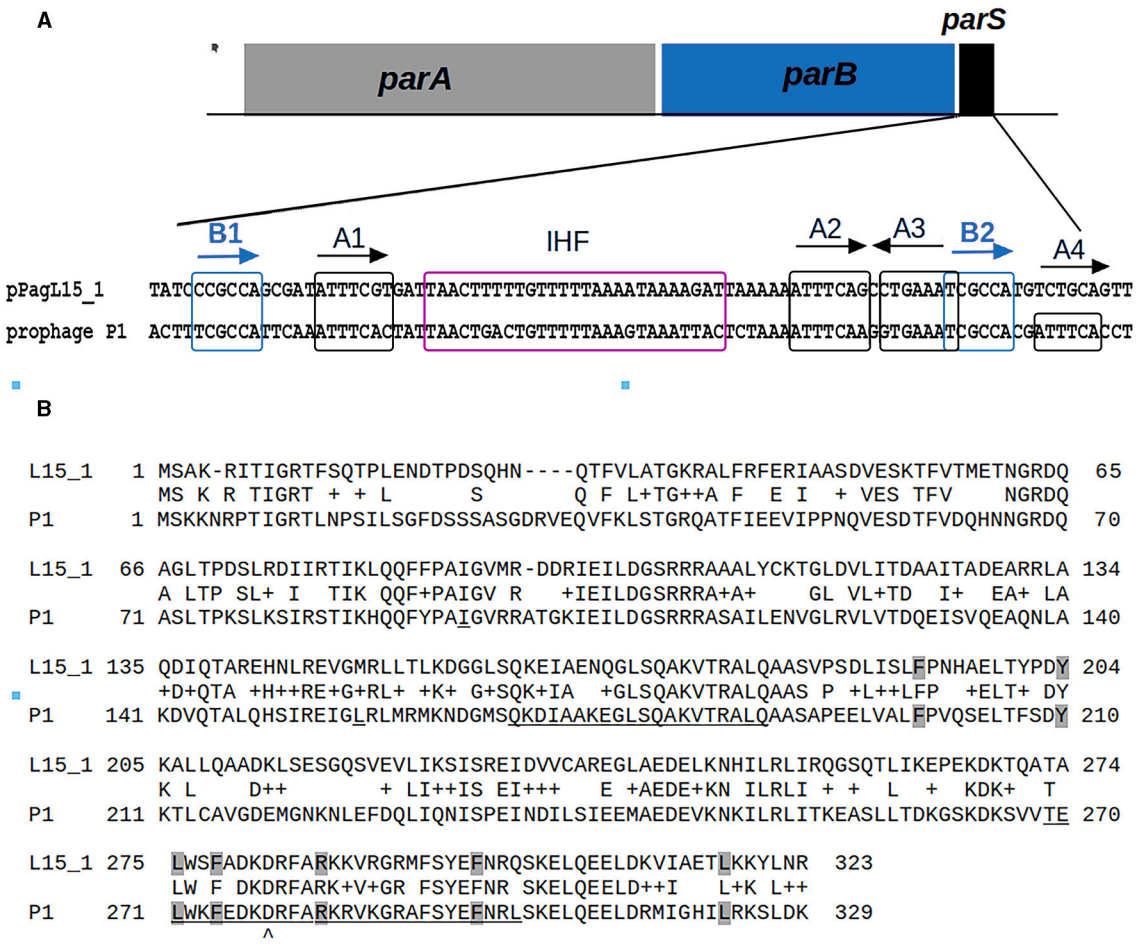

FIGURE 3
Similarities between the organization and sequence of the predicted partition cassette of pPagL15_1 plasmid and prophage P1. **(A)** Sequence alignment of the predicted centromere-like site of pPagL15_1 (*parS*$P_{pPagL15\_1}$) and the *parS* site of P1. A scheme of partition cassettes is above the alignment. Boxes A and B which are involved in the binding of P1 ParB, and the predicted and known IHF binding sites of pPagL15_1 and P1, respectively, are indicated. Boxes B, essential for partition incompatibility determination, are boxed in blue. **(B)** Alignment of amino acid sequences of predicted ParB protein of pPagL15 and ParB protein of P1. Amino acid residues of P1 ParB shown by mutational replacements as essential for binding with *parS* and their counterparts in pPagL15_1 ParB are shaded in gray. Regions of P1 ParB essential for the specific recognition of P1 *parS* are underlined. The aspartic acid residue of the P1 ParB, key for recognizing the second base of species-specificity determining BoxB2, is indicated below the alignment. The essential partition specificity and incompatibility determining regions of P1 ParB are indicated according to Radnedge et al. (1998) and Dabrazhynetskaya et al. (2009).

chloramphenicol-containing medium by colony PCR with primers specific for P1 *c1-100* Tn*9* genes and pPagL15_3 genes revealed that they contained only the *cat* gene of P1, and retained the pPagL15_3 plasmid.

3.6 P1 *c1-100* Tn*9* derivatives able to outcompete plasmid pPagL15_3 from the *P. agglomerans* IPAG312 cells

Replication or partition incompatibility leads to a random loss of any of the incompatible plasmids of a pair at cell divisions (Novick, 1987). The inability of P1 *c1-100* Tn*9* to replace the pPagL15_3 plasmid in the IPAG312 cells could suggest a mechanism protecting pPagL15_3 from the loss. We excluded that pPagL15_3 could be a mini-chromosome. Homologs of all *E. coli* K-12 substr. MG1655 proteins deposited in the database of essential *E. coli* gene products (https://shigen.nig.ac.jp/ecoli/pec/) could be identified among the predicted gene products of *P. agglomerans* L15 chromosome.

The pPagL15_3 plasmid encodes two proteins significantly similar to proteins of the canonical CcdACcdB type II TA system of F plasmid. The pPagL15_3 homolog of CcdA (WP_033781302.1; 78 aa) is 28% identical to F plasmid CcdA (WP_000813634.1; 72 aa), and the pPagL15_3 homolog of CcdB (WP_031594618.1; 104 aa) is 37% identical to the F plasmid CcdB (WP_031594618.1; 101 aa). Additionally, the amino acid sequences of pPagL15_3 CcdA and CcdB homologs contain amino acid sequence motifs characteristic of CcdA and CcdB family proteins, pfam motif PF07362 and PF01845, respectively. CcdB is a potent toxin that eliminates cells with plasmids that express its gene and do not contain the CcdA antitoxin (Bernard, 1996). To determine whether

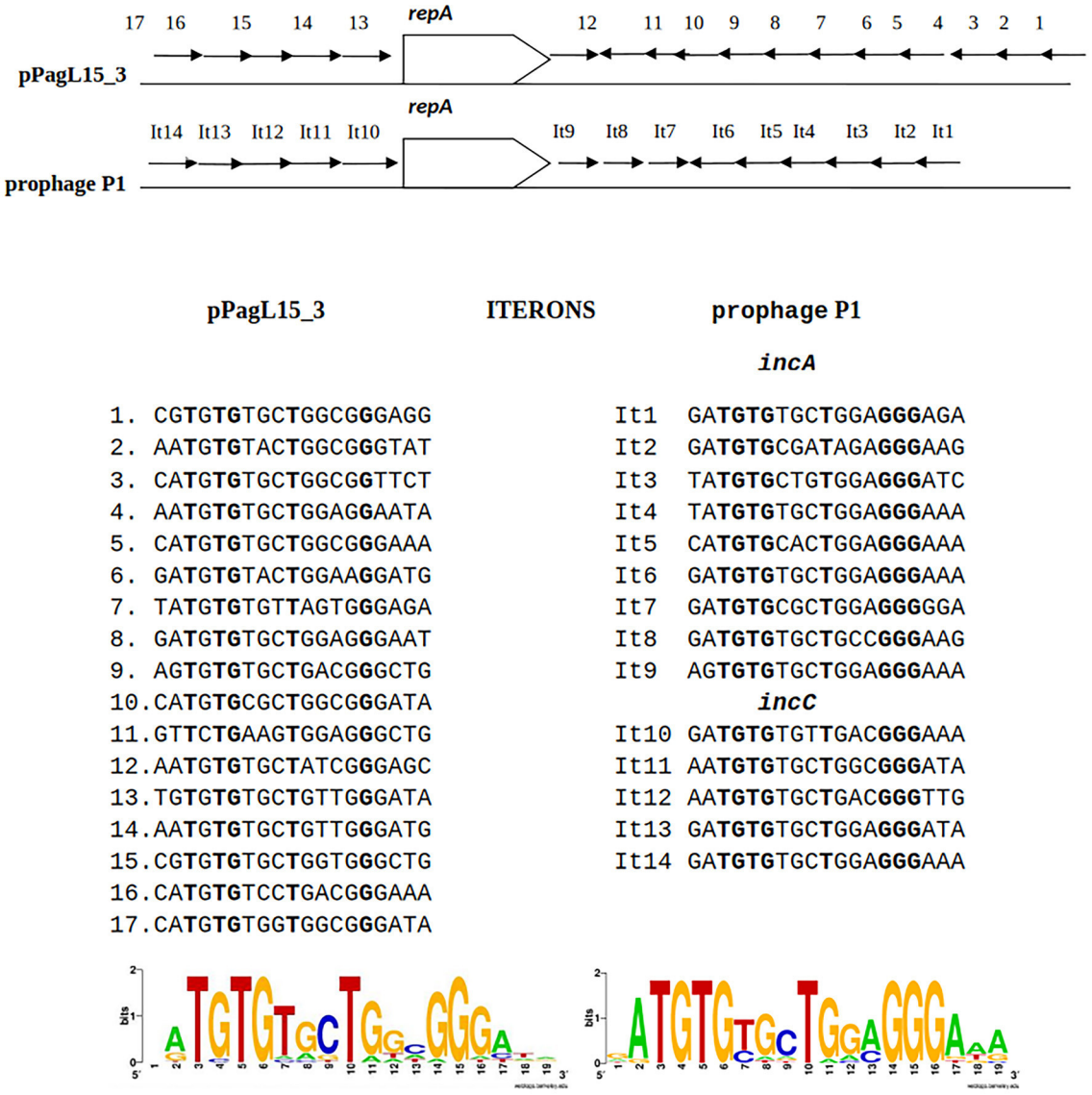

FIGURE 4
Similarities between the organization of the predicted replication initiation region of plasmid pPagL15_3 and the replication initiation region of plasmid-prophage P1. Arrows in the regions flanking the *repA* gene indicate the organization and direction of iteron sequences. Sequences of iterons of pPagL15_3 and prophage P1 and their logos are below the comparative scheme.

the inability of P1 *c1-100* Tn*9* to outcompete the pPagL15_3 plasmid from the IPAG312 cells could be due to the CcdB-mediated killing of cells that potentially lost the pPagL15_3, we constructed a derivative of P1 *c1-100* Tn*9* with the pPagL15_3 plasmid *ccdA* gene with its promoter inserted in the IS*1*L sequence of Tn*9*. When the IPAG312 cells were infected with the P1 *c1-100* Tn*9* IS*1*::$ccdA_{pPagL15\_3}$ bacteriophage, incubated to express the *cat* gene of Tn*9* and plated on medium with chloramphenicol, chloramphenicol-resistant colonies showed up after overnight incubation similar to the experiments with P1 *c1-100* Tn*9*. However, when we purified these colonies on a similar medium and used them to inoculate the LB medium with chloramphenicol, all of them grew to a stationary phase without noticeable growth retardation. To test whether the obtained clones could lose the pPagL15_3 plasmid after prolonged incubation under conditions selective for the P1 *c1-100* Tn*9* IS*1*::$ccdA_{pPagL15\_3}$ prophage, we restreaked them to M9 minimal medium supplemented with glucose, thiamine, and chloramphenicol, and then again on LA medium with chloramphenicol to obtain single colonies. Cells from the top of these colonies were used as a source of template DNA in colony PCR reactions with primers specific for P1 and pPagL15_3 DNA. In all tested cases, the amplicons were formed only with primers specific for P1, indicating that all tested clones acquired the P1 *c1-100* Tn*9* IS*1*::$ccdA_{pPagL15\_3}$ prophage and lost the pPagL15_3 plasmid (Supplementary Figure 7).

To verify whether the ability of P1 *c1-100* Tn*9* IS*1*::$ccdA_{pPagL15\_3}$ to replace the pPagL15_3 plasmid in the obtained clones resulted from the presence of the source of CcdA antitoxin in the modified P1 *c1-100* Tn*9* construct used

10.3389/fmicb.2024.1356206

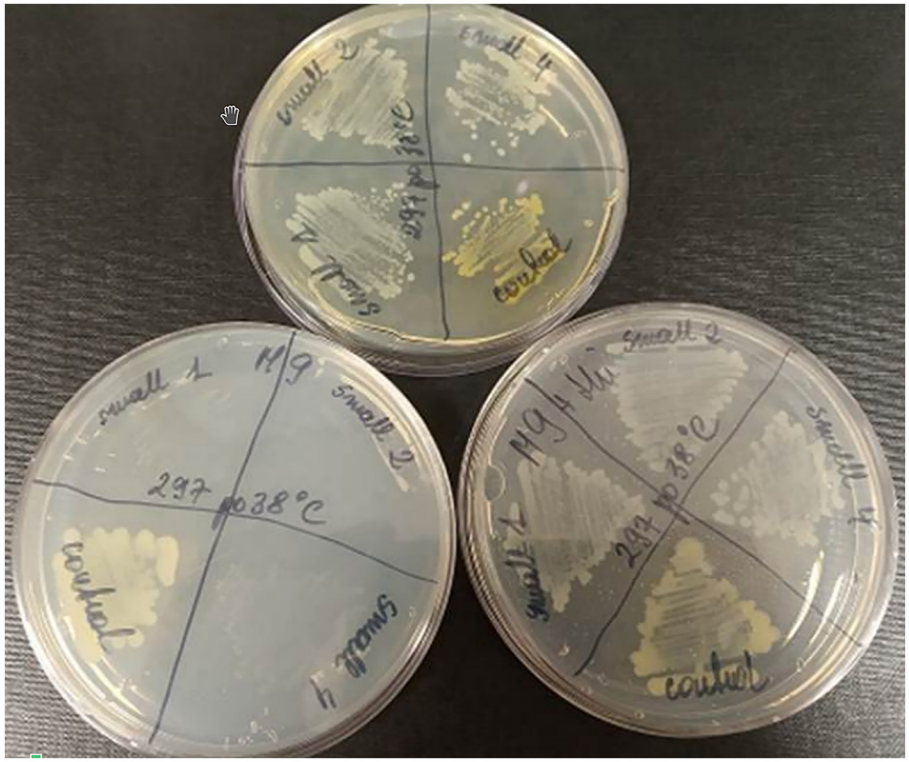

FIGURE 5
Curing of *P. agglomerans* L15 strain from the pPagL15_1 plasmid. Curing was based on screening for colonies that lost the ability to produce yellow stain (zeaxanthin) and to synthesize thiamine encoded by *crtX* and *thiOSGF* genes of pPagL15_1, respectively. The phenotypes of pPagL15_1-cured clones of L15 that were obtained after incubation of *P. agglomerans* L15 at 35°C for about 22 generations, plated on LB medium to obtain single colonies and screened for the presence of white clones. **(Upper plate)** shows differences in the colony color of pPagL15_1-cured clones and the parental L15 strain. Two plates at the bottom show the inability of pPagL15_1-cured clones to grow on a minimal M9 medium supplemented with glucose but without thiamine **(left plate)** and their ability to grow on a similar medium supplemented with thiamine **(right plate)**.

for curing, we constructed another P1 *c1-100* Tn*9* bacteriophage derivative with the kanamycin resistance cassette inserted in the IS*1*L sequence of Tn*9*. Surprisingly, the results were similar to those obtained with P1 *c1-100* Tn*9* IS*1*::$ccdA_{pPagL15\_3}$. The IPAG312 strain cells lysogenized with P1 *c1-100* Tn*9* IS*1*::km^R formed colonies on the LA medium with chloramphenicol and kanamycin. When cells of these colonies were used to inoculate LB medium with chloramphenicol and kanamycin, the optical density of the obtained cultures increased as expected. We attempted to cure them of pPagL15_3 plasmid by restreaking them on M9 solid medium with glucose, thiamine, kanamycin, and chloramphenicol and restreaking again on LA medium with chloramphenicol and kanamycin. When cells from colonies grown on LA plates with chloramphenicol and kanamycin were used as a source of template DNA in colony PCR with primers specific for P1 and for the PagL15_3 plasmid, the expected amplicons were obtained only with primers specific for P1, indicating that they lost the pPagL15_3 plasmid. One of the obtained lysogens cured of pPagL15_3 and containing P1 *c1-100* Tn*9* IS*1*::km^R prophage (designated by us as IPAG380) was used as a source of template DNA for long-read diagnostic shotgun WGS sequencing. Analysis of sequencing results confirmed that it represents a derivative of *P. agglomerans* IPAG312 strain cured of pPagL15_1 and pPagL15_3 plasmids and lysogenized with P1 *c1-100* Tn*9* IS*1*::km^R (Supplementary Table 7). Clearly, the reason for P1 *c1-100* Tn*9* being unable to stably lysogenize the IPAG312 strain was the IS*1*L sequence of the P1 mutant Tn*9*.

The IS1*L* sequence of Tn9 proved to be the only Tn*9* IS*1* sequence driving the mobility of Tn*9* (Chandler and Galas, 1983; Machida et al., 1983; Ahmed, 1984). Therefore, to determine whether IS*1*L by itself or the Tn*9* mobility driven by IS*1*L is the reason for the P1 *c1-100* Tn*9* inability to stably lysogenize *P. agglomerans* L15 or IPAG312, we infected the IPAG312 cells with a derivative of P1 *c1-100* Tn*9* containing the insertion of kanamycin resistance cassette in the non-essential *pdcB* gene and constructed by us previously (Bednarek et al., 2023). The infected cells could form colonies on the LA medium with kanamycin or with chloramphenicol and kanamycin. Moreover, when these colonies were used to inoculate liquid medium with kanamycin or chloramphenicol and kanamycin, their culture grew without any retardation, indicating that they formed stable lysogens. Consequently, our results show that the reason for P1 *c1-100* Tn*9* inability to stably lysogenize *P. agglomerans* IPAG312 cells is the mobility of its selective marker, namely the Tn*9* *cat* gene. The immobilization of Tn*9* or the enrichment of P1 *c1-100* Tn*9* with an immobile selective marker makes P1 a winner in the fight with incompatible plasmids to settle the L15 cells as the hosts.

3.7 The ability of P1 *c1-100* Tn*9* IS*1*::km^R to replace two incompatible plasmids and to develop lytically in the *P. agglomerans* L15 cells

To test whether the P1 *c1-100* Tn*9* IS*1*::km^R bacteriophage can stably lysogenize the *P. agglomerans* L15 strain and replace both plasmids of this strain incompatible with P1, we repeated the lysogenization procedure with this phage using the L15 strain as a recipient in the lysogenization. Similarly, as in the case of the IPAG312 strain, stable lysogens of L15 with P1 *c1-100* Tn*9* IS*1*::km^R could be obtained, and they could grow on LA medium with chloramphenicol and kanamycin as well as in liquid medium supplemented with these antibiotics. Moreover, after a few rounds of their streak plating on LA medium with chloramphenicol and kanamycin, they gave rise to colonies of cells cured of both pPagL15_1 and pPagL15_3 plasmids, as verified by PCR and by shotgun WGS sequencing (Supplementary Figure 7, Supplementary Table 7).

The acquisition of *P. agglomerans* L15 and IPAG312 strain derivatives cured of plasmids incompatible with P1 and lysogenized with P1 *c1-100* Tn*9* IS*1*::km^R prompted us to test whether P1 can develop lytically in the cells of these strains. Cultures of lysogens in liquid LB medium with chloramphenicol and kanamycin were grown with shaking until their optical density (OD_{600}) reached ~0.5. They were then quickly heated to 43°C to induce the prophage, incubated at 42°C with shaking for an additional 15 min, transferred to 33°C, and incubated for an additional 70 min with shaking. The aliquots of the cultures were serially diluted and spotted on a layer of indicator strain cells (*E. coli* N99) in LCA in Petri dishes. The plates were incubated overnight at 42°C and inspected for plaques. Surprisingly, in both cases, single plaques were obtained in contrast to the control samples in which we used the aliquots of the cultures of non-lysogens for spotting (Figure 6). To sum up, our results demonstrate that bacteriophage P1 can not only stably lysogenize *P. agglomerans* L15 cells but can also develop lytically in the cells of this strain. Additionally, the ability of P1 *c1-100* Tn*9* IS*1*::km^R to replace the pPagL15_1 and pPagL15_3 plasmids in the L15 strain confirms our predictions that each of these plasmid is incompatible with prophage P1.

3.8 Nucleotide sequence accession number

The genomic sequences of the *P. agglomerans* L15 chromosome, and the pPagL15_1, pPagL15_2, and pPagL15_3 plasmids were deposited in GenBank under the accession numbers CP034148, CP034149, CP034150, and CP034151, respectively.

4 Discussion

In this work, we showed that an epiphytic isolate of *P. agglomerans*—namely, the *P. agglomerans* L15 strain can be added to the list of bacteriophage P1 hosts. We also demonstrated that P1 can be a vector for transferring plasmids from a laboratory *E. coli* strain to the *P. agglomerans* L15 strain. Additionally, the determination of the complete *P. agglomerans* L15 genomic sequence, and the analysis of the L15 strain interaction with the P1 *c1-100* Tn*9* mutant phage allowed us to discover an unexpected influence of antibiotic selection pressure on the interplay between the incoming and resident mobile genetic elements and on breaking natural barriers protecting cells from the establishment of foreign DNA.

In *E. coli* K-12, P1 adsorbs to the terminal glucose in the outer core oligosaccharide of LPS (Franklin, 1969; Ornellas and Stocker, 1974; Yarmolinsky and Sternberg, 1988, and references therein). The core oligosaccharide of *P. agglomerans* LPS is highly diversified. In the case of several strains described, it is similar to that of *E. coli* in that it contains glucose in the core oligosaccharide (Karamanos et al., 1992; Lerouge and Vanderleyden, 2002; Kohchi et al., 2006; Hashimoto et al., 2017; Varbanets et al., 2019; Bulyhina et al., 2020). Therefore, it was unsurprising that P1 adsorption to *P. agglomerans* L15 cells was possible and similar to that of *E. coli* K-12 cells concerning time and efficiency (Supplementary Figure 1). Likely, not all *P. agglomerans* strains can adsorb P1, as not all contain glucose in their core LPS oligosaccharide (Varbanets et al., 2019). However, P1 requires only one receptor-binding protein (tail fiber) to adsorb to a host cell and inject its DNA (Liu et al., 2011; Lam et al., 2021). This offers a relatively simple system for phage specificity engineering by modifying tail fiber modules essential for the direct interaction of tail fibers with host receptors for a phage, as has been demonstrated recently (Lam et al., 2021). Additionally, two alternative forms of the C-terminal fragment of tail fiber protein, naturally encoded by the invertible C-segment of P1, enable the expression of two-tail fiber variants by P1 progeny (reviewed by Łobocka et al., 2004). Whether the alternative P1 tail-fiber variant may be required for the adsorption to *P. agglomerans* strains of atypical LPS core oligosaccharide structure remains to be found.

Despite the ability of P1 to adsorb to the L15 cells and the close phylogenetic relationship of *P. agglomerans* and *E. coli* (the best-known host of P1), we could not obtain stable L15 lysogens when we lysogenized L15 using the thermo-inducible P1 mutant, P1 *c1-100* Tn*9*, which carries the chloramphenicol resistance marker in Tn*9*. All obtained clones that became stably resistant to chloramphenicol with time carried only the chromosomally integrated and shortened versions of Tn*9*. It contained the chloramphenicol resistance marker but was depleted of the leftmost IS*1* sequence. Of the two IS*1* sequences at the ends of the Tn*9* transposon, the leftmost one (IS*1L*), preceding the *cat* gene promoter, is active, while the rightmost one (IS*1R)* is not, due to the transcriptional repression from the *cat* gene promoter (Chandler and Galas, 1983; Machida et al., 1983; Ahmed, 1984). We suppose that due to the presence in the L15 cells of two plasmids incompatible with P1 and the use of chloramphenicol to select lysogens, only cells in which Tn*9* transposed to the chromosome of L15 strain before the donor P1 loss could survive in the selective condition for a longer time. This could also be a reason why, despite similar adsorption efficiency of bacteriophage P1 *c1-100* Tn*9* to *E. coli* and *P. agglomerans* L15 cells, the number of colonies grown on selective medium after infection of *E. coli* was one order of magnitude higher than that grown after infection of *P. agglomerans* L15.

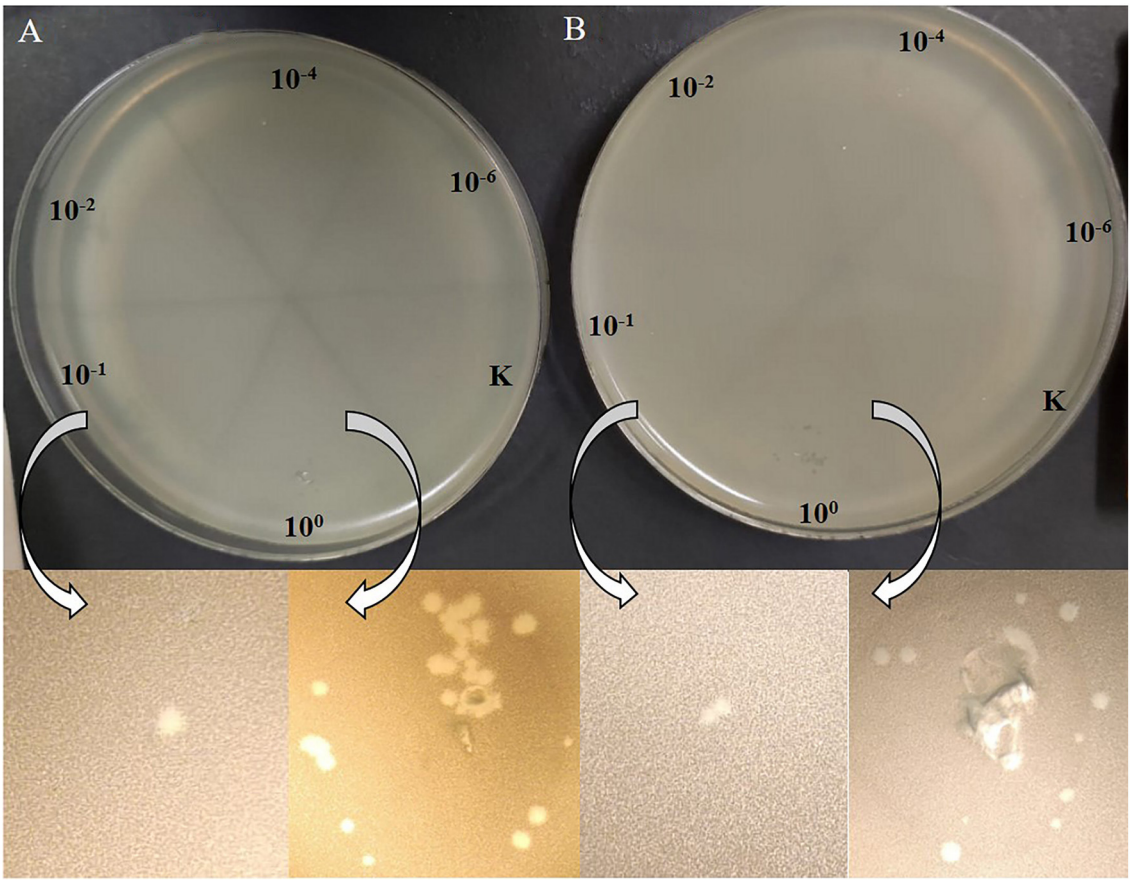

FIGURE 6
Plaques formed by P1 *c1 -100* Tn*9* IS*1*::km^{R} bacteriophage released from *P. agglomerans* L15 and *P. agglomerans* IPAG312 lysogens on the layer of *E. coli* N99 indicator strain cells. **(A)** IPAG312/P1. **(B)** L15/P1.

The truncated Tn*9* insertions in the L15 chromosome, in nine independent clones, were mapped to various sites of the region between pos. 3552017–3552106 of the *P. agglomerans* L15 genome corresponding to the promoter region and the 5′ end of a gene encoding the YdgH/BhsA/McbA-like domain-containing protein of unknown function (locus_tag CBF16_RS16745; Figure 1). The preferential insertion of Tn*9* in one locus is consistent with previous observations that while in general IS*1* and Tn*9* insert into easily denaturable regions with some specificity to the sequences homologous to the inverted terminal repeats (ITRs) of these elements (Galas et al., 1980; Miller et al., 1980), in some strains they insert preferentially in one locus (Il'ina et al., 1980). We found that the 7-nt sequence (TGCCAAC) present in the leftmost ITRs of both IS*1* sequences of P1 Tn*9* is also present at pos. 3552102 of the *P. agglomerans* L15 genome and marks the border between the L15-derived and Tn9-derived sequence in two of the analyzed clones. However, this sequence is present in 410 differently localized and differently oriented copies in the L15 chromosome, suggesting that its presence in the insertion region is either unimportant or is not the only factor responsible for selecting this insertion site.

The insertions of Tn*9* from P1 to the L15 chromosome studied in this work were always associated with deletions of the leftmost IS*1* sequence of Tn*9* and various parts of the Tn*9* region preceding the *cat* gene promoter. Additionally, they were mostly accompanied by the rearrangement in the remaining parts of this region in Tn*9*. This is consistent with previous observations indicating that the Tn*9* as well as IS*1* insertions cause alterations in the insertion target sites (Johnsrud et al., 1978; Ohtsubo and Ohtsubo, 1978; Calos and Miller, 1980; Meyer et al., 1980; Iida et al., 1981; Résibois et al., 1981; Gorb et al., 2011). The Tn*9* insertion in the P1 *c1-100* Tn*9* bacteriophage, which was used in this study, is at the resident IS*1* of P1 and contains the P1-derived IS*1* sequence at its left border (Galas et al., 1980; Łobocka et al., 2004). It was formed not by Tn*9* transposition to the genome of P1 but by two successive recombinations between the P1 IS*1* and the IS*1* sequences of R plasmid pSM14, which served as a donor of chloramphenicol resistance marker to P1 (Iida, 1983). Possibly, the P1 Tn*9* insertions in a single region of the *P. agglomerans* L15 strain are also formed by recombination.

We found that the epiphytic environmental *P. agglomerans* L15 strain can become proficient for the lysogeny with P1 *c1-100* Tn*9* phage if obstacles preventing the lysogeny can be overcome. The only obstacle preventing the lysogeny appears to be the mobility of the P1 Tn*9* transposon. One can assume that conditions promoting the transposition of Tn*9* to a chromosome remove the selective pressure to maintain the P1 prophage in the

freshly formed lysogens. Additionally, the accompanying deletion of the Tn*9* leftmost IS*1,* which is responsible for transposon mobility, prevents the reinsertion of truncated Tn*9* into the P1 genome. Together, this leads to the out-competition of P1 by the resident plasmids that are incompatible with it. We show that the immobilization of P1 Tn9 or the selection for a different immobile antibiotic-resistant marker inserted in the P1 *c1-100* Tn*9* genome, in addition to Tn*9,* reverts this scenario by enabling infecting P1 to outcompete both plasmids incompatible with it and to establish lysogeny. The antibiotic-dependent selective pressure to keep P1 in cells has a much stronger effect on the outcome of P1 infection than the presence in a cell of MazEF anti-phage defense system and of plasmids incompatible with P1. This may explain, at least in part, a surprisingly fast spreading of antibiotic resistance in bacteria grown in environments contaminated with antibiotics.

The P1 *c1-100* Tn*9* mutant has been widely used in studies on the host range of P1 (Yarmolinsky and Sternberg, 1988; Giermasińska and Łobocka, 2016, and references therein). Here, we show that even if bacteria can adsorb P1 and are metabolically compatible with P1 to support its lytic development or lysogeny, this mutant's failure to lysogenize them may result from the action of factors selective to cells in which Tn*9* transposed to a chromosome. Thus, negative results of attempts to obtain P1 *c1-100* Tn*9* lysogens should be verified using a P1 *c1-100* derivative carrying an immobile antibiotic resistance marker.

An unexpected result of our study was the discovery of how easily P1 could outcompete the two plasmids incompatible with it from the *P. agglomerans* L15 cells if only it contained an immobile selective marker. This observation could find practical use in the future. Large plasmids are common in *Pantoea agglomerans* and other species of *Pantoea* genus (Shetty et al., 2023). Only a few of them have been studied and found to significantly contribute to the versatility of *Pantoea* spp. strains. Our analysis of *Pantoea* strain sequences deposited in GenBank (accessed 2023-12-06) revealed that plasmids with partition cassette or replicon sequences highly similar to those of pPagL15_1 and pPagL15_3, respectively, are common in *Pantoea* strains representing various species. Eighty-eight *Pantoea* plasmids encode proteins with 72–100% identity over their entire length to ParB of pPagL15_1 plasmid (Supplementary Table 8). In all these proteins, amino acid residues of P1 ParB conserved in pPagL15_1 ParB and shown in P1 ParB to be essential for binding to *parS* and for the determination of P1 specific incompatibility are conserved (data not shown). It is worth noting that all the *Pantoea* P1 ParB homologs are encoded by *Pantoea* megaplasmids (Supplementary Table 8). Plasmids with replicon sequences highly similar to pPagL15_3 (100% coverage and over 90% of identity) and likely to be replicationally incompatible with P1 are less common in *Pantoea* strains. We detected such sequences in 19 *Pantoea* plasmid genomes deposited in GenBank (accessed November 13, 2023). Seventeen of them were detected in *P. agglomerans*, one in *Pantoea vagans,* and one in *Pantoea alfalfa* (data not shown). Curing bacteria from plasmids lacking phenotypic markers that are easy to select or differentiate in simple plate tests is typically a challenge, especially if their stability is high. Thus, the P1 *c1-100* Tn*9* IS*1*::km^R mutant with immobilized Tn*9* may be a ready-to-use tool in curing *Pantoea* strains from plasmids incompatible with P1 to facilitate their functional analysis.

Our results indicate that P1 can enrich the repertoire of molecular biology tools available for genetic manipulations in *P. agglomerans*. Certain plasmid-based tools have been described as suitable for such manipulations. Some, but not all, *P. agglomerans* strains can stably maintain *E. coli* pBR322 plasmid-based vectors and can be electroporated with derivatives of pBR322 (Wright et al., 2001). Some others can be electroporated with shuttle vectors constructed by cloning in the *E. coli* pUC18 plasmid of small cryptic plasmids identified in certain endophytic *P. agglomerans* strains (Andreote et al., 2008; de Lima Procópio et al., 2011). However, the use of the tools mentioned above is limited due to the limit of cloned insert size and the failure of their introduction to certain *P. agglomerans* strains.

Meanwhile, we demonstrated here using about 12 kb plasmid, just as an example, that P1 phages can transfer plasmids to some *P. agglomerans* strains by transduction. In this study, we used homologous recombination to insert a plasmid into P1 DNA without compromising the phage function of P1, which limited the size of the insert. However, P1 is a phage that mediates high-efficiency generalized transduction (Kenzaka et al., 2007; Thomason et al., 2007 and references therein). Its head can accommodate DNA of ~105 kb and can pack large plasmids or chromosomal fragments of up to this size if they contain sequences resembling the P1 *pac* site to initiate packaging (Sternberg and Maurer, 1991; Coren et al., 1995; Huang and Masters, 2014). Thus, our results showing the ability of P1 with the stable, selective marker to infect the *P. agglomerans* L15 cells productively open a possibility to use P1 to transfer genomic fragments or plasmids between various *P. agglomerans* strains and between *P. agglomerans* and other hosts of P1, especially model *E. coli* strains. The only described *P. agglomerans* phage that mediates generalized transduction is a flagellotrophic phage that could not infect a tested *E. coli* strain (Evans et al., 2010). The capacity of the P1 head makes this phage potentially proficient to transfer from *P. agglomerans* to *E. coli,* even large gene clusters, such as those that encode antibiotic synthesis pathways that have been identified in certain *P. agglomerans* strains (see Williams et al., 2020, and references therein). Comparison of the *P. agglomerans* L15 chromosomal sequence with the genomic sequence of the *E. coli* K-12 MG1655 strain (NC_000913) using BlastN revealed 775 fragments that encompass 22% of the *P. agglomerans* L15 chromosome and are ~91% identical to those of *E. coli,* including several fragments of 100% identity. Thus, the P1-mediated transfer of certain selectable *P. agglomerans* genomic fragments to *E. coli* could be possible.

Data availability statement

The datasets presented in this study can be found in online repositories. The names of the repository/repositories and accession number(s) can be found at: https://www.ncbi.nlm.nih.gov/genbank/, CP034148, CP034149, CP034150, and CP034151.

Author contributions

KG-B: Conceptualization, Formal analysis, Funding acquisition, Investigation, Methodology, Validation, Visualization, Writing – original draft, Writing – review & editing, Data curation. JG: Data curation, Investigation, Methodology, Validation, Writing – original draft, Resources, Software. ES: Investigation, Methodology, Software, Writing – original draft, Data curation. UG: Investigation, Writing – original draft. KŻ: Investigation, Writing – original draft. HR-B: Resources, Writing – original draft. RG: Resources, Methodology, Writing – original draft. MŁ: Methodology, Resources, Conceptualization, Formal analysis, Funding acquisition, Investigation, Project administration, Software, Supervision, Validation, Visualization, Writing – original draft, Writing – review & editing, Data curation.

Funding

The author(s) declare financial support was received for the research, authorship, and/or publication of this article. This work was supported by funds from the Warsaw University of Life Sciences (SGGW) internal grants no. 505-10-012400-A01080-99, 505-10-012400-K00394-99-40002, 505-10-012400-L00356-99, and 505-10-012400-M00289-99, for Ph.D. students; from the yearly Mazovian Voivodeship Marschal fellowship for KG-B in 2014, and the statutory funds of the Institute of Biochemistry and Biophysics of the Polish Academy of Sciences.

Acknowledgments

The authors thank dr. hab. Aneta Bartosik for providing the RK415 plasmid. A part of this study was presented at the Viruses of Microbes 2023 conference in Tbilisi, Georgia.

Conflict of interest

The authors declare that the research was conducted in the absence of any commercial or financial relationships that could be construed as a potential conflict of interest.

Publisher's note

Supplementary material

The Supplementary Material for this article can be found online at: https://www.frontiersin.org/articles/10.3389/fmicb.2024.1356206/full#supplementary-material

References

Abby, S. S., Néron, B., Ménager, H., Touchon, M., and Rocha, E. P. (2014). MacSyFinder: a program to mine genomes for molecular systems with an application to CRISPR-Cas systems. *PLoS ONE* 9:e110726. doi: 10.1371/journal.pone.0110726

Abeles, A. L., Friedman, S. A., and Austin, S. J. (1985). Partition of unit-copy miniplasmids to daughter cells. III. The DNA sequence and functional organization of the P1 partition region. *J. Mol. Biol.* 185, 261–272. doi: 10.1016/0022-2836(85)90402-4

Adams, M. H. (1959). *Bacteriophages*. New York, NY: Interscience Publishers Inc.

Ahmed, A. (1984). A deletion analysis of transposon Tn*9*. *J. Mol. Biol.* 173, 523–529. doi: 10.1016/0022-2836(84)90395-4

Altschul, S. F., Madden, T. L., Schäffer, A. A., Zhang, J., Zhang, Z., Miller, W., et al. (1997). Gapped BLAST and PSI-BLAST: a new generation of protein database search programs. *Nucleic Acids Res.* 25, 3389–3402. doi: 10.1093/nar/25.17.3389

Andreote, F. D., Rossetto, P. B., Souza, L. C., Marcon, J., Maccheroni, W. Jr., Azevedo, J. L., et al. (2008).Endophytic population of Pantoea agglomerans in citrus plants and development of a cloning vector for endophytes. *J. Basic Microbiol.* 48, 338–346. doi: 10.1002/jobm.200700341

Aziz, R. K., Bartels, D., Best, A. A., DeJongh, M., Disz, T., Edwards, R. A., et al. (2008). The RAST Server: rapid annotations using subsystems technology. *BMC Genom.* 9:75. doi: 10.1186/1471-2164-9-75

Bednarek, A., Cena, A., Izak, W., Bigos, J., and Łobocka, M. (2022). Functional dissection of P1 bacteriophage holin-like proteins reveals the biological sense of P1 lytic system complexity. *Int. J. Mol. Sci.* 23:4231. doi: 10.3390/ijms23084231

Bednarek, A., Giermasińska-Buczek, K., and Łobocka, M. (2023). Efficient traceless modification of the P1 bacteriophage genome through homologous recombination with enrichment in double recombinants: a new perspective on the functional annotation of uncharacterized phage genes. *Front. Microbiol.* 14:1135870. doi: 10.3389/fmicb.2023.1135870

Bernard, P. (1996). Positive selection of recombinant DNA by CcdB. *Biotechniques* 21, 320–323. doi: 10.2144/96212pf01

Bertani, G. (1951). Studies on lysogenesis. I. The mode of phage liberation by lysogenic *Escherichia coli*. *J. Bacteriol.* 62, 293–300. doi: 10.1128/jb.62.3.293-300.1951

Brettin, T., Davis, J. J., Disz, T., Edwards, R. A., Gerdes, S., Olsen, G. J., et al. (2015). RASTtk: a modular and extensible implementation of the RAST algorithm for building custom annotation pipelines and annotating batches of genomes. *Sci. Rep.* 5:8365. doi: 10.1038/srep08365

Bulyhina, T. V., Zdorovenko, E. L., Varbanets, L. D., Shashkov, A. S., Kadykova, A. A., Knirel, Y. A., et al. (2020). Structure of O-polysaccharide and lipid A of *Pantoea agglomerans* 8488. *Biomolecules* 10:804. doi: 10.3390/biom10050804

Calos, M. P., and Miller, J. H. (1980). Molecular consequences of deletion formation mediated by the transposon Tn*9*. *Nature* 285, 38–41. doi: 10.1038/285038a0

Carobbi, A., Di Nepi, S., Fridman, C. M., Dar, Y., Ben-Yaakov, R., Barash, I., et al. (2022). An antibacterial T6SS in *Pantoea agglomerans* pv. betae delivers a lysozyme-like effector to antagonize competitors. *Environ. Microbiol.* 24, 4787–4802. doi: 10.1111/1462-2920.16100

Chandler, M., and Galas, D. J. (1983). Cointegrate formation mediated by Tn*9*. *II. Activity of IS1 is modulated by external DNA sequences. J. Mol. Biol.* 170, 61–91. doi: 10.1016/s0022-2836(83)80227-7

Chattoraj, D. K., and Schneider, T. D. (1997). Replication control of plasmid P1 and its host chromosome: the common ground. *Prog. Nucleic Acid Res. Mol. Biol.* 57, 145–186. doi: 10.1016/S0079-6603(08)60280-9

Cole, S. T., and Guest, J. R. (1980). Genetic and physical characterization of lambda transducing phages (lambda frdA) containing the fumarate reductase gene of *Escherichia coli* K12. *Mol. Gen. Genet.* 178, 409–418. doi: 10.1007/BF00270492

Coren, J. S., Pierce, J. C., and Sternberg, N. (1995). Headful packaging revisited: the packaging of more than one DNA molecule into a bacteriophage P1 head. *J. Mol. Biol.* 249, 176–184. doi: 10.1006/jmbi.1995.0287

Dabrazhynetskaya, A., Brendler, T., Ji, X., and Austin, S. (2009). Switching protein-DNA recognition specificity by single-amino-acid substitutions in the P1 par family of plasmid partition elements. *J. Bacteriol.* 191, 1126–1131. doi: 10.1128/JB.01358-08

Dabrazhynetskaya, A., Sergueev, K., and Austin, S. (2005). Species and incompatibility determination within the P1par family of plasmid partition elements. *J. Bacteriol.* 187, 5977–5983. doi: 10.1128/JB.187.17.5977-5983.2005

Davidov, E., and Kaufmann, G. (2008). RloC: a wobble nucleotide-excising and zinc-responsive bacterial tRNase. *Mol. Microbiol.* 69, 1560–1574. doi: 10.1111/j.1365-2958.2008.06387.x

De Bruijn, F. J., and Bukhari, A. I. (1978). Analysis of transposable elements inserted in the genomes of bacteriophages Mu and P1. *Gene* 3, 315–331. doi: 10.1016/0378-1119(78)90041-0

De Coster, W., D'Hert, S., Schultz, D. T., Cruts, M., and Van Broeckh, C. (2018). NanoPack: visualizing and processing long-read sequencing data. *Bioinformatics* 34, 2666–2669. doi: 10.1093/bioinformatics/bty149

de Lima Procópio, R. E., Araújo, W. L., Andreote, F. D., and Azevedo, J. L. (2011). Characterization of a small cryptic plasmid from endophytic *Pantoea agglomerans* and its use in the construction of an expression vector. *Genet. Mol. Biol.* 34, 103–109. doi: 10.1590/S1415-47572010005000096

Delétoile, A., Decré, D., Courant,. S., Passet, V., Audo, J., Grimont, P., et al. (2009). Phylogeny and identification of Pantoea species and typing of *Pantoea agglomerans* strains by multilocus gene sequencing. *J. Clin. Microbiol.* 47, 300–310. doi: 10.1128/JCM.01916-08

Dubnau, D. (1999). DNA uptake in bacteria. *Annu. Rev. Microbiol.* 53, 217–244. doi: 10.1146/annurev.micro.53.1.217

Ershova, A. S., Rusinov, I. S., Spirin, S. A., Karyagina, A. S., and Alexeevski, A. V. (2015). Role of restriction-modification systems in prokaryotic evolution and ecology. *Biochemistry* 80, 1373–1386. doi: 10.1134/S0006297915100193

Evans, T. J., Crow, M. A., Williamson, N. R., Orme, W., Thomson, N. R., Komitopoulou, E., et al. (2010). Characterization of a broad-host-range flagellum-dependent phage that mediates high-efficiency generalized transduction in, and between, Serratia and Pantoea. *Microbiology* 156, 240–247. doi: 10.1099/mic.0.032797-0

Franklin, N. C. (1969). Mutation in galU gene of *E. coli* blocks phage P1 infection. *Virology* 38, 189–191. doi: 10.1016/0042-6822(69)90144-5

Fu, J. F., Ying, S. W., and Liu, S. T. (1997). Cloning and characterization of the ori region of pSW1200 of *Erwinia stewartii*: similarity with plasmid P1. *Plasmid* 38, 141–147. doi: 10.1006/plas.1997.1308

Galas, D. J., Calos, M. P., and Miller, J. H. (1980). Sequence analysis of Tn9 insertions in the lacZ gene. *J. Mol. Biol.* 144, 19–41. doi: 10.1016/0022-2836(80)90213-2

Gao, L., Altae-Tran, H., Böhning, F., Makarova, K. S., Segel, M., Schmid-Burgk, J. L., et al. (2020). Diverse enzymatic activities mediate antiviral immunity in prokaryotes. *Science* 369, 1077–1084. doi: 10.1126/science.aba0372

Giermasińska, K., and Łobocka, M. (2016). "Interaction of bacteriophage P1 with cells of selected plant pathogens of the genus Erwinia and related genera," in *Selected Issues of Chemistry, Physics and Biology*, eds. B. Zdunek and M. Olszówka (Lublin: Tygiel Press), 48–67.

Gilcrease, E. B., and Casjens, S. R. (2018). The genome sequence of *Escherichia coli* tailed phage D6 and the diversity of Enterobacteriales circular plasmid prophages. *Virology* 515, 203–214. doi: 10.1016/j.virol.2017.12.019

Goldberg, R. B., Bender, R. A., and Streicher, S. L. (1974). Direct selection for P1- sensitive mutants of Enteric Bacteria. *J. Bacteriol.* 118, 810–814. doi: 10.1128/jb.118.3.810-814.1974

Gorb, T. E., Kushkina, A. I., Ivanitsa, T. V., Lysenko, T. G., and Tovkach, F. I. (2011). Structural stability of DNA of the transposon derivatives of pCA25 plasmid. *Mikrobiol. Z.* 73, 53–57.

Grant, J. R., Enns, E., Marinier, E., Mandal, A., Herman, E. K., Chen, C. Y., et al. (2023). Proksee: in-depth characterization and visualization of bacterial genomes. *Nucleic Acids Res.* 51, W484–W492. doi: 10.1093/nar/gkad326

Grigoriev, P. S., and Lobocka, M. B. (2001). Determinants of segregational stability of the linear plasmid-prophage N15 of *Escherichia coli*. *Mol. Microbiol.* 42, 355–368. doi: 10.1046/j.1365-2958.2001.02632.x

Haft, D. H., DiCuccio, M., Badretdin, A., Brover, V., Chetvernin, V., O'Neill, K., et al. (2018). RefSeq: an update on prokaryotic genome annotation and curation. *Nucleic Acids Res.* 46, D851–D860. doi: 10.1093/nar/gkx1068

Hashimoto, M., Ichimura, T., Mizoguchi, H., Tanaka, K., Fujimitsu, K., Keyamura, K., et al. (2005). Cell size and nucleoid organization of engineered *Escherichia coli* cells with a reduced genome. *Mol. Microbiol.* 55, 137–149. doi: 10.1111/j.1365-2958.2004.04386.x

Hashimoto, M., Satou, R., Ozono, M., Inagawa, H., and Soma, G. I. (2017). Characterization of the O-antigen polysaccharide derived from *Pantoea agglomerans* IG1 lipopolysaccharide. *Carbohydr. Res.* 449, 32–36. doi: 10.1016/j.carres.2017.06.017

Hazan, R., and Engelberg-Kulka, H. (2004). *Escherichia coli* mazEF-mediated cell death as a defense mechanism that inhibits the spread of phage P1. *Mol. Genet. Genom.* 272, 227–234. doi: 10.1007/s00438-004-1048-y

Huan, Y. W., Fa-Arun, J., and Wang, B. (2022). The role of O-antigen in P1 transduction of *Shigella flexneri* and *Escherichia coli* with its alternative S' tail fibre. *J. Mol. Biol.* 434:167829. doi: 10.1016/j.jmb.2022.167829

Huang, H., and Masters, M. (2014). Bacteriophage P1 pac sites inserted into the chromosome greatly increase packaging and transduction of *Escherichia coli* genomic DNA. *Virology* 468–470, 274–282. doi: 10.1016/j.virol.2014.07.029

Humphrey, J., Seitz, T., Haan, T., Ducluzeau, A. L., and Drown, D. M. (2019). Complete genome sequence of *Pantoea agglomerans* TH81, isolated from a permafrost thaw gradient. *Microbiol. Resour. Announc.* 8, e01486–e01418. doi: 10.1128/MRA.01486-18

Iida, S. (1983). On the origin of the chloramphenicol resistance transposon Tn*9*. *J. Gen. Microbiol.* 129, 1217–1225. doi: 10.1099/00221287-129-4-1217

Iida, S., Marcoli, R., and Bickle, T. A. (1981). Variant insertion element IS1 generates 8-base pair duplications of the target sequence. *Nature* 294, 374–376. doi: 10.1038/294374a0

Iida, S., Streiff, M. B., Bickle, T. A., and Arber, W. (1987). Two DNA antirestriction systems of bacteriophage P1, darA, and darB: characterization of darA- phages. *Virology* 157, 156–166. doi: 10.1016/0042-6822(87)90324-2

Il'ina, T. S., Nechaeva, E. V., Pasynkova, L. N., Smirnova, N. I., and Smirnov, G. B. (1980). Tn9 integration sites and their effect on transposon properties. *Genetika* 16, 46–54.

Johnsrud, L., Calos, M. P., and Miller, J. H. (1978). The transposon Tn*9* generates a 9 bp repeated sequence during integration. *Cell* 15, 1209–1219. doi: 10.1016/0092-8674(78)90047-8

Jones, P., Binns, D., Chang, H. Y., Fraser, M., Li, W., McAnulla, C., et al. (2014). InterProScan 5: genome-scale protein function classification. *Bioinformatics* 30, 1236–1240. doi: 10.1093/bioinformatics/btu031

Kaiser, D., and Dworkin, M. (1975). Gene transfer to myxobacterium by Escherichia coli phage P1. *Science* 187, 653–654. doi: 10.1126/science.803710

Karamanos, Y., Kol, O., Wieruszeski, J. M., Strecker, G., Fournet, B., and Zalisz, R. (1992). Structure of the O-specific polysaccharide chain of the lipopolysaccharide of *Enterobacter agglomerans*. *Carbohydr. Res.* 231, 197–204. doi: 10.1016/0008-6215(92)84019-O

Kato, J., and Hashimoto, M. (2007). Construction of consecutive deletions of the *Escherichia coli* chromosome. *Mol. Syst. Biol.* 3:132. doi: 10.1038/msb4100174

Keller, C. M., Kendra, C. G., Bruna, R. E., Craft, D., and Pontes, M. H. (2021). Genetic modification of Sodalis species by DNA transduction. *mSphere* 6, e01331–e01320. doi: 10.1128/mSphere.01331-20

Kenzaka, T., Tani, K., Sakotani, A., Yamaguchi, N., and Nasu, M. (2007). High-frequency phage-mediated gene transfer among *Escherichia coli* cells, determined at the single-cell level. *Appl. Environ. Microbiol.* 73, 3291–3299. doi: 10.1128/AEM.02890-06

Kittleson, J. T., DeLoache, W., Cheng, H. Y., and Anderson, J. C. (2012). Scalable plasmid transfer using engineered P1-based phagemids. *ACS Synth. Biol.* 1, 583–589. doi: 10.1021/sb300054p

Klaiman, D., Steinfels-Kohn, E., Krutkina, E., Davidov, E., and Kaufmann, G. (2012). The wobble nucleotide-excising anticodon nuclease RloC is governed by the zinc-hook and DNA-dependent ATPase of its Rad50-like region. *Nucleic Acids Res.* 40, 8568–8578. doi: 10.1093/nar/gks593

Kohchi, C., Inagawa, H., Nishizawa, T., Yamaguchi, T., Nagai, S., and Soma, G. (2006). Applications of lipopolysaccharide derived from Pantoea agglomerans (IP-PA1) for health care based on macrophage network theory. *J. Biosci. Bioeng.* 102, 485–496. doi: 10.1263/jbb.102.485

Konddo, E., and Mitsuhashi, S. (1964). Drug resistance of enteric bacteria. IV. Active transducing bacteriophage P1 CM produced by the combination of R factor with bacteriophage P1. *J. Bacteriol.* 88, 1266–1276. doi: 10.1128/jb.88.5.1266-1276.1964

Lam, C. N., Mehta-Kolte, M. G., Martins-Sorenson, N., Eckert, B., Lin, P. H., Chu, K., et al. (2021). A tail fiber engineering platform for improved bacterial transduction-based diagnostic reagents. *ACS Synth. Biol.* 10, 1292–1299. doi: 10.1021/acssynbio.1c00036

Lee, S. I., Tran, T. D., Huynh, S., Parker, C. T., Hnasko, R., and McGarvey, J. A. (2021). Complete genome sequence of *Pantoea agglomerans* ASB05 using illumina and PacBio sequencing. *Microbiol. Resour. Announc.* 10:e0050121. doi: 10.1128/MRA.00501-21

Lennox, E. S. (1955). Transduction of linked genetic characters of the host by bacteriophage P1. *Virology* 1, 190–206. doi: 10.1016/0042-6822(55)90016-7

Lerouge, I., and Vanderleyden, J. (2002). O-antigen structural variation: mechanisms and possible roles in animal/plant-microbe interactions. *FEMS Microbiol. Rev.* 26, 17–47. doi: 10.1111/j.1574-6976.2002.tb00597.x

Lindow, S. E., Desurmont, C., Elkins, R., McGourty, G., Clark, E., and Brandl, M. T. (1998). Occurrence of indole-3-acetic acid-producing bacteria on pear trees and their association with fruit russet. *Phytopathology* 88, 1149–1157. doi: 10.1094/PHYTO.1998.88.11.1149

Liu, J., Chen, C. Y., Shiomi, D., Niki, H., and Margolin, W. (2011). Visualization of bacteriophage P1 infection by cryo-electron tomography of tiny *Escherichia coli*. *Virology* 417, 304–311. doi: 10.1016/j.virol.2011.06.005

Łobocka, M., and Gągała, U. (2021). "Prophage P1: an example of a prophage that is maintained as a plasmid," in *Bacteriophages*, eds D. R. Harper, S. T. Abedon, B. H. Burrowes, and M. L. McConville (Cham: Springer). doi: 10.1007/978-3-319-40598-8_54-1

Łobocka, M., and Yarmolinsky, M. (1996). P1 plasmid partition: a mutational analysis of ParB. *J. Mol. Biol.* 259, 366–382. doi: 10.1006/jmbi.1996.0326

Łobocka, M. B., Rose, D. J., Plunkett, G., Rusin, M., Samojedny, A., Lehnherr, H., et al. (2004). Genome of bacteriophage P1. *J. Bacteriol.* 186, 7032–7068. doi: 10.1128/JB.186.21.7032-7068.2004

Lorenzi, A. S., Bonatelli, M. L., Chia, M. A., Peressim, L., and Quecine, M. C. (2022). Opposite sides of *Pantoea agglomerans* and its associated commercial outlook. *Microorganisms* 10:2072. doi: 10.3390/microorganisms10102072

Machida, C., Machida, Y., Wang, H. C., Ishizaki, K., and Ohtsubo, E. (1983). Repression of cointegration ability of insertion element IS1 by transcriptional readthrough from flanking regions. *Cell* 34, 135–142. doi: 10.1016/0092-8674(83)90143-5

Matilla, M. A., Evans, T. J., Martín, J., Udaondo, Z., Lomas-Martínez, C., Rico-Jiménez, M., et al. (2023). Herbicolin A production and its modulation by quorum sensing in a *Pantoea agglomerans* rhizobacterium bioactive against a broad spectrum of plant-pathogenic fungi. *Microb. Biotechnol.* 16, 1690–1700. doi: 10.1111/1751-7915.14193

Meyer, J., Iida, S., and Arber, W. (1980). Does the insertion element IS1 transpose preferentially into A+T-rich DNA segments? *Mol. Gen. Genet.* 178, 471–473. doi: 10.1007/BF00270502

Miller, J. H. (1972). *Experiments in Molecular Genetics*. Cold Spring Harbor, NY: Cold Spring Harbor Lab Press.

Miller, J. H., Calos, M. P., Galas, D., Hofer, M., Büchel, D. E., and Müller-Hill, B. (1980). Genetic analysis of transpositions in the lac region of *Escherichia coli*. *J. Mol. Biol.* 144, 1–18. doi: 10.1016/0022-2836(80)90212-0

Millman, A., Melamed, S., Leavitt, A., Doron, S., Bernheim, A., Hör, J., et al. (2022). An expanded arsenal of immune systems that protect bacteria from phages. *Cell Host Microbe.* 30, 1556–1569.e5. doi: 10.1016/j.chom.2022.09.017

Murooka, Y., and Harada, T. (1979). Expansion of the host range of coliphage P1 and gene transfer from enteric bacteria to other gram-negative bacteria. *Appl. Environ. Microbiol.* 38, 754–757. doi: 10.1128/aem.38.4.754-757.1979

Novick, R. P. (1987). Plasmid incompatibility. *Microbiol. Rev.* 51, 381–395. doi: 10.1128/mr.51.4.381-395.1987.

Ohtsubo, H., and Ohtsubo, E. (1978). Nucleotide sequence of an insertion element, IS1. *Proc. Natl. Acad. Sci. U. S. A.* 75, 615–619. doi: 10.1073/pnas.75.2.615

Ornellas, E. P., and Stocker, B. A. (1974). Relation of lipopolysaccharide character to P1 sensitivity in *Salmonella typhimurium*. *Virology* 60, 491–502. doi: 10.1016/0042-6822(74)90343-2

Overbeek, R., Olson, R., Pusch, G. D., Olsen, G. J., Davis, J. J., Disz, T., et al. (2014). The SEED and the Rapid Annotation of microbial genomes using Subsystems Technology (RAST). *Nucleic Acids Res.* 42, D206–D214. doi: 10.1093/nar/gkt1226

Radnedge, L., Youngren, B., Davis, M., and Austin, S. (1998). Probing the structure of complex macromolecular interactions by homolog specificity scanning: the P1 and P7 plasmid partition systems. *EMBO J.* 17, 6076–6085. doi: 10.1093/emboj/17.20.6076

Rekosz-Burlaga, H., Borys, M., and Goryluk-Salmonowicz, A. (2014). Cultivable microorganisms inhabiting the aerial parts of *Hypericum perforatum*. *Acta Scientiar. Polonor. Hortor. Cult.* 13, 117–129.

Ren, J., Karna, S., Lee, H. M., Yoo, S. M., and Na, D. (2019). Artificial transformation methodologies for improving the efficiency of plasmid DNA transformation and simplifying its use. *Appl. Microbiol. Biotechnol.* 103, 9205–9215. doi: 10.1007/s00253-019-10173-x

Résibois, A., Toussaint, A., van Gijsegem, F., and Faelen, M. (1981). Physical characterization of mini-Mu and mini-D108. *Gene* 14, 103–113. doi: 10.1016/0378-1119(81)90152-9

Rosner, J. L. (1972). Formation, induction, and curing of bacteriophage P1 lysogens. *Virology* 48, 679–689. doi: 10.1016/0042-6822(72)90152-3

Sambrook, J., Fritsch, E. F., and Maniatis, T. (1989). *Molecular Cloning: A Laboratory Manual*. Cold Spring Harbor, NY: Cold Spring Harbor Laboratory.

Sergueev, K., Dabrazhynetskaya, A., and Austin, S. (2005). Plasmid partition system of the P1par family from the pWR100 virulence plasmid of *Shigella flexneri*. *J. Bacteriol.* 187, 3369–3373. doi: 10.1128/JB.187.10.3369-3373.2005

Shetty, S., Kamble, A., and Singh, H. (2023). Insights into the potential role of plasmids in the versatility of the genus Pantoea. *Mol. Biotechnol.* 2023:3. doi: 10.1007/s12033-023-00960-3

Smits, T. H., Rezzonico, F., Kamber, T., Goesmann, A., Ishimaru, C. A., Stockwell, V. O., et al. (2010). Genome sequence of the biocontrol agent *Pantoea vagans* strain C9-1. *J. Bacteriol.* 192, 6486–6487. doi: 10.1128/JB.01122-10

Sternberg, N. L., and Maurer, R. (1991). Bacteriophage-mediated generalized transduction in *Escherichia coli* and *Salmonella typhimurium*. *Methods Enzymol.* 204, 18–43. doi: 10.1016/0076-6879(91)04004-8

Streiff, M. B., Iida, S., and Bickle, T. A. (1987). Expression and proteolytic processing of the darA antirestriction gene product of bacteriophage P1. *Virology* 157, 167–171. doi: 10.1016/0042-6822(87)90325-4

Surtees, J. A., and Funnell, B. E. (2003). Plasmid and chromosome traffic control: how ParA and ParB drive partition. *Curr. Top. Dev. Biol.* 56, 145–180. doi: 10.1016/S0070-2153(03)01010-X

Tatusova, T., DiCuccio, M., Badretdin, A., Chetvernin, V., Nawrocki, E. P., Zaslavsky, L., et al. (2016). NCBI prokaryotic genome annotation pipeline. *Nucleic Acids Res.* 44, 6614–6624. doi: 10.1093/nar/gkw569

Tesson, F., Hervé, A., Mordret, E., Touchon, M., d'Humières, C., Cury, J., et al. (2022). Systematic and quantitative view of the antiviral arsenal of prokaryotes. *Nat. Commun.* 13:2561. doi: 10.1038/s41467-022-30269-9

Thissera, B., Alhadrami, H. A., Hassan, M. H. A., Hassan, H. M., Bawazeer, M., Yaseen, M., et al. (2020). Induction of cryptic antifungal pulicatin derivatives from *Pantoea agglomerans* by microbial co-culture. *Biomolecules* 10:268. doi: 10.3390/biom10020268

Thomason, L. C., Costantino, N., and Court, D. L. (2007). *E. coli* genome manipulation by P1 transduction. *Curr. Protoc. Mol. Biol.* 79, 1.17.1–1.17.8. doi: 10.1002/0471142727.mb0117s79

Tominaga, A., and Enomoto, M. (1986). Magnesium-dependent plaque formation by bacteriophage P1cinC(-) on *Escherichia coli* C and *Shigella sonnei*. *Virology* 155, 284–288. doi: 10.1016/0042-6822(86)90190-X

Varbanets, L. D., Bulyhina, T. V., Pasichnyk, L. A., and Zhytkevich, N. V. (2019). *Pantoea agglomerans* lipopolysaccharides: structure, functional and biological activity. *Ukr. Biochem. J.* 91, 5–20. doi: 10.15407/ubj91.01.005

Walker, J. T., and Walker, D. H. Jr. (1981). Structural proteins of coliphage P1. *Prog. Clin. Biol. Res.* 64, 69–77.

Walterson, A. M., and Stavrinides, J. (2015). Pantoea: insights into a highly versatile and diverse genus within the Enterobacteriaceae. *FEMS Microbiol. Rev.* 39, 968–984. doi: 10.1093/femsre/fuv027

Westwater, C., Schofield, D. A., Schmidt, M. G., Norris, J. S., and Dolan, J. W. (2002). Development of a P1 phagemid system for the delivery of DNA into Gram-negative bacteria. *Microbiology* 148, 943–950. doi: 10.1099/00221287-148-4-943

Williams, A. N., Sorout, N., Cameron, A. J., and Stavrinides, J. (2020). The integration of genome mining, comparative genomics, and functional genetics for biosynthetic gene cluster identification. *Front. Genet.* 11:600116. doi: 10.3389/fgene.2020.600116

Wilson, K. (2001). Preparation of genomic DNA from bacteria. *Curr. Protoc. Mol. Biol.* 2:2.4. doi: 10.1002/0471142727.mb0204s56

Wilson, M., and Lindow, S. E. (1994). Coexistence among epiphytic bacterial populations mediated through nutritional resource partitioning. *Appl. Environ. Microbiol.* 60, 4468–4477. doi: 10.1128/aem.60.12.4468-4477.1994

Wright, S. A., Zumoff, C. H., Schneider, L., and Beer, S. V. (2001). *Pantoea agglomerans* strain EH318 produces two antibiotics that inhibit *Erwinia amylovora in vitro*. *Appl. Environ. Microbiol.* 67, 284–292. doi: 10.1128/AEM.67.1.284-292.2001

Xu, S., Liu, Y. X., Cernava, T., Wang, H., Zhou, Y., Xia, T., et al. (2022). Fusarium fruiting body microbiome member *Pantoea agglomerans* inhibits fungal pathogenesis by targeting lipid rafts. *Nat. Microbiol.* 7, 831–843. doi: 10.1038/s41564-022-01131-x

Yamazaki, Y., Niki, H., and Kato, J. (2008). Profiling of *Escherichia coli* chromosome database. *Methods Mol. Biol.* 416, 385–389. doi: 10.1007/978-1-59745-321-9_26

Yarmolinsky, M., and Sternberg, N. (1988). "Bacteriophage Pl," in *The Bacteriophages, vol. 1*, ed. R. Calendar (New York, NY: Plenum Press), 291–438.

Yarmolinsky, M. B. (2004). Bacteriophage P1 in retrospect and prospect. *J. Bacteriol.* 186, 7025–7028. doi: 10.1128/JB.186.21.7025-7028.2004

Yarmolinsky, M. B., and Hoess, R. (2015). The legacy of Nat Sternberg: the genesis of Cre-lox technology. *Annu. Rev. Virol.* 2, 25–40. doi: 10.1146/annurev-virology-100114-054930

Frontiers in Microbiology

Explores the habitable world and the potential of microbial life

The largest and most cited microbiology journal which advances our understanding of the role microbes play in addressing global challenges such as healthcare, food security, and climate change.

Discover the latest Research Topics

See more →

Frontiers

Avenue du Tribunal-Fédéral 34
1005 Lausanne, Switzerland
frontiersin.org

Contact us

+41 (0)21 510 17 00
frontiersin.org/about/contact